

Tetsuo Tanabe *Editor*

---

# Tritium: Fuel of Fusion Reactors

# Tritium: Fuel of Fusion Reactors



Tetsuo Tanabe  
Editor

# Tritium: Fuel of Fusion Reactors



Springer

*Editor*

Tetsuo Tanabe

Interdisciplinary Graduate School  
of Engineering Sciences

Kyushu University  
Fukuoka  
Japan

ISBN 978-4-431-56458-4

ISBN 978-4-431-56460-7 (eBook)

DOI 10.1007/978-4-431-56460-7

Library of Congress Control Number: 2016954016

© Springer Japan 2017

This work is subject to copyright. All rights are reserved by the Publisher, whether the whole or part of the material is concerned, specifically the rights of translation, reprinting, reuse of illustrations, recitation, broadcasting, reproduction on microfilms or in any other physical way, and transmission or information storage and retrieval, electronic adaptation, computer software, or by similar or dissimilar methodology now known or hereafter developed.

The use of general descriptive names, registered names, trademarks, service marks, etc. in this publication does not imply, even in the absence of a specific statement, that such names are exempt from the relevant protective laws and regulations and therefore free for general use.

The publisher, the authors and the editors are safe to assume that the advice and information in this book are believed to be true and accurate at the date of publication. Neither the publisher nor the authors or the editors give a warranty, express or implied, with respect to the material contained herein or for any errors or omissions that may have been made.

Printed on acid-free paper

This Springer imprint is published by Springer Nature

The registered company is Springer Japan KK

The registered company address is: Chiyoda First Bldg. East, 3-8-1 Nishi-Kanda, Chiyoda-ku, Tokyo 101-0065, Japan

# Preface

After long and significant efforts of researchers on plasma confinement to realize controlled D-T nuclear fusion on Earth, now the International Tokamak Experimental Reactor (ITER) will soon be ready to demonstrate the fusion reaction producing energy. This research has taken a longer time in comparison with the rapid construction of successful nuclear fission reactors following the discovery of energy release in nuclear reactions. Nevertheless, to realize the fusion reactor as an energy source, many engineering-technological issues remain to be solved. It is unnecessary to say that the most important point is that the fusion reactor must be economically beneficial. The initial or capital cost to construct the fusion reactor is unavoidable, and most of the cost estimates so far indicate that a fusion reactor could be economical and repay its capital investment. But additional costs related to tritium fuel, or to sustaining fuel self-sufficiency in a D-T fusion reactor, and the trade-offs between tritium breeding and electricity production (or energy conversion) and tritium safety, are not small, and considerable effort will be required to reduce these costs. The main purpose of this book is to summarize recent efforts to establish fuel self-sufficiency in a D-T fusion reactor with strict regulation of tritium safety.

In 2013, a book entitled *Tritium in Fusion*, edited by S. Tosti and N. Ghirelli (Nova Publishers, NY, ISBN 978-1-62417-270-0) was published. It focused on the production and treatment of tritium in nuclear fusion equipment and aspects of measurements, dose assessment, and safety of tritium. The present book focuses on more practical aspects to realize a fusion reactor as an energy source. There is no doubt that safety is a concern in the tritium handling system described in the book cited above. To realize the fusion reactor as an energy source, however, there are additional issues related to tritium as a fusion fuel, and those are the subjects of the present book.

Although a tritium handling system has been established for military use, the system might not be directly applied to tritium systems for a fusion reactor, because the amount of tritium to be handled in the latter is much larger than in the former. In addition, owing to its limited availability, full recovery of tritium handled in any tritium subsystems in the fusion reactor is mandatory. For safety, tritium removal is

always required in any existing tritium handling system and removed tritium can be disposed of, whereas loss of tritium in the fusion reactor directly influences its fuel self-efficiency. Therefore, a significantly different approach is required in designing tritium handling in the fusion reactor.

This book is devoted to giving readers an idea and understanding of the characteristics of tritium for fusion in Part I, the current status of R&D on tritium fueling (including breeding) systems in Part II, and consideration of tritium safety in Part III.

In Part I (Chaps.1–5), Chap. 1, is an introductory chapter describing a fusion reactor focusing particularly on the use of tritium as a fuel, followed in Chap. 2 by the introduction of characteristics of tritium as a radioactive isotope of hydrogen. Chapters 3–5 summarize present knowledge of fuel (tritium) behavior in a fusion reactor. Because there is no reactor and tritium burning has not been realized yet, we have to extrapolate all present knowledge obtained from experiments and theories on large tokamaks of JET, JT-60U and TFTR, on various medium-size tokamaks, and in laboratory experiments on tritium behavior in reactor-size machines such as ITER and future power reactors. Chapters 3–5 thus describe overall tritium flow, tritium burning, and the behavior of fuel in a reactor, respectively.

In Part II (Chaps. 6–14), details of tritium handling and processing systems for tritium fueling and recycling maintaining tritium safety are described. Fueling is the key to maintaining burning plasma, as explained in Chap. 6. Both for tritium safety and fueling, tritium accountancy and measurements are indispensable, as described in detail in Chaps. 7 and 8. As discussed in Chap. 8, tritium measurement in plasma is not well established, and significant efforts are required. Tritium must be confined in any tritium handling system. Easy permeation by tritium of structural materials resulting in tritium contamination is a serious concern, noted in Chaps. 9 and 10. Isotope separation, explained in Chap. 11, is indispensable for fueling. To establish fuel self-efficiency, tritium breeding, and recovery are major concerns as set forth in Chaps. 12 and 13.

In Part III, major issues related to tritium safety are discussed. Chapters 14 and 15 deal with safety confinement of tritium and behavior of tritium released into the environment, with the important note that tritium safety for the public would be a minor concern in a fusion reactor.

This book is dedicated to the late Prof. Emeritus Masabumi Nishikawa of Kyushu University. During the editing process, we missed him who, as one of the most active tritium scientists in the world, had devoted significant effort to the initial editing of this book. His distinctive works on tritium breeding and tritium fuel systems for a fusion reactor were often referred to by numbers of scientists and engineers in many fields, not only tritium science and technology, but also plasma physics and reactor engineering and design. All authors of this book acknowledge his great work and leadership worldwide in tritium science and technology.

Finally, the editor wishes to thank all the authors for their qualified contributions to this book and acknowledges the support by Grant-in-Aid for Scientific Research, Ministry of Education, Culture and Sports, Priority area 467, “Tritium for Fusion” No. 19055008.

Fukuoka, Japan

Tetsuo Tanabe



# Contents

## **Part I Current Status of R&D on Tritium Fueling (Including Breeding) Systems**

<b>1</b>	<b>Introduction of a Nuclear Fusion Reactor</b>	3
	Tetsuo Tanabe	
<b>2</b>	<b>Characteristics of Tritium</b>	27
	Tetsuo Tanabe	
<b>3</b>	<b>Fuel Flow and Balance in a D-T Fusion Reactor</b>	49
	Tetsuo Tanabe and Masabumi Nishikawa	
<b>4</b>	<b>Burning Plasma</b>	73
	Yasuyuki Nakao	
<b>5</b>	<b>Behavior of Fuels in Reactor</b>	93
	Tetsuo Tanabe	

## **Part II Tritium Handling (Fueling) and Processing**

<b>6</b>	<b>Tritium Fueling System</b>	119
	Toshihiko Yamanishi	
<b>7</b>	<b>Tritium Measurement I—Tritium in Gas, Liquid, and Solid</b>	137
	Masanori Hara, Yoshinori Kawamura and Tetsuo Tanabe	
<b>8</b>	<b>Tritium Measurement II—Tritium in Plasma</b>	165
	Hideki Zushi	
<b>9</b>	<b>Permeation and Permeation Barrier</b>	207
	Yuji Hatano	
<b>10</b>	<b>Contamination and Decontamination</b>	231
	Kanetsugu Isobe	

<b>11 Isotope Separation System (ISS) . . . . .</b>	<b>243</b>
Toshihiko Yamanishi	
<b>12 Evaluation Method of Tritium Breeding Ratio Using Neutron Transport Equation . . . . .</b>	<b>257</b>
Hideaki Matsuura and Masabumi Nishikawa	
<b>13 Recovery of Tritium Bred in Blanket . . . . .</b>	<b>273</b>
Kazunari Katayama and Masabumi Nishikawa	
<b>Part III Tritium Issues Relating Safety</b>	
<b>14 Safety Confinement System . . . . .</b>	<b>297</b>
Kazunari Katayama and Masabumi Nishikawa	
<b>15 Behavior of Tritium Released to the Environment . . . . .</b>	<b>331</b>
Kazuyuki Noborio and Tetsuo Tanabe	
<b>Index . . . . .</b>	<b>357</b>

# Contributors

**Masanori Hara** Hydrogen Isotope Research Center, Organization for Promotion of Research, Toyama, Japan

**Yuji Hatano** Hydrogen Isotope Research Center, Organization for Promotion of Research, University of Toyama, Toyama, Japan

**Kanetsugu Isobe** Department of Blanket Systems Research, National Institutes for Quantum and Radiological Science and Technology, Fusion Energy Research and Development Directorate, Rokkasho Fusion Institute, Tokai, Ibaraki, Japan

**Kazunari Katayama** Interdisciplinary Graduate School of Engineering Sciences, Kyushu University, Kasuga, Fukuoka, Japan

**Yoshinori Kawamura** National Institutes for Quantum and Radiological Science and Technology, Fusion Energy Research and Development Directorate, Ibaraki, Japan

**Hideaki Matsuura** Department of Applied Quantum Physics and Nuclear Engineering, Kyushu University, Fukuoka, Japan

**Yasuyuki Nakao** Green Asia Education Center, Kyushu University, Kasuga, Fukuoka, Japan

**Masabumi Nishikawa** Interdisciplinary Graduate School of Engineering Sciences, Kyushu University, Kasuga, Fukuoka, Japan

**Kazuyuki Noborio** Hydrogen Isotope Research Center, University of Toyama, Toyama, Japan; Sakigake Semiconductor Co., Ltd, Kyoto, Japan

**Tetsuo Tanabe** Interdisciplinary Graduate School of Engineering Sciences, Kyushu University, Kasuga, Fukuoka, Japan

**Toshihiko Yamanishi** Department of Blanket Systems Research, National Institutes for Quantum and Radiological Science and Technology, Fusion Energy Research and Development Directorate, Rokkasho Fusion Institute, Aomori, Japan

**Hideki Zushi** Research Institute for Applied Mechanics, Kyushu University, Kasuga-City, Fukuoka, Japan

**Part I**

**Current Status of R&D on Tritium Fueling  
(Including Breeding) Systems**



# Chapter 1

## Introduction of a Nuclear Fusion Reactor

Tetsuo Tanabe

**Abstract** Most of energy resources on the earth are originated from energy given by the sun in which all energy is produced by nuclear fusion reactions. To build a small sun or to realize controlled fusion as an energy source on the earth has been a dream of human being. Owing to extensive research and development, the fusion reaction of Deuterium (D) and Tritium (T) soon comes in burning phase. Nevertheless, to realize a D-T fusion reactor as an energy source, lots of engineering issues still remain to be solved. Among all, T-relating issues are quite important, because T is hazardous due to its radioactivity and its resources are quite limited. In this chapter, after the introduction of nuclear fusion reactions, issues relating T to establish the D-T reactor as an energy source are summarized.

**Keywords** Fusion reactor · Fuel cycle · Tritium · Deuterium · T processing

### 1.1 Nuclear Fusion Reactions as an Energy Source

All energy on the earth except geothermal and tidal energies, and nuclear fission is originated from nuclear fusion in the sun. As shown in Fig. 1.1, nuclear fusion reactions in the sun are complicated but, as a whole, are represented by

$$4p + 2e^- = {}^4He + 6\gamma + 2\nu + 26.65 \text{ MeV}, \quad (1.1)$$

where p,  $e^-$ ,  ${}^4\text{He}$ ,  $\gamma$ , and  $\nu$  are a proton (an ionized hydrogen (H) atom), an electron, a Helium atom, gamma ray, and a neutrino, respectively [1]. Ordinary Hydrogen (H)<sup>1</sup>

---

<sup>1</sup>“Hydrogen” generally represents all hydrogen isotopes which are referred as protium (H), deuterium (D) and tritium (T), and proton (p), deuteron (d) and triton (t) for respective ions.

---

T. Tanabe (✉)

Interdisciplinary Graduate School of Engineering and Sciences, Kyushu University, 6-1,  
Kasuga-Koen, Kasuga, Fukuoka 816-8580, Japan

e-mail: tanabe@nucl.kyushu-u.ac.jp

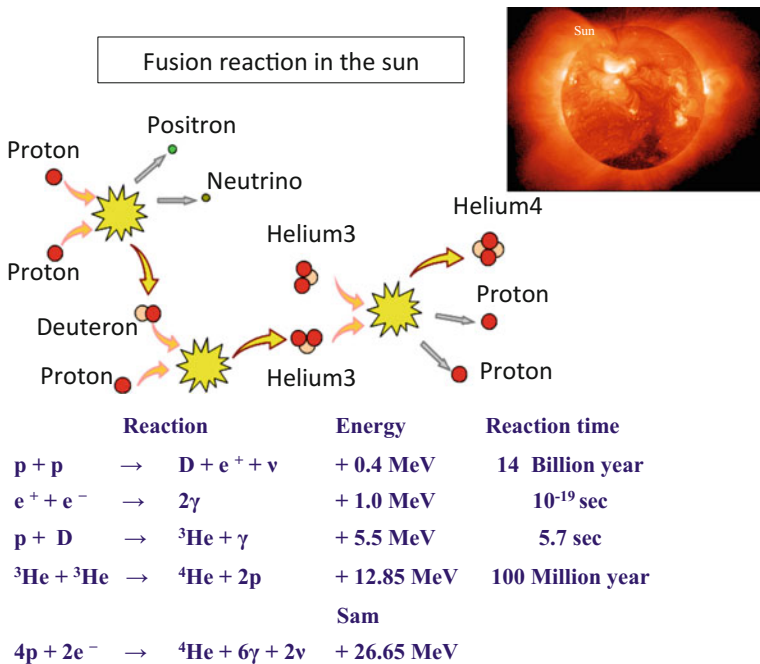


**Fig. 1.1** Fusion reactions in the sun

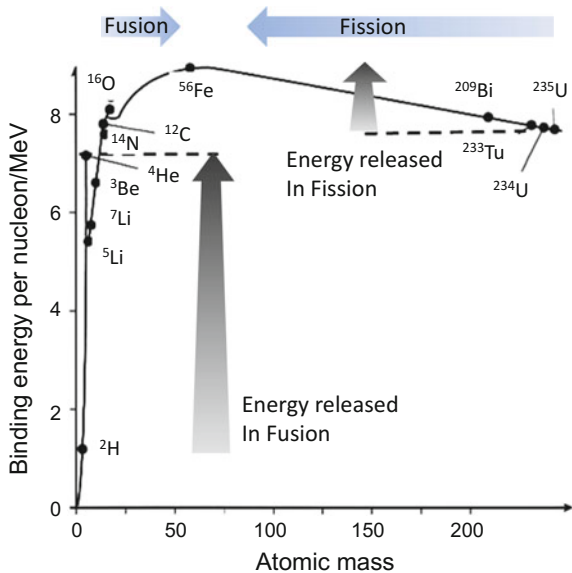
is the most abundant element in the sun (around 75 %) and the universe as well. H exists everywhere on the earth as the tenth abundant element with 0.14 % in weight and the third element in a human body (10 %) essentially as  $\text{H}_2\text{O}$  (water) [2]. Therefore, to realize this nuclear fusion as an inexhaustible source of energy for future or to make the sun on the earth has been a dream. Not only because fossil fuels presently used, such as petroleum, coal and natural gas, are exhaustible but also because the use of the fossil fuels inevitably results in the emission of carbon dioxide ( $\text{CO}_2$ ) and global warming is serious concern. But the dream has not easily come to true.

Various nuclear reactions, both fission and fusion reactions, are energy sources of stellar stars in space. In general, lighter elements can fuse and heavier elements are fissionable, if they are in high-energy state like in the stellar stars, as shown in Fig. 1.2. As depicted in the figure, iron (Fe) is the most stable element and mass differences ( $\Delta M$ ) of reactants and products are converted to energy ( $E$ ) according to famous Einstein's equation,

$$E = \Delta M \times c^2, \quad (1.2)$$

where  $c$  is the velocity of light. Operation of a D-T fusion reactor producing the fusion power of 1 GW for 1 year burns only 55.6 kg of T and 37 kg of D.

**Fig. 1.2** Nuclear energy released as a function of atomic mass

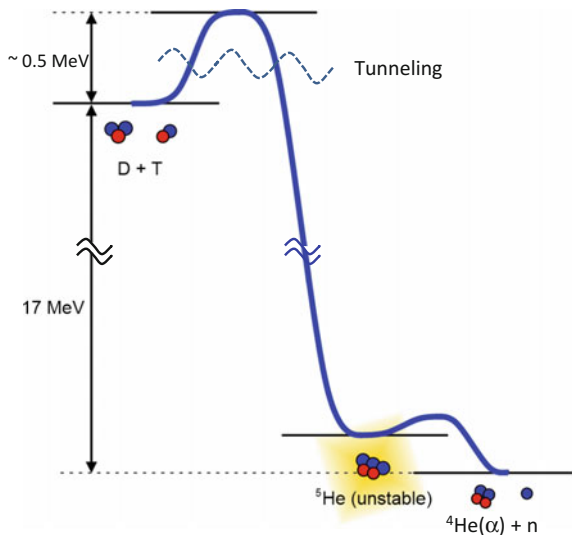


As for fusion reactions, there are quite many different fusion reactions. However, reactions using D, T,  $^3\text{He}$ ,  $^6\text{Li}$ ,  $^7\text{Li}$ , and  $^{11}\text{B}$  as fuels



seem to be realized on the earth.

**Fig. 1.3** Intermediate energy states of the DT fusion reaction

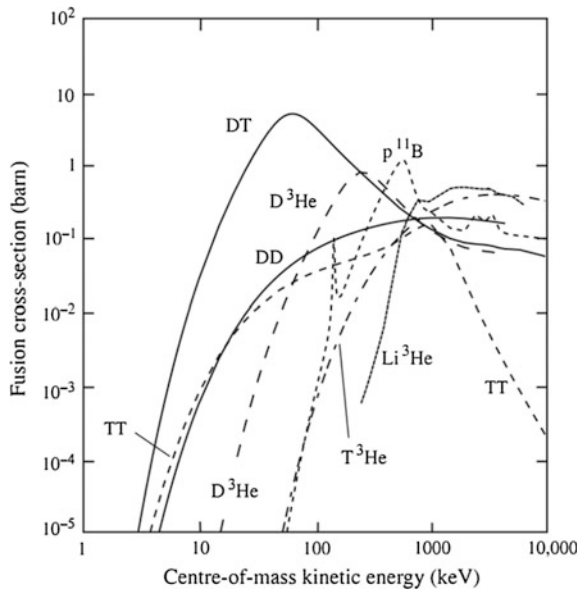


To induce these fusion reactions, reactants must be in higher energy states to overcome repulsive Coulomb force between them. Figure 1.3 shows energy states of the reactant and product for the D-T reaction (1.3) indicating the existence of around 1 MeV of Coulomb barrier between D and T to be overcome [1]. The reaction cross sections or the reaction rates are energy dependent as shown in Fig. 1.4 which gives 9 reactions having higher cross sections [2, 3]. Among all, the D-T reaction (1.3) requires the least energy to give the highest cross section at around a few tens keV. Because of the tunneling effect, energy required to induce the D-T reaction is much less than the Coulomb barrier of 1 MeV in Fig. 1.3. Therefore, realization of a D-T fusion reactor is the principal goal of the present fusion research.

Unfortunately, however, one of the reactants of the D-T reaction, T, is hazardous owing to its radioactivity. In addition, one of the products, neutron (n), activates structure materials such as ferrite and martensite steels to be radioactive and more hazardous than T. Furthermore, as described in the next chapter, T resources are very limited and artificial production or breeding of T in the reactor to satisfy fuel self-sufficiency is essential.

In the aspect of safety, any fusion reactions in which T and n are not involved would be better than the D-T fusion. In this respect, the D- ${}^3\text{He}$  reaction (1.7) which has the 2nd largest cross section as seen in Fig. 1.4 is very much attractive. Although the abundance of  ${}^3\text{He}$ , an isotope of ordinary  ${}^4\text{He}$ , is very poor on the earth with the abundance ratio of  $1.37 \times 10^{-4}\%$ , a fair amount of  ${}^3\text{He}$  exists on the surface of the moon and Venus. Hence, there is an ambitious plan to recover  ${}^3\text{He}$  from them or build D- ${}^3\text{He}$  reactors at their surfaces. In the D- ${}^3\text{He}$  reactor, however, a fair amount of T is always produced by D-D reactions (1.4) and accordingly T

**Fig. 1.4** Cross sections of various fusion reactions



handling systems similar to the D-T reactor are required for T to separate from the exhaust and to store safely.

Fusion reactions using Li and/or B as fuels [reactions (1.9–1.12)] are very much attractive. Natural lithium consisting of  $^6\text{Li}$  (natural abundance ratio of 7.5 %) and  $^7\text{Li}$  (natural abundance ratio of 92.5 %) is quite abundant in nature when recovery of lithium from the sea water is developed. Natural boron consisting of  $^{11}\text{B}$  (natural abundance ratio of 80 %) and  $^{10}\text{B}$  (natural abundance ratio of 20 %) is also abundant on the earth. Nevertheless, such fusion reactions require nearly 1000 keV plasma as seen in Fig. 1.4, which is far beyond the present research.

Thus, the establishment of the D-T fusion reactor is the primary goal. Various issues still remain and they are relating to the establishment of burning plasma, plasma materials interactions, materials, fuel cycles, power generation, T breeding, safety, and the reactor construction as the final target. This book focuses on the issues related to the fuel of tritium [4].

## 1.2 Development of the D-T Fusion Reactor

To induce the D-T reaction, D and T must be heated or in higher energy state as shown in Fig. 1.3. Since energetic particles are usually in ionized states and easily dissipated by electrostatic repulsive forces between them, they must come together over the Coulomb barrier or to be confined to continue the fusion reactions.

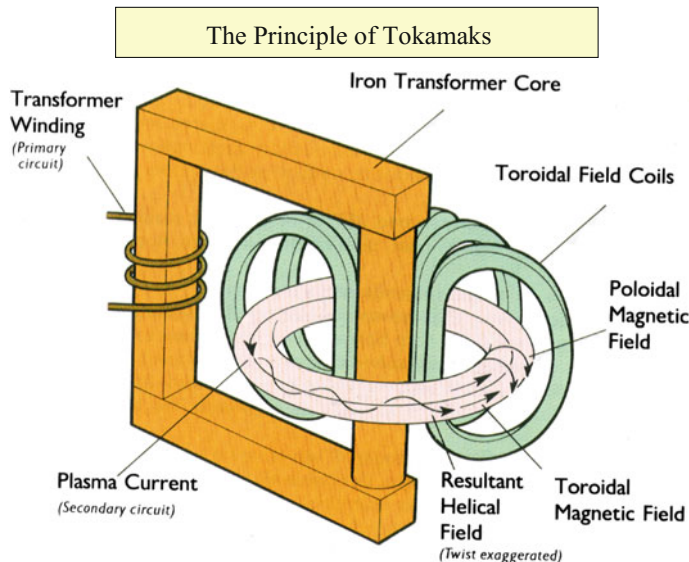
In order to overcome the Coulomb barrier between D and T, the fuel particles must be heated to a temperature of around 25 keV or 300 million degrees, under which conditions they are ionized and exist as plasma, a mixture of electrons and ions. To continue the fusion reactions, in addition, sufficient density and energy confinement are required, as specified by the Lawson criterion, or minimum value of [ion density ( $n_i$ ) multiplied by energy confinement time( $\tau_E$ )] for self-heating for fusion reactions. For DT,  $n_i \times \tau_E$  minimizes to be  $10^{20}/\text{m}^3 \text{ s}$  near the temperature 25 keV. Two different methods have been developed to confine plasma, i.e., a magnetic confinement fusion (MCF) system and an inertial confinement fusion (ICF) system. Brief introduction of the both systems is given below. It is out of scope of this book to describe details of MCF and ICF.

### ***1.2.1 Magnetic Confinement Fusion (MCF)***

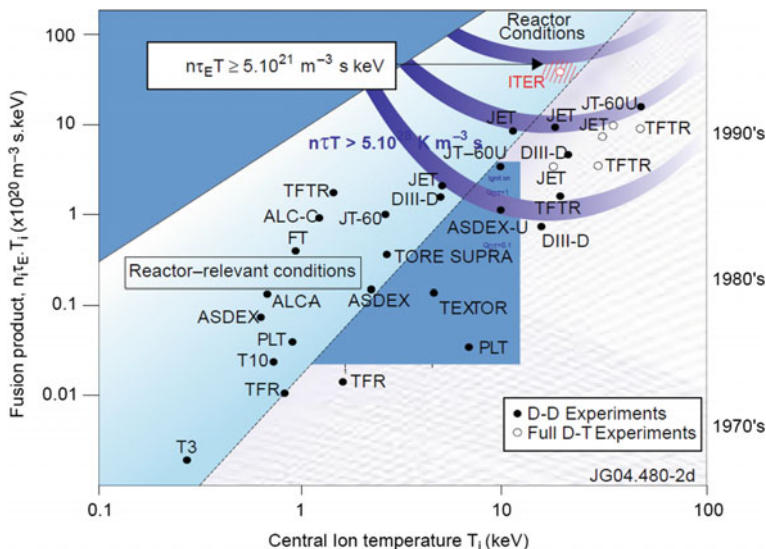
In MCF, high-energy plasma is contained in magnetic field by using the electrical conductivity of the plasma. The basic concept can be described by a fluid picture as a balance between magnetic pressure and plasma pressure, or in terms of individual particles gyrating along magnetic field lines. The simplest magnetic configuration is a solenoid, a long cylinder wound with magnetic coils producing magnetic field which forces electrons and ions to run parallel to the axis of the cylinder. The field confines them radially but allows escaping from the ends of the solenoid. To avoid the escaping or loss of them, various confinement schemes are proposed and two major confinements are now extensively studied, a tokamak system and a stellarator system.

Figure 1.5 shows the principle of the tokamak in which a large volume of high-temperature plasma is produced and confined in a toroidal shape by means of strong magnetic fields [5]. The original design principle was developed at the Kurchatov Institute in Moscow in the 1960s, and the tokamak system has become the most advanced magnetically confined fusion concept in the world. Figure 1.6 shows the fusion triple product ( $n_i \times \tau_E \times T_i$  (ion temperature)) achieved on different magnetic fusion facilities [6]. Each decade from 1970s to 1990s has given the gain in the triple product more than one order of magnitude to come close to the Lawson condition. Now ITER (International Thermonuclear Experimental Reactor) is under construction at St. Paul Lez Durance, France and will be ready within a several years to attain breakeven for energy production, i.e., the ratio of fusion energy output to input power ( $Q$ ) is one ( $Q = 1$ ). And  $Q = 10$  is the goal for ITER. Now, DEMO (DEMOstration Power Plant) is designed as a prototype commercial fusion reactor in several countries [7, 8].

The biggest stellarator machine is Large Helical Device (LHD) in National institute of Fusion Science in Japan [9], and the design activity to realize a reactor with the stellarator is under progress [10].



**Fig. 1.5** Principle of Tokamak [5]



**Fig. 1.6** Plasma confinement achieved on different fusion facilities, represented by triple product ( $n_i \cdot \tau_E \cdot T_i$ );  $n_i$  ion density,  $\tau_E$  Energy confinement time,  $T_i$  ion temperature (reprinted with permission from [5]). The fusion triple product achieved on different magnetic fusion facilities. The graph shows clearly that new facilities performed better than previous ones. The present large machines, from the point of view of the fusion product, have now achieved their engineering limits so that only the next step facility, ITER, can bring about decisive progress

### 1.2.2 Inertial Confinement Fusion (ICF)

In ICF, nuclear fusion reactions are initiated by heating and compressing a fuel target, typically in the form of a pellet which contains fuel, a mixture of D and T (see Fig. 1.7) [11]. To compress and heat the fuel, energy is delivered to the outer layer of the target using high-energy beams of laser light, electrons, or ions. (Most of present ICF devices use lasers.) The heated outer layer explodes outward, producing a reaction force against the remainder of the target, accelerating it inwards, compressing the target. This process is designed to create shock waves that travel inward through the target. When the input power is sufficient enough to compress and heat the fuel at the center, fusion reactions start. The energy released by the reactions will then heat the surrounding fuel to undergo fusion reactions. The principle was realized as a hydrogen atomic bomb in 1952. But the bomb is uncontrolled energy release and cannot be the energy source of the daily life. In ICF, nuclear fusions should be controlled as the energy source. Extensive works have been done to produce a condition known as “ignition” or fulfill the Lawson condition fusing a small fuel pellet, which is a millimeter-sized pinhead and contains around 10 milligrams of D-T fuels. NIF (National Ignition Facility) at Livermore CA, USA, is now under operation to demonstrate ICF being the energy source [12]. At present, its energy gain seems too small for ICF to be energy source.

Tritium technologies required for ICF are very similar to, or a little simpler than those for MCF, and most of tritium systems developed for MCF could be applied to ICF. Therefore, this book focuses on tritium science and technology for MCF. (“MCF fusion” is simply referred “fusion” hereafter.)

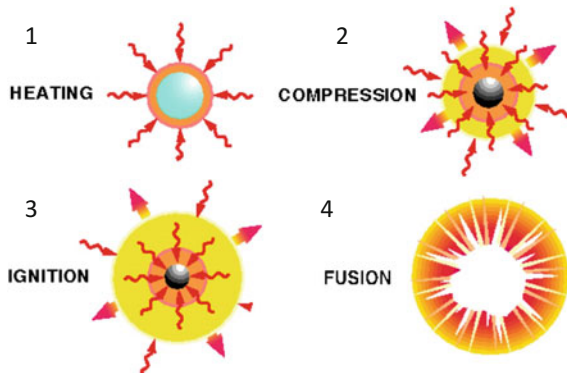


**Fig. 1.7** Stages of ICF (reprinted with permission from [11]). 1 Laser beams or laser-produced X-rays rapidly heat the surface of the fusion target, forming a surrounding plasma envelope. 2 Fuel is compressed by the rocket-like blowoff of the hot surface material. During the final part of the capsule implosion, the fuel core reaches 20 times the density of lead and ignites at  $1 \times 10^8$  °C. 3 Thermonuclear burn spreads rapidly through the compressed fuel, yielding many times the input energy. 4 Fusion

### 1.3 Energy Conversion in Fusion Reactor and Fission Reactor

Already 60 years have passed after finding that nuclear reactions give energy. Now fission reactors are well established as energy sources, while a fusion reactor seems to need still several tens years to be realized. Why so much longer time has been required for fusion than fission?

To give the answer, principles of energy conversion in a fusion reactor system and a fission reactor system are compared in Table 1.1. Different from any other energy sources, the fusion needs significant amount of energy to start burning or ignition, i.e., to make high-energy and high-dense plasma confined to satisfy the Lawson condition. The initial input power would be 1/3–1/4 of the fusion output power. Since a fusion reactor will be designed to produce the power of a few GW, each reactor may require a power station with the power of a few hundreds MW to

**Table 1.1** Comparison of fission reactor and fusion reactor

	Fission reactor	Fusion reactor
Reaction	$^{235}\text{U} + \text{n} \rightarrow \text{FP}_1 + \text{FP}_2 + 2\text{-}3 \text{n} + \gamma + \sim 200 \text{ MeV}$	$\text{D} + \text{T} = \text{n} + ^4\text{He} + 17.6 \text{ MeV}$
Characteristics	<ul style="list-style-type: none"> <li>– All of energy conversion, fuel breeding, and waste confinement are done in a fuel pin of diameter of <math>\sim 1 \text{ cm}</math></li> </ul>	<ul style="list-style-type: none"> <li>– An open tritium handling system with a huge volume</li> </ul>
Energy input	<ul style="list-style-type: none"> <li>– Nearly zero</li> </ul>	<ul style="list-style-type: none"> <li>– Requires huge energy to sustain burning plasma</li> </ul>
Energy conversion	<ul style="list-style-type: none"> <li>– Energy carried by fission products (FP, heavy ions) (<math>\sim 170 \text{ MeV}</math>) is deposited in fuel pins and removed by coolant surrounding the pin</li> </ul>	<ul style="list-style-type: none"> <li>– Energy carried by neutron (14 MeV) must be converted to heat in large volume of blanket system</li> </ul>
Fuel and ash	<ul style="list-style-type: none"> <li>– Both fuels (<math>^{235}\text{U}</math>) and ashes (FP) are encapsulated in small fuel pins from the start up—No extra systems for fueling and ash removal are required</li> </ul>	<ul style="list-style-type: none"> <li>– Requires continuous fueling system</li> <li>– Poor efficiencies of fueling and burning require large throughput</li> <li>– Requires continuous exhaust of He ash</li> </ul>
Fuel breeding and recovery	<ul style="list-style-type: none"> <li>– One fission produces 2–3 neutrons, easy to keep chain reactions and to breed fuels</li> <li>– Fuel pins retain both FP and new fissile</li> <li>– Spent fuels are reprocessed to recover them</li> </ul>	<ul style="list-style-type: none"> <li>– To keep breeding ratio more than 1, neutron multipliers (Be, Pb) are required</li> <li>– Tritium breeding and energy conversion must be done simultaneously</li> </ul>
Nuclear waste	<ul style="list-style-type: none"> <li>– Long life radioactive FPs and transuranium elements must be handled with special care and will be reposed deeply underground</li> </ul>	<ul style="list-style-type: none"> <li>– Waste is limited to activated structure materials and could be recycled</li> </ul>

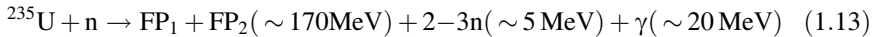
start up. In a fission reactor, no such high power is required and only removing control rods from the core could start the reactor.

Energy conversion systems for fission and fusion are completely different. In a fission reactor, energy produced by the fission reaction of U (Uranium) and neutron is carried by fission products (FPs) and transformed to thermal heat of coolant for electric power generation, while in a fusion reactor, energy carried by 14 MeV neutrons must be converted to the thermal heat of the coolant. At the same time, neutron is used to breed T to sustain fuel self-sufficiency as described below. Both fission and fusion leave nuclear wastes. Compared to long life nuclear wastes in fission including FPs and transuranium elements such as U, Np, Pu, which are serious concerns for radiation safety, activated structure materials by fusion neutron irradiation are less hazardous. Of course radioactivity of T requires special care, which is the main subject of this book.

In the following, energy conversion for both fusion and fission is briefly summarized.

### 1.3.1 Fission Reactor

In most of fission reactors using light water as coolant, energy produced by a nuclear reaction, around  $\sim 200$  MeV,



is distributed to FPs, which are nuclei with atomic numbers of around 40–50, neutrons, and  $\gamma$  rays, as indicated as the numbers in blankets in the equation [13].

Two or three neutrons produced by the reaction sustain chain reactions, and the reaction rate is easily controlled by removing the neutrons by boron (B) encapsulated in control rods with reactions such like,



It should be noted that the reaction can be used to produce T. Actually T production in nuclear reactors is considered, due to limited T resources.

Since the fission cross section is higher for lower energy neutrons, the neutrons produced by the fission reaction are decelerated by moderator, for which  $\text{H}_2\text{O}$  is used concurrently as coolant in a light water reactor (LWR). Accordingly, the energy of the neutrons is deposited in the coolant ( $\text{H}_2\text{O}$ ). However, its contribution in power generation is not large. The fuel of  $^{235}\text{U}$  is included in natural uranium only by 0.7 % and enriched to be a few % as fission fuel for LWR.  $^{238}\text{U}$  (99.3 %), the main component of the natural U, absorbs neutrons being transmuted to

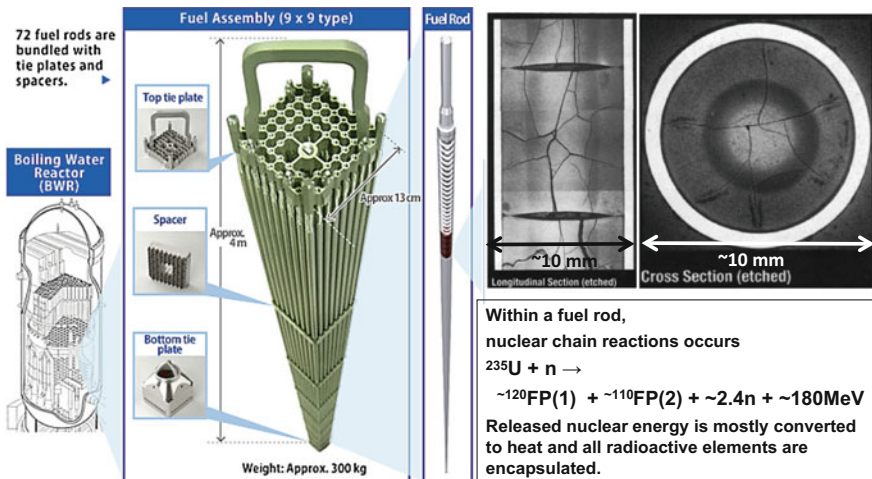


**Fig. 1.8** **a** Schematics of a boiling water type reactor and a fuel assembly (reprinted with permission from [14]) and **b** cross sections of a fuel pin (reprinted with permission from [15])

transuranic elements, like Pu, which are fissile and to be used in a fast breeder reactor but very much hazardous.

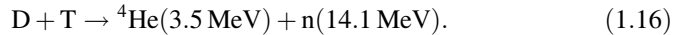
Because of heavy masses of FPs', their energies are mostly converted to heat in a fuel pin with a diameter of only around 10 mm and transferred to the H<sub>2</sub>O coolant in LWR flowing outside of the fuel pins to generate electricity (see Fig. 1.8 [14]). This means that energy conversion from dangerous nuclear energy to heat is done within a very small volume together with the confinement of hazardous FPs in the fuel pins (see Fig. 1.8b [15]). In addition, absorption of neutrons in B in the controlled rods decelerates the reaction rate and hence reaction control is simply done by insertion or extraction of the control rods. These points are all very much beneficial and reasons why a nuclear reactor was accomplished as energy source within rather short time.

One of the disadvantages of the fission reactor is that around 10 % of output power remains in the fuel pins as decay heat of the radioactive FPs just after the reactor shutdown, which requires continuous cooling for rather long time. Otherwise, the reactor core (bundles of the fuel pins) could melt down as such appeared in the Fukushima accident at 2011 in Japan due to the loss of coolant [16].

In this respect, fusion reactors are much safer than fission reactors, in which no fusion power remains after the reactor shutdown, as described below. Although structure materials are activated by neutron irradiation, their overall decay heat after the shutdown would not cause significant damage even at loss of coolant.

### 1.3.2 Fusion Reactor

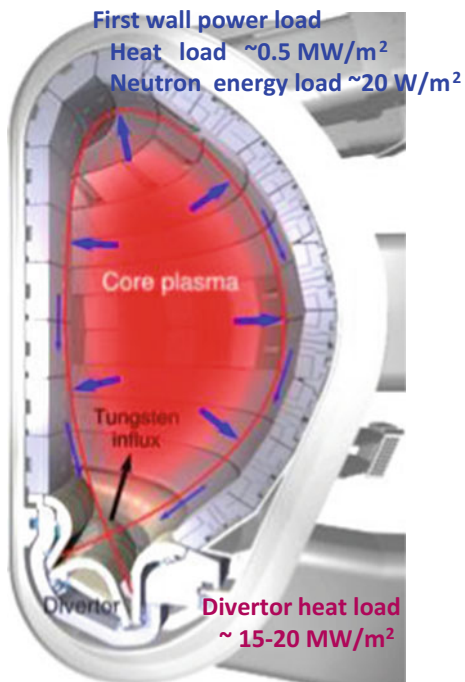
As already mentioned, the largest reaction rate appears in the D-T fusion reaction, which produces  ${}^4\text{He}$  and neutron having energy of 3.5 MeV and 14.1 MeV, respectively as,



Energy carried by  ${}^4\text{He}$  is used for plasma heating to maintain burning through its collisions with fuel ions ( $\text{D}^+$  and  $\text{T}^+$ ) and electrons, while energy carried by neutron (14 MeV) must be converted effectively to heat or electricity. Consequently, plasma-facing surfaces of a fusion reactor are subjected to high-energy neutrons. However, neutron energy deposition is volumetric and their energy is converted in blankets behind the first wall to thermal energy of the coolant for power generation.

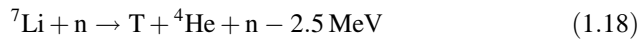
Energy used for plasma heating (1/3–1/4 of the output fusion power) must be removed; in other words, plasma-facing surfaces are subjected to very high heat load from the burning plasma as shown in Fig. 1.9. The heat load to the surface of divertor, which is installed for removal of He ash and fuel exhaust, becomes intolerably high for any materials. This is the one of the reasons for the selection of tungsten (W) having the highest melting point as plasma-facing materials. Still the heat load is too high and cooling of plasma temperature by impurity seeding is

**Fig. 1.9** Structure of tokamak type reactor core (Torous) and heat load to first wall and divertor



required. Although, plasma heat load to the first wall is much less than that to the divertor, energetic neutrons impinge to the first wall and their energy is superposed.

Furthermore, the neutrons are used to breed T using following reactions.



The reaction (1.17) produces one T per one neutron, while the reaction (1.18) produces one neutron which can be used again for both reactions. Since natural Li includes both  ${}^6\text{Li}$  and  ${}^7\text{Li}$  with their natural abundance ratio of 7.5–92.5, the natural Li can be used to breed T. Although the reaction (1.18) is beneficial for simultaneous production of T and neutron which can be used for T breeding again, the reaction requires energy (2.5 MeV) which in turn reduces the output power. Since the T resources are not enough as described in Chap. 2, the T breeding should have enough margins to compensate inventories of all T handling systems including a reactor vessel, pumps, and fuel processing and recycling systems, i.e., fuel self-sufficiency must be kept. To do this, neutron multiplication using beryllium (Be) or lead (Pb) is employed.



where  $A$  is a mass number of one of the isotopes of Pb which absorbs a neutron.

In a fusion reactor, the blanket system is set to surround the reactor core, in which conversion of neutron energy to heat must be done simultaneously with the T breeding. Because the neutron energy is very high, very thick materials are required to decelerate neutrons or convert their kinetic energy to heat transferred to coolant. Furthermore, recovering T bred in the blanket requires sophisticated systems. Thus, after confirming D-T burning in ITER, significant effort will be required to establish appropriate blanket systems to attain the energy conversion and T breeding simultaneously, which must be economically efficient [4].

14 MeV neutrons activate materials surrounding burning plasma. And the activated materials, mostly structure materials made of steels, radiate energy as  $\beta$  and  $\gamma$  rays for long after the reactor shutdown. Since the mass of the structure materials of the fusion reactor is much larger than that of the fission reactor, depository of the activated materials is concerned in addition to radiation safety. In this respect, development of low activation steels and utilization of SiC for structure materials is encouraged.

The overall residual energy or decay heat of the fusion reactor is far less than that of the fission reactor. In addition, no fusion power remains in a fusion reactor after shutdown. Thus, the meltdown of the fusion reactor can be avoided by inertial cooling. In this respect, fusion reactors are much safer than fission reactors.

Nevertheless, lots of scientific and technical issues relating T remain to realize the fusion reactor as an energy source. In particular, to keep T safety and to establish fuel sufficiency in T breeding are two of the most important ones. The purpose of this book is to give information relating tritium science and technologies to realize a D-T fusion reactor as an energy source.

Thus, the mechanism of energy conversion from nuclear energy to thermal energy (or to raise temperature of the coolants, whatever they are, any liquids including water, gases, or even liquid metals) is quite different between a nuclear reactor and a fusion reactor. Nevertheless, it should be noted that once the nuclear energy is converted to the thermal energy, there is no large difference in volume energy density between the two reaction systems. In fission reactors, nuclear energy is converted to heat of the coolant in quite small volume with energy density of 0.1–1.0 W/cm<sup>3</sup>, while fusion energy is converted in its whole volume of around 1000 m<sup>3</sup> of the reactor with energy density of 0.1–1.0 GW/1000 m<sup>3</sup>. Both energy densities are nearly the same.

## 1.4 Fusion Reactor System—A Huge Open T Handling System

Figure 1.10 shows schematic of electric power generation by a fusion reactor [7]. As described above, energy conversion in the fusion reactor system is quite different from that in the fission reactor system widely used as an energy source.

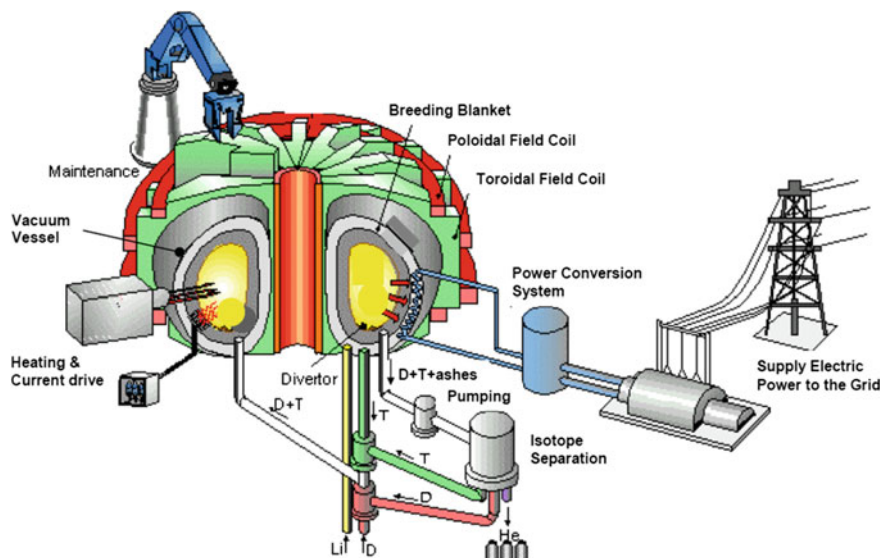


**Fig. 1.10** Schematic of electric power generation by a fusion reactor (reprinted with permission from [7])

Moreover, using T as its fuel, safety requirements for the fusion are also quite different from that for the fission.

In the fission reactor, its fuel is simply encapsulated in fuel pins so as the radioactive FPs are also enclosed in the pins. All fuels are loaded in the reactor at the beginning of reactor operation. Any failures of the fuel pins are easily detected by monitoring the radio-activity of cooling water, and removing of the FPs from or cleaning of the cooling water is one of the most important issues during its normal operation. Emergency cooling is one of the key safety features and its failure could cause serious environmental damages such happened at reactors in Fukushima [16] and Three Mile Island [17].

In a D-T fusion reactor, D and T are continuously fueled in its huge reactor vessel or tokamak system and recovered mostly as gaseous form together with He ash and other gases added intentionally or unintentionally. Owing to poor burning efficiency, only a few % of the throughput fuel would be burned, and the amounts of both the fuel throughput and exhaust are quite large.

For safety, T must be contained physically and confined following the regulation law of T in a reactor system specified by ICRP [18]. Because of easily dissipating nature of hydrogen gas, it is hardly possible to avoid leak, permeation, and consequent contamination of T. Therefore, any T handling systems require decontamination of T or detritiation.

T fueling and recycling systems, which use mostly established techniques, can be built for ITER or even a reactor without very high hurdles and, hence, T plant is not likely on a critical schedule path toward the first D-T plasma in ITER [19]. Nevertheless, the amount of T handled in ITER or a reactor will be so large that only tiny amount of T release from any T handling systems by leakage, permeation, and cross contamination is hardly avoidable. Hence, detritiation systems are indispensable and accordingly a D-T fusion reactor will be a huge open T handling system, which we have never experienced, and quite different from small glove box systems for handling small amount of T, for example, tracer usage.

## 1.5 Safety Issues in a Fusion Reactor

### 1.5.1 General Safety

Inherent safety and environmental sustainability are key benefits of fusion compared to fission. Because there is no chain reactions like fission and the reaction is thermally self-limiting with limited burning time, a few seconds without refueling. Low residual decay heat of the few-MW level requires no additional external cooling upon system shutdown.

In fission reactors, significant amount of hazardous radioactive FPs and transuranium elements, such as Pu and Np with quite long decay times are produced, while both toxicity and lifetime of T fuel in fusion reactions are much less

than above-mentioned radioactive materials in fission. However, neutrons activate structure materials and the total volume of the activated wastes will be similar or larger than the fission reactor. Currently, materials are not optimized for low activation under neutron irradiation. In future, the activated material can be recycled for reuse after 50–100 years and material optimized for low activation can be readily recycled for use in fusion power plant reactors. In case of active cooling system failure, decay heat from activated materials is low enough that all in-vessel components can be cooled by natural convection and reactor “meltdown” is physically impossible.

Therefore, most of the safety issues are related to radioactivity of T and the activated structure materials. Since the activated materials are not movable, most serious movable hazards involve the T fuel itself and activated dusts containing T resulting from erosion of plasma-facing components, which are discussed in Chap. 5.

The consequence of a “design basis accident” would be suspension of operations and possibly fire. Electricity would cease to be produced, but there would be no offsite impact. The consequences of accidents significantly beyond the design basis are well within the regulatory limits, and radiation dose of radiological workers and of the public can be below the limits specified by ICRP [15]. In ITER, public safety might not be a serious concern. Concerns are mostly for safety of workers in reactor site, and it does not seem easy to keep T contamination below regulatory level, owing to speciality of tritium as a radioactive hydrogen isotope, which can be easily exchanged with H in ubiquitous water on the earth. Thus, the safety concerns of the fusion reactor are quite different from those of fission products mostly metals.

### 1.5.2 Safety Issues Relating Tritium

In a D-T fusion reactor, only 55.6 kg of T and 37 kg of D are burned (consumed) per 1 GWth year. (GWth is energy released by fusion reactions and GWe for electricity). Since utilization of T is strictly restricted by law with accountancy (or under regulation) of a few tens Bq. T must be physically contained and confined following the regulation law of T in any nuclear systems. Details of T safety in a fusion reactor are described in Part III (Chaps. 14 and 15). Here, it is briefly summarized.

T handling in small scale is well established, and various manuals have been published, such as the Tritium Handbook published by DOE [20, 21], considering to use T as medical diagnostics and sign illumination, especially “EXIT” signs. Few T facilities have handled such large amount of T to be used in ITER and DEMO. In 2007, Savannah River Laboratory has opened a new Tritium Extraction Facility (TEF) [22], in which the amount of T handled is rather large but does not likely exceed 10 kg. We will face to new and never experienced problems to handle such large amount of T used in ITER or a fusion reactor. They are mostly related to T inventory in a reactor vessel and T recycling systems, and precise T accountancy.

As noted in Fig. 2.1 in Chap. 2, the existence of T can be easily detected with  $\beta$ -electrons, while no one method can cover the quantitative analysis in wide range. Moreover, T retained in materials can be detected only within  $\mu\text{m}$  range from their surface due to very shallow escaping depth of the  $\beta$ -electron. At very high concentrations, decay heat makes calorimetric measurements of T in the materials possible, but the accuracy of the measurements is only two or three digits. Loss of 0.1 % is never allowed in regulation, but it is quite hard to account T with the accuracy in more than three digits. Ironically, the loss itself can be detected, but it is difficult to determine how large the loss from the total mass handled.

In addition, T handling has been done mostly at room temperature (RT) except for T reservoirs (T stored in metals), and no cooling system has been required. While most of fusion systems as an energy source must be operated at temperatures well above RT with cooling water/gas systems (except for ice pellets manufacturing and isotopes separation). Therefore, absorption, desorption, and permeation of T in materials of any reactor component can be unavoidable. The permeation and leakage result in T contamination of T handling systems and of any coolants or cooling water. Most of those T problems are directly connected to the safety of operators and/or professionals. But, as already mentioned, public safety does not seem to become a significant problem in normal reactor operation, because the T emission to outside of the reactor site can be easily kept below the safety limit. Even in severe accident, T level at the public boundary can be kept below the regulation limit, which is the base for the maximum in-vessel T inventory of 1 kg in ITER.

Nevertheless, T contamination of materials surfaces is one of the most important concerns and understanding of the contamination mechanism is quite important to reduce and/or remove the contamination (decontamination). Because of chemical nature, T can be easily transferred from a highly contaminated surface to lower contaminated or non-contaminated surfaces, leading to cross contamination or multi-step contaminations in T handling systems. In ITER, safety handling of a divertor cassette, which will be the largest component in the reactor vessel, is the most serious concern [23]. The cassette retains very high levels of T on their surfaces, which easily transfers to arms or gloves of remote-handling systems or glove boxes and is highly activated by neutron irradiation. Once the surface of the device/equipment in the systems is contaminated, T can be easily transferred to any materials attaching. Figure 2.8 in Chap. 2 shows an example of cross contamination remaining fingerprints of T activity on metal plates in a glove box, in which heavily contaminated materials were handled [23].

The most important mechanism of the cross contamination is isotope exchange reactions of T with the ubiquitous lighter hydrogen isotope, protium (H), in water to become HTO and hydrocarbons in atmosphere to become OBT (Organic Bound Tritium).

Tritium disintegration at skin is not so important owing to thin penetration depth of the  $\beta$ -electrons, but T can penetrate into a human body by the isotopic exchange reactions with light water in tissues to be very hazardous. Once T is going in human body and tissues, a few weeks are needed to be isotopically replaced by H from

drinking water. In this respect, OBT is more hazardous and requires more time to be removed than HTO. In Chap. 2, mechanisms of isotopic replacement are discussed in detail.

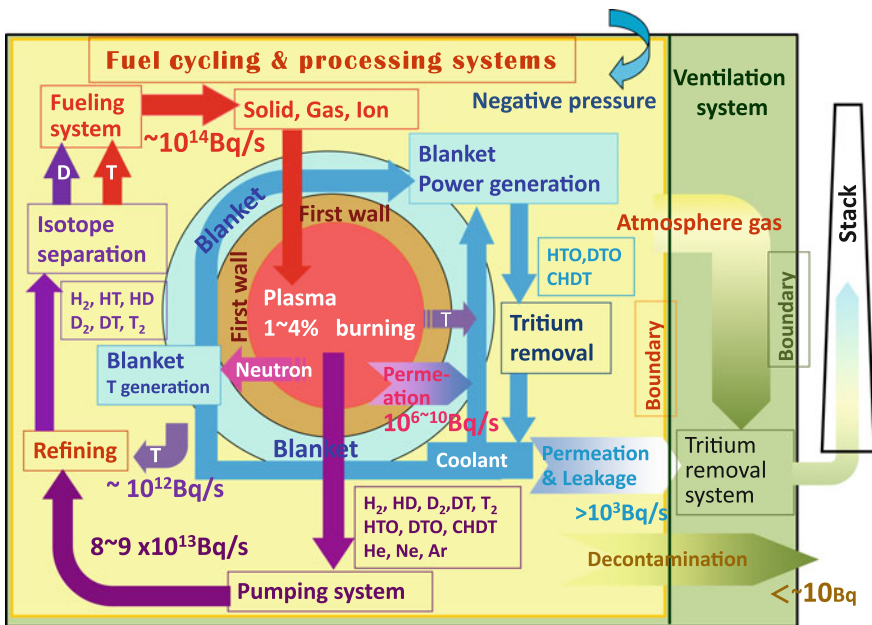
## 1.6 T Fuel Cycling and Processing Systems

Figure 1.11 is a schematic drawing of T fuel cycling and processing systems with blanket to generate power and to breed T simultaneously. For the safety reasons, T in a reactor will be limited to only a few kg or radioactivity of around  $10^{17}$  Bq [24, 25]. Since burning efficiency is likely to be several % as discussed in Chap. 3, required throughput into the reactor is more than 25 times of T burned. In the figure, fuel throughput is  $\sim 10^{14}$  Bq/s, following the maximum fuel throughput of ITER,  $200 \text{ Pa m}^3 (\sim 2.5 \text{ g})/400 \text{ s}$  (one ITER discharge). In present tokamas, 1–10 % ( $\sim 1 \times 10^{13}$  Bq/s) of input fuels are retained on/in the plasma-facing walls. Accordingly,  $\sim 90$  % of the throughput fuel,  $\sim 9 \times 10^{13}$  Bq/s, is exhausted and refueled after reprocessing (refinement and isotope separation). In blanket systems,  $\sim 10^{12}$  Bq/s must be bred, because the amount of bred T must exceed that of burned T.

In the aspect of T confinement for the safety, there are at least two boundaries, one between the vacuum vessel (or reactor) and the blanket (or tritium processing) systems and the other between the tritium processing system and environment. T is transferred either by permeation and leakage and/or cross contamination through the boundary. Since public exposure to T is regulated at a level as tiny as a few Bq/cm<sup>2</sup>, T must be strictly confined in a reactor system with accountancy of an order of pg (picogram). Considering the throughput of  $\sim 10^{14}$  Bq/s, each boundary should reduce T level by orders of  $10^6$ .

Passive barriers consisting of process piping, jacketed vessel, guard or second barrier piping [26] are taken into account in ITER tritium systems [25]. Nevertheless, the decommission factor (DF) of  $10^{-6}$  seems hardly possible by a single step. One can apply permeation barriers. Yet, the permeation reduction factor of 3 (orders) has been attained by oxide film coatings, and so on, but the reliability of the barrier effect is rather poor. Since permeation flux of 1/1 to 1/100 of the incidents flux was attained in PDP (plasma-driven permeation) experiments [27], T permeation to cooling channels in the divertor region will be quite large due to extremely large particle fluxes and significant amount of T can be piled up in the cooling systems.

The easy isotopic replacement gives additional problems for T permeated through process piping. The permeated T readily reacts with surface contaminants to produce hazardous tritiated water and/or hydrocarbons. In particular, ferrite, a low activation structure candidate material, has very high T permeability and needs permeation barrier with the permeation reduction of 5-6 orders of magnitude which is not attained yet. For a water-cooling system, permeated T from the plasma-facing surface or blanket to the coolant water easily produces HTO, resulting diluted tritiated water from which T recovery is very cost-consuming.



**Fig. 1.11** Schematic drawing of T fuel cycling and processing systems with blanket to generate power and to breed T simultaneously. Amount of tritium flowing in fuel cycling and processing systems is also given

In the water-cooling system, there is another problem. Water corrosion at the cooling side surfaces results in H uptake, and H can permeate counter direction (higher temperature side) to dilute fuels (D and T). This can be reduced if the permeation barrier is built at the cooling side. On the other hand, the permeation barrier at the cooling side increases fuel retention.

Glove boxes or something like housing would be the second boundary. However, T permeation in gloves must also be considered on handling of large amount of T. In addition, one should be careful on multi-step or multistage cross contaminations, which would require more than two steps use of the glove box. The cross contamination is also a serious concern for remote-handling system. i.e., once remote hands touch contaminated components in tokamak, like a divertor cassette, the hands and/or gloves are immediately contaminated and the contamination will be transferred to other components to be handled.

Generally, qualitative analysis with the accuracy of more than 3 digits is hardly possible. Therefore, the loss of  $10^{-3}$  is out of accountancy in higher concentration T handling side, though this cannot be accepted in regulation. While the leakage of this amount through the boundary to lower T handling side can be detected and can be dealt with to fulfill the regulation.

T breeding in the blanket should have enough margins to compensate the inventory in all T systems including a reactor vessel and T decay as well. To

enhance the recovering rate of T produced in the blanket, addition of water vapor ( $H_2O$ ) is well known to be effective, but T diluted in  $H_2O$  needs lots of energy to be recovered, which increases fusion energy cost.

## 1.7 Critical Issues Relating T Handling

In a D-T fusion reactor, 55.6 kg ( $\sim 10^{18} \text{Bq}$ ) T is burned (consumed) per 1 GWth year fusion energy. The form of tritium handled includes ice pellets ( $\sim 20 \text{ K}$ ), gas at RT (300 K) (both for fueling), energetic neutrals and ions (for neutral and ion beam heating) and plasmas, of which temperatures are ranging from  $10^1$  to  $10^9 \text{ K}$ . Therefore, the interactions of T with materials used in the reactor or T confinement systems include various physics and chemistry. The radioactivity of T generates additional problems due to  $\beta$ -electron emission and/or radiation heat, such as excited state chemistry and non-equilibrium thermodynamics. Figure 1.12 summarizes science and technology related to T in fusion reactor systems and their dependence on the amount and energy of T [4]. T issues are related to (1) T plasma or T in ionized and excited states, (2) Effects of  $\beta$  electron emission and/or radiation heat, (3) Defect formation by electron excitation and He production, (4) Easy adsorption, solution, diffusion, and permeation in materials, (5) Easy isotope replacement with ubiquitous H in water and hydrocarbons in atmosphere, and so on. There remains difficulties in T accountancy or quantitative analysis. Ironically,

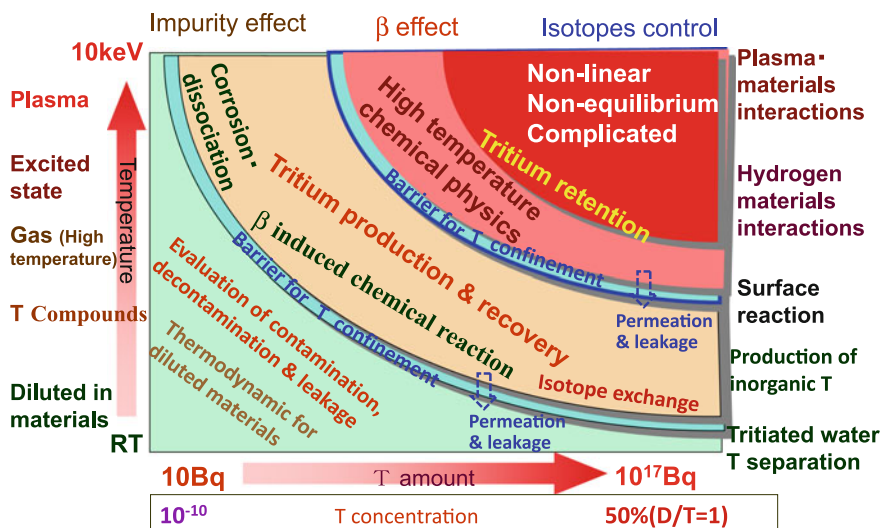


**Fig. 1.12** Science and technology related to tritium in fusion reactor systems and their dependence on the amount and energy of tritium [4]

detection of low level of T ( $1\text{--}10^7$  Bq) is rather easy by the  $\beta$ -counting method, though we can detect only T at surface and in subsurface within a few  $\mu\text{m}$ . PVT measurements are same as D analysis. For large amount, a radiation heat measurement works but is time-consuming and includes large error.

Tritium handling system, which uses mostly established techniques, can be built for ITER or even reactor. However, we will face to new problems in handling of huge amount of T for D-T burning, which we have never experienced up to now. Some of them can be listed as follows:

- T safety compatible with T economy
- Power generation compatible with T breeding
- Limited T resource and small margin in T breeding
- Poor burning efficiency requiring huge throughput
- Optimization and control of D-T fueling to keep efficient D-T burning
- Difficulty of quantitative analysis of D and T in plasma and in materials
- Unknown isotope effects between D and T in burning plasma and T recycling systems
- Large in-vessel inventory hard to remove
- Unavoidable permeation and leakage in T handling systems
- Refinement of fuel (or removal of impurity from fuel)
- Easy transfer of contamination
- Significantly large DF required (more than  $10^{-6}$ )
- T safety required under severe accidents

As noted in Chap. 14, T confinement is a key issue for safety and should be realized with multiple confinements following Defense in Depth concept. In Fig. 1.12, one can note that three regions are separated with barriers for T confinement. However, T can permeate or leak through the barrier. Hence, reduction of the permeation or leakage is a key.

Most of those T problems are directly related to the safety of operators and/or professionals. But public safety does not seem to become serious problems. All chapters in this book consider these points to a greater or lesser extent.

## 1.8 Summary

Recent advances in confinement of high-energy hydrogen plasma have made D-T fusion reactions mostly be ready as an energy source. In order to establish a D-T fusion reactor, converting the fusion energy to electricity and/or heat, having an enough margin in T breeding, and insuring T safety must be simultaneously achieved. Characteristics of the D-T fusion reactor are to convert energy (14 MeV) of neutrons produced by D-T reactions to heat or electricity and simultaneously to use them for breeding T fuel. Thus, energy conversion in the D-T fusion reactor is

completely different from that of a fission nuclear reactor, and various engineering issues remain to be solved.

ITER is targeting the breakeven in energy gain ( $Q = 1$ ) in physics phase. Its technical phase is devoted to solving technical issues described here. In particular, handling of huge amount of T as a fuel will require a significant effort to ensure that the radiation dose of radiological workers and of the public is as low as reasonably achievable (ALARA) and below the limits specified by the International Commission on Radiological Protection (ICRP).

In addition, T resources are very limited. Not only for the safety reason but also for avoiding the shortage of T resources, T retention in a reactor must be kept as small as possible and T breeding should have enough margins to compensate the inventory in all T systems including the reactor vessel and pumps.

## References

1. <http://www.stanford.edu/~rhamerly/cgi-bin/Ph240/Ph240-2.php>
2. P. Clark Souers, *Hydrogen Properties for Fusion Energy* (University of California Press, California, 1986)
3. S. Atzeni, J. Meyer-ter-Vehn, The physics of inertial fusion beam plasma interaction, hydrodynamics, hot dense matter, Int. Ser. Monogr. Phys. **125** (2004)
4. T. Tanabe, Tritium fuel cycle in ITER and DEMO: issues in handling large amount of fuel. J. Nucl. Mater. **438**, S19–S26 (2013)
5. <http://www.laetusinpraesens.org/iter/iter8.php>
6. J. Mlynar, Focus on: JET, EFD-R(07)01, p. 179 (2007)
7. D. Maisonnier, I. Cook, P. Sardain et al., DEMO and fusion power plant conceptual studies in Europe. Fusion Eng. Des. **81**, 1123–1130 (2006)
8. K. Tobita, S. Nishio, M. Enoda, et al., Nucl. Fusion, **49**, 075029 (10 pp) (2009)
9. <http://www.lhd.nifs.ac.jp/en/>
10. A. Sagara, T. Goto, J. Miyazawa, N. Yanagi, T. Tanaka, H. Tamura, R. Sakamoto, M. Tanaka, K. Tsumori, O. Mitarai, S. Imagawa, T. Muroga, The FFHR design group, design activities on helical DEMO reactor FFHR-d1. Fusion Eng. Des. **87**, 594–602 (2012)
11. <http://iter.rma.ac.be/en/physics/how2doit/Inertial/index.php>
12. <https://lasers.llnl.gov/news/photon-fusion/2014/february>
13. D. Bodansky, *Nuclear Energy, Principle, Practices, and Prospect* (American Inst. Phys, 1996)
14. <http://www.nfi.co.jp/e/product/prod02.html>
15. H. Stehile, J. Nucl. Mater. **153**, 3–15 (1988)
16. <http://www.iaea.org/newscenter/focus/fukushima/>
17. <http://www.nrc.gov/reading-rm/doc-collections/fact-sheets/3mile-isle.html>
18. ICRP, The 2007 recommendations of the international commission on radiological protection. ICRP Publication 103. Ann ICRP **37**, 2–4 (2007)
19. M. Glugla, D.K. Murdoch, A. Antipenkov et al., Fusion Eng. Des. **81**, 733 (2006). (references therein)
20. DOE Handbook, Tritium Handling and Safety Storage, DOE-HDBK-1129-99, USDOE, March 1999
21. DOE Handbook, Radiological Training for Tritium Facilities, DOE-HDBK-1105-96, USDOE, Dec 1996
22. <http://www.srs.gov/general/news/factsheets/tf.pdf>

23. T. Tanabe, *Fusion Eng. Des.* **87**, 722–727 (2012)
24. Technical basis for the ITER final design. Document series No. 24, IAEA, Vienna (2002)
25. D. Babineau, S. Maruyama, R. Pearce, M. Glugla, B. Li, B. Rogers, S. Willms, G. Piazza, T. Yamanishi, S.H. Yun, L. Worth, W. Shu, Review of the ITER fuel cycle, in *Proceedings of 23rd IAEA Fusion Energy Conference*, ITR/2-2, 11–16 Oct 2010
26. L. Cadwallader, T. Pinna, Reliability estimation for double containment piping, in *Proceedings of 20th ANS Topical Meeting on the Technology of Fusion Energy*, INL/CON-12-24848, Nasshville, TN, USA, 27–31 Aug 2012
27. R.A. Kerst, W.A. Swansiger, Plasma driven permeation of tritium in fusion reactors. *J. Nucl. Mater.* **122&123**, 1499–1510 (1984)



# Chapter 2

## Characteristics of Tritium

Tetsuo Tanabe

**Abstract** For any energy sources, fuel is a concern. In a DT fusion reactor, deuterium (D) and tritium (T) are fuels. Since hydrogen in natural water contains 0.016 % D, we can extract it from the water mostly by means of electrolysis. T, a radioactive hydrogen isotope decaying to  ${}^3\text{He}$  by emission of a  $\beta$ -electron and an antineutrino ( $\bar{\nu}$ ) with a half-life of 12.323 year, is generated by cosmic rays and also by nuclear reactions (atomic bombs and nuclear reactors) after the Second World War. Because of its short lifetime, natural abundance of T is very small. Therefore T, as a fuel of the D-T fusion, must be artificially produced. Although handling and processing of hydrogen is well established in industrial scales, owing to its radioactivity, special care is required for safety in handling T. In this chapter, characteristics of T as a radio isotope of hydrogen are introduced, focusing important properties of T as the fuel of a fusion reactor. Particular focuses are given to handling of large amount of radioactive T, behavior of T in burning plasma, and T breeding in blanket to attain fuel self-sufficiency, all of which we have never experienced.

**Keywords** Hydrogen · Deuterium · Tritium · Properties · Characteristics · Radioactivity · Resources

### 2.1 Hydrogen Isotopes

#### 2.1.1 Hydrogen, Deuterium, and Tritium

Hydrogen is the lightest chemical element on the periodic table with chemical symbol H and atomic number 1, and the most abundant element in the universe. There are three isotopes of hydrogen, the most common isotope of hydrogen,

---

T. Tanabe (✉)

Interdisciplinary Graduate School of Engineering and Sciences,  
Kyushu University, 6-1, Kasuga-Koen, Kasuga, Fukuoka 816-8580, Japan  
e-mail: tanabe@nucl.kyushu-u.ac.jp

termed protium (name rarely used, symbol  $^1\text{H}$  or simply H) constituted of a single proton and an electron, heavy hydrogen termed deuterium ( $^2\text{H}$ , usually D) involving one neutron into protium and tritiated hydrogen termed tritium ( $^3\text{H}$ , usually T) involving two neutrons. H and D are stable isotopes, while T is a radioisotope decaying with the half-life of 12.323 year. More heavier hydrogen isotopes can be synthesized, but they are not stable with half-lifetimes of less than a zeptosecond ( $10^{-21}$  s) [1].

Main physical properties of H, D, and T are given in Table 2.1 [2, 3]. Because of the large mass differences among them, isotopic differences of those physical properties (isotopic effects) are pronounced much more than isotopic effects of any other elements. At standard temperature and pressure (STP; 0 °C, 101.325 kPa), hydrogen isotopes are a colorless, odorless, tasteless, nonmetallic, highly combustible diatomic gas with the molecular formula of  $\text{H}_2$ ,  $\text{D}_2$ , and  $\text{T}_2$ . When three gases are coexisting, total of 6 isotopes,  $\text{H}_2$ ,  $\text{HD}$ ,  $\text{HT}$ ,  $\text{D}_2$ ,  $\text{DT}$ , and  $\text{T}_2$  appear. However, the basic exchange between  $\text{D}_2$  and  $\text{T}_2$  for fusion fuels, for example,



does not take place automatically. Some catalysts or raising temperature accelerates the exchange reaction. The equilibrium constant K of the reaction (2.1) changes with temperature and given by

$$\Delta G = -RT \ln K, \quad \text{or} \quad K = [\text{DT}]^2 / [\text{D}_2] * [\text{T}_2], \quad (2.2)$$

**Table 2.1** Comparison of physical properties of  $\text{H}_2$ ,  $\text{D}_2$ , and  $\text{T}_2$  gases [3]

	$\text{H}_2$	$\text{D}_2$	$\text{T}_2$
Abundance (in atomic form)	99.985 %	0.016 %	$10^{-18}$
Density ( $\text{kg m}^{-3}$ ) at STP (0 °C, 101.325 kPa)	0.08988	0.180	0.2705
Heat of vaporization ( $\text{kJ mol}^{-1}$ )	0.904	1.24	1.39
Boiling point (BP) (K)	20.271	23.67	25.04
Liquid density at BP ( $\text{kg m}^{-3}$ )	70.99	163.83	255.6
Heat of fusion ( $\text{kJ mol}^{-1}$ )	0.117	0.197	0.250
Melting point (MP) (K)	13.99	18.73	20.62
Solid density at M.P. ( $\text{kg m}^{-3}$ )	86.3	196.7	45.35 mol/L
Triple point (TP)	13.804 K, 7.030 kPa	18.69 K, 17.13 kPa	20.62 K, 21.6 kPa
Critical point (CP)	32.976 K, 1.293 MPa	38.26 K, 1.65 MPa	40.44 K, 1.85 MPa
Density at CP ( $\text{mol/m}^3$ )	15,200	16,700	17,700
Solid heat capacity at TP ( $\text{J mol}^{-1} \text{K}^{-1}$ )	6.2	11.8	16.1
Bond energy ( $\text{kJ mol}^{-1}$ )	435.9	443.4	446.9

using the molar fraction of each molecule.  $K = 0$  at 0 K, and  $K = 4$  at infinitely high temperature. In an equimolar mixture of D and T, molar fractions are 0.25, 0.25, and 0.5 for  $D_2$ ,  $T_2$ , and DT, respectively. In a fusion reactor system,  $H_2$  always remains in the fuel as an impurity, but equilibrium constants for mixture of three isotopes, H, D, and T, were not measured nor calculated. Because of the significant mass differences, gas flow, in particular, evacuation rates for three isotopes are quite different and could influence fuel recycling in the reactor.

There exist two different spin isomers of hydrogen diatomic molecules that differ by the relative spin of their nuclei [3]. In the  $H_2$  molecule, the spins of the two hydrogen nuclei (protons) couple to form a triplet state known as ortho-hydrogen termed o- $H_2$  with parallel spins, and a singlet state known as para-hydrogen termed p- $H_2$  with antiparallel spins.

At STP, hydrogen gas contains about 25 % of p- $H_2$  and 75 % of o- $H_2$  (or 1/3 in their ratio), which is referred as the “normal form,” n- $H_2$ . For  $D_2$  and  $T_2$ , the ratios are 2/1 and 1/3, respectively. The equilibrium ratio changes with temperature. At 0 K, p- $H_2$ , o- $D_2$ , and p- $T_2$  account 100 % in equilibrium. Thermal properties of pure p- $H_2$  differ from those of n- $H_2$ . The difference in thermo-physical properties of isomers of  $T_2$  would influence the formation process of ice pellets for fueling.

Since hydrogen readily forms covalent compounds with most nonmetallic elements, most of the hydrogen on the earth exists in molecular forms such as water and/or organic compounds. Hydrogen is mostly produced by steam reforming of natural gas and less often from more energy-intensive hydrogen production methods like the electrolysis of water. Most hydrogen is employed near its production site, with the two largest usages being fossil fuel processing (e.g., hydro-cracking) and ammonia production, mostly for the fertilizer market. Hydrogen is mainly used in petroleum and chemical industries. Quite recently,  $H_2$  is used as energy carrier with energy density of 120 MJ/kg to give clean energy, and application of hydrogen fuel cell for cars has started.

Hydrogen is a concern in metallurgy as it can embrittle many metals [4], which makes the design of pipelines and storage tanks complicating. Nevertheless, the mechanism of hydrogen embrittlement is not clarified yet, and hence, hydrogen embrittlement should be taken into account for reactor design. Hydrogen is easily dissolved in and permeate through metals. For utilization of T in fusion, the dissolution and permeation are quite important problems for T inventory and confinement from the aspect of radiation safety of which details are discussed in this book.

### 2.1.2 *Tritium, a Radioactive Hydrogen Isotope*

Tritium decays to  $^3He$  with emissions of a  $\beta$ -electron and an antineutrino ( $\bar{\nu}$ ) with a half-life of 12.323 year [3],



According to the decay rate, 1 g of T is equivalent to  $3.5574 \times 10^{14}$  Bq and about 5.5 % is disappearing during its storage in a year by the decay. The energy of the emitted  $\beta$ -electrons is widely distributed with the maximum of 18.6 keV and average of 5.7 keV as shown in Fig. 2.1 [3]. The integrated decay heat, 324 mW/1gT, is not very large, but could influence melting of ice pellets used for fueling, and enhance thermal release of T from heavily T-loaded materials. Small particles containing certain amount of T are charged up by the emission of electrons and show unexpected movement due to electrostatic force [5].

Owing to its low energy, the effect of the  $\beta$ -electrons on human beings is very weak compared to other radioactive materials. Hence, T had been used under very mild regulation or sometimes without regulation. “EXIT” signs for emergency and luminous watches commonly used are driven by T with electroluminescence. Usually, no thick shielding is required to handle T, though direct touching is prohibited.

The detection of T retained on materials surfaces is rather easy with using the  $\beta$ -counting method, which has the detection limit and/or accuracy of several Bq/cm<sup>2</sup> on solid surfaces and around 0.1 Bq/cm<sup>3</sup> in water. However, the  $\beta$ -electron counting is limited to below  $\sim 10^9$  Bq or mg order of T. Furthermore, T retained in the bulk of solid materials is quite hard to detect, because the  $\beta$ -electron can penetrate through or escape from the solid materials only a few  $\mu\text{m}$  in depth. (Its maximum range in air is 6 mm and less than 1  $\mu\text{m}$  in metals.) Therefore, movable T in the solid, mostly in metals, causes safety problems.

For much larger amount of T, mass and/or pressure measurements, the same way to measure other hydrogen isotopes, are employed (see Fig. 2.2). For highly concentrated T in liquids and solids, its decay heat allows a calorimetric measurement, but its accuracy is only  $10^{-2}$ – $10^{-3}$ . At present, T measurements except for the

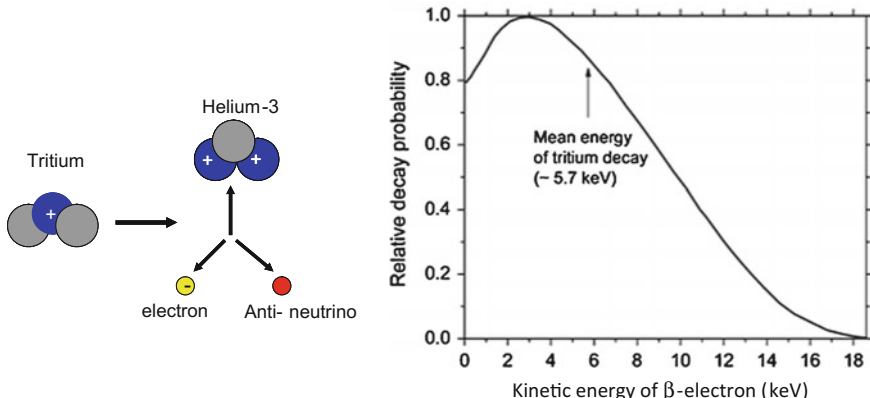


**Fig. 2.1** Decay scheme of T and energy distribution of  $\beta$ -electrons emitted at T decay

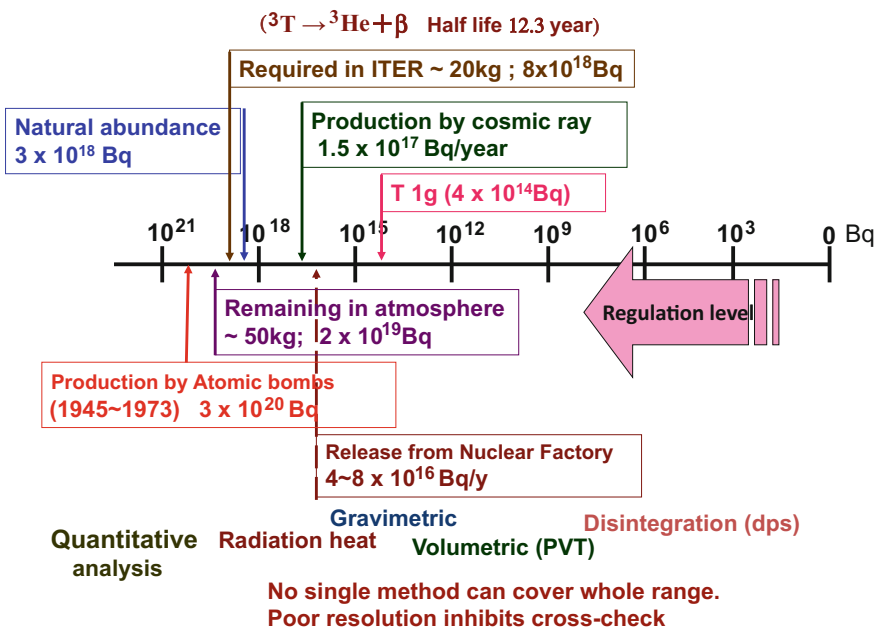


**Fig. 2.2** Tritium abundance and measurements [6]

$\beta$ -counting give the accuracy of only 2–3 digits and any loss of T less than 0.1 % is hardly possible to detect. Therefore, attaining exact T accountancy in a fusion reactor seems quite hard and significant efforts are required to comply with the safety regulation. Details of quantitative analysis of T are given in Chap. 7.

Since public exposure to T is regulated at a level as tiny as a few  $\text{Bq/cm}^2$ , T must be strictly confined in T handling systems. But it is quite hard in reality, because T having the same nature as hydrogen easily dissolves in and permeates through materials resulting in easy leakage. T escaping from the handling system by permeation and leakage contaminates materials outside the system. Hydrogen permeation is described in Chap. 9. Furthermore, once T escapes from the system, it is easily replaced with H in ubiquitous water to make HTO and in organic molecules to make OBT (Organic Bound Tritium). Both are more hazardous than HT.

## 2.2 Tritium Resources

For any energy system, resources of fuel are critical. Since hydrogen in natural water or standard mean ocean water (SMOW) contains 0.016 % deuterium (D) (see Table 1), we can extract D from the water mostly by means of electrolysis. Because

the surface waters of earth contain more than 1 billion tons of D, D can be considered to be a practically infinite fuel resource.

In nature, T is produced by cosmic rays, mostly high-energy neutrons as,



At the same time, T decays with half-life of 12.3 years or around 5 %/year. Consequently, the amount of T is balanced between the production and the decay resulting nearly constant concentration of  $10^{-18}$  in natural hydrogen (T/H) which is referred as tritium unit (TU). Thus, the total abundance of T on the earth is around of several kg ( $\sim 3 \times 10^{18}$  Bq) (see Fig. 2.2), existing with chemical form of HTO [7]. Before Partial Test Ban Treaty at October 1963, nuclear weapon tests produced much more T than natural abundance. Afterward, such artificially produced T has been decaying to the present level of  $\sim 50$  kg. Still every nuclear reactor is releasing  $\sim 10^{14}$  Bq/year.

Since T is a critically important component for nuclear weapons, it is produced in nuclear fission reactors, for example, in heavy water cooled reactors,



and in a special rod containing  $^{10}\text{B}$  or  $^6\text{Li}$  in light water cooled reactors,



Reaction (2.6) is used in CANDU (CANada Deuterium Uranium) reactors, and produced T is commercially available for peaceful use, while reaction (2.8) is mostly for T in military use.

The total T inventory for the military use is estimated to be around 600 kg at maximum during the early 1970s. Due to various tests of nuclear weapons, T concentration in environment was about 6000 times higher than the natural abundance at 1963 just before the stop of nuclear weapon test at Partial Test Ban Treaty. Afterward, the natural abundance decayed significantly and nearly comes back to the level of old days when no T was artificially produced. Still commercial light water reactors are releasing T around 1 g/year/ 1 reactor.

According to Ref. [8], the total T inventory or reserve in USA for nuclear weapons was estimated to be 60–100 kg at 1984 and the amount would not change very much afterward or has very likely decreased as evidenced by current shortage of  $^3\text{He}$ , of which considerable amount has been recovered from nuclear facilities as a decay product of T.

Now an important question arises, that is, how much T is burned in a fusion reactor? From a simple calculation according to the famous Einstein equation,

$E = \Delta M c^2$ , where  $E$  is released energy given by the D-T reaction,  $\Delta M$ , the mass of D and T burned (disappeared), and  $c$  is the velocity of light, 56 kg of T is burned per GW year of fusion power (GWth) for a D-T reactor. (About one-third of the fusion power is converted to electric power represented by GWe.) Currently, around 100 g of T is produced per year in a standard CANDU reactor and 20–25 kg T (mainly in Canada) will be available for operation of ITER. Still the amount of initial inventory in ITER, which is the amount of T simply dissolve in materials used in ITER and immobilized (hard to recover), is quite uncertain, but could be significantly large, as discussed in Chap. 3. This means that at present we have no T reserves for DEMO.

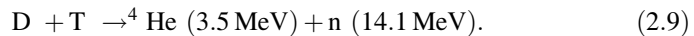
Therefore, any fusion reactor should breed T in its blanket system and the T breeding should have enough margins to compensate T inventory in its tritium systems and the 5 %/year decay (fuel self-efficiency) and reserve for new reactors.

In addition, as discussed in Chap. 3, very poor burning efficiency in a tokamak fusion reactor requires huge amount of total throughput and hence rather large reserve. By using an optimized blanket system, overall T breeding ratio (TBR) in a fusion reactor is expected to be around 1.2 at maximum [9]. In this respect, overall T retention rate in a reactor system including T recovering, refining, isotope separation, and refueling systems must be below 0.1.

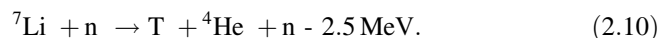
## 2.3 Tritium as Fuel of D-T Reactor

As described in previous section, it is difficult to get sufficient amount of T even for DEMO. T must be bred by a nuclear reactor or an accelerator with nuclear reactions using Lithium (Li). Since the attainable breeding ratio does not seem to quite high as discussed in Chap. 3, T retained in any T systems in a reactor should be recovered not only for T safety but also for T economy.

As described in Chap. 1, the energy released by D-T reactions is distributed to  ${}^4\text{He}$  and neutron,

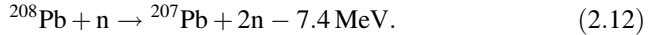


The energy of  ${}^4\text{He}$  is to be used for heating plasma to sustaining the D-T burning and the energy carried by neutron is transformed to heat in a blanket system for electricity or other use, like hydrogen production. At the same time, neutron is used to breed T as



Since, as described in Chap. 1, natural Li includes both  ${}^6\text{Li}$  and  ${}^7\text{Li}$  with their natural abundance ratio of 7.5–92.5, utilization of Li in the blanket seems easily to

give breeding ratio of more than 1. To get enough margin on T breeding, neutron multipliers, such as Be and Pb are planned to use in the blanket,



However, the neutron multipliers (Eqs. 2.10–2.12) require external energy, and their usage in the blanket reduces the output power. By using the optimized blanket system, the overall T breeding ratio in a fusion reactor could be around 1.2 at maximum. In this respect, the overall T recovering rate from the reactor vessel and other T processing systems must be kept as large as possible, above around 0.95; otherwise, T fuel for the 2nd reactor is not constructed. At the moment, this seems very hard owing to large in-vessel T inventory as described later.

## 2.4 Isotope Effects Among Atoms and Molecules

Various properties of hydrogen isotopes are summarized and tabulated in a book by Souers [3]. In Table 2.1, some properties important for fusion application are summarized.

Because of large mass differences among the three hydrogen isotopes (H, D, and T), isotope effects are most appreciable in properties relating to the velocities of ions, atoms and molecules, and vibration and rotation of atoms and molecules.

Simple molecular kinetics tells that an average velocity  $\bar{v}$  of a gas molecule with its mass  $m$  at temperature  $T$  and pressure  $P$  is given by,

$$\bar{v} = \sqrt{\frac{8kT}{\pi m}} \quad (2.13)$$

where  $k$  is the Boltzmann constant. Therefore, the velocity differences among the three hydrogen isotopes of H<sub>2</sub>, D<sub>2</sub>, and T<sub>2</sub> are,

$$\overline{v_H}/\overline{v_D} = \sqrt{2} \quad (2.14)$$

$$\overline{v_H}/\overline{v_T} = \sqrt{3} \quad (2.15)$$

and

$$\overline{v_D}/\overline{v_T} = \sqrt{3/2} \quad (2.16)$$

Since incident flux  $J$  to the surface of a gas container is given by gas density  $n$  times its velocity  $\bar{v}$

$$J = n\bar{v}/4 = \frac{P}{(2\pi mkT)^{1/2}} \quad (2.17)$$

Accordingly, incident flux ratios under the same pressure are given as,

$$J_H/J_D = \sqrt{2} \quad (2.18)$$

and

$$J_H/J_T = \sqrt{3} \quad (2.19)$$

These differences appear in reaction rates of any chemical reactions including hydrogen. Isotope separation with using the different fluxes is one of the most useful applications. A turbomolecular pump shows significantly larger pumping speed for D<sub>2</sub> than H<sub>2</sub>. It should be noted that the sensitivity factors of a vacuum ionization gage are also square root mass dependences for all hydrogen isotopes, because the gage measures the molecular fluxes but not the pressure of gases directly. Better confinement time of D than H in plasmas is a well-known and an important isotope effect. All those differences influence the amounts of D and T confined in plasma, and simple fueling with equimolar mixture of D and T does not ensure the most effective D-T burning.

Observed isotope effects between H and D often deviate from such square root mass ratios. For T, little observations have been reported and extrapolation of the isotope effects between H and D to those for D and T might not be correct. Behaviors of D and T fuels are discussed in detail at Chap. 5.

#### **2.4.1 Hydrogen in Plasma (Atoms and Ions)**

Different from the kinetic properties given above, differences in electronic properties, ionization, excitation of electrons for atoms and molecules among three isotopes are quite small as given in Table 2.2. This will make distinction of D and T in boundary plasmas difficult as described in the next section. In burning plasma, fuels are fully ionized in core plasma, while neutral atoms and molecules are mixed in boundary plasma. Since heavier ions are confined better in plasma, the mass difference strongly influences confinement times of deuteron (D<sup>+</sup>) and triton (T<sup>+</sup>) and also evacuation speeds as described above. This requires special care on fueling of D and T in plasma core to maintain high burning efficiency, and hence, determination of D/T ratio in the plasma core is critically important.

Optical emissions from excited atoms and molecules are one of the most important diagnostics to characterize boundary plasmas. Hydrogen in the boundary plasma is usually observed by Balmer series emissions. In particular,  $\alpha$ - and  $\beta$ -emissions are used to determine recycling of fuels at plasma-facing surfaces, the

**Table 2.2** Balmer series emissions of H, D, and T [3]

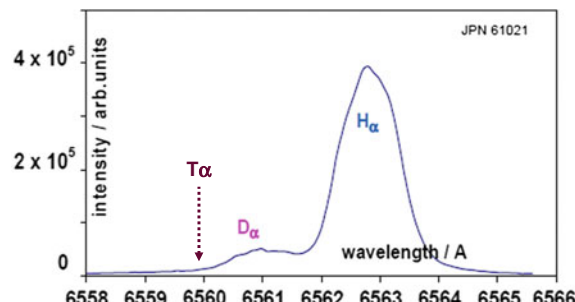
Balmer lines	H (nm)	D (nm)	T (nm)	H–D (nm)	H–T (nm)
$\alpha$	656.28529	656.10104	656.04166	0.18425	0.24363
$\beta$	486.1362	486.00028	485.9563	0.13592	0.1799
$\gamma$	434.04946	433.92829	433.88902	0.12117	0.16044
$\delta$	410.1765	410.06191	410.02479	0.11459	0.15171
$\epsilon$	397.0072	396.89992	396.86329	0.10728	0.14391
IP ( $\text{cm}^{-1}$ )	109,678.76	109,708.608	109,718.538	-29.844	-39.774
IP (eV)	13.598	13.602	13.603	3.7001 meV	4.9313 meV

ratio of incoming and/or outgoing fluxes. And also temperature of the boundary hydrogen plasma can be determined by the intensity ratios of the Balmer series emissions.

Since electronic structures of three isotopic atoms (H, D, and T) are not much influenced by the differences of atomic masses, the differences in electron energy levels of excited states and ionization energy of each atom are within 3–5 meV and differences in wave lengths of Balmer lines emission are within 0.1–0.2 nm as given in Table 2.2. To distinguish three isotopes in plasma by observation of the Balmer series emission, a spectrometer with very fine resolution is required. Figure 2.3 is an example of the fine-resolution optical measurement in JET [10].  $\text{H}\alpha$  and  $\text{D}\alpha$  were mostly separated. Nevertheless, it seems difficult to quantify concentration of H, D, and T, or any isotope with lower concentration becomes difficult to detect quantitatively.

In burning plasma, because of high temperature, fuel particles of D and T are fully ionized giving no optical emissions except Bremsstrahlung. Therefore, it is quite hard to know concentrations of D and T in the burning core which is indispensable to control D–T burning though fueling ratio of D/T. Since in a D–T fusion reactor, D–D reactions always accompany with D–T reactions, neutrons accordingly produced can be separated with their energies, 2.4 and 14 meV. Hence, measurements of neutron energy distribution in a reactor is expected to be used for a diagnostic to determine, burning rate and D/T ratio in the burning plasma, though it does not seem easy.

**Fig. 2.3** Balmer lines emission observed at boundary plasma of D and H mixture in JET (reprinted with permission from [10])



### 2.4.2 Molecules

As already described, various hydrogen molecules are distinguished. Considering nuclear spins, they are o-H<sub>2</sub>, p-H<sub>2</sub>, HD, HT, o-D<sub>2</sub>, p-D<sub>2</sub>, DT, o-T<sub>2</sub>, and o-T<sub>2</sub>. Since the differences caused by the nuclear spins are only appreciable at very low temperatures, they are not considered in handling of fusion fuels, except for making ice pellets for the fueling. Hence, 6 molecules H<sub>2</sub>, D<sub>2</sub>, T<sub>2</sub>, HD, HT, and DT are generally separated. H is not the fuel but always remains as an impurity and hard to remove any handling systems of D and T. A few percentage of H is expected to be in the exhausted fuels from a reactor vessel.

As described above, translational motion, molecular vibration, and rotation are significantly different among 6 isotope molecules and they influence their thermal properties of their gases, liquids, and solids. The rotational and vibrational levels of hydrogen molecules are quantized and owing to quantum effects, three isotopes show complete different energy levels as shown in Fig. 2.4 [3]. One can note that the ratio of the zero point vibration energies of H and T is just 0.58 equal to their square root mass ratio. Molecular hydrogen spectroscopy in boundary plasma of TEXTOR shows that observed spectra for pure H and pure D discharges agree quite well with the theoretical ones, while the spectral lines for H and D mixtures are overlapping and difficult

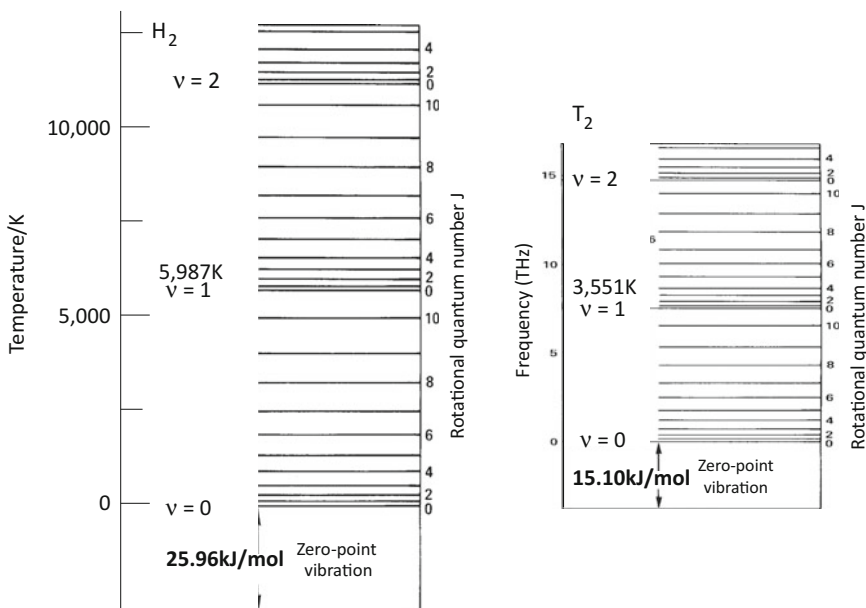


**Fig. 2.4** Vibrational and rotational energy levels of isolated H<sub>2</sub> and T<sub>2</sub> (reprinted with permission from [3])

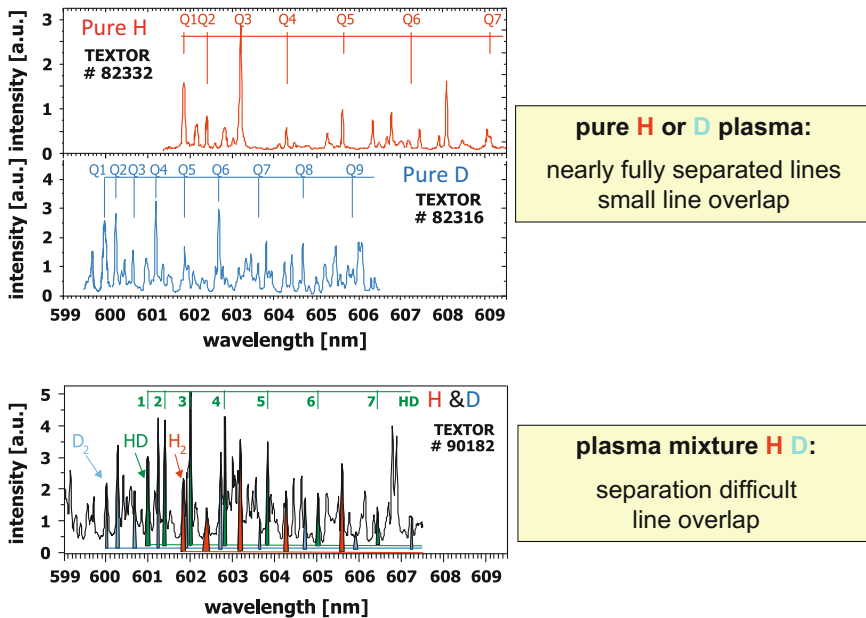


**Fig. 2.5** Examples of molecular spectra obtained from plasmas of pure H, pure D, and HD mixture in TEXTOR (reprinted with permission from [11]). For pure H or D, no overlap in dominant lines, while many lines overlap for mixture of H and D to make separation difficult

to separate (see Fig. 2.5 [11]). Hence, molecular spectroscopy seems challenging to be applied for quantitative analysis of H, D, and T in boundary plasmas.

For quantitative analysis of  $H_2$ , HD, HT,  $D_2$ , DT, and  $T_2$  in gases near room temperature, Raman spectroscopy can be applied to distinguish the differences of rotational energy levels of each molecule, which is described in Chap. 12.

The different rotational and vibrational levels give different heat capacity and thermal conductivity of ice pellets of  $D_2$  and  $T_2$ . The heat capacity of solid hydrogen shows quite good square root mass dependence as shown in Fig. 2.6 [12]. As noted above, spin isomers of o- $D_2$ , p- $D_2$ , DT, o- $T_2$ , and o- $T_2$  give different thermo-physical properties. This directly influences manufacturing the ice pellets, and the decay heat of T could enhance melting behavior and ablation or evaporation flux of D and T in fueling by DT pellets.

Since most of the isotope effects in interaction of hydrogen and materials include surface kinetics, differences in hydrogen fluxes to and from solid surface among three isotopes should be taken into account.

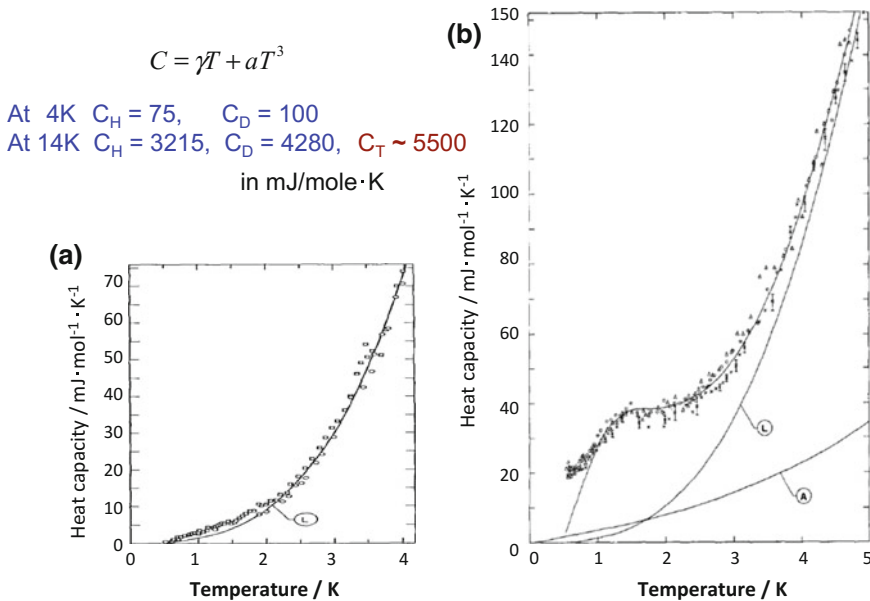


**Fig. 2.6** Temperature dependence of heat capacity of H and D (reprinted with permission from [12]). **a** Pure H<sub>2</sub>. Solid curve labeled L (proportional T<sup>3</sup>) is the lattice contribution. **b** Pure D<sub>2</sub>. Upper curve is theoretical specific heat including lattice contribution given by L and the contribution of empty calorimeter given by A

### 2.4.3 Hydrogen Properties in Materials

Among various properties of hydrogen in materials, solubility, diffusivity, and permeability are quite important not only for T safety but also for T fuel self-sufficiency. Interaction of hydrogen and materials has been one of the most important subjects in materials science, too.

Compared to other elements, hydrogen is easily dissolved or trapped and migrates in materials. Hydrogen properties in materials have been extensively studied, because of its importance in hydrogen embrittlement which is one of the causes of the materials failure in large structure, bridges, ships, gas tanks, and so on [4].

Since hydrogen solution and permeation are likely proportional to incident flux, the isotopic effects in solubility (S) and diffusivity (D) would be proportional to the square root of mass ratio, i.e.,

$$S_H/S_D = \sqrt{2} \quad (2.20)$$

and

$$S_H/S_T = \sqrt{3} \quad (2.21)$$

and

$$D_H/D_D = \sqrt{2} \quad (2.22)$$

and

$$D_H/D_T = \sqrt{3} \quad (2.23)$$

Similar isotope effects are often observed in hydrogen permeability  $\Phi$  as

$$\Phi_H/\Phi_D = \sqrt{2} \quad (2.24)$$

In diffusion-controlled permeation, permeability is represented by,

$$\Phi = SD \quad (2.25)$$

According to the isotope effects in  $S$  and  $D$ , however, Eq. (2.25) is not possible; that is, the isotope effect could not be represented such simple equations.

Large mass differences among hydrogen isotopes result in large difference in their quantized rotational and vibrational states. Contradictions among  $\Phi$ ,  $D$ , and  $S$  are most likely owing to neglecting of the isotope effects in the rotational and vibrational states in solids. Actually significantly large isotope effects originating from quantum effects are observed in diffusion coefficients at temperature far below RT as given in Fig. 2.7. The diffusion coefficients do not follow single Arrhenius relationship in their temperature dependence, and the upper shift at lower temperatures is attributed to the quantum tunneling effect. Because of the lightest mass of protium, among the

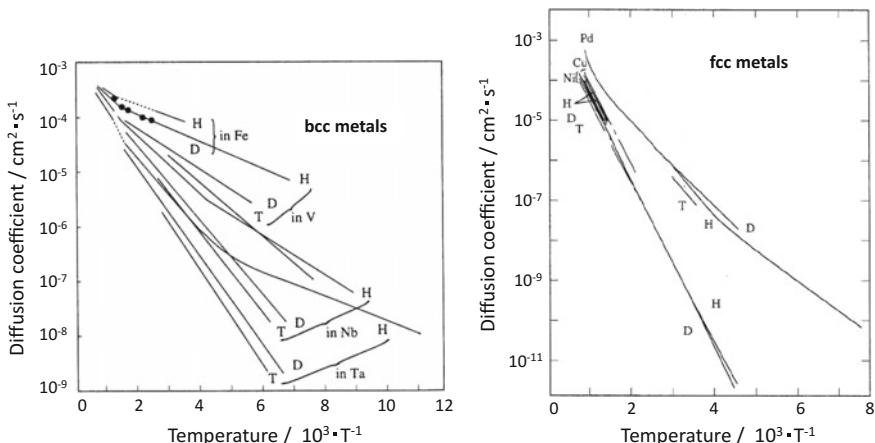


**Fig. 2.7** Comparison of diffusion coefficients of H, D, and T in some metals

three isotopes, the quantum effect is the most appreciable. Above the room temperature, the difference becomes less and the differences in not only diffusivity but also solubility and permeability of H, D, and T are within the factor of the square root mass ratio, which is in most case near the experimental error. Therefore, isotope differences in handling of large amount of gases of H, D, and T are not likely over the square root of their mass ratio.

Isotopic effects between H and D are also appreciable in the interactions of hydrogen and materials such as reflection, reemission, diffusion, and trapping. In a fusion reactor, plasma-facing materials are exposed to T plasma or subjected to high-energy T ions and atoms. The isotopic effects among high-energy hydrogen isotopes, in particular between D and T, have not been studied yet. Their difference in confinement time, recycling at the plasma-facing surface, and evacuation could largely influence in burning efficiency.

In case of handling T as a tracer, T sometimes gives anomalous isotope effects mainly caused by isotope exchange with H in ubiquitous water as discussed in the next section.

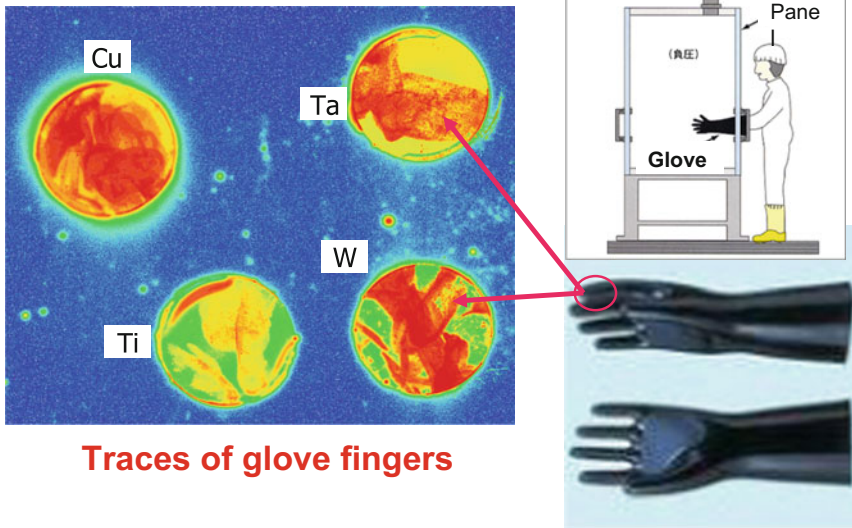
## 2.5 Contamination by Isotope Exchange Reactions

### 2.5.1 *Isotopic Replacement on Solid Surface as a Cause of T Contamination*

Contamination of materials surfaces by T is one of the most important safety concerns and understanding of the contamination mechanism is quite important to reduce and/or remove the contamination (detritiation). Due to reactive nature of hydrogen, T can be easily transferred from a highly contaminated surface to lower contaminated or noncontaminated surfaces, leading to cross-contamination or multistep contaminations in T handling systems. In ITER, safety handling of a divertor cassette, one of the largest components, is the most serious concern [13]. The cassette retains very high levels of T on their surfaces, which easily transfers to arms or gloves of remote handling systems or gloves boxes. Once the surface of the device/equipment in the systems is contaminated, T can be easily transferred to any materials next to be handled. Figure 2.8 shows an example of cross-contamination remaining fingerprints of T activity on metal plates in a glove box in which heavily contaminated materials were handled [14]. Gloves as essential equipment in a T handling system are always contaminated and T on the glove surface is immediately transferred to noncontaminated materials. The cross-contamination is caused by easily replacement of T with the ubiquitous lighter hydrogen isotopes such as protium (H)/deuterium (D) in water and hydrocarbons in atmosphere. The consequence is multistage contamination and sequential reduction of the contamination by second and third glove-boxes might not so effective.

### Easy transfer of T contamination

Metal plates exposed to D plasma in TPL and handled in a T handling glove box



Possible contamination by permeation

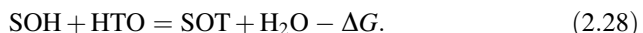
**Fig. 2.8** T contamination of metal surfaces caused by handling in a glove box [14]. High T activity appeared as the traces of the gloves

The most important mechanism of the cross-contamination is isotope exchange reactions of T with the ubiquitous lighter hydrogen isotope, protium (H), in water to become HTO and hydrocarbons in atmosphere, as given in following reactions,



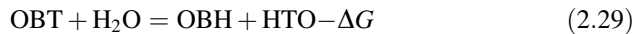
Similar to the reaction (2.27), T involved inorganic molecules, referred as Organic Bound Tritium (OBT) easily remains in a human body and more hazardous than HTO.

Such isotopic replacements easily proceed at any solid surface (*S*) as



for tritiated water case. This is the main cause of the contamination of the gloves in Fig. 2.8. In addition, T and HTO are very easy to permeate through metals and organic materials, respectively, which also cause the T contamination.

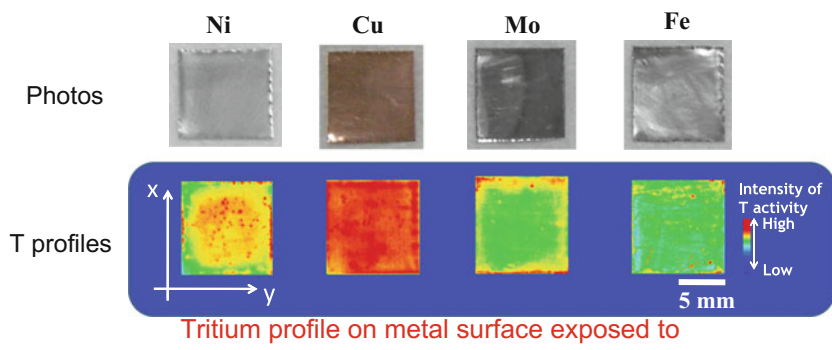
Tritium disintegration at skin is not so important owing to thin penetration depth of the  $\beta$ -electrons, but T can penetrate into a human body by isotopic replacement with light water in tissues to be very hazardous. Once T is going in human body and tissues, a few weeks are needed to be isotopically replaced by H from drinking water as,



On the contrary, dipping in water and/or wiping with wet papers of the T-contaminated surface is very effective for detritiation. For example, drinking beer is very efficient to enhance the replacement of T in a human body. It is also well known that the addition of water vapor is very much effective to recover T in structure and breeding materials and on the surface of any materials, but T diluted in water is very hard or needs lots of energy to be recovered, which increases fusion energy cost.

Owing to those easy surface replacement, surface T concentration is not necessarily to be the same as that in the bulk as shown in Fig. 2.9 [15]. In the figure, the surface T levels are compared for various metals in which tritiated hydrogen was dissolved at 873 K. One can note that the surface T concentrations are quite different with the solubility. That is because, the surface of most of metals was oxidized with different level (or different oxide thickness) and the amount of

Behavior of T on solid surface is often separated form that of bulk  
(Only T within a few  $\mu\text{m}$  can be detected)



	Ni	Cu	Mo	Fe
<b>Surface T conc. (Arb. unit)</b>	1070	2380	811	704
<b>H solubility at 873K (H/M)</b>	$10^{-3}$	$10^{-5}$	$10^{-7}$	$10^{-5}$

Fig. 2.9 Examples of T profiles on metal surfaces exposed to T gas [15]

retained OT is higher for more oxidized surface. However one should be careful that once some of the surface T was smeared out, T was supplied from the bulk by diffusion and the surface T level recovered easily. Of course if bulk T concentration was very high, the surface-segregated T could be neglected.

### ***2.5.2 Isotopic Replacement with Residual or Impurity H in Materials***

Any materials retain hydrogen as an impurity with more than a few tens ppm. Therefore, the isotopic replacement described in the previous section is not limited to the surface. Easy diffusion of hydrogen in the bulk enhances the replacement. In case of H in industrial use, the replacement of H retained in the materials or ubiquitous water with H throughput does not matter. The H throughput into an H processing/handling system is much larger than the amount of H on surface and in bulk of the materials used in the system and tiny loss is not accounted. For T safety, on the other hand, any T retained in the system should be accounted. Furthermore, since absolute amount of T handled in most of the T systems is much less than the amount of H in industrial systems, T retained in the systems does matter. This is quite important in T handling system and T measuring systems and described in Chap. 3 in more detail.

Since the bulk replacement is diffusion-limited process strongly dependent on material's temperature, its replacement rate is generally much slower than that of the absorption and surface replacement and is not appreciable at RT. However, in the fusion reactor vessel probably operated at 700–800 K, the contribution of the isotopic replacement of T with H in bulk would have significant contribution on T retention owing to quite large volume of the vessel. Furthermore, T escaping from the plasma impinges and is retained in a little deep inside of the plasma-facing materials. This enhances the isotopic replacement with H in bulk. The bulk T inventory is discussed in Chaps. 3 and 5.

## **2.6 Effect of $\beta$ -Emission on T Behavior**

Liquid  $T_2O$  is corrosive due to self-radiolysis. The  $\beta$ -particles travel only about 6  $\mu m$  in water and deposited energy during the travel causes decomposition of water molecules (water radiolysis) to produce gaseous hydrogen (including HT) and redox-active products including highly reactive hydroxyl radicals ( $\cdot OH$  and  $\cdot OT$ ). This is one of the main causes for T to be hazardous and is discussed in Part III.

Here only direct effect of  $\beta$ -emission on behavior of T fuel is described. In reactions including T, anomaly owing to  $\beta$ -emission and recoil He atoms is sometimes claimed. However, due to the small penetration of  $\beta$ -electron, its direct influence on neighboring T is hardly observed. Instead, the electron colloid with neighboring molecules or atoms, whatever chemical forms, electron excitation of themselves or neighbors could lead some reactions which are not possible thermally like the self-radiolysis. This kind of reaction is highly possible to occur at solid surfaces in water including T or solid surface including T in gas. The reaction caused by the electron excitation could be either reductive or oxidative.

Quite recently, a corrosion test in rather high-dense tritiated water has shown corrosion enhancement [16]. The direct effect of the T decay to T including molecules must be quite seldom unless T concentration is quite high or T is not diluted in H or D. When T concentration in materials is very high, deposited electron energy raises the materials temperature, often referred as decay heat. The decay heat of pure T is 324 mW/g or  $67.5 \times 10^{-3}$  cal/g s, which will cause its temperature rise of 1 K for a few 10 s seconds. The decay heat is not quite large but would influence ice pellet production. The effect of decay heat was observed as enhanced T release from graphite tiles used in T discharges in JET.

If isolated particle retains certain amount of T, electron emission makes the particle charging up and the behavior of the particle becomes controlled by static electric field [17].

## 2.7 Tritium Issues in Burning Plasma and Self-sufficiency of Fuels

The burning efficiency in a fusion fuel cycle is, unfortunately, very poor; only a few % or less of input tritium in the reactor vessel burns and the majority must be exhausted and recovered to recycle. However, as described in Sect. 2.2, T resources are not enough even for a DEMO reactor. Therefore, T should be artificially produced or bred in a blanket of a fusion reactor. Since T decays about 5 % a year, T breeding in the blanket should have enough margins to compensate not only the T inventory in all T handling systems, but also the disappearance by the decay.

With using an optimized blanket system, overall T breeding ratio in a fusion reactor is expected to be around 1.2 or a little less. In this respect, the in-vessel T retention rate ((fueling – (burning + recovering))/fueling) must be below 0.1. Otherwise, T for the second reactor is not generated. At the moment, it seems very hard to make the in-vessel fuel retention rate to be below 0.1, as described later.

Suppose the burning efficiency is  $\sim 3$  %, to burn 56 kg/year of T for 1GWth of fusion power, total throughput becomes  $\sim 1800$  kg/year. Accordingly, fuel retention rate must be below 0.05 % to keep the in-vessel T inventory below 1 kg required for the safety in ITER. It is of course not necessary to reserve 1800 kg of T

at one time. But T inventory in other T systems than the vacuum vessel should be also taken into account.

In the present plasma devices, light hydrogen (H) always remains in the deuterium fueling operation, of which origin was discussed in the previous section. Whatever the sources are, contamination of D and T by H is unavoidable and additional effort to remove H in an isotope separation process is required. For enhancement of radiative cooling of the plasma and also for disruption mitigation, impurity seeding such as Ne and Ar will be employed, which could significantly dilute the fuels. In addition, various chemical forms of hydrocarbons will be formed from carbon plasma-facing materials and impurity carbon in W, if they are used. Thus, D and T fueled into the vacuum vessel are exhausted as a heavily contaminated gas of D and T with H, hydrocarbons and inert gasses (He, Ne, and Ar). Since only D and T must be recycled, the exhaust gas must be recovered, refined, isotopically separated, and refueled. One should remind that this is requested from the self-fuel efficiency but not from the safety.

As noted in Sect. 2.4, behaviors of D and T not only in the plasma but also in materials are significantly different from each other: for instance, confinement times, fueling efficiencies, escaping fluxes from the plasma, retention rates in materials, evacuation rates from VV, and so on. Therefore, the fueling rate is necessarily the same and must be optimized to attain the highest burning efficiency. Because of very poor fueling efficiency of gas puff [18], T is injected mainly by pellets and NBI, while D would be fueled by gas puff and NBI [19]. Such different fueling between D and T does not assure homogeneous mixing of D and T in plasmas. Therefore, it will not be easy to maintain the appropriate D/T ratio in the plasma for continuing the highest burning efficiency. The concentration of D and T in the burning plasma must be separately measured to achieve feedback fueling independently. It is, however, quite difficult to measure the concentration of D and T separately. Separate detection of neutrons with energies of 14 MeV (produced by D-T reactions) and of 2.4 MeV (D-D reactions) is one of the most promising ways, but the signal does not necessarily give spatial distribution of D/T ratio in the plasmas. Different confinement times of D and T would result in their inhomogeneous distribution particularly in their radial distribution.

Furthermore, retention rates of D and T in the plasma-facing wall is not necessarily the same and release rates from the wall may be different as well. This means that if some local thermal load like an ELM hits the wall, thermal release of D and T is different in their amounts and this disturbs the D/T ratio in the plasma. Owing to the huge wall inventory, a small change in the D/T ratio of the wall retention could cause significant change in the D/T ratio of the burning plasma. Thus, we are going to face difficulty in controlling the D/T ratio in the plasma to attain and keep efficient burning. Again, the initial phase of ITER discharges using H and D shall be used intentional control of H/D ratio in plasmas.

## 2.8 Summary

Hydrogen properties important for fusion application are described. Because of large mass differences, isotope effects among H, D, and T in dynamic behaviors relating atomic and molecular motions are quite large. In particular, differences of confinement in plasma, retention in plasma-facing wall, permeation, and pumping speed between D and T would require independent controls in fueling of D and T to keep D-T burning to be efficient. Unfortunately, however, D/T ratio in the burning is quite hard to observe (determine). The fueling and burning control are one of the most difficult remaining issues to be solved in ITER. Poor T resources also require appropriate fueling, breeding, and full recovering of T to recycle the fuel to attain the fuel self-sufficiency.

For handling of massive amount of T as the fuel, effects of  $\beta$ -electrons emitted at the decay are not concerned, except the 5 % disappearance by the decay. In storage and for safety, the decay could give some impacts through electron excitation by the  $\beta$ -electrons. Self-radiolysis of tritiated water is one of the most important effects, because it is the main cause of hazard of T for human bodies. Isotope exchange of T with H in ubiquitous water molecules, in particular, adsorbed on solid surfaces results in easy cross-contamination. Charging up small particles retaining T with high concentration could be another cause of the contamination.

Nevertheless, the decay heat of 324 mW/1 gT is rather small and would not give significant effect in handling of massive amount of T except at very low temperature for making ice pellets.

## References

1. [http://en.wikipedia.org/wiki/Isotopes\\_of\\_hydrogen](http://en.wikipedia.org/wiki/Isotopes_of_hydrogen)
2. <http://en.wikipedia.org/wiki/Hydrogen> and references therein
3. P.C. Souers, *Hydrogen Properties for Fusion Energy* (University of California Press, California, 1986)
4. R.P. Gangloff, B.P. Somerday (ed.), *Gaseous Hydrogen Embrittlement of Materials in Energy Technologies, The Problem, its Characterization and Effects on Particular Alloy Classes* (Woodhead Publishing, Sawston, 2012). ISBN: 978-1-84569-677-1
5. C.H. Skinner, G.A. Gentile, L. Ciebiera, S. Langish, *Fusion Sci. Technol.* **45**, 11–14 (2004)
6. T. Tanabe, Tritium handling issues in fusion reactor materials. *J. Nucl. Mater.* **417**, 545–550 (2011)
7. S. Tosti, N. Ghirelli, *Tritium in Fusion—Production, Uses and Environmental Impact* (Nova Publishers, NY, 2013)
8. T.B. Cochran, W.M. Arkin, R.S. Norris, M.H. Hoenig, *Nuclear Weapon Data Book, vol. II, US Warhead Production* (Ballinger Publishing Co., Pensacola, 1987)
9. M.E. Sawan, M.A. Abdou, *Fusion Eng. Des.* **81**, 1131–1141 (2006)
10. A. Pospieszczyk, S. Brezinsek, A. Meigs, G. Sergienko, M. Stamp, JET-EFDA contributors, 32nd EPS Conference on Plasma Phys. Tarragona, 27 June–1 July 2005 ECA vol. 29C, P-2.011 (2005)

11. S. Brezinsek, P.T. Greenland, Ph Mertens, A. Pospieszczyk, U. Samm, B. Schweer, G. Sergienko, Formation of HD molecules in the boundary layer of TEXTOR. Phys. Sci. **T103**, 63–67 (2003)
12. R.J. Roberts, J.G. Dauntourna, J. Low Temp. Phys. **6**, 97–129 (1972)
13. T. Tanabe, Fusion Eng. Des. **87**, 722–727 (2012)
14. T. Tanabe, J. Nucl. Mater. **417**, 545–550 (2011)
15. T. Otsuka, T. Tanabe, Fusion Eng. Des. **85**, 1437–1441 (2010)
16. M. Oyaizdu, K. Isobe, T. Hayashi, T. Yamanishi, Effect of tritiated water on corrosion behavior of SUS304. Fusion Sci. Technol. **60**, 1515–1518 (2011)
17. C.H. Skinner, Tritium Retention and Removal in Tokamaks, in: *Proceedings of 2nd ITER International Summer School: Confinement*, ed. by S.-I. Itoh, S. Inagaki, M. Shindo, M. Yagi (American Institute of Physics, 2009), pp. 127–145
18. J. Miyazawa, S. Masuzaki, H. Yamad et al., J. Nucl. Mater. **313–316**, 534–538 (2003)
19. M.E. Sawan, M.A. Abdou, Plasma Fusion Eng. Des. **81**, 1131–1144 (2006)

# Chapter 3

## Fuel Flow and Balance in a D-T Fusion Reactor

Tetsuo Tanabe and Masabumi Nishikawa

**Abstract** Because of radioactivity of tritium (T), special cares for safety are required. In addition, limited resources of T require fuel self-sufficiency in a fusion reactor. Accordingly, accurate T accountancy, i.e., to know quantitatively how much T is in throughput, exhausted, and retained in all T handling systems in a reactor is required. At the same time, T retention in any systems should be minimized, or T retained in the systems should be recovered as much as possible. In this chapter, fuel flows and balances in all fuel processing/handling subsystems of a reactor are introduced referring deuterium (D) flow in present experimental tokamaks, which are using D as operating gas. Subsequently, current designs of the fueling and recycling systems of a fusion reactor are introduced and required conditions to keep T safety and fuel self-sufficiency are considered.

**Keywords** Tritium · Fuel flow · Inventory · Processing system · Safety · Self-sufficiency

### 3.1 Fuel Flow in a D-T Fusion Reactor

#### 3.1.1 Overall Fuel Flow at Steady State Burning

Figure 3.1 shows a schematic diagram of D and T fuel flow at steady state burning. Fuel throughput ( $\phi_D$ ,  $\phi_T$ ) (g/s) will be separately controlled to optimize burning efficiency. Only minor part of the throughput is going into plasma with fueling efficiencies of  $f_D$  and  $f_T$  and burns to produce helium (He) and neutrons (n) with burning efficiency of  $b$ . The D-T reaction produces 14 MeV neutron and 3.5 MeV He. The former is used for production of T and electric or thermal power, and the latter for heating to sustain burning plasma. Thermalized He must be evacuated to

---

T. Tanabe (✉) · M. Nishikawa  
Interdisciplinary Graduate School of Engineering and Sciences,  
Kyushu University, 6-1, Kasuga-Koen, Kasuga, Fukuoka 816-8580, Japan  
e-mail: tanabe@nucl.kyushu-u.ac.jp

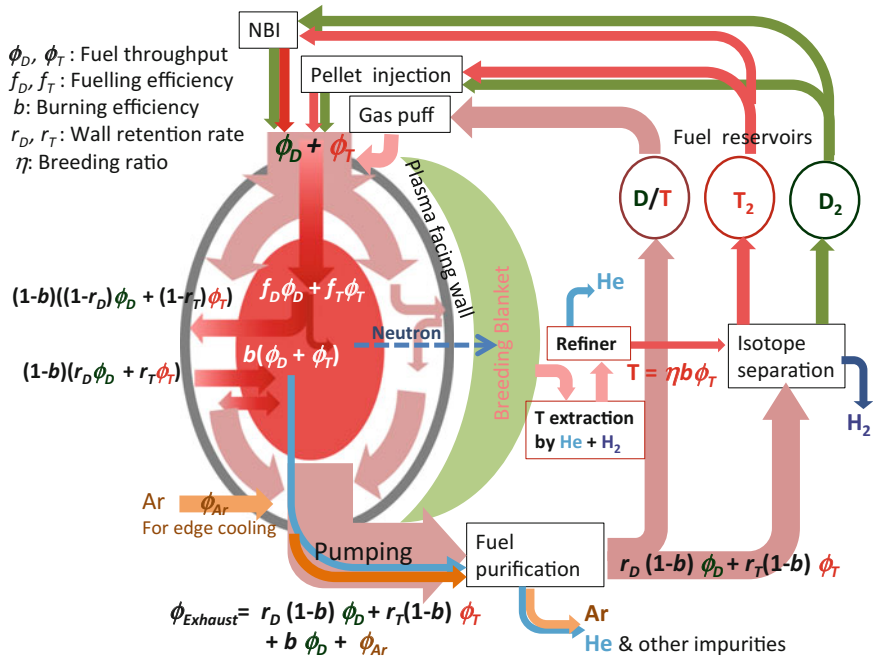


**Fig. 3.1** Schematic diagram of fuel flow in a fusion reactor at steady state burning. Fuel throughput ( $\phi_D$ ,  $\phi_T$ ) will be separately controlled to optimize the burning. Only minor part of throughput is going into plasma with fueling efficiencies of  $f_D$  and  $f_T$  for D and T, respectively, and burns with burning efficiency,  $b$ , producing He and neutrons. Some fuels are escaping from plasma and impinge into plasma-facing wall and retained there, and remainders are released as fuels again. Recycling coefficient ( $r$ ) defines the retention rate of fuels in the wall as  $(1 - r)$

avoid the dilution of the fuels in the burning plasma. For enhancement of radiative cooling of the burning plasma and also for disruption mitigation, impurity seeding such as Ne and Ar will be employed [1], which should be also exhausted. In addition, various chemical forms of hydrocarbons will be formed from carbon as a plasma-facing material, if it is used, and  $H_2$  and  $H_2O$  always remain as residual gas in a vacuum system. Thus, the most of D and T fueled are exhausted as a heavily contaminated gas with H,  $H_2O$ , various hydrocarbons, and inert gasses (He, Ne and Ar).

Some fuels are escaping from plasma and impinge into plasma-facing wall, and some are retained. The recycling coefficient ( $r$ ) defined as the flux ratio of incident and outgoing fuels at the surface of the plasma-facing wall gives the fuel retention rate as  $(1 - r)$ . In present tokamaks, the fueling efficiency is 10–30 % and the burning efficiency defined as the ratio of throughput to production rate of He or neutrons is likely to be several percent as discussed in Chap. 4. Neutrons are going to blanket systems to breed T with a breeding ratio,  $\eta$ , defined as the ratio of the number of produced neutron to that of bred T atoms. The breeding ratio, which is

strongly influenced by geometrical structure, breeding materials, neutron multipliers of the blanket system, does not likely exceed 1.2.

Since the exhausted gas includes various impurities, refinement of the exhausted gas, i.e., the removal of the impurities, is required for its reuse as fuels (fuel recycling). In order to reduce the load on an isotope separation system, refined D and T gas mixture would be refueled without D/T separation. Still separate fueling of D and T is necessary for burning control. D can be supplied from outside, while T recovered from the blanket followed by refining and isotope separation shall be used.

### 3.1.2 Quantification of Fuel Flow Rate

Figure 3.2 shows simplified fuel flow with normalized fuel throughput of 100 fuel particles ( $50(D) + 50(T)$ ) per unit time at steady state burning [2]. In the figure, the burning efficiency, the fuel retention rate in a vacuum vessel (VV), and the T breeding ratio are set to be 0.05, 0.02, and 1.2, respectively, as desirable values. For the total throughput of  $50/50(D/T)$ , only  $5/5$  fuels are burned to produce 5 neutrons

#### Fuel balance in a reactor

assuming burning efficiency of 10%,  
fuel retention rate of 2%, and breeding rate of 1.2

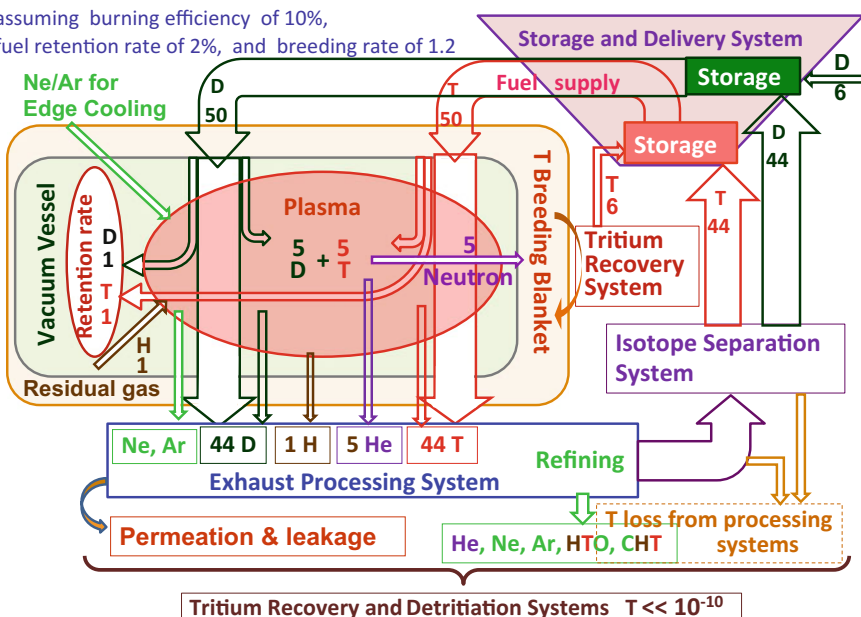


**Fig. 3.2** Specified fuel flow with throughput of 50 D and 50 T. Overall burning efficiency, fuel retention rate in vacuum vessel, and breeding ratio are assumed to be 10, 2, and 1.05 %, respectively. (See text)

with energy of 14 MeV, and 1/1(D/T) is retained in VV. Consequently, 44/44(D/T) are exhausted. In present plasma apparatuses, light hydrogen (H) is always remaining in their deuterium fuelling operation. Its origin is partly residual H<sub>2</sub>O in vacuum. Since any materials retain H as impurity in their bulk, their usage in vacuum gives always out-gassing of H<sub>2</sub> and H<sub>2</sub>O. Another source is back-feed from vacuum pumps. Whatever the sources are, contamination of D and T by H is unavoidable and additional effort to remove H in an isotope separation process is required as discussed in Chaps. 6 and 11.

Neutrons produced by the D-T reactions enter into blanket systems to deposit their energy to coolant for power generation and to breed T simultaneously. In the Fig. 3.2, under the assumption of the breeding rate of 1.2, 6 T atoms are bred from 5 neutrons. As a whole, 50 (=44 + 6) T could be recovered for the refueling of 50 T. D can be employed from outside. Therefore, in this simplified case, the fuel self-sufficiency is attained. In the figure, no losses in all fuel processing systems are assumed. However, this is unrealistic and a few % losses would be unavoidable in recovering of T in all T handling systems. Moreover, both the fuel retention rate of 2 % in the vacuum vessel and the breeding ratio of 1.2 seem optimistic or difficult to attain. Hence, to keep the fuel self-sufficiency is not easy, which is discussed in detail in this chapter.

Corresponding to Fig. 3.2, detailed values of fuel flows with the throughput of 50/50 (D/T) are given in Table 3.1 for all T processing systems (Exhaust Processing System (EPS), Tritium Recovery System from blanket (TRS), Isotope Separation System (ISS), and Storage and Delivery System (SDS)). In Fig. 3.3, schematic of ITRE Tritium plant is given for reference. Details of the T processing systems are described in Chap. 6.

In any T processing systems, losses by wall retention, leakage, and permeation are unavoidable. In the Table 3.1, the losses of 0.05, 0.1, and 0.1 % are assumed for EPS, TRS and ISS, respectively. Accordingly, in EPS, 43.8/43.8 (D/T) out of 44/44 will be transferred to SDS directly or via ISS. To reduce operational load on ISS, the refined fuel with 43.8/43.8 (D/T) could be directly refueled as mixed fuels. Since D/T (5/5) is burned, new fuels with the same amount are required. D can be supplied from outside (recovered from sea water as described in Chap. 2) with enough margin, while T bred and recovered in TRS (5.9 out of 6 T produced) and isotopically separated in ISS shall be used. In the table, the total T recycled would be 49.7–49.3. This does not satisfy the fuel self-sufficiency. Considering T loss by its decay (5 %/year) in SDS, improvement of the burning efficiency, reduction in wall retention rate in a reactor, and recovering efficiency in all other systems are indispensable.

In Fig. 3.2 and Table 3.1, the same fueling rates are assumed for T and D. As described in Chaps. 2 and 5, however, behaviors of D and T would be significantly different with each other not only in plasma, but also in materials, owing to their very large mass difference. In other words, confinement times, fuelling efficiencies, escaping fluxes from plasma, retention rates in materials, and evacuation rates from the vacuum vessel must be all different for D and T. A simple kinetic theory indicates that the square root of mass ratio of D/T could be correlated to those

**Table 3.1** Fuel flow in each subsystem at steady state burning for fuel throughput of 50 D and 50 T with burning efficiency of 5 %, fueling efficiency of 10 % and breeding ratio of 1.2

		D	T	H/H <sub>2</sub> O	He	Ne, Ar, and other impurities (For divertor cooling)	Remarks
Vacuum vessel (Tokamak system)		Throughput (Input)	50	50		2	For 3 GWth annual, 168 kgT/y will be burned. This requires throughput of 1680 kgT/y
		Wall retention	1	1* <sup>3</sup>			
		Output (Exhaust)	44	44	1/1	5	
Exhaust processing system (EPS)		Throughput (Input)	44	44	1/1	5	2 + 1
		Retention or loss	0.2	0.2			99.5 % recovery
		Output	43.8	43.8	1(H)		
Tritium recovery system from blanket (TRS)		T production rate		6			T Breeding ratio 1.2
		Processing gas			700* <sup>1</sup>		* <sup>1</sup> Either H or H <sub>2</sub> O is required to recover T from blanket
		Retention or loss		0.06			99 % recovery
		Output		5.9* <sup>2</sup>			* <sup>2</sup> For refueling
Isotope separation system (ISS)		Input	43.8	43.8	1		
		Retention or loss	0.04	0.04			99 % recovery
		Output	43.4				Isotopically separated (not necessary to be 100 % pure)
Storage and delivery system (SDS)		Input	43.4	43.4 + 5.9* <sup>2</sup>			D and T are separately stored
		External supply	>6.6	* <sup>3</sup>			* <sup>3</sup> Requires reduction in Wall retention from 1 to 0.3
		Reserve* <sup>4</sup> (stored in forms of metal hydride)	150	150			* <sup>4</sup> Reserves = 3 times of throughput
		Output (fueling)	50	50			

### ITER Tritium Plant

The tritium plant is composed of a fuel processing and tritium removal systems.

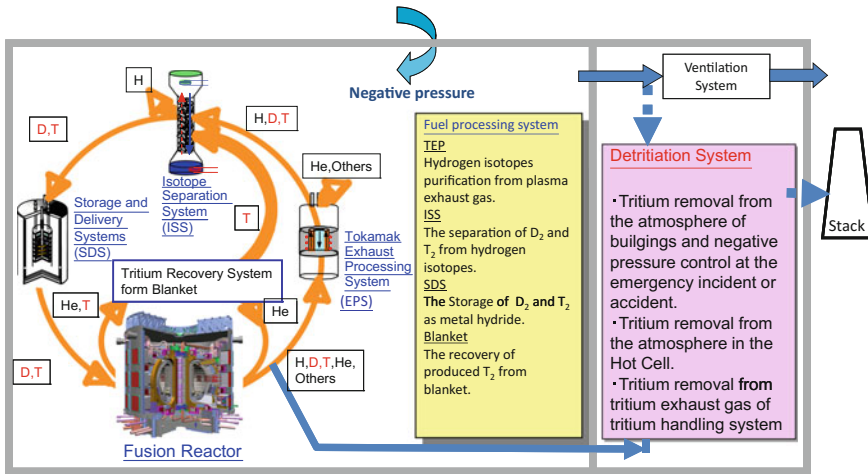


**Fig. 3.3** Schematics of ITER T plant consisting or a reactor, a tokamak exhaust processing system (TEP), a T recovery system from blanket (TRS), an isotope separation system (ISS), and storage and delivery systems (SDS). All subsystems are located in buildings or glove boxes kept at negative pressure and equipped with ventilation systems supported by detritiation systems

properties as described in Chap. 2, but more or less no data are available for D and T until now.

Furthermore, the different confinement times of D and T in burning plasma would result in their inhomogeneous radial distribution. Therefore, it must not be easy to keep appropriate D/T ratio in the burning plasma to get the highest burning efficiency. The concentrations of D and T in the burning plasma must be separately measured to make feedback fueling of D and T independently. It is, however, quite difficult to measure the concentrations of D and T in plasma separately and a new task for ITER as discussed in Chap. 8.

The retention rates of D and T in the plasma-facing wall are not necessarily the same, so as their release rates from the wall are. Behavior of fuels in the plasma-facing wall is separately described in Chap. 5. Thus, we are going to face difficulty of controlling D/T ratio in the burning plasma to attain and keep efficient burning. However, until now no systematic efforts have been done to control two isotopes, even for H/D in plasma. All these problems remain to be solved in ITER.

In the following, detailed fuel flows in a fusion reactor focusing to T are described with special cares on its radioactivity. Particularly, requirements of precise T accountancy in all T handling systems and the fuel self-sufficiency in a fusion reactor are taken into consideration. Although handling of D/T mixture might give additional difficulty in the fuel flow control, it is not considered here.

## 3.2 Tritium Processing Systems for a Fusion Reactor

### 3.2.1 Specialty in T Processing or Handling Systems Owing to Its Radioactivity

Processing or handling techniques of large amount of hydrogen in chemical plants are well established. Hence, no special techniques are required for T processing/handling in general [3–5]. However, because of its radioactivity, T handling is strictly regulated by law. T inventory or residue in any T systems must be accounted, unless it is below regulation levels, for example, several tens Bq/cm<sup>3</sup> of T in gas phase and a few hundredth Bq/cm<sup>3</sup> of T in water. (1 Bq of T is equivalent to  $2.8 \times 10^{-15}$  g). The detail of the regulation is described in Chap. 14. T, as a hydrogen isotope, easily dissolves in any materials, diffuses into deep, and permeates through them [6]. Furthermore, T can be easily replaced isotopically with H in ubiquitous water and inorganic/organic H compounds adsorbed on materials surfaces, resulting in surface contamination as discussed in Chap. 2. Therefore, the contaminations of materials surface and atmosphere by T are serious concerns.

The amount of T handled in a fusion reactor is in kg order, about three orders of magnitude less than that of H in industrial use of tons order. Nevertheless, its radioactivity requires special cares for safety, such as precise T accountancy in all tritium handling sub-systems, T leakage, and permeation from the subsystems. Furthermore, owing to poor T resources, establishment of the fuel self-sufficiency in a D-T fusion reactor is essential. Therefore, T must be bred in a blanket system with enough margins and bred T must be recovered from the blanket as much as possible. T retention or residual T in any T handing subsystems must be minimized or throughput T into any subsystems must be fully recovered, 99 % or above.

As already noted, any small amount of T remaining in a system must be accounted. Generally, T throughput in a T handling system is much less than the volume of the system. Consequently, T is piling up in the system until the concentrations of T in the throughput and in the system becomes the same as shown in Fig. 3.4a. The amount of T indicated as  $W_a (=W_b)$  in the figure is referred as system inventory, which is recoverable afterward as seen in the figure. This kind of system inventory is important in a T processing system having large volume such as an isotope separation system.

The system inventory is not limited to the volume, but surface of the system wall and inside of the wall materials often retain much larger amount of T owing to its high chemical reactivity and easy isotopic replacement with ubiquitous hydrogen (H) on materials surface and dissolved in bulk. Any materials retain H as an impurity with its concentration of a few tens of ppm or above. Moreover, any materials surfaces hold water molecules as adsorbates. Such pre-existing hydrogen and absorption/adsorption of T in materials surpass the system inventory described above and delay the establishment of the steady state as shown in Fig. 3.4b. In other words, T piles up in the chamber and the total piled-up amount in the system is far larger than the throughput, resulting significantly large T inventory in the

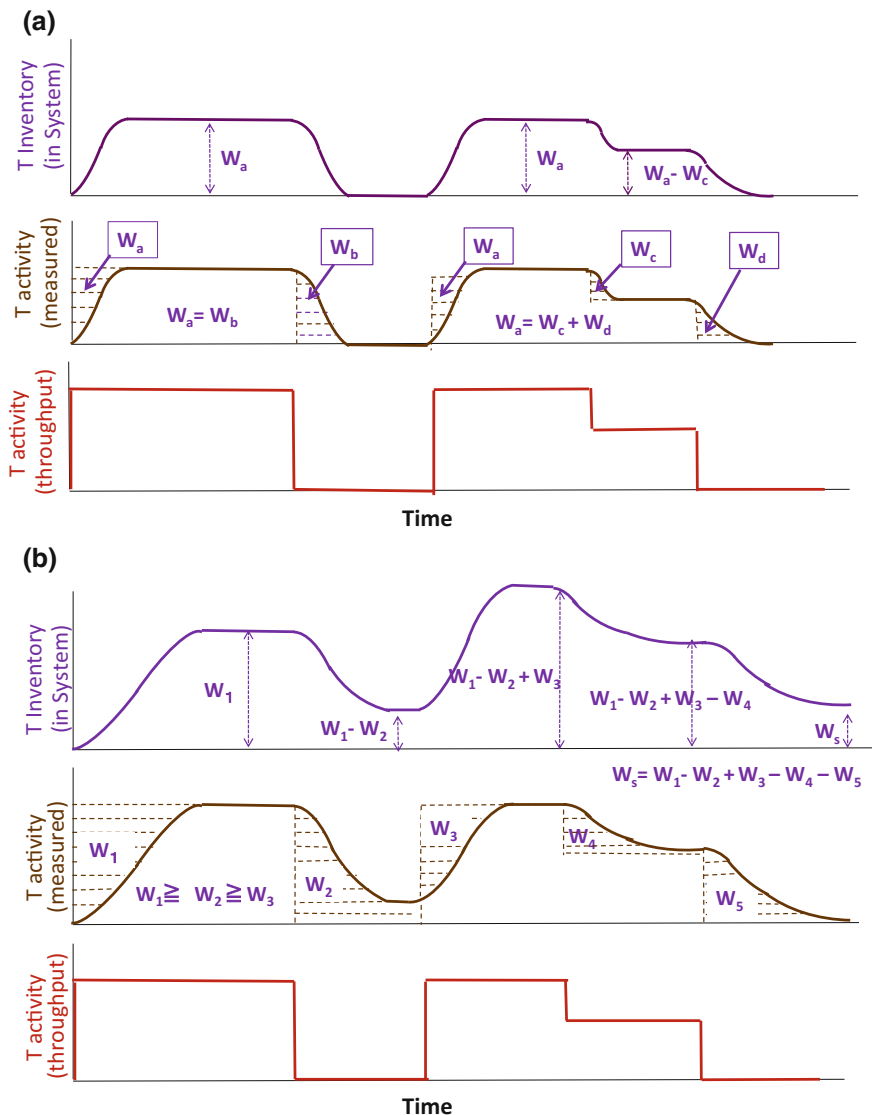


**Fig. 3.4** Time sequences of T concentration in output and inventory of a system corresponding to change of T concentration in throughput given at the bottom, with (a) and without (b) adsorption/absorption of the system wall

plasma-facing wall and other tritium processing systems. Furthermore, such inventory is usually hard to recover.

Changing the system inventory with time gives a problem in measurements of T in gas phase by an ionization chamber as well-known as the memory effect. The T

activity detected by the ionization chamber is initially much less than the actual T activity in the throughput gas as shown in Fig. 3.4b, or a little longer time is required to get a real or correct T activity in the throughput. When the T activity in the throughput gas changes, the variation of the measured T activity is not straightforward to the changes or does not follow the changes as described in the figure. When the input T activity is reduced to zero, the measured activity does not drop to zero immediately but continues to decrease long. Contrarily, once gas with high activity of T is introduced into the chamber, measurements of low activity gas are prohibited long by release of remaining T in the chamber.

This memory effect caused by T holding in any T handling systems becomes less appreciable for higher T activity in the throughput or larger throughput, and for smaller volume of the system. More details on the memory effects on T measurements are given in Chap. 7. Again, it should be noted that little care is paid on the system inventory in hydrogen industries, because it is negligibly small compared to its huge throughput.

The T inventory in a system should be accounted for safety regulation. However, as discussed in Chap. 2, quantitative analysis of T in the bulk is hardly possible, so as the T inventory in T handling systems. By integrating the difference of the T concentration in the throughput and the exhaust, the T inventory of a system can be estimated. However, the accuracy of the T measurement in gas or liquid is limited within 3 or 4 digits. This means that the loss of 1 g T from a T handling system can hardly be detected when 1 kg of T is handled in it.

It should be noted that any residual H<sub>2</sub> gas in H handling systems must be cared to avoid “hydrogen explosion.” Since the hydrogen explosion can occur for hydrogen gas in air with wide concentration ranges of 4.1–74.2 %, the concentration of H<sub>2</sub> gas in any atmosphere in the H handling systems must be monitored according to regulation law. In this respect, the fusion reactor cannot be exceptional. In a fusion fuel system, D and T are generally handled as a pure gas and leakage from the system is concerned for both T safety and hydrogen explosion. In addition, incursion of air into the system is also a concern.

In a fusion reactor, T inventory in the vacuum vessel becomes much larger than the throughput, not only because the vessel is quite large, but also because energetic T escaping from the plasma impinges directly into the plasma-facing materials and could pile up in their bulk.

Thus, the T inventory in a reactor, in general, is composed of three components as given in Fig. 3.4b. (i) “initial inventory” given by  $(W_1 - W_2)$  that piles up at the beginning and immobilized (ii) “dynamic inventory” corresponding to  $W_2$  that is the inventory during discharge at a steady state and (iii) “static inventory” corresponding to  $W_5$ , which remains after discharge. The difference between the initial inventory and the static inventory is due to the different retention (residence) time of T in the system. The retention time changes with temperature. In case of high temperature metallic wall, in which hydrogen diffuses easily, the difference could be small.

In most of preset tokamaks, which are operated with D, and its PFM covered by carbon at RT or a little above, the initial inventory is quite large compared to the

dynamic inventory which can be determined from the release of D after the discharge [7, 8]. The static inventory increases with discharge duration and part of them is immobilized and integrated amount of the static inventory for long time would be quite large. In particular, as described below, the isotopic exchange with impurity H in the plasma-facing materials would have significant contribution in the initial and static inventories. For example, if some of the impurity H with  $\sim 10$  ppm in  $10^3$  tons of fusion reactor materials were replaced by T, the system retention could be easily over few kg of T [6], significantly larger than the allowable T inventory in ITER, only 1 kg, for the regulation in France [9]. The detailed mechanism of the fuel retention is given in Chap. 5.

### **3.2.2 Tritium (Fuel Processing) System in ITER and a Reactor**

ITER requires total of 15–18 kg T, which can be supplied by Canada. Since the natural abundance of T is too small to recover, T must be artificially produced, usually with using an accelerator or in a heavy-water-cooled nuclear reactor. One CANDU (CANada Deuterium Uranium) reactor [10] is producing only 100–200 gT/y. Hence, T is very expensive, \$31,000/g or more. While cost for depository of T, at present, is more expensive, probably 100 times higher than the price of T, though this is not considered yet. In D–T burning phase of ITER, the maximum throughput for one discharge is limited to be  $200 \text{ Pa m}^3/400 \text{ s}$  ( $\sim 2.5 \text{ g}$ ) and that in-vessel T inventory, 1 kg, or allowable safety limit, 700 g. Since the current estimation of the fuel retention rate in the vacuum vessel (VV) is nearly 20 % [7, 8], allowable discharge numbers before the in-vessel T inventory exceeds the allowable safety limit of 700 g is only 1400 (=700/0.5). This means that T removal from VV is required for every 1400 discharges. Although various methods have been proposed to remove the in-vessel T, the most appropriate method is not developed yet [11].

The T fuel processing system of ITER, which use mostly established techniques, can be built or even for a reactor without very high hurdles and, hence, is not likely on a critical schedule path toward the first D–T plasma in ITER [3–5, 12]. The fuel processing system of ITER is composed of several subsystems as shown in Fig. 3.3. The system for a reactor will not be much different from those for ITER except Blanket System (BS), which will not be installed in early phase of ITER operation. As already noted in Table 3.1, the system is consisted of Reactor System (VV), EPS, TRS, and SDS. In ITER, electric power generation is not targeted, and BS will be installed only for testing T breeding and recovery. For a fusion reactor, BS includes capabilities of both T breeding and heat exchange for the power generation.

The reactor and other T processing subsystems are set in rooms or hot cells negatively pressurized and equipped with a ventilation system for detritiation of coolant water, atmospheric gases and other gases used for ventilation. The detritiation is quite important and discussed in Chaps. 10 and 14. ITER has claimed that T confinement is achieved through multipassive barriers and use of active systems [4, 13]. However, as shown in Fig. 2.8 in Chap. 2, multistage cross-contaminations could easily result in spreading of contamination. Hence, multistage handlings in huge-sized glove boxes would be required for maintenance of a reactor and its large components such as divertor cassettes.

Public safety does not seem to become significant problem because the emission to outside of the reactor site can be easily kept below the safety limit. Unfortunately, however, quantitative estimations of inventory in each subsystem, amount of permeation and leakage, and accompanying contamination are quite hard. [See Part III (Chaps. 14 and 15)].

In the following, each subsystem is shortly described. Details of each system are given in Part II (Chaps. 6–13). For fueling, there are four candidate systems, gas puff (GP), pellet injection (PI), neutral beam injection (NBI) and compact toroidal injection (CTI) systems [14]. In the pellet injection system, ice pellets of fuels with a volume of around 1 cc will be produced. Not all delivered fuel into PI is solidified and the remainder will be exhausted and recovered. In NBI, ~100 keV neutral beam is produced to inject into plasma. The main purpose of NBI in a reactor is to heat plasmas but fuel throughput by NBI would not be large. To recover the remainder in NBI, large evacuation capability (pumping speed) is required and accordingly fuels in plasma chamber can be evacuated through large port of NBI. Therefore, NBI seems better not to use in a reactor for T safety and fuel self-sufficiency, though NBI is the main heating system in ITER. Fueling methods in a reactor are still under discussion.

Exhausted or pumped-out fuels are refined in TEP to remove He ash, impurities like residual H<sub>2</sub>, H<sub>2</sub>O and some hydrocarbons and inert gases, like N<sub>2</sub>, Ne, and Ar seeded to enhance radiation cooling. D and T are isotopically separated, if fueling of pure D and T are required. Although, it is not clear how to control D/T ratio in burning plasma yet, mixed fueling with D and T together will be preferable, to reduce both operation cost of ISS and its T inventory.

In the physics phase of ITER operation, BS will not be installed, while in the engineering phase various different concept of BS will be tested mainly for T breeding. The details of BS for a reactor will be presented in Chaps. 6 and 13.

To keep the fuel self-sufficiency, T inventory in all T processing systems should be minimized. In addition, full recovery of bred T in BS is critically important. To do this, adding H<sub>2</sub> (D<sub>2</sub>), or H<sub>2</sub>O (D<sub>2</sub>O) in a carrier gas is quite effective and T is recovered as diluted hydrogen gas (HT or DT) or water (HTO or DTO). In case of oxide breeders, T is recovered mostly as the water. Hence, T recovering from BS should be separately done from refining and isotope separation systems in main fuel recycling system.

### 3.3 Tritium Flow and T Inventory in Subsystems

In a T processing (handling) system, its throughput ( $\phi_{\text{System}}^{\text{in}}$ ), exhaust ( $\phi_{\text{System}}^{\text{out}}$ ), leakage ( $\phi_{\text{System}}^{\text{leak}}$ ) and inventory ( $R_{\text{System}}$ ) at a time  $t$  is balanced as

$$R_{\text{System}} = \int_0^t (\phi_{\text{System}}^{\text{in}} - \phi_{\text{System}}^{\text{out}} - \phi_{\text{System}}^{\text{leak}}) dt, \quad (3.1)$$

After a certain time, the system becomes steady state, and consequently  $R_{\text{System}}$  becomes constant or saturated to show no more change. Then,

$$\phi_{\text{System}}^{\text{in}} = \phi_{\text{System}}^{\text{out}} + \phi_{\text{System}}^{\text{leak}} \quad (3.2)$$

Define a characteristic or residence time, “ $\tau$ ”, of the system as time required for  $R_{\text{System}}$  becomes as  $1/e \times R_{\text{System}}^{\text{Steady}}$  (the inventory at the steady state) as,

$$1/e = \int_0^\tau (\phi_{\text{System}}^{\text{in}} - \phi_{\text{System}}^{\text{out}} - \phi_{\text{System}}^{\text{leak}}) dt / \int_0^\infty (\phi_{\text{System}}^{\text{in}} - \phi_{\text{System}}^{\text{out}} - \phi_{\text{System}}^{\text{leak}}) dt \quad (3.3)$$

Then the T inventory in the system can be approximated to be its throughput multiplied by  $\tau$ ,

$$R_{\text{System}}^{\text{Steady}} \approx \tau \times \phi_{\text{System}}^{\text{in}} \quad (3.4)$$

In ordinary H plants, as discussed in the previous section, H throughput is quite large, or its residence time is quite small. Accordingly the H inventory or residue in the H plants ( $R_{\text{System}}^{\text{Steady}}$ ) does not matter or can be neglected. However, in a T handling system, all four terms do matter owing to radioactivity of T and its inventories in any subsystems shall be always accounted.

As shown in Fig. 3.4a or b, T inventory in a fusion reactor is roughly divided into two categories, mobile (dynamic or recoverable) and immobile (static or hardly recoverable) ones, though the difference between the two is only due to their different length of the residence times. T retention in VV is mostly caused by the wall retention and immobile, while that in BS and ISS is mostly volumetric and categorized to mobile one.

Table 3.2 gives expected residence times ( $\tau$ ) and T inventories for each subsystem in a fusion reactor at steady operation with the power of 3 GWth under the assumption of fueling efficiency, burning efficiency and T breeding rate in BS being 20, 5, and 120 %, respectively. A specialty in T handling systems of a fusion reactor lies in quite large differences of the residence times and T inventories among the

**Table 3.2** Estimation of T inventory in each subsystem for fusion power of 3 GW with burning efficiency of 5 % (burning of  $\sim 5.3$  mg (T)/s), fueling efficiency of 10 % and breeding ratio of 1.2

Subsystem		T throughput mg(T)/s	Residence time/s	T inventory g (T)	Remarks
Vacuum Vessel (VV)	Burning plasma	25	$\sim 2$	$\sim 1$	Confinement time
	Divertor	80	$\sim 10$	$\sim 15$	Pumping speed
	Wall retention	1	$\sim 10^{3*}$	?	*1 discharge time
Tritium recovery system from blanket (TRS)	Flow system	6.4	$\sim 10^3$	$\sim 60$	Breeding ratio = 1.2
	Batch system		$10^3\text{--}10^7$	$\sim 6000$	
EPS (Exhaust processing system)	Cryo-pump	99	$10^3\text{--}10^5$		Depends on operation of Cryosorption pump
	Refinery	99	$\sim 3$	$\sim 4.5$	Purification by Pd membrane
Fueling	Gas puff	70	$\sim 10$	$\sim 10$	Compression
	Pellet	35	$\sim 10^4$	$\sim 5000$	Pellet production
Isotope Separation System (ISS)		10	$\sim 10^4$	$\sim 1000$	D/T separation time
Reserve		5.3	$2.6 \times 10^6$	$13.7 \times 10^3$	30 days

subsystems. Nevertheless, the T inventories in all subsystems shall be accounted. The details on numbers in Table 3.2 are discussed in the following sub-sections.

### 3.3.1 Tritium Throughput at Steady State

To get the fusion output power of 3 GWth or 1 GWe, around 35 kg of T is burned annually equivalent to 5.3 mg/s or  $3.6 \times 10^{14}$  Bq/s. Because of low burning efficiency, only a few % of fueled T will be burned. This requires T throughput of 106 ( $=25 + 80 + 1$ ) mgT/s ( $7.2 \times 10^{16}$  Bq/s) under accountancy (or under regulation) of a few tens Bq. The majority of the throughput is recovered (pumped out from VV) by EPS. Since, as already noted, the fueling efficiency is very poor, only 25 mgT/s is going in the plasma (assuming the fueling efficiency to be 20 % in Table 3.2), the majority of the fuel (80 mg/s) does not enter the burning plasma and directly exhausted. The wall retention, 1 mgT/s (assumed to be 1 % of the throughput in Table 3.2), is quite uncertain. Consequently, 99 ( $=106 - 5.3 - 1$ ) mg/s is pumped

out as the exhausted fuels. Since the exhausted fuels include H, D, T, He and other impurities, it should be refined, isotopically separated and then recycled.

Even if the most of the wall retention could be recovered after the discharge, some should remain and pile up for long time to become huge in-vessel T inventory. For the fuel self-sufficiency, the wall retention should be minimized or recovered as discussed later.

The reactor is surrounded by blanket systems (BS) to convert energy carried by neutrons to heat for electric power generation and to breed T simultaneously. Different from a fission reactor, in which most of the released energy by nuclear reactions is deposited in fuel pins with a diameter of only around 10 mm, quite large volume is required to convert energy of neutrons (14 MeV) to heat, as noted in Chap. 1.

Since, T resources are very limited, T breeding in BS should have enough margins to compensate T losses by burning, decay, non-recoverable wall retention, permeation and leakage. In addition, T in all subsystems permeates through their walls into coolant or surrounding atmosphere. In particular, ferrite, a low activation structure candidate material, has very high T permeability and needs permeation barriers with the permeation reduction in 5–6 orders of magnitude as discussed in Chap. 9. Permeated T readily reacts with surface adsorbents to produce hazardous tritiated water and/or hydrocarbons according to the reactions as described in Chap. 2. In a water cooling system, permeated T from the plasma-facing surface or blanket to the coolant water is easily converted to HTO, resulting huge volume of diluted tritiated water from which T recovery is very cost consuming.

Although lithium (Li) can work as a coolant and tritium breeder simultaneously [15], the extraction of T from Li is very difficult. Hence a Lithium Lead (LiPb) eutectic alloy for which T recovery is rather easy, could be promising coolant [16]. Simultaneous implementation of electric power generation, T breeding and T safety still need significant R&D efforts and the three must be optimized.

### **3.3.2 Tritium Inventory in Each Sub-system**

For T safety, accurate accountancy of T inventory in each subsystem is “must.” For T fuel self-sufficiency, as discussed above, reduction in T inventories in a reactor and enhancement of T recovery from blanket are critical. The largest uncontrolled T inventory will appear in the VV (except for SDS, of which T inventory can be controlled). T inventories of other subsystems are not as large as that of VV, and their characteristic times are much shorter, too. Nevertheless, integrated losses in all subsystems could be large, even if their loss rates would be as low as below 1 %, which does not seem easy, and large effort is required. Although the T inventory in BS is not large, full recovery of bred T is critical to attain the fuel self-sufficiency.

### 3.3.2.1 Vacuum Vessel of a Reactor

T in burning plasma is either in excited or ionized state, and T in scrape-off plasma surrounding the burning plasma mainly consists of molecules with some ionized and excited ones having much higher temperature than surface temperatures of plasma-facing wall. Accordingly, interactions of T in the scrape-off plasma and the wall surface are not that of thermalized T (gaseous T) and the wall.

In a fusion reactor, as discussed several times, only small amount of fuel throughput is going into plasma and burned. The fuelling efficiencies for gas puff, NBI, and pellet injection are not the same, but for simplicity, the efficiencies are unified into one value of around 20 % or  $\sim 25$  mg/s in Table 3.2. Therefore, large part of the fuel throughput (80 mg/s) is pumped out through scrape-off layers and divertor.

Fuels escaping from the plasma impinge to PFM surfaces, and some are retained. Introducing a recycling coefficient,  $r$ , the fuel retention rate is given by  $1 - r$ . In Table 3.2,  $r$  is assumed to be 0.99. As described in Chap. 5, the fuel retention in the plasma-facing wall is mostly owing to fuels incorporated in redeposited wall materials once eroded somewhere at plasma-facing surfaces. Since the redeposition at plasma shadowed area (they are not re-eroded) linearly increases with discharge time, so as the fuel retention increases. In the present large tokamaks, the fuel retention rate is reported to be 5–20 % of the throughput. This is not acceptable from the aspect of the fuel self-sufficiency in a reactor. However, it is well-known that lower recycling is better to attain good plasma performance. Long pulse operations in a reactor would not allow the low recycling or large wall pumping, because wall retention must be saturated anyhow. Therefore, establishment of good plasma performance under low retention regime is one of the most important research issues of ITER. The fuel retention rate in VV is most uncertain part of T inventory and will be discussed separately in Chap. 5.

### 3.3.2.2 Tokamak Exhaust and Blanket Systems

Fuels going to be burned are far less, i.e., burning efficiency defined as  $b$  in Fig. 3.1 is likely to be of few %, which is determined either cross-section of D-T reactions or allowable He level in the burning plasma. The detail of fuel burning is given in Chap. 4. In Table 3.2,  $b$  is assumed to be 5 %. According to the Fig. 3.1, burning flux or neutron production rate is given by  $b\phi$ . Multiplying a breeding rate of  $\eta$ , T production rate becomes  $\eta b\phi$ . In Table 3.1,  $\eta$  is assumed to be 1.2, and consequently, 6.3 mg/s of T is produced in BS.

Except the wall retention and burning, fuel throughput (99 mg/s) is exhausted to the main pumping system and refined to be pure fuel gases. The refining system is also used for T recovered from BS, which adds some inventory in Table 3.1.

T inventory in BS changes with recovering methods. In case of in situ recovering by flowing through of cover gas, the inventory is quite small, but this requires handling of huge amount of the cover gas and enrichment of diluted T in it. In case of recovery by a batch system, T recovery is much easier than the flow system, and the inventory varies significantly depending on the timing of recovery.

### 3.3.2.3 Other Systems (Fueling, Isotope Separation, Delivering, and Reserve)

As already mentioned, methods of fuelling include NBI, Pellet, and Gas puff, and every method has its own residence time. Because of the longest time to produce ice pellets, the T inventory of the pellet injection system must be the largest. The residence time of the isotope separation system would be a few hours. Since the system requires large electricity, the amount of D and T to be separated should be as small as possible. In this respect, fuelling of mixed gas of D and T is highly recommended. However, to control D/T ratio in the burning plasma to give the best performance, some amount of D and T must be separately fuelled which forces to make isotope separation anyhow.

### 3.3.2.4 The Total T Inventory

Summing up T inventories in all subsystems in Table 3.2, the total T inventory in a reactor at the steady state operation would be  $\sim 20$  kg. This does not include the initial inventory required to establish the steady state burning from the start-up of the reactor, which is quite uncertain.

In some reactor designs proposed, a few detailed estimations of T inventory have been reported in [2] as shown in Table 3.3 for DEMO (J05) at JAERI by Nakamura et al. [17, 18], a magnetic confinement (MCF) reactor and an inertial confinement (ICF) reactor by the author. Though the table is still quite unsatisfied, two estimations for DEMO (J05) and the MCF reactor are quite different except for the reservoir in which the largest inventory appears. The inventories in Table 3.3 are for burned fuels of 30 days. It is significant to note that the total T inventory estimated in Table 3.2 under crude assumptions agrees well with the estimations in Table 3.3 (around 20 kg). Even the value is similar to the initial T preparation for ITER (15–18 kg T). Considering small resources of T, artificial or intentional T production in fission reactors will be required; even if the fuel self-sufficiency can be established in each reactor. It should be noted again that these estimations do not include the initial inventory in which the in-vessel inventory dominates as discussed in Chap. 5.

**Table 3.3** Tritium inventory estimated for DEMO(j05) of JAERI [24,25], a MCF reactor and an ICF reactor [2]

	DEMO(j05) after 5 years operation (Nakamura) [24,25]	MCF reactor at steady state (Nishikawa) [6]		ICF (D-TKYO-Fast) at steady state (Nishikawa) [6]	
Output (electricity)	3 GWth(1 GWe)	3 GWth (1 GWe)		3.6 GWth (1.2 GWe)	
T burning (kg/day)	0.4	0.4		0.48	
Burning efficiency		3 %		30 %(max)	
Reserve (storage) in main fuel cycle (for 30 days)		12 kg		14.4 kg	
Retention in breeder	1.2 g (LiO <sub>2</sub> )	$x_0 = 0.4 \times (\text{TBR}-1) \times \text{days of operation}$		$y_0 = 0.48 \times (\text{TBR} - 1) \times \text{days of operation}$	
Storage in waste		w		z	
Retention in		Mobile (active)	Immobile (static)	Mobile (active)	Immobile (static)
Main fuel cycle	2–46 g (Divertor) 0.2–75 g (First wall)	2.5–5.5 kg	x <sub>1</sub>	1.2–2.6 kg	y <sub>1</sub>
Blanket system	0.8–400 g	0.01–0.4 kg	x <sub>2</sub>	b <sub>1</sub>	y <sub>2</sub>
Power generation system (coolant)		a	x <sub>3</sub>	b <sub>2</sub>	y <sub>3</sub>
		(2.6–5.8) kg + a	$\Sigma x_i$	(1.2–2.6) kg + $\Sigma b_i$	$\Sigma y_i$
Total <sup>a</sup>		$\sim 15 \text{ kg} + \sum x_i + w$		$\sim 16 \text{ kg} + \sum y_i + z$	

<sup>a</sup>Total is the summation of storage in waste, mobile inventory, and immobile inventory

### 3.4 Tritium Balance for Fuel Self-sufficiency

As noted in the previous chapter, there is no practical external source of T for fusion energy development beyond ITER. All subsequent DT experimental devices and power plants have to breed their own T. Therefore, attaining T self-sufficiency is necessary for self-sustaining fusion plants operating on the DT fuel cycle and has been extensively studied focusing on breeding [19–21]. Different from previous works, this section considered the fuel self-sufficiency from the viewpoint of losses from all T processing systems.

### ***3.4.1 T Inventory and Loss***

Previous sessions focus on the balance of fuel flow at the steady state burning employing residence times in all subsystems. For consideration of fuel self-sufficiency, time integration of fuel retentions and any losses in all subsystems are required. Among all, the wall retention seems the largest, if the fuel retention rate keeps constant with a value of more than 0.1 as expected in ITER, and recovering of T from VV is mandatory for the fuel self-sufficiency. Since the recovery from VV cannot be done continuously, the in-vessel T inventory significantly varies with the frequency and the efficiency of the recovering. Other inventories in all subsystems also change with their operational scenarios. Those systems having shorter residence time or easier T recovery do not have significant influence on the fuels self-sufficiency. However, owing to T decays around 5 %/year, longer residence time or longer time storage results in loss of T, which, in turn, depresses the fuel self-sufficiency.

In this respect, T recovery scenario from BS and operational scenario of refining and isotope separation systems are quite important. T inventory in BS changes with breeding materials and removal mechanisms. In addition, T extractions by continuous processing and batch processing result in completely different T inventory. The continuous operation keeps the T inventory low and constant, while the T recovery is hard because recovered T is diluted in large amount of cover (carrier) gas. T recovery by the batch operation is easier, but frequency or operation period of one batch changes the amount of recovered T and the T inventory as well. For easier recovery, longer accumulation of bred T in BS is better. On the other hand, T loss by its decay is no more negligible. Therefore, one should optimize the batch operation for its operation frequency. T inventory in the isotope separation system also changes with separation methods/mechanisms.

T inventories in any subsystems are generally recoverable but the recovering process always accompanies some losses. Usually the recovering efficiency of more than 99.5 % seems quite hard to attain. The residue of 0.5 % does matter, because all of the fuel throughput should be processed. According to the required fueling, 102 mgT/s, for a reactor with 3 Gwth as given in Table 3.2, the fuel retention rate of 0.5 % results in the accumulation of 0.51 mgT/s, this means that after 11.5 days of full continuous operation, the in-vessel T inventory would exceed T regulation limit of 1 kg for ITER. This suggests that the fuel retention rate should be less than  $3 \times 10^{-4}$  to keep the in-vessel T inventory below 1 kg for 1 year continuous operation, which is referred again in the following section.

In any T processing systems, losses by permeation and leakage of T are unavoidable and quite hard to recover as the fuel. The losses in the T processing systems are finally going into water, resulting in T-contaminated water. Depending on the T activity of the contaminated water, they are either diluted to be released into the environment or stored as is or after condensation by evaporation. In a fusion reactor, permeated T from VV to cooling channel might not small enough to

ignore for the fuel self-sufficiency and for T safety, and then permeation barriers would be required as discussed in Chap. 9.

### 3.4.2 Establishment of Fuel Self-sufficiency

This section describes how T losses influence the fuel self-sufficiency and gives suggestions to improve the fuel self-sufficiency. To establish the fuel self-sufficiency, it is essential that the amount of T bred in BS exceeds the amount of T consumption by burning and T loss by decay. In addition, T recovery from VV and loss by permeation and leakage should be also taken into account.

The T consumption/losses in a fusion reactor consist mainly of the following:

- (1) Consumption by D-T burning,
- (2) Loss as T retention in VV,
- (3) Loss by  $\beta$  decay of T within the residence time in T handling systems,
- (4) Loss due to permeation and leakage through first wall materials or piping materials, and
- (5) Preservation for the initial inventory of subsequent fusion reactors to be constructed.

The last one is due to the shortage of T resources in nature. As discussed in Fig. 3.2, the initial inventory, i.e., from the start-up to steady state phase is likely quite large. This indicates that significant amount of T shall be preserved at the start-up phase in addition to the reserve for the steady state operation given in Table 3.2, even it could be recovered afterward.

To discuss the fuel self-sufficiency, various parameters/values shall be quantified, which are burning efficiencies, breeding ratios, recovering efficiencies in all subsystems. In Table 3.1, the recovering efficiencies are assumed to be 99–99.5 % and no recovery of the wall retention. Accordingly, T breeding ratio of 1.2 is required in simple calculation. For full recovery, the ratio could be reduced to 1.1.

Furthermore, blanket covering ratio, i.e., how much surface area of VV is covered by blanket systems, or ratio of neutrons going and not going into BS, which totally depends on the reactor design. Until now, however, all these values are quite uncertain. Therefore, we introduce a parameter,  $\eta_{\text{required}}$ , representing the tritium breeding ratio required to establish the D-T reactor with the fuel self-sufficiency, which is defined by the total amount of T consumption rate divided by the T burning rate.

BS is the only place to produce T, and the T breeding ratio attainable in BS,  $\eta_{\text{attainable}}$ , is obtained from multiplication of the efficiency in neutron usage in T generation reaction and the efficiency in the recovering process of bred T. The details of the neutron efficiency in T breeding and the efficiency in recovery of bred T are discussed in Chaps. 4 and 12, respectively. If we could make  $\eta_{\text{attainable}}$  be larger than  $\eta_{\text{required}}$ , the fuel self-efficiency is attained. However, the both

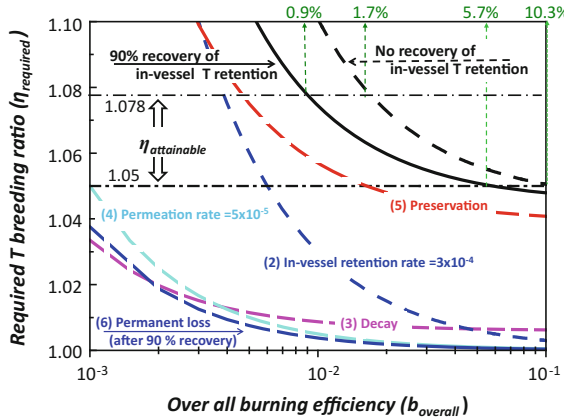


**Fig. 3.5** Dependence of required breeding rate ( $\eta_{\text{required}}$ ) on overall burning efficiency. Dashed lines of (2)–(5) are breakdowns into respective losses written as the texts and (6), the permanent loss in VV after 90 % recovery. If the attainable breeding ration increased from 1.05 to 1.078, required burning efficiency could be reduced to 0.9 % from 5.7 % in case of 90 % recovery of the in-vessel T retention (See text). If the in-vessel T is not recovered, required burning efficiency becomes significantly large

parameters are difficult to estimate from present knowledge or experiences, because T behavior in a reactor is not fully understood, and parameters required for estimation of T balance in a power reactor are not clarified yet. For instances, the overall T burning efficiency in VV has quite large uncertainty, though it is one of the most important parameters in discussion of the T balance. Therefore, no detailed scenarios to attain the fuel self-sufficiency have been proposed yet. Only Nishikawa et al. [22, 23] have demonstrated how  $\eta_{\text{required}}$  changes with the burning efficiency ( $b_{\text{overall}}$ ) for a reactor with 3 Gwth as Fig. 3.5.

In order to maintain the steady state nuclear burning of  $T_{\text{burn}}$  (gT/s) which is determined by the thermal output of a fusion reactor, the required fuel throughput into VV,  $\phi_T$ , whatever the fueling methods are, is given by

$$\phi_T = T_{\text{burn}} / b_{\text{overall}}, \quad (3.5)$$

where  $b_{\text{overall}}$ , the overall burning efficiency of T introduced into VV, includes both the fueling efficiency and the burning efficiency. The burning efficiency corresponds to the theoretical T burn up related to the  $Q$  value of a fusion reactor given in Chap. 4.

To get the figure, there are several assumptions as follows:

- (i) Preservation for a succeeding 3 Gwth reactor (equivalent to T burned in 57 days of operation) being prepared for 3 years operation,
- (ii) Loss by permeation and leakage being  $5 \times 10^{-5}$  of the throughput,
- (iii) Loss by retention in VV being  $3 \times 10^{-4}$  of the throughput.

The figure compares two cases, one with 90 % recovery of the in-vessel T retention and the other without the recovery. Depending on  $b_{overall}$ , required T throughput varies so as all losses assigned as curves (1)–(5) in the figure corresponding to (1)–(5) given above.

The value of  $\eta_{attainable}$  would be a little smaller than 1.05, which is employed as the target value of the net TBR in the present design of a DEMO reactor of JAEA [17, 18, 24]. As seen in the figure, for  $\eta_{attainable}$  being 1.05, the burning efficiency should be more than 5.7 % in case of the 90 % recovery, while 10.3 % in case of no recovery. The burning efficiency of more than 5 % does not seem easily attained. However,  $\eta_{attainable}$  changes with the blanket coverage. BS hardly covers whole areas of VV and some neutrons escape without T breeding.  $\eta_{attainable}$  of 1.05 in the figure is estimated for the blanket coverage of 0.75. If the blanket coverage could be increased to 0.77, the overall  $\eta_{attainable}$  became 1.078. Then required burning efficiency is less than 0.9 % for the 90 % recovery case and 1.7 % for no recovery case.

In conclusion, the establishment of the fuel self-sufficiency is quite hard for realistic values of  $\eta_{attainable}$ , 1.05, and increases in both the burning efficiency and the blanket coverage are dispensable to attain the fuel self-efficiency and to keep reservation for succeeding reactors. Still the in-vessel retention is a concern. At present, it seems quite hard to be less than  $1 \times 10^{-2}$  owing to incorporation of T in redeposited layers at plasma shadowed area, and frequent removals would be required. The removal of T from the redeposited layers at the plasma shadowed area remains unsolved yet.

### 3.5 Summary

Because of radioactivity of T, special cares for radiation safety are required in processing/handling of large amount of T. In addition, limited resources of T require fuel self-sufficiency in a fusion reactor. Accordingly, accurate T accountancy, i.e., to know quantitatively how much T is in throughput, exhaust and is retained in all T systems, is required. At the same time, T inventory (T retention) in any T handling/processing systems should be minimized, or T should be recovered as much as possible. In this chapter, fuel flows in a fusion reactor at a steady state operation are considered. Subsequently, current designs of fuel flow in a fusion reactor are introduced and required conditions to keep T safety and fuel self-sufficiency are considered.

Various factors influence the fuel self-sufficiency. It is needless to say the importance of increasing both the burning efficiency and the blanket coverage, and reducing the T inventory in all T handling systems. In addition, from engineering aspect, operational scenarios of all T handling systems, e.g., extraction of T from BS, T retention in ISS, and T storage SDS shall be optimized to get the maximum efficiency in their operations and also to reduce the total T inventory in a reactor system.

Even under the optimized operation of all systems, both increase of the burning efficiency and the blanket coverage are dispensable to attain the fuel self-efficiency and to keep reservation of T for succeeding reactors.

## References

1. A. Kallenbach, M. Bernert, R. Dux et al., Impurity seeding for tokamak power exhaust: from present devices via ITER to DEMO. *Plasma Phys. Control Fusion* **55**, 124041 (2013)
2. T. Tanabe, Tritium fuel cycle in ITER and DEMO: issues in handling large amount of fuel. *J. Nucl. Mater.* **438**, S19–S26 (2013)
3. M. Glugla, D.K. Murdoch, A. Antipenkov et al., ITER fuel cycle R&D: consequences for the design. *Fusion Eng. Des.* **81**, 733–744 (2006)
4. D. Babineau, S. Maruyama, R. Pearce, et al., in Review of the ITER fuel cycle. In *Proceedings of 23rd IAEA Fusion Energy Conference*, ITR2/2, Daejeon, Republic of Korea
5. I.R. Cristescu, I. Cristescu, L. Doerr et al., Tritium inventories and tritium safety design principles for the fuel cycle of ITER. *Nucl. Fusion* **47**, S458–S463 (2007)
6. T. Tanabe, Tritium handling issues in fusion reactor materials. *J. Nucl. Mater.* **417**, 545–550 (2011)
7. J. Roth, E. Tsitrone, A. Loarte et al., Recent analysis of key plasma wall interactions issues for ITER. *J. Nucl. Mater.* **390–391**, 1–9 (2009)
8. E. Tsitrone, B. Pegourie, Y. Marande et al., Multi machine scaling of fuel retention in 4 carbon dominated tokamaks. *J. Nucl. Mater.* **415**, s735 (2011)
9. D. Murdoch, M. Glugla, T. Hayashi et al., Evolution of ITER Tritium confinement strategy and adaptation to Cadarache site conditions and French regulatory requirements. *Fusion Eng. Des.* **83**, 1355–1358 (2008)
10. [http://www.candu.org/candu\\_reactors.html](http://www.candu.org/candu_reactors.html)
11. C.H. Skinner, Tritium retention and removal in tokamaks, ed. by in: S.-I. Itoh, S. Inagaki, M. Shindo, M. Yagi *Proceedings of 2nd ITER International Summer School: Confinement, 2009*, Amer. Inst. Phys, pp. 127–145
12. Technical basis for the ITER final design Document Series No.24, IAEA Vienna 2002
13. D. Murdoch, S. Beloglazov, P. Boucquey et al., ITER design review: Tritium issues fusion. *Sci. Technol.* **54**, 3–8 (2008)
14. R. Raman, K. Itami, Conceptual design description of a CT fueler for JT-60U. *J. Plasma Fus. Res.* **76**, 1079–1087 (2000)
15. A. Yu, I.V. Sokolov, A.A. Altovkij, Borisov et al., RF TBMs for ITER tests, *Fusion Eng. Des.* **81** (2006) 425 and references there in
16. C.P.C. Wong, S. Malang, M. Sawan, et al., An overview of dual coolant Pb–17Li breeder first wall and blanket concept development for the US ITER-TBM design, *Fusion Eng. Design*, **81** (2006) 461–467, and references there in
17. H. Nakamura, D. Sakurai, S. Suzuki et al., Case study on tritium inventory in the fusion DEMO plant at JAERI. *Fusion Eng. Des.* **81**, 1339–1345 (2006)
18. K. Tobita, S. Nishio, M. Enoda et al., Design study of fusion DEMO plant in JARI. *Fusion Eng. Des.* **81**, 1151–1158 (2006)
19. M.A. Abdou, E.L. Vold, C.Y. Gung, Deuterium-Tritium fuel self-sufficiency infusion reactors. *Fusion Technol.* **9**, 250–285 (1986)
20. M.E. Sawan, M.A. Abdou, Physics and technology conditions for attaining tritium self-sufficiency for the DT fuel cycle. *Fusion Eng. Des.* **81**, 1131–1144 (2006)
21. L.A. El-Guebaly, S. Malang, Toward the ultimate goal of tritium self-sufficiency: technical issues and requirements imposed on ARIES advanced power plants. *Fusion Eng. Des.* **84**(12), December 2009, Pages 2072–2083 and references therein

22. M. Nishikawa, T. Tanabe, Study on the fuel balance of a DT reactor. *Fusion Eng. Des.* **85**, 987–991 (2010)
23. M. Nishikawa, Study on Tritium balance in a D-T fusion reactor. *Fusion Sci. Technol.* **57**, 120–128 (2010)
24. K. Tobita, S. Nishio, M. Enoeida et al., Compact DEMO, SlimCS: design progress and issues. *Nucl. Fusion* **49**, 075029 (2009)



# Chapter 4

## Burning Plasma

Yasuyuki Nakao

**Abstract** This chapter gives a brief introduction to thermonuclear burning of fusion core plasmas. To begin with, we discuss some fusion reactions important for energy production on Earth. For each reaction, the reaction *Q*-value, the graph of reaction cross-section, and the kinetic energies of reaction products are given. After explaining the necessity of plasma for energy generation, we introduce a concept of thermonuclear reaction and define the reaction rate parameter (or *reactivity* in short). The reactivity curves are also shown as a function of the plasma temperature. Magnetic confinement and inertial confinement are two main approaches to achieve the fusion core plasma. Necessary conditions for thermonuclear ignition in these schemes are described. Finally, we give rough estimates of the fractional burn-up of fuel in core plasmas.

**Keywords** Thermonuclear burning · Fusion core plasma · Magnetic confinement · Inertial confinement · Fractional burn-up

### 4.1 Nuclear Fusion Reactions and Cross-Sections

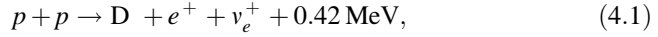
*Nuclear fusion* is a process in which two light nuclei fuse into a heavier one. Amount of energy that is equal to the difference in the total rest-mass energy before and after the reaction is released in the process. This energy is called the *reaction Q-value*. In order to fuse, the two nuclei must overcome their mutual Coulomb repulsive force. The cross-sections for fusion reactions thus tend to drop with decreasing kinetic energy in the center-of-mass system. However, once the two nuclei overcome the Coulomb barrier, fusion becomes likely, as the two overlapping nuclei quickly reach a minimum energy state.

---

Y. Nakao (✉)

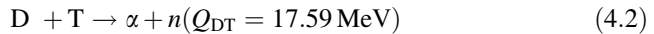
Green Asia Education Center, Kyushu University, 6-1 Kasuga-Koen,  
Kasuga, Fukuoka 816-8580, Japan  
e-mail: nakao@nucl.kyushu-u.ac.jp

In the Sun and other stars, the principal nuclear reactions begin with the conversion of hydrogen into deuterium [1]:



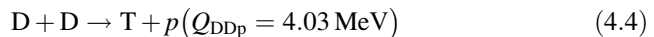
where  $p$ ,  $D$ ,  $e^+$ , and  $\nu_e$  denote proton, deuteron, positron, and electron neutrino, respectively. If the subsequent annihilation of the positron ( $e^+$ ) with an ambient electron is added, the total energy release becomes 1.44 MeV. Anyway this first-step reaction occurs very rarely because it involves weak interaction (a proton changes to a neutron); its cross-section is immeasurably small (about  $10^{-53} \text{ m}^{-2}$  at 1 MeV, for example). The reaction using ordinary hydrogen ( $p$ ) is thus useless as an energy source on Earth.

The main fuels for controlled fusion are the hydrogen isotopes, i.e., deuterium ( $D$ ) and tritium ( $T$ ). The D-T reaction



has advantages over other fusion reactions using hydrogen isotopes. The reaction  $Q$ -value (shown in the parentheses) is the largest of the reactions between hydrogen isotopes, and the cross-section at low energy is considerably large. This is because at energies below the height of Coulomb potential barrier  $B^1$ , the D-T reaction predominantly proceeds via the formation of an excited state of compound  ${}^5\text{He}$  nucleus, which gives a strong resonance in the cross-section (see Fig. 1.3 in Chap. 1). Deuterium occurs naturally in water with the abundance ratio of 0.015 %, but tritium is not available from natural sources, and therefore, one has to produce it in an artificial way.

The D-D reactions

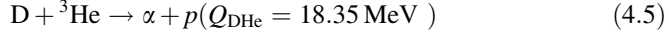


are nearly equally probable. The cross-sections at 10–100 keV energies are about 100 times smaller than that for the D-T reaction. It should be noted that the D-D reactions accompany secondary D-T and  $D-{}^3\text{He}$  reactions.

Fusion fuels consisting of the mixtures of hydrogen isotopes and light nuclei (helium-3, lithium, boron, etc.) are called ‘advanced fusion fuels.’ For these fuels, the probability that the incident particle penetrates the Coulomb potential barrier is much lower than in the case of hydrogen isotopes only, leading to smaller cross-sections at sub-barrier energy. Among this group of reactions, the  $D-{}^3\text{He}$  reaction

---

<sup>1</sup>For D-T reaction,  $B \approx 0.4 \text{ MeV}$ .



would be most interesting because it does not involve radioactive fuel and releases no neutrons. At high energy, the cross-section is intermediate between those of D-T and D-D. It should be noted that natural abundance ratio of  ${}^3\text{He}$  is quite small (about  $10^{-4}\%$ ). Moreover, D- ${}^3\text{He}$  fusion would anyhow produce T and emit neutrons ( $n$ ) due to the D-D reactions.

In controlled fusion reactions, the reacting particles have energies in the range from 1 to several tens of keV. The initial kinetic energies are thus small enough compared with the  $Q$ -values. In such a case, due to conservation of energy and momentum, the energy released by the reaction (i.e.,  $Q$ -value) is distributed between two reaction products in quantity inversely proportional to their masses. Thus, in the case of the D-T reaction, for example, the product neutron carries away 80 % of the released energy, that is

$$E_n = \frac{m_\alpha}{m_n + m_\alpha} Q_{\text{DT}} \approx 14.1 \text{ MeV}, \quad (4.6)$$

while the remaining 20 % (about 3.5 MeV) is contained in the  $\alpha$ -particle.

The most important quantity for the analysis of nuclear processes would be the *reaction cross-section*, which is a measure of the probability per pair of particles for the occurrence of the reaction. The cross-section is denoted by  $\sigma$  and has the dimensions of area (hence is called cross-section). Most fusion reactions occur at energies below the height of Coulomb potential barrier  $B$ . In this case, the influence of repulsive Coulomb potential is significant, and the energy dependence of the reaction cross-sections  $\sigma(E)$  comes mainly from two factors. One is the barrier penetration factor (i.e., tunneling probability)  $P(E)$ , which is usually given by WKB calculation<sup>2</sup> as follows:

$$P(E) \propto \exp\left(-\sqrt{\frac{E_G}{E}}\right) \quad (4.7)$$

with  $E_G$  being the Gamov energy and  $E$  the total kinetic energy in the center-of-mass (CM) system. The Gamov energy is defined by

$$E_G = 2\mu c^2 \left( \frac{\pi Z_1 Z_2 e^2}{\hbar c (4\pi \epsilon_0)} \right)^2, \quad (4.8)$$

where  $\mu (= m_1 m_2 / (m_1 + m_2))$  is the reduced mass of the two-particle system and  $Z_j$  ( $j = 1, 2$ ) is the atomic number of species  $j$ ;  $c$ ,  $e$ ,  $\hbar (= h/2\pi)$ , and  $\epsilon_0$  are the velocity of light in vacuum, the elementary charge, Planck's constant, and the electric permittivity of free space, respectively. Another factor is the geometrical

---

<sup>2</sup>A semi-classical method in quantum mechanics.

cross-section, which is written as follows:

$$\sigma_{\text{geom}}(E) = \pi \lambda^2 = \pi \frac{\hbar^2}{2\mu E}. \quad (4.9)$$

Here,  $\lambda$  is the reduced de Broglie wavelength. Up to this stage,  $\sigma(E) \propto \sigma_{\text{geom}}(E) P(E)$ . By extracting the part ‘ $1/E$ ’ out of  $\sigma_{\text{geom}}(E)$  and introducing one more quantity  $S(E)$  called *astrophysical S-factor*, the fusion cross-section is expressed as a product of three factors:

$$\sigma(E) = S(E) \frac{1}{E} \exp\left(-\sqrt{\frac{E_G}{E}}\right). \quad (4.10)$$

The S-factor is a weakly varying function of the energy (unless resonances at sub-barrier energies occur) and is determined experimentally. It represents the intrinsically nuclear parts for the occurrence of the reaction, whereas the other two factors represent well-known energy dependences that are non-nuclear in nature [1].

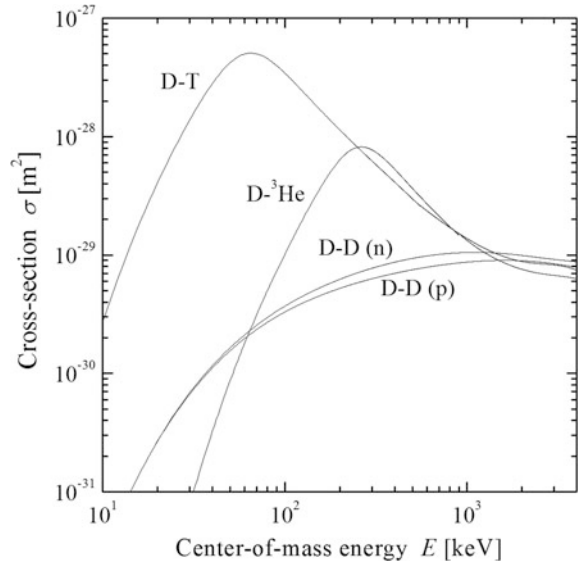
Some basic physics issues for understanding fusion cross-sections are concisely described in Bosch and Hale [2]. Based on R-matrix theory, they evaluated the cross-sections and improved parameterization formulas for the four reactions  $T(d, n)^4\text{He}$ ,  $D(d, n)^3\text{He}$ ,  $D(d, p)\text{T}$ , and  $^3\text{He}(d, p)^4\text{He}$ . Here, for example,  $T(d, n)^4\text{He}$  is an alternative way of indicating the D-T reaction (Eq. 4.2).

Figure 4.1 shows the cross-sections of these reactions, reproduced using the formulas given in [2], as a function of the CM energy. The D-D reactions do not have resonances, and their cross-sections monotonically increase with energy in the interval of our interest. In contrast, the cross-sections of the D-T and D- $^3\text{He}$  reactions have a strong energy dependence accompanying the maximum, which is the characteristic of the reactions via compound nucleus formation. The energies at which the maxima of cross-sections lie are far below the Coulomb barrier height  $B$ , indicating that the fusion reactions essentially occur through the quantum mechanical tunneling effect.

## 4.2 Fusion Reaction Rates in Plasmas

To utilize nuclear fusion for energy production, the fuel should be in the plasma state. In an ordinary state of matters, it is difficult to cause a number of fusion reactions. This is because most of the reactant’s kinetic energies are quickly lost in the processes such as excitation and ionization of the constituent atoms, and dissociation of the molecules; the cross-sections for atomic and molecular processes are larger by several orders of magnitude than those for fusion reactions. These unfavorable processes can be avoided if the fuel is in the plasma state. In high-temperature plasmas, a certain fraction of the plasma ions can have energies high enough to overcome (penetrate) the Coulomb potential barrier. Because

**Fig. 4.1** Cross-sections of four important fusion reactions as a function of center-of-mass energy



thermal motion energies of the plasma ions are used to induce fusion reactions, the process is called *thermonuclear fusion*.

To calculate the rate of fusion reactions in plasma, one should take into account the velocity distributions of the reacting particles. An important quantity here is the *reaction rate parameter* (or *reactivity*)  $\langle \sigma v \rangle$ , the product of the reaction cross-section  $\sigma(v)$ , and the relative velocity  $v$  averaged over the velocity distributions of two reacting species. If the two species are labeled by 1 and 2, with number densities  $n_1$  and  $n_2$ , respectively, the *fusion reaction rate* (i.e., the number of fusion reactions per unit time per unit volume) is given by

$$R = \frac{1}{1 + \delta_{12}} n_1 n_2 \langle \sigma v \rangle_{12}. \quad (4.11)$$

Here, the Kronecker symbol  $\delta_{ij}$  (defined as  $\delta_{ij} = 1$  if  $i = j$  and  $\delta_{ij} = 0$  otherwise) is introduced to properly take into account the case of reactions between ‘like particles’ (particles of the same species). Without the factor including  $\delta_{ij}$ , each reaction between like particles is counted twice.

The reactivity stands for the probability of reaction per unit time per unit density of target nuclei, being written as follows:

$$\langle \sigma v \rangle_{12} = \iint f_1(\mathbf{v}_1) f_2(\mathbf{v}_2) \sigma(v) v d\mathbf{v}_1 d\mathbf{v}_2, \quad (4.12)$$

where  $v = |\mathbf{v}_1 - \mathbf{v}_2|$ , and  $f_j(\mathbf{v}_j)$  is the unit-normalized velocity distribution of species  $j$  ( $j = 1, 2$ ) in the laboratory system. Assuming that the velocities of both species are given by the Maxwell–Boltzmann distribution with a same temperature  $T$ ,

$$f_j(\mathbf{v}_j) d\mathbf{v}_j = \left( \frac{m_j}{2\pi kT} \right)^{3/2} \exp\left( -\frac{1}{2} m_j v_j^2 / kT \right) d\mathbf{v}_j, \quad (4.13)$$

Equation (4.12) is put into explicit form:

$$\langle \sigma v \rangle_{12} = \left( \frac{m_1 m_2}{4\pi^2 k^2 T^2} \right)^{3/2} \iint \exp\left( -\frac{m_1 v_1^2 + m_2 v_2^2}{2kT} \right) \sigma(v) v d\mathbf{v}_1 d\mathbf{v}_2. \quad (4.14)$$

It is convenient to change the variables of the integration from  $\{\mathbf{v}_1, \mathbf{v}_2\}$  to  $\{\mathbf{v}, \mathbf{c}\}$ , where  $\mathbf{c}$  is the velocity of the center of mass of the two reacting particles. In this transformation, the Jacobian is unity so that  $d\mathbf{v}_1 d\mathbf{v}_2 = d\mathbf{v} d\mathbf{c}$ . Furthermore, the total kinetic energy of reacting particles in the laboratory system,  $(1/2)m_1 v_1^2 + (1/2)m_2 v_2^2$ , is replaced by  $(1/2)\mu v^2 + (1/2)(m_1 + m_2)c^2$ , the sum of the kinetic energy of the particles with respect to the center of mass *plus* the energy of motion of the center of mass. With these results inserted into Eq. (4.14), the integrals separate so that

$$\begin{aligned} \langle \sigma v \rangle_{12} &= \left( \frac{m_1 m_2}{4\pi^2 k^2 T^2} \right)^{3/2} \int \exp\left( -\frac{1}{2} \mu v^2 / kT \right) \sigma(v) v d\mathbf{v} \\ &\quad \times \int \exp\left( -\frac{m_1 + m_2}{2kT} c^2 \right) d\mathbf{c} \\ &= 4\pi \left( \frac{\mu}{2\pi kT} \right)^{3/2} \int_0^\infty \exp\left( -\frac{1}{2} \mu v^2 / kT \right) \sigma(v) v^3 dv. \end{aligned} \quad (4.15)$$

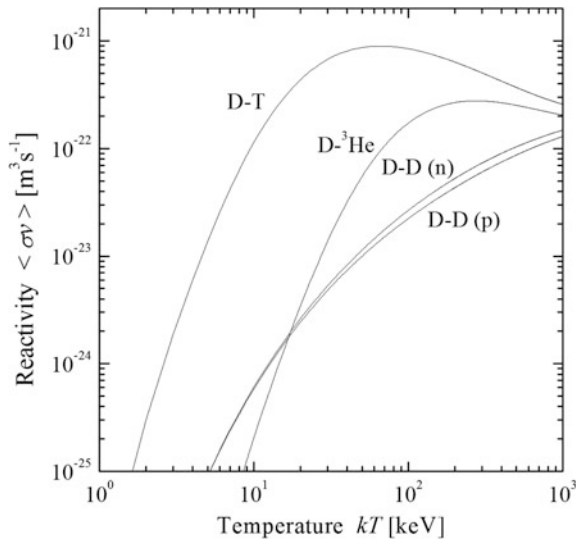
Here, the isotropic velocity distributions are assumed. With a further change of a variable from  $v$  to  $E (= \mu v^2 / 2)$ , the energy in the CM system, we obtain the final form of the reactivity:

$$\langle \sigma v \rangle_{12} = \left( \frac{8}{\pi \mu} \right)^{1/2} \frac{1}{(kT)^{3/2}} \int_0^\infty E \exp(-E/kT) \sigma(E) dE. \quad (4.16)$$

Thus, the reactivity is a function only of the plasma temperature. It can be shown that for temperature  $kT \ll E_G$ , the Gamov energy defined by Eq. (4.8), the integrand has a maximum at  $E_G$  (unless resonances at sub-barrier energies occur). This implies that most of the contribution to the reactivity is done by the particles having high energy around  $E_G$ . Given the fusion cross-section data, the reactivity can be precisely evaluated by means of numerical integration.

Figure 4.2 shows the values of  $\langle \sigma v \rangle$  for the reactions of interest for controlled fusion, i.e.,  $T(d, n)^4\text{He}$ ,  $D(d, n)^3\text{He}$ ,  $D(d, p)\text{T}$ , and  $^3\text{He}(d, p)^4\text{He}$ , as a function of plasma temperature  $kT$ . In the temperature range that is likely achievable in a thermonuclear fusion reactor, the D-T reaction is clearly favorable; it has the largest reactivity among these four reactions. The D-T reactivity has a broad peak at about 64 keV. Thanks to this peak, the D-T reactivity turns out to be far larger than that of any other reaction whenever the plasma temperature is a few tens of keV.

**Fig. 4.2** Reactivities of four important fusion reactions as a function of plasma temperature



Using the reactivity and the densities of reacting species, one can calculate the *fusion power density*  $P_{\text{fus}}$  (the energy released by fusion reactions per unit time per unit volume in the plasma). For a D-T plasma of  $n_D = (1 - \gamma) n_i$  and  $n_T = \gamma n_i$  ( $0 < \gamma < 1$ ), for example,

$$P_{\text{fus}} = n_D n_T \langle\sigma v\rangle Q_{\text{DT}} = (1 - \gamma) \gamma n_i^2 \langle\sigma v\rangle Q_{\text{DT}}. \quad (4.17)$$

### 4.3 Ignition Condition and Requirement for Magnetic Confinement Fusion

The essence of the controlled thermonuclear fusion is to confine the plasma of hydrogen isotopes for a long time so that the fusion reaction rate becomes large enough to generate the desired power. Two major schemes to achieve this goal are *magnetic confinement fusion* (MCF) and *inertial confinement fusion* (ICF). The basic principle of MCF is that in a magnetic field, charged particles move gyrating along the line of magnetic force. The transverse motions are nearly suppressed, and it is therefore possible to confine the plasma particles by using an appropriately designed magnetic field. The most established magnetic confinement device at present is *tokamak*. In this section, we derive a necessary condition for steady-state operation of MCF plasma on the basis of a simple power-balance model. The condition for ICF plasma is discussed in the next section. An excellent introduction to MCF is found in Stacey [3]. As for tokamak, see Wesson [4].

The minimum plasma temperature required is roughly estimated from a comparison of the fusion power density  $P_{\text{fus}}$  with the radiated power density  $P_{\text{br}}$  due to *bremstrahlung* (*braking radiation*). The latter is a process in which the Coulomb

scattering of plasma electrons by the ions produces accelerations which in turn give rise to the emissions of electromagnetic radiation. The radiated energy per unit time per unit plasma volume is given by

$$P_{\text{br}} = \frac{16}{3} g \frac{Z_i^2 n_i n_e e^6}{(4\pi\epsilon_0)^3 m_e c^3 \hbar} \left( \frac{2\pi k T_e}{3m_e} \right)^{1/2} = C_b Z_i^2 n_i n_e \sqrt{k T_e}, \quad (4.18)$$

where  $g$  represents the Gaunt factor, being used to take into account the relativistic as well as quantum mechanical effects [5]. The values of various constants are incorporated in  $C_b$ , and  $C_b = 5.35 \times 10^{-37}$  if  $n_i$  and  $n_e$  are measured in  $\text{m}^{-3}$ ,  $k T_e$  in keV, and  $P_{\text{br}}$  in  $\text{W/m}^3$ ;  $C_b = 3.34 \times 10^{-21}$  if  $P_{\text{br}}$  is changed to be in  $\text{keV/m}^3 \text{ s}$ . From  $P_{\text{fus}} \geq P_{\text{br}}$ , the plasma temperature above which the fusion output exceeds the bremsstrahlung loss is estimated to be 4.3 keV. The plasma temperature thus should be at least above 5 keV. (This also applies to ICF plasma.)

On the other hand, plasma density  $n (=n_i =n_e)$  is limited by the strength of the magnetic field. Due to the macroscopic equilibrium and stability of plasma as a fluid, the ratio  $\beta$  of the plasma pressure to the external magnetic pressure cannot exceed the limit value— $\beta$  limit:

$$\beta = \frac{n_i k T_i + n_e k T_e}{B_0^2 / 2\mu_0} \leq \beta_{\max} \rightarrow n \leq \frac{1}{2kT} \beta_{\max} (B_0^2 / 2\mu_0). \quad (4.19)$$

The limit value  $\beta_{\max}$  varies depending on the plasma confinement scheme. For a tokamak, typically  $\beta_{\max} \leq 10\%$ . With typical values of  $B_0 \approx 6 \text{ Wb/m}^2$ ,  $\beta_{\max} 5\%$ , and  $kT \approx 15 \text{ keV}$  used in Eq. (4.19), the density  $n$  is estimated to be of the order of  $10^{14} \text{ cm}^{-3}$ . In the case of tokamak, the plasma operating density is also restricted by the so-called *Greenwald limit* [6]. Although physics of this density limit has not been completely clarified yet, the empirical formula constructed by experimental tokamak database is expressed as follows:

$$\frac{n_{20}}{I_P(\text{MA})/\pi a(\text{m})^2} < 1 \rightarrow n_{20} < n_{20 \text{ lim}} = \frac{I_P(\text{MA})}{\pi a(\text{m})^2}, \quad (4.20)$$

where  $I_P$  is the plasma current,  $a$  the plasma minor radius, and  $n_{20}$  the electron density in the unit of  $10^{20} \text{ m}^{-3}$ . For the ITER ‘inductive’ operation scenario,  $n_{\text{lim}}^{(GW)}$  is estimated to be  $1.2 \times 10^{20} \text{ m}^{-3}$ , which is comparable to  $n_{\text{lim}}^{(\beta)}$ , the value of the  $\beta_{\max}$  density limit.

Now, we discuss the operating condition of a D-T fusion plasma with density  $n = n_i (= 2n_D = 2n_T) = n_e$  and temperature  $T = T_i = T_e$ . At steady state, a constant power  $P_{\text{fus}}$ , given by Eq. (4.17), is produced in the plasma by D-T fusion reactions, 20 % of which is carried by  $\alpha$ -particles ( $\alpha$ -particle power  $P_\alpha$ ):

$$P_\alpha = \frac{1}{4} n^2 \langle \sigma v \rangle E_\alpha. \quad (4.21)$$

Remaining 80 % is carried away by neutrons (*neutron power*  $P_n$ ):

$$P_n = \frac{1}{4} n^2 \langle \sigma v \rangle E_n, \quad (4.22)$$

and is converted to thermal power in the blanket region surrounding the plasma.

The power  $P_\alpha$  and an external *auxiliary heating power*  $P_{\text{aux}}$  are delivered to the plasma to maintain the operating condition, compensating the power losses due to (1) electromagnetic radiation and (2) transport across the magnetic field (i.e., thermal conduction and convection). An important measure here is the *plasma fusion multiplication* (or briefly the *plasma Q-value*)  $Q_p$  defined by

$$Q_p = \frac{P_{\text{fus}}}{P_{\text{aux}}}. \quad (4.23)$$

The plasma  $Q$ -value is a measure of the efficiency of a fusion reactor. Using  $Q_p$ , the auxiliary heating power is expressed as  $P_{\text{aux}} = P_{\text{fus}}/Q_p$ . The main mechanism of radiation loss is bremsstrahlung, and the loss power is hence given by Eq. (4.18). In a global way, the power loss due to the transport is written in terms of the *energy confinement time*  $\tau_E$  as follows:

$$P_{\text{trans}} = \frac{(3/2)n_i kT_i + (3/2)n_e kT_e}{\tau_E} = \frac{3nkT}{\tau_E}. \quad (4.24)$$

In order to maintain the steady state, the total loss power ( $P_{\text{br}} + P_{\text{trans}}$ ) must be compensated by the plasma heating power ( $P_\alpha + P_{\text{aux}}$ ), that is

$$\frac{1}{4} n^2 \langle \sigma v \rangle E_\alpha + \frac{P_{\text{fus}}}{Q_p} = C_b n^2 \sqrt{kT} + \frac{3nkT}{\tau_E}. \quad (4.25)$$

Making use of Eq. (4.17), the expression for  $P_{\text{fus}}$ , and relation  $E_\alpha = Q_{\text{DT}}/5$ , this condition is finally rewritten in the form:

$$n\tau_E = \frac{12kT}{\left(\frac{1}{5} + \frac{1}{Q_p}\right)\langle \sigma v \rangle Q_{\text{DT}} - 4C_b \sqrt{kT}}. \quad (4.26)$$

The product of the plasma density and energy confinement time,  $n \tau_E$ , is called *confinement parameter*. The right-hand side of Eq. (4.26) is the function of the temperature  $T$  only. The equation represents the *ignition* (or *burning*) *condition* and reveals that for steady-state burning at a specified temperature, the value of  $n \times \tau_E$  has to equal the value given by the right-hand side at that temperature.

Somewhat different representation is the *Lawson criterion* [7], where it is assumed that the fusion output power  $P_{\text{fus}}$  and the power lost from the plasma ( $P_{\text{br}} + P_{\text{trans}}$ ) are converted into thermal power and then into electric power.

A certain fraction ( $=\eta$ ) of the converted power is injected into the plasma as a heating power, that is

$$\eta \left( P_{\text{fus}} + P_{\text{br}} + \frac{3nkT}{\tau_E} \right) = P_{\text{br}} + \frac{3nkT}{\tau_E}. \quad (4.27)$$

Using Eqs. (4.17) and (4.18) for  $P_{\text{fus}}$  and  $P_{\text{br}}$ , respectively, the Lawson criterion is written as follows:

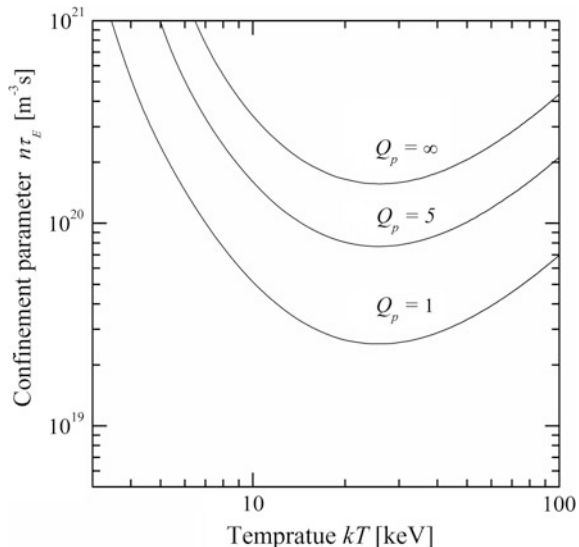
$$n\tau_{E,L} = \frac{12kT}{\frac{\eta}{1-\eta} \langle \sigma v \rangle Q_{\text{DT}} - 4C_b \sqrt{kT}}. \quad (4.28)$$

It is easily observed that the Lawson criterion ( $n\tau_{E,L}$ ) with  $\eta \approx 0.5$  leads to the confinement requirement (i.e.,  $n\tau_E$ ) at  $Q_p \approx 1$ .

For the above power-balance model, we assumed an idealized core state, i.e., equimolar DT plasma ( $\gamma = 1/2$ ) without impurities. In actual fusion reactors, however, DT mixtures are not always equimolar, and therefore, measurement and control of the DT molar fraction is quite important (see Chap. 8). Moreover, some impurity ions would be present even in the core region. They come mainly from the surrounding wall and carry some bound electrons. In such cases, we have to take into account an additional energy loss due to radiation from the impurities (mainly line radiation).

Figure 4.3 shows the values of the confinement parameter  $n\tau_E$  required for the cases of  $Q_p = 1$  (*breakeven*),  $Q_p = 5$ , and  $Q_p = \infty$  (*self-ignition*). Each curve has a minimum at  $kT \approx 25$  keV, and for self-ignition, it is about  $2 \times 10^{20} \text{ m}^{-3} \text{ s}$ .

**Fig. 4.3** Confinement parameter required for steady-state operation of MCF plasma as a function of temperature

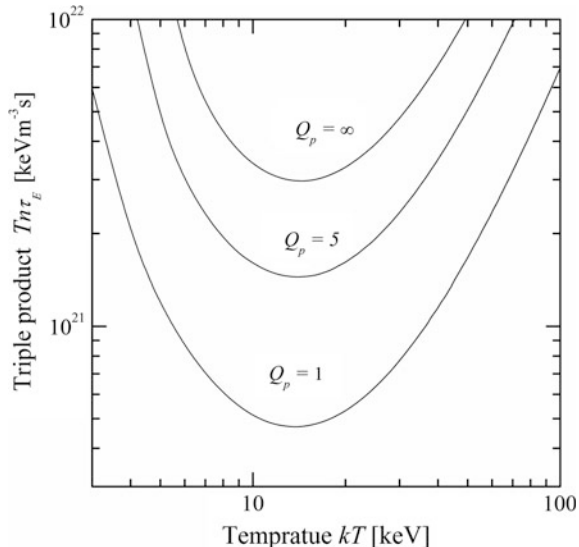


One more interesting quantity would be  $T n \tau_E$ , the product of plasma temperature (in keV), density, and energy confinement time, given by Eq. (4.26) multiplied by  $T$ . This is known as the *triple product* and is used to evaluate the progress in MCF research (i.e., the nearness of confined plasma to the ignition or burning condition). The temperature dependences of the triple product given in Fig. 4.4 for several values of  $Q_p$  are almost symmetrical with respect to  $kT \approx 15$  keV and are roughly regarded as flat in a wide temperature range (8–25 keV), which is just the merit of using this parameter. For self-ignition, the required  $T n \tau_E$  is about  $3.5 \times 10^{21}$  keV m<sup>-3</sup> s.

It should be noted here that values of confinement parameter  $n \tau_E$  or triple product  $T n \tau_E$  or the relations such as Eq. (4.28) are useful only when we set up a rough objective for fusion core plasma. Possible (or permitted) values of the density  $n$  and the energy confinement time  $\tau_E$  depend on features of the confinement device adopted. As for limitations imposed on the density, we discussed briefly in the preceding paragraph. The confinement time also depends on details of the device and is affected by various quantities and parameters including the size and shape of plasma, magnetic field, density, plasma current, and heating power. A lot of efforts have been made toward clarifying the physics of plasma confinement, and the establishment of the confinement law is still the most important issue in controlled fusion research.

Plasma temperatures ( $>10$  keV) needed for fusion burning have been achieved in many facilities. By the middle of the 1990s, plasma conditions near (or around) breakeven  $Q_p = 1$  were achieved in three major tokamaks (TFTR, JET, and JT-60). The further step aiming at the demonstration of fusion-energy-producing plasmas is to be taken by ITER [8].

**Fig. 4.4** Fusion triple product required for steady-state operation of MCF plasma as a function of temperature



## 4.4 Ignition Condition and Requirement for Inertial Confinement Fusion

Another approach to achieve controlled fusion is ICF. In this scheme, driver beams (laser, ion beams, and so on) are focused upon hydrogen isotope-filled targets to compress and heat the fuel to fusion temperatures. The inertia of fuel is used to ‘confine’ it long enough for fusion reactions to occur.

The sequence of processes in conventional laser-driven ICF might be as follows. (1) The laser beams from many directions irradiate uniformly a target (a small sphere containing fuel). The outer layer of the target is immediately heated and forms a plasma atmosphere, which continues to absorb the laser radiation. (2) The plasma rapidly *ablates* (blows off), and by Newton’s 3rd law, the remaining target is accelerated inward and compresses the fuel inside. (3) The beam irradiation is designed in such a way that during the final stage of the implosion, a ‘hot’ (5–10 keV) central core surrounded by a ‘cold’ ( $\leq$  a few keV) ultra-dense fuel layer is created. (4) The  $\alpha$ -particles resulting from the fusion reactions in the central hot region deposit their energy to the surrounding dense fuel. This contributes to additional heating, and thermonuclear burn propagates outward until a fair fraction of the fuel is exhausted. The above sequential processes, (1)–(4) are repeated at a rate of a few hertz so that a continuous fusion power is produced. ICF is thus characterized by its ‘extremely high density’ ( $n > 10^{32} \text{ m}^{-3}$ ), ‘extremely short period’ ( $\tau < 10^{-8} \text{ s}$ ), and ‘pulse operation,’ being quite different from MCF. For detailed explanation of ICF, see Atzeni and Meyer-ter-Vehn [9].

The simplified energy flow in an ICF reactor system is as follows. A *driver energy*  $E_d$  is delivered to the target, which releases an amount of *fusion energy*  $E_{\text{fus}}$ . The *energy gain*  $G$  of the target is hence

$$G = \frac{E_{\text{fus}}}{E_d}. \quad (4.29)$$

The fusion energy released is first converted into thermal energy in the surrounding blanket and then converted into electricity with efficiency  $\eta_{\text{el}}$ . A certain fraction ( $\eta_{\text{rec}}$ ) of the electric power is recirculated for feeding the driver, which has an efficiency  $\eta_d$  of converting the recirculated power into the beam energy. The energy balance for this cycle is written as follows:

$$\eta_d \eta_{\text{rec}} \eta_{\text{el}} G = 1. \quad (4.30)$$

Taking  $\eta_{\text{el}} \approx 40\%$  and requiring  $\eta_{\text{rec}} \leq 25\%$  to obtain a sufficient amount of usable net energy, we obtain the condition

$$\eta_d G \geq 10. \quad (4.31)$$

For laser driver,  $\eta_d \approx 10\%$  could be achieved. Then, the target gain required for power production is  $G \geq 100$ .

In usual operating conditions (a few shots per second), the magnitude of fusion energy release per shot,  $E_{\text{fus}}$ , has to be limited to a few GJ in order to keep the reactor vessel from being damaged. Burn of 1 mg DT releases 337 MJ of fusion energy. Then, if a fuel burn-up of 20–30 % is assumed, the mass of fuel pellet has to be restricted to a few 10 mg [9].

In order to burn such small fuel masses and to obtain an enough energy gain ( $\geq 100$ ) at a reasonable driver energy level, it is essential to compress the fuel to extremely high densities (above 1000 times the solid density of DT fuel). For high gain, it is also important to ignite only a small fraction of the fuel. (Heating of entire fuel to the ignition temperature leads to an excessive requirement on the driver energy.) The ‘hot spot’ created must be large and hot enough to heat the surrounding cold fuel and to generate sufficient amount of fusion energy for explosive burn propagation.

Before discussing the ignition condition, we here refer to a confinement parameter of ICF fuel. Let us consider a plasma sphere consisting of compressed DT fuel, and for simplicity, suppose that it has uniform density  $\rho$  (ion number density  $n_0$ ) and temperature  $kT$  at time  $t = 0$ , with a free boundary at radius  $R_f$ . The plasma sphere expands in the form of a *rarefaction wave*, the front of which propagates inward (from the surface) with the sound velocity  $C_s = (2kT/m_i)^{1/2}$ . The *effective confinement time* of this plasma sphere is given as the time interval in which the wave front advances about one-fourth of the radius  $R_f$ , that is

$$\tau_{\text{eff}} = \frac{R_f}{4C_s}. \quad (4.32)$$

The factor ‘1/4’ is somewhat arbitral but reflects the fact that when the rarefaction wave travels one-fourth of  $R_f$ , the amount of remaining fuel decreases below a half. Using the relation  $n_0 = \rho/m_i$  and Eq. (4.32), the confinement parameter is expressed in terms of  $\rho R$ , the product of mass density and radius of the compressed fuel:

$$n_0 \tau_{\text{eff}} \approx \frac{1}{4m_i C_s} \rho R. \quad (4.33)$$

Now let us consider the ignition condition of the compressed DT fuel with a nearly isobaric configuration. The ‘ignition’ may be defined by a state that the temporal rate of increase in the internal energy (or temperature) of the hot spot is significant so that the burn wave propagates without any external heating. The rate of change in the internal energy per unit volume of the hot region is determined by the balance between the  $\alpha$ -particle heating power  $P_\alpha$  and loss powers due to the radiation ( $P_{\text{br}}$ ), electron thermal conduction ( $P_C$ ), and fuel expansion ( $P_W$ ), that is

$$\frac{d}{dt} 3nkT = P_\alpha - (P_{\text{br}} + P_C + P_W). \quad (4.34)$$

The expressions for  $P_\alpha$  and  $P_{\text{br}}$  are Eqs. (4.21) and (4.18), respectively. If we use the cgs unit except for  $kT$  which is in keV, these powers are rewritten (in the unit of erg/cm<sup>3</sup> s) as follows [9]:

$$P_\alpha = \frac{1}{4} \left( \frac{\rho}{m_i} \right)^2 \langle \sigma v \rangle E_\alpha = A_\alpha \rho^2 \langle \sigma v \rangle, \quad A_\alpha = 8.04 \times 10^{40}; \quad (4.35)$$

$$P_{\text{br}} = C_b \left( \frac{\rho}{m_i} \right)^2 \sqrt{kT} = A_{\text{br}} \rho^2 \sqrt{kT}, \quad A_{\text{br}} = 3.05 \times 10^{23}. \quad (4.36)$$

The remaining loss powers,  $P_C$  and  $P_W$  (both in erg/cm<sup>3</sup> s), can be calculated by [9]

$$P_C \approx - \frac{\kappa \nabla(kT) S}{V} \approx A_C \frac{(kT)^{7/2}}{R^2}, \quad A_C = 4.1 \times 10^{19}; \quad (4.37)$$

$$P_W \approx \frac{3p v_{\text{exp}}}{R} \approx A_W \frac{\rho(kT) C_s}{R}, \quad A_W = 2.3 \times 10^{15}. \quad (4.38)$$

Here,  $S/V (=3/R)$  is the surface-to-volume ratio of the plasma sphere. The expansion velocity  $v_{\text{exp}}$  was approximated by  $C_s = (2kT/m_i)^{1/2}$ . For ignition, it is necessary at least that

$$P_\alpha > P_{\text{br}} + P_C + P_W. \quad (4.39)$$

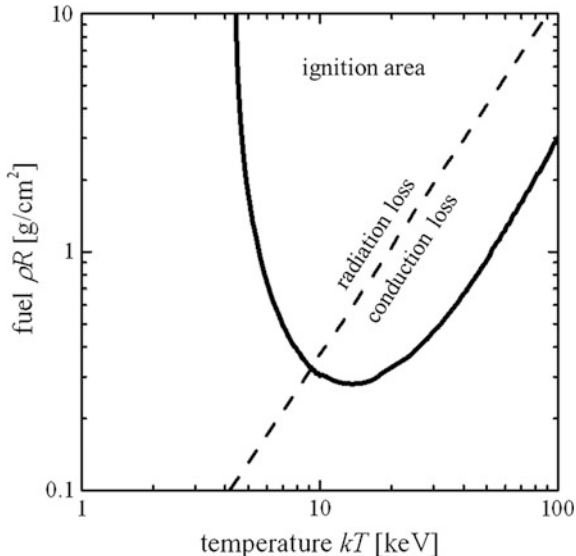
Substituting Eqs. (4.35)–(4.38) into Eq. (4.39) and then multiplying the both sides by  $R^2$ , we obtain the inequality of second degree [9]

$$(A_\alpha \langle \sigma v \rangle - A_{\text{br}} \sqrt{kT}) (\rho R)^2 - A_W C_s kT (\rho R) - A_C (kT)^{7/2} > 0. \quad (4.40)$$

Figure 4.5 shows the ignition boundary resulting from Eq. (4.40) on the  $kT - \rho R$  plane. When the plasma temperature is low, the radiation is the main power loss mechanism to determine the ignition boundary. At higher temperatures, the thermal conduction becomes dominant. The influence of the fuel expansion is small in the case that the hot region is surrounded by dense cold layer of fuel. It is observed that the minimum  $\rho R$  of the hot region is about 0.3 g/cm<sup>2</sup> at  $kT \approx 10$  keV. For ignition and sufficient burning, however, larger  $\rho R_{\text{hot}}$  should be attained. The ignition boundary as shown in Fig. 4.4 corresponds to the  $n \tau_E - kT$  curve for MCF plasma at  $Q_p \approx 1$ .

ICF study has advanced steadily too, with progress including the fuel compression to more than 600 times the solid density, completion of major facilities, etc. Among the facilities, NIF at Lawrence Livermore National Laboratory (USA) is of the largest scale, being based on *indirect drive* using conventional central hotspot ignition with the laser driver energy of 2 MJ. The fusion gain  $G$  still remains to be of the order of 0.01, but NIF aims to attain  $G \sim 10$  [10].

**Fig. 4.5** Ignition boundary of compressed DT fuel with a nearly isobaric configuration. (Provided by T. Johzaki)



Along with the conventional approach to ignition of ICF, over in recent two decades, there has been an increasing interest in alternative approaches such as *fast ignition* (FI) and *shock ignition* (SI) [11]. In FI, an ultra-high-power and short-pulse laser acts as a spark plug to ignite a compressed fuel of moderate size. In SI, a fuel shell is imploded with a low implosion velocity, and then, a strong shock wave is launched at the end of the laser pulse to initiate ignition in the compressed fuel core. These schemes are expected to make it possible to obtain high fusion gains with moderate driver energies.

## 4.5 Fractional Burn-up of Fuel in Core Plasma

At the end of this chapter, we roughly estimate the *fractional burn-up* of DT fuel both in MCF and ICF schemes. First, let us consider MCF burning core plasmas. In this case, the fractional burn-up  $f_b$  is defined as the ratio of the fuel depletion rate due to fusion reactions to the rate of fuel injection into the core plasma region, that is

$$f_b = \frac{\text{depletion rate}}{\text{injection rate}} = \frac{2 \times \frac{1}{4} n^2 \langle \sigma v \rangle}{S_{\text{inj}}} \quad (4.41)$$

The factor ‘2’ in the numerator accounts for the number of fuel particles lost per reaction. At steady state, the loss of fuel particles due to reactions and cross-field diffusion from the core is compensated by injection. The fuel injection rate is thus

$$S_{\text{inj}} = \frac{1}{2} n^2 \langle \sigma v \rangle + \frac{n}{\tau_p}. \quad (4.42)$$

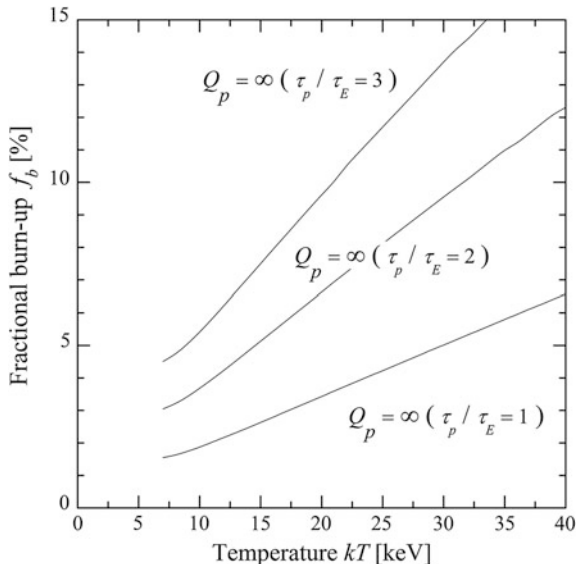
Here,  $\tau_p$  is the particle confinement time. Substituting Eq. (4.42) into Eq. (4.41), we can write  $f_b$  in the following form:

$$f_b = \frac{\frac{1}{2} n^2 \langle \sigma v \rangle}{\frac{1}{2} n^2 \langle \sigma v \rangle + \frac{n}{\tau_p}} = \frac{\langle \sigma v \rangle}{\langle \sigma v \rangle + \frac{2}{n \tau_E (\tau_p / \tau_E)}}. \quad (4.43)$$

In this expression, the reactivity  $\langle \sigma v \rangle$  is a function of the plasma temperature  $T$  only (see Fig. 4.2). The confinement parameter  $n \tau_E$  required for steady-state burning depends on  $T$  and also on  $Q_p$  (plasma  $Q$ -value), and is shown in Fig. 4.3. Only unknown quantity is  $\tau_p / \tau_E$ , the ratio of two confinement times. It is obvious that  $\tau_p \geq \tau_E$  because the power loss due to the transport  $3nkT/\tau_E$  contains the contribution from convection (i.e.,  $1/\tau_E = 1/\tau_p + 1/\tau_{\text{conduction}} + \dots$ ). So, if an arbitrary value above unity (e.g., 2–3) is used for the confinement time ratio  $\tau_p / \tau_E$ , a rough estimate of the fractional burn-up  $f_b$  is obtained.

Figure 4.6 shows  $f_b$  for the case of  $Q_p = \infty$  as a function of plasma temperature. The value of  $f_b$  increases with the temperature. Larger confinement time ratio  $\tau_p / \tau_E$  gives larger  $f_b$ . When  $kT = 20$  keV (10 keV) and  $\tau_p / \tau_E = 2$ , for example,  $f_b \approx 7\%$  (4%). If  $\tau_p / \tau_E$  were set to be unity,  $f_b \approx 3\%$  (2%); almost the same  $f_b$  values were previously derived by Stacey [12], where the operating regime of D-T fusion plasma was discussed under the condition that  $B = 10$  Wb/m<sup>2</sup>,  $\beta = 5\%$ , and  $\tau_p = \tau_E$ . In a recent report [13], based on considerations from more engineering side, the value of  $f_b$  has been estimated to be about 6% when  $kT = 20$  keV.

**Fig. 4.6** Fractional burn-up of DT fuel in MCF core plasma as a function of temperature



In reactor engineering studies, it may be usual to use the *burning efficiency*  $F_B$  which is defined as the ratio of burned fuel to the throughput fuel. The relation between the fuel throughput (per unit time per unit volume)  $S_{\text{thr}}$  and our injection rate  $S_{\text{inj}}$  used in Eq. (4.41) is  $S_{\text{inj}} = S_{\text{thr}} \times \eta_f$ , where  $\eta_f$  is the *fueling efficiency*, the fraction of throughput fuel that gets to the core region. Thus,  $F_B = \eta_f \times f_b$  and  $\eta_f < 1$ . Although unknown at present, the fueling efficiency  $\eta_f$  is one of the important parameters for reactor system design.

Actually, a fusion reactor will be operated at  $Q_p < \infty$ , a state below self-ignition. Lower  $Q_p$  gives smaller  $f_b$  because the value of confinement parameter  $n\tau_E$ , appearing on the right-hand side of Eq. (4.43), becomes small with decreasing  $Q_p$ . Thus, in MCF, the burning efficiency would be less than 10 % even when the perfect fueling ( $\eta_f = 1$ ) should be attained.

Let us turn to the case of ICF fuel. We here suppose again a compressed DT plasma sphere which has uniform density  $\rho$  and temperature  $T$  at time  $t = 0$ , with a free boundary at radius  $R_f$ . The fractional burn-up of fuel  $f_b$  is then obtained from

$$f_b = \frac{n_0 - n(\tau_{\text{eff}})}{n_0}, \quad (4.44)$$

where  $n(t)$  is the number density of the fuel ions at time  $t$ ,  $n_0 = n(0)$ , and  $\tau_{\text{eff}}$  is the effective confinement time given by Eq. (4.32). The rate of fuel depletion due to fusion reactions is

$$\frac{dn}{dt} = -\frac{1}{2}n^2\langle\sigma v\rangle. \quad (4.45)$$

To integrate Eq. (4.45) with the initial condition  $n(0) = n_0$ , we assume that the temperature in main part of the plasma sphere does not change within the confinement time  $\tau_{\text{eff}}$ . Then,

$$n(t) = \frac{n_0}{1 + \frac{1}{2}n_0\langle\sigma v\rangle t}. \quad (4.46)$$

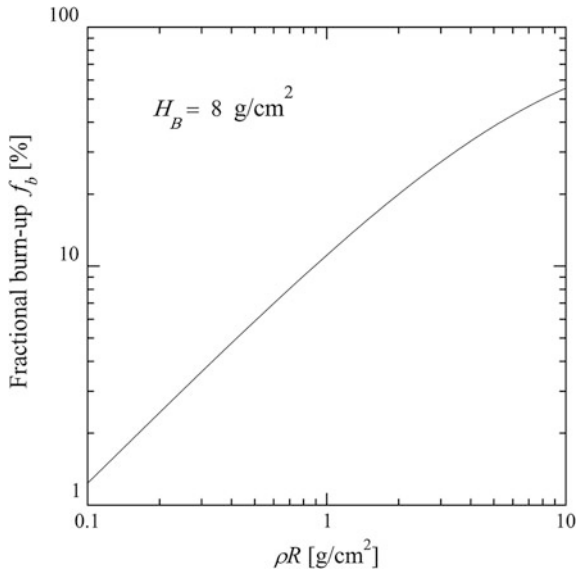
Substituting this  $n(t)$  into Eq. (4.44), we obtain

$$f_b = \frac{\frac{1}{2}n_0\langle\sigma v\rangle\tau_{\text{eff}}}{1 + \frac{1}{2}n_0\langle\sigma v\rangle\tau_{\text{eff}}}. \quad (4.47)$$

Using Eq. (4.33), the fractional burn-up is rewritten in the following form:

$$f_b = \frac{\rho R}{\rho R + H_B}, \quad (4.48)$$

**Fig. 4.7** Fractional burn-up of compressed DT fuel as a function of confinement parameter



where  $H_B$  is the *burn parameter* defined by

$$H_B = \frac{8m_i C_s}{\langle \sigma v \rangle}. \quad (4.49)$$

The burn parameter is a weakly varying function of the plasma temperature. When  $kT = 20\text{--}100$  keV,  $H_B = 7\text{--}10$  g/cm<sup>2</sup>. Here, we choose  $H_B = 8$  g/cm<sup>2</sup> as a reference value.

As is illustrated in Fig. 4.7, the fractional burn-up  $f_b$  is a monotonic increasing function of  $\rho R$ , ‘confinement parameter’ of the compressed fuel. When  $\rho R = 0.3$  g/cm<sup>2</sup>, which is a minimum of  $\rho R_{\text{hot}}$  for ‘self-heating,’  $f_b \approx 3\%$ . In future ICF reactors,  $\rho R$  values of compressed fuel would be of 2–3 g/cm<sup>2</sup> and hence  $f_b = 20\text{--}30\%$ . Conversely, in order to burn about 30 % of the fuel,  $\rho R \approx 3$  g/cm<sup>2</sup> is required. Thus, the fractional burn-up of ICF reactor fuel is one order of magnitude larger than that of MCF fuel.

## 4.6 Summary

Over the past 50 years, tremendous progress has been made in MCF research. Plasma conditions near the breakeven ( $Q_p = 1$ ) were achieved in major three tokamaks, and the achieved values of fusion triple product are within a factor of 10 of that required for large-scale fusion power production. The next step is to be taken by ITER. Its major goal is the realization of burning plasma or, more definitely, the

production of fusion power of  $\sim 500$  MW at a state that  $Q_p \approx 10$  for several hundred sec. The possibility to let flow fully steady current in the plasma will also be tested. Another important objective is to confirm the reactor engineering issues, one of which is handling of kg-class tritium as a fuel.

ICF has also advanced with impressive progress including the fuel compression to high densities, the increase in laser driver power, the completion of major facilities, and the proposal of alternative approaches. In 2013, NIF achieved an important milestone; it was confirmed that the *fuel gain* (the ratio of fusion energy released to the energy applied to fuel capsule) exceeded unity for the first time [14], although the energy gain  $G$  of the target still remains to be of the order of  $10^{-2}$ . Anyway, the first *fusion ignition* will be achieved by ICF.

A further step beyond ITER or NIF is taken by considering a fusion demonstration facility. In MCF, for example, the major research and development issues would include the following: validation of predictability and controllability for burning plasmas, design and development of plasma facing components capable of long-range operation at high-power density, development of breeding blankets, and materials technology for high neutron irradiation. Clarification of the physics of plasma confinement is still the most important issue. In particular, establishment of a scaling law for the particle confinement time  $\tau_p$  as well as clarification of the fueling efficiency  $\eta_f$  is quite important in relation to the fuel cycle and reactor system design.

It would be useful to note again that the fractional burn-up  $f_b$  of MCF fuel in core plasmas remains below 10 %. Accordingly, the burn efficiency  $F_B (= \eta_f \times f_b)$  would be less than 10 % even when the perfect fueling (i.e.,  $\eta_f = 1$ ) should be attained. In contrast, the fractional burn-up of ICF reactor fuel is one order of magnitude larger than that of MCF fuel.

To put the fusion energy into use, conceptual design studies of several demonstration reactors are vigorously being done. In the studies, increase in efficiency in both fueling and burning is ‘must’ to keep fuel self-sufficiency together with insuring T safety as discussed in Chap. 3.

**Acknowledgments** The author would like to acknowledge useful comments and discussions with Dr. M. Nakamura (Japan Atomic Energy Agency), Assoc. Prof. T. Johzaki (Hiroshima Univ.), and Assoc. Prof. H. Matsuzura (Kyushu Univ.), and also thank Dr. V.T. Voronchev (Moscow State Univ.) and Prof. T. Tanabe (Kyushu Univ.) for helpful suggestions and a critical review, respectively.

## References

1. D.D. Clayton, *Principles of Stellar Evolution and Nucleosynthesis* (University of Chicago Press, Chicago, 1968)
2. H.S. Bosch, G. Hale, Nucl. Fusion **32**, 611 (1992)
3. W.M. Stacey Jr., *Fusion: An Introduction to the Physics and Technology of Magnetic Confinement Fusion* (Wiley, New York, 1984)

4. J. Wesson, *Tokamaks*, 3rd edn. (Clarendon, Oxford, 2003)
5. For example, J.D. Jackson, *Classical Electrodynamics* (John Wiley and Sons, 1962)
6. M. Greenwald, J.L. Terry, S.M. Wolfe, S. Ejima, M.G. Bell, S.M. Kaye, G.H. Neilson, Nucl. Fusion **28**, 2199 (1988)
7. J.D. Lawson, Proc. Phys. Soc. **70B**, 6 (1957)
8. For example, D. Meade, Nucl. Fusion **50**, 014004 (1992)
9. S. Atzeni, J. Myer-ter-Vehn, *The Physics of Inertial Fusion* (Clarendon Press, Oxford, 2004). See also, H. Azechi, *Concept of Laser Fusion*, in J. Plasma Fusion Res. **81**, Suppl., 2 (2005) in Japanese
10. E.I. Moses et al., Nucl. Fusion **49**, 104022 (2009)
11. For example, M. Tabak et al., Nucl. Fusion **54**, 054001 (2014)
12. W.M. Stacey Jr., Nucl. Fusion **13**, 843 (1973)
13. D. McMorrow, *Tritium*, JSR-11-345 (JASON Program Office, The MITRE Corporation, Virginia, Nov. 2011)
14. O.A. Hurricane et al., Nature **506**, 343 (2014)

# Chapter 5

## Behavior of Fuels in Reactor

Tetsuo Tanabe

**Abstract** This chapter is devoted to describe the behavior of fuels (D and T) in a reactor vessel. As given in Chap. 3, D and T are fueled in a reactor vessel with gas-puffing, pellet injection, or NBI. Among the total fuel throughput, only a few % are going into burning plasma, confined with the particle confinement time of a few second and exhausted or recycled. While the remaining part of the throughput is transported through scrape-off layers surrounding the burning plasma to evacuation pumps. Hence, all surfaces of the reactor vessel are exposed to neutral fuel gas with a pressure of a few Pa at the first wall and a few tens to a few hundreds Pa at the divertor. In addition, plasma facing surfaces are exposed to energetic particles, both ions and charge exchanged neutrals escaping from the plasma. The interaction of the gas with the surface is not special but just those occurring in a container with hydrogen gas inside. However, the interactions with the energetic particles and the plasma facing surfaces give significant effect both to the plasma and to the surfaces. A terminology “plasma wall interaction or plasma surface interaction” is often used for the interactions of energetic particles with surface but seldom to include the interactions of thermalized or residual gas with surface. Accordingly, the fuel retention in the plasma facing wall, which is quite important for T safety and fuel self-efficiency, is not understood well and quite difficult to evaluate, as already discussed in Chap 3.

**Keywords** Erosion · Deposition · Plasma facing surface · Plasma surface interactions · Retention · Recycling · Tritium · Deuterium · Carbon · Tungsten

---

T. Tanabe (✉)

Interdisciplinary Graduate School of Engineering and Sciences, Kyushu University,  
6-1, Kasuga Koen, Kasuga, Fukuoka 816-8580, Japan  
e-mail: tanabe@nucl.kyushu-u.ac.jp

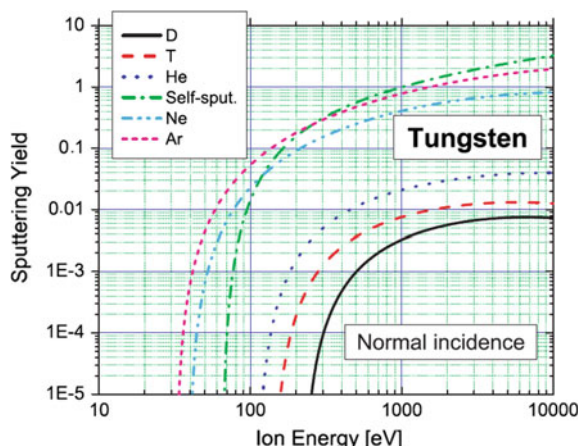
## 5.1 Erosion and Impurity Production by Plasma Wall Interactions

### 5.1.1 Physical Sputtering

Plasma facing surfaces are exposed to energetic particles escaping from plasma as well as residual gas mostly composed of fuels (D and T). When the energy of the impinging particles exceeds the threshold energy to displace surface atoms, the surface atoms are sputtered to leave the surface, which is referred to as physical sputtering. The threshold energy is larger for heavier surface atoms, and sputtering yield is larger for heavier impinging particles. Since plasma always contains impurities such as carbon (C), oxygen (O), and helium (He) produced by D-T reactions, the physical sputtering by these impurities is significantly larger than that by fuel ions. Figure 5.1 shows sputtering yields of tungsten (W) [1] by hydrogen and some impurities, which is most likely to be used as the plasma facing surface of a fusion reactor. The sputtering yields by hydrogen isotopes are by far less than those by the impurities including the self-sputtering. Therefore, the sputtering by the impurities is the main cause of both erosion of the plasma facing surface and plasma contamination by sputtered atoms.

The sputtered atoms are ionized in boundary plasma (or scrape-off layers). The ionized atoms successively gyrate along the magnetic field lines and mostly returned to the surface to be redeposited nearby (referred to as prompt redeposition) or transferred along the scrape-off layers to be redeposited somewhere on the plasma facing surface and shadowed area, and/or exhausted from the reactor. Some of the ionized atoms penetrate deep into plasma and confined as impurity ions. Repetitive processes of erosion by sputtering and redeposition cause long-range material transport. Those redeposited at plasma shadowed surfaces such as gaps of plasma facing tiles and vacuum ducts are simply piled up without resputtering.

**Fig. 5.1** Sputtering yields for tungsten by hydrogen and some impurities at normal incidence angle (reprinted with permission from [1])



In the redeposited layers, fuel particles are easily incorporated, often referred to as codeposition with fuel particles. Therefore, the incorporation of the fuel in the redeposited materials at the plasma shadowed area is the dominant cause of T retention in the reactor vessel (in-vessel T retention) and concerned.

### 5.1.2 Chemical Sputtering

When plasma facing wall is made of materials reactive to hydrogen, like carbon, material surface can be eroded by chemical reaction with hydrogen (chemical sputtering) producing volatile reaction products, like  $\text{CH}_4$ , additionally to physical sputtering. Figure 5.2a shows the incident energy dependence of carbon sputtering

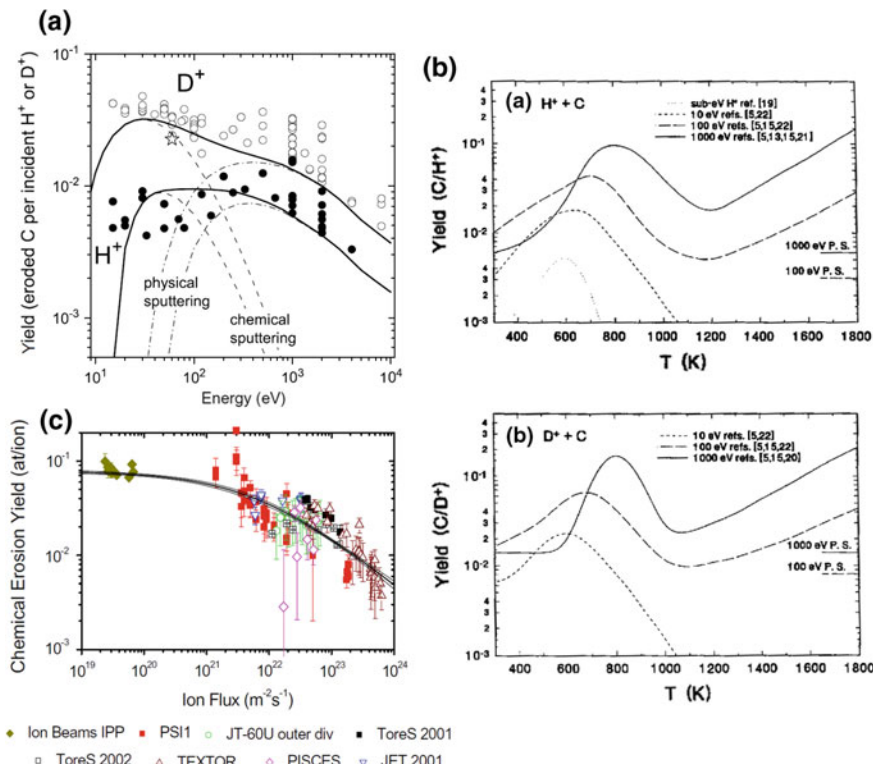


**Fig. 5.2** a Sputtering yields for carbon by hydrogen (reprinted with permission from [2]), b erosion yields due to hydrogen and deuterium impacts of carbon according to Haasz and references therein (reprinted with permission from [3]), and c flux dependence of the chemical erosion yield of carbon for maximum erosion temperature and 30 eV  $\text{D}^+$  determined from different plasma experiments (reprinted with permission from [3])

by H and D ions with the separation of physical sputtering and chemical sputtering [2]. One can see that the chemical sputtering dominates at lower incident energies without the thresholds. Since the chemical reactions between H and C change with temperature, the chemical sputtering yields of C show strong temperature dependence with its maximum yield at around 800 K as shown in Fig. 5.2b [3]. This is because the reaction rate to produce  $\text{CH}_4$  increases with temperature, while  $\text{CH}_4$  becomes unstable at higher temperatures. The decomposition of  $\text{CH}_4$  is used to manufacture pyrolytic carbon and diamond films. Different from physical sputtering, chemical sputtering of C shows flux dependence as shown in Fig. 5.2c [3]. With increasing the ion flux, the chemical sputtering yields significantly decreases. In reactor condition with the ion flux of nearly  $10^{24}/\text{m}^2\text{s}$ , more than one order of magnitude less than those for lower flux. The reason for the reduction is not fully understood, yet.

The chemical stability of C–H bond is also the cause of the H incorporation in carbon-redeposited layers or high H retention. Since  $\text{BeH}_2$  is observed when Be is exposed to H plasma [4], chemical sputtering and enhanced retention are caused by redeposited Be layers. Erosion and redeposition of Be are quite important in JET [5], because Be is used as the first wall. However, its low melting temperature does not allow to use Be as the first wall in a fusion reactor and no discussion for Be as PFM is given in this book. Be is used as neutron multiplier in blanket system as given in Chaps. 6 and 12.

Hydrocarbons, mainly methane, as the products of the chemical erosion of C, are emitted to plasma and ionized. But most of them are promptly redeposited by gyration in strong magnetic field at the vicinity of the eroded area to make redeposited layers. (prompt redeposition). It should be noted that hydrogen concentration (in H/C atomic number ratio) in redeposited layers is different from the ratio of incident fluxes of H and C. Because hydrogen flux impinging to the surface ( $\phi_H$ ) is much larger than impinging carbon flux ( $\phi_C$ ), i.e.,  $\phi_H/\phi_C \gg 4$ , the maximum H/C in stable hydrocarbons, most of incident hydrogen is reemitted. Accordingly, H/C in the redeposited layers is controlled by their temperature; the higher the temperature, the lower the H/C. This is the reason to use “redeposition and redeposited layers” but not “codeposition and codeposited layers” in this book. If H/C exceeds around 1, the layers become volatile, resulting in the chemical sputtering.

In present tokamaks, as shown in Fig. 5.3, most of the first wall and the outer divertor are eroded and the inner divertor redeposited. Repetitive processes of erosion and redeposition transport carbon eroded at the outer divertor and the first wall to the inner divertor. At plasma shadowed area, such as gaps of armor tiles and pumping ducts, the redeposited layers are not subjected to plasma and continue to grow in their thickness. Large erosion by chemical sputtering and large T retention in the redeposited layers are the main reasons to exclude carbon materials as its PFM in ITER.

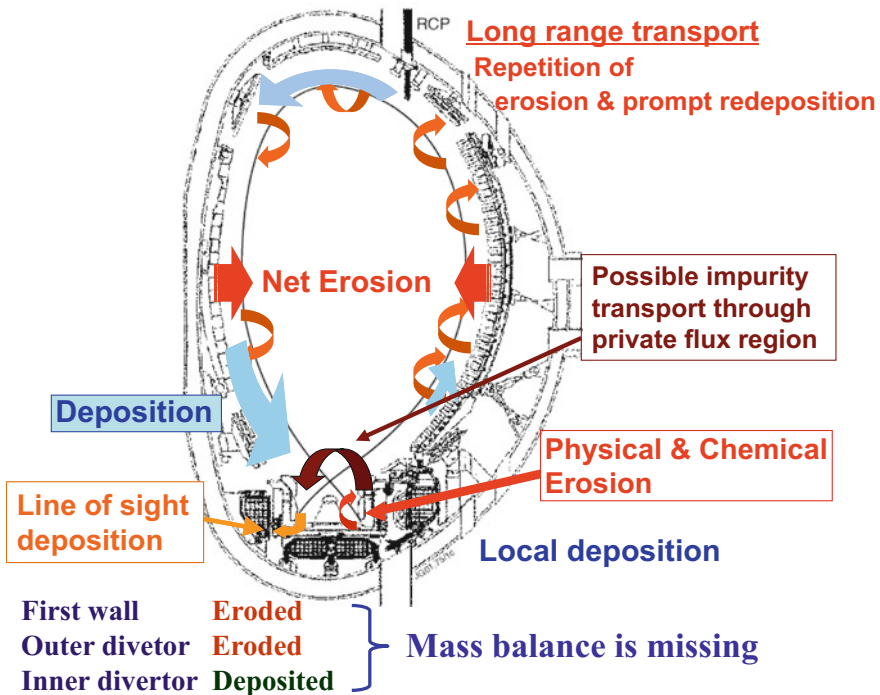
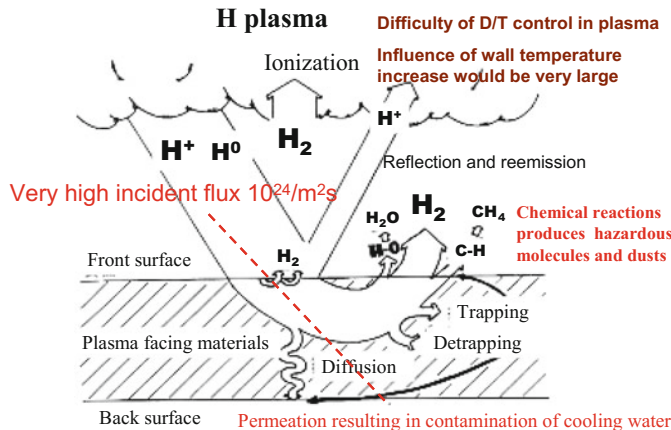


Fig. 5.3 Erosion, deposition, and materials transport in Tokamak

## 5.2 Hydrogen Recycling at Plasma Facing Surface

### 5.2.1 Metals

Hydrogen recycling at plasma facing surface (PFS) has been quite important for density control or maintaining plasma in good condition. In general, low recycling scheme, i.e., most of the impinging fuel particles being retained in plasma facing materials (PFM) with little reemission (referred to as wall pumping), is favorable for easy density control by fueling only. In order to attain the large wall pumping, in most of the present tokamaks, “wall conditioning” to remove hydrogen retained in PFS has been routinely made by He discharges after certain numbers of main plasma discharges [6]. However, long-pulse or steady-state operation in a fusion reactor would not keep the low recycling regime, and fuel accumulation in PFS continues to increase up to the saturation of fuels in PFS. This means plasma operation in high recycling regime is dispensable, which is not well established yet and one of the important research targets in ITER. Accumulation of the fuel particles in PFM means large T inventory, which also concerns for T safety and fuel self-sufficiency, as already discussed in Chap. 3. Although techniques developed for the wall conditioning may be used to reduce the T inventory, processing or



**Fig. 5.4** Schematics of behavior of hydrogen at plasma facing wall [7]

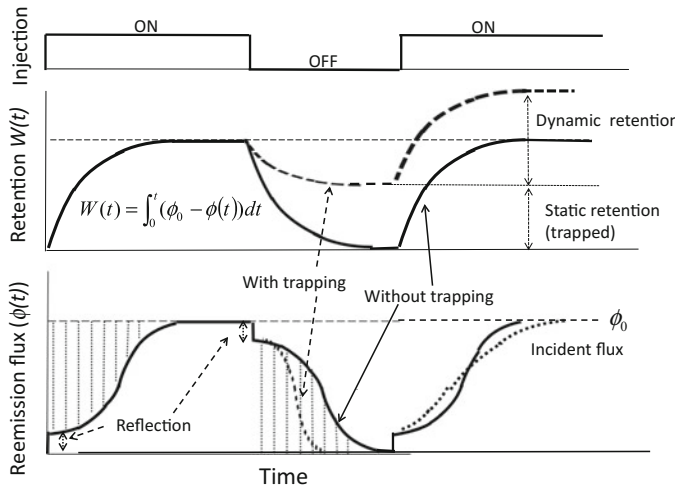
refinement of removed T is concern, for example, He grow discharge results in huge amount He gas containing T becoming unwanted load on refinement of exhausted fuels.

Figure 5.4 shows the general features of hydrogen recycling at PFM (metals) [7]. Energetic hydrogen ions and neutrals escaping from plasma impinge to PFS. Except directly reflected ones which are a few tens % of the impinging flux, the impinging fuel ions and neutrals are injected into the material within a certain depth referred to as projected range (varied depending on the incident energy). Most of the injected fuel particles diffuse back to the front (injected) surface (reemission), and remaining migrates or diffuses in to be dissolved or trapped, and permeates to the back surface to be released as  $H_2$  molecules.

Figure 5.5 schematically shows time sequences of reemission flux of injected fuels from the plasma facing wall and retention in the wall. Except direct reflection of incident particle, the figure is quite similar to Fig. 3.3 in Chap. 3. The reemission flux increases with time and finally comes to the steady state where the impinging particle flux balances with the reemitted flux plus the permeated flux. Generally, the latter is quite small and not considered for fuel recycling but does matter for T safety as discussed later. Dotted area in the figure corresponds to the amount of the fuel particles retained (dissolved and trapped) in PFM

$$W(t) = \int_0^t (\phi_0 - \phi(t)) dt \quad (5.1)$$

and plotted in the middle of the figure. If there is no H trapped, all retained are subsequently released after the termination of the injection. While if some are



**Fig. 5.5** Schematics of reemission and retention of implanted fuel particles

trapped as indicated as bold dotted lines in the figure, the reemission after the termination of the plasma exposure decays earlier than that without the trapping.

Because energetic fuel particle injection produces new defects in PFM, which can trap fuels subsequently injected, the true steady state is hardly attained. Nevertheless, the retention rate or difference between the injected flux and reemitted one becomes less and less toward the saturation. Hence, after a certain time of the injection, the remitted flux becomes nearly constant equivalent to the incident flux. However, the integrated amount of the retained flux or the injected fluence becomes quite large. It is quite difficult to evaluate  $W(t)$  accurately after the long time of plasma exposure. In principle, the integration of the flux balance Eq (5.1) gives the  $W(t)$ . However, the accuracy of the measurements of  $\phi(t)$  only 2 to 3 digits does not allow the reliable evaluation of  $W(t)$ .

As indicated in the figure, the total retention during the injection includes two components: “dynamic retention” and “static retention.” The former is directly connected to the fuel recycling and the latter to the T inventory. The latter decreases with increasing temperature, because trapped fuels can be detrapped thermally. Irradiation of energetic ions and neutrons produces various defects such as interstitials and vacancies, their clusters or dislocation loops, and bubbles, which work as additional trapping sites to increase significantly the static retention or in-vessel T inventory, especially for W [8].

Although the permeated flux is tiny compared to the injected flux, the permeated T in the cooling water is concerned for safety and free permeation is not allowed. Hence, the formation of permeation barrier is an important R&D task [9], which is described in Chap. 9.

### 5.2.2 Carbon Materials

Reemission behaviors for carbon and metals are basically similar as described in Fig. 5.5. However, the reemission for carbon materials (C) includes methane resulting from chemical sputtering and causing significant surface recession (erosion). In addition, retention properties in C are quite different from those of metals. As shown in Fig. 5.5, significant amount of injected fuels into the metals is released after the termination of the injection, i.e., the difference between the dynamic retention and the static retention is not large. In contrast, injected H in C is trapped near the projected range making C–H bond, and very small diffusivity in C inhibits the migration of H into the bulk, while their porous nature allows hydrogen molecules to penetrate deep through open pores, resulting in hydrogen profiles given in Fig. 5.6. This means that residual fuel gases in a reactor vessel can penetrate through the whole thickness of a carbon tile, resulting in all carbon grain surfaces being saturated with hydrogen. However, H can hardly penetrate through the grains. Actually, T was observed at the back side of carbon tiles used in DT discharge campaign in JET Mark-IIA divertor [10].

As shown in Fig. 5.4, recycled hydrogen including reflected ions and neutrals, and reemitted molecules easily return to plasma. If some impurities such as carbon and oxygen exist on the plasma facing surface, reemitted hydrogen can react with them to make hydrogen compounds such as  $\text{CH}_4$  and  $\text{H}_2\text{O}$ , respectively. In C, impinging hydrogen is bound to carbon atoms until the hydrogen concentration

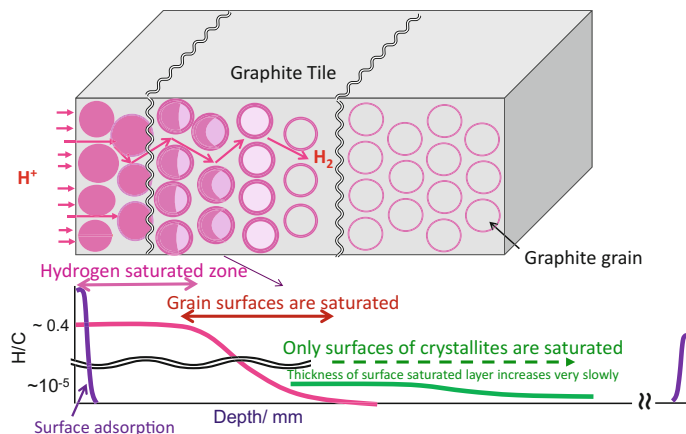


**Fig. 5.6** Mechanism of H retention in carbon materials. Different from metals, the carbon materials are constructed of graphite like grain particles and fillers to be filtrated. H Migration of H impinging to them can be separated to two different schemes. One is directly impinging into the particles. But diffusion is too slow for H to penetrate deeper than its projected range. The other is penetration  $\text{H}_2$  molecules recombined at the particle surfaces into deep inside through open pores among the particles. Therefore two different depth profiles appear; one as that in the particles and the other in whole depth of the material

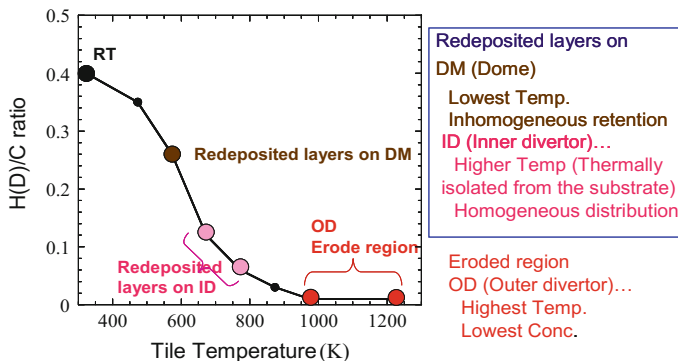


**Fig. 5.7** Temperature dependence of observed D/C ratio in eroded and redeposited plasma facing carbon tiles of JT-60 together with a saturation concentration of H (given by atomic ratio of H and C ( $H/C$ )) implanted in carbon. [18]

attains a saturation level (see Fig. 5.7). The saturation concentration in C at RT is as high as  $\sim 0.4$  in  $H/C$  atom ratio. Hence, the full coverage of plasma facing surfaces by C would result in significantly large T inventory, and the utilization of C as PFM is excluded in ITER.

When hydrogen concentration exceeds the saturation concentration, H subsequently impinging is either recombined to be reemitted as  $H_2$  molecules, or released making volatile hydrocarbons such as  $CH_4$ , which is the origin of the chemical sputtering. Furthermore, the hydrocarbons produced by the chemical sputtering enter into boundary plasma and impinge again to make redeposited carbon layers. Repetitive processes of erosion and deposition cause long-range transfer of carbon atoms, and as a whole, the first wall is mostly eroded and the inner divertor and plasma shadowed area are deposited as shown in Fig. 5.3. Redeposited carbon layers on the plasma shadowed area are saturated with H and D, which become the dominant in-vessel T inventory as discussed in the next section.

Since any hydrocarbons are not stable at elevated temperatures, which is the reason for the reduction of chemical sputtering above around 800 K, the saturation concentration at elevated temperatures decreases appreciably and becomes similar level to that of metals (See Fig. 5.7).

Irrespective of metals or C, the wall inventory is larger by several orders of magnitude than the total number of fuel particles in plasma. Hence, only tiny change in the wall inventory strongly influences the plasma performance, and accordingly, the density control of plasmas becomes difficult for the saturated walls. This is the reason why the low recycling or wall pumping scheme, i.e., small reemission before the establishment of the steady state is preferred to obtain good plasma confinement. Since long-pulse or steady-state operations exclude the low recycling regime, it is one of the most important tasks of ITER to confirm the steady-state operation with the saturated wall being possible.

In the following, H retention and carbon deposition in present large machines are summarized. Unfortunately, little systematic data for H retention with metallic

plasma facing wall are available. Now, JET is operating with W divertor and Be first wall. Compared to the full carbon wall of the previous JET, the metallic wall results have shown larger dynamic retention and less static retention [11]. The results are quite reasonable, corresponding to larger diffusion in metals allowing deep penetration during the discharge to enhance the wall pumping and easy desorption after the discharge.

## 5.3 Hydrogen Retention and Carbon Deposition in Present Tokamaks

### 5.3.1 *Summary of Deuterium Retention in Present Tokamaks Using D Discharges*

Current estimation of T retention in ITER is based on the studies of D retention in tokamaks with DD discharges (deuterium plasma heated by deuterium neutral beam), of which plasma facing surfaces are mostly composed of C. The results of these studies are summarized in this section [12–15].

In most tokamaks, as already discussed, carbon tiles at outer divertor area are eroded and those at the inner divertor area deposited by the eroded carbon. But materials balance between the erosion at the outer divertor and the deposition at the inner divertor is missing as shown in Fig. 5.3. The former is less than the latter, and the missing mass is likely compensated by erosion at the first wall of the main chamber, for which no systematic measurements have been made. The carbon redeposition occurs by repetitive processes of erosion and prompt redeposition of the eroded carbon as already discussed. In addition, there appears line-of-site deposition at remote areas from plasma, tile gaps or tile sides, and divertor opening for pumping. The deposition in tile gaps is much larger for surface-eroded tiles compared to that for surface-deposited tiles [16], which is the evidence of prompt redeposition of eroded materials.

D is incorporated in the redeposited layers. But this is not due to simultaneous deposition (codeposition) of eroded carbon with D. The concentration of D in the redeposited layers is modified afterward. Generally, injecting D flux to PFM from plasma is significantly higher than that of impurity carbon flux. Accordingly, most of the injected D is spontaneously reflected and/or reemitted and only part of the incoming D remains in the redeposited C layers with a saturation concentration of 0.4 in D/C at maximum (see Fig. 5.7) [17, 18]. Except far-remote area from plasma, the redeposited carbon layers are subsequently exposed to boundary plasmas. Moreover, if the temperature of the redeposited carbon layers is raised, part of the retained D is desorbed [16].

The situation for the eroded region is the same, i.e., the surface is saturated with D with the saturation concentration determined by the surface temperature but not the injected flux ratio of D and C. In eroded area, because of the surface recession, the thickness of the surface-saturated layers would be limited only at near-surface

regions and would not linearly increase with time [19]. It also suggests that the isotopic ratios of retained hydrogen near-surface layers are always equilibrated with those of the incoming hydrogen isotope fluxes (H/D/T), when different hydrogen isotopes are impinging. And the depth attaining this equilibrium is quite thick owing to the porous nature of carbon materials, and is increased by temperature rise. Hence, D retention in plasma facing surfaces (both eroded and redeposited) would be significantly reduced by isotopic replacement by HH discharges subsequently made after DD discharges as observed in JT-60U [19].

Table 5.1 summarizes carbon deposition and D retention rates in current tokamaks [12–15]. As seen in the table, the fuel retention rates of 3–50 % are found using gas balance measurements. A lower retention rate ( $\sim 10\%$ ) is often obtained using postmortem analysis of plasma facing tiles. Since carbon erosion and deposition rates are nearly the same for most tokamaks, the fuel retention rates are totally dependent on the temperatures of plasma facing surface or operation temperature owing to the temperature dependence of the saturation concentration of H in the redeposited layers. Accordingly, JT-60U operated at the highest temperature (523–573 K) shows the lowest retention rate. Sometimes, JT-60U showed wall saturation, i.e., 0 % retention rate.

**Table 5.1** Carbon deposition and fuel retention rates in current large tokamaks [12–15]

Device/campaign	Carbon deposition rate (C/s)	Fuel retention rate (D-T/s)	Fuel retention fraction	Remarks
JETMK-IIA divertor (DTE)	$6.5 \times 10^{20}$	$5.8 \times 10^{20}$ (D/C = 0.8)	0.17 (in DTE1) 0.11 (in DTE2)	– T retention after non-mechanical cleaning – T retention after long-term outgassing and mechanical removal of accessible T deposit
JETMK-IIB divertor (DTE)	$4.3 \times 10^{20}$	$1.25 \times 10^{20}$ (D/C = 0.3)	0.03	– D retention from postmortem analysis
TFTR DT Campaign			0.16	
ASDEX-Upgrade (DD)	$3.5 \times 10^{20}$		0.035 0.1	– D retention from postmortem analysis – D retention from fuel balance
TEXTOR (DD)	$2.5 \times 10^{20}$	$1.6 \times 10^{19}$	0.08	– D retention from postmortem analysis
Tore Supra (DD)		$2.5 \times 10^{20}$	0.5	– D retention from fuel balance in dedicated long-pulse discharges
JT-60U (DD)	$3 \sim 6 \times 10^{20}$ (only plasma facing area)	$5.3 \times 10^{18}$ (D/C = 0.02)	0.0 (for saturated wall)	– Wall saturation appeared at 573 K operation

DD D discharges with D NBI heating

Unfortunately, ITER will be operated at around 423 K, which is much lower than the reactor operation temperature (above  $\sim 700$  K) or even that of JT-60U (573 K). Accordingly, D retention in its redeposited carbon layers would be significantly large. Other tokamaks (except JET) operated at near RT show similar retention rates of 10–20 %. The largest retention was observed in Tore Supra, which has water-cooled divertor/limiter blades at the bottom of its tokamak vessel [20].

### **5.3.2 Tritium Retention on Plasma Facing Materials Caused by DT Experiments in TFTR and JET**

The first DT plasma operation or introduction of T in D plasmas was done at 1993 in TFTR in which most of plasma facing surfaces were covered by carbon armor tiles [21]. One of the most important information from the DT operation is that around 20 % of T introduced was remained in the TFTR vessel in spite of significant effort to remove it [22]. A very high fuel retention rate of  $\sim 50$  % was also observed in Tore Supra operated at RT in Table 5.1. This confirms that appreciable amount of T is retained in the redeposited layers, which are continuously growing on plasma shadowed area (no erosion) and in tile gaps very near or line of site to eroded tiles.

Following TFTR, JET initiated the full DT shots [23] as a divertor machine (referred to as DTE campaign) and again T incorporation in redeposited carbon layers dominated the in-vessel T retention [24]. Figure 5.8 shows how T was distributed on JET Mark-II divertor tiles used in the DTE campaign [25]. The highest T level was observed on the BN4 tile and the T profile well corresponded to the profiles of the redeposited carbon. In addition, the poloidal sides of the BN4 tile and the BN7 tile as indicated by dotted squares were shadowed from plasma by vertical divertor tiles and covered by thick redeposited carbon layers. Consequently, T levels were very high. The non-uniformities in the T distribution in the redeposited layers as indicated in squares in BN4 and BN7 tiles are mostly due to the exfoliation of the redeposited carbon layers. Behind the redeposited layers, T retention was quite small, which confirms the T retention in the redeposited layers. Furthermore, the toroidal sides of the BN4 and BN7 tiles indicated by the dotted circles were shadowed by neighboring tiles owing to the tile alignment as indicated at the bottom right of Fig. 5.8 and covered by redeposited carbon as indicated in the figure.

### **5.3.3 Behavior of Tritium Produced by D-D Reactions**

During DD plasma discharges, T is produced by D-D reactions. Although the amount of T produced is quite small, both retention and exhaust of T are concerned for T safety. Significant effort was paid to remove T retained in a vacuum vessel

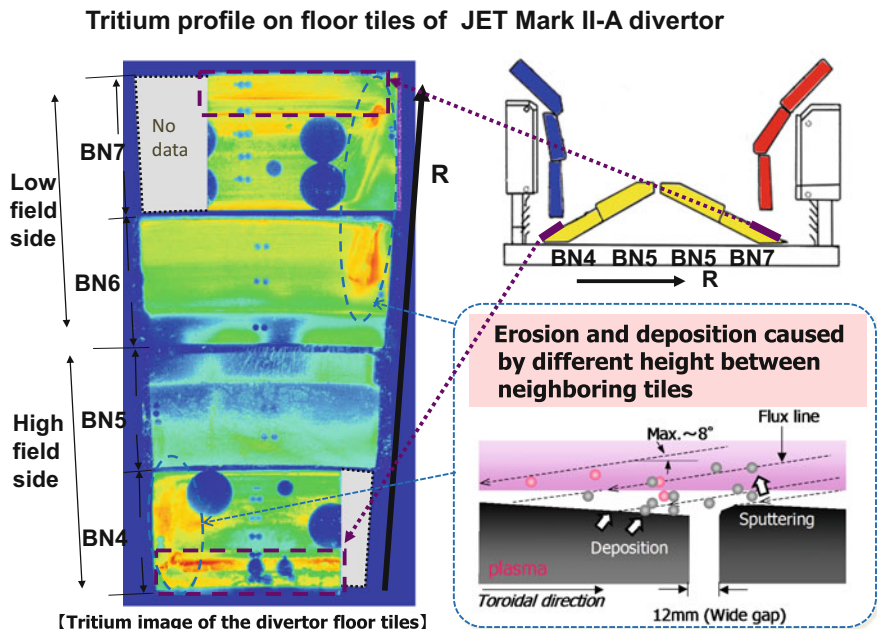


**Fig. 5.8** Tritium retention and carbon deposition on Mark II-A divertor tiles used in DTE campaign in JET [26]. Holes in the T profiles are owing to the drilling of the tile for combustion measurement of T. Non-uniform T distribution on the bottom of BN4 tile (in dotted square) is owing to the exfoliation of redeposited carbon layers remaining little T

after the DD discharges, using HH discharges, He cleaning discharges, and isotopic replacement with HTO (moisture). However, behavior of T attracted little attention, because T was believed to behave similar as H and D. However, retention studies on T produced by D-D reactions in TEXTOR, JT-60U, and ASDEX-Upgrade [26] have shown that T behaves differently from fueled H and D. A significant part of T produced by the D-D reactions, which initially has energy of 1 MeV, did not fully lose their energy in the plasma and directly impinged on the depth of around 10  $\mu\text{m}$  of PFM. Actually, T profiles retained on all PFS surfaces of JT-60U after the DD discharges were quite consistent with the area profiles of calculated impinging flux of high energy T by the OFMC code [11]. Around 10 % of T was directly injected into a little deep and retained with the depth profile shown in Fig. 5.9 [27, 28]. Of course, the remaining T is thermalized in plasma and retained at eroded surface or incorporated in the redeposited carbon layers similarly as H and D. However, those T retained near surfaces were isotopically replaced by H and/or D, subsequently impinging on the surface. Thus, the main part of T retained in the plasma facing tiles after DD + HH discharges in JT-60U was a little deep implanted ones as shown in depth profiles of H, D, and T for an eroded tile of JT-60U in Fig. 5.9. Nevertheless, at plasma shadowed or remote area, T was retained in redeposited

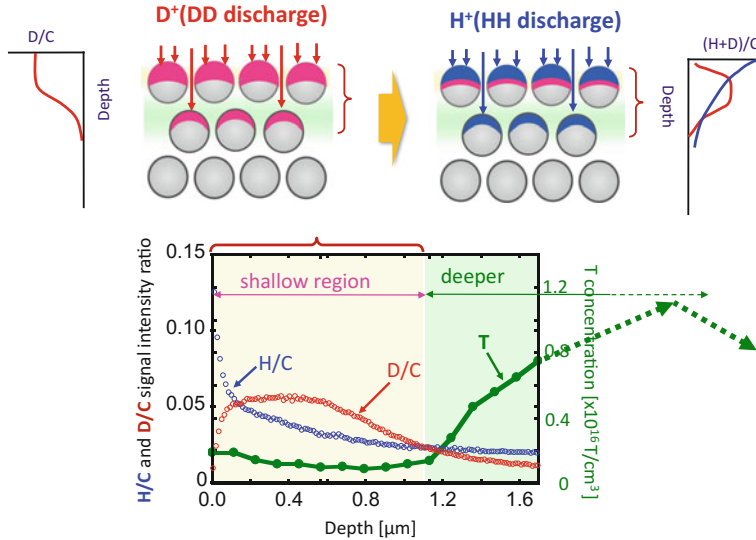


**Fig. 5.9** Depth profiles of H, D, and T in a JT-60 carbon tiles exposed to DD discharges and HH discharges subsequently made for T removal. By the HH discharges, D retained during the DD discharges was isotopically replaced as shown in the top. Note that T concentration is is several orders of magnitude less than H and D concentrations [29]

carbon layers escaping from the isotopic exchange [29]. Therefore, behavior of T produced in DD discharge tokamaks does not directly correlate with that in a D-T reactor.

### 5.3.4 Estimation of In-Vessel Tritium Inventory in ITER

Evaluation of hydrogen retention in present tokamaks is of the highest priority to establish a database and a reference for ITER. Figure 5.10 is the latest evaluation for in-vessel T retention for ITER given by Roth et al. [30]. In the figure, the T retention rate for full carbon covered ITER is  $\sim 20\%$ , which is consistent with the data given in Table 5.1 for most of present carbon tokamaks. Therefore, ITER has decided not to use C divertor in its initial HH discharge phase. Utilization of W divertor instead of the C divertor would significantly reduce the fuel retention rate as seen in the figure. That is owing to less erosion and hence less redeposition compared with C. Only a few hundreds of shots would exceed the allowable level of the in-vessel T inventory and stop ITER operation for T removal, though the estimation in Fig. 5.10 includes very large error and uncertainty.

Another important question not solved yet is whether the fuel retention saturates or not. In Fig. 5.10, two dotted lines indicate linear and square root increases of the

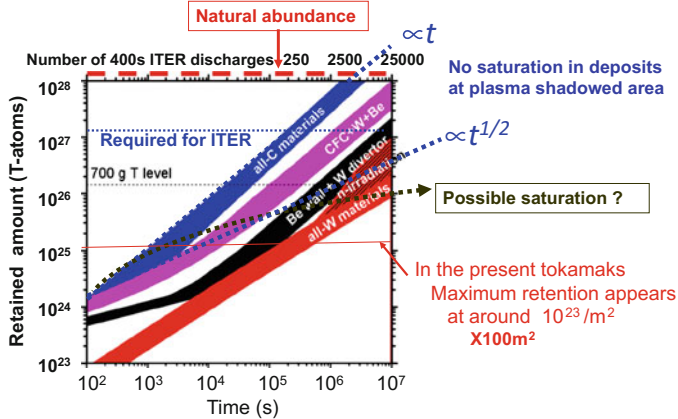


**Fig. 5.10** Estimation of accumulation of T inventory in ITER by Roth et al. [30]

fuel retention with discharge time. In case of the linear increase, the in-vessel T inventory of ITER would exceed the allowable T level after a few thousand shots. The infinite retention increase must not happen, and somehow the retention must saturate. Actually, D in eroded divertor tiles of JT-60U saturates as shown in Fig. 5.7 [18]. Even D in the redeposited layers on plasma facing surfaces seems to saturate (not shown here). However, the redeposition at plasma shadowed area has no chance to be heated or eroded, and the fuel retention would continue to increase.

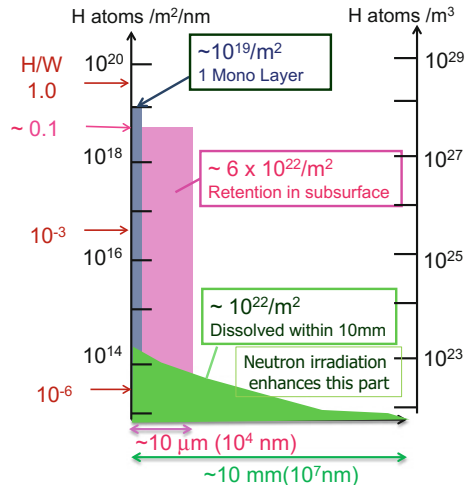
It should be mentioned that T breeding cannot compensate such high T inventory. Hence, reduction of the in-vessel T inventory and/or T removal/recovery is the most important task for the fuel self-sufficiency as well as for T safety as discussed in Chap. 3.

## 5.4 Hydrogen Retention in Tungsten

As described above, in a reactor using C as PFM, incorporation of T in the redeposited C layers dominates overall T retention, while, in a reactor using tungsten (W) as PFM, T retention in redeposited W layers is expected to be much less, owing to low sputter erosion of W by fuels. Nevertheless, bulk retention in W, i.e., T dissolved and trapped in W bulk, is not likely small as that of C. Because diffusion coefficient of T in W is quite large, T easily diffuses in and is dissolved at deep in bulk. Moreover, defects produced by neutron irradiation in the reactor would work as T trapping sites to increase the bulk T retention [31, 32].

Peculiarity of H retention in W appears as significantly large trapping in near surface, making H saturated surface layers with H/W of 0.001–0.1 depending on the temperature [33]. The formation of the surface-saturated layers is attributed to the production of trapping sites by energetic hydrogen injection from plasma and/or

**Fig. 5.11** Schematic of depth profile of H retained in W [33]



stress field caused by highly concentrated hydrogen in W themselves. Figure 5.11 schematically shows the depth profile of H retained in W [33]. The thickness of the surface-saturated layers can grow far over the implanted depth of incident fuel ions. The saturated layers over 100  $\mu\text{m}$  thick could accumulate T over ITER safety limits because of its extremely high flux.

Deep penetration would contribute to the total retention for very high fluences. Neutron irradiation produces additional defects in the bulk [32], which works as trapping sites and enhances bulk retention significantly. Different from C, H dissolved and trapped in W in deeper region would not be easily subjected to isotope replacement. Reemission and permeation at the steady state are not likely to be influenced by trapped T. However, T permeation in W is one of the most important safety concerns, of which details are described in Chap. 9.

## 5.5 In-Vessel T Inventory of a Fusion Reactor

As given in Table 2 of Chap. 3, a little detailed estimation on T inventories has been made for DEMO(J05) at JAERI and a magnetic confinement (MFC) reactor and an inertial confinement (ICF) reactor designed in Japan with output powers of 3 GWth and fuel reserves for 30 days [34]. Though the values in the table include large scattering and uncertainties, the total T inventories in the three reactors for the steady-state operation with 3 GWth and the fuel reserves of 30 days converge to around 20 kg.

Among the inventories in all subsystems, the in-vessel inventory has the largest uncertainty. The inventories in other systems except the breeding blanket are likely extrapolated or interpolated from well-established hydrogen technology. Hence, the

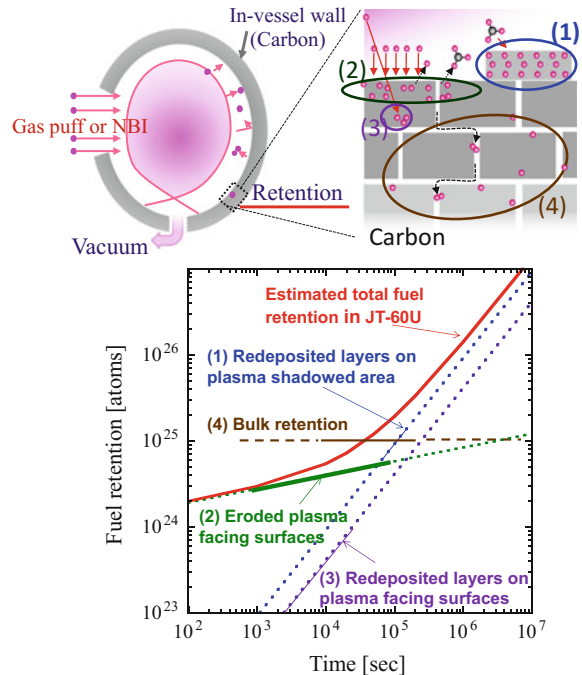
estimation of the in-vessel inventory based on the present knowledge of hydrogen retention in large tokamaks is quite important. However, as already discussed, the present tokamaks have been operated with the wall pumping scheme and the wall retention rates (or pumping rate) in tokamaks using C as their plasma facing walls are quite large as shown in Table 5.1. For the fuel self-sufficiency, such large fuel retention rate cannot be acceptable. The retention rate in a reactor should be less than  $10^{-4}$ . We have to reduce the fuel retention rate more than two orders of magnitude. Again, that is the main reason to exclude C and to employ W as PFM of the reactor. Nevertheless, without knowing the causes or mechanisms of the wall retention, the reduction of the wall retention is hard to realize. In the following, details of the fuel retention mechanism in the present tokamak are described.

### **5.5.1 Fuel (H and D) Retention in Present Large Tokamaks**

In present tokamaks, significant imbalance between throughput and output of fuels (mostly measured by deuterium) is observed, i.e., 5–20 % of the input fuels are continuously retained and immobilized in the vacuum vessel as shown in Table 5.1 [35]. Such in-vessel fuel retention is mostly caused by the incorporation of fuels in redeposited materials (codeposition) at plasma shadowed area. Accordingly, estimation of T inventory in ITER as given in Fig. 5.9 was made based on erosion and redeposition simulations. However, depending on the model and PFM, the estimation scattered more than three orders of magnitude [30].

In order to make more precise evaluation, we have to know the retention mechanisms in detail. For any PFM, the retention mechanisms can be categorized into 4 regimes, i.e., retentions in (1) redeposited layers on plasma facing surfaces and (2) that at plasma shadowed area, (3) eroded area and (4) bulk [36, 37]. Separation of (1) and (2) is only caused by temperature difference; temperature of the former is much higher, and accordingly, the fuel concentration is less than the latter. Figure 5.12 shows how those components change with discharge time in JT-60U; solid lines are measured data, and dotted lines are their extrapolations [38, 39]. It should be noted that this is the only one comprehensive experimental data set for the change of fuel retention with discharge time (fluence) in a whole tokamak with the separation of H and D. Still, the fluence in JT-60U is much smaller compared to that of ITER, and linear extrapolations as indicated by dotted lines are dispensable. Local retention mechanisms of H in C are schematically shown on the top of Fig. 5.12. The largest T retention is incorporation of T with redeposited materials. T retention in the eroded surfaces is generally small, but the total eroded surface areas are quite large, because most of the first wall surfaces in large tokamaks are eroded, and the integrated T retention over the whole eroded area becomes quite large. In JT-60U, the total D + H retention in their eroded area was comparable to that in the redeposited layers. Different from the latter, the retention in the eroded area tends to saturate or grow very slowly. Therefore, in a reactor, the

**Fig. 5.12** Time dependences of fuel retentions divided into 4 components observed in JT-60U. Solid lines are experimentally observed data [16, 36]



T retention in the eroded surface would contribute only to the initial inventory, even though it could account to kg order.

Bulk retention is different depending on the PFM materials. Since C and plasma splayed W coatings are porous, retention at the surface layers of all grains (inner surface) dominate the bulk retention irrespective of the thickness, while penetration (diffusion) through grain is quite different, i.e., more or less no penetration in graphite grain while gradual diffusion in the W layers. Bulk retention in metallic materials is dominated by the penetration into deep by diffusion as discussed in Sect. 5.4, which will result in the increase of the T retention with square root dependence of incident fluence as indicated in Fig. 5.9. Moreover, T retained in the deep inside of the metallic materials is quite hard to remove.

As indicated in Fig. 5.7, saturation concentration significantly decreases with temperature. Considering the operating temperature of a reactor, which should be 700–800 K for electric power generation, the fuel retention rates could be one or two orders of magnitude less than those given in Table 5.1, which were determined for the present tokamaks mostly operated at RT or a little higher. Even so, the fuel retention rate is still too large to attain the fuel self-sufficiency. And recovery of the in-vessel T inventory would be required not only for the T safety but also for the fuel economy. The importance of recovery of the in-vessel T is discussed in Chap. 3.

### 5.5.2 T-Related Issues on the In-Vessel T Inventory

Evaluations of the in-vessel fuel inventory have been mostly done by the integration of local retentions in redeposited layers and/or near surfaces assuming toroidal symmetry in tokamaks. Although the bulk retention should have certain contribution, it has been scarcely assessed. The bulk retention in the plasma facing materials must be very small in its concentration. Nevertheless, its integrated amount over the full volume of the plasma facing materials and vacuum vessel could not be small. Here, the maximum bulk retention for metallic PFM is estimated according to the crude assumptions as follows. It is well known that outgassing rates from metals are ranging from  $10^{-6}$  to  $10^{-3}$  Pa m<sup>3</sup>/m<sup>2</sup> s [38]. Taking  $10^{-5}$  Pa m<sup>3</sup>/m<sup>2</sup> s as the outgassing rate from plasma facing surfaces with their surface area of 1000 m<sup>2</sup>, the total outgassing rate would be  $10^{-2}$  Pa m<sup>3</sup>/s. This seems negligible compared to the max fuel throughput in ITER of 200 Pa m<sup>3</sup>/s. ( $\sim 2.5$  g) [39].

Since the source of the H outgassing is very likely H retained in the materials as impurity, it might be reasonable to assume that tritium uptake in the bulk proceeds just opposite to the outgassing. Then, about  $10^{-2}$  Pa 3/s (0.1 mg/s) orders of tritium would be continuously retained in the bulk, i.e., every ITER discharge (400 s) would remain 0.4 g of T in the bulk and 25,000 shots pile up 1 kg. This estimation is too extreme. However, following another estimation would probe this T pileup scenario is realistic.

Consider that any materials retain H as an impurity with more than 10 ppm. Suppose T can be replaced by the impurity H, though reaction rate totally depends on the diffusion time. Then, 10 ppm T could be dissolved in the bulk at steady state. This suggests that the usage of 1000 tons of structure materials for a reactor could result in 10 kg of T at the maximum. This type of T inventory is well known in the detection of T by an ionizing chamber as a memory effect, i.e., initially introduced T to the ionization chamber and piping disappeared and certain time is required to start the detection, and the detection continues for while after stopping the T introduction as explained in Chap. 3.

From the aspect of T safety, this type of inventory is often categorized to be immobilized T inventory and might not be a serious safety concern, but kg orders of T would disappear in the bulk of structure materials of all T handling systems at the starting phase of every reactor. This will be discussed later again.

Difficulty in conducting the quantitative analysis of T in the in-vessel components adds additional problems. It is ironical that the accuracy in detecting low levels of T (below  $10^9$  Bq) by its  $\beta$  decay is better than that in the very high levels which are determined by mass and/or pressure measurements and calorimetry with the accuracy of only  $10^{-2}$  to  $10^{-4}$  (see Fig. 5.1). In addition, one cannot detect the T existing in solid deeper than a few  $\mu\text{m}$ . The easy isotopic exchange of T with ubiquitous hydrogen in water and hydrocarbons at materials surfaces can significantly affect the analysis.

### 5.5.3 Isotopic Effects

Isotopic effects appear as clear differences in blister formations on irradiated metal surface with H and D ions [40] owing to their different damaging rate. Although isotopic effects in behaviors of D and T should appear not only in plasmas but also in materials, they have been hardly studied. Large mass difference between D and T would give appreciable differences in confinement times, fueling efficiencies, escaping fluxes from plasma, retention rates in materials exposed to DT plasmas, evacuation rates from the vessel, and so on [41]. As described in Chap. 2, the simple kinetic theory suggests the dependences of the square root of the mass ratio of D/T on those properties, but more or less no quantitative data for the isotopic effects for D and T in plasmas and in materials are available until now.

Due to the isotopic effects, it must not be easy to keep the appropriate D/T ratio in plasma to continue the most efficient burning or to keep D-T burning efficiency the highest without independent fueling of D and T. To do this, concentrations of D and T in the burning plasma must be separately measured to make feedback to fueling possible. It is, however, quite difficult to evaluate or analyze the amount of D and T separately in the burning plasma. Different confinement times of D and T in plasma would result in their inhomogeneous distribution particularly in radial distribution (see Chap. 8).

Furthermore, retention rates of D and T in plasma facing wall are not necessarily the same as their release rates from the wall are. This means that if some local thermal load like ELM hits the wall, thermally released D and T are different in their amounts and disturb the D/T ratio of the plasma. Owing to the huge wall inventory, a small change in its D/T ratio in PFM would cause a significant change in the D/T ratio of the plasma. Thus, we are going to face difficulty of controlling the D/T ratio in burning plasma.

Until now, few systematic studies using intentionally mixed hydrogen (H and D) plasma have been conducted. Only in JT-60U, retentions of all hydrogen isotopes of H, D, and T have been systematically studied and proved that all isotopes do not necessarily behave similar and their behaviors reflect the history of plasma operations. In D operating tokamaks, a few % of H always remained in their D discharges after intense D discharges [11, 37]. For the study of D plasmas, effects of the few % H are negligible [8], but from T aspects, it is unacceptable. In the initial phase of ITER, discharges with an intentional control of H/D ratios should be made.

## 5.6 PFM Materials Selection for a Reactor

The in-vessel T inventory must be kept as small as possible, not only for safety reason but also for fuel self-sufficiency. In the present tokamaks of which plasma facing materials are mostly carbon, the fuel retention rates in their vacuum vessel

are significantly large, i.e., nearly 20 % of fueled hydrogen is continuously piled up [10, 11]. Considering the T decay of around 5 %/year, the retention rate must be kept far less than the decay. Otherwise, D-T reactors cannot be an economical energy source. Of course it is believed that ITER or any reactors should be operated under the steady-state condition and the in-vessel T inventory must be saturated. Unfortunately, however, the current estimation shows no saturation for any materials combinations of Be, C, and W, owing to the continuous piling up of hydrogen in the redeposited layers formed at remote area and bulk retention. The removal of T in the redeposited layers at the plasma shadowed area is not easy, and methods for reduction and recovery (removal) of the in-vessel T inventory are still under development and need large efforts.

From the concerns of large T retention in C, ITER decided not to use C. In the present ITER design, materials selected are Be for the first wall and W for the divertor. However, utilization of W bulk below their DBTT could result in the total failure through the cracking from W to cooling tubes. Hence, we should keep C materials as an alternative for plasma facing materials (PFM) for a reactor [34, 42].

According to the present estimation of the in-vessel T inventory, it seems impossible to keep it below 1 kg, ITER safety limit, after certain period of operation. Therefore the periodic removal or reduction of the in-vessel T inventory will be indispensable. Therefore, the total T retention might not be a good figure of merit for the selection of PFM in a reactor. And readiness to remove T once retained should be taken into account. Carbon, at ITER operation temperature, retains larger amount of T compared with Be and W, while T retention is limited to plasma facing surface area and inner surfaces and in-grain retention is quite low. Accordingly, T retained in carbon is rather easily replaced by hydrogen isotopes subsequently impinging. Even T in the redeposited layers could be replaced isotopically, if their temperature was above 800 K.

In the aspect of T management, carbon if used above 800 K (in a reactor) seems better than W. Heavy neutron activation of W would result in much dangerous dust than carbon. Dimensional change of carbon by neutron irradiation was claimed, but intentional and periodic replacement in the occasion of reactor maintenance would relieve the problem. As such, figure of merit for the selection of PFM of DEMO reactor might be reconsidered [34].

## 5.7 Summary

Plasma facing surfaces are subjected to fuel ions and neutrals escaping from scrape-off (boundary) plasmas together with thermalized and residual fuel gases. Since the fuel ions and neutrals are in higher energy states and/or having larger kinetic energy, their impacts on the surface result in “plasma wall interactions,” mainly surface erosion and impurity production by sputtering, and fuel recycling and retention in plasma facing materials.

Because of the lighter mass of hydrogen fuels, impurity production by their surface sputtering is small compared with sputtering by other impurities such as C and O. However, chemical sputtering of C and Be, if they are used as PFM of a reactor, causes heavy erosion and also plasma contamination. Furthermore, eroded materials are redeposited to make redeposited layers which retain significant amount of T. In particular, the layers redeposited at plasma shadowed area are simply piling up to increase the T inventory monotonically with discharge time. This is one of the most serious concerns to use C as PFM.

Different from C, erosion of W by physical sputtering of fuels is quite small. Seeded gases such as Ne and Ar for plasma edge cooling and impurities such as C and O enhance the erosion, and redeposited W layers would retain T. Nevertheless, the dominant T retention mechanism in W is bulk retention caused by solution and trapping of T in W bulk. Most of the T dissolved in the bulk would be released after plasma discharge, while trapped T, in particular those at newly introduced trapping sites by neutron damage, would remain long and could be significantly large T inventory. Below  $\sim 700$  K or reactor operating temperature, T inventory caused by C redeposition would exceed that in W bulk. At higher temperature, the relation will be reversed according to a recent review [34].

Quite recently, ITER has decided to exclude C divertor and to employ the full W divertor and full Be coverage of the first wall in its reactor vessel. Therefore, there remains no chance to use C to investigate its behavior in reactor relevant conditions. Because of its low melting temperature, Be is not likely the PFM of a reactor. This means W is the only candidate material of PFM in a fusion reactor. As discussed in this chapter, the T removal (recovery) from the PFM becomes critical. This could lead to different criteria for PFM selection, and R& D efforts on other PFM candidate materials, including C, should be continued.

In any materials used as PFM, T removal is critically important and various techniques have been proposed. Nevertheless, no technique is established, because retention mechanism in reactor relevant conditions are not fully understood, which requires significant R&D efforts.

The retention characteristics should show isotope effects among H, D, and T and their differences would influence the fueling of D and T to optimize the burning. Establishment of fueling control techniques of D and T to optimize the burning would be an additional important task in ITER in addition to the reduction of T inventory.

## References

1. Y. Yamamura. et al., Report of the IPP Nagoya, IPPJ-AM-26, 1983
2. C. Hopf, W. Jacob, J. Nucl. Mater. **342**, 141–147 (2005)
3. A. A. Haasz, J. A. Stephens, E. Vietzke et al. Atomic and plasma-material interaction data for fusion, Part A, **7**, 9–63 (1998)
4. J. Roth et al., J. Nucl. Mater. **337–339**, 970 (2005)
5. C. Björkas, K. Vörtler, K. Nordlund et al., New J. Phys. **11**, 123017 (2009)

6. G.F. Matthews, M. Beurskens, S. Brezinsek et al., Phys. Scr. **T145**, 014001 (2011)
7. M. Shimada, R.A. Pitts, J. Nucl. Mater. **415**, S1013–S1016 (2011)
8. T. Tanabe, J. Nucl. Mater. **417**, 545–550 (2011)
9. T. Tanabe, Phys. Scr. **T159** (014044), 12 (2014)
10. T. Tanabe, Fusion Eng. Des. **87**, 722–727 (2012)
11. T. Tanabe, N. Bekris, P. Coad et al., J. Nucl. Mater. **313–316**, 478–490 (2003)
12. G.F. Matthews, J. Nucl. Mater. **438**, S2–S10 (2013)
13. T. Tanabe, Tritium management in a fusion reactor—safety, handling and economical issues, eds. by S.-I. Itoh, S. Inagaki, M. Shindo, M. Yagi. Proceeding of 2nd ITER International Summer School: Confinement, American Institute of Physics, 112–126 (2009)
14. V. Philipps, Phys. Scr. **T123**, 24–32 (2006)
15. T. Tanabe, K. Masaki, K. Sugiyama, et al. Phys. Scr. **T138** (014006), 9 (2009)
16. E. Tsitrone, J. Nucl. Mater. **363–365**, 12–23 (2007)
17. K. Sugiyama, T. Tanabe, C.H. Skinner et al., Phys. Scr. **T108**, 68–71 (2004)
18. T. Shibahara, T. Tanabe, Y. Hirohata et al., J. Nucl. Mater. **357**, 115–125 (2006)
19. T. Tanabe, K. Masaki, K. Sugiyama, M. Yoshida, Phys. Scr. **T138** (014006), 9 (2009)
20. T. Tanabe, K. Sugiyama, T. Shibahara et al., J. Nucl. Mater. **390–391**, 705–708 (2009)
21. B.B. Pégouriéa, C. Brosset, E. Delchambre et al., Phys. Scr. **T111**, 23–28 (2004)
22. Michael D. Williams, Fusion Eng. Design **36**, 135–142 (1997)
23. C.H. Skinner et al., J. Nucl. Mater. **241–243**, 214–226 (1997)
24. P. Andrew et al., J. Nucl. Mater. **266–269**, 153–159 (1999)
25. R.-D. Penzhorn, J.P. Coad, N. Bekris et al., Fusion Eng. Des. **56**, **57**, 105–116 (2001)
26. K. Sugiyama, K. Miyasaka, T. Tanabe et al., J. Nucl. Mater. **313–316**, 507–513 (2003)
27. K. Masaki, K. Sugiyama, T. Tanabe, J. Nucl. Mater. **313–316**, 514–518 (2003)
28. K. Sugiyama, T. Tanabe, K. Miyasaka et al., J. Nucl. Mater. **329–333**, 874–879 (2004)
29. M. Yoshida, T. Tanabe, K. Sugiyama et al., Fusions Sci. Technol. **60**, 1560–1563 (2011)
30. K. Sugiyama, T. Tanabe, K. Masaki, N. Miya, J. Nucl. Mater. **367–370**, 1248–1253 (2007)
31. J. Roth, E. Tsitrone, T. Loarer et al., Plasma Phys. Control. Fusion **50**, 103001 (2008)
32. M. Shimada, G. Cao, Y. Hatano, T. Oda, Phys. Scr. **T145**, 014051 (2011)
33. Y. Hatano, M. Shimada, V.K. Alimov et al., J. Nucl. Mater. **438**, S114–S119 (2013)
34. T. Tanabe, Physica Scripta, **T159** (2014) 014044 (12p)
35. T. Tanabe, J. Nucl. Mater. **438**, S19–S26 (2013)
36. V. Philipps, J. Nucl. Mater. **363–365**, 12–23 (2007)
37. M. Yoshida, T. Tanabe et al., J. Nucl. Mater. **417**, 620–623 (2011)
38. M. Yoshida, T. Tanabe, A. Adachi et al., J. Nucl. Mater. **438**, S1261–S1265 (2013)
39. D. Hoffman, B. Singh, J.H. Thomas, *Handbook of Vacuum Science and Technology*. (Academic Press, 1998)
40. ITER Technical Basis 2002, ITER EDA, Documentation Series No. 24, IAEA, Vienna, 2002
41. N. Enomoto, S. Muto, T. Tanabe et al., J. Nucl. Mater. **385**, 606–614 (2009)
42. S. Higashijima, The JT 60 Team. J. Plasma Fusion Res. **75**, 1297–1304 (1999). (in Japanese)



**Part II**

**Tritium Handling (Fueling)**

**and Processing**



# Chapter 6

## Tritium Fueling System

Toshihiko Yamanishi

**Abstract** A fusion reactor requires a tritium (T) fueling system. The T fueling system consists of subsystems for fuel injection, vacuum pumping, fuel cleanup, isotope separation, fuel storage, blanket, and water detritiation. The fuel gas (T and deuterium (D)) is supplied by the fuel injection system and is exhausted by the vacuum pumping system. The exhausted gas is processed by the fuel cleanup system and the isotope separation system. Impurities, such as helium, water, and hydrogen (H), are removed by the above systems, and T and D are supplied again as the fuel gas through the storage system. The blanket system has a significant function that produces T from neutron and T breeder materials. The blanket system processes T thus produced and send it as fuel. A large amount of tritiated water is produced in a T-removal system and a coolant system. T in water is recovered by the water detritiation system and is sent as fuel again. In this chapter, the above T fueling system is described in detail. Some future R&D subjects in the T fueling system for a fusion reactor are also mentioned.

**Keywords** Tritium · T · Tritium fuel system · Fuel cleanup system · Isotope separation system · Storage system · Blanket system · Water detritiation system

### 6.1 Introduction

In a fusion reactor, only a few percentage of the D-T gas supplied into the plasma burns, so that the rest of the D-T gas is exhausted (pumped) and must be recycled as the fuel. Tritium (T) is a hydrogen isotope, so that it easily replaces with H contained in water and organic compounds. Hence, the D-T gas dominates in the exhausted gas; some T is exhausted as the form of tritiated water and organic

---

T. Yamanishi (✉)

Department of Blanket Systems Research, National Institutes for Quantum and Radiological Science and Technology, Rokkasho Fusion Institute, Rokkasho, Japan

e-mail: yamanishi.toshihiko@qst.go.jp

compounds. In addition, He ash produced by D-T reactions and some other inert gases such as Ne and Ar seeded for plasma edge cooling come into the exhausted gas. These impurity gases must be removed.

Not only for the fuel self-sufficiency, but also for T safety, exhausted T must be fully recovered and its release to the environment should be kept as low as reasonably achievable (ALARA). H, the most abundant hydrogen isotope, always appears as an impurity in the fuel D-T stream and requires additional effort to be removed in a hydrogen isotope separation system.

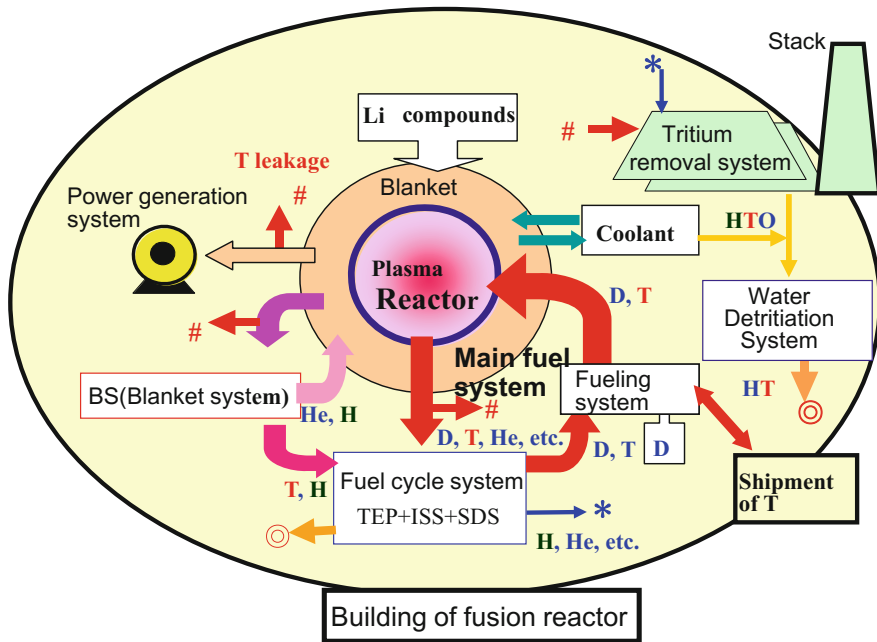
To establish the fuel self-sufficiency, a T breeding mechanism is essential in a fusion reactor. Several blanket modules, which have lithium compounds as a T breeding material and beryllium compounds as a neutron multiplier, are installed surrounding a reactor core. T produced in the modules is recovered by a processing system. The blanket system consists of the modules and the T-processing system. The recovery efficiency must be nearly 100 % to attain the fuel self-sufficiency as already discussed in Chap. 3.

It is thus essential to establish a compact and effective fuel processing system for a fusion reactor and a little detail of the T fueling system is described in this chapter.

## 6.2 Structure of Tritium Fueling System

Figure 6.1 shows a T flow diagram in a fusion reactor. The system is mainly composed of a main fuel system, a blanket system, and a T-removal system with a water detritiation system. The main fuel system consists of a fueling system and a fuel cycle system. The fueling system consists of a vacuum pumping system and a fuel injection system. The fuel cycle system consists of a TEP (Tokamak Exhaust System), an ISS (isotope separation system), and a SDS (storage and delivery system).

Generally, the main fuel system is a combination of chemical processes. One of the significant features of the system is that radioactivity of T does not allow its leakage and requires recovery of the leaked T. For T safety, a series of T-removal systems is prepared to confine T in a fusion reactor facility. All the components in T-processing systems should have a leak tight structure to avoid T leakage as low as reasonable achievable (ALARA). Even if T was released into a fusion reactor building by an accident or by a miss-operation, the amount of T released to the environment should be controlled to be less than a regulation value and should be decreased to be ALARA. Some maintenance works are required for T-contaminated components, and these components would be dismantled. Some amount of T would be released through the maintenance works. To confine T, the maintenance works would be carried out in a hot cell, whose atmosphere is maintained at a negative pressure. The atmosphere gas in the hot cell is further circulated through the T-removal system. In the T-removal system, T released into the atmosphere of the hot cell is oxidized by a catalyst reactor and removed by a molecular sieve dryer or a scrubber column. A regeneration process of the molecular sieve dryer produces tritiated water. Therefore, installation of the detritiation system with the water



TEP: Tokamak Exhaust Processing system

ISS: Isotope Separation System

SDS: Storage and Delibery System

**Fig. 6.1** Schematic of T flow in a fusion reactor

detritionation system consisting of scrubber and molecular sieve dryer is essential. For a fusion reactor, when T level in coolant water exceeds the regulation level owing to T permeation, the coolant water should be also processed by the water detritiation system as shown in Fig. 6.1. T recovered by the water detritiation system is sent to the fuel cycle system to reuse as fuel. The detritiated water is exhausted to the environment.

ITER is the first device which equips the abovementioned main fuel system [1]. In some previous plasma devices carrying out T experiments such as TFTR and JET, T fueled into their plasmas was not recycled, while ITER will be the first system to reuse fueled T. Furthermore, the first test trial of recovery of bred T in the blanket will be done in its technical phase. For instance, to obtain 1 GWe output from a fusion reactor, the amount of T fueled into the reactor (throughput) will be 10 kg/day in the case where the conversion factor of energy from heat to electricity is 1/3 and a burning efficiency of T is 4 %. We must establish the fueling system with such high T throughput in a fusion reactor. A series of demonstration tests of a test blanket module is a main subject in ITER for a next-generation machine and a DEMO reactor. Hence, basic studies of the blanket have been carried out under the BA (Broader Approach) activity in JA and EU [2].

## 6.2.1 Fueling System

### 6.2.1.1 Fuel Injection System

DT fueling into burning plasma is one of the key issues for stable fusion reactor operation. In case of the magnetic confinement, there are two types of techniques depending on the energy of fueling particles. One is the high-energy particle injection, such as neutral beam injection (NBI), which is also used for plasma heating. Recently, compact toroidal injection [3] is also proposed using small plasma of fuel, instead of NB. The other is ambient or lower temperature particle injection, such as gas puffing or pellet injection. For any fueling in magnetically confined fusion, it is a main issue how to fuel into the core plasma without cooling down the core plasma. Inertially confined fusion uses a spherical solid target. The fuel gas of D-T is condensed into the spherical porous polycarbonate form.

In ITER, about 300 mol/h of D-T (50–50 %) gas is charged into the plasma. About 20 % D-T is charged by the high-temperature particle injection such as NBI, 25 % D-T is charged by the pellet injector, and the gas puffing supplies the rest of D-T. For a DEMO reactor, these percentages will be modified to obtain maximum burning efficiency.

#### (1) Neutral Beam Injection

This technique consists of collisional heating of plasma particles by injected high-energy neutral particles. The technique is also used for fueling into the core plasma. In a neutral beam injection (NBI) system, fuel particles are first ionized and accelerated, and then neutralized to inject through the strong magnetic field of plasma. Either positive or negative ions can be used and they have to be accelerated to >1 MeV before the neutralization. To get higher efficiency in the neutralization, negative ions are mainly used. In the case of ITER (0.5GW<sub>th</sub>), for example, 40 A of negative deuteron beam is required to accelerate to 1 MeV, so that a few 10 cm<sup>3</sup>(stp)/s of deuterium is injected if neutralization efficiency is about 60 %.

#### (2) Compact toroidal injection [3]

This technique is an injection method of small fuel plasma produced outside of the reactor core with high speed of a few 100 km/s. Because the fuel plasma can be injected close to the center of the core plasma, it is expected to get high fusion reaction efficiency.

#### (3) Gas puffing

This is the most popular fueling technique with injection of fuel gas through high-speed electromagnetic valves (piezo valves) with response time of less than 1 s. In order to supply the fuel gas uniformly into the vacuum vessel, several gas-puffing ports with the piezo valves are installed.

#### (4) Pellet injection [4]

This technique is an injection of solid pellets of fuels. First, the pellets are made by pushing out solidified deuterium and/or tritium through piston or screw from the cylinder cooled by liquid He followed by cutting to be an adequate size. Then the pellets are accelerated by either centrifuge, gas gun, or rail gun methods. The centrifuge method can inject a few mm pellet with velocity of 1 km/s by a few 10 Hz, using high-speed rotated arm with high reliability. The gas gun, using 1–10 MPa of hydrogen or He, is demonstrated a few km/s of pellet velocity. Theoretically, the rail gun would inject the pellet with higher velocity than other methods.

### 6.2.1.2 Vacuum Pumping System

The pumping technology is very important to maintain fusion reactions by exhausting fuel mixture and transferring them to a T-processing plant. In a magnetic fusion reactor, R&D issues are to develop pumping systems to tolerate strong magnetic and high radiation fields, and to attain large pumping speed of about 300 mol/h of D–T fuel gas from the vacuum chamber as described in the previous section. Characteristics of major possible pumps are summarized as follows.

#### (1) Turbo molecular pump [5]

This pump compresses gas molecules by a high-speed rotor and exhausts them to the downstream. Continuous operation of the pump is achievable. However, there is a concern on reduction of rotational speed of a metallic rotor in the strong magnetic field by eddy current. To avoid the effect of the magnetic field, recently, a ceramic rotor using SiN<sub>4</sub> has been developed. Moreover, gas-bearing and gas turbine rotation are selected as alternatives of magnetic-bearing and electric motor rotation, respectively, which promise more reliable performances in the strong magnetic field. In order to fabricate a pump with larger pumping capacity, a larger ceramic rotor is required. Progress of ceramic material technology is awaited.

#### (2) Cryosorption pump

This pump evacuates gas molecules by sorption on the cryopanels cooled at about 4 K. Since the pump has no mechanically working parts, it is quite beneficial to use in strong magnetic field. Because of limited capacity in the sorption of the cryopanel, however, its periodical regeneration by thermal desorption of the absorbed gases is required. This does not allow its continuous operation but forces its batch operation. Owing to its operational ability under the strong magnetic field, ITER selects a series of cryopumps with periodic switching operations.

#### (3) Metal jet diffusion pump [5]

In an inertially confined fusion reactor, it is quite important to ensure a stable operation of their evacuation pumps under vapors evaporated from liquid breeder covering the first wall, such as Li and LiPb. A metal jet diffusion pump using liq. Pb

has been investigated for operation in such circumstance. The pump has no mechanical working parts and is compatible with metal vapor and even dust. Its structure is very simple and allows high-temperature operation different from an oil diffusion pump. Scale-up demonstration is a further issue.

### (5) Roughing pump

All pumps except the cryopump require roughing pumps. To have capability to handle T, oil-free pumps are favorable. This is because tritiated oil would be produced as waste by easy isotopic replacement of H in the oil by T; it is not easy task to measure the T concentration in the oil. Pumps of scroll and reciprocating types without usage of the oil are available [6].

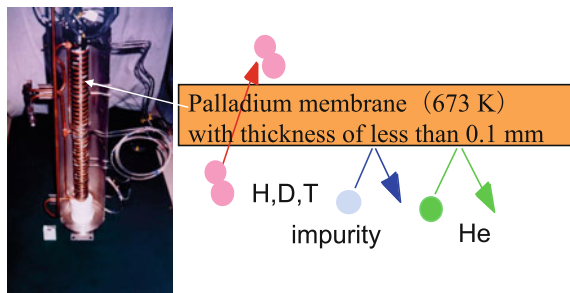
## 6.2.2 *Fuel Cycle System*

### 6.2.2.1 TEP (Tokamak Exhaust Process)

As shown in Fig. 6.1, the exhaust gas from a fusion reactor contains three types of gases, fuel gases (D and T) that were not burned in plasma, the fusion reaction product (He) and impurities such as water vapor, methane and other hydrocarbons, hydrogen molecule, and other rare gases intentionally added for cooling of plasma edge (Ne and Ar). The impurities such as water vapor, methane, and other hydrocarbons are mainly produced by the interactions between the plasma and the plasma-facing surface of materials. The exhausted gases from the reactor must be refined (purified to be pure hydrogen mixture by removing impurities) before sending to an isotope separation system (ISS), which can handle only highly purified hydrogen isotopes. For the refinement, a palladium diffuser made of a Pd alloy with thickness of only 0.1 mm is applied (See Fig. 6.2). Only hydrogen isotopes dissolve and permeate the diffuser above 673 K. In order to avoid hydrogen embrittlement of pure Pd, a Pd–Ag alloy with a few % of silver metal (Ag) is used as the diffuser. In an ordinary chemical plant for H refining, the diffuser is used under pressurized hydrogen atmosphere while a high-pressurized fuel should be avoided in a T-handling system to eliminate T permeation. Therefore, operational pressure of the diffusers for the refinement of the fuel is near atmospheric pressure or below, and the inside of the tubes is evacuated to recover permeated pure hydrogen isotopes [7]. Although a long-time operation of the diffuser has been a concern, because of possible embrittlement by the accumulation of  ${}^3\text{He}$  as the decay product inside of the tubes, its durability has been confirmed by the long-term tests carried out under the collaboration between Japan Atomic Energy Research Institute and Los Alamos National Laboratory [8] quite recently.

The residual gases, which do not permeate through the palladium diffuser, still contain some T with chemical form of water and hydrocarbons, which do not allow their direct release to the environment. Therefore, they must be further processed to

**Fig. 6.2** Photograph and conceptual diagram of palladium diffuser



### Palladium diffuser

A cylindrical palladium membrane is set at the center of the chamber. The trunk of the chamber is evacuated by a vacuum pump, and hydrogen gas permeates from the membrane to the trunk.

remove T to be ALARA. Some systems have been developed and proposed for this purpose. In ITER, a train of a catalytic reactor and a palladium membrane reactor has been applied [1]. The catalytic reactor is packed with platinum catalyst which converts methane/water to hydrogen gas by the following methane cracking/water-gas shift reaction [9],



The palladium membrane reactor promotes the isotope exchange reaction between T included in the impurities and hydrogen (H) gas,

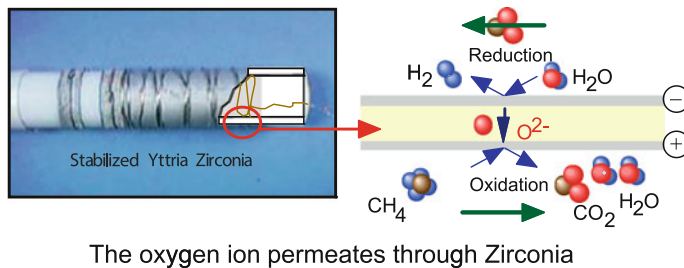


Figure 6.3 shows the conceptual structure of the palladium membrane reactor [10]. The hydrogen gas permeates through the Pd tube and reacts with impurities at the Pd metal surface. The HT gas produced by the reaction (6.3) permeates through the Pd tube again.

The catalytic reactor has a disadvantage that an appreciable amount of carbon dust will be produced by the methane-cracking reaction to remain in the reactor. As alternatives of the catalytic reactor, advanced or new technologies have been applied. An electrolysis cell is a promising method. Figure 6.4 shows the basic structure of a ceramic electrolysis cell using a membrane of yttria-stabilized zirconia. The water vapor is decomposed to hydrogen and oxygen ions by the

**Fig. 6.3** Schematic of palladium membrane reactor





**Fig. 6.4** Basic concept of ceramic electrolysis cell

electrolysis. The oxygen ions permeate to the other surface of the membrane electrode by electric potential gradient in it and oxidize methane to water vapor and  $\text{CO}_2$  as shown in Fig. 6.3 [11].

The detritiation factor (DF) is defined as the ratio of T concentrations at the inlet and at the outlet of the system. The gas processed by TEP is finally released to the environment as shown in Fig. 6.1. In the fuel cycle system, T concentration in processed gasses is quite high ( $10^{10} \text{ Bq}/\text{cm}^3$ ). On the other hand, T concentration in the released gas to the environment must be less than the regulation value ( $90 \text{ Bq}/\text{cm}^3$ ). Therefore, the DF value of TEP is as large as  $10^6$  in ITER, and still the outlet gas of TEP is further processed by a detritiation system, whose required DF would be larger than 100.

### 6.2.2.2 Isotope Separation System (ISS)

This technology is described in detail in Chap. 11, so that the system is briefly explained. Several methods have been developed for separation of hydrogen isotopes, such as gas chromatography, a cryogenic distillation column, and a thermal diffusion method. The cryogenic distillation column has been only the system that can be applied to the fusion fuel system. This is because the column can process a large amount of flow rate with a high separation factor in comparison with the other methods. In ITER, the cryogenic distillation column will be applied [1].

### 6.2.2.3 Storage and Delivery System (SDS)

In a fusion reactor, D-T fuels can be stored in metal beds as hydrides. ITER will take pulsed operation with discharge time of around 400 s. Therefore, D and T recovered from a cryogenic isotope separation system are stored temporally in the beds and then delivered as fuel in a reactor adjusting the pulsed operation. In a DEMO reactor, a continuous operation is planned so that the above temporally storage operation is not required. However, accumulation and storage of T are required to store T produced in blanket. In addition, fuel preservation is required during the maintenance/inspection of the reactor.

There are many hydride-forming metals, such as uranium, titanium, zirconium, and their alloys. Metal hydrides have their own equilibrium dissociation pressure varying with temperature, i.e., a hydride dissociates and releases hydrogen with a constant pressure at a higher temperature, while recombines to the hydride to store hydrogen. For the safe handling of T, it is better that the equilibrium dissociation pressure at room temperature (RT) is reasonably low (easy hydriding) and it is about 0.1 MPa at 773 K (easy dissociation). In this respect, uranium is one of the bests and has been used in many T-handling facilities. However, uranium as a nuclear material requires a complicated regulation control to use. From this reason, the alloy of zirconium (Zr) and cobalt (Co) has been developed and used as a T storage bed in TPL/JAEA. In recent two decades, T storage in ZrCo bed has been successfully demonstrated. The hydrogen equilibrium dissociation pressure of ZrCo is about 1 mPa at RT and is about 100 kPa at 623 K. 100 g of ZrCo can store about 1 mol of D-T gas [12].

For T accountancy to ensure the accordance of its regulation rule, determination of T inventory in all T-processing systems of a fusion reactor is necessary. As mentioned above, all of the fuel is stored (reserved) to the storage beds during the maintenance/inspection period. We can know the total amount T in a fusion reactor from the measurements of the amount of T preserved in all storage beds. To do this, a volumetric method is used, collecting all T released by heating the storage beds in gas reservoir with a fixed volume (V) and measuring gas pressure (P) to give  $n = pV/RT$ . However, this method requires a long time and includes an error owing to other hydrogen isotopes (H and D) included as an impurity in the bed. In order to avoid these disadvantages (long-time operation, error of residual hydrogen), a special T storage bed has been developed with a self-accounting function, such as in-bed gas flowing calorimetry shown in Fig. 6.5. In this system, a He cooling loop

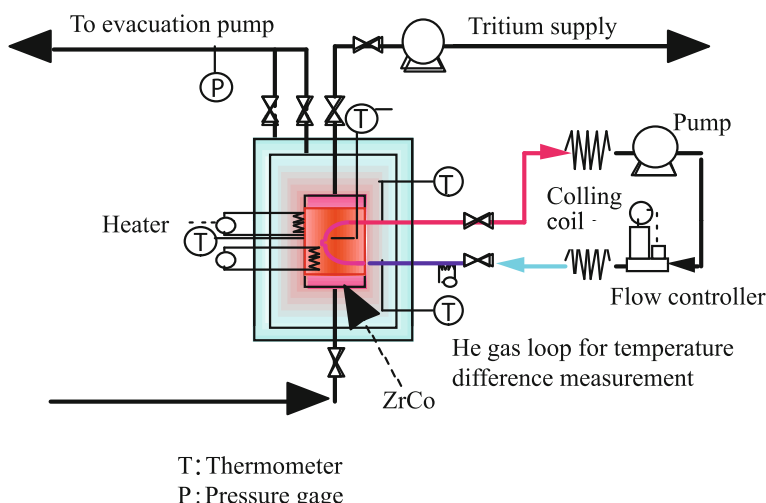


**Fig. 6.5** T storage bed having T accountancy system

to remove decay heat of T is introduced in a storage bed and the difference between the inlet and outlet temperature of He of the loop caused by the decay heat is measured. By making a calibration curve between the temperature differences and the decay heat of T stored in the bed, the T inventory in the bed can be monitored in any time. The TPL/JAEA has demonstrated that accuracy of the T inventory in the bed determined by this method is within 99.9 % of a full bed capacity [12]. Therefore, this method is selected to account T in T storage beds in ITER.

## 6.3 Blanket System

A set of blanket modules is installed in a vacuum vessel facing the plasma. Various different concepts of a blanket system are proposed as described in Chap. 13. A typical solid breeder blanket system uses lithium and beryllium compounds as a T breeder and a neutron multiplier, respectively. T produced in the blanket is recovered by a carrier gas, for example, helium gas with some hydrogen added for its easy recovering. The amount of T bred and recovered should be larger than that consumed (burned). The full recovery of bred T is not easy and requires significant efforts as described in the next section. Without knowing mechanisms of T release (reaction) from the breeding materials, it is hard to develop an appropriate blanket system to satisfy the fuel self-sufficiency. Therefore, intensive works shall be done for that [2].

### 6.3.1 Tritium Recovery Technology from Blanket

In case of a solid breeder blanket, bred T is recovered by a carrier (or sweeping) gas. A gas stream of He would flow through the packed region of breeder (lithium oxides) pebbles in a blanket module (see Fig. 6.6). Basically, the chemical form of T released from the lithium oxides is water vapor because of the thermal decomposition of the surface hydroxyl group in their surface region. From the viewpoint of safety, handling high-level tritiated water is not favorable. In addition, the recovered T should finally be in elemental form (hydrogen form) to be used as the fuel. Hence, the addition of hydrogen ( $H_2$ ) in the He sweep gas has been proposed as the first concept. The isotope exchange reactions at the surface of lithium oxides enhance T recovery, and T is mainly recovered as hydrogen gas form with a small amount of water vapor. The amount of T generated in the blanket is determined by the fusion power and the tritium breeding ratio (TBR).

T-recovering efficiency varies with the flow rate of the sweep gas and partial pressure (or concentration) of  $H_2$  in it. As described in the next section, for T recovery from the sweep gas, there would be an optimum partial pressure of T in a sweeping gas at the outlet of the blanket. Therefore, if the partial pressure of T at the outlet of the blanket is decided, the flow rate of the helium sweep gas and the

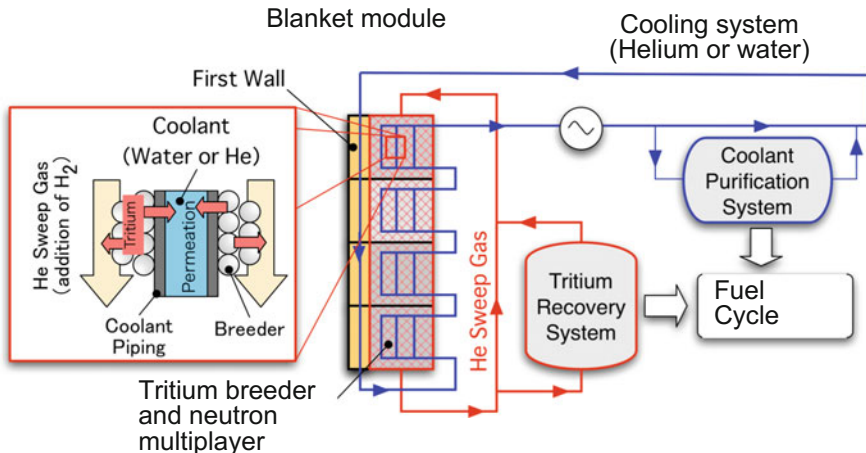


**Fig. 6.6** A schematic diagram of T recovery system and coolant purification system for blanket

amount of hydrogen gas (H) added could be calculated [13]. The partial pressure of T at the outlet of the blanket should be determined by considering the T inventory and the T leakage to the coolant. Instead of H, the addition of deuterium (D) to the helium sweep gas has also been proposed. However, the use of deuterium has not been adopted, because recovering T from H (or isotope separation of T and H) is much easier than that of T from D owing to larger mass difference in the former.

### 6.3.2 Recovery of Hydrogen Isotopes of Elemental Form

Since the addition of H<sub>2</sub> in sweep gas enhances T release as the elemental chemical form HT and T<sub>2</sub>, their recovery or removal from the sweep gas is required, which is the theme of this section. Nevertheless, some T is released as the water vapor, HTO, as described in the previous section. The recovery of HTO from the sweep gas is described in the next section. The probable candidate techniques to recover H<sub>2</sub> and HT from the sweep gas are (1) permeation, (2) hydrogen sorption in metals (alloys), and (3) cryosorption.

Concerning the permeation, utilization of the palladium diffuser is the most probable method [14] and is planned to use in the TEP system of ITER. In the case of the blanket system, the partial pressure of T is much smaller than that in the TEP system, and it may not work effectively and a new idea is required to use it [15].

Hydrogen absorption in hydride-forming metals described in the previous section can be applied for the hydrogen recovery. In this section, we assume to use particles of zirconium alloys (ZrCo, ZrNi) in the hydrogen recovery system. The system is composed of several columns packed with the zirconium alloys. The sweep gas is introduced into the column, and the alloys selectively absorb hydrogen

isotopes from the sweep gas and other impurities. To recover the absorbed hydrogen isotopes, the column should be heated so that the alloys desorb them. Since repetitive processes of absorption (hydriding) and desorption (dehydriding) pulverize the alloy, the column should equip filtration of the pulverized fine particles. The water vapor deteriorates the performance of the packed column by the oxidation of the alloy and, hence, must be removed before the gas is introduced to the column.

The cryosorption is a technique to use cryogenic adsorption of hydrogen for refinement of or removal of impurities from hydrogen. A porous adsorbent such as a synthesized zeolite shows large adsorption capability of hydrogen isotopes at liquid nitrogen (liq. N<sub>2</sub>) temperature. When the He sweep gas containing the elemental form of hydrogen isotopes is introduced into the zeolite packed column kept at liq. N<sub>2</sub> temperature, the hydrogen isotopes are selectively adsorbed on the zeolite [16]. This method was applied to the T removal from the exhaust gas of helium glow discharge of JET and ITER vacuum vessels [17]. Recovery of hydrogen adsorbed in the bed is simply done by removing liq. N<sub>2</sub> that is much easier than that in the metal-packed column requiring heating.

### **6.3.3 Recovery of Hydrogen Isotopes of Water Form**

As mentioned above, T produced in the blanket can mainly be recovered as HT. However, a small amount of T still remains as HTO. Therefore, removal or recovery of HTO from the sweep gas is quite important task. After getting HTO, reduction of HTO to get elemental form of hydrogen isotopes is required. In the following, some possible methods for the recovery of HTO and the reduction of HTO are briefly introduced.

As described above, the water vapor can be recovered by porous adsorbent such as synthesized zeolite packed in a column. In this case, different from the cryogenic adsorption of hydrogen gas, the temperature of the column can be ambient or at room temperature.

To reuse T in recovered HTO as a fuel, conversion of the chemical form of T from HTO to HT is needed. A possible method is to use a catalyst bed, where T in HTO is isotopically replaced with H in H<sub>2</sub> gas,



Electrolysis of HTO is also an important way. In the blanket system, the T concentration is very high. To avoid a large T inventory, we must choose an electrolysis cell which has a small water inventory. A recently developed electrolysis cell made by organic compounds has a small water inventory. However, it is difficult to apply the organic electrolysis cell because of the radioactive effect of T. A ceramic such as YSZ yttria-stabilized zirconia, which can be used in the TEP system, may be applicable [16] because of its large durability against the T

radiation. Utilization of the perovskite type ceramic is also promising. This type ceramic is a kind of a fuel cell and hence can directly extract hydrogen from water molecules. Some basic studies on the T recovery system using the hydrogen pump have recently been carried out [18, 19].

## 6.4 Water Detritiation System

As mentioned above, an appreciable amount of tritiated water is produced in the T-removal system. Furthermore, T permeation through cooling tubes to coolant water results in a large amount of tritiated water. The T concentration in the coolant water would be low; however, it is still too high to discard to the environment directly. The most promising method of T removal from the tritiated water is to use chemical exchange columns [20]. For hydrogen isotope separation, there are several chemical exchange reactions: (1) water vapor–hydrogen ( $\text{H}_2\text{O}-\text{H}_2$ ); (2) water vapor–hydrogen sulfide ( $\text{H}_2\text{O}-\text{H}_2\text{S}$ ); and (3) hydrogen–ammonium ( $\text{H}_2-\text{NH}_3$ ) [20]. Among the three reactions, the first one is most suitable for the T removal as HT from the tritiated water. Although the second one needs no catalyst and is applied for the recovery of deuterium from natural water, the production of HTS should be concerned. The reaction of (3) is also unfavorable because of the production of  $\text{NH}_2\text{T}$ . The chemical exchange columns have been developed, constructed, and operated for the purpose of T recovery of some heavy water power plants in Canada and in Korea [21, 22]. For ITER, a modified type of chemical exchange column has been developed [23]. Figure 6.7 shows a conceptual diagram of the chemical exchange column [23] for a fusion reactor. A hydrogen gas flow is produced at the electrolysis cell and flows to the top of the column. T in hydrogen is moved to water vapor by the following reaction:  $\text{HT} + \text{H}_2\text{O} \text{ (vapor)} = \text{H}_2 + \text{HTO} \text{ (vapor)}$ . The water vapor flow is accompanied by the hydrogen flow from the electrolysis cell. T in the water vapor flow is further moved to a water flow from top of the column by the vapor–liquid equilibrium



The separation factor for the reaction between the water vapor and hydrogen reaches about 5 at 323 K. Accordingly, the hydrogen flow contacts the water stream counter currently as shown in Fig. 6.7. To make reflux flows within the column, an electrolysis cell, which produces a hydrogen flow from water, set at the bottom of the column to produce the hydrogen flow from bottom of the column. A natural water flow is also supplied from the top of the column to make the reflux flows within the column as shown in Fig. 6.7. An ordinary platinum catalyst can promote the reaction between hydrogen and water vapor. However, the catalyst loses its function when the surface of the catalysts is covered by water. Hence, hydrophobic catalysts made by organic compounds are used in the chemical exchange column [24]. In addition, the water flow passes through the path made at the center of the

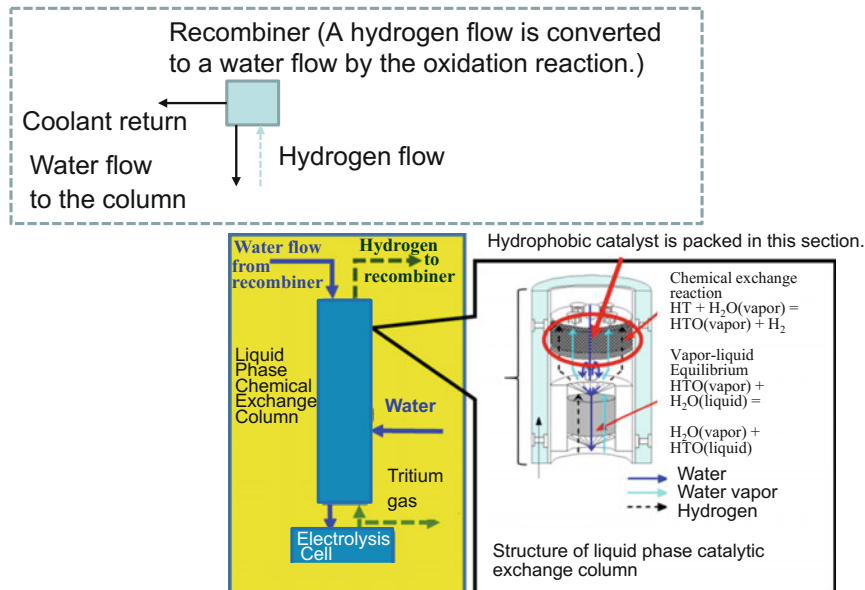


**Fig. 6.7** Typical conceptual flow diagram of water deuterium system of fusion reactor

catalyst section. The water flow is not in contact with the catalysts and does not wet the surface of the catalysts as shown in Fig. 6.7. A serious disadvantage of the chemical exchange column is that the processing flow rate is not so large. (The maximum processing flow rate would be 60–100 kg/h for a column.) This is because it is difficult to develop an electrolysis cell treating a large flow rate. As described in the preceding section, a modified chemical exchange column has been developed for a fusion reactor. Only a difference between the columns of heavy water power plants and those of fusion reactor is whether or not there is a recombiner (see Fig. 6.7). The recombiner is set at the top of the column and produces a water flow from the hydrogen flow from the bottom of the column. The water flow is returned to the column from the top of the column, and a part of water flow is returned to use coolant again. For ITER, we do not need to process the coolant water, since T concentration in the coolant is expected to keep being small during ITER operation period. The hydrogen flow is directly discarded to the environment from the top of the column and is not required to produce the water flow. Hence, the recombiner is excluded, and natural water is supplied from the top of the column instead of that from the recombiner.

For a DEMO reactor, a larger flow rate of coolant water should be processed. This is because the DEMO reactor has a full-scale breeding blanket system, and the system would be operated for a long time. The amount of coolant water of the blanket system is large, and the concentration of T in the coolant would also be large. A large amount of T would permeate to the coolant because of the long operation period. ITER has some test blanket modules only, and these modules are

operated for a limited period. One of the possible options to handle the large flow rate of the coolant water is to apply a combination system as shown in Fig. 6.8 [23]. A water distillation column is introduced prior to the exchange column to process a large flow rate of the cooling water. The water distillation column recovers T by the difference of boiling point of water isotopes ( $H_2O$  and  $HTO$ ). T is concentrated to the bottom of the column. The function of the water distillation column is to prevent to increase the T concentration of the cooling water: No large separation factor is necessarily required for the column. By applying the water distillation column, we can reduce the flow rate to the chemical exchange column to 1/10–1/100. Table 6.1 shows typical separation factors of the water distillation column. Although we do not need a larger separation factor for the water distillation column, it is quite effective to develop a more compact system prior to the exchange column. The size of the water distillation column is still large (~50 m) [23]. For the DEMO reactor, an adsorption column as an alternative to the water distillation column has been proposed in which the synthesis zeolite is used as adsorbent [25]. The amount of T water vapor ( $HTO$ ) adsorbed is larger than that of water vapor ( $H_2O$ ). By using the difference between  $HTO$  and  $H_2O$  on the amount of adsorption on the zeolite,  $HTO$  and  $H_2O$  can be separated. An electrolysis cell is also proposed for T removal from the tritiated water with using a membrane of the ion exchange resin. A resin named Nafion shows one of the best performances for separation of hydrogen isotopes. To apply it for T separation, its radiation hardness to exposure of  $\beta$ -electrons of T should be considered. A set of data on its durability to tritiated water has been measured, and it has been proved that the Nafion can be used for two years under ITER condition (9.25 TBq/kg) [26].

**Fig. 6.8** Structure of chemical exchange column

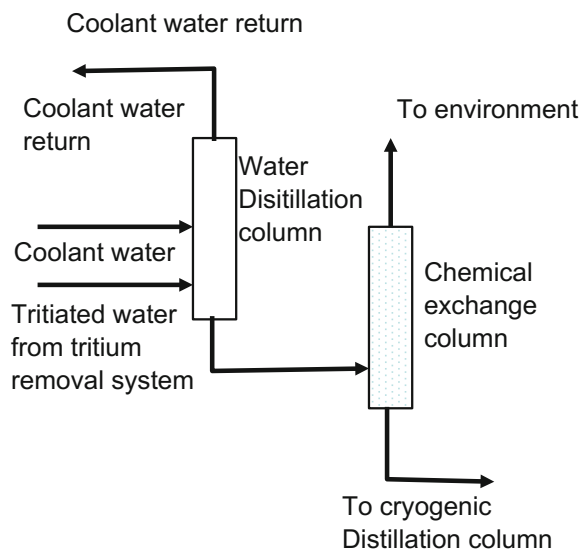


**Table 6.1** Separation factor of water distillation column

Temperature(K)	298	333	353	373
Pressure of H <sub>2</sub> O (kPa)	3.17	19.9	47.3	101.3
Pressure of HTO (Pa)	2.89	18.86	45.5	98.5
Separation factor = Ratio of pressure	1.095	1.056	1.04	1.029

## 6.5 Future R&D

A series of basic R&D studies on the T fueling system has been completed, and the design of the T fueling system for ITER has been carried out. The system could handle a large amount of T safely following the regulation row. However, to design a DEMO fusion reactor, further R&D studies are required to realize a compact and economic T fueling system in addition to safe handling of T. Any T-handling systems must be installed in confinement systems such as glove boxes, rooms, and a building. Therefore, a large T confinement system would be required for a large T fueling system and a large T-removal system. The large T-removal system produces a large amount of tritiated water. Hence, it is still one of the significant goals to decrease the size of any T-handling systems with the improvement of system performance.

## References

1. M. Glugla et al., *Fusion Eng. Des.* **82**(2007), 472–487 (2007)
2. T. Yamanishi et al., *Fusion Eng. Des.* **87**, 890–893 (2012)
3. K. Suzuki, *J. Plasma Fus. Res.* **76**, 288–291 (2000)
4. H. Hiratsukia, *J. Plasma Fus. Res.* **76**, 1189–1192 (2000)
5. T.T. Abe et al., *Vacuum* **41**(1990), 1992–1995 (1990)
6. T. Hayashi et al., *Fusion Eng. Des.* **28**, 357–360 (1995)
7. H. Yoshida, *Nucl. Technol./Fusion*, **3**, 471–474 (1983)
8. S. Konishi et al., *Fusion Eng. Des.* **18**, 33–36 (1991)
9. R.D. Penzhorn et al., *Fusion Technol.* **14**, 450–453 (1988)
10. M. Glugla, et al., in *Proceedings of 19th SOFT*, Lisbon, Portugal, 16–21 Aug 1996
11. K. Isobe, *Fusion Sci. Technol.* **41**, 988–991 (2005)
12. T. Hayashi et al., *Fusion Sci. Technol.* **41**, 801–804 (2002)
13. Y. Kawamura et al., *Fusion Sci. Technol.* **48**, 654–657 (2005)
14. M. Nishikawa et al., *J. Nucl. Sci. Technol.* **33**, 504–510 (1996)
15. M.M. Enoeda et al., *Fusion Technol.* **26**, 664–667 (1994)
16. T. Yamanishi et al., *Fusion Sci. Technol.* **48**, 63–66 (2005)
17. M. Enoeda et al., *Fusion Technol.* **28**, 591–596 (1995)
18. Y. Kawamura et al., *Fusion Eng. Des.* **82**, 113–121 (2007)
19. Y. Kawamura et al., *Fusion Eng. Des.* **83**, 625–633 (2008)
20. G. Vasaru, *Tritium Isotope Separation*, Chap. 5. (CRC Press, 1993)

21. S.K. Sood, et al., Ontario Hydro, Toronto, Canada. Fusion Technology Experience at Ontario Hydro's Darlington Tritium Removal Facility And Heavy Water Upgraders (1998)
22. K.M. Song, et al., Installation of liquid phase catalytic exchange columns for the Wolsong tritium removal facility (2007)
23. Y.Y. Iwai et al., *Fusion Sci. Technol.* **41**, 1126–1130 (2002)
24. S. Isomura et al., *Fusion Technol.* **14**, 518–521 (1998)
25. Y.Y. Iwai et al., *Fusion Sci. Technol.* **45**, 532–540 (2008)
26. Y.Y. Iwai et al., *Fusion Sci. Technol.* **42**, 636–642 (2005)



## Chapter 7

# Tritium Measurement I—Tritium in Gas, Liquid, and Solid

Masanori Hara, Yoshinori Kawamura and Tetsuo Tanabe

**Abstract** Since tritium (T) handled in fusion environment distributes so widely in its concentration and chemical form, no single T-measuring method can cover the wide concentration ranging from environment level (a few Bq) to carrier free level (GBq or above) and distinguish various tritiated compounds (gas, water, and organics). In principle, any methods used for hydrogen measurements can be used for T measurements. However, safety requirements owing to the radioactivity of T give limitation in the measurements. Furthermore, electric noises caused by  $\beta$ -electrons emitted at T decay often disturb the measurements. On the other hand, they are allowed to use the radioactivity measurement. Nevertheless, their energy is so low to make their detection difficult. In this chapter, the principle of T detection and measurements is introduced, and its applications are described targeting quantitative analyses of wide ranges of T in gas, liquid, and solid separately. In a fusion reactor, T in plasma is a new target to be quantified, which is described in Chap. 8, separately.

**Keywords** Ionization chamber • Liquid scintillation counter • BIXS • Calorimeter • Imaging plate • Combustion method • Smear test

---

M. Hara (✉)

Hydrogen Isotope Research Center, Organization for Promotion of Research,  
University of Toyama, Toyama, Japan  
e-mail: masahara@ctg.u-toyama.ac.jp

Y. Kawamura

Fusion Energy Research and Development Directorate,  
National Institutes for Quantum and Radiological Science and Technology,  
Ibaraki, Japan  
e-mail: kawamura.yoshinori@qst.go.jp

T. Tanabe

Interdisciplinary Graduate School of Energy and Sciences,  
Kyushu University, Fukuoka, Japan  
e-mail: tanabe@nucl.kyushu-u.ac.jp

## 7.1 Introduction (Hydrogen and Tritium Detection)

Since tritium (T) is one of hydrogen isotopes, all methods for detection and/or qualitative analysis of hydrogen can be applied for T measurements. In addition, T can be readily detected by its disintegration ( $\beta$  decay emitting an electron) or a radiation measurement. The sensitivity of T detection by the radiation measurement is better than those of stable hydrogen isotopes by conventional methods by several orders of magnitude. The detection limits of several  $\text{Bq cm}^{-2}$  on solid surfaces and  $0.01 \text{ Bq cm}^{-3}$  in water are attained. However, the radiation measurements except calorimetry are inapplicable to a very high concentration of T. For much large amount of T, mass and/or pressure measurements (referred as conventional methods hereafter) are employed, which are ordinarily used to measure the stable hydrogen isotopes. The calorimetry allows measurements of the released energy of the T disintegration (decay heat), but its accuracy is only 2–3 digits. All present T measurements except the radiation measurements give only 3–4 digits in accuracy, and the change in T concentration less than 0.1 % is hardly possible to detect.

Among various radiation measurements, gas ionization detectors such as an ionization chamber and a proportional counter are particularly beneficial to detect and to quantify T in gas phase. However, they cannot be applied to detect T in solids or liquids, because the escaping depth of the  $\beta$ -electrons in solids or liquids is only a few  $\mu\text{m}$  and those emitted inside of them cannot escape from their surfaces. Measurements of T in solids or liquids require special techniques. The combustion method, in which T in materials is fully combusted to HTO vapor to be measured by a liquid scintillation counter, is a special technique for the qualitative analysis of T in materials.

For pure hydrogen gas containing T, volumetric (PVT method) and gravimetric methods are reliable. However, to obtain the absolute amount of T, its concentration in the gas should be separately measured. If a sample gas contains hydrogen isotopes or other hydrogen compounds, identification of all chemical species included is required.

Nondestructive analysis of hydrogen in solids or liquids is hardly possible. There are several reasons for that. Hydrogen diffusion is fast enough to enhance hydrogen release with a little increase of temperature. Secondary ion mass spectrometry (SIMS) is one of the important methods to know the depth profile of hydrogen in materials with isotopic separation. However, readily diffusive release of hydrogen from solid surface by the probe beam heating prohibits the quantitative analysis of hydrogen. Any beam probe methods using electrons, ions, and laser always accompany some hydrogen release by the beam heating. The binding energy of 1 s electron of hydrogen is too low to employ electron spectroscopy such as X-ray photoelectron spectroscopy (XPS) and Auger electron spectroscopy (AES). Methods using electronic or magnetic field can be used, but sensitivity for hydrogen atom is too small to detect trace amounts of hydrogen.

T has been used as a tracer of hydrogen to investigate behavior of H and interactions of H with materials. In such cases, the amount of T handled is too small

to measure with conventional hydrogen detection techniques. Radiation measurements are employed instead. On the other hand, in the fuel cycling system of a fusion reactor as described in Chap. 1, the amounts of T handled are too much to count the disintegration of T. Consequently, conventional methods used for the analysis of normal hydrogen have to be employed. No single method can cover very wide ranges of T concentration in a fusion reactor. Therefore, appropriate methods should be chosen depending on the concentration of T to be measured. To quantify T in plasma core, special or totally different techniques are required, of which details are described in the next chapter.

Following sections describe methods and their applications, conventional ones used for analysis of ordinary hydrogen (H and D), and radiation measurements specified to T. Additionally described are how these methods are applied in a fusion reactor facilities to measure/analyze T in gas, liquid (water), and solid phases, separately.

## 7.2 Techniques for Tritium Measurements

Figure 7.1 shows various techniques of T measurements with the separation of direct physical methods and radioactivity measurements. In general, the direct physical methods and the radioactivity measurements can be applied for higher activity levels of T and for lower activity levels of T, respectively. The applicability of these methods depends on the physical and chemical forms of T samples to be analyzed. In a fusion reactor, various states and forms of T are existing; they are T in gas phase, liquid phase, solid phase, and even plasma. Depending on the phases, different techniques are required. Therefore, the measurement techniques shall be properly selected in view of both the physical and the chemical forms of samples to obtain an accurate and reliable value. Particular concern in T measurements is

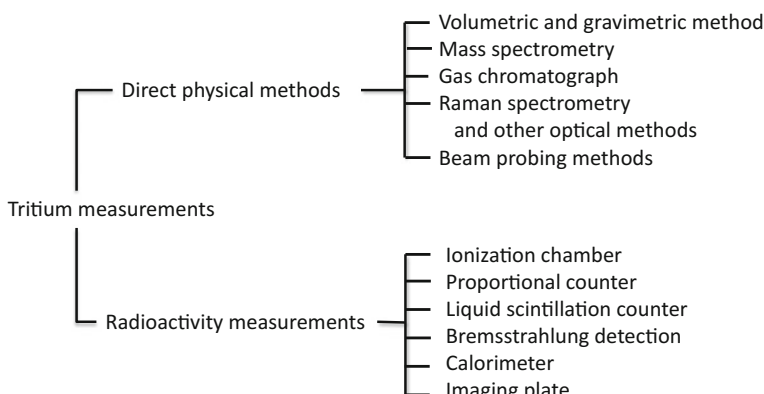


**Fig. 7.1** Classification of tritium measurement methods

contamination of measuring systems by T. The contamination disturbs succeeding measurement appearing as the memory effect.

### 7.2.1 Direct Physical Methods

#### 7.2.1.1 Volumetric and Gravimetric Measurements

The amount of T ( $n$ ) in gaseous form at 1 bar of pressure and above 300 K can be evaluated from the ideal gas law,  $PcV = nRT$ , where  $P$ ,  $V$ , and  $T$  are pressure ( $P$ ), volume ( $V$ ), and temperature ( $T$ ) of sample gas including T with the concentration ( $c$ ). To assay the gaseous T, the sample gas is loaded into an evacuated container with its volume of  $V$  through a valve. The pressure of the sample gas in the container is measured at a given temperature. The temperature of the sample gas should be accurately measured, because the uncertainty of the temperature leads to less accuracy in  $n$ . For example, the uncertainty of temperature measurement of 1 K near room temperature turns out to be 0.3 % of uncertainty in  $n$ . Since the volumetric measurement cannot provide the partial pressure or concentration of T species in the sample gas, its chemical composition should be separately determined with using mass spectrometry, Raman spectrometry, gas chromatography, and other techniques.

In a fusion reactor, T fuel must be recovered and reused. All T in the system is once stored or fully recovered in a metal hydride bed or a gas reservoir. The volumetric method is readily applied for the measurement of T in the gas reservoir. In case of a T stored bed, the gravimetric method can be used. Mass difference of the stored bed before and after storage directly gives the mass of stored hydrogen isotopes. The gravimetric method is generally used for a pure T gas handling system and even for a mixed gas of H and T, if their concentration ratio is known.

#### 7.2.1.2 Mass Spectrometry

There are various types of mass spectrometers to identify and to quantify gas species. Owing to radioactivity of T, particular cares are required to use mass spectrometry for the analysis of T-containing gas: (1) increasing noise level of a mass spectrometer due to the  $\beta$ -electrons from the T compounds adsorbed on surfaces of any components of the mass spectrometer [1], (2) the memory effect, as already described in Chap. 3, disturbs successive measurements after a measurement of high concentration T gas. The individual detection of all isotopes of hydrogen and helium requires high resolution over 1000 in mass spectrometry, because the molecular masses of HT, D<sub>2</sub>, and <sup>4</sup>He are quite close with each other (4.0239, 4.0282, and 4.0026, respectively) as listed in Table 7.1 [2–4]. High-resolution mass spectrometers are commercially available for both sector and quadrupole types.

**Table 7.1** Required minimum resolution to separate each isotopologue of hydrogen molecules and He in QMS [4]

Species	Mass (Da)	$H_2^+$	${}^3He^+$	$HD^+$	${}^4He^+$	$HT^+$	$D_2^+$	$T_2^+$
$H_2^+$	2.01565	–	3.0	3.0	2.0	2.0	2.0	1.5
${}^3He^+$	3.016029319	2.0	–	512.4	4.1	4.0	4.0	2.0
$HD^+$	3.021926779	2.0	511.4	–	4.1	4.0	4.0	2.0
${}^4He^+$	4.002602	1.0	3.1	3.1	–	189.2	157.3	3.0
$HT^+$	4.02387427	1.0	3.0	3.0	188.2	–	930.5	3.0
$D_2^+$	4.028203558	1.0	3.0	3.0	156.3	929.5	–	3.0
$T_2^+$	6.03209854	0.5	1.0	1.0	2.0	2.0	2.0	–

To make the quantitative measurement by a mass spectrometer, two important factors must be taken into account: One is a sensitivity factor of a detector for a targeted molecule, and the other is its fragmentation into smaller ones. Watanabe et al. [5] have determined relative sensitivity factors of all isotopologues of hydrogen molecules normalized to that of  $H_2$  for a quadrupole mass spectrometer (QMS) equipped with a Faraday cup but without a secondary electron multiplier (SEM) as listed in Table 7.2. The relative sensitivity factors of  $H_2$ , HD, and  $D_2$  are nearly the same, while those for HT and DT are a little different and that of  $T_2$  is significantly smaller than those of the other isotopologues of hydrogen molecules. Titov [4] reported that the relative sensitivity factors of the isotopologues of hydrogen molecules exponentially decrease with increase in their molecular mass [4]. The relative sensitivity factors should be occasionally calibrated by measurements of stable hydrogen isotopes. Although the fragmentation pattern is the other important factor for the quantitative analysis, those of HT, DT, and  $T_2$  are hardly reported.

QMSs often equip with SEM to enhance their sensitivity. SEM amplifies the number of electrons induced by mass-analyzed ions. It should be noted that the  $\beta$ -electron emitted from T could induce secondary electrons to be electronic noises in SEM [1, 2]. The electric noise becomes appreciable owing to the accumulation of T by adsorption on the dynodes of SEM after its cumulative use for T detection and disturbs the sensitivity. Although the adsorbed T on the dynodes can be partly removed by baking [6], full removal is quite hard. Thus, employment of SEM for the detection of T compounds sometimes prohibits their quantitative analysis. The

**Table 7.2** Relative sensitivities of a mass spectrometer for hydrogen isotopes ( $R_M^X = S_M^X / S_M^{H_2}$ ) determined by Watanabe et al. [5]

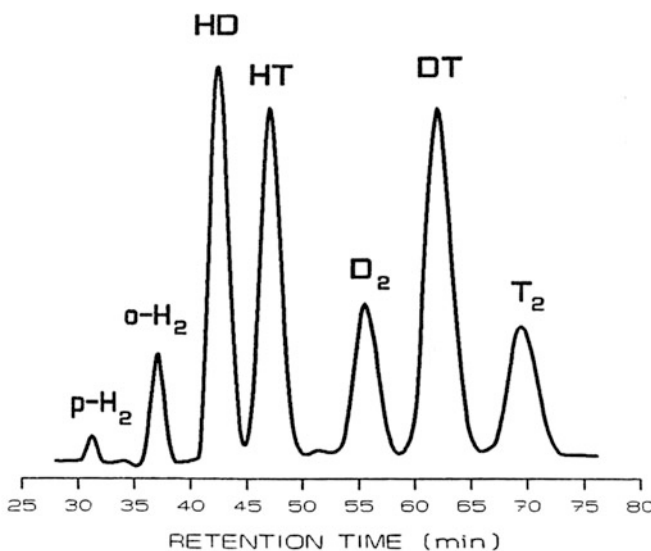
Isotopes	M/e	$R_M^X = S_M^X / S_M^{H_2}$
$H_2$	2	1.00
HD	3	$1.09 \pm 0.06$
$D_2$	4	$0.99 \pm 0.03$
HT	4	$1.06 \pm 0.06$
DT	5	$0.96 \pm 0.04$
$T_2$	6	$0.88 \pm 0.03$

influence of T radioactivity on mass analysis of gases including high T concentration is not well investigated, and more examinations are required.

### 7.2.1.3 Gas Chromatography and Raman Spectroscopy

Gas chromatography [7–11] and Raman spectroscopy [12–15] have been used for the quantitative analysis of the composition of gaseous samples containing T. Since many textbooks of gas chromatography and Raman spectroscopy are available in various languages, only key issues on their applications for the analysis of T-containing gases are briefly described here.

To separate hydrogen isotopes by a gas chromatograph, it is well known that iron oxide is doped on packing materials in its column such as activated alumina, molecular sieves, and silica gel [7–11]. In addition, the column is cooled at a cryogenic temperature. Figure 7.2 shows an example of six isotopologues of hydrogen molecules which are separated by a gas chromatography [11]. Since impurities contained in analyzed gases condense or adsorb on the packing material



Adsorbent:	Molecular Sieve 5A	Laboratory:	Merck
Carrier Gas:	Helium 5.6	Flow Rate:	48 ml/min
Column:	2 mm ID x 2.5 m	Temperature:	-155 °C
Sample:	H / D / T	Sample Volume:	0.035 ml NTP

**Fig. 7.2** An example of gas chromatographic separation of all isotopologues of hydrogen molecules under the conditions given at the bottom of the figure (Reprinted with the permission from [11])

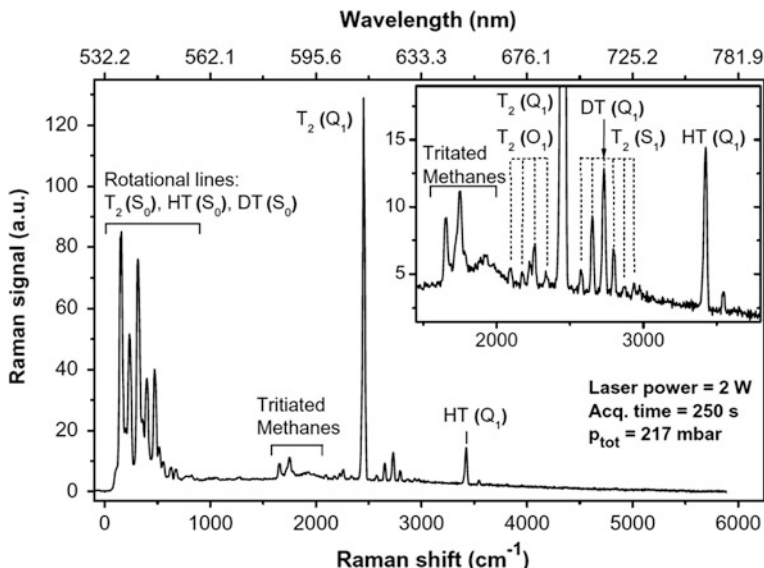


**Fig. 7.3** Raman spectrum of flowing gas sample containing  $T_2$ , DT, HT, and tritiated methane species ( $CT_4$ ,  $CHT_3$ , and  $CDT_3$ ) (Reprinted with permission from [14])

at the cryogenic temperature, they have to be removed before the gas analysis or to bypass the column. When the column captures large amount of impurities, it loses its function and reactivation of the column is required to remove adsorbed impurities with heating the column under an inert gas stream.

The laser Raman spectrometry provides several advantages for the analysis of hydrogen isotope molecules: (1) non-contacting and nondestructive analyses providing less contaminants, (2) superior discrimination ability of isotopologues of hydrogen molecules [12], and (3) on-site process line analysis. In the Raman spectrometry, an optical cell and optical paths are carefully designed. Since the Raman scattering generates the faint light emission with a wavelength very close to that of the intense incident light, optical paths, optical windows, the brightness, the resolution of spectrometer, and the detector must be optimized. The Raman spectroscopy is used as an in-line T monitor in Tritium Laboratory in Karlsruhe, Germany, and an example of spectrum of flowing gas sample containing  $T_2$ , DT, HT, and tritiated methane is shown in Fig. 7.3 [14].

## 7.2.2 *Detection of Disintegration of T*

### 7.2.2.1 Characteristics of Electrons Emitted from T

T decays into  ${}^3\text{He}$  by emitting a  $\beta$ -electron (hereafter referred simply as the  $\beta$ -electron) having energy of 18.6 keV at maximum and 5.7 keV in average. (see Fig. 2.1 in Chap. 2). The kinetic energy of the  $\beta$ -electrons in a material will be dissipated by collisions with electrons bound in constituent atoms or molecules of the material to excite and/or ionize them. Alternatively, the  $\beta$ -electron is deflected by the electromagnetic field of the nuclei in the material, and it loses kinetic energy with emitting electromagnetic wave (photons) referred as “bremsstrahlung” or “braking radiation”. After the  $\beta$ -electron fully loses its energy by these two energy loss processes, it is captured in the orbital of the atoms or molecules. Generally, the energy loss is dominated by the ionization process, while the production of bremsstrahlung increases with increasing the atomic number of the constituent element of the material.

The penetration length of an electron until it fully loses its energy is known as an extrapolated range. The extrapolated range,  $R_e$  [g cm $^{-2}$ ], of an electron with energy  $\varepsilon$ [MeV] is given by a following empirical equation by Flammersfield [16],

$$R_e = 0.11 \left( \sqrt{1 + 22.4\varepsilon^2} - 1 \right) \quad (7.1)$$

The range of the  $\beta$ -electron ( $\varepsilon = 18.6$  keV) in dry air at the standard pressure is estimated to be 0.35 cm, while that in aluminum is only 1.57  $\mu\text{m}$ . Such short range prohibits the  $\beta$ -electron escaping from a material and makes the detection of the  $\beta$ -electron in the material quite hard as already noted in Chap. 2. Nevertheless, the  $\beta$ -electrons are used for the detection of T retained in the material within the range from its surface. In addition, the bremsstrahlung emission can be used for the detection of T. Although the bremsstrahlung photon generated in deeper depth than the range of the  $\beta$ -electron can be detected, the generation efficiency of the bremsstrahlung photon is less than that of the ionization process.

To detect the  $\beta$ -electron, consideration of its energy loss before escaping from a material is important. When an electron having energy  $\varepsilon$  travels in a material to the x-direction, it loses energy as,

$$-\frac{\partial \varepsilon}{\partial x} = S(\varepsilon) \quad (7.2)$$

where  $S(\varepsilon)$  is referred as a stopping power.

The stopping power can be divided into two factors, i.e., that caused by electron excitation and photon emission including bremsstrahlung emission as:

$$S(\varepsilon)_{\text{tot}} = S(\varepsilon)_{\text{electron}} + S(\varepsilon)_{\text{photon}} \quad (7.3)$$

The subscripts “tot”, “electron”, and “photon” correspond to the total stopping power, and stopping powers are caused by electron excitation (ionization process) and photon emission (bremsstrahlung), respectively. The stopping power of the electron excitation and the photon emission is correlated [16] as

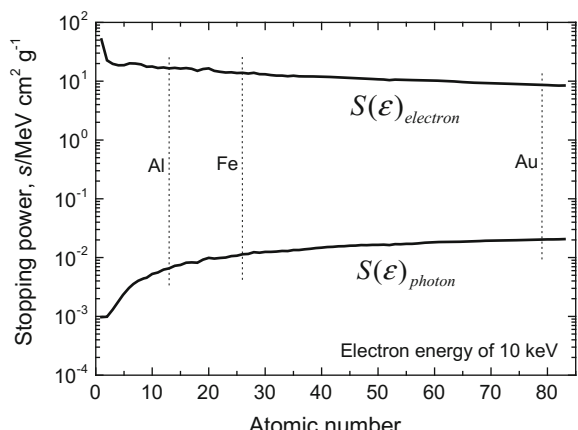
$$S(\varepsilon)_{\text{photon}} = \frac{Z\varepsilon}{\alpha} S(\varepsilon)_{\text{electron}}, \quad (7.4)$$

where  $Z$  is the atomic number of a constituent element of the material, and  $\alpha$  is a proportional factor which depends on the energy of electrons. Usually,  $S(\varepsilon)_{\text{photon}}$  is much smaller than  $S(\varepsilon)_{\text{electron}}$ . For example, in a metal,  $\alpha$  is given to be about 750 for electrons with energies of MeV region. According to Eq. (7.4),  $S(\varepsilon)_{\text{photon}}$  increases with increasing the atomic number. However, Eq. (7.4) cannot be applied for low-energy electrons like the  $\beta$ -electrons of T. The stopping power for electrons having energies below around 10 keV is calculated by a simulation code like ESTAR [17]. Figure 7.4 shows the dependence of stopping powers on the atomic number. The stopping power of ionization,  $S(\varepsilon)_{\text{electron}}$ , is much larger than that of bremsstrahlung,  $S(\varepsilon)_{\text{photon}}$ . In a heavy metal like gold,  $S(\varepsilon)_{\text{photon}}$  is only 1/400 of  $S(\varepsilon)_{\text{electron}}$ . For lighter materials, the energy loss by the photon emission becomes less as shown in Fig. 7.4. More detailed values are given in a reference [18].

Comparing with the  $\beta$ -electron, the bremsstrahlung photons penetrate much longer in a material which is beneficial to detect T in it. Energy of the bremsstrahlung photons  $h\nu$  is given as

$$h\nu = E_i - E_f \quad (7.5)$$

**Fig. 7.4** Changes of stopping powers of electron excitation and photon emission with atomic numbers of absorbers for 10 keV electrons



where  $h$  is the plank constant,  $E_i$  is the energy of the incident electron before the deflection, and  $E_f$  is the energy after the deflection. In case of the highest energy transfer of the  $\beta$ -electron, the photon energy is 18.6 keV, of which wavelength is given by

$$\lambda = \frac{hc}{hv} = \frac{12.4 \times 10^{-10}[\text{keVm}]}{18.6[\text{keV}]} = 0.67 \times 10^{-10}[\text{m}] \quad (7.6)$$

Since energy transferred to the bremsstrahlung photons can change from the maximum to 0, the wavelength of the bremsstrahlung photons distributes from  $0.67 \times 10^{-10}$  m to infinity.

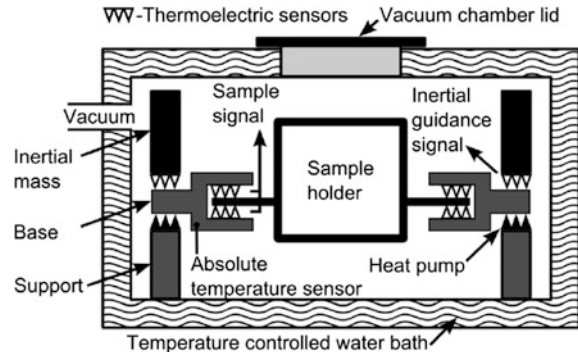
In the following sections, 5 methods used for T measurements relating to the  $\beta$ -electron are briefly explained. They detect (1) energy lost or deposited in a material (calorimetry), (2) secondary ions and electrons generated by the  $\beta$ -electron in gas (ionization chamber), (3) photons generated in a scintillator (scintillation counter), (4) bremsstrahlung photons (Beta ray-Induced X-ray Spectrometry, BIXS) in a material, and (5) the  $\beta$ -electron escaping from the material ( $\beta$ -electron counting and/or an imaging plate method).

### 7.2.2.2 Calorimetry

Deposited energy of the  $\beta$ -electrons in a material is turned to be decay heat and raises the material temperature. Although the decay heat of T ( $0.91 \text{ pW Bq}^{-1}$  or  $324 \text{ mW g}^{-1}$ ) is not large, it is fully deposited into the material retaining T owing to the very short range of the  $\beta$ -electron. Therefore, measurements of the decay heat of T retained in a sample with using a calorimeter give the absolute amount of T, and the method is referred as calorimetry.

The calorimetry can accept various kinds of samples: gas, liquid, solid, and their mixtures. However, the small decay heat does not allow the measurement of lower activity T (low T concentration). The calorimetry for T measurements has been developed and used worldwide in tritium laboratories. Recently, a dual cell, near-isothermal (heat flow) calorimeter is developed [19], which makes precise measurements of the heat flow, and detection limit is much improved compared to traditional single cell calorimeters. The newest one in Tritium Laboratory in Karlsruhe is described by Bükk-Deme et al. [20] and schematically shown in Fig. 7.5. Calorimetry is planned to use as an in situ T monitor of a T storage tank in ITER [21]. Since the calorimeter detects any heat, any chemical reactions accompanying emission/absorption of heat should interfere. Therefore, chemically active species, if they are included, should be converted into the stable ones [19].

**Fig. 7.5** Schematics of upgraded TLK tritium calorimeter, IGC-V0.5, with inertial guidance (Reprinted with the permission from [20])



### 7.2.2.3 Ionization Chamber

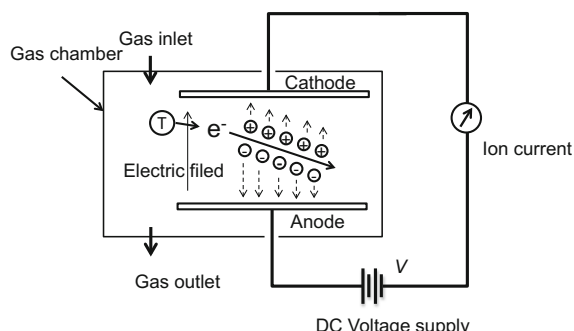
An ionization chamber is a gas-filled radiation detector widely used for the detection of ionizing radiations: X-ray, gamma ray, and energetic particles. The ionization chamber detects charge (electrons and ions) induced by the ionizing radiation [22]. There are two types in the detection of the charge: one is a simple ionization type such as an ionization chamber, and the other is a gas multiplication type such as a proportional counter.

The ionization chamber is one of the simplest devices for radioactivity measurements. A typical ionization chamber consists of a detection chamber and electrodes in it. The concept of the ionization chamber for the T measurement is schematically shown in Fig. 7.6. The electrodes provide an electric field which prevents the recombination of ions and electrons generated by the  $\beta$ -electron, and the electric field accelerates the ions and electrons toward the electrodes inducing ionization current to be measured.

The ionization current,  $i$  [A], induced by the radioactivity,  $a$  Bq  $[s^{-1}]$ , is expressed as:

$$i = \frac{feE_\beta a}{W} \quad (7.7)$$

**Fig. 7.6** Schematics of ionization chamber operation for gaseous T



where  $f$  is a collection efficiency of ions,  $e$  [C] is the elementary charge,  $E_\beta$ [eV] is the averaged energy of the  $\beta$ -electron, and  $W$  [eV] is the formation energy of an ion pair in a gas filling the chamber (referred as “W-value”). The W value of fast electrons for dry air is known to be 33.8 eV and that for helium is 41.3 eV [22]. Therefore, the ionization current changes with the gas species filled in the chamber. According to Eq. (7.7), for instance, the number of ion pairs in dry air generated by an electron with energy of 18.6 keV is

$$18.6 \times 10^3[\text{eV}] / 33.8[\text{eVion}^{-1}] = 550[\text{ions}] \quad (7.8)$$

Therefore, a 18.6 keV electron coming into the chamber per second induces the ionization current given by

$$\begin{aligned} 550[\text{ions}] \times 1.602 \times 10^{-19}[\text{C}] &= 8.81 \times 10^{-17}[\text{Cs}^{-1}] \\ &= 8.81 \times 10^{-17}[\text{A}] \end{aligned} \quad (7.9)$$

Volume of the ionization chamber is an important factor to determine the detection limit. Considering air containing  $0.1 \text{ Bq cm}^{-3}$  of T-emitting  $\beta$ -electrons with the average energy of 5.6 keV, the required chamber volume to obtain 10 fA as the ionization current is calculated to be

$$\begin{aligned} \frac{5.6 \times 10^3[\text{eV}]}{33.8[\text{eVion}^{-1}]} \times 0.1[\text{Bqcm}^{-3}] \times V[\text{cm}^3] \times 1.602 \times 10^{-19}[\text{C}] &= 10 \times 10^{-15}[\text{A}] \\ V &= 3.8 \times 10^3[\text{cm}^3] \end{aligned} \quad (7.10)$$

where 100 % of the collection efficiency,  $f$ , is assumed. Although larger chamber volume gives larger ionization current, a smaller volume is better for T safety, reducing sample gas volume and surface contamination. Therefore, the chamber volume must be optimized considering T radioactivity to be measured [23].

A proportional counter uses the same principle, but it requires an additional gas (referred as a proportional gas) and a higher electric field to amplify the ionization current. Although the proportional counter has higher sensitivity compared with the ionization chamber, the addition of the proportional gas is unsuitable for an in-line monitor. Hence, the ionization chamber is used as a process gas monitor in gaseous T handling systems. It should be noted that the ionization chamber does not work under vacuum condition.

#### 7.2.2.4 Liquid Scintillation Analyzer

Liquid scintillation analyzer (LSA) is one of the most important methods to measure the  $\beta$ -electron of T. Since the range of the  $\beta$ -electron is quite short even in air, a liquid sample having T is directly mixed with a liquid scintillator to effectively

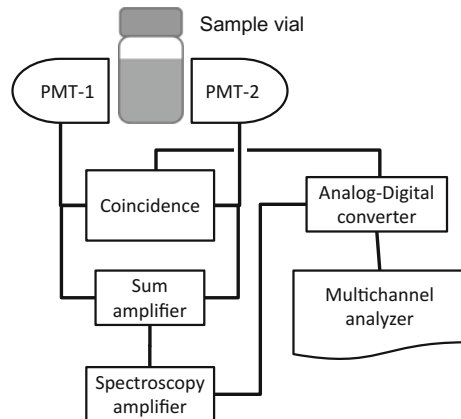


**Fig. 7.7** Schematic diagram of modern liquid scintillation analyzer

induce scintillation. The scintillation cocktail which includes the scintillator and the sample will be measured by LSA. A schematic diagram of LSA is given in Fig. 7.7 [24], where two photomultipliers (PMTs) are equipped to convert the flash of the scintillation into electric current pulses. Taking coincident selection of two pulses from PMTs, those pulses caused by the disintegration are separated from background noises in the system. After amplification of the pulses, their pulse heights are analyzed with a multichannel analyzer to get the pulse height spectrum and the disintegration rate.

The mechanism to give scintillation (scintillation process) is shown in Fig. 7.8. The energy of radiation released with the disintegration of a radionuclide is absorbed by the solvent of scintillator. The absorbed energy is transferred to a fluor (scintillator), and then, the excited fluor relaxes via emitting the photon referred as the scintillation. The intensity and frequency of the scintillation are proportional to the energy of the radiation and the disintegration rate of a radionuclide, respectively. However, not all the energy of the radiation is converted into the scintillation photon. There are two dominant processes in the energy dissipating other than the scintillation: They are referred as “chemical quenching” and “color quenching”. These processes are shown in Fig. 7.8. The former is caused by any other energy dissipation in the scintillation cocktail than the energy transfer to the fluor. This process results from unwanted concomitants in the scintillation cocktail. The color quenching is caused by colored substances in the scintillation cocktail. Both processes must be taken into account to determine the disintegration rate of sample. The chemical quenching can be corrected by using a quenched standard set. For  $^{3}\text{H}$  or  $^{14}\text{C}$ , the quench standard sets are commercially available. For other radionuclides, the quenched standard set should be prepared by oneself. There is no widely established way to correct the color quenching. In case that a radioactive sample is colored, it should be decolorized or be diluted before the cocktail preparation.

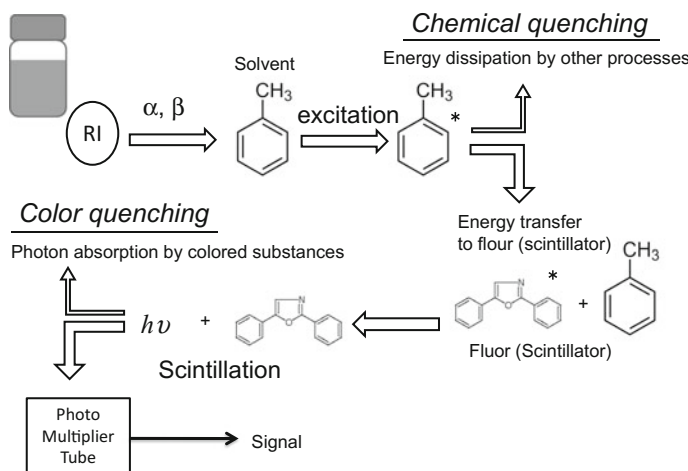


**Fig. 7.8** Liquid scintillation process together with chemical and color quenching processes

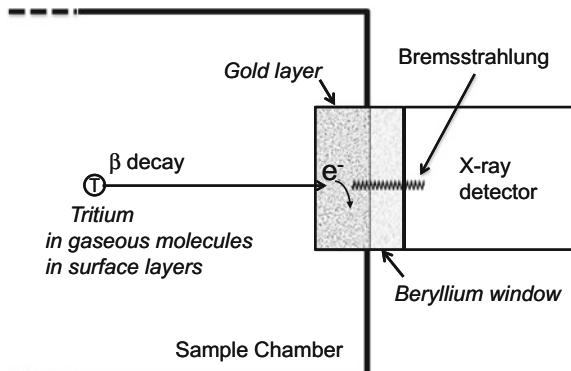
Therefore, selection and preparation of a sample and scintillation cocktail are quite important to obtain accurate and reproducible results as described later (Sect. 7.5.2).

### 7.2.2.5 Bremsstrahlung Measurements

Comparing with energy loss by ionization process, that by radiative stopping process,  $S(\varepsilon)_{\text{photon}}$ , including bremsstrahlung is smaller as shown in Fig. 7.4. Nevertheless, the bremsstrahlung caused by T in materials is used for T detection. The radiation can be detected with X-ray detectors such as a NaI scintillation detector and a Ge detector. Since the penetration length of the bremsstrahlung induced by the  $\beta$ -electron is longer than its range, the measurement of the bremsstrahlung allows to know T existing in a little deeper region of materials and allows to determine depth profile of T. Thus, T measurements using the bremsstrahlung have unique features and are referred as Beta ray-Induced X-ray Spectrometry (BIXS).

The application of BIXS for T measurements in gas is described here. To enhance the intensity of the bremsstrahlung, a high atomic number material should be selected as an absorber (see Fig. 7.4). Therefore, designing of a measurement system is essentially important [25–29]. In a gaseous T measurement by BIXS, Matsuyama et al. [25–28] have succeeded to improve the detection efficiency by using a gold-plated beryllium window as shown in Fig. 7.9. The gold layer effectively converts the kinetic energy of the  $\beta$ -electron into the bremsstrahlung, and its thickness is adjusted to be  $8.0 \times 10^{-8}$  m referring the range of the  $\beta$ -electron having the average energy of 5.6 keV. The number of bremsstrahlung photons is proportional to the number of the  $\beta$ -electrons that enter the gold layer.

**Fig. 7.9** Mechanism of BIXS for measurement of T in gas phase



The geometry including the volume of the sample chamber is optimized to have enough numbers of the  $\beta$ -electrons entering the gold layer. The gas pressure in the chamber should be also adjusted, because the penetration depth of the  $\beta$ -electron in the sample gas decreases with increasing its pressure. Therefore, the pressure dependence of the counting efficiency must be calibrated for each measurement system. No BIXS systems to measure T in gas phase are commercially available. BIXS is also established for the measurements of T in near surface region of a solid and separately described in Sect. 7.6.2.2.

### 7.2.2.6 Tritium Imaging

Radionuclide imaging is called “autoradiography”. T distribution on material surface can be measured by the autoradiography. Conventional autoradiography uses photographic emulsion. The reduction of silver halide in the emulsion by radiation (the  $\beta$ -electron) makes a latent image. The latent image is fixed by the development process to give T distribution as an image. The T autoradiography has been used to observe local accumulation of hydrogen in steels for its importance in the study of hydrogen embrittlement. Recent advances in photoelectric devices allow to use an imaging plate (IP) instead of the photographic emulsion for T imaging. IP has the photostimulable phosphor layer (PSP) made of  $BaFBr:Eu^{2+}$ . PSP stores the energy of the incident  $\beta$ -electron to IP and records its position. The stored energy in PSP is released by the photostimulation of He–Ne laser as photostimulated luminescence (PSL). By contacting IP to a material surface retaining T, the distribution of T on the surfaces is imaged to IP. The PSL intensity is proportional to the T radioactivity at a given position, and it can be converted into T activity by using a reference standard of T. However, the PSL intensity decreases with time after the exposure of radiation as known “fading”. The fading is moderated by keeping IP at a lower temperature after the exposure.

Tritium imaging plate technique (TIPT) is very convenient to get the distribution of T on the surface. The surface of the conventional IP is covered by protective

layers to allow multiple uses. Since the protective layers prevent T penetration to the phosphor layer, IP for T imaging does not have the protective layer. Hence, a very thin film is inserted between IP and a sample to avoid the T contamination of IP. In high-level T measurements, the contamination of IP by T permeating through the film should be concerned. A suitable application of IP to determine T profile on plasma-facing tiles used in D-D discharging plasmas is given in Fig. 5.8 in Chap. 5.

### 7.3 Amount and Chemical Form of T Handled in a Nuclear Fusion Facility

Figure 7.10 schematically shows fuel cycle systems of a nuclear fusion plant. In the figure, chemical species of T flowing through are also given. As described in Chap. 1, around 56 kg T is burned in a year to give 1 GWe by a D-T fusion reactor. Because of poor burning efficiency, T fuel throughput would be kg/day and nearly the same amount of the fuel throughput except those consumed by burning is retained in plasma-facing wall and/or exhausted. Fueling will be made by either or all of gas puff, ice pellet injection, and neutral beam injection of pure T and/or mixture of D and T. Therefore, major parts of the fuel cycle systems handle gaseous form of fuels. The exhaust from the reactor is low-pressure gas including He and some other impurities such as Ne, Ar, water (HTO), and hydrocarbons [or Organically Bound Tritium (OBT)]. Both D and T in the exhausted gases are

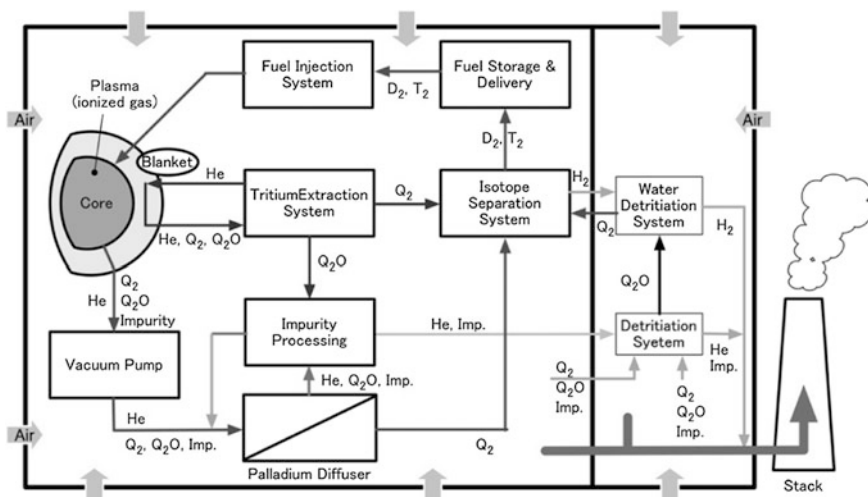


**Fig. 7.10** T fuel flow in a nuclear fusion plant. Chemical forms of T flowing through are indicated, referring all isotopologues of hydrogen molecules ( $H_2$ , HD,  $D_2$ , HT, DT, and  $T_2$ ) as  $Q_2$  and water molecules as  $Q_2O$

refined and separated in the isotope separation system. D and T extracted are transported to the fuel storage system to reuse as fuels (discussed in Chap. 6).

In any T handling systems, T released or leaked from the system should be minimized. Gaseous hydrogen isotopes easily leak from joints for piping or permeate through a material wall. Therefore, the concept of multiple confinement as described in Chap. 14 is adopted to prevent T release and to reduce radiological hazards. To realize this, T handling facilities and inside of glove boxes (GB) should be kept at negative pressure compared to the atmospheric pressure surrounding them. Furthermore, atmospheric gases in any T handling rooms and glove boxes are continuously ventilated to remove T (connected to T decontamination systems). In the T decontamination systems, all T compounds are converted into HTO by a catalytic oxidation, and HTO is captured by an adsorbent. T is transferred into water coolant by a leakage or a permeation. Accordingly, fair amount of HTO always exists in the water coolant. HTO is decontaminated by a water detritiation system (WDS). After T level in the detritiated water and/or gases is reduced to less than the regulation level, the detritiated water is released to the environment.

In any T handling systems, T accountancy for radiological safety is a quite important matter, so that T must be monitored or quantitatively accounted. In the following sections, T analyses in a fusion reactor plant will be described with the separation of T in gas phase, in liquid phase, and in solid phase. T analysis in plasma is also a quite important and a new particular task, which is described in Chap. 8 separately.

Generally, techniques or methods to measure T have been well developed, and they can be used or there are no other ways than to use them in a fusion plant. Nevertheless, the amount of T handled in a reactor is quite huge, and T accountancy is so strict. Significant improvement of them and invention of new techniques are required particularly for the determination of T inventory in a reactor.

## 7.4 T in Gas Phase (in Fuel Cycle System)

In a nuclear fusion reactor, pure T<sub>2</sub> or DT mixture gas will be handled with gas pressure ranging from vacuum to several atmospheres. On the other hand, T concentration in atmosphere of rooms and of glove boxes should be maintained as low as reasonably achievable. Therefore, T measurements need to cover so wide concentration range that no single method can cover. An appropriate measurement method depending on the T concentration and/or T processing system should be selected. In the following, measurements of T in gas phase are described separately for high and low T concentrations.

### 7.4.1 High-Level Measurements for T Process Systems

A volumetric method can determine the amount of gases including T. Since the volumetric method cannot determine the gas composition, T concentration in the gas should be separately measured by Raman spectrometry, gas chromatography, mass spectrometry, or other methods. The Raman spectrometry can be used as process monitoring to determine T compounds in the gas [13–15]. The gas chromatography is one of the most powerful techniques for quantitative analysis of T in any gas including T. However, it requires a gas sampling system with using a carrier gas. The analyzed gas must be detritiated before it is exhausted [7, 8, 10].

The mass spectrometer also requires a gas sampling system mostly with a pumping system. Selection of the pumping system is an important issue. An ion pump is unsuitable for pumping the mixed gas of noble gases and T compounds. Because it preferentially evacuates hydrogen gases, while noble gases are hardly evacuated. Therefore, the gas composition is changed by pumping with an ion pump.

An ionization chamber can be employed as a process monitor in any gaseous T handling system. The gaseous T can be directly or partly introduced into the chamber, and the exhausted gases return to the system. Since T concentrations in the processed gases are not necessarily suitable for the measurement by the ionization chamber as described in the previous section, the ionization chamber requires a suitable chamber volume and the electric field adjusted. It should be mentioned that ionization chambers do not work under vacuum conditions. The bremsstrahlung measurement is also a candidate for the quantitative analysis of T in the gas phase [25–29]. Different from the ionization chamber, this method is suitable for low-pressure condition because the  $\beta$ -electrons are readily stopped by coexistence gaseous molecules in the chamber.

For the selection of any methods described above as T monitoring, the gas pressure is an important factor.

### 7.4.2 Low-Level Measurements for Atmosphere

The above-mentioned methods are hard to apply to measure directly T diluted in gases with low T concentration and require condensation or accumulation of T. The most reliable method to measure the low T concentration in the gas phase is to use a trap system to condensate T compounds. They are converted into HTO by a direct or a catalytic oxidation, and HTO is trapped by the system. The concentration of HTO is determined by LSA. The concept of the trap system is schematically shown in Fig. 7.11. A sample gas is introduced in two traps which capture water components in the gas. Then, remaining gaseous T components, HT,  $\text{CH}_3\text{T}$ , and other T compounds are oxidized by an oxidizer (oxidation bed) to convert T included in them into HTO and trapped in additional two traps. In the oxidizer, copper oxide is

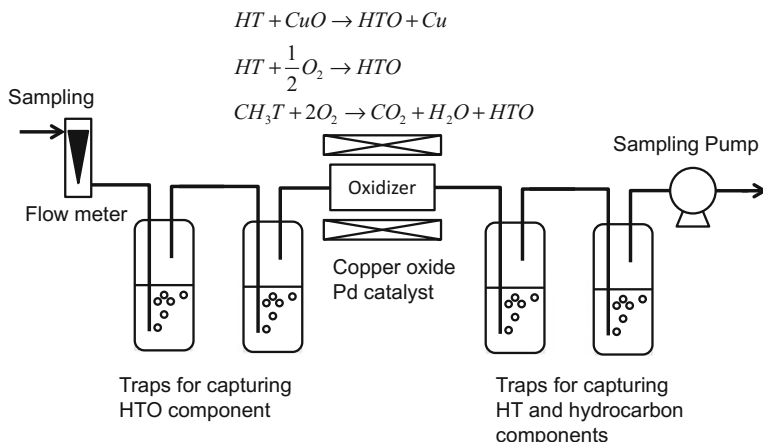


**Fig. 7.11** Tritium sampling system for measurement of T in air

used for the sample gas containing no oxygen molecules and a palladium catalyst is used for the sample gas containing oxygen molecules, T in air, for an example. The T concentration in the trapped water is determined by LSA. The detection limit of T with the trap method can be significantly improved with increasing the amount of the trapped water by introducing larger amount of the sample gas.

In the measurements of T in the gas phase by using an ionization chamber and/or a proportional counter, particular cares are required for the existence of HTO as an impurity in a sample gas. Since the adsorption of HTO on any surfaces of a detector is unavoidable, the accumulation of adsorbed HTO on the surface of the system disturbs measurements. This phenomenon is referred as “memory effect” and is significant in succeeding measurements after once high-level T is introduced into the system. There are two methods to reduce the memory effect: One is the substitution or removal of adsorbed HTO by the isotope exchange reaction, i.e., by introducing  $H_2O$  into the system, and the other is the thermal desorption (baking the system). In either way, it is difficult to completely eliminate the memory effect.

## 7.5 T in Liquid Phase and/or Tritiated Water

Handling of very high level of tritiated water requires special cares. Mainly because HTO is quite hazardous to the human body compared with HT, nearly 10,000 times. Another is a self-radiolysis, i.e., the  $\beta$ -electron decomposes  $H_2O$  into hydrogen and oxygen molecules accompanying the formation of various radicals [30]. Accumulation of hydrogen molecules in tritiated water for longtime storage would be a latent hazard for the handling. Therefore, the handling of the high level of tritiated water is generally done in the specially designed isolated space.

### 7.5.1 High-Level Measurements

Calorimetry is one of the most reliable ways to measure T activity in high-level tritiated water [31] and a specially designed calorimeter measures 100 MBq of HTO [32]. The inside surface of the sample cell of the calorimeter is covered with an inactive layer to prevent the chemical reaction of its surface with tritiated water [32]. Other radioactivity measurement methods can be used for high-level HTO. However, due to the upper limit of the radiation counting, dilution of sample is required to reduce the activity to be an appropriate level for the counting method. This not only brings error in measurements, but also requires additional care for safety. Thus, a great care in sampling or sample preparation is required.

### 7.5.2 Low-Level Measurements: Sample Preparation for Liquid Scintillation Analysis

As already described in Sect. 7.2.2.4, LSA is widely used for the measurements of T in liquid samples. Nevertheless, LSA requires special cares in sample preparations. In reference [33], Thomson wrote “*Correct sample preparation in LSA is essential for both accurate and reproducible analysis, and no amount of instrumental sophistication can ever fully compensate for the problems attendant to badly prepared sample.*” Here, the sample preparation means obtaining homogeneous, colorless, and less quenching scintillation cocktail. To use LSA for a quantitative analysis of T, a quenching in the cocktail, a selection of both vial and scintillator are concerned and they are described in the following.

The effects of chemical quenching in colorless cocktail can be corrected by using a suitable quenched standard set. On the other hand, correction of color quenching is not well established. A colored sample is subjected to bleach treatment or dilution to make a colorless cocktail.

Various types of liquid scintillators with different characteristics are commercially available. To make the homogeneous sample cocktail, which is indispensable for LSA, selection of the scintillators is quite important considering characteristic of samples, such as (1) aqueous or organic, (2) pH, and (3) salinity. Correction of the quenching in LSA is also important which is made by using the quench correction curve employing an appropriate quenched standard set [34]. The detailed restriction of LSA and the preparation of sample cocktails are reported by Verrezen et al. [35, 36].

Utilization of plastic vials sometimes gives unexpected problems, referred as “wall effect” [24, 36]. This effect prevents the quenching correction by using an external gamma source. Most of modern scintillators overcome this problem [24, 36].

Both the photoluminescence and the chemiluminescence in the cocktail prohibit obtaining the accurate and reproducible data [24]. They give additional pulses on

pulses caused by T in LSA. Usually, they are appreciable just after the sample preparation. However, they tend to decrease with time. Therefore, observation of the attenuation of the total luminescence could separate their disturbance on T measurements.

## 7.6 T in Solid Phase

The detection of T in a solid except very near surface region is hardly possible, because the  $\beta$ -electron cannot escape from the inside of the solid. Only calorimetry allows to measure the amount of T in the solid, if it is sufficiently large. Otherwise, T must be extracted from the solid to be analyzed by using other methods. Various techniques such as combustion, thermal desorption, chemical etching, physical sputtering, and mechanical cutting are employed for the T extraction from the solid for a quantitative analysis. T localized near surface region can be observed by the detection of the  $\beta$ -electrons. Various ion beam analyses usually used for H analysis in near surface region can be also used for T analysis. They are SIMS, Rutherford backscattering spectrometry (RBS), an elastic recoil detection analysis (ERDA), a nuclear reaction analysis (NRA), and so on.

### 7.6.1 T in Bulk

The combustion method is applied for the quantitative analysis of T in flammable samples [33, 37]. By combustion, T retained in a sample is converted into HTO and captured with a liquid trap or a cold trap. The captured HTO is measured by LSA. Figure 7.12 schematically shows a combustion system having two furnaces and two liquid traps. The flammable sample is heated in the first furnace under oxygen

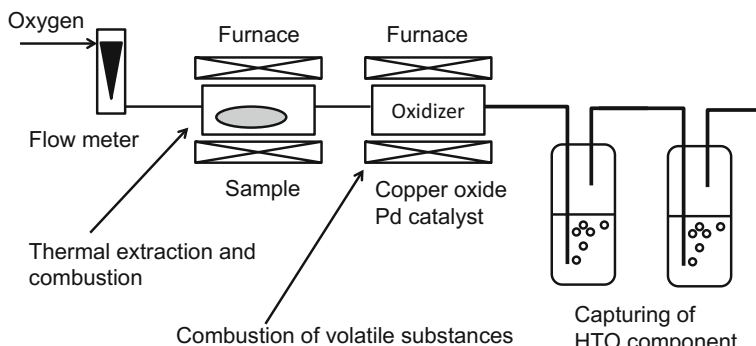


**Fig. 7.12** Apparatus for T extraction from a sample by the combustion method

stream to release HTO and other volatile compounds including T. The T compounds are fully combusted into HTO in the second furnace (oxidizer), and HTO is captured by the traps. The oxidizer plays an important role to fully oxidize volatile species, because the volatile species enhance both chemical and color quenching. Automatic combustion systems are commercially available [33].

The combustion system shown in Fig. 7.12 can be used also for nonflammable samples. Under inert gas stream instead of oxygen, higher temperature heating causes thermal desorption of T from the sample. The desorbed T is fully oxidized by using copper oxides as an oxidizer. The method is useful for the measurement of T in metals [38].

If a sample is a material soluble in acid, chemical etching can be applied. The sample is immersed in an acid solution to release T into the solution. Then, T in the solution is measured by LSA. It should be noted that dissolved metallic ions often color and increase salinity. Only limited scintillators are applied for high acidity and salinity solutions. The chemical etching of metals could release undesired gaseous hydrogen including T. In order to avoid the generation of the gaseous hydrogen, chemical etching by sodium persulfate instead of the acid solution is proposed [39].

### ***7.6.2 T on Surface and in Subsurface Regions***

T measurements of surfaces of any T handling systems are quite important for the contamination control for handling facility and the radiological safety. The  $\beta$ -electrons can be measured by a specially designed  $\beta$ -counter which equips an ultrathin window or window less to allow low-energy  $\beta$ -electrons to penetrate into its detector. Recently, BIXS is also used for surface T measurements. Owing to longer penetration depth of X-ray induced by the  $\beta$ -electron compared to that of the  $\beta$ -electron itself, BIXS detects T retained in a little deeper region than that the  $\beta$ -counter does. IP technique is also a newly developed technique to image T distribution on a surface.

In a fusion reactor, T accountancy is quite important both for T safety and for T self-sufficiency. The largest T retention appears in plasma-facing surfaces. At present, it is estimated from the balance between fuel supply into and its exhaust from a reactor vessel. However, its accuracy is quite poor, and hence, the development of techniques to quantify the T retention in the reactor vessel is urgent.

#### ***7.6.2.1 Ion Beam Analysis***

Surface analyses using ion beams including SIMS, RBS, NRA, ERDA, and AMS (Accelerator Mass Spectrometry) are powerful methods for detecting hydrogen in near surface region.

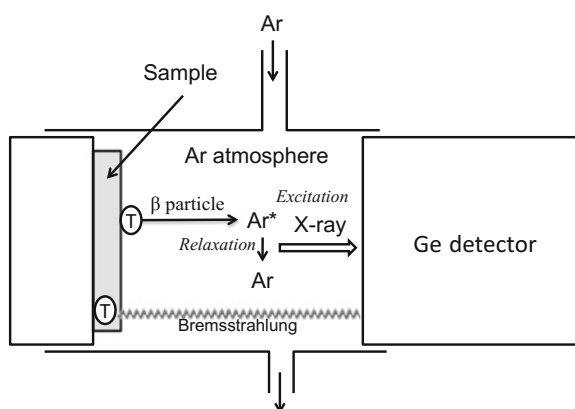
These methods have been applied for the depth profiling of H and D implanted in subsurface layers of candidate plasma-facing materials by many researchers.

They can simultaneously measure all hydrogen isotopes. Therefore, they can be applied for T analysis without any modification. The NRA [40] and the AMS [41] have been used for the detection of low level of T in materials. Nevertheless, all these methods require an ion source or an accelerator which is installed in vacuum chamber with a large volume. T released from a sample causes T contamination of their ion source, chamber wall and detection systems as well. Therefore, these ion beam analyses are not likely to be used as a standard detection technique of high-level T in near surface region.

### 7.6.2.2 Beta Ray-Induced X-Ray Spectrometry (BIXS)

BIXS has been successfully applied for the surface T measurements [42, 43]. Different from gaseous T measurements described in Sect. 7.2.2.5 (See Fig. 7.9), the surface T measurement utilizes characteristic X-rays as schematically shown in Fig. 7.13. The  $\beta$ -electrons emitted from material surface excite Ar atoms in atmosphere. Excited Ar atoms relax emitting their characteristic X-rays, which is detected by an X-ray detector such as a Ge detector. Since the  $\beta$ -electrons in a material induce both bremsstrahlung and characteristic X-rays of its constituent elements, the energy spectrum consists of the characteristic X-ray peaks and the broad component (bremsstrahlung) as shown in Fig. 7.14a, which is a typical BIXS spectrum of a 316 stainless steel (SS 316) sample retaining T. The spectrum consists of Ar(K $\alpha$ ) peak induced in atmospheric Ar gas, characteristic X-rays of Cr, Fe, and Ni, major constituents of SS 316, and continuum (1–12 keV bremsstrahlung induced in SS316 and Ar gas). The peak intensity of Ar(K $\alpha$ ) appeared at 3 keV is proportional to T concentration on the surface. Since the bremsstrahlung is caused by continuous energy loss of the  $\beta$ -electrons in a material as given by Eq. (7.2), BIXS spectrum can give the depth profile of T [44]. The depth profile obtained from the bremsstrahlung is shown in Fig. 7.14b. The depth profile shows that significant amount of T is localized at the surface and some T dissolved in the bulk. Thus,

**Fig. 7.13** Mechanism of BIXS for measurement of T at solid surface and in subsurface



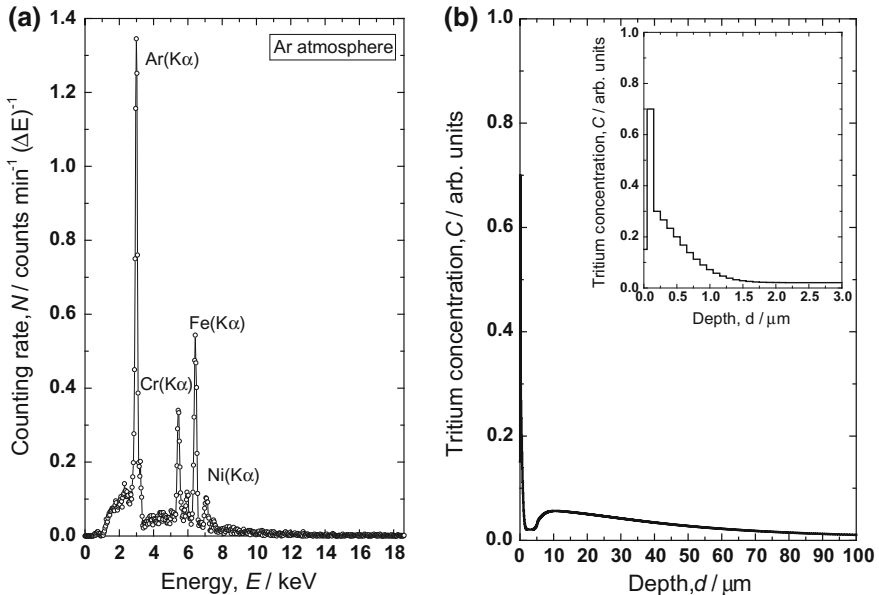


**Fig. 7.14** **a** Typical energy spectrum of photons given by BIXS for T retaining SS 316 sample and **b** depth profile reconstructed from continuum. Courtesy of Masao Matsuyama

BIXS spectrum provides various information of T in the subsurface region. However, BIXS is not applicable for large area measurements due to the limited size of the Ge detector.

### 7.6.2.3 Imaging Plate (IP)

An imaging plate technique gives surface distribution of T. An imaging plate (IP) directly attaches a sample surface retaining T. Consequently, T retained within the range of the  $\beta$ -electrons can be detected. IP also detects bremsstrahlung and characteristic X-rays induced by the  $\beta$ -electrons. However, their influence can be usually neglected, because the energy deposited into IP by them is much smaller than that of the  $\beta$ -electrons. On the other hand, insertion of a film between IP and the sample surface with thickness enough to shield the  $\beta$ -electrons but to allow the penetration of the characteristic X-rays and the bremsstrahlung makes detection of T in much deeper region possible. In 1998, Saito et al. [45] measure T distribution on metal surface applying IP instead of autoradiography using a classical photographic emulsion. Thereafter, IP is widely used for the studies of the interaction between T compounds and material surfaces. In particular, the behavior of T introduced into JET and TFTR discharges has extensively studied by IP as described in Chap. 5 [46–48] and an example is given in Fig. 5.8.

The disadvantage of IP to apply for T imaging is its potential cross-contamination by T due to the direct contact of IP to a sample. Insertion of a protective film between IP and the sample, which must be thin enough to allow the  $\beta$ -electrons to penetrate through but thick enough to suppress T permeation, protects the T contamination of IP, while reduces the sensitivity of IP.

#### 7.6.2.4 Swipe Assay

Swipe assays are widely used in order to monitor surface contamination of T handling rooms and laboratories [33]. The swipe assays are referred as smear or wipe tests. The assay is performed by swabbing potentially contaminated surfaces with a media capable of adsorbing/absorbing radioactivity such as a paper filter, a cotton swab, a cloth, and a glass fiber filter. This method is used to know the contamination of the large area at once. T taken on the surface of the wipe media is measured by an appropriate detection system. LSA is usually used with immersing the media directly in a liquid scintillator. If the media and/or T taken are soluble in the scintillation cocktail, all activity can be measured, while if not, the counting efficiency is concerned [33]. In addition, the results always include some uncertainty, because T of the contaminated surface is not necessarily transferred fully to the media by swabbing. The results could be altered by swiping manners, such as contacting times, contacting pressure, and surface roughness. This is particularly important to determine whether the T contamination at the specific location is over or below the regulation level. Nevertheless, the swipe assay is convenient to specify the contaminated areas and often used routinely in radiological controlled area.

## 7.7 Summary and Future Prospects

In any T handling systems, T accountancy for the radiation safety is very strict, so that T must be accurately quantified. Furthermore, any T release from the system and T contamination should be monitored. Therefore, techniques and/or methods of T measurements or T monitoring have been developed to be employed in the T processing/handling systems of a fusion reactor. In this chapter, T measurements are introduced by separating physical methods and radioactivity measurements. The amount of T handled in a reactor is huge, and T accountancy is strict so that concentration range of T to be measured is quite wide. Consequently, significant improvement of currently available T-measuring techniques and new techniques is indispensable. Furthermore, there are no ways to quantify T in solids nondestructively except calorimetry. The determination of the amount of T retained in system walls including plasma-facing surfaces remains to be solved. Contamination and/or memory effect of measuring systems caused by the measurements of high level of T are also a concern. In addition, strong radiation field induced by neutron activation of reactor materials prevents T detection by disintegration. Thus, research and

development for T measurements in a fusion reactor are one of the important tasks for T operation in ITER.

## References

1. H. Miyake, K. Ichimura, M. Matsuyama et al., Development of a Tritium compatible mass spectrometer. *Fusion Eng. Des.* **10**, 417–421 (1989)
2. R.E. Ellefson, W.E. Moddeman, H.F. Dylla, Hydrogen isotope analysis by quadrupole mass spectrometry. *J Vac. Sci. Technol.* **18**, 1062–1067 (1981)
3. J. Sreekumar, T.J. Hogan, S. Taylor et al., Quadrupole mass spectrometer for resolution of low mass isotopes. *J. Am. Soc. Mass Spectrom.* **21**, 1364–1370 (2010)
4. V.V. Titov, Isotopic quadrupole mass spectrometry of hydrogen and helium. *J. Radioanal. Nucl. Chem.* **174**, 205–222 (1993)
5. K. Watanabe, H. Miyake, M. Matsuyama, Relative sensitivities of Bayard-Alpert gauges and a quadrupole mass spectrometer for hydrogen isotope molecules. *J. Vac. Sci. Technol.* **A5**, 237–241 (1987)
6. K. Ichimura, M. Matsuyama, K. Watanabe, Adsorption and desorption of tritium on material for secondary electron multiplier. *J. Nucl. Sci. Technol.* **21**, 56–60 (1984)
7. R. Lässer, A.C. Bell, B. Grieveson et al., The analytical gas chromatographic system of the JET active gas handling system—Tritium commissioning and use during DTE1. *Fusion Eng. Des.* **47**, 333–353 (1999)
8. C. Genty, R. Schott, Quantitative analysis for the isotopes of hydrogen—H<sub>2</sub>, HD, HT, D<sub>2</sub>, DT and T<sub>2</sub>—by gas chromatography. *Anal. Chem.* **42**, 7–11 (1970)
9. M. Saeki, T. Hirabayashi, Y. Aratono et al., Preparation of gas chromatographic column for separation of hydrogen isotopes and its application to analysis of commercially available tritium gas. *J. Nucl. Sci. Technol.* **20**, 762–768 (1983)
10. R. Lässer, M. Glugla, S. Grünhagen et al., Use of gas chromatography in the tritium laboratory Karlsruhe. *Fusion Sci. Technol.* **41**, 515–519 (2002)
11. R. Vogd, H. Ringel, H. Hackfort et al., Gas chromatographic separation of hydrogen isotopes on molecular sieves. *Fusion Nucl. Technol.* **14**, 574–578 (1988)
12. M. Sturm, M. Schlösser, R.J. Lewis et al., Monitoring of all hydrogen isotopologues at tritium laboratory Karlsruhe using Raman spectroscopy. *Laser Phys.* **20**, 493–507 (2010)
13. S. Fischer, M. Sturm, M. Schlösser et al., Monitoring of tritium purity during long-term circulation in the KATRIN test experiment LOOPINO using laser Raman spectroscopy. *Fusion Sci. Technol.* **60**, 925–930 (2011)
14. S. Fischer, M. Sturm, M. Schlösser et al., Laser Raman spectroscopy for KATRIN. *Nucl. Phys. B* **229–232**, 492 (2012)
15. M. Schlösser, S. Rupp, H. Seitz et al., Accurate calibration of the laser Raman system for the Karlsruhe tritium neutrino experiment. *J. Mole. Struct.* **2013**, 61–66 (1044)
16. M.F. L'Annunziata, Nuclear radiation, its interaction with matter and radioisotope decay, in ed. by M.F. L'Annunziata *Handbook of Radioactivity Analysis*, 2nd edn. (Academic Pr, Amsterdam, 2003)
17. M.J. Berger, J.S. Coursey, M.A. Zucker, et al., *Stopping-Power and Range Tables for Electrons, Protons, and Helium Ions*. 2014, <http://www.nist.gov/pml/data/star/index.cfm>
18. L. Pages, E. Bertel, H. Joffre et al., Energy loss, range, and Bremsstrahlung yield for 10-keV to 100 MeV electrons in various elements and chemical compounds. *Atomic Data* **4**, 1–127 (1972)
19. R. Collé, Classical radionuclide calorimetry. *Metrologia* **44**, S118–S126 (2007)
20. A. Bükkí-Deme, C.G. Alecu, B. Kloppe, et al., First results with the upgraded TLK tritium calorimeter IGC-V0.5, *Fusion Eng. Des.* **88**, 2865–2869 (2013)

21. K.M. Song, S.H. Sohn, M.H. Chang et al., Effect of tritium storage vessel and aluminum secondary container on calorimeter performance. *Fusion Sci. Technol.* **60**, 1010–1013 (2011)
22. G.F. Knoll, Ionization chamber. in *Radiation Detection and Measurement*, 4th edn. (John Wiley and Sons, Inc, 2010)
23. M. Matsuyama, A small ionization chamber appropriate to tritium processing systems. *Fusion Eng. Des.* **18**, 91–96 (1991)
24. M.F. L'Annunziata, Liquid scintillation analysis: principles and practice. in ed. by M.F. L'Annunziata *Handbook of Radioactivity Analysis*, 2nd edn. (Academic Press, Amsterdam, 2003)
25. M. Matsuyama, H. Arai, T. Yamazaki, et al., In-situ measurement of high level tritium by Bremsstrahlung counting method (II) characteristics of a beryllium windows. *Annl. Rept. Hydrogen Isot. Res. Center Toyama Univ.*, **13**, 51–61 (1993)
26. M. Matsuyama, K. Watanabe, T. Yamazaki, Improvement of a Bremsstrahlung counting method for measurements of gaseous Tritium. *Fusion Technol.* **28**, 1045–1049 (1995)
27. W.M. Shu, M. Matsuyama, T. Suzuki et al., Characteristics of a promising Tritium process monitor detecting Bremsstrahlung X-rays. *Nucl. Instr. Meth. Phys. Res. A* **521**, 423–429 (2004)
28. M. Matsuyama, Y. Torikai, M. Hara et al., New technique for non-destructive measurements of Tritium in future fusion reactors. *Nucl. Fusion* **47**, S464–S468 (2007)
29. M. Rölling, F. Priester, M. Babutzka et al., Activity monitoring of a gaseous Tritium source by beta induced X-ray spectrometry. *Fusion Eng. Des.* **88**, 1263–1266 (2013)
30. S. Heinze, T. Stoltz, D. Ducret et al., Self-radiolysis of tritiated water: experimental study and simulation. *Fusion Sci. Technol.* **48**, 673–679 (2005)
31. T. Genka, K. Kobayashi, N. Takeuchi et al., A twin type heat flow microcalorimeter for radioactivity measurements. *Radioisotopes* **37**, 115–158 (1987)
32. M. Matsuyama, K. Takatsuka, M. Hara, Sensitivity of a specially designed calorimeter for absolute evaluation of Tritium concentration in water. *Fusion Eng. Des.* **85**, 2045–2048 (2010)
33. J. Thomson, Sample preparation techniques for liquid scintillation analysis. in ed. by M.F. L'Annunziata *Handbook of Radioactivity Analysis*, 2nd edn. (Academic Pr, Amsterdam, 2003)
34. J. Thomson, Use and preparation of quench curves. LSC Application Note. 2002, PerkinElmer Life Science P11399
35. F. Verrezen, H. Loots, C. Hurtgen, A performance comparison of nine selected liquid scintillation cocktails. *Appl. Radiat. Isot.* **66**, 1038–1042 (2008)
36. F. Verrezen, H. Loots, C. Hurtgen, in *A Performance Comparison of Nine Selected Liquid Scintillation Cocktails*. SCK•CEN-BLG-1052 (2008)
37. P.E. Warwick, D. Kim, I.W. Crouace et al., Effective desorption of Tritium from diverse solid matrices and its application to routine analysis of decommissioning materials. *Anal. Chim. Acta* **676**, 93–102 (2010)
38. I.W. Croudace, P.E. Warwick, D. Kim, Using thermal evolution profiles to infer Tritium speciation in nuclear site metals: an aid to decommissioning. *Anal. Chem.* **86**, 9177–9185 (2014)
39. P. Warwick, The measurement of Tritium in steel. *Anal. Commun.* **35**, 157–160 (1998)
40. K. Ochiai, T. Hayashi, C. Kutsukake et al., Measurement of Deuterium and Tritium retentions on the surface of JT-60 divertor tiles by means of nuclear reaction analysis. *J. Nucl. Mater.* **329–333**, 836–839 (2004)
41. M. Friedrich, W. Pilz, G. Sun et al., Tritium depth profiling by AMS in carbon samples from fusion experiments. *Phys. Scr.* **94**, 98–101 (2001)
42. M. Matsuyama, T. Tanabe, N. Noda et al., Nondestructive measurement of surface Tritium by  $\beta$ -ray induced X-ray spectrometry (BIXS). *J. Nucl. Mater.* **290–293**, 437–442 (2001)
43. M. Matsuyama, T. Murai, K. Watanabe, Quantitative measurement of surface Tritium by  $\beta$ -ray induced X-ray spectrometry (BIXS). *Fusion Sci. Technol.* **41**, 505–509 (2002)

44. J. Long, Z. An, Comparison of reconstruction methods of depth distribution of Tritium in materials based on BIXS. *Nucl. Instr. Method Phys. Res. B* **267**, 1852–1855 (2009)
45. H. Saitoh, T. Hishi, T. Misawa et al., Quantitative visualization of Tritium distribution in Vanadium by Tritium radioluminography. *J. Nucl. Mater.* **258–263**, 1404–1408 (1998)
46. T. Tanabe, N. Bekris, P. Coda et al., Tritium retention of plasma facing components in Tokamaks. *J. Nucl. Mater.* **313–316**, 478–490 (2003)
47. K. Hashizume, J. Masuda, T. Otsuka et al., Diffusion behavior of Tritium in V-4Cr-4Ti alloy. *J. Nucl. Mater.* **367–370**, 876–881 (2007)
48. T. Otsuka, M. Shimada, R. Kolasinski et al., Application of Tritium imaging plate technique to examine Tritium behavior on the surface and in the bulk of plasma-exposed materials. *J. Nucl. Mater.* **415**, S769–S772 (2011)

# Chapter 8

## Tritium Measurement II—Tritium in Plasma

Hideki Zushi

**Abstract** In D-T burning plasma, the fueled ion density ratio  $n_D/n_T$  is a key parameter to control the fusion output power. The requirements in ITER are briefly described, namely the range of density ratio, spatial locations (core, edge, wall, and divertor), and spatial/time resolutions. Diagnostic methods on neutrons from D-T reactions, the radio waves sensitive to the effective mass, charge exchange neutral flux of fuel particles, and passive and active spectroscopies for Balmer–Fulcher lines of fuel neutrals are introduced. Diagnostic principles, instrument of measurements, experimental results achieved in experimental devices, and prospects for ITER are described for each method.

**Keywords** Neutron • Microwave • Charge exchange • Spectroscopy

### 8.1 Introduction

In a fusion reactor, throughput of fuels (deuterium (D) and tritium (T)) is distributed in burning plasma (plasma core), edge plasma (Scrape off layers), and plasma facing materials and remaining exhausted. Although the amount of T in plasma (core and edge) is not large compared to T inventory in the plasma facing component, controls of the throughput (D and T) and their concentration ratio in the plasma core are critically important to keep efficient D-T burning. Therefore, diagnostics (measurement systems) to determine concentration profiles of D and T in the burning plasma shall be installed.

In the previous chapter, techniques and/or methods for quantification of T in all T handling or processing systems in a fusion reactor are introduced from the aspect of tritium accountancy and safety. However, none of them can be applied to quantify D and T in plasma, because they are in ionized or excited states.

---

H. Zushi (✉)

Research Institute for Applied Mechanics, Kyushu University,  
6-1 Kasuga-Koen, Kasuga-City, Fukuoka 816-8580, Japan  
e-mail: zushi@riam.kyushu-u.ac.jp

To observe T in plasma, either detection of emitting photons or particles from the plasma or probing with injection of photons or energetic particles into the plasma as probes is used. Molecular spectroscopy observes hydrogen molecules in excited states rotationally and vibrationally with separation of all isotopologues. Atomic spectroscopy for excited atoms in boundary plasmas (observation of emission of Balmer lines and Lyman lines) is well established. Charge exchange neutrals escaping from plasma are also used. However, no direct photon emission from fully ionized ions in core plasma excludes such spectroscopic measurements, and probing techniques, using high-energy neutrals, lasers, and electromagnetic waves, are used. Nevertheless, no diagnostics have been fully developed for the determination of the concentration profiles of D and T in burning plasma, yet. ITER would be the first test bed to do that.

In this chapter, T diagnostics planned to use in ITER are introduced. Then candidate diagnostics to separately determine the concentrations of D and T in burning plasma are described.

## 8.2 Requirements for Tritium Diagnostics in ITER [1]

In ITER under the tight restriction of T usage, burning experiment has to be carried out. The following operating scenario is considered to access the D/T burning plasma;

- (1) H phase inductive; ohmic L-mode; limited H-mode.
- (2) D phase; inductive; ELMy H-mode.
- (3) D/T phase; inductive; ELMy H-mode.

Plasma current is raised inductively and sustained by using a transformer for the tokamak start-up. Here L and H modes mean the low and high confinement performance modes in tokamak plasma. The good plasma confinement will result in a steepened pressure profile at the plasma edge. When the pressure gradient exceeds a critical value, so-called edge-localized modes (ELMs) are destabilized. Under the controlled ELMy modes operation scenario is considered. First phase (1) of operation is a hydrogen, non-nuclear phase and aiming at full commissioning of the tokamak systems. Operation will be inductive, mainly L-mode with some limited operation in H-mode. The next phase (2) will be a deuterium phase in which fusion reactions will occur. The operation mode is inductive, ELMy H-mode. In phase (3), high-power D/T plasma will be operated in the ELMy H-mode. Since fusion powers of 400 MW and fusion burn times of >300 s are expected, extension of the diagnostics will be inevitably required with respect to T. For example, gas pressure and composition in the main chamber, divertor and duct, fuel ratio ( $n_T/n_D$ ) in

plasma core and edge, and D and T influxes ( $\Gamma_D$ ,  $\Gamma_T$ ) in the divertor and main chamber are required.

The measurement requirements for the D/T fueling ratio and other related items have been specified in detail and the specifications required to meet all of the ITER operating modes are shown in Table 8.1.

**Table 8.1** Parameters specified for ITER condition

Parameter	Diagnostic region	Parameter range	Time resolution	Spatial resolution	Accuracy
Gas pressure and composition in the main chamber		$10^{-4}$ – 20 Pa $A = 1$ – 100 $\Delta A = 0.5$	1 s 10 s	Several points Several points	20 % during pulse 50 % during pulse
Gas pressure and gas composition in ducts		<7 kPa $A = 1$ – 100 $\Delta A = 0.5$	100 ms 1 s	Several points Several points	20 % during pulse 20 % during pulse
Fuel ratio in plasma core ( $n_T/n_D$ )	$r/a < 0.9$	0.1–10	100 ms	a/10	20 %
Fuel ratio in the edge ( $n_T/n_D$ ) ( $n_H/n_D$ )	$r/a > 0.9$ $r/a > 0.9$	0.1–10 0.01–0.1	100 ms 100 ms	Radial integral Radial integral	20 % 20 %
Core He density ( $n_{He}/n_e$ )	$r/a < 0.9$	1–20 %	100 ms	a/10	10 %
D, T influx in the divertor		$10^{19}$ – $10^{25}$ atoms/s	1 ms	50 mm	30 %
Fuel ratio in the divertor ( $n_T/n_D$ ) ( $n_H/n_D$ )		0.1–10 0.01–0.1	100 ms 100 ms	Integral Integral	20 % 20 %
$n_H/n_D$ ratio in the core		0.01–0.1	100 ms	a/10	20 %
D, T influx in main chamber		$10^{18}$ – $10^{20}$ atoms/ $m^2 s$	100 ms	Several poloidal and toroidal locations	30 %

In this table, He and H are not injected as source of plasma and they are the fusion products via following fusion processes. (From Table 2 in [1])

### 8.3 Diagnostics for Fuel Density Ratio $n_T/n_D$ and Particle Flux Ratio $\Gamma_T/\Gamma_D$

The diagnostics for the determination of fuel density ratio,  $n_T/n_D$ , have been developed based on the nuclear reaction and diagnostic methods depending on the charge and mass. In this section, neutron measurements, electromagnetic measurements, particle measurements, and spectroscopic measurements are described. The principles, instruments, and measurement results will be presented. Prospects for ITER will be also discussed.

#### 8.3.1 Neutron Diagnostics to Determine $n_T/n_D$ at the Plasma Center [2]

##### *Principle:*

In the D-T fusion, plasma neutrons are created by following two nuclear reactions:



The neutron production rate  $S$  (neutrons/m<sup>3</sup>/s) is given, respectively, for D-T and D-D reactions,

$$S_{DT} = n_D n_T \langle \sigma v \rangle_{DT}, \quad (8.3)$$

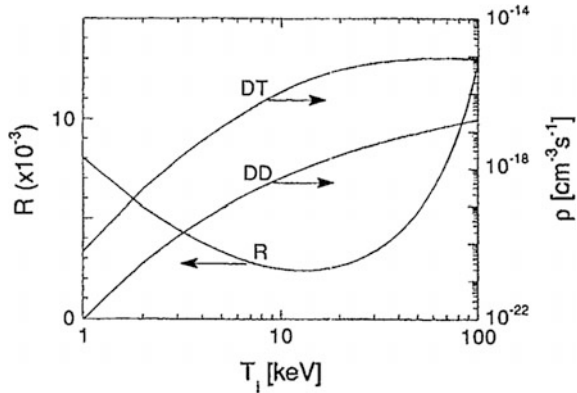
$$S_{DD} = \frac{1}{2} n_D n_D \langle \sigma v \rangle_{DD}, \quad (8.4)$$

where  $\langle \sigma v \rangle$ , depending on the ion temperature  $T_i$ , is the Maxwellian rate coefficient for each reaction. The fuel density ratio  $n_D/n_T$  is expressed by two reactions (8.3) and (8.4) as

$$\frac{n_D}{n_T} = 2 \frac{S_{DD} \langle \sigma v \rangle_{DT}}{S_{DT} \langle \sigma v \rangle_{DD}}. \quad (8.5)$$

In Fig. 8.1,  $\langle \sigma v \rangle_{DT}$ ,  $\langle \sigma v \rangle_{DD}$  and their ratio  $R$  are plotted as a function of  $T_i$ . The latter determines the relative intensity of dd and dt neutron emission peaks, where dd and dt are the neutrons produced by D-D reactions and D-T reactions,

**Fig. 8.1**  $\langle\sigma v\rangle_{DT}$ ,  $\langle\sigma v\rangle_{DD}$ , and its ratio  $R = \langle\sigma v\rangle_{DD}/2\langle\sigma v\rangle_{DT}$  are plotted as a function of  $T_i$ . (Reprinted with permission from [2])



respectively. The line integrated intensities ( $I_{DT}$ ,  $I_{DD}$ ) into dt and dd neutrons along a path crossing the D–T plasma are, respectively, given as

$$I_{DT} = k \int dl (n_D n_T \langle\sigma v\rangle_{DT}), \quad (8.6)$$

and

$$I_{DD} = k \int dl \left( \frac{n_D^2}{2} \langle\sigma v\rangle_{DD} \right), \quad (8.7)$$

where  $k$  is a constant. The density profiles of D and T are described by  $n_D(r) = n_D(0)f_D(r)$  and  $n_T(r) = n_T(0)f_T(r)$ , respectively. If the shape of profiles is the same,  $f_D(r) = f_T(r) = f(r)$ , then the fuel density ratio at the plasma center can be decided as follows:

$$\frac{n_D(0)}{n_T(0)} = 2 \frac{I_{DD} \int f_D(r)^2 \langle\sigma v\rangle_{DD}(T_i(r)) dl}{I_{DT} \int f_T(r)^2 \langle\sigma v\rangle_{DT}(T_i(r)) dl} \sim \frac{I_{DD}}{I_{DT}} \frac{1}{R(T_{i0})} \frac{l_{DD}}{l_{DT}}, \quad (8.8)$$

where  $l_{DD}$  ( $l_{DT}$ ) is the effective path length.

#### Method and Instruments:

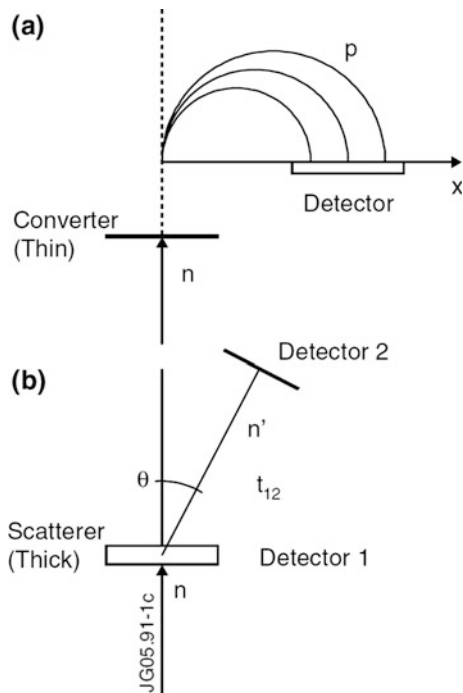
Since neutrons are produced by the D–D reaction (8.1) and D–T reaction (8.2) with quite different rates and different energy which are referred as dd (2.5 MeV neutrons) and dt (14 MeV neutrons), respectively, hereafter, the detection systems are required to have different detection efficiency ( $\varepsilon$ ) and energy resolution ( $\Delta E/E$ ).  $\varepsilon$  for dd detector must be a factor of  $10^2$  greater than that for dt to compensate for the lower dd production rate. On the other hand,  $\Delta E/E$  can be set relative to the thermal Doppler broadening which is 2.6 times greater for dd than for dt at  $T_i = 4$  keV.

The principle of the measurement is schematically shown in Fig. 8.2 [3]. One is a magnetic proton recoil spectrometer (MPRS). This consists of a thin film to convert neutron to proton (a convertor foil), a quadrupole-dipole magnet, and a detector array. This method is based on proton counting in a position sensitive detector. For a tandem type, the first MPRS is for dt and the second for dd.

Another one is a time-of-flight (TOF) spectrometer, which is characterized by its relatively compact size and no influence from the magnetic field [4]. The detector D1 is a scintillator (BC422Q, BC404) with the luminous decay time of 0.7 ns. The detector D2 is another scintillator (BC400, NE102A). These two detectors consist of a TOF sphere. The D2 detector should therefore be ring-shaped to achieve the maximum catching efficiency of the selected scattered neutrons coming from D1. Scattering angle  $\theta$  is 45° and a distance is 1.2 m.

For the TOF system, a fast discrimination electric circuit is required for D-D events, because D1 is suffered from high counting rates and D-T events are two-three orders of magnitude larger than D-D events. An example circuit is shown in Fig. 8.3. High pulse-height signals detected by D1 and D2 are the D-T events, while low pulse-height ones are the D-D events. A discrimination window, lower and upper levels (LLD and ULD), works as a band-pass filter for later ones.

**Fig. 8.2** Principles for measuring neutron energy base on counting of momentum analyzed recoil protons in a space sensitive detector of the MPR (a) and using the recorded time delay  $t_{12}$  of signals from two detectors for scattered neutrons of TOF (b) techniques. (Reprinted with the permission from [3])



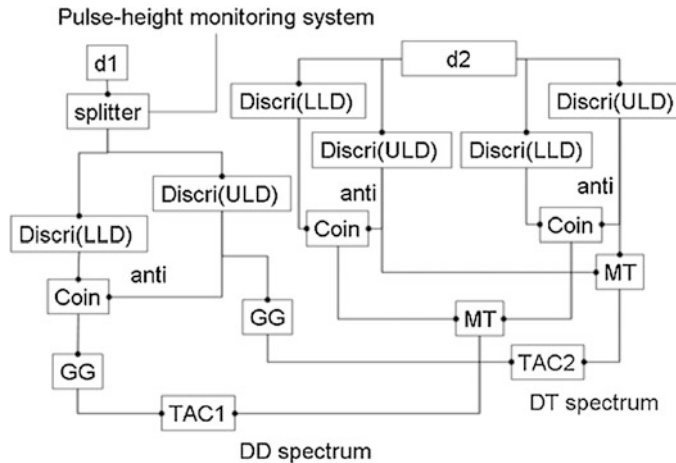


**Fig. 8.3** Electric circuit for a TOF spectrometer. *Discri* is discriminator, *Coin* 2-fold coincidence, *GG* dual-gate generator, *MT* mean timer, *TAC* time-to-pulse height convertor. (Reprinted with the permission from [5])

### Results:

An example of an MPRS spectrum for  $dt$  observed in a JET pulse No: 42982 is shown in Fig. 8.4 [3]. The spectrum is fitted with three spectral components representing a thermal component (TH) and two supra-thermal (epithermal ET and high-energy HE). SC is due to the scattered neutron flux, which constitutes a few percent admixture of the measured neutron flux.

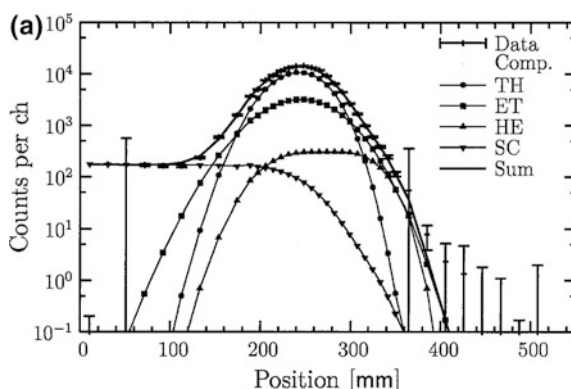


**Fig. 8.4** Example of an MPR recorded spectrum for the 14 meV neutron emission from JET discharge #42982 representing record high fusion energy produced (a). The spectrum is fitted with three spectral components representing a thermal reaction component (TH) and two supra-thermal component [epithermal (ET) and high energy (HE)]; a fourth component represents contribution from scattered (SC) neutrons. (Reprinted with the permission from [3])

In order to verify the principle of the TOF system, a D-T neutron beam produced in fusion neutronics source (FNS) facility in JAERI has been used. The FNS neutron beam consists of dt and dd with energies of 14.21 and 2.66 MeV, respectively. Scattering angle  $\theta$  is  $45^\circ$  and a distance between two detectors is 1.2 m. The counting yield is defined as the ratio of the count rate to the incident neutron flux. The dt and dd incident fluxes are evaluated as  $3.65 \times 10^5$  and  $8.37 \times 10^3$  (n/cm<sup>2</sup>/s), respectively, by a neutron activation method using  $N_b$  and  $N_b + I_n$  activation foils. Two spectra are clearly separated and counting yields are  $1.4 \times 10^{-3}$  and  $2.4 \times 10^{-5}$  (counts cm<sup>2</sup>/s), respectively, as shown in Fig. 8.5 [5].

### **Prospection to ITER**

In Table 8.1, the requirements for the fuel density ratio measurement are a spatial resolution of  $a/10$ , where  $a$  is the plasma minor radius, time resolution of 100 ms, and accuracy of 20 % in the fuel ion density ratio range of 0.1–10. For neutron measurements, the requirements for the time resolution and the accuracy mean a counting rate capability of 250 counts/s for dd peak. Under the standard operation in ITER with  $n_D = n_T$  and  $T_i = 20$  keV, the production rate of dt ( $S_{DT}$ ) is 200 times higher than that of dd ( $S_{DD}$ ). This suggests the ratio of the neutron production rate ( $S_{DT}/S_{DD}$ ) to be 20–2000 in the range of fuel ion density ratio of 0.1–10. The measurement geometry and collimation system should be selected so that the dd peak in the neutron energy spectra is not covered with the scattered/energy-degraded neutron originating from dt neutrons. According to the above results, the TOF system must be located at a position of at least the evaluated incident flux range in ITER. However, pileup may occur on the first detector under the maximum incidence neutron flux. The smaller TOF sphere and division of the first detector may solve this problem [4].

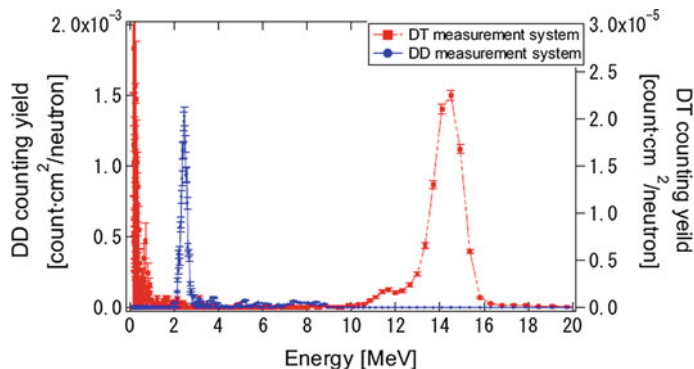


**Fig. 8.5** dt and dd spectra with the TOF spectrometer. (Reprinted with the permission from [5])

### 8.3.2 Electromagnetic Diagnostics for $n_T/n_D$ in the Core Plasma

In this subsection, reflectometry and an MHD spectroscopy (toroidal Alfvén eigenmode (TAE) measurements) are introduced.

#### 8.3.2.1 Ion–Ion Hybrid Layer Reflectometry [6]

##### *Principle:*

The phase velocity  $V_{ph\perp} = \omega/k_\perp$  of the fast Alfvén wave propagating across the magnetic field  $B$  is equal to the Alfvén speed,  $V_A$ ,

$$V_{ph\perp} \sim V_A = B/\sqrt{4\pi\rho}, \quad (8.9)$$

where  $\omega$  is the frequency,  $k_\perp$  is the wave number perpendicular to the magnetic field,  $\rho = n_D M_D + n_T M_T$  is the mass density in the DT mixture plasma. The measurement of wave phase (wavelength) by an interferometer gives the mass density.

For local measurement of the T density, the following relation of the ion–ion hybrid resonance and cutoff frequencies is used. The index of refraction perpendicular to the magnetic field is given by

$$N_\perp^2 = \frac{RL}{S}, \quad (8.10)$$

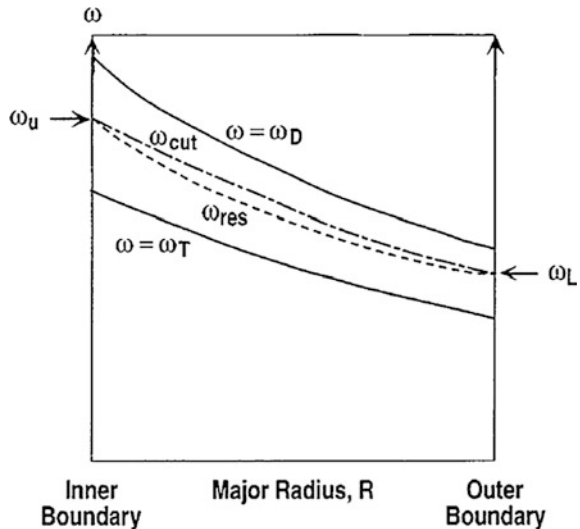
where  $R = 1 - \sum_s (\omega_{ps}^2/\omega(\omega + \omega_{cs}))$ ,  $L = 1 - \sum_s (\omega_{ps}^2/\omega(\omega - \omega_{cs}))$  and  $S = (R + L)/2$  have been introduced in Stix [7].  $\omega_{ps}$  and  $\omega_{cs}$  are the plasma frequency and cyclotron frequency of species  $s$ , respectively. The resonance and cutoff conditions are given by  $S = 0$  ( $N_\perp \rightarrow \infty$ ), and  $R = 0$ , or  $L = 0$  ( $N_\perp \rightarrow 0$ ), respectively. When  $C_D$  ( $C_T$ ) represents the concentration fraction of D (T) to the electron density and the quasi-neutral condition  $n_e = n_D + n_T$ , ( $C_D + C_T = 1$ ) is assumed,  $S = 0$  (ion–ion hybrid resonance) and  $L = 0$  (ion–ion hybrid cutoff) conditions give the following relations, respectively,

$$\omega_{res} = \left( \frac{3 - C_D}{3 + (3/2)C_D} \right)^{1/2} \omega_D, \quad (8.11)$$

$$\omega_{cut} \sim \omega_D C_T + \omega_T C_D = (1 - C_D/3)\omega_D, \quad (8.12)$$

where  $\omega_{res}$  is the resonance frequency;  $\omega_{cut}$ , the cutoff frequency;  $\omega_D$ , the D ion cyclotron frequency; and  $\omega_T (= 2/3\omega_D)$ , the T ion cyclotron frequency, respectively. In a nonuniform magnetic field,  $B \propto 1/R$  in a tokamak,  $\omega_{res}$  and  $\omega_{cut}$  depend on  $R$  (the major radius) schematically shown in Fig. 8.6. For a given frequency  $\omega$  in

**Fig. 8.6** Ion cyclotron frequencies of D and T,  $\omega_D$  and  $\omega_T$ , and resonance  $\omega_{res}$  and cutoff  $\omega_{cut}$  frequencies as a function of tokamak major radius. (Reprinted with the permission from [6])



the Alfvén wave range, the position of the ion-ion hybrid resonance and cutoff layers,  $R_{res}$  (IIHRL) and  $R_{cut}$  (IIHCL), are uniquely determined by the concentration fraction. Since the fast Alfvén wave launched inward from the outer boundary is reflected at  $R = R_{cut}$  and goes back to the outer boundary, the measurement of the reflected waves gives the local  $C_D$  ( $R_{cut}$ ).

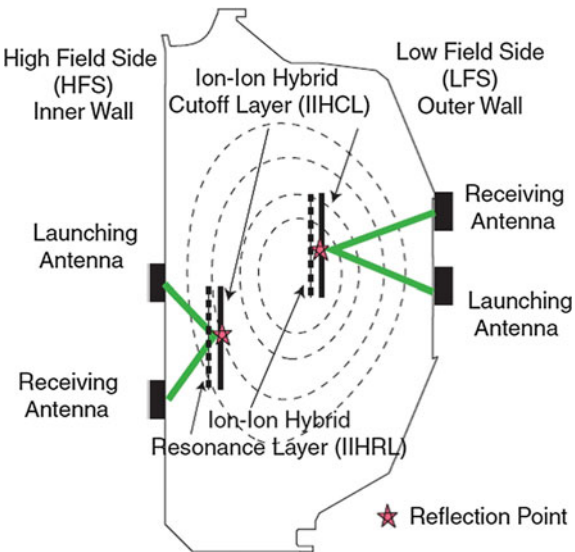
#### **Method and instruments:**

A superheterodyne reflectometer has been used to determine  $R_{cut}$  by measuring a round trip time delay, i.e., the phase difference between the launched wave and reflected one in an H-D plasma [8]. Two sets of reflectometer are schematically shown in Fig. 8.7. The launching and receiving antennas are one-turn toroidal loops with cross-sectional areas of  $8\text{--}17 \text{ cm}^2$  and these relatively small loops launch a broad wavenumber spectrum parallel to the magnetic field,  $S(k_{||})$ , centered about  $\sim 0$ . A 20 mW electromagnetic wave is launched perpendicular to the magnetic field with a frequency of 14–23 MHz and an intermediate frequency (IF) of 4 MHz is analyzed. The time of flight for the wave is measured as it travels from a launching antenna to the IIHCL and then reflects back to a receiving antenna. The launching and receiving antennas are located on the midplane at nearly identical toroidal angles but are displaced poloidally by 35 cm for the low field side (LFS) experiment, and 57 cm for the high field side (HFS) experiment. In this case, the cutoff frequency is decided by

$$\omega_{cut} \sim (1 - C_H/2)\omega_H, \quad (8.13)$$

where  $C_H$  and  $\omega_H$  are a fraction of the hydrogen and the H ion cyclotron frequency, respectively. Plotting  $X = a \cos(\phi)$  vs  $Y = b \sin(\phi)$  yields the phase ( $\phi$ ) of the data signal and the time variation in  $\phi = \omega/c \int N dl$  forms loops. In the case of

**Fig. 8.7** Elevation of DIII-D illustrating the basic concept. Waves are launched by graphite tile antennae near the midplane, reflect off the IIHCL, and are received by a nearby graphite tile antenna. Waves launched from the LFS encounter the cutoff layer prior to the ion-ion hybrid resonance layer. Waves launched from the HFS must tunnel through the resonance layer in order to reflect off the cutoff (refraction neglected). The dashed lines represent plasma flux surfaces. (Reprinted with the permission from [8])



LHS, launching when  $\omega_{\text{cut}}$  is decreased with increasing  $C_H$ , the IIHCL approaches to  $\omega_D$ . Since the propagation length is increased and the phase difference is increased, one can see the counterclockwise loops. On the other hand, when  $C_H$  is reduced,  $\omega_{\text{cut}}$  is increased and the IIHCL becomes  $\omega_H$ . Thus, the phase is decreased and the loops rotate in the clockwise direction.

### Results:

The LFS experiments were performed in DIII-D tokamak, as shown in Fig. 8.8. Hydrogen gas was puffed into from 300 to 700 ms during the current ramp-up phase. Since DIII-D operates normally with D, an unknown quantity of D is released from the walls during the discharge. Additional fueling is provided by D neutral beam injection. The toroidal field was 1.9–2.1 T. The signals were noisy from 300 to 500 ms. The noisy signal may be caused by the relatively large antenna gaps or by poor plasma stability (many minor disruptions are evident on the central soft X-ray signals) or both [panel (c)]. Just before the  $D^0$  neutral beam injection commences at 500 ms, a minor disruption occurs; thereafter, the signal becomes less noisy as the outer plasma edge grows closer to the antennas and plasma stability improves [panel (d)]. The phase inferred from the X and Y components first decreases to zero, while hydrogen gas is puffed into the discharge and then abruptly reverses direction when the gas puff ceases and D particle sources predominate [see panel (e)]. Representative polar plot of the phase  $\phi$  from X-Y signals for LFS experiments is shown in Fig. 8.9. A star symbol ( $\phi \sim -\pi/2$ ) is  $t = 325$  ms, corresponding to the  $H_2$  puff; then, the phase rotates in the counterclockwise direction and stops at the diamond after  $2\pi$  circulation, whose trend is consistent with the expected behavior for the  $C_H$  increment. Figure 8.10 shows the hydrogen concentration inferred by three independent diagnostics for one of the discharges in the

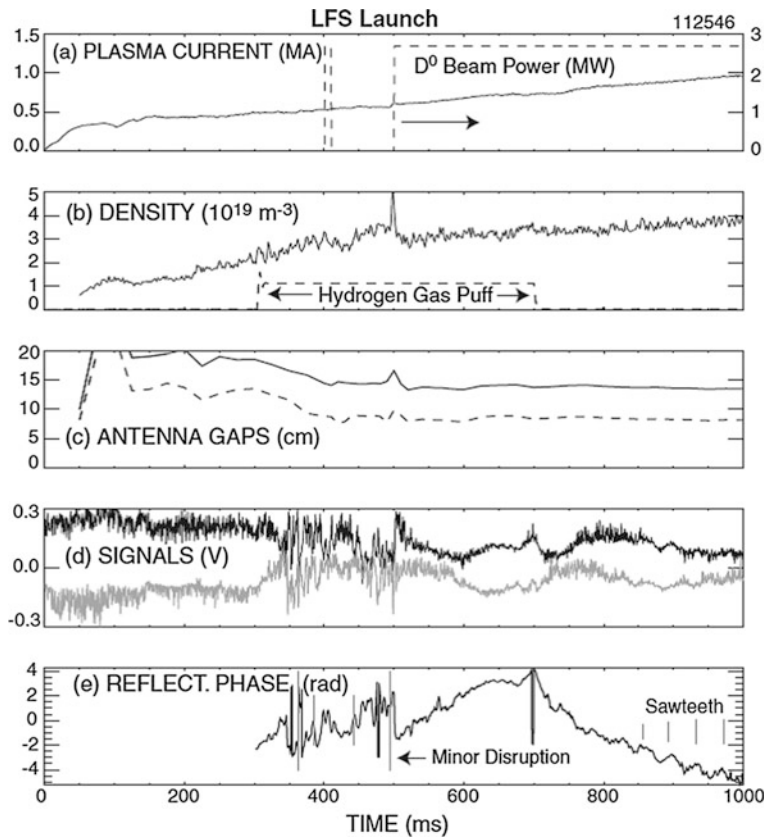


**Fig. 8.8** Time evolution of parameters. **d** X and Y mixed signals of the reflectometer, with a dc offset introduced for clarity, and **e** the inferred reflectometer phase (after 3.5 ms boxcar smoothing). Increasing phase in this figure corresponds to a counterclockwise rotation in Fig. 8.4. (Reprinted with the permission from [8])

**Fig. 8.9** Phase-space diagram between 325 and 400 ms for the X-Y mixed signals shown in Fig. 8.8. For a LFS launch, a counterclockwise rotation is expected when the hydrogen concentration increases. (Reprinted with the permission from [8])

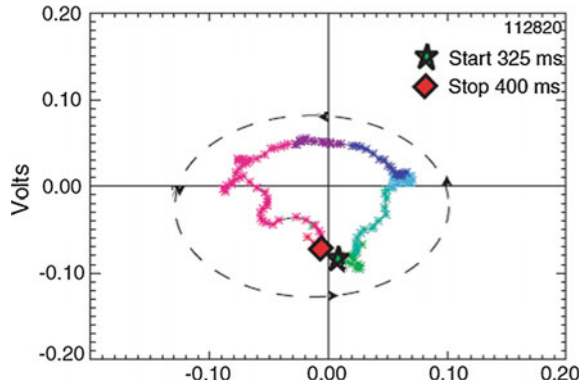
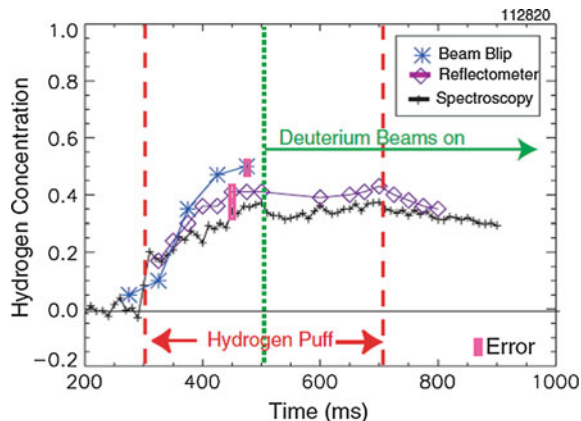


**Fig. 8.10** Time evolution of the hydrogen concentration inferred from the ion-ion hybrid reflectometer diagnostic (black diamond). A hydrogen gas puff begins at 300 ms and ends at 700 ms; (Reprinted with the permission from [8])



LFS experiment. In this discharge, phase tracking first occurs at 4 ms after the hydrogen gas puff begins, indicating that the IIHCL entered the plasma at this time. This observation provides a calibration phase for the reflectometer signal, and so the subsequent evolution of  $C_H$  is determined by the reflectometer signals alone.

### Prospection to ITER

The application of the reflectometry to ITER is examined within the framework of cold plasma theory [9]. The major radius dependence of the various frequencies and of the index of refraction  $n$  is similar. However, since the wavelength is a smaller fraction of the minor radius, WKB approximation will be more valid. A 28 MHz wave reflects from the cutoff layer at  $\omega_{\text{cut}} \sim (1 - C_D/3)\omega_D = (1 + C_T/2)\omega_T$  in the plasma interior ( $R \sim 7$  m). Several issues have been listed. First, it is noted that this technique cannot independently determine  $C_D$ . All ions with the same charge-to-mass ratio ( $e/m$ ) contribute equally to the cutoff frequency, so alpha ash and any fully ionized impurities are indistinguishable from D ions. Independent measurements of the densities of the major impurities or those of  $Z_{\text{eff}}$  are required to determine  $C_D$ . Second important issue is optimization of the launching and receiving antennas. In DIII-D, the simple single-turn loops with a broad  $S(k_{||})$  are employed. In order to avoid the contribution to the signal associated with unwanted, more complex, ray paths, an antenna having a narrower  $k_{||}$  spectrum and multiple receiving antennas should be deployed to ensure reception of the desired bundle of rays.

### 8.3.2.2 MHD Spectroscopy (Toroidal Alfvén Eigenmodes) [10]

**Principle:**

The frequency of the toroidal Alfvén eigenmodes (TAEs) is given by

$$\omega_{\text{TAE}} \sim \frac{V_A}{2\pi q R} = \frac{1}{2\pi q R} \frac{B}{\sqrt{4\pi \sum_i n_i M_i}} \quad (8.14)$$

where  $q(r) = m/n$  is the safety factor;  $m$  and  $n$  the poloidal and toroidal mode numbers. Fast particles, including alpha particles and other fusion products and injected beam ions, can destabilize these modes. Their velocities are of the order of  $V_A$  and pressures  $n_f T_f$  are comparable to the pressure  $n_i T_i$  of bulk ions. Here  $n_f$  ( $\ll n_i$ ) and  $T_f$  ( $\gg T_i$ ) are the density and temperature of the fast particles. External antennas can excite these waves. According to the square root dependence on the plasma mass in Eq. (8.14), the plasma effective mass can be also inferred from the measurement of the resonant frequency of Alfvén eigenmodes (AEs), such as TAEs, in the gap centered at  $\omega_{\text{TAE}}$  [10]. Because of the low-frequency range of the modes that are used for diagnostic purposes, this approach is referred to as magnetohydrodynamics (MHD) spectroscopy. Since the effective atomic mass  $A_{\text{eff}}$  in D-T plasma is given by

$$A_{\text{eff}} = \frac{2n_D + 3n_T}{n_e} = 2C_D + 3C_T = 2 + C_T, \quad (8.15)$$

the TAE frequency is described in terms of  $C_T$ ,

$$\omega_{\text{TAE}}(r) \propto \frac{1}{2\pi q(r)R} \frac{B(r)}{\sqrt{4\pi n_e(r)A_{\text{eff}}}} = \frac{1}{2\pi q(r)R} \frac{B(r)}{\sqrt{4\pi n_e(r)(2 + C_T)}} \quad (8.16)$$

If  $q(r)$  and  $n_e(r)$  are unchanged in a series of plasma,  $C_T$  can be deduced from measured  $\omega_{\text{TAE}}^{\text{DT}}(C_T)$ . For pure D-D plasma  $\omega_{\text{TAE}}^{\text{DD}} = \omega_{\text{TAE}}(C_T = 0)$  can be measured. Thus,

$$C_T = 2 \left( \frac{\omega_{\text{TAE}}^{\text{DD}}}{\omega_{\text{TAE}}^{\text{DT}}} \right)^2 - 2 \quad (8.17)$$

**Method and instruments:**

TAEs with the low toroidal mode numbers can be driven by saddle coils, as shown in Fig. 8.11. These modes can be excited externally whose amplitudes are large enough to be detected, whereas low enough to avoid significant perturbations

to the plasma equilibrium and transport. When the local Alfvén resonance condition  $\omega_{\text{TAE}}(r) = k_{\parallel}v_A(r)$  is satisfied at a position  $r$ , the wave-plasma resonant interaction occurs (continuum damping). Thus, excited waves are anticipated to be strongly damped in plasmas of high elongation and edge magnetic shear, hence becoming undetectable during the divertor phase of the discharge. To overcome these limitations, a structure optimized for the excitation and detection of AEs with  $n \leq 15$  is being planned. A sketch of the proposed design is shown in Fig. 8.11. Four of the eight antennas will be driven at the same time, chosen to obtain the specific spectrum of toroidal mode number needed for a given experiment.

### Results:

A result of MHD spectroscopy or TAE diagnostics in JET is shown in Fig. 8.12, where the measurement of the density fraction  $n_T/(n_D + n_T) = A_{\text{eff}} - 2$  is performed in a series of discharges with similar equilibrium characteristics. TAEs with  $n = 1$  mode was excited. In this case, direct estimation of  $n_T/(n_D + n_T)$  was made purely from experimental measurements. The contribution from impurities on  $A_{\text{eff}}$  was neglected.  $\omega_{\text{TAE}}^{\text{DD}}$  was calculated from the average density ( $n_e$ ),  $q = 1.5$  and  $A_{\text{eff}} = 2$ . Figure 8.12 suggests a good agreement with edge spectroscopic measurements for two discharges (42844, 42870) with different D/T relative concentrations, although their time evolutions were somewhat different.

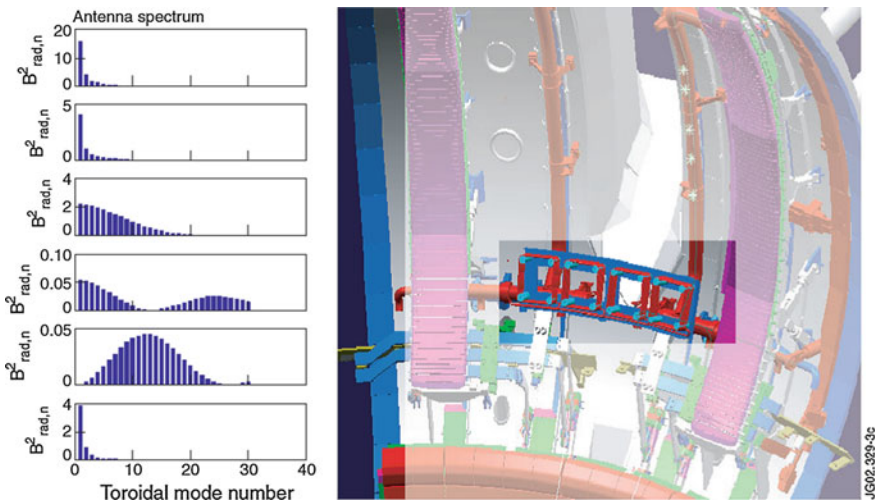


**Fig. 8.11** A sketch of four of the eight AE antennas designed along with the expected geometrical toroidal mode number spectrum for a number of possible phase combinations, for the radial component of the magnetic field. A second block of four antennas will be installed diametrically opposed in the vacuum vessel. (Reprinted with the permission from [10])

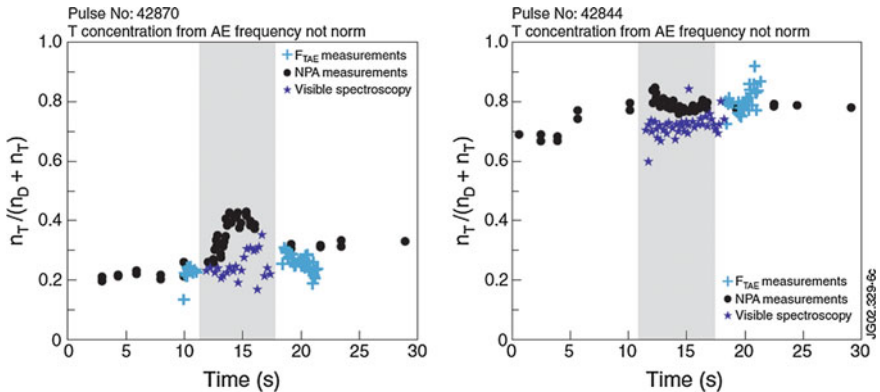


**Fig. 8.12** Estimate of D/T ratio from the measured frequency of an externally excited  $n = 1$  TAE compared with visible spectroscopic data (intensity ratio of  $T_2$  to  $D_2$  lines) and with results from the neutral particle analyzer. (Reprinted with the permission from [10])

### Prospection to ITER

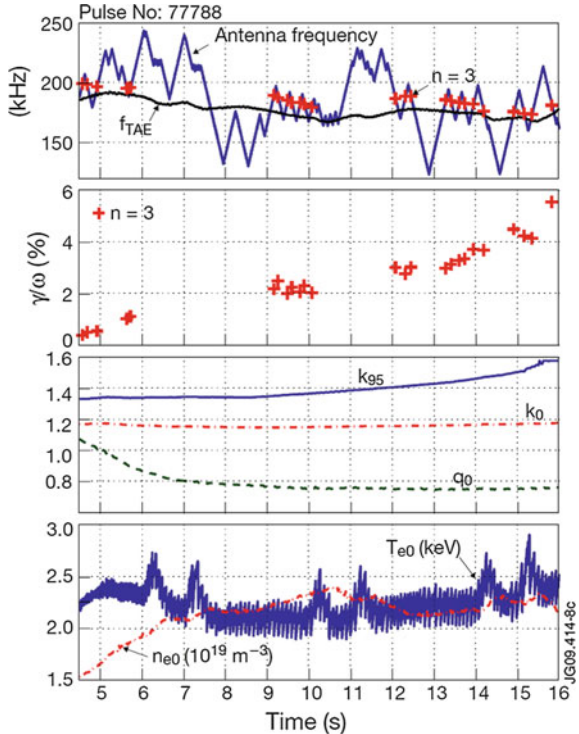
This active TAE diagnostic tool provides a measure of the mass density in the region where the mode is localized and can be used to determine the D/T ratio. Using eight compact antennas, damping rate measurements were carried out in JET [11]. The antenna system is capable of exciting AE's over a wide range of frequencies (50–500 kHz) and toroidal mode numbers ( $n = 0$ –15). In elongation scan experiment, the damping rates of  $n = 3$  TAEs is increased as a function of the edge elongation factor  $\kappa$  to 5 % at high  $\kappa$ , as shown in Fig. 8.13. The excited magnetic field per ampere decreases from  $0.6 \text{ GA}^{-1}$  at the antenna mouth to less than  $0.01 \text{ GA}^{-1}$  for  $r/a < 0.5$ . It suggests that the coupling to core-localized modes is very weak. However, the real-time tracking on individual modes is ensured.

### 8.3.3 Neutral Particle Analyzer (NPA) Measurement for $n_D/n_T$ in the Intermediate Region [12]

#### Principle:

In a tokamak, neutral atoms, which are externally fueled or coming from the chamber walls (recycling), interact with plasma ions resulting charge exchange. These processes create new neutrals with higher energy compared with those of the fueled and recycling ones. Ionization by electron and ion impacts causes neutrals to be ceased. When the neutral particle analyzer (NPA) views a plasma along a path (from  $r = -a$  to  $r = a$ ), the flux of atoms  $\Gamma_{a=\text{H,D,T}}$  (particles/m<sup>2</sup>/s/sr) ejected at the

**Fig. 8.13** Damping rate measurements of  $n = 3$  TAEs during an edge elongation scan. Here,  $\kappa$  is the elongation and  $q$  is the safety factor,  $T_e$  is the electron temperature and  $n_e$  is the electron density, with the suffixes “0” and “95” indicating core and edge values, respectively. (Reprinted with the permission from [11])



velocity  $v$  from the plasma can be evaluated by the path integration of local emissivity  $\varepsilon_a(x, v)$ , ion velocity distribution function  $f_i(x, v)$ , and transmission coefficient  $\eta_a(x, v)$ , as follows:

$$\Gamma_a(v) = \int_{-a}^a dx \varepsilon_a(x, v) f_i(x, v) \eta_a(x, v) = \int_{-a}^a dx (\langle \sigma_{cx} v_i \rangle n n_0 + \langle \sigma_{recom} v_e \rangle n^2) f_i(x, v) \eta_a(x, v), \quad (8.18)$$

where  $n_0(x)$  is the neutral density,  $n(x)$  the plasma density with an assumption of  $n(x) = n_e(x) = n_i(x)$ ,  $\langle \sigma_{cx} v_i \rangle$  and  $\langle \sigma_{recom} v_e \rangle$  are charge exchange and recombination rate coefficients, respectively, and  $v_i$  and  $v_e$  the thermal velocity of ions and electrons, which are much larger than the mean velocity  $v$  of atoms. Brackets  $\langle \rangle$  mean average over assumed Maxwell velocity distributions. The function  $f_i(x, v)$  is assumed to be locally Maxwellian and is approximated by

$$f_i(x, v) = f_i(x_0(v)) \delta(x - x_0(v)). \quad (8.19)$$

The local transmission coefficient for neutrals  $\eta_a(x, v)$  born at  $x$  to penetrate along the path from  $x$  to a (detector position) is given by taking into account recharge exchange and ionization processes,

$$\eta_a(x, v) = \exp \left( \frac{1}{v} \int_a^x dx' (\langle \sigma_{cx} v \rangle n + \langle \sigma_e v \rangle n + \langle \sigma_{ion} v \rangle n) \right), \quad (8.20)$$

where  $\langle \sigma_e v \rangle$  and  $\langle \sigma_{ion} v \rangle$  are electron and ion ionization rate coefficients, respectively.

Thus, the flux of the atoms integrating the effective path length of  $l$  becomes

$$\Gamma_a(v) \sim \eta_a(x_0, v) [\langle \sigma_{cx} v \rangle n_0(x_0) + \langle \sigma_{recom} v_e \rangle n(x_0)] n_i(v) l. \quad (8.21)$$

In the 1–10 keV energy range, the two terms inside the square brackets do not depend on the isotope chosen. Thus, for the isotope density ratio, one may write

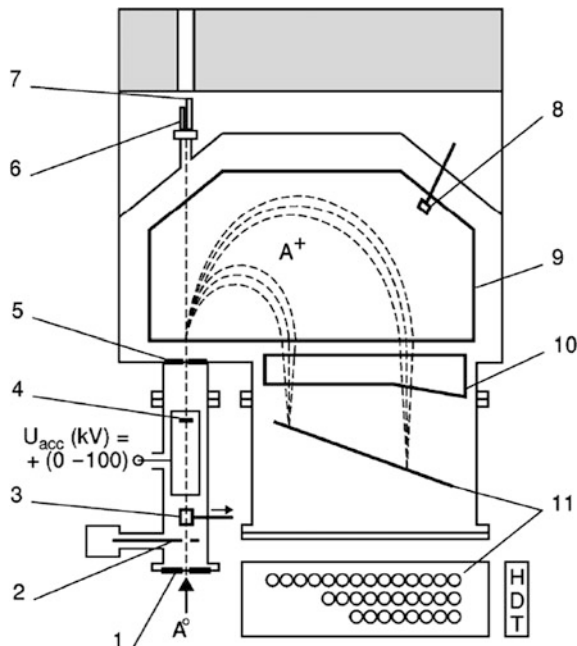
$$\frac{n_H(E)}{n_D(E)} = \frac{1}{\sqrt{2}} \frac{\Gamma_H(v)}{\Gamma_D(v)} \frac{\eta_D(x_0, v)}{\eta_H(x_0, v)}, \quad (8.22)$$

where  $\frac{1}{\sqrt{2}}$  is a correction factor for mass difference at the given energy. Since NPA can analyze energy spectra of fast neutrals ( $H^0$ ,  $D^0$ , and  $T^0$ ) escaping from the plasma and these atoms of different energies come from different radial positions inside the plasma, precious information about the isotope composition profile is contained in the NPA-detected signal.

### **Method and instruments:**

Figure 8.14 shows an NPA [called ISotope SEParator (ISEP)] layout used in JET [13]. It consists of three main chambers such as acceleration, magnet, and detection. The acceleration chamber consists of an input aperture, a collimator slit mechanism, a removable calibration aid, a thin carbon stripping foil supported on nickel mesh, and an output aperture. Elements of the magnet and detector chambers are a light emission diode for detector testing, optical laser for alignment, a Hall probe, the magnet that gives a nonuniform field, an electrostatic condenser that gives a nonuniform electric field, and a detector array. A neutral atom with mass  $A$  enters into the entrance slit (2 mm  $\varphi$ ) of the acceleration chamber. The positive electrode of the accelerator consists of a hollow polished stainless steel cylinder with 8-mm apertures on the axis at the both ends. The secondary ion  $A^+$  can be created through the thickness of 30 nm and diameter of 12 mm  $\varphi$  carbon stripping foil mounted inside the cylindrical electrode close to the exit end. A thin nickel mesh with 90 % transmission supports the foil. Acceleration voltage of  $U_{acc} = +0 \sim 100$  kV is used, and the secondary ions formed by the stripping foil are

**Fig. 8.14** ISEP layout showing the input aperture (1), adjustable collimator (2), calibration aid (3), stripping foil (4), output aperture (5), a light emitting diode (6), alignment laser (7), Hall probe (8), electromagnet (9), electrostatic condenser (10), and the detector flange (11) with scintillator/PMT detector assemblies. (Reprinted with the permission from [13])



accelerated in the gap between the cylindrical electrode and aperture (5) ( $8 \text{ mm } \phi$ , which is at ground potential.  $A^+$  is deflected through  $180^\circ$  in the magnet chamber (9). The magnet gap increases from 9 mm at the entrance to 29 mm at the back edge of the poles. The shape of the gap is designed to give the best two-dimensional focusing of the ions entering the electrostatic analyzer (10).

### Results:

In a typical JET shot, observed energy spectra of H and D at a specified time were shown in Fig. 8.15 [12]. Although the energy distribution of H was the Maxwellian like, that of D deviated above 10 keV, because of D beam injection. The NPA density ratio taken for the same JET shot was analyzed and compared with other diagnostics in Fig. 8.16. The spectrum for D was limited below 10 keV and two signals for H and D were time integrated ( $\sim 1 \text{ s}$ ) to increase the statistical accuracy. Since the NPA signal is modeled by Eq. (8.18), the radial location of the density ratio has been deduced with the help of the model flux. The horizontal error bars correspond to the FWHM of the emissivity  $\varepsilon_a(x, v)$  profiles given by the model for each considered energy. Here the FWHM means the spatial region of the plasma from within which 67 % of atoms of a particular energy are emitted. In Fig. 8.16,  $\varepsilon_a(x, E)$  have been analyzed at two extreme energies, 5 and 9.9 keV. For 5 keV, it peaks at  $r/a = 0.65$  extending from  $r/a = 0.45$  to 0.75, and for 9.9 keV, it peaks at

**Fig. 8.15** Energy distribution of hydrogen flux (straight lines) and deuterium flux (dashed lines), for discharge 55867,  $t = 7.945$  s. (Reprinted with the permission from [12])

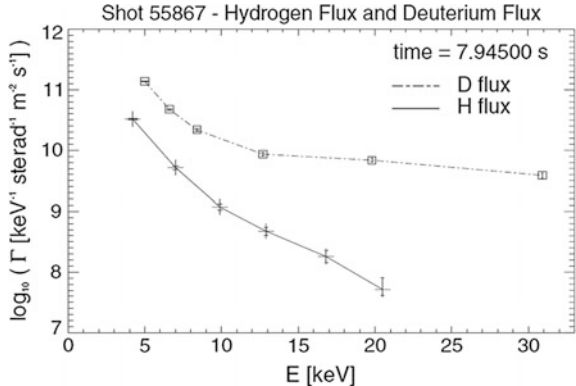
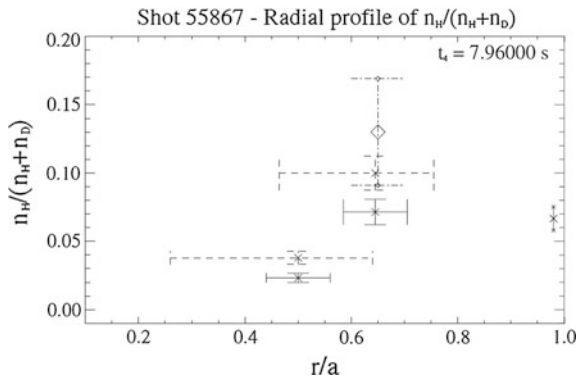


**Fig. 8.16** Results of density ratio for discharge 55867,  $t = 7.96$  s. Three NPA results (times symbols, with large horizontal error bars) are reported, together with the TAE value (diamond at  $r/a = 0.65$ ) and the spectroscopic measurement at the plasma edge (times symbol, at  $r/a \sim 1$ ). (Reprinted with the permission from [12])



0.5 from  $r/a = 0.25$  to 0.65. Solid horizontal bars are calculated ones by integrating over a fraction corresponding to only  $0.1a$  around the peak position. Particles at 9.9 keV are ejected from  $r/a = 0.5$  and the density fraction  $n_H/(n_H + n_D)$  is 2 %. On the other hand, particles at 5 keV are leaving from the plasma position at  $r/a = 0.65$  and the resultant density ratio is 7 %. These values are a half of 12 % by TAE method ( $r/a = 0.65$ ) and almost the same range of that by spectroscopy ( $r/a = 0.95$ ).

### Prospection to ITER

The error analysis of the fueling ratio is carried out based on the numerical simulation methods [14]. The dotted horizontal line in Fig. 8.17 shows the ITER requirement of  $\pm 10$  % accuracy in the determination of the T/D fuel ratio. In ITER, the transmission coefficients  $\eta_a$  for atoms of 100 keV and 2 MeV were 0.0026 and 0.49 from the plasma center  $r/a = 0$ , and 0.05 and 0.7 from half of the plasma

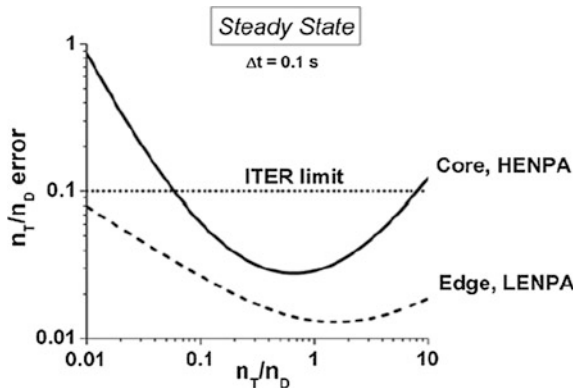


**Fig. 8.17** Steady-state scenario. Errors of  $n_T/n_D$  measured by HENPA in the core ( $r/a < 0.5$ ) and by LENPA at the edge ( $r/a > 0.5$ ) of plasma versus the isotope ratio. Horizontal dotted line—level of  $\pm 10\%$  accuracy of  $n_T/n_D$  ratio. HENPA count rates are integrated over energy ranges 1.3–2 MeV for  $D^0$  atoms and 0.5–1.4 MeV for  $T^0$  atoms. LENPA count rates of  $D^0$  and  $T^0$  atoms are taken for energy 100 keV (energy width of the channel is 3 %). (Reprinted with the permission from [14])

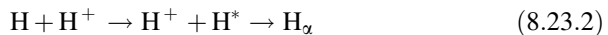
radius  $r/a = 0.5$ , respectively. A tandem of two neutral particle analyzers will be used for detection of the neutral fluxes. Low energy (LENPA) serves to measure  $D^0$  and  $T^0$  atoms within the energy range 10–200 keV. High energy (HENPA) serves to measure  $D^0$  atoms in the energy range 0.1–2.0 MeV and  $T^0$  atoms in the range 0.1–1.4 MeV. The former measures the density ratio at the edge ( $r/a > 0.5$ ) and the latter in the core ( $r/a < 0.5$ ). Both detection efficiencies are achieved as a function of energy by taking into account  $\varepsilon_a$ ,  $\eta_a$ , real geometrical factors, and conversion of the incoming atomic flux to the counting rate. The neutron noise is taken into account. Thus, below the required time resolution of 0.1 s the error of the density ratio was evaluated in Fig. 8.17. In the simulations, the T/D density ratio within the range 0.01–10 (it corresponds to the full variation range of the T/D ratio in ITER) was varied. In order to achieve the statistical accuracy, HENPA spectra were integrated in the 1.3–2 meV energy range for the deuterium, which is above the  $D^0$  beam injection energy, and in the 0.5–1.4 meV range for tritium. Since  $\varepsilon_a(r, E)$  for these high-energy particles is mostly concentrated in the core region  $r/a < 0.5$ , the energy integration procedure does not change significantly the origin of the neutral fluxes. Thus, HENPA satisfies the ITER requirement accuracy ( $\pm 10\%$ ) if the fuel ratio value varies in the range 0.06–8. On the other hand, because of the high counting rates for LENPA the energy integration is not necessary. The  $\varepsilon_a(r, E)$  at 50, 100, and 200 keV is fairly well separated at  $r/a = 0.8, 0.6$ , and 0.4, respectively. For the LENPA thermal spectra (100 keV), the FWHM of  $\varepsilon_a(r)$  was  $r/a = \pm 0.2$ . It can be concluded that LENPA provides the measurement of the fuel ratio in a periphery ( $r/a > 0.5$ ) in the whole range of 0.01–10.

### 8.3.4 Spectroscopic Diagnostic for $n_D/n_T$ and $\Gamma_D/\Gamma_T$ in the Edge

#### 8.3.4.1 Passive Balmer Alpha Diagnostics for the Edge Plasma [15]

**Principle:**

The atomic velocities of the fuel ions, arising from dissociation, electron impact excitation, and charge exchange, are mapped in the Doppler-broadened Balmer line profiles.



The Balmer line emission intensity can be described by  $\int dl n_3 h v_{32} A_{32}$ , where  $n_3$  is the population density of the principle quantum level  $n = 3$ ,  $h$  and  $v_{32}$  are Planck's constant and the emission frequency, respectively, and  $A_{32}$  is the Einstein transition probability. According to a simple coronal model,  $n_3$  is determined by balancing the electron impact excitation from the ground state and spontaneous transitions from the level  $n = 3$ . From the rate equation in steady state, the following relation

$$\frac{dn_3}{dt} = n_e n_0 \langle \sigma v \rangle_{1-3} - n_3 \sum_{i < 3} A_{3i} = 0, \quad (8.24)$$

is derived and the photon flux  $\phi_\alpha$  (photons/m<sup>2</sup>/s/sr) is given

$$\phi_\alpha = \frac{1}{4\pi} \int dl n_e n_0 \langle \sigma v \rangle_{1-3} \frac{A_{32}}{\sum_{i < 3} A_{3i}} = \frac{1}{4\pi} \int dl n_e n_0 X B, \quad (8.25)$$

where  $X = \langle \sigma v \rangle_{1-3}$  is the excitation rate coefficient and  $B = A_{32} / \sum_{i < 3} A_{3i}$  is the branching ratio.

The wave length of tritium Balmer alpha,  $T_\alpha$ , 656.045 nm, is slightly shifted from that of deuterium Balmer alpha  $D_\alpha$ , 656.104 nm due to small difference in the reduced mass of the nucleus/electron system. This wavelength difference is a factor of 3 smaller than the separation between  $H_\alpha$  and  $D_\alpha$  and is comparable to the Doppler width of the lines. Thus, using a spectrometer with high wavelength resolution, the density fraction can be derived by the measurement of the  $H_\alpha$ ,  $D_\alpha$ , and  $T_\alpha$  emission intensities,

$$\frac{n_T}{n_H + n_D + n_T} = \frac{T_\alpha}{H_\alpha + D_\alpha + T_\alpha} \quad (8.26)$$

Here, path integration effects are ignored. However, as discussed in later subsection, the Zeeman effects on the Balmer lines will give the local information on the  $H_{\alpha}$ ,  $D_{\alpha}$ , and  $T_{\alpha}$  emissions.

### **Method and instruments:**

The setup used for the detection of Doppler-broadened Balmer lines in TFTR is shown in Fig. 8.18 [15]. Emitted light from TFTR was collected by a telescope and transmitted via a fiber optics to the data-acquisition room. In order to avoid the Zeeman splitting effects, only  $\pi$  component is selected by a polarizer. On exiting the fiber, the light from the plasma was recollimated, filtered with a 1-nm band-pass filter, and reinjected into a second fiber. The maximum transmission wavelength of the filter was set to the  $D_{\alpha}$  wavelength by tilting the filter. A Fabry–Perot interferometer was used to spectrally resolve the  $H_{\alpha}$ ,  $D_{\alpha}$ ,  $T_{\alpha}$  emissions. The free spectral range of the Fabry–Perot interferometer was set to 0.7 nm with a resolution of 0.023 nm. The Fabry–Perot interferometer was set to scan over two orders every 200 ms and then the spectrum was detected by a photomultiplier.

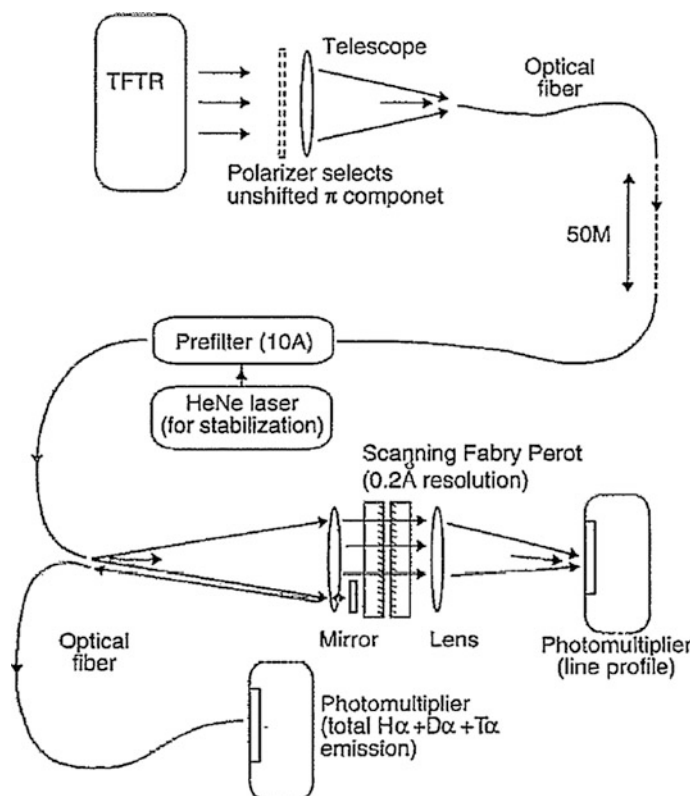


**Fig. 8.18** Experimental setup in TFTR. (Reprinted with the permission from [15])

### Results:

Before D-T experiment in TFTR,  $D_\alpha$  and  $H_\alpha$  profiles in H-D plasma were examined in  $D^0$ -beam injection plasma with a small amount of hydrogen recycled from the wall. Expected  $T_\alpha$  profiles are overlaid to them according to two simulation results with  $C_T = 6\%$  and  $24\%$ .  $H_\alpha$  can be used to evaluate the density ratio even for  $C_H \sim 10\%$ . At T concentrations above 20 %, a clear separate peak emerges, while below that level, the  $T_\alpha$  line is apparent in a “bulge” in the longer wavelength side of the  $D_\alpha$  profile. This is due to the small wavelength difference and reduction of the line width of  $T_\alpha$  by  $\sqrt{2/3}$ . To estimate the level at which  $T_\alpha$  would be detectable, a line fitting with two temperatures (warm and cold) was used. This fits the complete  $H_\alpha - D_\alpha - T_\alpha$  profile to 6 Gaussians. Thus, the reproducibility of the line profiles in different deuterium discharges was found to be 0.02 % integrated over the region of the expected  $T_\alpha$  wavelength. In D-T plasma (73453), the  $H_\alpha - D_\alpha - T_\alpha$  profile was measured and compared with the  $H_\alpha - D_\alpha$  line profile in H-D plasma (73443), as shown in Fig. 8.19. The subtraction of the  $H_\alpha - D_\alpha - T_\alpha$

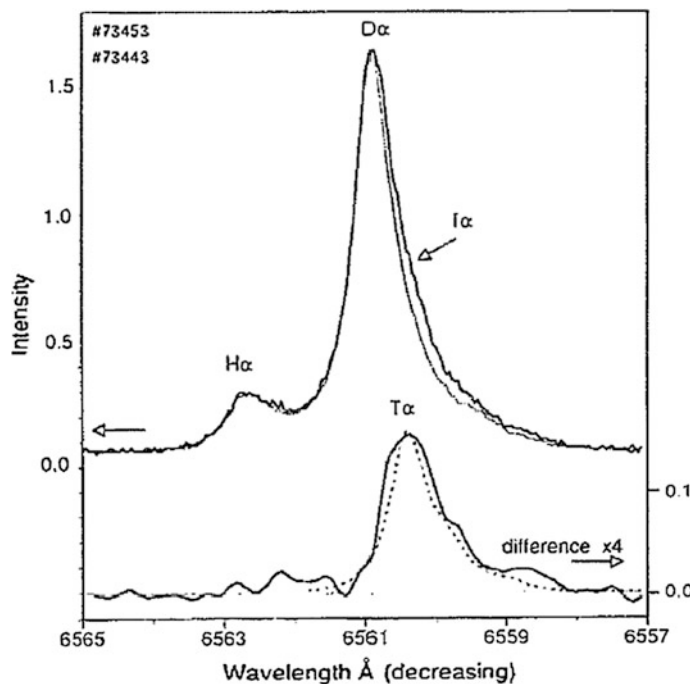


**Fig. 8.19** Upper traces show a comparison of the normalized line profiles from discharge 73453 in ***bold*** and an earlier deuterium comparison discharge (73443, thin trace) before tritium NBI. The displacement on the short wavelength side of the profile is due to  $T_\alpha$ . The lower traces show the difference between these profiles magnified by a factor 4 (scale on the right-hand side) and (*dotted*) a  $T_\alpha$  profile predicted by DEGAS. The difference profile was smoothed with a filter function to remove noise features beyond the instrumental spectral resolution. (Reprinted with the permission from [15])

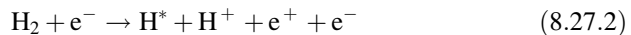
profile from the  $H_\alpha - D_\alpha$  line profile reveals  $T_\alpha/(H_\alpha + D_\alpha + T_\alpha)$  of  $\sim 2\%$ . The maximum level of  $T_\alpha/(H_\alpha + D_\alpha + T_\alpha)$  of 7.5 % was found in a D-NBI discharge (73454) immediately following T-NBI plasma (73453). This suggests that the recycling affects the density ratio. The Monte Carlo neutral transport code, DEGAS, is used to evaluate  $H_\alpha - D_\alpha - T_\alpha$  profile. The result is overlaid by a dotted curve.

### 8.3.4.2 Passive Molecular Fulcher-Band Spectroscopy for Molecular Flux [16]

**Principle:**

As described in Introduction, understanding of the surface release molecular flux  $\Gamma_M$  ( $\text{mol}/(\text{m}^2/\text{s})$ ) for all isotopologues of hydrogen molecules ( $\text{H}_2$ ,  $\text{HD}$ ,  $\text{D}_2$ ,  $\text{HT}$ ,  $\text{DT}$ ,  $\text{T}_2$ ) is important to control the fueling ratio, because in a fusion plasma most of the fueling gas mixture—tritium and deuterium—will enter the plasma via recycling from PFCs.

The loss events for recycling molecules are listed by the following Franck–Condon dissociation, dissociative ionization, and dissociative excitation processes.



In the high temperature ( $T_e > 10 \text{ eV}$ ), molecular formation by means of recombination is negligible. Thus,  $\Gamma_M$  can be deduced from line emissions of excited atoms produced with the above processes in high-temperature plasmas, if the photon flux  $\phi_M$  ( $\text{photons}/(\text{m}^2/\text{s}/\text{sr})$ ) is equivalent to the number of molecular loss events per second, as follows [17].

$$\Gamma_M = D_{\text{eff}} / X_M B_M \phi_M, \quad (8.28)$$

where  $D_{\text{eff}}$  is the effective dissociation rate coefficient and  $X_M B_M$  is the effective emission rate (excitation rate  $X_M = \langle \sigma v \rangle_{\text{exc}}$  and the branching ratio  $B_M = A_{\text{Fulcher}} / \sum_{i < p} A_{pi}$ ) of the transition.  $D_{\text{eff}}/X_M B_M$  means dissociation events per photon. The Fulcher- $\alpha$ -band is the strongest in the visible range which is a rovibrational transition between the two excited electronic states  $3p\ ^3\Pi_u$  and  $2s\ ^3\Sigma_g^+$ . According to the simple rate equation for the  $n_3$  population density between the electronic excitation from the ground level and spontaneous emission from  $n = 3$  to  $n = 2$ , the following relation can be derived in steady state as

$$\frac{dn_3}{dt} = n_e n_{\text{H}_2} X_{2s^3\Sigma_g^+ - 3p^3\Pi_u} - \frac{2}{7} n_3 \sum_{i < 3} A_{3i} = 0, \quad (8.29)$$

and the intensity of the Fulcher emission is given by

$$I_{\text{Fulcher}} = \frac{1}{4\pi} n_3 A_{\text{Fulcher}} h\nu_{\text{Fulcher}} = \phi_{\text{Fulcher}} \frac{7}{2} n_e n_{\text{H}_2} X_{2s^3} \sum_g {}^+ -3p^3 \Pi_u B_{\text{Fulcher}}, \quad (8.30)$$

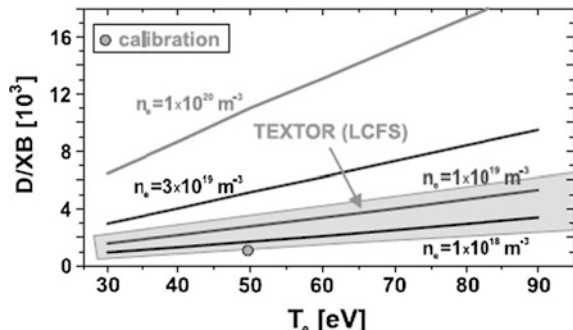
where  $2/7$  is the ratio of the statistical weight of the upper level  $d^3\Pi_u$  state to the sum of all six states,  $A_{\text{Fulcher}}$  ( $\sim 2.5 \times 10^7 \text{ s}^{-1}$ ) is the Einstein transition probability for the Fulcher emission, and  $n_{\text{H}_2}$  denotes the molecular hydrogen density. Based on the collisional radiative (CR) model, the calculated results of  $D_{\text{eff}}/X_M B_M$  are shown in Fig. 8.20. The contribution of each vibrational level to the total intensity is determined by the rotational population within that level. Depending on the selection rules for rotational transitions, there are three branches  $P$  ( $\Delta J = -1$ ),  $Q$  ( $\Delta J = 0$ ), and  $R$  ( $\Delta J = +1$ ), where  $J$  represents the rotational quantum number. According to the sum rule for the transition probabilities, measuring only  $Q$ -branch and doubling its intensity are sufficient for the determination of the intensity of one vibrational level.

In addition to normal isotopologues, the following molecules HD, HT, and DT are formed and contribute to the total released molecular flux  $\Gamma_M$ . The spectrum of six isotopic species of molecular hydrogen observed in gas discharge is shown in Fig. 8.21 [18]. Because of the different masses of nuclei  $T_2:TD:TH:D_2:HD:H_2 = 6.5:4.4:3.2$  differences in the energy of vibrational and rotational levels occur. The difference between vibrational levels decreases for higher masses and the whole spectrum becomes close to the  $v = 0$  level. A non-negligible number of heteronuclear molecules are produced though at isotopologue ratios of only a few percent for the minority species.

#### **Method and instruments:**

Systems used for molecular spectra measurements in TEXTOR are shown in Fig. 8.22 [19]. Observation is done on a graphite test limiter ( $0.12 \text{ m} \times 0.08 \text{ m}$ ,  $r = 0.07 \text{ m}$ ) inserted at the last closed flux surface, LCFS, of tokamak plasma. Molecules released from the limiter surface were measured by the spectrometer

**Fig. 8.20** CRMOL calculations for the conversion factor  $D/X_B$ . (Reprinted with the permission from [17])



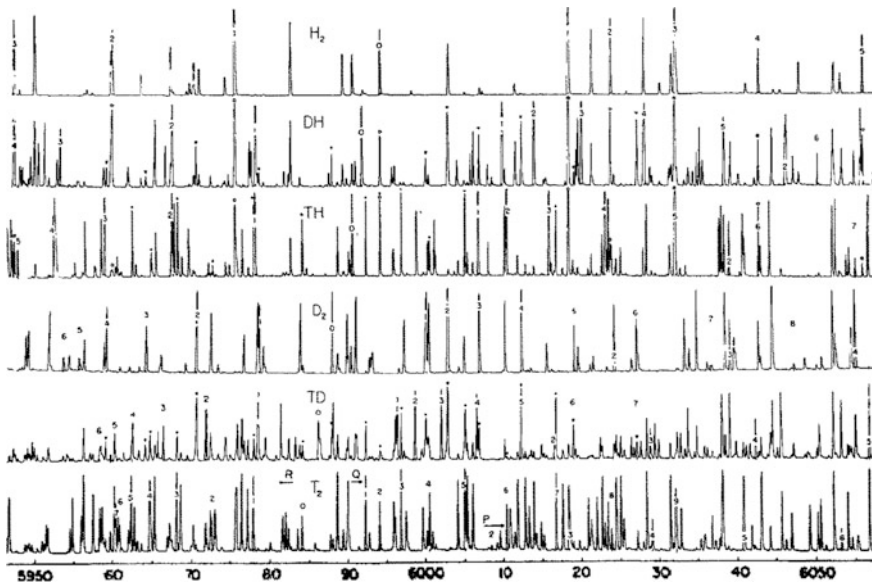


**Fig. 8.21** Comparison of the spectrum near 6000 Å of the six isotopic species of molecular hydrogen. The lines of the  $0- > 0$  band of  $3p\ ^3\Sigma -> 2s\ ^3\Sigma$  are indicated. Many lines of different origin are interspersed. The illustrated section is one of the simplest in the spectrum. (Reprinted with the permission from [18])

system 3. Part of the light of the main optical path is deflected by mirror MH3, coupled with a quartz optical fiber and, finally by means of a lens system, imaged onto the entrance slit ( $50\ \mu\text{m}$ ) of a  $0.8\ \text{m}$  spectrometer in Littrow arrangement. The spectrometer, which functions on the principle of auto-collimation, is equipped with a single apochromatic lens (150 mm diameter) in front of the Echelle grating. The Al-coated grating ( $165\ \text{mm} \times 150\ \text{mm}$ ), with a blaze angle of  $46^\circ$ , is ruled with 1200 grooves per millimeter. An optical multichannel analyzer system, which consists of an intensified linear diode array with 1024 pixels and a detector controller, is used for detection. Each pixel of the array is  $25\ \mu\text{m}$  wide and  $2.5\ \text{mm}$  high. The detector was cooled to  $-10\ ^\circ\text{C}$ , and the exposure time is set to 200 ms. The spectrometer is operated in second order. The resolving power,  $\lambda/\Delta\lambda$ , of the system, which is experimentally determined by the measurement of an effective Gaussian instrumental line profile with the aid of a Geissler discharge tube, is approximately 13,000 at 600 nm. The wavelength range covered amounts to 8 nm in one recording.

### Results:

To describe the molecule release from the plasma facing materials PFCs, a simple surface recombination model combined with the chemical law of mass

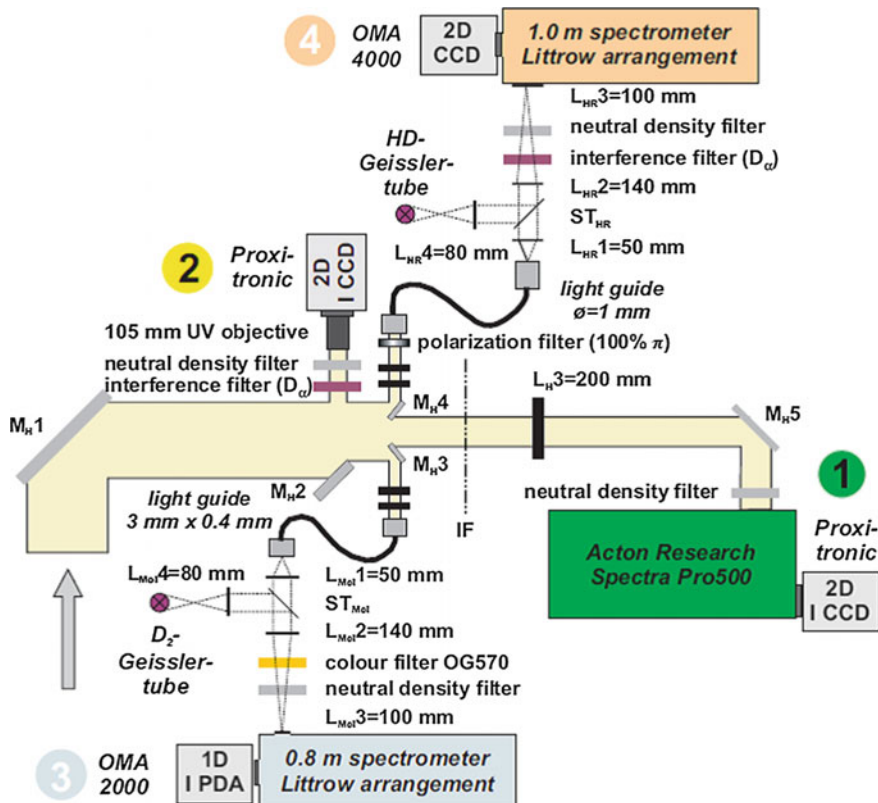


**Fig. 8.22** Schematic view of the optical paths for four observation systems located at the horizontal diagnostic port. (Reprinted with the permission from [19])

action between H<sub>2</sub>, D<sub>2</sub>, HD is introduced [16]. Each concentration of isotopologues is described as follows:

$$\begin{aligned}
 C_{\text{H}2}(C_D) &= \frac{1}{1 + \frac{C_D}{1-C_D} \frac{K_1}{K_2} + \left(\frac{C_D}{1-C_D}\right)^2 \frac{1}{K_2}}, \\
 C_{\text{HD}}(C_D) &= \frac{1}{1 + \frac{1-C_D}{C_D} \frac{K_2}{K_1} + \frac{C_D}{1-C_D} \frac{1}{K_1}}, \\
 C_{\text{D}2}(C_D) &= \frac{1}{1 + \frac{1-C_D}{C_D} K_1 + \frac{C_D}{1-C_D} K_2}.
 \end{aligned} \tag{8.31}$$

Here the surface recombination coefficients  $k_{\text{H}2}$ ,  $k_{\text{HD}}$ ,  $k_{\text{D}2}$ , and equilibrium constants  $K_1 = k_{\text{H}2}/k_{\text{D}2}$  and  $K_2 = k_{\text{HD}}/k_{\text{D}2}$  are used for a H<sub>2</sub>, HD, and D<sub>2</sub> reaction system. When  $K_1 = K_2 = 1$ , the isotopologues concentration is simply determined.

The maximum of the HD production, which means then one-third of the total molecular release, is reached at  $C_D = 50\%$ . The other two-thirds of the molecules are then equivalently distributed on  $D_2$  and  $H_2$ .

Figure 8.23 shows the Q-branches ( $v = 0-3$ ) up to  $J = 8$  as a reference spectrum of HD in a low  $H_2$  concentration, marked by the low intensity of the  $H_2$  lines, whereas the concentration and the spectrum of  $D_2$  dominates, but the HD lines are also visible. According to Eq. (8.31), the HD intensity corresponds roughly to a D-concentration range between 75 and 95 %. The spectrum obtained in a deuterium plasma with additional heating by means of an H neutral beam represents the case where all isotopologues have comparable intensity. This case corresponds to the middle concentration range. However, it should be stressed that this simple analysis provides only a qualitative view. For a quantitative analysis of  $\Gamma_M$ , the rotational and vibrational populations for all species have to be taken into consideration.

Isotope ratio was examined in the following procedure. Firstly, the test limiter was well baked and then saturated with D. The total exposure duration was 50 s. The test limiter was then removed from the vessel and stored in a vacuum tank. Secondly, the chamber wall is conditioned by means of glow discharge and subsequent H discharges. The global isotope exchange was carried out. The ration D/(H+D) was changed from 0.95 to 0.45, measured at the main limiter. Finally, the test limiter was again positioned at the plasma boundary. Figure 8.24 shows the corresponding time evolution of the relative intensities of the isotopologue Q (0, 0) Fulcher- $\alpha$  for the first discharge. Since the surface of the test limiter is saturated by D, it is observed that the local isotope ratio on the test limiter changes toward the global one. In Fig. 8.24b at  $t = 1.4$  s, which is characterized by the fast removal of the surface saturated D, the decrease in the fraction of  $D_2$  Fulcher- $\alpha$  intensity from 0.40 to 0.3 and simultaneously the increase of the  $H_2$  intensity from 0.25 to 0.35 are observed. The intensity of HD is almost constant at 0.35, which is qualitatively consistent with the model result at  $C_D \sim 0.5$ .

The passive diagnostic methods can be extended to local measurement using the Zeeman patterns in the spectral shape. In TRAIM-1M, the Zeeman split in the

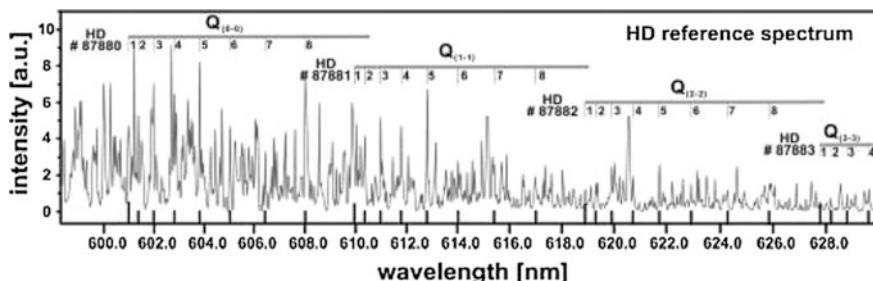
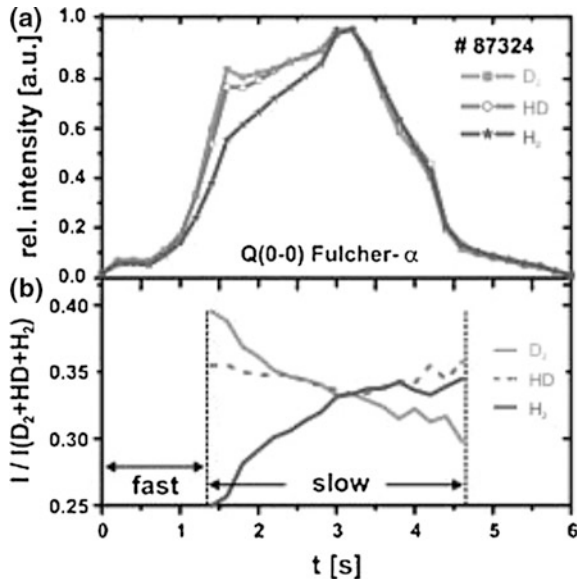


**Fig. 8.23** Fulcher-band system of HD was observed in front of the test limiter. The first lines of each Q-branch ( $v = 0-3$ ) of the diagonal transitions are marked. (Reprinted with the permission from [16])

**Fig. 8.24** Time evolution of the Fulcher- $\alpha$  intensity of all three isotopomers during the upright molecular release from a saturated surface. (Reprinted with the permission from [16])



Fulcher (Balmer) lines has been observed. The spectra of separately measured  $\pi$  and  $\sigma$  polarization components and those measured without the polarizer are shown in Fig. 8.25. The spectra are well fitted by the Zeeman pattern with a magnetic field of 6.68 T. The expected spatial resolution was  $\sim 6$  mm determined from a fitting error of 0.05 T at  $B_t = 6.68$  T [20]. The example is compared with the magnetic measurement of the plasma axis, shown in Fig. 8.26. The error bars of the measurements correspond to the standard deviations of the fitting procedure.

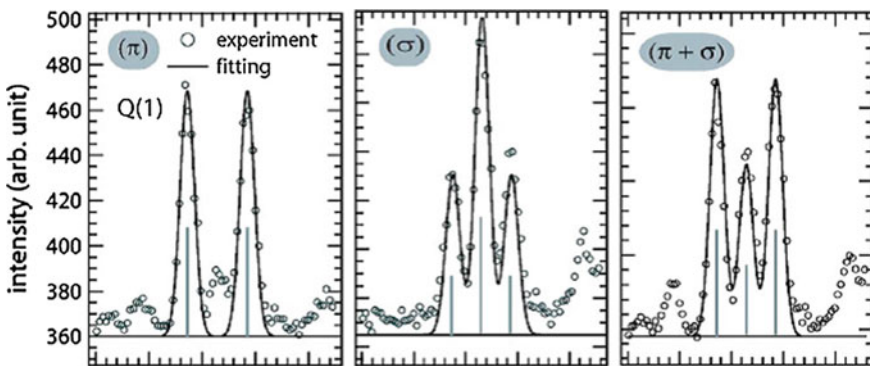
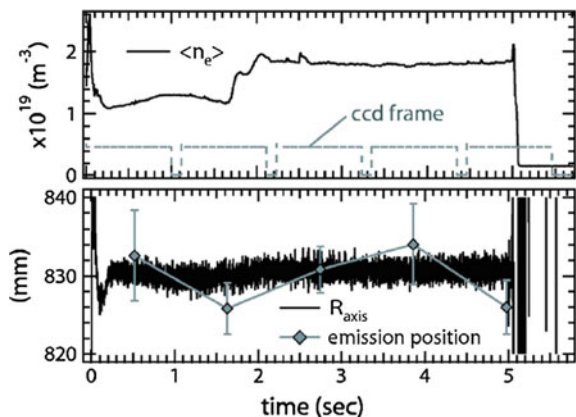


**Fig. 8.25** Expanded Fulcher Q (1) spectra ( $v'-v'' = 0-0$ ). (Reprinted with the permission from [20])

**Fig. 8.26** Temporal evolution of the line-averaged density, CCD shutter frame, horizontal position of the magnetic axis ( $R_{\text{axis}}$ ), and the evaluated position of the molecular emission using the Zeeman effects. (Reprinted with the permission from [20])



### Prospect to ITER:

In ITER, a passive H-alpha spectroscopy system, equatorial visible/infrared wide angle viewing system (WAVS), will be installed to study the fuel density ratio ( $n_T/n_D$  and  $n_H/n_D$ ) at the edge and divertor [21]. This WAVS measures Balmer series lines (transitions of principal quantum number from  $n = 8$  to  $n = 2$ ) emitted from hydrogen isotopes in the wavelength range of 370–660 nm. The fuel density ratio at the edge is evaluated by measured intensity ratio of  $T_2/D_\alpha$ ,  $H_2/D_\alpha$ , including molecular lines. Since the optical mirrors and light-transferring tubes in WAVS will be directly irradiated with neutrons, gammas, and energetic ions/particles, material choice and their electrical and optical properties are key issues for spectroscopy. Figure 8.27 shows four views covered with WAVS [22, 23]. These areas cover all heating ports, shine-through area, upper target strike area, and the inner divertor target including part of the dome and the baffle and of half of the rest of the first wall evenly distributed. In total, the WAVS will be composed of 15 lines of sight (LOS) and 15 optical systems transferring the light from the PFCs through the diagnostic shielding module (DSM) in the port plug up to detectors located in the port cell. The proposed optical design (Fig. 8.28) uses mirrors inside the port plug, sapphire windows on the port closure plate, a field lens, a Cassegrain telescope, dichroic filters to split visible (VIS) and infrared (IR) lines, and some lenses in the port interspace, a dogleg behind the bioshield and more lenses in the port cell up to the camera. Port plug 4 vertical doglegs are used to minimize the neutron leakage. The divertor view is achieved with  $2560 \times 3200$  pixels and others  $1280 \times 1600$  pixels. The spatial resolution is 3 mm on the divertor. The frame rate of camera is 100 Hz. [22].

First mirrors are key components of the optical systems. Full-scale circular actively cooled mirrors (109 mm in diameter) with flat shape have already been designed, manufactured, and polished with blanks of stainless steel and TZM (molybdenum alloy) with nickel interlayer and reflective thick coating (3–5  $\mu\text{m}$ ) of

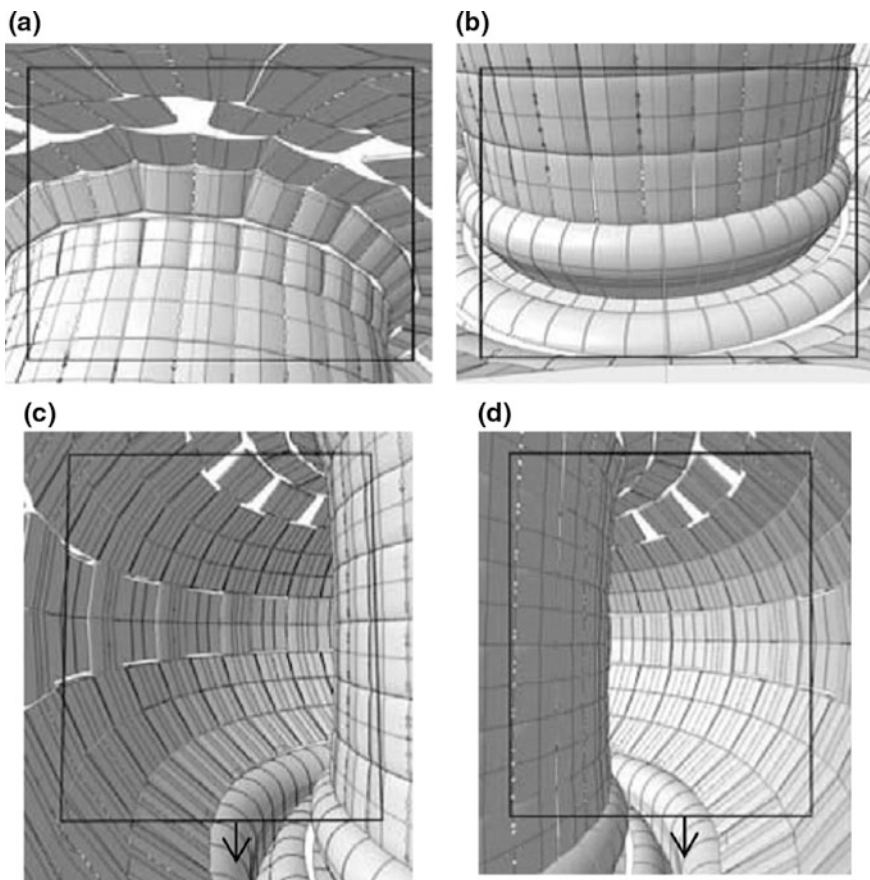


**Fig. 8.27** Four views of WAVS—including new upper target view (a); note that (b) has 2 times higher resolution than others and (c) and (d) are not yet optimized for best coverage of the outer divertor targets (arrows). (Reprinted with the permission from [22])

rhodium and molybdenum. The reflectivity for  $4.5\ \mu\text{m}$  thickness is calculated 0.78 and 0.58 at  $650\ \text{nm}$ , respectively. Using the finite element method, the thermo-mechanical study of the TZM mock-up has been performed [24]. When a plasma radiation flux of  $0.5\ \text{MW/m}^2$  is applied during  $400\ \text{s}$ , the maximum temperature rise is lower than  $25\ ^\circ\text{C}$  at the water flow rate of a few meters per second. Initial temperature was set at  $0\ ^\circ\text{C}$  and its deformation after removal of the defocus which is the main induced default is limited to  $0.016\ \mu\text{m rms}$ . In present experimental devices, the reduction in performance of the first mirror has been systematically investigated [25]. In LHD, it has been analyzed that the deposits on the mirror consisted of Fe, FeO, and C, originating from the stainless steel duct and LHD interior having stainless steel walls and carbon divertor and the specular reflectivity,

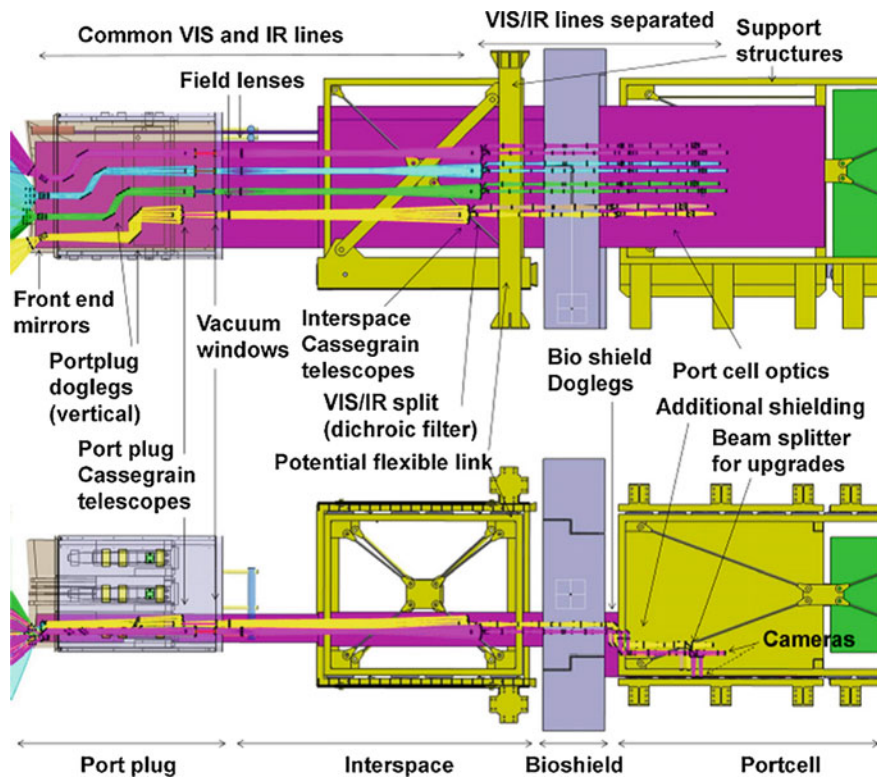


**Fig. 8.28** WAVS side view (*top*) and top view (*bottom*). (Reprinted with the permission from [23])

dropped significantly from 0.7 to 0.1 at 1  $\mu\text{m}$ . The optical shutter to protect the erosion and deposition of the first mirror is being under the conceptual design stage and an in situ cleaning system, if possible, is also deemed necessity [23].

### 8.3.4.3 Active Diagnostics CXRS and BES (Charge eXchange Recombination and Beam Emission Spectroscopies) [26]

#### *Principle:*

In the burning plasma, the fueling into the core region is considered to be done by fast neutral beams. Different from the passive Balmer- $\alpha$  emission (originated from the electron impact excitation), which is restricted with the emission from the edge, the neutral beam has diagnostic potential to measure intense Balmer- $\alpha$

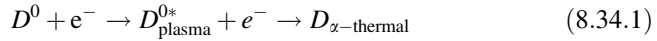
emission in the core. The  $D_{\alpha\text{-ACX}}$  line associated with the fast neutrals is emitted in plasma by the following active charge exchange process,



Here  $D_{\text{plasma}}^{0*}$  means the excited state of D atom. The active CX photon flux  $\phi_{\alpha\text{-ACX}}$  is given by

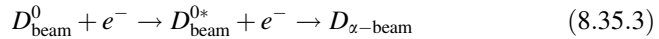
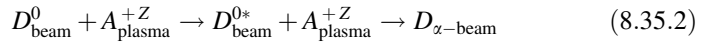
$$\phi_{\alpha\text{-ACX}} = \frac{1}{4\pi} n_d n_{\text{beam}} \langle \sigma v \rangle_{\text{cx}} \Delta l, \quad (8.33)$$

where  $\Delta l$  is the path length and bracket must be calculated by taking the velocity distribution functions for bulk ions and beam particles into account. This emission line is overlaid on the emission due to the electron impact excitation and passive charge exchange excitation with the neutral  $D^0$  recycled from the wall. The former and latter are named “cold” and “warm” components, depending on their radial location.



In order to obtain the ACX component above two spectra must be subtracted from the observed spectrum.

The beam Balmer- $\alpha$  emission  $D_{\alpha\text{-beam}}$  via the following three collisional processes can be also observed in the vicinity of Balmer- $\alpha$  line [27].



These processes are dominant by collisional excitation of the beam atoms with fuel deuterons, fully stripped impurities and electrons. Line emissions caused by the neutral beams is Doppler-shifted depending on the velocity of the injected particles and on the angle between the beams and the viewing lines. The beams intersect the magnetic field lines at some angle and a strong magnetic field is therefore experienced by the neutrals in their center of mass frame. The  $v_{\text{beam}} \times B$  Lorentz electric field perturbation causes the  $D_{\alpha\text{-beam}}$  line (motional Stark emission, MSE) to split into 15 Stark components ( $0\sigma, \pm 1\sigma, \pm 2\sigma, \pm 3\sigma, \pm 4\sigma, \pm 5\sigma, \pm 6\sigma, \pm 7\sigma$ ), 9 of which are usually strong enough to be observed. Since the beam consists of three energy fraction ( $E_0$ ,  $E_0/2$  and  $E_0/3$ ), corresponding to  $D^+$ ,  $D_2^+$ ,  $D_3^+$  in the positive-ion source of the beam injectors, three Stark components appear at different

Doppler shifts. Thus, the Balmer- $\alpha$  photon flux  $\phi_{\alpha-\text{BE}}^i$  from the  $i$ th energy fraction of beam particles is described by

$$\phi_{\alpha-\text{beam}}^i = \frac{1}{4\pi} n_e n_{\text{beam}}^i \langle \sigma v^i \rangle_{\text{BE}}^{\text{eff}} \Delta l \quad (8.36)$$

The effective emission rate  $\langle \sigma v \rangle^{\text{eff}}$  for impact excitation of fast neutrals at  $E_0 = 40 \text{ keV/amu}$  has been calculated as a function of the density. At  $n_e = n_i = 5 \times 10^{19} \text{ m}^{-3}$   $\langle \sigma v \rangle^{\text{eff}}$  is  $\sim 1.8 \times 10^{-15} \text{ m}^3/\text{s}$ , which is almost double the electron impact excitation rate at  $T_e = 10 \text{ keV}$  [27].

Using Eqs. (8.33) and (8.36), the deuteron fraction can be deduced from the ratio of the measured photon fluxes and effective emission rates as follows:

$$C_D = \frac{\phi_{\alpha-\text{ACX}}}{\sum_i \left( \phi_{\alpha-\text{beam}} \langle \sigma v \rangle_{cx}^{\text{eff}} / \langle \sigma v \rangle_{\text{BE}}^{\text{eff}} \right)^i} \quad (8.37)$$

### **Method and instruments:**

In Fig. 8.29, the diagnostics beam system in JET is schematically shown [28]. A plane view of the JET tokamak shows the NBI assemblies at the torus octant 8. In

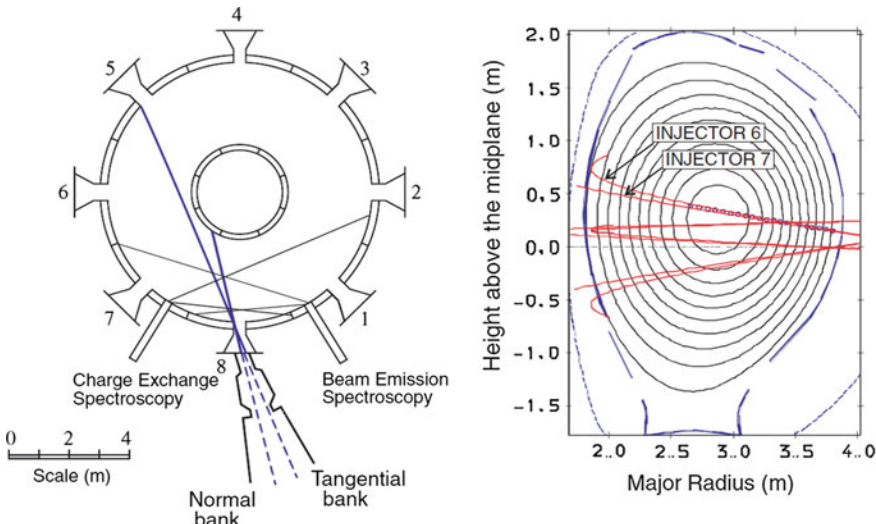


**Fig. 8.29** Plan view and side elevation of the JET tokamak. The figure on the *left* illustrates the location of the observation ports for charge exchange and beam emission spectroscopies. The figure on the *right* shows the typical trajectories of each neutral injector; particular attention should be drawn to diagnostic injectors 6 and 7, which are annotated. (Reprinted with the permission from [28])

Fig. 8.29 (right figure), the projection of the neutral beams and a typical set of observation positions (major radius  $R$ , height above the midplane  $Z$ ) are denoted by dots. An optical head collects light along a set of nearly horizontal viewing lines intersecting the neutral beams of octant 8. The light is separated into two orthogonal polarization components ( $\sigma$  and  $\pi$ ) for simultaneously measurements of both components. To measure the polarization angles of the Stark multiplet, 4 pairs of fibers to a spectrometer, pair of polarizing beam splitters, collimating lens, and half-wave plate are used. The polarization plane of the linearly polarized incident light is rotated by a (zero-order) half-wave plate in order to maximize the sensitivity of the measurement. The collimating lenses are used to image different plasma locations onto optical fibers, on top of which an assembly of polarizing beam splitter cubes is mounted. They separate the linearly polarized light into two orthogonal components, each of which gives a full Stark spectrum. With this technique, four radial positions are observed simultaneously needing eight detection channels.

### Results:

In D beam heating JET plasma, the spectrum in the vicinity of D Balmer- $\alpha$  is shown in Fig. 8.30 [29]. “A” corresponds to the cold edge emission, from whose Doppler width  $T_D \sim 40$  eV was evaluated. “B” is present only with the D beams

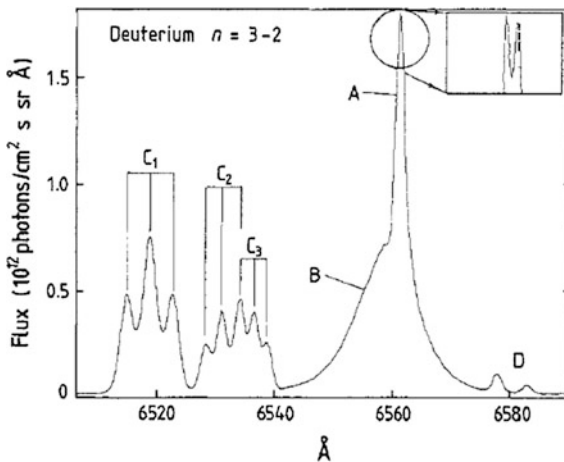


**Fig. 8.30** Spectrum in the vicinity of deuterium Balmer- $\alpha$  with the neutral beams active. JET pulse no 14825; toroidal magnetic field,  $B_t = 2.7$  T. “A,” cold plasma edge feature-inset is from pulse no 17719 at higher resolution; “B,” plasma deuterium charge exchange induced emission feature; “C<sub>1</sub>,” deuterium emission from the full energy fraction; “C<sub>2</sub>,” half-energy fraction; “C<sub>3</sub>,” third energy fraction; and “D,” CII emission from the edge. (Reprinted with the permission from [29])

and is the primary charge exchange component at the beam-plasma-viewing line intersection. Although the passive charge exchange component is observed, after subtracting them from “B”  $T_D \sim 2.7$  keV was evaluated. This part is characterized by an asymmetric blue wing with respect to the cold component. Although the light is emitted from the bulk ions, this asymmetry is principally due to the favoring of charge transfer to plasma deuterons commoving with beam because of the rapid fall of the charge exchange cross sections for relative velocity  $v > 1.5 v_{\text{Bohr}}$  ( $v_{\text{Bohr}}$  is the Bohr orbital speed = 25 keV/amu). “C” is characterized by Doppler-shifted emission from the beam deuterons. Three components (C1, C2, C3) are associated with the full, half, and third energy components. For H, D-mixed plasma CX spectrum has been analyzed in the TEXTOR H-beam injection experiment [30]. The CX beam spectrum in the vicinity of H and D Balmer- $\alpha$  lines are simulated using the six Gaussian profiles modeling edge, PCX, and ACX spectra for H and D as shown in Fig. 8.31. From the intensity ratio of these components, it is considered that the local H/D ratio is different. In a JET D-T plasma, since two sets of normal and tangential injection beams were used (see Fig. 8.32), more complicated  $D_\alpha - T_\alpha$  spectra were taken with different viewing angles as shown in Fig. 8.29. Each energy fraction of beam particles gives 9 visible motional Stark emission lines, and then 27 components are totally distributed. Thus, the spectral entity in the red side encompasses 54 beam emission components originated from two beam lines. Four passive edge features (representing D and T impact excitation and passive CX for D

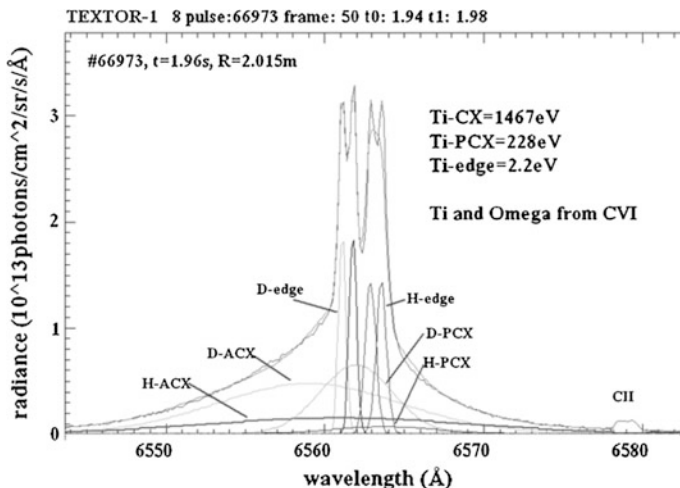


**Fig. 8.31** CX Balmer- $\alpha$  spectrum in a TEXTOR hydrogen scan. Doppler width and shift of CX component are taken from CVI analysis. Note that the local isotope amplitude ratio H/D may be different for CX, PCX, and edge lines. Zeeman splitting is applied to edge lines only. (Reprinted with the permission from [30])

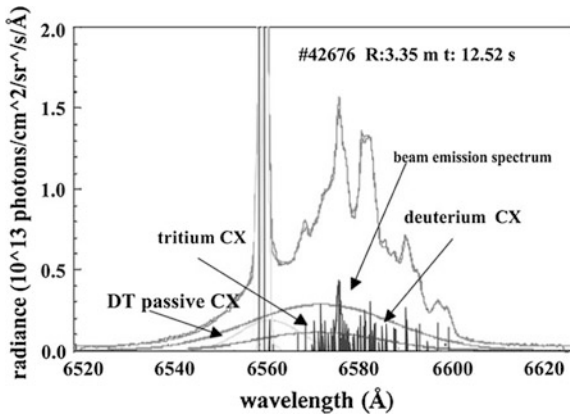


**Fig. 8.32** A combined presentation of beam features and thermal CX components of isotopes deuterium and tritium in a JET D-T pulse. Full modeling of beam features based on geometry, magnetic field, and plasma density and temperature as well as the usual input of carbon ion temperature has enabled initial estimates leading to a global minimum. D and T are assumed have the same temperature and toroidal speed. The weakest parts in the modeling of the composite spectrum are the D and T PCX features. (Reprinted with the permission from [30])

and T) near 656 nm and two active core CX features whose peaks are  $\sim 657$  nm are fitted by Gaussian profiles. Atomic modeling of the beam emission excitation including the real geometry of beam and plasma interaction is inevitable. In this case,  $T/(T + D)$  is deduced 0.25.

#### Prospect to ITER:

In ITER, the two neutral heating beams (0.5 MeV/amu 18 MW) and a dedicated diagnostic neutral beam (0.1 MeV/amu, 3.6 MW) are available as active beam diagnostics. There are two CXRS systems: (a) an edge CXRS system covering the outer region of the plasma ( $1 > r/a > 0.4$ ) using an equatorial observation port, and (b) a core CXRS system for the very core ( $0 < r/a < 0.7$ ) using a top observation port, as shown in Fig. 8.33. Thus, optimum radial resolution (20 mm at  $r/a = 0$  and 58 mm at  $r/a = 0.7$ ) is ensured for each system with the radial resolution better than  $a/30 \sim 66$  mm.

The doping neutral beams DNB are injected as total 1280 beam-lets from the 560 mm  $\times$  1518 mm ion grid assembly [31]. Although each beam-let causes motional Stark effects (MSE), the overall result of the angular spread with the beam-let divergence of 5 mrad is a significant smearing of the  $\pi$  and  $\sigma$  multiplet fine structure. The total beam spectrum is the result of a superposition of characteristic MSE spectra. The beam Balmer- $\alpha$  spectrum is calculated in Fig. 8.34, which consists of D- and T-ACX spectra and MSE. This result is obtained at  $r/a = 0.3$ , D:

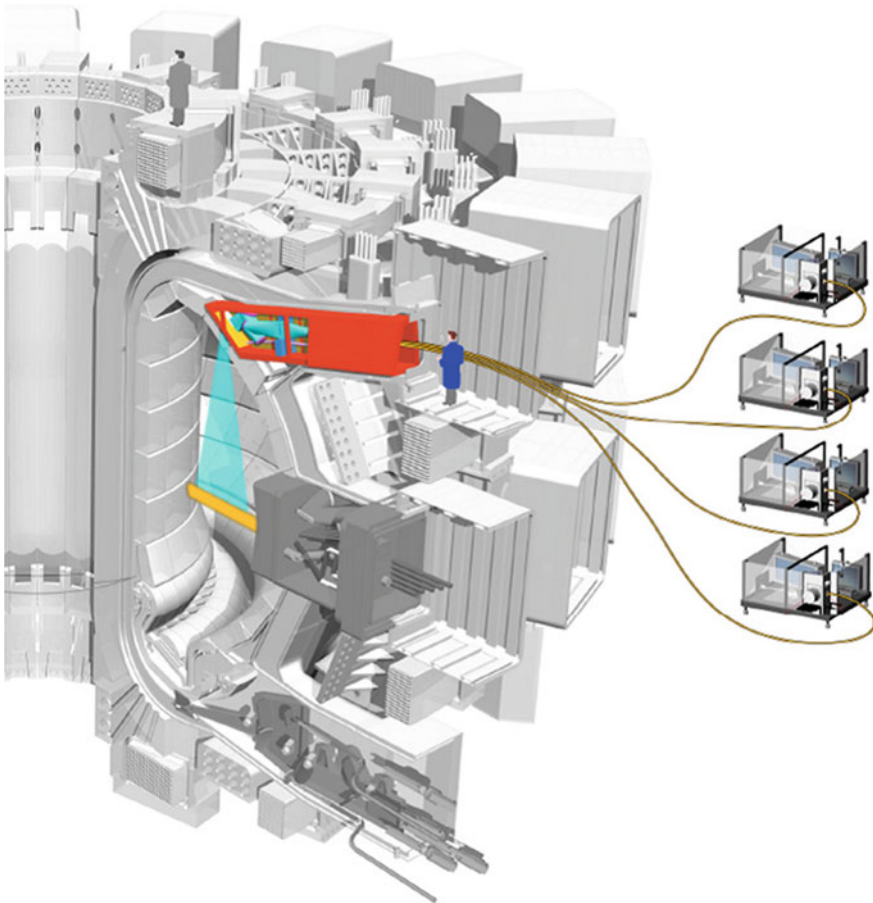


**Fig. 8.33** ITER CXRS diagnostic showing U-port periscope. DNB injection in E-port 4 and a schematic link to high-throughput spectrometers one for each radial channel. (Reprinted with the permission from [31])

$T = 1:1$ ,  $B = 5.3$  T and U-port diagnostic port. Error analysis has been done for the fueling ratio. The local fuel mixture ratio is achieved from modeling the ACX. In this analysis, a beam modulation scheme, which reduces the errors for the free parameters significantly by separating active and passive features, has been proposed. Figure 8.35 shows the error evaluation for a local  $T/(T + D)$  ratio measurement. The error below 5 % is ensured for  $0.1 < C_T < 0.6$  at  $r/a = 0.3$  with  $n_d + n_t = 7.6 \times 10^{19} \text{ m}^{-3}$ .

**Fig. 8.34** Finite beam modeling of the DNB MSE spectrum and active D-T thermal CX feature in U-port-3. Location  $r/a = 0.3$ , D:T = 1:1, B = 5.3 T. The broad CX feature represents the two bulk ions D and T. (Reprinted with the permission from [31])

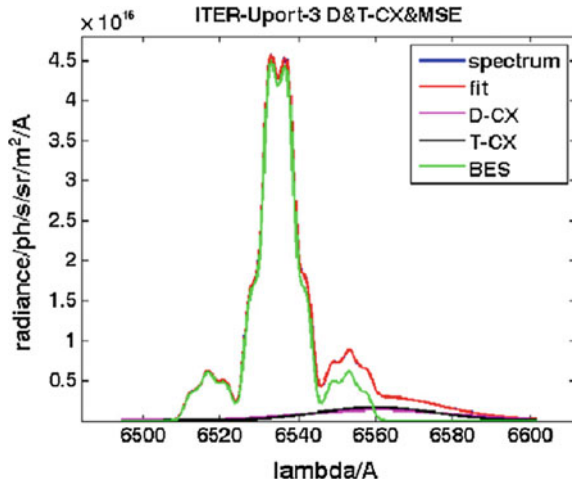
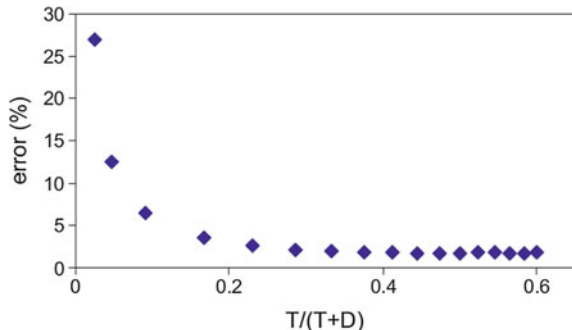


**Fig. 8.35** Error analysis: Scan of fuel mix T/(T + D) with  $n_d + n_t = 7.6 \times 10^{19} \text{ m}^{-3}$  at  $r/a = 0.3$ . (Reprinted with the permission from [31])



## 8.4 Summary and Conclusion

In order to control the fusion power, the information about the ion density ratio  $n_D/n_T$  is one of the inevitable parameters. Although the radial profiles of fueled ions are determined by the transport in the core and edge, it has been known that recycling performance with respect to the chamber walls dominates the global fuel ratio. No single method gives the radial profile, because of the significant difference in energy of fuel particles along the radial direction. Under such conditions, the measurements of  $n_D/n_T$  should be done separately at the core, edge, divertor, and walls. Representative diagnostic methods are selected and reviewed. Physical principle, typical instruments, experimental results, current status, and progress toward ITER are introduced for each method. The particle diagnostics are neutrons from D-T and D-D reactions and passive method of the fuel neutral particle flux from charge

exchange reactions. The former is sensitive to the core density ratio and the latter to that from the intermediate to the edge. Using the effective mass sensitive properties of the Alfvén waves, the reflection of the externally launched waves and resonant generation of the driven waves are characterized by the relatively good spatial resolution. It is also concluded that passive and active spectroscopies of Balmer and Fulcher lines will give the local information well. It is concluded that spatial and time resolutions of the above methods satisfy basically the ITER requirements at present.

However, in ITER severe noises from strong steady magnetic field, neutron, and gamma rays on the electric circuits of diagnostic instruments are forecasted. Lifetime of the optical instruments, severe maintenance environment, remote operation of the instruments, and in situ calibration continue to be priority issues.

## References

1. ITER Physics, Nuclear Fusion, **47** Chap. 7 (2007) S337–384
2. J. Kallne, P. Batisoni, G. Gorini, Rev. Sci. Instrum. **62**, 2871–2874 (1991)
3. L. Giacomelli et al., Nucl. Fusion **45**, 1191–1201 (2005)
4. K. Okada, K. Kondo et al., Rev. Sci. Instrum. **77**, 10E726 (2006)
5. K. Okada, K. Kondo et al., J. Plasma Fusion Res. SERIES **8**, 666–669 (2009)
6. H. Ikeji et al., Rev. Sci. Instrum. **68**, 478–479 (1997)
7. T. Stix, Waves in Plasmas, AIP 1992, p. 7
8. G.W. Watson et al., Plasma Phys. Controlled Fusion **46**, 471–487 (2004)
9. W.W. Heidbrink et al., Rev. Sci. Instrum. **75**, 3862–3864 (2004)
10. A. Fasoli et al., Plasma Phys. Controlled Fusion **44**, B159–B172 (2002)
11. T. Panis, et al., Nuclear Fusion, **50** 084019 (9 pp) (2010)
12. D. Bettella et al., Plasma Phys. Controlled Fusion **45**, 1893–1907 (2003)
13. V.I. Afanasyev et al., Rev. Sci. Instrum. **74**, 2338–2352 (2003)
14. V.I. Afanasyev et al. Plasma Phys. Controlled Fusion **55**, 045008(10 pp) (2013)
15. C.H. Skinner et al., Rev. Sci. Instrum. **66**, 646–648 (1995)
16. S. Brezinsek et al., Phys. Scr. **T103**, 63–67 (2003)
17. S. Brezinsek et al., J. Nuclear Material **313–316**, 967–971 (2003)
18. G.H. Dieke, J. Molecular Spectroscopy **2**, 494–517 (1958)
19. S. Brezinsek et al., Plasma Phys. Controlled Fusion **47**, 615–634 (2005)
20. T. Shikama et al., Phys. Plasma **14**, 072509 (2007)
21. T. Sugie et al., J. Plasma Fusion Res. **79**, 1051–1061 (2003)
22. R. Reichle et al., Rev. Sci. Instrum. **83**, 10E520 (2012)
23. S. Salasca et al., Fusion Eng. Design **96–97**, 932–937 (2015)
24. M. Joanny et al., Rev. Sci. Instrum. **81**, 10E108 (2010)
25. A. Litnovsky, et al., Nuclear Fusion, **49** 075014(8 pp) (2009)
26. J. Svensson, M. von Hellermann, R.W.T. Konig, Plasma Phys. Controlled Fusion **43**, 389–403 (2001)
27. W. Mandl et al., Plasma Phys. Controlled Fusion **35**, 1373–1394 (1993)
28. H. Anderson et al., Plasma Phys. Controlled Fusion **42**, 781–806 (2000)
29. A. Boileau, M. von Hellermann et al., J. Phys. B: At. Mol. Opt. Phys. **22**, L145–L152 (1989)
30. M. von Hellermann et al., Phys. Scr. **T120**, 19–29 (2005)
31. M. von Hellermann et al., Nucl. Instrum. Methods Phys. Res. **A 623**, 720–725 (2010)



# Chapter 9

## Permeation and Permeation Barrier

Yuji Hatano

**Abstract** Because of their small sizes in molecular and atomic forms, hydrogen isotopes easily dissolve in a solid material and permeate through it. The permeation through a container material is a critical issue against safe confinement of tritium. On the other hand, it is common to employ a permeation technique for the separation of hydrogen isotopes from other gaseous species. In this chapter, elemental processes of permeation of hydrogen isotopes through metals and ceramics are explained together with the possible isotope effects on them. Fundamental equations describing the hydrogen permeation through materials under the exposure to gas and plasma are given. The hydrogen permeation under the corrosive environment is also discussed. Characteristics of hydrogen dissolution, diffusion, and permeation in metallic and ceramic materials important for fusion are summarized together with the peculiarity of the hydrogen permeation under the fusion reactor environments.

**Keywords** Tritium • Hydrogen isotopes • Permeation • Surface • Diffusion

### 9.1 Elemental Processes of Permeation

#### 9.1.1 Permeation of Gaseous Hydrogen Isotopes

Elemental processes of tritium (T) permeation are similar to those of hydrogen (H) and deuterium (D). Hence, these hydrogen isotopes are just described as “hydrogen” in this chapter unless distinction between isotopes is necessary. Permeation of gaseous hydrogen is driven by pressure difference between the upstream and downstream sides of a material. The permeation process involves dissolution of hydrogen impinging on the material, diffusion to the opposite side,

---

Y. Hatano (✉)

Hydrogen Isotope Research Center, Organization for Promotion of Research,  
University of Toyama, Gofuku 3190, Toyama 930-8555, Japan  
e-mail: hatano@ctg.u-toyama.ac.jp

and release. Hydrogen dissolves in the form of either molecules and atom or ions, depending on the type of the material. The molecular dissolution is observed for polymers, whereas dissolution in the forms of atoms or ions is typical for metals and dense ceramics. The form of hydrogen dissolution in a material can be understood from the dependence of the concentration of dissolved hydrogen  $C_H$  [mol m<sup>-3</sup>] on the hydrogen gas pressure  $P$  [Pa] under the equilibrium conditions:  $C_H = K_S P$  (Henry's law), if hydrogen dissolves in the molecular form; and  $C_H = K_S P^{0.5}$  (Sieverts' law [1]), if hydrogen dissolves in the form of atoms. Here,  $K_S$  is the solubility [mol m<sup>-3</sup> Pa<sup>-1</sup> or mol m<sup>-3</sup> Pa<sup>-0.5</sup>]. Because metals and ceramics are more important for tritium confinement and separation, the attention is focused on hydrogen permeation through metals and ceramics in the following part of this chapter.

Waelbroeck et al. [2] have published a review report on hydrogen permeation in fusion environments. In the report, they summarized hydrogen permeation phenomena and proposed formulas for several rate-limiting cases. In the following, widely accepted models to describe hydrogen permeation behavior under the hydrogen gas atmosphere, hydrogen plasma, and ion irradiation are described in detail.

Schematic potential energy diagram of metal–hydrogen systems and elemental processes of permeation are shown in Fig. 9.1. Vibrational and rotational energy states are omitted in the figure for simplicity (see also Fig. 9.5). In principle, the rate constants of the elemental processes shown in this figure can vary with the concentrations of hydrogen at the surface and in the bulk of a material. However, in the discussion described below, the rate constants are assumed to be independent of the hydrogen concentrations for simplicity. In other words, the hydrogen concentrations at the surface and in the bulk are assumed to be sufficiently low. The flux of hydrogen molecules impinging on the upstream surface  $J_{in}$  [mol m<sup>-2</sup> s<sup>-1</sup>] at the gas pressure  $P$  is given by the kinetic theory of gases as

$$J_{in} = P / \left( N_A \sqrt{2\pi m_{H_2} k_B T} \right), \quad (9.1)$$

where  $N_A$  is the Avogadro constant [mol<sup>-1</sup>],  $m_{H_2}$  is the mass of a hydrogen molecule [kg],  $k_B$  is the Boltzmann constant [J K<sup>-1</sup>], and  $T$  is the absolute temperature [K]. Hydrogen molecules impinging on the material surface are dissociated with probability of  $\alpha_m$  and then absorbed in the bulk.  $\alpha_m$  is referred as the dissociative sticking probability and expressed as  $\alpha_m = \alpha_{m0} \exp(-2E_C/RT)$  where  $\alpha_{m0}$  is the pre-exponential factor and  $E_C$  is the activation energy for dissociative sticking per hydrogen atom. The values of  $\alpha_m$  and  $E_C$  are sensitively dependent on a chemical state of surface;  $\alpha_m \sim 1$  and  $E_C \approx 0$  for clean surfaces of transient metals, whereas significant drop of  $\alpha_m$  accompanied with large increase in  $E_C$  is induced by adsorption of impurities such as carbon, oxygen, and sulfur [3]. For example, in the case of Pd,  $\alpha_m = 0.3\text{--}0.6$  and  $E_C \approx 0$  for the clean surface, while  $\alpha_m = 10^{-5}\text{--}10^{-3}$  and  $E_C \approx 17.2$  kJ mol<sup>-1</sup> for the sulfur-covered surface at about

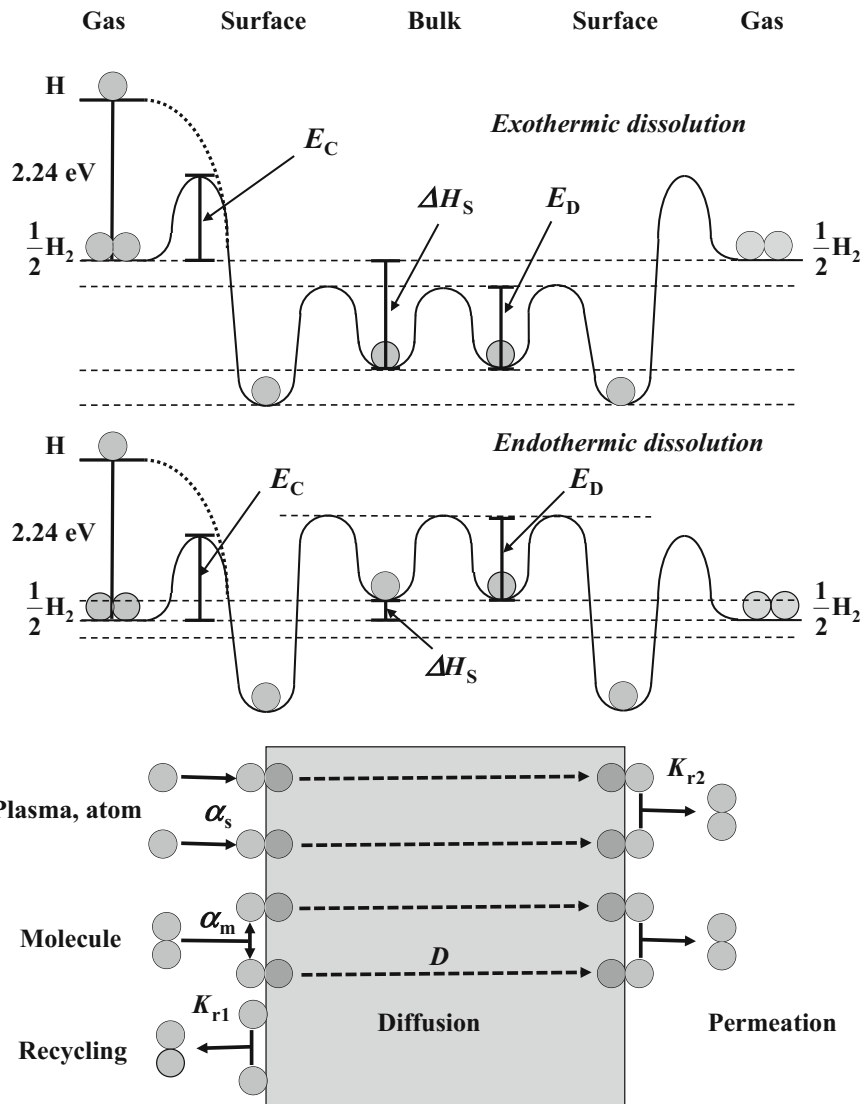


**Fig. 9.1** Schematic potential diagram of hydrogen–metal systems and elemental processes of plasma- and gas-driven permeation.  $E_C$  is the activation energy for dissociative sticking of hydrogen molecules,  $\Delta H_S$  is the enthalpy of hydrogen solution, and  $E_D$  is the activation energy for diffusion.  $\alpha_s$  is the sticking probability of hydrogen atoms or ions, and  $\alpha_m$  is that of molecules.  $K_{r1}$  and  $K_{r2}$  are the recombination rate constant for hydrogen atoms at the upstream surface and that at the downstream surface, respectively

430–1000 K [4]. The release of hydrogen molecules from a metal surface is mostly a second-order reaction, and the flux of the released hydrogen molecules,  $J_r$  [ $\text{mol m}^{-2}\text{s}^{-1}$ ], is expressed as

$$J_r = 2K_r C_H^2, \quad (9.2)$$

where  $K_r$  is the surface recombination rate constant and  $C_H$  is hydrogen volume concentration [ $\text{mol m}^{-3}$ ] in a subsurface layer. In principle, areal surface concentration [ $\text{mol m}^{-2}$ ] of hydrogen must be considered. However, permeation is the process involving bulk diffusion, and, for simplicity, it is common to use the hydrogen volume concentration in a subsurface region under the assumption of surface–subsurface equilibrium. Hence, the dimension of  $K_r$  is [ $\text{m}^4 \text{s}^{-1}$ ]. Surface recombination is a process consisting of several elemental processes and there are different models on  $K_r$  [3, 5]. Under the equilibrium condition,  $C_H = K_S P^{0.5}$ , and absorption and desorption fluxes should be balanced:

$$2\alpha_m J_{in} = 2K_r C_H^2. \quad (9.3)$$

Substitutions of Eqs. (9.1) and (9.2) into (9.3) give the correlation between  $\alpha_m$  and  $K_r$  as

$$\alpha_m = K_r K_S^2 N_A \sqrt{2\pi m_{H2} kT}. \quad (9.4)$$

Both the values of  $\alpha_m$  and  $K_r$  are sensitively dependent on the surface conditions including impurity concentrations. Eq. (9.4) indicates that the variations of  $\alpha_m$  and  $K_r$  cannot be independent with each other.

Dissolved hydrogen atoms occupy interstitial sites (tetrahedral sites or octahedral sites) in the bulk of metals [6]. The solubility  $K_S$  is expressed as

$$K_S = \exp(\Delta S_S/R) \exp(-\Delta H_S/RT), \quad (9.5)$$

where  $\Delta S_S$  is the entropy of solution and  $\Delta H_S$  is the enthalpy of solution. It should be noted that  $\Delta H_S$  can be positive or negative (about  $-100$  to  $+100 \text{ kJ mol}^{-1}$  for metals [6]) because hydrogen dissolves exothermically or endothermically, depending on a material, as shown in Fig. 9.2 [6–8]. Diffusion process in the bulk normally follows the Fick's first and second laws. Diffusivity  $D$  [ $\text{m}^2 \text{s}^{-1}$ ] is described as

$$D = D_0 \exp(-E_d/RT), \quad (9.6)$$

where  $D_0$  is a pre-exponential factor and  $E_d$  is the activation energy for diffusion.

Here, hydrogen permeation through a thin metal plate with thickness of  $L$  [m] is considered. The particle balance at the upstream and downstream surfaces can be written as

$$2\alpha_{m1} J_{in1} = \frac{2\alpha_{m1} P}{N_A \sqrt{2\pi m_{H2} kT}} = 2K_{r1} C_{H1}^2 - D \left. \frac{\partial C_H}{\partial x} \right|_{x=0} \quad (\text{for upstream}), \quad (9.7)$$

and

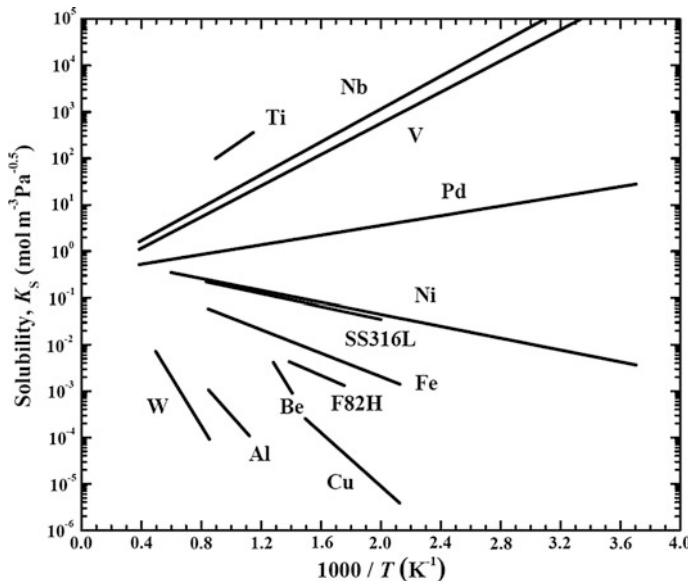


**Fig. 9.2** Temperature dependence of hydrogen solubility in selected metallic materials calculated with data provided in Table 1.1 in [5], Table A.2 in [6], and Table 2 in [7]

$$-D \frac{\partial C_H}{\partial x} \Big|_{x=L} = 2K_{r2}C_{H2}^2 - 2\alpha_{m2}J_{in2} = J_P \quad (\text{for downstream}). \quad (9.8)$$

Subscripts 1 and 2 indicate the upstream side and the downstream side, respectively (generally  $J_{in1} \gg J_{in2}$ ), and  $x$  is the distance from the upstream surface. The first term in the right-hand side of Eq. (9.7) shows the recycling flux [ $\text{mol m}^{-2} \text{s}^{-1}$ ] from the upstream surface, and  $J_P$  is the permeation flux [ $\text{mol m}^{-2} \text{s}^{-1}$ ]. In a steady state, the uniform concentration gradient of hydrogen is established throughout the thickness of the plate, and the flux of hydrogen atoms being absorbed in the plate is equal to the sum of fluxes being released from upstream and downstream surfaces of the plate. Hence,

$$2\alpha_{m1}J_{in1} + 2\alpha_{m2}J_{in2} = 2K_{r1}C_{H1}^2 + 2K_{r2}C_{H2}^2, \quad \text{and} \quad (9.9)$$

$$J_P = D \frac{C_{H1} - C_{H2}}{L} = 2K_{r2}C_{H2}^2 - 2\alpha_{m2}J_{in2}. \quad (9.10)$$

If the driving pressure is high and the surface is relatively clean, the absorption flux should be significantly larger than the diffusion flux. Under such conditions, the permeation is controlled by diffusion process (diffusion-limited permeation), and  $C_H$  in the upstream and downstream subsurface practically reaches the equilibrium values. Here, Eq. (9.10) can be approximately rewritten as [9]

$$J_P = DK_S \frac{P_1^{0.5} - P_2^{0.5}}{L}. \quad (9.10')$$

If  $P_1 \gg P_2$ , then  $C_{H1} \gg C_{H2}$ , as schematically shown in Fig. 9.3. Hence,  $J_P = DK_S P_1^{0.5}/L$ . The product of  $D$  and  $K_S$  is called as “permeability” [ $\text{mol m}^{-1} \text{s}^{-1} \text{Pa}^{-0.5}$ ] and given as

$$DK_S = D_0 \exp\left(\frac{\Delta S_S}{R}\right) \exp\left(-\frac{E_d + \Delta H_S}{RT}\right). \quad (9.11)$$

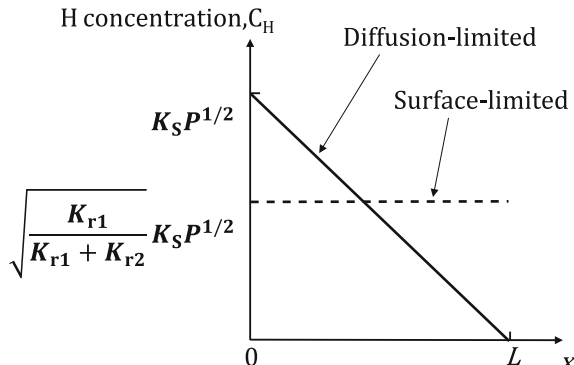
The activation energy for permeation  $E_P$  is expressed as  $E_P = E_d + \Delta H_S$ .  $E_d$  takes a positive value, whereas  $\Delta H_S$  can be positive or negative, as described above. Hence,  $E_P$  can also be positive or negative depending on the sign and the absolute value of  $\Delta H_S$  as shown in Fig. 9.4, in which the values of permeability were calculated using separately determined  $D$  and  $K_S$  given in [6–8]. Isotope effects in  $D$  and  $K_S$  will be described later.

If the driving pressure is low and/or the surface is not clean enough, the absorption flux is not necessarily large enough in comparison with diffusion flux, and hence, the permeation rate can be limited by surface reactions under the certain conditions. In the surface-limited regime, the gradient of  $C_H$  in the bulk is negligibly small, as shown in Fig. 9.3, because of relatively fast diffusion in the bulk of a material;  $C_{H1} \approx C_{H2} \approx C_H$ . If the hydrogen pressure of the downstream side is negligibly low, the permeation flux  $J_P$  is expressed as

$$J_P = 2K_{r2}C_H^2 = 2\alpha_m J_{in1} \frac{K_{r2}}{K_{r1} + K_{r2}}. \quad (9.12)$$

If the surface recombination rate constants are the same for both surfaces ( $K_{r1} = K_{r2}$ ), a half of absorbed hydrogen flux is released from the upstream surface and the other half permeates to the downstream side. Because  $\alpha_m = K_{r1}K_S^2 N_A \sqrt{2\pi m_{H2} kT}$  and  $J_{in} = P/(N_A \sqrt{2\pi m_{H2} kT})$ ,

**Fig. 9.3** Concentration profiles of hydrogen during gas-driven permeation (GDP) under the diffusion-limited regime (solid line) and surface-limited regime (dashed line)



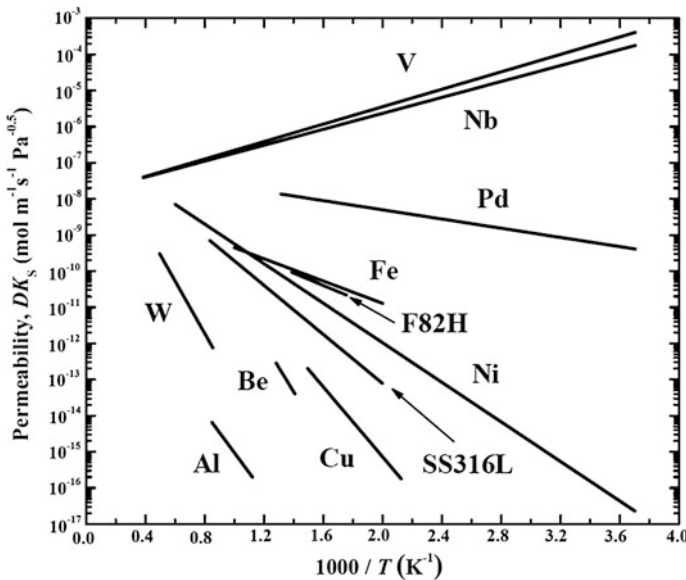


**Fig. 9.4** Temperature dependence of hydrogen permeability of selected metallic materials calculated with data provided in Tables 1.1, 5.2, and 5.3 in [5], Tables A.1 and A.2 in [6], and Table 2 in [7]

$$J_P = 2 \frac{K_{r1} K_{r2}}{K_{r1} + K_{r2}} K_S^2 P. \quad (9.13)$$

In the surface-limited regime, the permeation flux is proportional to  $P$ , whereas that in the diffusion-limited regime is in proportion to  $P^{0.5}$ .

The time transient of  $J_P$  is given by solving Fick's second law under the given initial and boundary conditions:

$$\frac{\partial C}{\partial t} = D \frac{\partial^2 C}{\partial x^2}, \quad \text{and} \quad (9.14)$$

$$J_P = -D \left. \frac{\partial C_H}{\partial x} \right|_{x=L}. \quad (9.15)$$

In the diffusion-limited permeation, Eq. (9.14) can be solved by assuming constant subsurface hydrogen concentrations  $C_{H1} = K_S P_1^{0.5}$  and  $C_{H2} = K_S P_2^{0.5}$ . Analytical solutions for Eq. (9.14) under the different boundary conditions are given in [10]. The change in  $C_H$  and  $J_P$  with time  $t$  in a transient state of the surface-limited permeation is discussed in [11].

### 9.1.2 Plasma-Driven Permeation

Plasma-facing materials of a fusion reactor will be exposed to ions and atoms of hydrogen isotopes. Different from molecular hydrogen, hydrogen ions and atoms in plasma do not need to be dissociated at the surface to enter into the material. Dissociation energies for H<sub>2</sub>, D<sub>2</sub>, and T<sub>2</sub> molecules are 4.478, 4.556, and 4.591 eV, respectively [12], and ionization energies of H, D, and T are about 13.6 eV [13]. The values of these dissociation and ionization energies are clearly larger than  $\Delta H_s$  for metals (up to about +100 kJ mol<sup>-1</sup> or up to about +1 eV per atom, as described above). Hydrogen ions and atoms having such high potential energies are referred as suprathermal particles hereafter. Because the hydrogen ions and atoms are dissolved exothermically into almost all materials, the sticking probability for the suprathermal particles,  $\alpha_s$ , is significantly higher than that of molecules in thermal energy,  $\alpha_m$ , in most cases [4, 14]. In addition, the temperature dependence of  $\alpha_s$  is far weaker than that of  $\alpha_m$ . For example, Hatano et al. [15] examined  $\alpha_s$  and  $\alpha_m$  of D and D<sub>2</sub> on Nb surface covered by a single layer of oxygen adatoms in a temperature range from 300 to 1800 K. A value of  $\alpha_s$  was 0.25, and this probability was independent of temperature in the examined range, whereas  $\alpha_m$  increased from  $2 \times 10^{-7}$  to  $6 \times 10^{-5}$  with increase in temperature at the maximum oxygen coverage. Because of such large value of  $\alpha_s$  for suprathermal hydrogen particles, the permeation flux  $J_p$  for “plasma-driven permeation (PDP)” is, in general, significantly larger than that of “gas-driven permeation (GDP)” discussed in the previous section at comparable impinging flux [4, 15].

The suprathermal hydrogen particles entering into a material are immediately thermalized. In other words, their interactions with a material are non-equilibrium process, and hence,  $C_H$  under the plasma exposure must not follow Sieverts’ law. If their kinetic energies are sufficiently low, their projected range is negligibly small. In the diffusion-limited regime,  $\alpha_s J_{in}$  is almost balanced with  $J_r$ , and hence,  $C_H$  is expressed as

$$C_H = (\alpha_s J_{in} / K_{r1})^{0.5}. \quad (9.16)$$

Because  $J_p = D \frac{C_H}{L}$ ,  $J_p$  for PDP is dependent on surface state of the upstream even under the diffusion-limited regime. The change in  $J_p$  with time in a transient state is expressed by Fick’s second law [Eq. (9.14)]. However, because the chemical reactivities of hydrogen ions and atoms are higher than those of molecules, the surface state of a material can be modified by plasma exposure [16]. Therefore,  $C_H$  in the upstream subsurface can vary with time.

Equation (9.12) is rewritten for PDP under the surface-limited regime as

$$J_p = 2K_{r2}C_H^2 = \frac{K_{r2}}{K_{r1} + K_{r2}} \alpha_s J_{in}. \quad (9.17)$$

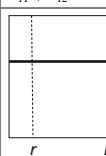
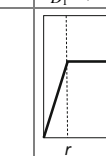
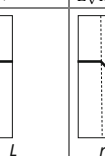
The change in  $J_p$  with time in a transient state is also discussed in [11]. Again, the variation of  $K_{r1}$  under the plasma exposure results in change in  $J_p$  for PDP.

The suprathermal hydrogen particles with high kinetic energy are implanted to a certain depth called as the projected range,  $r$ . A part of implanted hydrogen diffuses back to the upstream side, and the other part diffuses to the downstream side. The emission rates of hydrogen isotopes from the upstream and downstream sides can be limited by diffusion process in the bulk or recombination process at the surfaces. Therefore, the permeation phenomena can be separated into four regimes depending on the combinations of rate-limiting steps: recombination/recombination (RR), recombination/diffusion (RD), diffusion/recombination (DR), and diffusion/diffusion (DD). Doyle [17], and Brice and Doyle [18] summarized the variation of the permeation flux  $J_p$  for these extreme cases, as shown in Table 9.1. The concentration profiles of hydrogen in those regimes are also shown in this table.

### 9.1.3 Permeation Under the Corrosive Environment

Under the water corrosive environment ( $Q_2O$  where  $Q = H, D$ , and  $T$ ), hydrogen permeation occurs, though the permeation rate is far lower than that caused by environment of hydrogen in the elemental forms ( $Q_2$ ). This is because the free energy of formation of water is more negative than that of hydrogen dissolution in metals, and therefore, the metals cannot “extract” hydrogen atoms from water molecules. Nevertheless, many of metal oxides are thermodynamically more stable than water, and hence, various metals can take oxygen atoms from water molecules to form oxides and liberate hydrogen atoms. A part of the hydrogen atoms thus liberated recombines into molecules, while a remaining part dissolves into metals after permeating through the oxide layer. It is well known that hydrogen uptake during oxidation in water or steam and consequent hydrogen embrittlement are one of the main degradation mechanisms of Zr alloys used as cladding tubes of nuclear

**Table 9.1** Steady-state permeation flux  $J_p$  and hydrogen concentration profiles for PDP with energetic particles [16, 17]

Regime	RR	DR	RD	DD
$J_p$	$\frac{K_{r2}}{K_{r1} + K_{r2}} \alpha_s J_{in}$	$\frac{r^2 K_{r2}}{D_1} (\alpha_s J_{in})^2$	$\frac{D_2}{L\sqrt{K_{r1}}} \sqrt{\alpha_s J_{in}}$	$\frac{r D_2}{L D_1} \alpha_s J_{in}$
Concentration profile				

$J_{in}$  is incident flux of energetic particles, and  $\alpha_s$  is the sticking probability.  $D$  and  $K_r$  are diffusivity and surface recombination rate constant, and suffixes of 1 and 2 indicate the upstream and downstream sides, respectively. In the concentration profiles, hydrogen permeates from left (upstream) to right (downstream) side

fuels. Interestingly, the oxidation tests of Zr alloys in steam and a steam–H<sub>2</sub> mixture gas at 573–873 K showed that only hydrogen atoms liberated by water dissociation were absorbed into the substrate metal if the oxide layer was not porous [19]. These observations indicate that permeation of hydrogen is possible when the water corrosion of metals takes place. Indeed, Hayashi et al. [20–22] observed permeation of deuterium through Fe, Ni, and stainless steel membranes under the exposure to D<sub>2</sub>O. They reported that Au coating on the D<sub>2</sub>O-exposed membrane surface to prevent oxidation significantly suppressed the deuterium permeation. Oyaizu et al. [23] examined tritium permeation through F82H steel under the exposure of He gas including small amount of T<sub>2</sub>O vapor (20–100 kBq/cc corresponding to 0.006–0.1 Pa) at temperatures from 563 to 878 K. They reported extremely slow but obvious tritium permeation accompanied by the formation of magnetite and hematite. These observations suggest that the permeation caused by corrosion by water either HTO, DTO, or T<sub>2</sub>O can induce chronic release of tritium from fusion systems. In a water-cooled blanket system, corrosion of its structural material by cooling water and consequent hydrogen permeation to breeding zone can result in dilution of bred tritium, as described below. Similar hydrogen permeation is possible during corrosion by other gases such as H<sub>2</sub>S and aqueous solutions. It is well known that corrosion of metals in acid solutions accompanies evolution of H<sub>2</sub> gas. Before recombining into H<sub>2</sub> molecules, some of H atoms produced by cathodic reaction ( $H^+ + e^- \rightarrow H$ ) enter in metals [24]. In alkaline solution, production of hydrogen atoms followed by dissolution in metals takes place by the following reaction:  $H_2O + e^- \rightarrow H + OH^-$ . Thus, hydrogen permeation flux is used as a corrosion monitor [25]. These electrochemical reactions have been used for permeation measurements of hydrogen isotopes through metals [26].

## 9.2 Permeation Behaviors in Metals and Ceramics

### 9.2.1 General Characteristics of Hydrogen Permeation Through Metals

As described in Eq. (9.11), hydrogen permeability is given as a product of the solubility  $K_S$  and the diffusivity  $D$ . The values of  $K_S$  for several selected metallic materials are shown in Fig. 9.2 [6–8]. Evidently, the solubility  $K_S$  shows clear correlation to group numbers in the periodic table of elements. Elements in groups 3, 4, and 5 show negative enthalpy of solution  $\Delta H_S$ , and hence,  $K_S$  for those elements is high in comparison with elements in other groups. Elements in groups 1 and 2 form stable hydrides, but their  $K_S$  are relatively low [6].  $\Delta H_S$  in the majority of group 6–12 elements are positive, and hence,  $K_S$  in these metals is relatively low. An important exception is Pd in group 10;  $\Delta H_S$  for Pd is −10 kJ/mol [6], which makes Pd an excellent permeation membrane material, as described later.

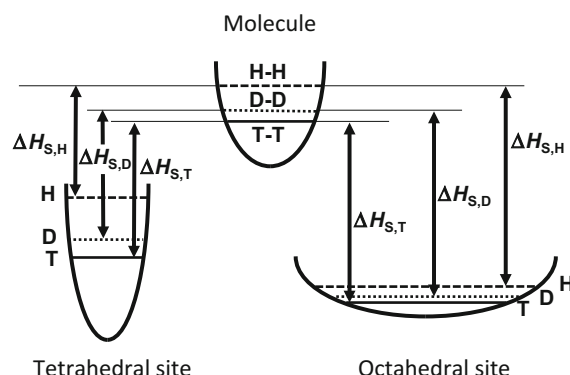
Large difference in zero-point vibration energies  $E_{\text{vib}}$  among H, D, and T [12] is most likely to be the cause of isotope effects in  $K_S$ . In the quantum harmonic oscillator approximation, vibrational energy is given by

$$E_{\text{vib}} = \left( n + \frac{1}{2} \right) h v_0 = \left( n + \frac{1}{2} \right) \frac{h}{2\pi} \sqrt{\frac{K_F}{\mu}}, \quad (9.18)$$

where  $v_0$  is the normal frequency of vibration,  $K_F$  is the force constant, and  $\mu$  is the reduced mass. Therefore, a lighter hydrogen isotope has higher vibrational energy (see also Fig. 2.4 in Chap. 2). In most cases, hydrogen atoms occupy octahedral sites (O-sites) in metals with the face-centered cubic (fcc) structure such as Pd and tetrahedral sites (T-sites) in those with the body-centered cubic (bcc) lattice such as Ta [6]. The volume space of O-sites in fcc metals is larger than that of the T-sites in bcc metals if lattice constants are comparable. Therefore, the shape of potential well for hydrogen in the former is more gentle having smaller  $K_F$  than that in the latter, as shown in Fig. 9.5. It means that the difference in vibration energy between H, D, and T is smaller in the fcc metals than the bcc metals. It is known that lighter hydrogen isotope shows larger  $K_S$  in the case of Pd [12], whereas smaller  $K_S$  was observed for a lighter isotope in the case of Nb and Ta [27]. This obvious difference in isotope effects can be qualitatively explained by the difference in the value of  $K_F$  between hydrogen molecule and interstitial site in a metal. As shown in Fig. 9.5, if the differences in the vibrational energies among H, D, and T in a molecule are larger than those in a metal lattice (like Pd), then  $|\Delta H_{S,H}| > |\Delta H_{S,D}| > |\Delta H_{S,T}|$ . The opposite correlation,  $|\Delta H_{S,H}| < |\Delta H_{S,D}| < |\Delta H_{S,T}|$ , is obtained if the differences in the vibrational energies among H, D, and T in a molecule are smaller than those in a metal lattice (like Ta).

The diffusivity of hydrogen isotopes in selected metals are shown in Fig. 9.6a (bcc metals) and b (fcc metals) [6]. In general, the diffusivity in bcc metals is higher than that in fcc metals especially at low temperatures. This is because the distance between neighboring T-sites in bcc metals is shorter than that between neighboring

**Fig. 9.5** Schematic description of potential wells (solid curves) and zero-point vibration energies of H, D, and T in a  $\text{Q}_2$  molecule, octahedral and tetrahedral sites of metals, and consequent isotope effects on the enthalpy of solution,  $\Delta H_S$



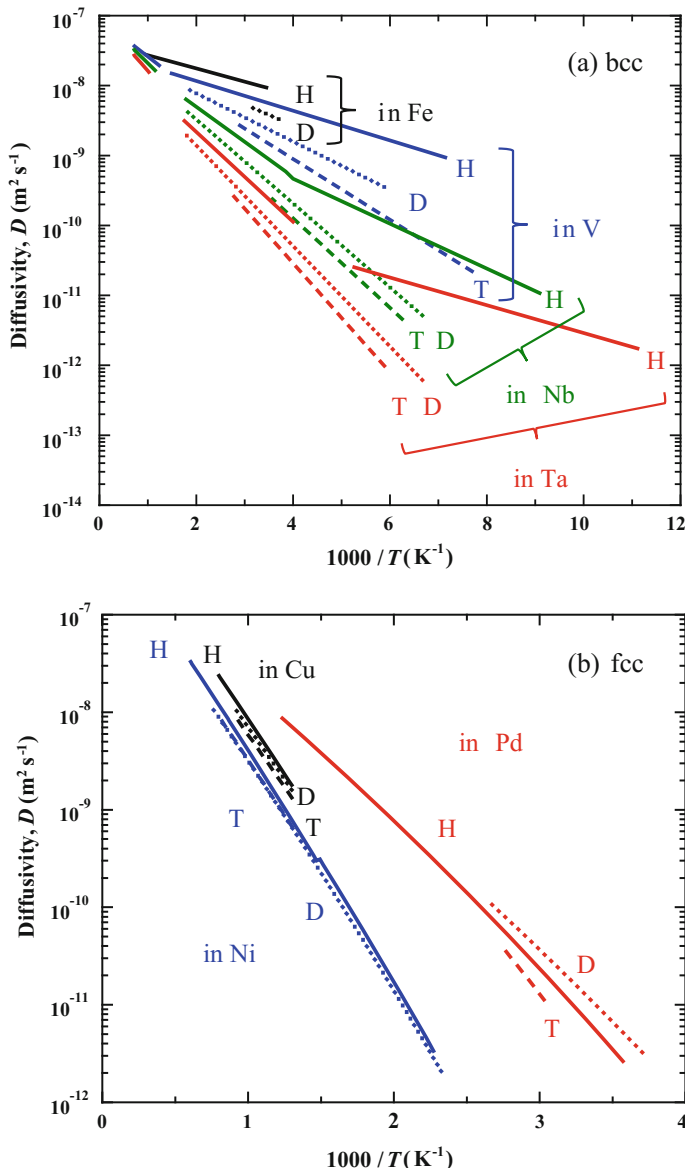


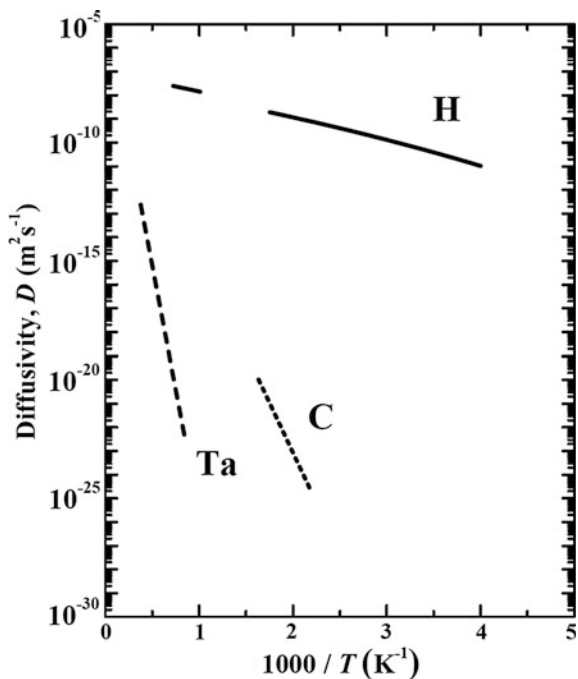
**Fig. 9.6** Temperature dependence of diffusivity of H, D, and T in selected bcc (a) and fcc (b) metals calculated with data provided in Tables 5.2. and 5.3 in [5]

O-sites in fcc metals, and there are no intervening metal atoms in the diffusion path [6]. In metals with the hexagonal-close-packed (hcp) structure, measured hydrogen diffusivity is comparable to but smaller than that in fcc metals [6]. Clear isotope effects are observed in hydrogen diffusivity; the value of diffusivity for heavier

isotopes is smaller than that of lighter isotopes. The isotope effects in bcc metals are larger than those in fcc metals and those expected from the classical diffusion mechanism ( $D_0 \propto m^{-1/2}$ ). Diffusion mechanisms of hydrogen isotopes in pure metals and simple alloys have been discussed in detail by Fukai in [6]. Diffusivity of hydrogen in metals is higher than that of other elements by orders of magnitudes. For example, diffusivity of H [28, 29] and C [30] in Ta is shown in Fig. 9.7 together with the self-diffusivity of Ta [31]. Taking the diffusivity of H in V,  $2 \times 10^{-9} \text{ m}^2 \text{ s}^{-1}$ , and that of C,  $1 \times 10^{-21} \text{ m}^2 \text{ s}^{-1}$ , at 573 K, the diffusion length defined as  $\sqrt{2Dt}$  reaches 1 mm for H with diffusion time of 250 s, whereas the diffusion time becomes millions of years for C at this temperature. It means that, from a practical point of view, solely hydrogen is permeable through metals. This is the reason for that metal membranes are widely used for hydrogen separation from other gases or purification. On the other hand, such high diffusivity causes tritium leak due to permeation.

Permeability of hydrogen ( $=DK_S$ ) in selected metals is shown in Fig. 9.4 [6–8]. Group 5 metals (V, Nb, and Ta) show large values of permeability because of the combination of large diffusivity and negative enthalpy of solution. However, in general, permeation rates observed in experiments are far lower than those expected from the permeability because of surface contamination. These metals are reactive not only to hydrogen but also to impurities such as carbon, oxygen, and sulfur, and surface reactions of hydrogen (dissociation and recombination) are strongly

**Fig. 9.7** Comparison of diffusivity of H [26, 27], C [28], and Ta (self-diffusion) [29] in Ta



retarded by adsorption of such impurities, as described above. The effects of impurities are not negligible even in an ultra-high vacuum at elevated temperatures because of surface segregation of impurities from the bulk [15]. Since Pd is a noble metal, its susceptibility to the influence of impurities is significantly far less than other metals. Therefore, Pd is widely used as a base material of the hydrogen permeation membrane for purification of hydrogen isotopes.

### 9.2.2 *Metals and Alloys Important for Fusion*

The data on hydrogen diffusivity and solubility for fusion reactor materials are summarized by Reiter et al. [7]. Therefore, the list of data is omitted here, and solely, the permeation characteristics of selected materials are described.

Reduced activation ferritic/martensitic (RAFM) steels such as F82H (Japan) and Eurofer (EU) steels are candidates of structural materials of a tritium breeding blanket. Because of their body-centered structures, the permeation behaviors of hydrogen through the RAFM steels are similar to those through pure Fe and characterized by relatively high diffusivity and low solubility in comparison with austenitic stainless steels. However, significant difference from Fe can be observed in apparent diffusivity at temperatures  $<500$  K; the apparent diffusivity in the RAFM steels is lower than that in pure Fe due to hydrogen trapping at defects such as dislocations and fine precipitates [8]. Those traps do not affect the permeation rate in a steady state because the steady state is achieved after attainment of local equilibrium between trapping and detrappling. However, the duration of time necessary to attain the steady state significantly increases by trapping. Hydrogen permeability of various ferritic alloys and steels has been reviewed by Jung [32].

Austenitic stainless steels are generally more resistant against corrosion and hydrogen embrittlement than ferritic steels and hence used in various locations of a fusion reactor including tritium processing plants. Because of its fcc structure, hydrogen permeation in the austenitic stainless steels is more similar to that in Ni than Fe and characterized by relatively high solubility and low diffusivity [6]. Because of far larger activation energy for diffusion, hydrogen permeability in the austenitic steels is significantly lower than that in ferritic steels at temperatures  $<600$  K. The difference becomes smaller as temperature increases.

Vanadium alloys including a V-4Cr-4Ti alloy are candidate structural materials for liquid Li blanket concept. As V has large hydrogen solubility and diffusivity, the alloys have large hydrogen permeability:  $10^{-10}$ – $10^{-7}$  mol m $^{-1}$  s $^{-1}$  Pa $^{-0.5}$  at 423–1073 K [33–35]. Nevertheless, tritium leak by permeation should not be an issue for the liquid Li blanket concept because of strong chemical affinity of Li to hydrogen isotopes. However, tritium permeation barrier is necessary to use the alloys for other blanket concepts.

Tungsten (W) is a leading candidate of plasma-facing materials of a fusion reactor. Solubility of hydrogen in W is very low due to its large positive enthalpy of solution [36], and hence, gas-driven permeation through W is low in comparison with other metals except at very high temperatures [37, 38]. Plasma-driven permeation experiments have been performed to examine diffusion and surface reactions of hydrogen in W [39–46]. The diffusivity of hydrogen in W has been determined by several researchers [47], but only very limited data on  $K_S$  [36, 38] and  $K_r$  [39, 40] are available. The permeation rate in a transient state through W is also strongly affected by trapping effects of defects [39]. The group in Osaka University reported that the temperature dependence of the steady-state permeation rate under the ion implantation is sensitively and complicatedly influenced by impurities (He, C, and N) in the ion beams [42–46]. Nakamura et al. [48] examined PDP of deuterium and tritium and reported that no significant isotope effects were observed in the permeation rates in a steady state.

The majority of available data on diffusivity and solubility were measured at elevated temperatures. At lower temperatures including room temperature, the permeation mechanism may be different and the values of  $J_P$  may disagree with those expected by extrapolating the data obtained at elevated temperatures. Indeed, Maienschein et al. [49] measured tritium permeation through various metals at 323 K and reported that the permeation rates for Cu, Au, Al, Mo, and W were significantly higher than extrapolations of high-temperature data in the literature. They ascribed these observations to transport of tritium along short-circuiting paths such as grain boundaries or other lattice defects. Ikeda et al. [50, 51] also observed a relatively high permeation rate at around room temperature for W. On the other hand, they reported that the permeation rate through Ni at around room temperature agreed well with extrapolations of high-temperature data. The difference between Ni and W indicates that the contributions of the short-circuiting paths are more significant for materials with low hydrogen solubility. One has to be careful in predicting low temperature tritium permeation rate using high-temperature data for low solubility materials.

### 9.2.3 *Ceramics and Permeation Barrier Materials*

Most ceramic materials such as oxides and carbides show very low permeability of hydrogen if they are not porous. Therefore, those materials have been recognized as candidates of permeation barrier coatings. Excellent reviews on hydrogen permeation through ceramics and their applications to permeation barrier have been given by Hollenberg et al. [52] and Causey et al. [53]. As shown in these reviews, the data on diffusivity, solubility and permeability of hydrogen in the ceramics reported in the literature scatter in a wide range. For example, diffusivity and solubility data for

SiC summarized in [54] scatter in 5–6 orders of magnitude at 773–873 K. Barrier efficiency of ceramic coatings on various substrate materials are also widely scattered [52]. Because the ceramics are brittle, one of the possible reasons for the data scattering is the influence of cracks and pores playing the roles of short-circuiting paths for molecular hydrogen. Grain boundaries can also act as the short-circuiting paths for hydrogen atoms. Chikada et al. [55] examined barrier efficiency of  $\text{Er}_2\text{O}_3$  coating on a ferritic steel and found that the permeability through the  $\text{Er}_2\text{O}_3$  coating decreased with reduction in the grain boundary density in the coating. They examined deuterium distributions in the coating by using nanoscale secondary ion mass spectroscopy and confirmed that deuterium was concentrated at the grain boundaries [56]. They concluded that the grain boundaries acted as the short-circuiting paths for hydrogen in  $\text{Er}_2\text{O}_3$  [55, 56]. On the other hand, impurity atoms and/or additive elements in ceramic materials act as traps against hydrogen. Anyway, hydrogen permeation in ceramic materials is appreciably influenced by extrinsic factors.

Deviation from stoichiometric composition of a ceramic can be an intrinsic factor important for its hydrogen permeability, although this information is missed in most papers of hydrogen permeation studies. It is known that amounts of hydrogen incorporated in TiC, ZrC, HfC, VC, and NbC increase with decrease in  $[\text{C}]/[\text{M}]$  ratio where M indicates metallic elements; in other words, this amount increases with increase in  $x$  of  $\text{MC}_{1-x}$  [57]. Gringoz et al. [58] examined electrochemical hydrogen absorption and desorption of  $\text{TiC}_{0.9}$  and  $\text{TiC}_{0.6}$  and observed reversible absorption and desorption solely for the latter. The reported diffusivity of H in  $\text{TiC}_{0.6}$  was as high as  $3 \times 10^{-16} \text{ m}^2\text{s}^{-1}$  even at room temperature [58]. These observations suggest that stoichiometric TiC and non-stoichiometric  $\text{TiC}_{1-x}$  are completely different materials from the viewpoint of hydrogen permeation although both of them have NaCl-type crystal structure. Hence, the characterization of the deviation from stoichiometric composition of ceramics is necessary to understand their hydrogen permeability.

Chikada et al. [59] examined deuterium permeation through RAFM steel disks having  $\text{Er}_2\text{O}_3$  coatings on one side or both sides. The one-side coating reduces the permeation rate by a factor of  $10^2$ , while the both side coating by a factor of  $10^4$ – $10^5$ . The activation energy for permeation for the one-side coated samples was 60–61 kJ mol<sup>-1</sup>, while that for the both-side coated sample was 117 kJ mol<sup>-1</sup>. Namely, the barrier efficiency of two  $\text{Er}_2\text{O}_3$  layers was the product of that of each layer, while the activation energy was the sum. The mechanisms underlying these correlations have not been understood in detail. Nevertheless, it is clear that fabrication of permeation barrier coatings on both sides of a material is far more effective than that on one side. Hatano et al. [60] prepared  $\text{ZrO}_2$  coatings as thin as 180 nm on both sides of disks of a ferritic steel and observed significant reduction in deuterium permeation rate ( $\sim 1/1000$ ). This observation also indicates the effectiveness of coating fabrication on both sides.

### 9.3 Important Remarks on Permeation Under the Fusion Conditions

Schematic description of hydrogen transport in the fusion reactor first wall is shown in Fig. 9.8. Impinging of fuel particles onto plasma-facing material or armor material induces PDP to a coolant. GDP of tritium takes place from breeding zone to a coolant in a blanket system. If water is used as the coolant and corrosion of structural material occurs, permeation of hydrogen from coolant zone to breeding zone is possible. GDP and corrosion-induced permeation discussed above take place in any tritium systems. Because of peculiarity of fusion environments described below, there are several issues that need to be considered to understand tritium permeation in fusion reactor materials.

#### 9.3.1 Temperature Gradient

The discussion described above was based on the implicit assumption that temperature of a material is uniform throughout its thickness. However, in reality, large

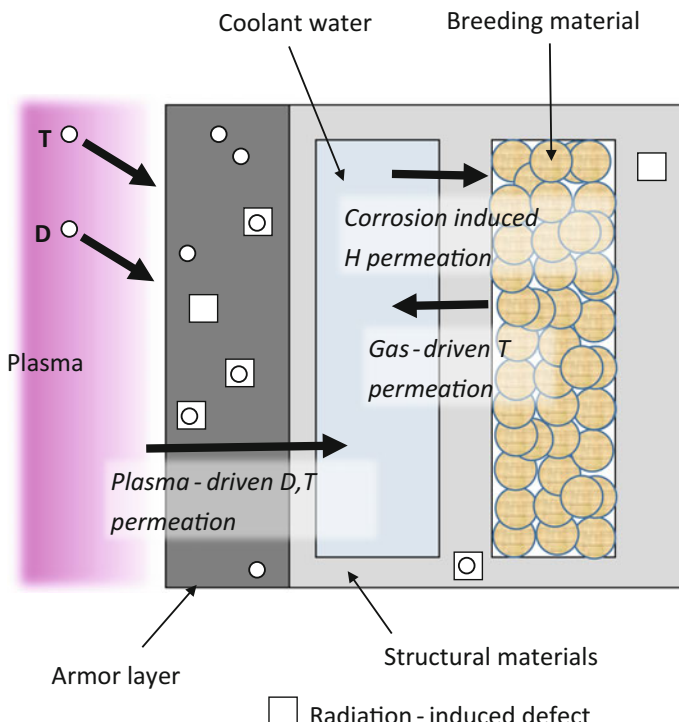


**Fig. 9.8** Schematic description of tritium and hydrogen transport in a first wall and breeding blanket of a fusion reactor

temperature gradient appears in divertor, first wall, and blanket system having cooling channels. Diffusion flux  $J_d$  in the material under the temperature gradient is referred as thermomigration and given by [61]

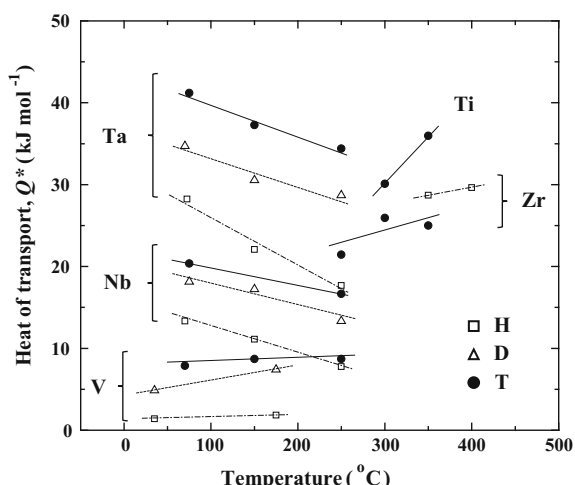
$$J_d = -D \left( \frac{\partial C}{\partial x} + \frac{Q^* C \partial T}{RT^2 \partial x} \right), \quad (9.19)$$

where  $Q^*$  is the heat of transport. Despite that  $Q^*$  is the most important parameter to understand the thermomigration, data available in the literature are very limited. Sugisaki et al. [62] measured  $Q^*$  of hydrogen isotopes in Ti, Zr, V, Nb, and Ta as summarized in Fig. 9.9. As shown in the figure,  $Q^*_T > Q^*_D > Q^*_H$  in group 5 metals (V, Nb, and Ta). In other words, the permeation of tritium can be more sensitively influenced by the temperature gradients than those of hydrogen and deuterium. Hence, the accumulation of  $Q^*$  data for tritium in candidate fusion reactor materials is required for precise evaluation of tritium permeation under the fusion conditions.

### 9.3.2 Radiation Effects

Materials used in a reactor vessel are exposed to intensive irradiation of high-energy neutrons and other radiations. The high-energy neutrons induce displacement damages and consequently defects such as vacancies and voids. The formation of the defects results in retardation of hydrogen diffusion and increase in retention due to trapping effects. For example, Hatano et al. [63, 64] examined deuterium trapping in W irradiated with neutrons in a fission reactor using a linear plasma machine and reported significant increase in deuterium retention (up to 0.8 at%) and

**Fig. 9.9** Heat of transport  $Q^*$  of hydrogen isotopes in Ti, Zr, V, Nb, and Ta [61]



retardation of diffusion. Such trapping effects do not influence the permeation in a steady state, as mentioned above. Nevertheless, the diffusion and permeation in the walls of pulse-operated devices are certainly affected by those traps.

Enhancement of hydrogen diffusion by radiation has been reported for oxides including MgO [65], TiO<sub>2</sub> [66] and Al<sub>2</sub>O<sub>3</sub> [67]. As mentioned previously, oxides are potential candidates of permeation barrier materials. The radiation-induced diffusion may deteriorate barrier efficiency. As described in [52, 53], there are several papers reporting the results of in-pile tests for permeation barriers. The barrier efficiency observed in the in-pile tests was clearly deteriorated compared with that observed in laboratory tests. Because the in-pile tests require complicated experimental setup, the mechanisms of the deterioration have not been fully understood. Nevertheless, as discussed in [52], radiation-induced diffusion is one of the potential causes of the deterioration. Anyway, the tests under the irradiation are indispensable for the application of the permeation barriers.

### 9.3.3 Partial Pressure of Tritium

In order to minimize the leak and permeation, tritium is generally handled at a pressure significantly lower than the ambient pressure in many tritium handling systems or facilities. The rate-limiting steps of GDP can vary with a driving pressure, as described above. According to Strehlow and Savage [68] who measured GDP of deuterium through various metals and alloys under a wide range of the driving pressure (0.1 Pa–100 kPa), the rate-limiting step of GDP is the diffusion process in the metal bulk at a higher pressure and it changes to the diffusion process in oxide films on the surface and then penetration through cracks and other imperfections in the oxide films as pressure drops. The observations of Zarchy and Axtmann [69] who performed tritium permeation experiments for 304 stainless steel with a driving pressure of 10<sup>-5</sup>–10<sup>-7</sup> Pa agreed with the model proposed by Strehlow and Savage [68]. At an extremely low driving pressure, permeation rate should be limited by hydrogen uptake rate at the upstream side surface [69].

It should be noted that the rate-limiting step of permeation depends on not only material, temperature and driving pressure but also contents of impurities (e.g., H<sub>2</sub>O and O<sub>2</sub>) in hydrogen gas. Therefore, one has to understand that the estimation of tritium permeation rate at low driving pressure using the literature data is always accompanied by considerable uncertainty. Nevertheless, in GDP, the diffusion-limited regime gives the maximum permeation rate at given pressure and temperature. Therefore, the estimation of tritium permeation rate from the literature data of diffusivity and solubility provides a result on the safe side.

## 9.4 Summary

Elemental processes of hydrogen permeation in solid materials under the exposure to hydrogen gas, plasma, and water were described. Several useful equations describing gas- and plasma-driven permeation were given. Characteristics of hydrogen diffusion, dissolution, and permeation in metals including isotope effects were summarized. Permeation behaviors of hydrogen isotopes in selected fusion reactor materials were reviewed. Understanding of the effects of sharp temperature gradients and neutron irradiation on tritium diffusion and retention, and tritium permeation under the low partial pressures were identified as remaining issues.

## References

1. A. Sieverts, Über Lösungen von Gasen in metallen. Z. Elektrochem. **16**, 707–713 (1910). doi:[10.1002/bbpc.19100161706](https://doi.org/10.1002/bbpc.19100161706)
2. F. Waelbroeck, P. Wienhold, J. Winter, E. Rota, T. Banno, Influence of bulk and surface phenomena on the hydrogen permeation through metals. KFA Jülich Report JüL-1966 (1984), Jülich
3. M.A. Pick, K. Sonnenberg, A model for atomic hydrogen-metal interactions—application to recycling, recombination and permeation. J. Nucl. Mater. **131**, 208–220 (1985). doi:[10.1016/0022-3115\(85\)90459-3](https://doi.org/10.1016/0022-3115(85)90459-3)
4. A.I. Livshits, M.E. Notkin, A.A. Sammartsev, Physico-chemical origin of superpermeability —Large-scale effects of surface chemistry on “hot” hydrogen permeation and absorption in metals. J. Nucl. Mater. **170**, 79–94 (1990). doi:[10.1016/0022-3115\(90\)90329-L](https://doi.org/10.1016/0022-3115(90)90329-L)
5. P.M. Richards, Surface-limited hydrogen release and uptake in metals. J. Nucl. Mater. **152**, 246–258 (1988). doi:[10.1016/0022-3115\(88\)90333-9](https://doi.org/10.1016/0022-3115(88)90333-9)
6. Y. Fukai, *The Metal-Hydrogen System Basic Bulk Properties* (Springer, Berlin Heidelberg, 1993)
7. F. Reiter, K.S. Forcey, G. Gervasini, A compilation of tritium-material interaction parameters in fusion reactor materials, EUR 15217 EN (1993)
8. E. Serra, G. Benamati, O.V. Ogorodnikova, Hydrogen isotopes transport parameters in fusion reactor materials. J. Nucl. Mater. **255**, 105–115 (1998). doi:[10.1016/S0022-3115\(98\)00038-5](https://doi.org/10.1016/S0022-3115(98)00038-5)
9. O.W. Richardson, J. Nicol, T. Parnell, The diffusion of hydrogen through hot platinum. *Philos. Mag.* **8**(1904), 1–29. doi:[10.1080/14786440409463168](https://doi.org/10.1080/14786440409463168)
10. J. Crank, *The Mathematics of Diffusion* (Oxford University Press, Oxford, 1975)
11. I. Ali-Khan, K.J. Dietz, F.G. Waelbroeck, P. Wienhold, The rate of hydrogen release out of clean metallic surfaces. J. Nucl. Mater. **76–77**, 337–343 (1978). doi:[10.1016/0022-3115\(78\)90167-8](https://doi.org/10.1016/0022-3115(78)90167-8)
12. R. Lässer, *Tritium and Helium-3 in Metals* (Springer-Verlag, Berlin Heidelberg, 1989)
13. J.D. Garcia, J.E. Mace, Energy level and line tables for one-electron atomic spectra. J. Opt. Soc. Am. **55**, 654–661 (1965). doi:[10.1364/JOSA.55.000654](https://doi.org/10.1364/JOSA.55.000654)
14. F. Waelbroeck, I. Ali-Khan, K.J. Dietz, P. Wienhold, Hydrogen solubilisation into and permeation through wall materials. J. Nucl. Mater. **85–86**, 345–349 (1979). doi:[10.1016/0022-3115\(79\)90514-2](https://doi.org/10.1016/0022-3115(79)90514-2)
15. Y. Hatano, K. Watanabe, A.I. Livshits, A. Busnyuk, V. Alimov, Y. Nakamura, K. Hashizume, Effects of bulk impurity concentration on the reactivity of metal surface: Sticking of hydrogen molecules and atoms to polycrystalline Nb containing oxygen. J Chem Phys **127**, 204707 (2007). doi:[10.1063/1.2804874](https://doi.org/10.1063/1.2804874)

16. Y. Hatano, H. Nakamura, H. Furuya, M. Sugisaki, Influence of surface impurities on plasma-driven permeation of deuterium through nickel. *J. Vac. Sci. Technol. A* **16**, 2078–2083 (1998). doi:[10.1116/1.581313](https://doi.org/10.1116/1.581313)
17. B.L. Doyle, A simple theory for maximum h inventory and release: a new transport parameter. *J. Nucl. Mater.* **111–112**, 628–635 (1982). doi:[10.1016/0022-3115\(82\)90277-X](https://doi.org/10.1016/0022-3115(82)90277-X)
18. D.K. Brice, B.L. Doyle, Simultaneous gas- and plasma-driven hydrogen transport in solids. *J. Vac. Sci. Technol. A* **5**, 2311–2314 (1987). doi:[10.1116/1.574442](https://doi.org/10.1116/1.574442)
19. B. Cox, Hydrogen absorption by Zircaloy-2 and some other alloys during corrosion in steam. *J. Electrochem. Soc.* **109**, 6–12 (1962). doi:[10.1149/1.2425334](https://doi.org/10.1149/1.2425334)
20. T. Hayashi, K. Isobe, H. Nakamura, K. Kobayashi, Y. Oya, K. Okuno, M. Oyaizu, Y. Edao, T. Yamanishi, Hydrogen isotope behavior transferring through water metal boundary. *Fusion Sci. Technol.* **60**, 369–372 (2011)
21. T. Hayashi, H. Nakamura, K. Isobe, K. Kobayashi, M. Oyaizu, T. Yamanishi, Y. Oya, K. Okuno, Hydrogen isotope permeation from cooling water through various metal piping. *Fusion Eng. Des.* **87**, 1333–1337 (2012). doi:[10.1016/j.fusengdes.2012.03.009](https://doi.org/10.1016/j.fusengdes.2012.03.009)
22. T. Hayashi, K. Isobe, H. Nakamura, K. Kobayashi, Y. Oya, K. Okuno, M. Oyaizu, Y. Edao, T. Yamanishi, Hydrogen isotope behavior on a water–metal boundary with simultaneous transfer from and to the metal surface. *Fusion Eng. Des.* **87**, 1520–1523 (2012). doi:[10.1016/j.fusengdes.2014.03.069](https://doi.org/10.1016/j.fusengdes.2014.03.069)
23. M. Oyaizu, K. Isobe, H. Nakamura, T. Hayashi, T. Yamanishi, Permeation behavior of tritium through F82H steel. *J. Nucl. Mater.* **417**, 1143–1146 (2011). doi:[10.1016/j.jnucmat.2011.03.002](https://doi.org/10.1016/j.jnucmat.2011.03.002)
24. L.S. Darken, R.P. Smith, Behaviour of hydrogen in steel during and after immersion in acid. *Corrosion* **5**, 1–16 (1949). doi:[10.5006/0010-9312-5.1.1](https://doi.org/10.5006/0010-9312-5.1.1)
25. F. Dean, Hydrogen flux measurements in petrochemical application, in *Techniques for Corrosion Monitoring*, ed. by L. Yang (Woodhead Publishing, Cambridge, 2008)
26. M.A.W. Devanathan, Z. Stachurski, The adsorption and diffusion of electrolytic hydrogen in palladium. *Proc. Roy. Soc. A* **270**, 90–102 (1962). doi:[10.1098/rspa.1962.0205](https://doi.org/10.1098/rspa.1962.0205)
27. K. Fujita, Y.C. Huang, M. Tada, The studies on the equilibria of Ta-H, Nb-H, and V-H systems. *J. Jpn. Inst. Met.* **43**, 601–610 (1979)
28. Z.H. Qi, J. Völkl, R. Lässer, H. Wenzl, Tritium diffusion in V, Nb and Ta. *J. Phys. F* **13**, 2053–2063 (1983). doi:[10.1088/0305-4608/13/10/015](https://doi.org/10.1088/0305-4608/13/10/015)
29. T. Eguchi, S. Morozumi, Diffusion of hydrogen at high temperatures in the group V transition metals and alloying effect on the diffusion. *J. Jpn. Inst. Met.* **41**, 795–802 (1977)
30. R.W. Powers, M.V. Doyle, Diffusion of interstitial solutes in the group V transition metals. *J. Appl. Phys.* **30**, 514–524 (1959). doi:[10.1063/1.1702398](https://doi.org/10.1063/1.1702398)
31. P.E. Pawel, T.S. Lundy, The diffusion of Nb<sup>95</sup> and Ta<sup>182</sup> in tantalum. *J. Phys. Chem. Solids* **26**, 937–942 (1965). doi:[10.1016/0022-3697\(65\)90180-0](https://doi.org/10.1016/0022-3697(65)90180-0)
32. P. Jung, Compositional variation of hydrogen permeability in ferritic alloys and steels. *J. Nucl. Mater.* **238**, 189–197 (1996). doi:[10.1016/S0022-3115\(96\)00448-5](https://doi.org/10.1016/S0022-3115(96)00448-5)
33. O.G. Romanenko, I.L. Tazhibaeva, V.P. Shestakov, AKh Klepikov, Y.V. Chikhray, A.V. Golosanov, B.N. Kolbasov, Hydrogen gas driven permeation through vanadium alloy VCr<sub>6</sub>Ti<sub>5</sub>. *J. Nucl. Mater.* **233–237**, 376–380 (1996). doi:[10.1016/S0022-3115\(96\)00034-7](https://doi.org/10.1016/S0022-3115(96)00034-7)
34. R.E. Buxbaum, R. Subramanian, J.H. Park, D.L. Smith, Hydrogen transport and embrittlement for palladium coated vanadium–chromium–titanium alloys. *J. Nucl. Mater.* **233–237**, 510–512 (1996). doi:[10.1016/S0022-3115\(96\)00239-5](https://doi.org/10.1016/S0022-3115(96)00239-5)
35. I.V. Shkolnik, T.V. Kulsartov, I.L. Tazhibaeva, V.P. Shestakov, Investigation of the surface element composition influence on hydrogen permeability through vanadium alloy VCr<sub>4</sub>Ti<sub>4</sub>. *Fusion Sci. Technol.* **34**, 868–871 (1998)
36. R. Frauenfelder, Solution and diffusion of hydrogen in tungsten. *J Vac Sci Technol* **6**, 388–397 (1969). doi:[10.1116/1.1492699](https://doi.org/10.1116/1.1492699)
37. A.P. Zakharov, V.M. Sharapov, E.I. Evko, Hydrogen permeability of mono- and polycrystals of molybdenum and tungsten. *Fiz.-Khim. Mekh. Mater.* **9**, 29–33 (1973)

38. G. Benamati, E. Serra, C.H. Wu, Hydrogen and deuterium transport and inventory parameters through W and W-alloys for fusion reactor applications. *J. Nucl. Mater.* **283–287**, 1033–1037 (2000). doi:[10.1016/S0022-3115\(00\)00202-6](https://doi.org/10.1016/S0022-3115(00)00202-6)
39. R.A. Anderl, D.F. Holland, G.R. Longhurst, R.J. Pawelko, C.L. Tybus, C.H. Sellers, Deuterium transport and trapping in polycrystalline tungsten. *Fusion Technol.* **21**, 745–752 (1992)
40. Yu. Gasparyan, M. Rasinski, M. Mayer, A. Pisarev, J. Roth, Deuterium ion-driven permeation and bulk retention in tungsten. *J. Nucl. Mater.* **417**, 540–544 (2011). doi:[10.1016/j.jnucmat.2010.12.119](https://doi.org/10.1016/j.jnucmat.2010.12.119)
41. H.T. Lee, E. Markina, Y. Otsuka, Y. Ueda, Deuterium ion-driven permeation in tungsten with different microstructures. *Phys. Scr.* **T145**, 014045 (2011). doi:[10.1088/0031-8949/2011/T145/014045](https://doi.org/10.1088/0031-8949/2011/T145/014045)
42. H.Y. Peng, H.T. Lee, Y. Otsuka, Y. Ueda, Ion-driven permeation of deuterium in tungsten by deuterium and carbon-mixed ion irradiation. *Phys. Scr.* **T145**, 014046 (2011). doi:[10.1088/0031-8949/2011/T145/014046](https://doi.org/10.1088/0031-8949/2011/T145/014046)
43. H.T. Lee, H. Tanaka, Y. Otsuka, Y. Ueda, Ion-driven permeation of deuterium through tungsten under simultaneous helium and deuterium irradiation. *J. Nucl. Mater.* **415**, S696–S700 (2011). doi:[10.1016/j.jnucmat.2010.12.023](https://doi.org/10.1016/j.jnucmat.2010.12.023)
44. Y. Ueda, H.T. Lee, H.Y. Peng, Y. Otsuka, Deuterium permeation in tungsten by mixed ion irradiation. *Fusion Eng. Des.* **87**, 1356–1362 (2012). doi:[10.1016/j.fusengdes.2012.03.006](https://doi.org/10.1016/j.fusengdes.2012.03.006)
45. H.Y. Peng, H.T. Lee, Y. Otsuka, Y. Ueda, Effect of tungsten and carbon surface mixed layer on deuterium permeation in tungsten. *J. Nucl. Mater.* **438**, S1063–S1066 (2013). doi:[10.1016/j.jnucmat.2013.01.233](https://doi.org/10.1016/j.jnucmat.2013.01.233)
46. H.T. Lee, M. Ishida, Y. Otsuka, Y. Ueda, The influence of nitrogen on deuterium permeation through tungsten. *Phys. Scr.* **T159**, 014021 (2014). doi:[10.1088/0031-8949/2014/T159/014021](https://doi.org/10.1088/0031-8949/2014/T159/014021)
47. T. Tanabe, Review of hydrogen retention in tungsten. *Phys. Scr.* **T159**, 014044 (2014). doi:[10.1088/0031-8949/2014/T159/014044](https://doi.org/10.1088/0031-8949/2014/T159/014044)
48. H. Nakamura, T. Hayashi, T. Kakuta, T. Suzuki, M. Nishi, Tritium permeation behavior implanted into pure tungsten and its isotope effect. *J. Nucl. Mater.* **297**, 285–291 (2001). doi:[10.1016/S0022-3115\(01\)00635-3](https://doi.org/10.1016/S0022-3115(01)00635-3)
49. J.L. Maienschein, F.E. McMurphy, V.L. Duval, Increase of tritium permeation through resistant metals at 323 K by lattice defects. *Fusion Technol.* **14**, 701–706 (1988)
50. K. Ikeda, T. Otsuka, T. Tanabe, Determination of hydrogen diffusivity and permeability in W near room temperature applying a tritium tracer technique. *J. Nucl. Mater.* **415**, S684–S687 (2011). doi:[10.1016/j.jnucmat.2010.12.007](https://doi.org/10.1016/j.jnucmat.2010.12.007)
51. K. Ikeda, T. Otsuka, T. Tanabe, Hydrogen permeation in metals near room temperature by a tritium tracer technique. *J. Nucl. Mater.* **417**, 568–571 (2011). doi:[10.1016/j.jnucmat.2010.12.116](https://doi.org/10.1016/j.jnucmat.2010.12.116)
52. G.W. Hollenberg, E.P. Simonen, G. Kalinin, A. Terlain, Tritium/hydrogen barrier development. *Fusion Eng. Des.* **28**, 190–208 (1995). doi:[10.1016/0920-3796\(95\)90039-X](https://doi.org/10.1016/0920-3796(95)90039-X)
53. R.A. Causey, R.A. Karnesky, C.S. Marchi, Tritium barriers and tritium diffusion in fusion reactors. *Compr. Nucl. Mater.* **4**, 511–549 (2012). doi:[10.1016/B978-0-08-056033-5.00116-6](https://doi.org/10.1016/B978-0-08-056033-5.00116-6)
54. G.A. Esteban, A. Perujo, F. Legarda, L.A. Sedano, B. Riccardi, Deuterium transport in SiC/ $\beta$ -SiC composites. *J. Nucl. Mater.* **307–311**, 1430–1435 (2002). doi:[10.1016/S0022-3115\(02\)01282-5](https://doi.org/10.1016/S0022-3115(02)01282-5)
55. T. Chikada, A. Suzuki, T. Kobayashi, H. Maier, T. Terai, T. Muroga, Microstructure change and deuterium permeation behavior of erbium oxide coating. *J. Nucl. Mater.* **417**, 1241–1244 (2011). doi:[10.1016/j.jnucmat.2010.12.283](https://doi.org/10.1016/j.jnucmat.2010.12.283)
56. R. Sato, T. Chikada, H. Matsuzaki, A. Suzuki, T. Terai, K. Sugiyama, Measurement of hydrogen isotope concentration in erbium oxide coatings. *Fusion Eng. Des.* **89**, 1375–1379 (2014). doi:[10.1016/j.fusengdes.2014.01.074](https://doi.org/10.1016/j.fusengdes.2014.01.074)
57. G.W. Samsonow, W.W. Morosow, Carbohydride der Übergangsmetalle. *Monats Chem.* **102**, 1667–1678 (1971)

58. A. Gringoz, N. Glandut, S. Valette, Electrochemical hydrogen storage in  $TiC_{0.6}$ , not in  $TiC_{0.9}$ . *Electrochim. Commun.* **11**, 2044–2047 (2009). doi:[10.1016/j.elecom.2009.08.049](https://doi.org/10.1016/j.elecom.2009.08.049)
59. T. Chikada, A. Suzuki, C. Adelhelm, T. Terai, T. Muroga, Surface behaviour in deuterium permeation through erbium oxide coatings. *Nucl. Fusion* **51**, 063023 (2011). doi:[10.1088/0029-5515/51/6/063023](https://doi.org/10.1088/0029-5515/51/6/063023)
60. Y. Hatano, K. Zhang, K. Hashizume, Fabrication of  $ZrO_2$  coatings on ferritic steel by wet-chemical methods as a tritium permeation barrier. *Phys. Scr.* **T145**, 014044 (2011). doi:[10.1088/0031-8949/2011/T145/014044](https://doi.org/10.1088/0031-8949/2011/T145/014044)
61. P.G. Shewmon, *Diffusion in Solids* (McGraw-Hill, New York, 1963)
62. M. Sugisaki, H. Furuya, H. Sekiya, K. Hashizume, Thermal diffusion of tritium and protium in alpha phase of zirconium. *Fusion Technol.* **14**, 723–728 (1988)
63. Y. Hatano, M. Shimada, VKh Alimov, J. Shi, M. Hara, T. Nozaki, Y. Oya, M. Kobayashi, K. Okuno, T. Oda, G. Cao, N. Yoshida, N. Futagami, K. Sugiyama, J. Roth, B. Tyburska-Püschel, J. Dorner, I. Takagi, M. Hatakeyama, H. Kurishita, M.A. Sokolov, Trapping of hydrogen isotopes in radiation defects formed in tungsten by neutron and ion irradiations. *J. Nucl. Mater.* **438**, S114–S119 (2013). doi:[10.1016/j.jnucmat.2013.01.018](https://doi.org/10.1016/j.jnucmat.2013.01.018)
64. Y. Hatano, M. Shimada, T. Otsuka, Y. Oya, VKh Alimov, M. Hara, J. Shi, M. Kobayashi, T. Oda, G. Cao, K. Okuno, T. Tanaka, K. Sugiyama, J. Roth, B. Tyburska-Püschel, J. Dorner, N. Yoshida, N. Futagami, H. Watanabe, M. Hatakeyama, H. Kurishita, M. Sokolov, Y. Katoh, Deuterium trapping at defects created with neutron and ion irradiations in tungsten. *Nucl. Fusion* **53**, 073006 (2013). doi:[10.1088/0029-5515/53/7/073006](https://doi.org/10.1088/0029-5515/53/7/073006)
65. Y. Chen, M.M. Abraham, H.T. Tohver, Radiation-induced diffusion of hydrogen and deuterium in  $MgO$ . *Phys. Rev. Lett.* **37**, 1757–1760 (1976). doi:[10.1103/PhysRevLett.37.1757](https://doi.org/10.1103/PhysRevLett.37.1757)
66. Y. Chen, R. Gonzalez, K.L. Tsang, Diffusion of deuterium and hydrogen in rutile  $TiO_2$  crystals at low temperatures. *Phys. Rev. Lett.* **53**, 1077–1079 (1984). doi:[10.1103/PhysRevLett.53.1077](https://doi.org/10.1103/PhysRevLett.53.1077)
67. R.G. Macaulay-Newcombe, D.A. Thompson, Ion beam analysis of deuterium-implanted  $Al_2O_3$  and tungsten. *J. Nucl. Mater.* **258–263**, 1109–1113 (1998). doi:[10.1016/S0022-3115\(98\)00098-1](https://doi.org/10.1016/S0022-3115(98)00098-1)
68. R.A. Strehlow, H.C. Savage, The permeation of hydrogen isotopes through structural metals at low pressures and through metals with oxide film barriers. *Nucl. Technol.* **22**, 127–137 (1974)
69. A.S. Zarchy, R.C. Axtmann, Tritium permeation through 304 stainless steel at ultra-low pressures. *J. Nucl. Mater.* **79**, 110–117 (1979). doi:[10.1016/0022-3115\(79\)90437-9](https://doi.org/10.1016/0022-3115(79)90437-9)



# Chapter 10

## Contamination and Decontamination

Kanetsugu Isobe

**Abstract** Handling of radioisotopes often accompanies their transfer to handling equipment/tools and its environment, referred as contamination. If the transferred radioactivity is higher than regulation level, its removal or decontamination is required. Except very high energy radiation and neutron from radioisotopes, exposure to the radiation generally does not transfer the radioactivity, in other words, no activation of the handling tools and the environments occurs. Since tritium (T), a radioisotope of hydrogen, is chemically active, T handling always resulting in T contamination of handling tools and environments. Hence, direct T handling of workers is prohibited and handling tools are always required. This chapter focuses to contamination and decontamination of T for solid materials. T contamination of workers which is mostly caused by internal exposure through inhalation and/or skin absorption of tritiated water or vapor is described in Chap. 15 based on the details of safety regulation of T given in Chap. 14.

**Keywords** Tritium gas • Tritiated water • Solid • Contamination • Decontamination • Detritiation

### 10.1 Tritium Contamination

Any materials used in T handling systems are more or less contaminated by T, which is one of the most important safety concerns. Once materials, devices, and equipment in any T handling systems are contaminated, they have to be decontaminated for maintenance/repairing, replacement, disposal, and decommission. Although disposal of T-contaminated waste or tritiated waste is one of quite

---

K. Isobe (✉)

National Institutes for Quantum and Radiological Science and Technology,  
Fusion Energy Research and Development Directorate,  
Department of Blanket Systems Research, Rokkasho Fusion Institute,  
Shirakatahirane 2-4, Tokai, Ibaraki 319-1195, Japan  
e-mail: isobe.kanetsugu@qst.go.jp

important safety issues, it is well established and documented [1–3]. Hence, the disposal of tritiated waste is not treated in this chapter. This section focuses contamination, and the next section, decontamination.

Since contaminations of fluid (water and gas) and of solid are quite different, they are separately discussed in the following.

### ***10.1.1 Water and Gas***

This section briefly explains contamination and decontamination of gases used in ventilation or atmosphere of any T handling systems and liquid mostly used as coolant. T permeation from the first wall and blanket systems to coolant through cooling channel, resulting heavy contamination T of the coolant, is a serious concern. Therefore, T permeation barrier seems indispensable, which is separately described in Chap. 9. Water contaminated by T is just referred as tritiated water and how it is produced and how it is decontaminated are discussed in Chap. 14 (Sect. 14.2.4.2 Detritiation system).

Gases used for ventilation of any T handling systems are tritiated, i.e., inclusion of small amount of HT, HTO, tritiated hydrocarbons, and other tritiated gases. In most cases, the gases used for the ventilation are circulated with filtration and finally exhausted from a stack with dilution to keep their T activity below the regulation level. For highly activated case, the gases are oxidized and resulting HTO is recovered in a cold trap or absorption bed. Details of T recovery are given in Chap. 13.

### ***10.1.2 Solid***

This section focuses to T contamination of solid materials. The characteristic of contamination and decontamination of T totally depend on chemical nature of materials to be contaminated and T or hydrogen, mostly abundant as hydrogen gas, water, or any types of hydrocarbons and materials. Generally, the T contamination of materials takes place by the following processes:

- Surface uptake (such as adsorption),
- Inclusion and dissolution into subsurface,
- Dissolution into bulk (internal diffusion in dissolved state and migration among trapping sites).

These three processes appear quite differently depending on chemical form of tritium and character (physical and chemical properties) of materials, their surface states, and material's temperature. In the next section, details of each term are described.

### 10.1.2.1 Surface Uptake or Adsorption

In most cases, the first step of contamination is interactions of tritiated gases and surface of solid, and consequently, the tritiated molecules in the gases are adsorbed at the surface releasing some energy called adsorption energy. Depending on the values of the adsorption energy, physical adsorption (less than  $\sim 10$  keV) and chemical adsorption (above  $\sim 10$  keV) are distinguished. In the physical adsorption, chemical states of adsorbates (tritiated molecules) are not changed, while in the chemical adsorption chemical reactions of the adsorbates with atoms on the solid surface sometimes occur. An HT molecule can be either physically adsorbed as HT or chemically adsorbed as H and T to be bound to atoms of the solid surface.

Similarly, any solid surface adsorbs HTO physically or chemically. In chemical absorption, bond breaking of HTO into H or T and OH or OT to be bound to the surface occurs. Since solid surface, usually, absorbs ubiquitous water ( $H_2O$ ) both physically and chemically, isotopic replacement of T in newly adsorbed tritiated molecules with H in preadsorbed  $H_2O$  molecules appears as significant surface contamination by T. Bonding with impurity atoms included in materials such as C, O, and S also enhances T uptake.

### 10.1.2.2 Inclusion in Subsurface

Once T is chemically adsorbed on the surface, its isotopic replacement with H in ubiquitous water or some surface reactions to make HTO would increase the amount of physically adsorbed HTO as multi-layers and/or in pores. Formation of hydroxides with surface atoms and impurities increases surface uptake of TO and consequently increases surface roughness which could also enhance adsorbed amount of HTO. Furthermore, T released at reaction of HTO and surface atoms to make their oxide can penetrate into subsurface layers. This is one of the most important processes of T uptake on the surface of cooling channels using water as coolant.

In organic materials, particularly polymers often used as gaskets and windows in T handling systems and wears for T protection, HTO can easily penetrate in them and physisorbed on their pore surfaces owing their porous nature. Oxide ceramics and concrete can also uptake HTO in their open pores. Contamination of concrete is also caused by isotopic replacement of T with its structure water.

### 10.1.2.3 Inclusion in Bulk

Once T is included into subsurface with chemical form of an atom or ion, it diffuses into bulk according to its concentration gradient. Hydrogen diffusion and solubility in metals are generally much larger than those in other materials so as the T uptake. In addition, the amount of T retained in metal bulk becomes much larger than that retained at surface and in subsurface layers. During the diffusion process, some T is

trapped at defects, impurities, and precipitates in metals. In bcc metals, whose H solubility is much less than that of FCC metals, trapping is significant and could be main cause for their T inventory. Once T is trapped, it is hardly detrapped to make decontamination difficult. T dissolved in oxides (or ceramics) could migrate or diffuses in bulk as  $T^+$  or  $OT^-$  and electric field would enhance their migration. However, the diffusion/migration rate is much less than that in metals. Hence, some oxides are used as permeation barrier as discussed in Chap. 9.

As described above, T contamination of solid is caused by T uptake in solid surface and solution and trapping in solid bulk. Contamination processes caused by gases, water, and organically bound tritium (OBT) are summarized in Table 10.1. OBT, such as tritiated methane and tritiated acid, also causes tritium contamination. Because it was measured in the Fusion experimental tours, the interest of OBT has been increasing with respect to understanding tritium behavior in a fusion reactor. In any case, chemical form of T and chemical nature of solid significantly change how T is bound to their surface and in bulk or changes binding energy. T inclusion in bulk is significantly different among polymers, ceramics, concrete, and metals.

The existence of surface layers, such as oxide, deposition, and coating film, also influences on the contamination procedure. It is well known that some deposited layers can catch the large amount of T, while some oxide layers can prevent the dissolution and diffusion of T into the bulk. The studies about hydrogen isotope permeation, dissolution, and diffusion have been extensively carried out not only in nuclear and but also in other science and engineering fields. The information from the previous works is important when we consider the contamination behavior.

In addition of the influence of materials, there are various other factors affecting the contamination procedure. Radiochemical reaction is one of the important examples.  $\beta$ -electrons emitted at disintegration of T make radiochemical reactions

**Table 10.1** Summary of T contamination of solid

	Adsorption		Inclusion in subsurface	Inclusion in bulk
	Physisorption	Chemisorption		
Gas (HT)	Physisorption (HT)	Chemisorption (HT) Isotopic replacement with H in surface water (HTO)	Trapping Chemical reaction with surface-segregated impurities (T-S or TO-S)	Dissolution and trapping as an atom or ion (All kinds of materials)
HTO	Physisorption as surface water (HTO)	Chemisorption (HTO) Chemically bound to surface atoms (TO-S)		Dissolution and Trapping of T released by surface corrosion
OBT	Physisorption as OBT	Chemical reaction with surface adsorbates	Chemical reaction with surface-segregated impurities	Adsorption in open pores (ceramics and organic materials)

S corresponds to solid atom

with others. For example, in tritiated water, decomposition of the water produces H and OH radicals which could enhance either reduction or oxidation. Accordingly, surface of materials used for T storage could be subjected to change its chemical nature for longtime storage or storage of high activity T. Furthermore, decay heat of T increases the temperature of the materials which force the cooling of T storage bed.

## 10.2 Decontamination

Since decontamination of fluids (gas and liquid) is generally the same as T recovery from gas and liquid described in Chap. 6, this section focuses decontamination of solids.

As described above, T contamination is somehow ascribed to bonding of T to atoms and molecules at surface and in bulk of solid materials. Hence, decontamination can be performed by either physical removal or chemical debonding. Accordingly, various methods for T decontamination have been proposed and examined so far. A typical example of physical decontamination is scrapping or removing the contaminated area. Although physical sputtering using energetic ions is promising way to remove T-contaminated surface layers, it is difficult to apply for decontamination of T handling equipment/tools. Followings are usually used decontamination methods, and their combinational uses are often employed.

For physical methods;

- (a) Purging or blowing-off by liquid or gas,
- (b) Mechanical wiping and/or scrapping-off.  
And for chemical methods;
- (c) Desorption by evacuation,
- (d) Desorption by heating,
- (e) Isotopic exchange or chemical replacement.

Gas purging or blowing-off is one of the simplest ways to remove physisorbed water. Blow-off by water is quite effective because the water enhances replacement of HTO on surface by H<sub>2</sub>O. Since the amount of adsorbate shows pressure-dependent isotherm, evacuation to lower pressure generally encourages their desorption. A simple evacuation is not effective to remove chemisorbed T. Heating for bond breaking and/or desorption is quite effective. However, heating and evacuation of materials with large volume is not realistic. Isotopic exchange or chemical replacement is a major decontamination method, particularly effective for removal of HTO absorbed on surface both physically and chemically. This method is also useful for polymers, while the decontamination of concrete might be difficult owing to huge amount of its structure water and T dilution in it. Hence, surface of the concrete in T handling systems is usually covered with water shedding paint. Table 10.2 shows summary of effectiveness of decontamination methods usually employed in T handling facilities. The table suggests that a suitable method should be selected depending on the chemical state of T and properties of contaminated materials. Combinational uses are also common.

**Table 10.2** Summary of effectiveness of decontamination methods usually used

Decontamination method		Blow-off by inert gas	Evacuation	Physical sputtering	Heating	Replacement with H <sub>2</sub>	Replacement with H <sub>2</sub> O	Electrolysis
Origin of contamination	Mechanical scraping							
Physisorbed as HT	○	○	○	○	○ Flash ramp	○	○	—
Chemisorbed as T-S or TO-S	△	×	×	○	△ Laser heating	○	○	
T dissolved or trapped in bulk	×	×	△	×	○ Bulk heating	△ at high T	—	—
Physisorbed as HTO	△	○	○	○	○ Flash ramp	×	○	—

## 10.3 Specific Examples of Contamination and Decontamination

As described above, contamination and decontamination procedures are different with materials, and some examples for metals and organic materials are separately given below.

### 10.3.1 Metal

Contamination and decontamination processes have been investigated in T handling facilities in the world. To understand those processes, fundamental data on hydrogen isotope solubility and diffusivity in materials used in the facilities are quite important. In particular, those in metallic materials are quite important because they are used as structure materials of any T handling systems. Therefore, interactions of T and stainless steels as candidate fusion reactor structure materials have been extensively studied. In the following, some investigations are introduced. Interactions of tritiated water and 304 SS were reported by Longhurst [4]. They revealed that HT converts relatively quickly to HTO on its surface at both an ambient and elevated temperature. And the T uptake process consists of surface adsorption and isotopic exchange with preexisting surface-bound water. The effects of alloying and changes of their microstructures on T behavior in various austenitic stainless steels were reported by J. Chêne et al. [5]. They found that T absorption/desorption at the austenitic stainless steels varied with the microstructure and that precipitates and intermetallic phases in the steels trap T. Nishikawa and his colleagues [6, 7] studied the T absorption and desorption for tubes of stainless steel, copper, and aluminum as candidate cooling tubes. They have confirmed that a significant amount of T is captured at the surface of the tubes owing to isotopic replacement of T in a flowing gas in the tube and preexisting OH bases strongly bound to its surface [6] and subsequently determined the amount of adsorbed water [7] and reaction rates of the isotopic replacement on the tube surface of 304SS [6].

Aiming to develop decontamination processes, desorption behavior and T distribution on stainless steel surface have been studied [8–10]. They showed that T was enriched at the surface and its distribution and release were controlled by T diffusion in metals. These results suggest the importance of the T diffusion in bulk for decontamination. M.J. Quinlan et al. tried decontamination of purge gases with adding  $H_2O$  or  $H_2O_2$  and found that the addition of  $H_2O_2$  improved the decontamination process [11].

### 10.3.2 *Organic Materials*

Contamination and decontamination processes of organic materials including polymers and oils have not been studied well comparing with those of metals. One of the reasons is difficulty of T measurement in those materials by the liquid scintillation method, because T in those materials disturbs the scintillation process by quenching as described in Chap. 7. Studies of the interaction of polymers with T have another difficulty. Heavy T contamination of polymers should be avoided, because irradiation with  $\beta$ -electrons released by T disintegration degrades their materials properties. Nevertheless, utilization of polymer in T handling systems is indispensable which requires on-site verification of the polymers for both contamination and decontamination.

Sazonov et al. [12] improved the liquid scintillation method to avoid errors associated with scintillation quenching. They measured liquid–liquid isotope exchange and absorption on pump oil with nuclear magnetic resonance (NMR) spectroscopy. Borysow et al. [13] also used NMR and studied surface-enhanced exchange reaction of hydrogen isotopes with water and oil. They used additional method, Raman spectroscopy to determine contents. Understanding of T interaction with organic materials and behavior of T included in them are quite important. However, they have not been examined well and new experiments are awaited.

### 10.3.3 *Actual T Handling Systems*

T has been used at many facilities in the world and each facility has been accumulated experience and knowledge to handle large amount of T. Nevertheless, they are very much limited. In CANDU type nuclear reactors, which use heavy water ( $D_2O$ ) as moderate coolant, about 200 g of T produced in  $D_2O$  by reactions with neutrons has been extracted in every year. In the reactor, radioisotopes having much stronger radiation than T are more concerned. Among various fusion experimental machines, Joint European Tours (JET) in UK and Tokamak Fusion Test Reactor (TFTR) in USA used T as fuels. Any tokamak machines operating with D are contaminated with T produced by D-D reactions and they have to be decontaminated. In these machines, T-contaminated components were decontaminated for reuse, maintenance, or decommission, and the decontamination procedures were documented [14, 15].

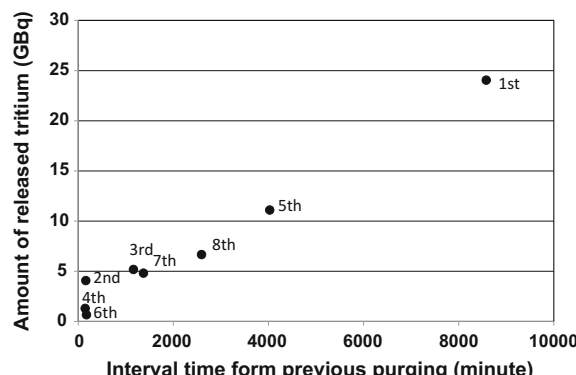
There are several laboratories in the world where large amount of T can be handled. The Tritium Laboratory Karlsruhe in Germany has accumulated their experience of T handling and reported that various unexpected contaminations appeared inside or components of any T handling systems. One example is significant contamination of an electrical insulator [16]. It is also well known that T

contamination of gloves and glove boxes after handling large amount of T requires particular care for their succeeding use (see Fig. 2.8 in Chap. 2).

In Japan, Tritium Processing Laboratory (TPL) of Japan Atomic Energy Agency (JAEA) has been handling significant amount of T from pure T to diluted T with its activity of up to kBq in gases form or water since 1988 [17]. Accordingly, their T handling systems are contaminated by T. Therefore, replacement, maintenance, and repairing of their components were required occasionally. Before to do these, the system should be decontaminated. In the following, decontamination procedures in TPL are summarized. A typical decontamination method employed is gas purging, first by dry gas followed by atmospheric gas containing moisture (water vapor). T concentration in the purge gas was monitored during the decontamination. Even after the T activity in dry purged gas became less than the regulation level to allow the system open in atmosphere, the T activity in the atmospheric gas purged succeeding to the dry gas purging dramatically increased. Furthermore, breaks of the purging, or taking interval of the decontamination caused recovery of the T activity at the surface of the components due to diffusional release of T from bulk. Figure 10.1 shows how T activity in the purged gas of vacuum pumping line changed with time intervals between two purgings in TPL of JAEA. Each purging was performed with atmospheric air for 1 h and all purged (exhausted) gas was collected in a hold tank, which makes determination of the amount T released by every purging. The number in figure shows turn of the purging. As seen in the figure, even after 4 times of the purging, the amount of released T by the purging increased with the interval time. This indicates that initially most of the T was retained in the bulk and the T release was compensated by diffusional supply of T from the bulk. Thus, T once taken into the bulk is hard to remove and requires longer time for decontamination.

This point is particularly important for disposal of decontaminated materials and decommission in the context of hard detection of T in materials as pointed out in Chap. 7. Once the surface of the materials was decontaminated to the allowable level of T activity for their disposal, the surface T activity could restore the T activity prior to the decontamination.

**Fig. 10.1** Variation of the amount of T released during a purging with interval time between two succeeding purgings



## 10.4 Summary and Future Prospect

Handling of T always accompanies contamination of any materials used in handling equipment or tools, which, in turn, requires their decontamination for reuse and even for decommission. In general, the decontamination can be made by reversal processes of contamination, which are realized as decontamination by some physical methods. In most cases, however, simple reverse processes are not possible, because T uptake at the solid surface accompanies some chemical reactions or release of adsorption energy. Therefore, chemical states of T and chemical character of materials to be contaminated vary chemical state of T uptake into the materials. Therefore, contamination procedures are significantly different among the organic materials, polymers, ceramics, glasses, and metals. Accordingly, the decontamination of these materials often requires different methods or techniques. As described, in numbers of T handling facilities in the world, T contamination has been unescapable and T decontamination has been routinely performed. Nevertheless, different T handling systems and their different materials have given different contamination behavior and require different decontamination procedures. Accordingly, experiences and knowledge accumulated up to now are neither well organized nor archived. In addition, unfortunately, the amount of T handled in all present T handling facility is far less than that used in a fusion reactor and simple extrapolation of present experiences and knowledge could not be applied to T handling in the reactor. Therefore, database of basic properties of materials relating their interactions with T are still needed to understand the contamination procedure and to develop decontamination methods. Construction of T handling system would not be technically difficult, while actual operations must be carefully done. ITER is only one actual test bed for the T handling in a reactor.

## References

1. DOE-HDBK-1192-2008, Tritium handling and safe storage, December, 2008
2. F. Mannone, in *Management of tritium-contaminated wastes, a survey of alternative options*, Commission of European Communities, Joint Research, CD-NA-12526-EN-C, 1990
3. IAEA Technical reports series No. 421, Management of waste containing tritium and carbon-14, ISBN 92-0-114303-6
4. G.R. Longhurst, in *Tritiated water interaction with stainless steel*, INL/EXT-07-12584
5. J. Chêne, P. Trabuc, O. Gastaldi, Tritium release and trapping in austenitic stainless steels: role of microstructure and desorption anneal. *Fusion Sci. Technol.* **54**, 510–514 (2008)
6. M. Nishikawa, T. Takeishi, Y. Kawamura et al., Tritium mass balance in the piping system of a fusion reactor. *Fusion Technol.* **21**, 878–882 (1992)
7. T. Shiraishi, S. Odoi, M. Nishikawa, Adsorption and desorption behavior of tritiated water on the piping Materials. *J. Nucl. Sci. Tech.* **34**, 687–694 (1997)
8. A.I. Markin, E.A. Azizov, N.I. Siromyatnikov et al., Research of the tritium saturation, isotope diffusion and decontamination of stainless steel using magnetic microscopy. *Fusion Sci. Technol.* **54**, 489–492 (2008)

9. S. Naoe, Y. Torikai, R.-D. Penzhom et al., Transport of tritium in SS316 at moderate temperatures. *Fusion Sci. Technol.* **54**, 515–518 (2008)
10. T. Otsuka, T. Tanabe, Hydrogen release from ferritic/martensitic stainless steel. *Fusion Sci. Technol.* **54**, 541–544 (2008)
11. M.J. Quinlan, W.T. Shmayda, S. Lim et al., Effects of H<sub>2</sub>O abd H<sub>2</sub>O<sub>2</sub> on thermal desorption of tritium from stainless steel. *Fusion Sci. Technol.* **54**, 519–522 (2008)
12. A.B. Sazonov, G.V. Vereteninikova, E.P. Magomedbekov, Interaction of tritium with oils and tritiatied waste oil decontamination. *Fusion Sci. Technol.* **54**, 584–587 (2008)
13. J. Borysow, M. Eckart, M. Fink, Surface enhanced exchange reactions of hydrogen isotopes with water and Fomblin oil. *Fusion Sci. Technol.* **54**, 580–583 (2008)
14. P. Edwards, N. Davies, A. Loving et al., in *Operation, Maintenance and decontamination of the JET Torus Access Facilities*, EFDA-JET-CP(01)09/04
15. E. Perry, J. Chrzanowski, C. Gentile et al., in *Decommissioning of the Tokamak Fusion Test Reactor*, PPPL-3895
16. C.J. Caldwell-Nichols, H.-D. Adami, N. Bekris et al., Post service examination of a tritium pemeator and from the CAPER facility at the Tritium Laboratory Karlsruhe. *Fusion Sci. Technol.* **54**, 599–602 (2008)
17. Y. Naruse, Yuji Matsuda, K. Tanaka, Tritium process laboratory at the JAERI. *Fusion Eng. Des.* **12**, 293–317 (1990)



# Chapter 11

## Isotope Separation System (ISS)

Toshihiko Yamanishi

**Abstract** In a fusion reactor, Hydrogen (H) always exists as an impurity of the fuel. A water detritiation and a blanket fuel system produce a large amount of hydrogen. The hydrogen gas must be released to the environment without tritium (T). High purity deuterium (D) and T are required as fuel of fusion reactor. The fusion reactor thus needs an isotope separation system having a large separation factor. A cryogenic distillation method (column) has been developed for this purpose. In this chapter, the cryogenic distillation method (column) is described in detail. The separation basis and the structure of the column are first introduced. One of the most important subjects is to develop simulation method of the column and is described in detail. A set of experimental data of the columns are also described in detail. Some future R&D subjects are then described. Although the cryogenic distillation is the most promising for a fusion reactor, some other methods can be applicable for fusion-related facilities. From this viewpoint, other methods such as thermal diffusion are also briefly introduced.

**Keywords** Tritium, T • Isotope separation system • Cryogenic distillation • Stage model • Thermal diffusion

### 11.1 Introduction

In a fusion reactor, as noted in previous chapters, only small fraction of fueled D and T into plasma burns and remaining is exhausted and recycled. In the exhaust, D and T are fully mixed. For burning control, independent fueling of D and T is indispensable. This requires a D and T separation system. In a fusion reactor, hydrogen (H) always exists as an impurity of the fuel. In addition, a large amount of H gas will be used for a water detritiation system and the blanket system. Therefore,

---

T. Yamanishi (✉)

National Institutes for Quantum and Radiological Science and Technology Fusion Energy Research and Development Directorate, Rokkasho Fusion Institute, Aomori, Japan  
e-mail: yamanishi.toshihiko@qst.go.jp

the isotope separation system in a fusion reactor should have high separation factors for the separation of these hydrogen isotopes. Moreover, owing to the poor resources of T, most of T must be recycled through the isotope separation system. In ITER, T recovering rate must be above 90 %. At the same time, since the hydrogen (H) gas is finally exhausted to the environment, the T concentration in the H gas from the isotope separation system should be as low as reasonable achievable (mole fraction of T less than  $10^{-10}$ ). This requires significantly high separation factors. The flow rate of the isotope separation system of a fusion reactor reaches to  $\sim 300$  mol/h. Several methods have been developed for the separation of hydrogen isotopes such as gas chromatography, thermal diffusion, laser method, and cryogenic distillation. Among all, only the cryogenic distillation method can meet the above conditions (large flow rate and separation factor) [1] and is most likely used in a fusion reactor. In this chapter, several simulation methods and a set of experimental data of the cryogenic distillation columns are described in detail.

## 11.2 Cryogenic Distillation System

ITER will employ a cryogenic distillation column for the isotope separation in its fuel cycle system [2]. The distillation column system has been well established and applied in chemical industries. To apply the column for T separation from hydrogen isotope mixture, two important issues must be solved: One is, as mentioned above, to have a large separation factor in the column and another is to work under the mixture of six hydrogen isotopes ( $H_2$ , HD, HT,  $D_2$ , DT, and  $T_2$ ). A column cascade composed of several columns, four columns for ITER, with some equilibrators designed as shown in Fig. 11.1. Two feed flows are supplied to the cascade: a feed flow from TEP (Tokamak Exhaust Process) and a feed flow from the water detritiation system. The feed flow from TEP contains  $H_2$ , HD, HT,  $D_2$ , DT, and  $T_2$ . The feed flow from the water detritiation system contains  $H_2$ , HD, and HT. From these two feed flows, the cascade produces three flows: A top flow from column 2 is discarded to the environment, since the flow contains  $H_2$  and HD (essentially free from T), a top flow from column 2 is a product flow of  $D_2$  with small amounts of DT, and a bottom flow from column 4 is a product flow of  $T_2$  with small amount of DT. The equilibrators are a kind of catalytic reactors (often uses Pt catalyst beds) to promote the isotopic exchange reactions:  $2DT \leftrightarrow D_2 + T_2$  and  $HT + D_2 \leftrightarrow HD + DT$ .

The column consists of three components: a condenser at the top of the column, a packed section at the middle of the column, and a reboiler at the bottom of the column (See Fig. 11.2). The condenser produces a liquid hydrogen flow by cooling the hydrogen gas using helium coolant at  $\sim 20$  K. The reboiler regenerates a hydrogen vapor flow from the liquid hydrogen in the reboiler with an electric heater. The vapor and the liquid flow counter-currently contacting with each other in the packed section. In the packed section, packing materials (such as Dixon Ring) exist to get a large surface area and to disperse the liquid flow. An isotope

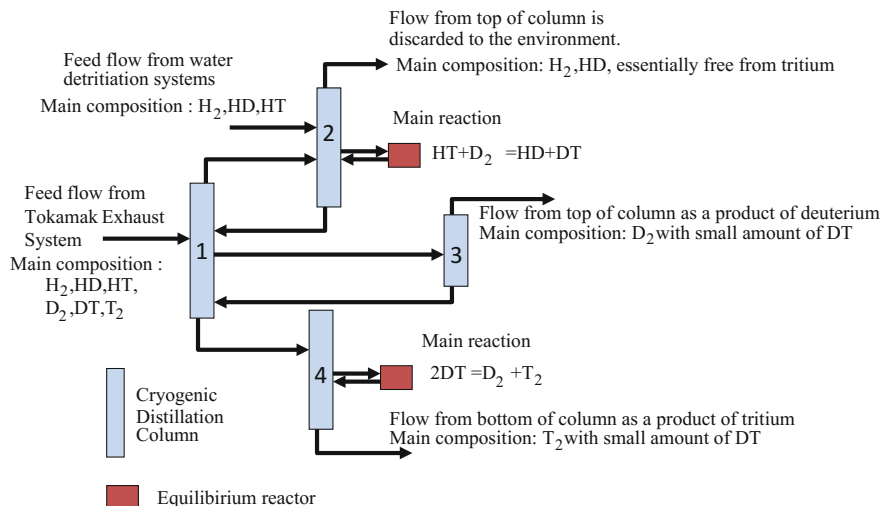


**Fig. 11.1** Cryogenic distillation column cascades for hydrogen isotope separation of ITER

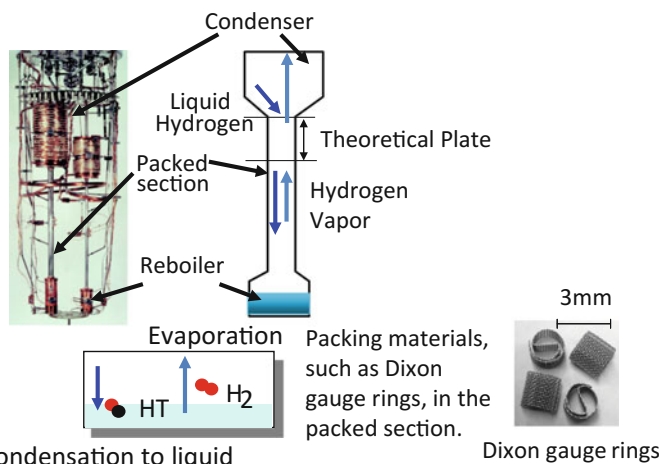


**Fig. 11.2** Structure and concept of cryogenic distillation system

having lower boiling point tends to move to the vapor flow and is finally enriched into the condenser. On the other hand, an isotope having higher boiling point is moved to liquid and is finally enriched into the reboiler. The difference in the boiling points among the hydrogen isotopes is relatively large (H<sub>2</sub> = 20 K, T<sub>2</sub> = 25 K). Although the height of the column designed for ITER is in the range of 3–5 m to get a large separation factor, the diameter of the columns is quite small (0.05 ~ 0.1 m) because of small feed flow rates. A series of designing methods to determine the height and the inner diameter of the column will be described latter.

### 11.3 Simulation Method

The distillation system is a well-established technique. Nevertheless, its application to separate T requires significant R&D. There are limitations to make distillation column experiments using T with a realistic scale, because of the radioactivity of T, which inhibits easy access to and inspection of the column to get a series of data under wide and various conditions. In addition, complicated devices, such as the helium refrigerant system, are needed to operate the column even for a small experimental scale column. It is thus quite important to develop or establish a simulation method to design the column. As mentioned above, the cryogenic distillation column in the fuel cycle system must have a large separation factor. The T concentration in the flow discarded to the environment should be maintained at extremely low values. In ITER, atom fraction of T should be less than  $1 \times 10^{-10}$ , while the atom fraction of T in the flow of T product is required to be more than 90 %. To satisfy these requirements, it is significant to study a control system of the column, and a simulation of column system is indispensable for this purpose.

A stage model has been applied to simulate operation of the distillation column. In this model, the column is assumed to be composed of several theoretical stages. Figure 11.3 shows a typical stage model of the cryogenic distillation column at steady state for total reflux operation; i.e., no feed is supplied, and no exhaust. The relations between compositions (mol fractions) of liquid and vapor phases can be expressed as two lines in Fig. 11.3 for actual operation and equilibrium. As shown in the inset of Fig. 11.3, liquid flow 1 and vapor flow 4 enter into the theoretical stage. Vapor flow 2 and liquid flow 3 leave the stage. The composition of flow 1 is equal to that of flow 2, and flow 3 has the same composition as flow 4. The composition of flow 2 is equilibrated with that of flow 3. For a typical operation at the steady state, flows are withdrawn from the top and the bottom of the column as products, and multiple feed flows are supplied as shown in Fig. 11.4. According to the figure, we can obtain the following equations for mass balances around the  $j$ th stage [3].

$$L_{j-1}x_{i,j-1} + V_{j+1}y_{i,j+1} + F_jz_{i,j} = (L_j + U_j)x_{i,j} + (V_j + W_j)y_{i,j}, \quad (11.1)$$

$$\begin{bmatrix} B_{i,1} & C_{i,1} & \cdots & \cdots \\ A_{i,1} & B_{i,2} & C_{i,2} & \ddots & \vdots \\ \cdots & \cdots & \cdots & A_{i,N-1} & B_{i,N} \end{bmatrix} \begin{bmatrix} x_{i,1} \\ \vdots \\ x_{i,N} \end{bmatrix} = \begin{bmatrix} D_{i,1} \\ \vdots \\ D_{i,N} \end{bmatrix}, \quad (11.2)$$

$$A_{i,j} = L_{j-1}, \quad B_{i,j} = -(V_j + W_j)K_{i,j} - (U_j + L_j), \quad C_{i,j} = V_{j+1}K_{i,j+1}, \quad D_{i,j} = -F_jz_{i,j}, \quad (11.3)$$

$$y_{i,j} = K_{i,j}x_{i,j}, \quad (11.4)$$

where

$L_j$  Liquid flow rate from the  $j$ th stage,

**Fig. 11.3** Stage model of cryogenic distillation column at steady state under total reflux operation

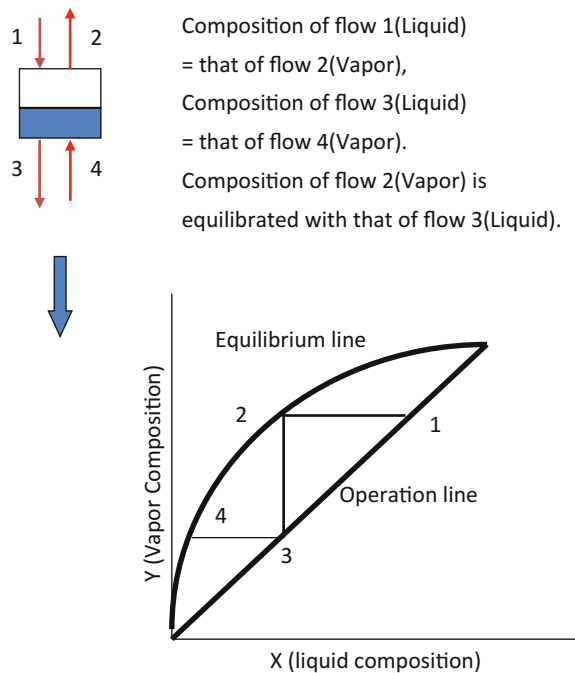
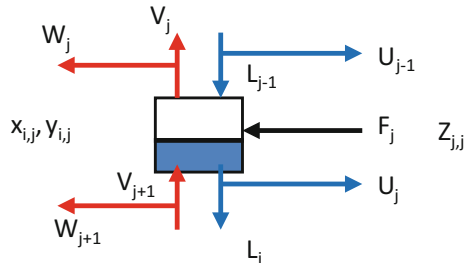


**Fig. 11.4** Mass balance for a component  $i$  around  $j$ th stage for simulation



- $V_j$  Vapor flow rate from the  $j$ th stage,
- $F_j$  Feed flow rate to the  $j$ th stage,
- $U_j$  Side cut liquid flow rate from the  $j$ th stage,
- $W_j$  Side cut vapor flow rate to the  $j$ th stage,
- $Z_{i,j}$  Mole fraction of the  $i$ -component of feed flow to the  $j$ th stage,
- $x_{i,j}$  Mole fraction of the  $i$ -component of liquid flow from the  $j$ th stage,
- $y_{i,j}$  Mole fraction of the  $i$ -component of vapor flow from the  $j$ th stage,
- $K_{i,j}$  Vapor–liquid equilibrium coefficient of the component  $i$  at the  $j$ th stage

The above basic equations from a tri-diagonal matrix can be simply solved by the tri-diagonal method. To solve the equations rigorously, we must consider the heat balance around each stage [4]. However, the effect of the heat balance is not so

large for the cryogenic distillation columns of the hydrogen isotope separation and can be neglected. The followings are the solution procedure of the tri-diagonal method.

- (1) Suppose the liquid compositions for all the stages to be the composition of the main feed flow. Input initial values for flow rates of feed flows, flow rates of liquid and vapor flows, and column pressure. The pressure drop is also considered.
- (2) Suppose temperatures for all the stages within the column to be the boiling point of the main feed flow, which can be calculated from its composition and the column pressure. Corresponding to the temperature, pressure, and liquid composition values, all the vapor–liquid equilibrium coefficients can be calculated for all the stages.
- (3) Calculate values of the tri-diagonal matrix in Eq. (11.2).
- (4) Solve the matrix and obtain a set of new liquid composition values.
- (5) Recalculate the temperature from the composition.
- (6) Iterate calculation processes from (3) to (5).

When the summation of the mass balances around all the stages converges to a certain value, the calculation is terminated.

Since a large separation factor is needed for the column of a fusion reactor, it is often difficult to get a suitable set of solutions by the tri-diagonal method only. To solve this problem, several studies have been carried out. The most effective method is the Newton–Raphson method [5]. A set of new functions are derived to get a convergence for Eq. (11.2).

$$S_j = \sum_{i=1}^m K_{ij}x_{ij} - 1, \quad (11.5)$$

$$\begin{aligned} S_1(T_1 &\dots T_N) &= 0 \\ S_j(T_1 &\dots T_N) &= 0 \\ S_N(T_1 &\dots T_N) &= 0, \end{aligned} \quad (11.6)$$

$$\begin{bmatrix} \frac{\partial S_1}{\partial T_1} & \dots & \frac{\partial S_1}{\partial T_N} \\ \vdots & \ddots & \vdots \\ \frac{\partial S_N}{\partial T_1} & \dots & \frac{\partial S_N}{\partial T_N} \end{bmatrix} \begin{bmatrix} \Delta T_1 \\ \vdots \\ \Delta T_N \end{bmatrix} = - \begin{bmatrix} S_1 \\ \vdots \\ S_N \end{bmatrix}, \quad T_j = T_j + \Delta T_j, \quad (11.7)$$

where  $T_j$  = Temperature at the  $j$ th stage,  $m$  = Number of components, and  $N$  = Number of total theoretical stages of the column.

The above equations can be solved by the following manner.

- (1) Suppose the liquid compositions for all the stages to be a composition of the main feed flow. Input initial values for flow rates of feed flows, flow rates of

liquid and vapor flows, and column pressure. The pressure drop is also considered.

- (2) Suppose temperature distribution within the column to be the same as that for the liquid, all the vapor–liquid equilibrium coefficients can be calculated.
- (3) Calculate values of the tri-diagonal matrix in Eq. (11.2).
- (4) Solve the matrix and obtain a set of new composition distribution.
- (5) Numerically evaluate partial differential matrix.
- (6) Evaluate Jacobian matrix for the above matrix.
- (7) Evaluate  $\Delta T$  values.
- (8) Recalculate temperature for all the stages.
- (9) Iterate calculation processes from (3) to (7)

If the summation of the mass balances for all the stages converges to a certain value, the calculation would be terminated. This method gives us a set of solutions more rapidly in comparison with that of the tri-diagonal method. However, the calculation sometimes fails to converge. As mentioned above, the boiling point of the main feed flow is used for the initial temperature values. To get the convergence, it has been found that the initial temperature values for the column should be carefully selected. The temperatures at the top and the bottom of the column are rigorously assigned from the designed top and bottom compositions. From the top and bottom temperatures of the column, the temperature values for all the stages can be determined by proportional partitions. However, the calculation may fail to converge, even if the above method is applied, for the case where the T concentration at the top of the column is quite small. It means that the concentrations of all the hydrogen isotopes, except T at the upper part of the column, are almost unchanged. Accordingly, the temperature in the upper part of the column is also almost constant. For such case, we need to employ temperatures at middle of the column as well as the top and bottom temperatures [4]. Some simulation methods apart from the stage model have also been developed, and some references are introduced here [6, 7].

For the dynamic simulation of the column, in the framework of the stage model, the basic equations can be expressed by a set of ordinary differential equations from the mass balance for each stage in accordance with Fig. 11.4.

$$L_{j-1}x_{i,j-1} + V_{j+1}y_{i,j+1} + F_jz_{i,j} = (L_j + U_j)x_{i,j} + (V_j + W_j)y_{i,j} = H_j \frac{dx_{i,j}}{dt}, \quad (11.8)$$

The above equations can be solved numerically by some methods such as the Runge–Kutta method or the improved Euler method [8]. To simulate dynamic variation of product composition of the column, we can discuss a control system of the column [8].

To solve Eqs. (11.2) and (11.8) numerically, several parameters for liquid and vapor of hydrogen isotopes are required. The vapor–liquid equilibrium coefficient,  $K$ , and the enthalpies of the liquid and the vapor can be expressed by the following

equations, and the remaining values for all the fittings,  $c$ ,  $B^0$ ,  $m$ ,  $u$ ,  $v$ , and  $w$ , are listed in Tables 11.1, 11.2, and 11.3 [9].

$$y_{i,j} = K_{i,j}x_{i,j}, \quad (11.9)$$

$$K_{i,j} = \gamma_{i,j} \frac{p_{ij}^*}{P_j}, \quad (11.10)$$

$$p_{ij}^* = c_{i1} + c_{i2}T_j + c_{i3}T_j^2 + c_{i4}T_j^3 + c_{i5}T_j^4, \quad (11.11)$$

$$\gamma_{i,j} = \exp\left(\frac{G_i^E}{RT_j}\right) \exp\left\{\frac{(P - p_i^*)}{RT_j} B_i^*\right\}, \quad (11.12)$$

$$G_i^E = \sum_j x_j A_{i,j} - \Delta G, \quad \Delta G = \frac{1}{2} \left( \sum_i \sum_j x_i x_j A_{i,j} \right), \quad (11.13)$$

**Table 11.1** Values of coefficients used in Eq. (11.10)

Isotope	$c_1$	$c_2$	$c_3$	$c_4$	$c_5$
H <sub>2</sub>	102.21	-8.0435	-6.19	$-7.65 \times 10^{-3}$	$1.47 \times 10^{-3}$
HD	-446.444	79.6609	-4.996	0.105456	$3.68 \times 10^{-4}$
HT	-111.567	25.6927	-1.6786	$1.41 \times 10^{-2}$	$1.22 \times 10^{-3}$
D <sub>2</sub>	87.3386	-9.45373	0.692576	$-5.56 \times 10^{-2}$	$1.88 \times 10^{-3}$
DT	-294.74	50.219	-2.68292	$2.67 \times 10^{-2}$	$1.07 \times 10^{-3}$

**Table 11.2** Values of coefficients used in Eq. (11.13)

Isotope	$B^0$ (m <sup>3</sup> /mol K <sup>m</sup> )	m
H <sub>2</sub>	-0.0113	-1.44
HD	-0.0159	-1.52
HT	-0.0196	-1.58
D <sub>2</sub>	-0.025	-1.64
DT	-0.031	-1.7
T <sub>2</sub>	-0.0395	-1.77

**Table 11.3** Values of coefficient used in Equations (11.15) and (11.16)

Isotope	$u_L$ (J/mol K)	$u_V$ (J/mol K)	$v_L$ (J/mol K <sup>2</sup> )	$v_V$ (J/mol K <sup>2</sup> )	$w_L$ (J/mol K <sup>3</sup> )	$w_V$ (J/mol K <sup>3</sup> )
H <sub>2</sub>	24.8541	-4.99084	-5.99924	1.05635	0.166775	-0.014288
HD	30.2796	-4.86434	-7.19218	0.98718	0.191934	-0.010527
HT	-140.901	-6.02617	6.09091	1.07677	-0.0628662	-0.011593
D <sub>2</sub>	-164.891	-4.5884	7.28923	1.0208	-0.0842047	-0.013502
DT	-188.582	-11.3101	8.76987	1.62254	-0.106162	-0.021248

$$B_i^* = B_i^0 T_i^m, \quad (11.14)$$

where  $\gamma_{i,j}$  = a coefficient of the  $i$ -component at the  $j$ th stage representing deviation from the Raoult's law,  $P_j$  = Pressure at the  $j$ th stage, and  $p_{i,j}^*$  = Vapor pressure of pure  $i$ -component at the  $j$ th stage.

$$A_{i,j} = A_{i,j}^0 T^{-1.33}, \quad (11.15)$$

$$\begin{aligned} A_{1,2}^0 &= 580, A_{1,3}^0 = 1060, A_{1,4}^0 = 1580, A_{1,5}^0 = 2320, A_{1,6}^0 = 2900, A_{2,3}^0 = 110, \\ A_{2,4}^0 &= 350, A_{2,5}^0 = 750, A_{2,6}^0 = 1120, A_{3,4}^0 = 90, A_{3,5}^0 = 350, A_{3,6}^0 = 620, \\ A_{4,5}^0 &= 120, A_{4,6}^0 = 300, A_{5,6}^0 = 60, \end{aligned}$$

$$H_i^* = u_{L,i}T + v_{L,i}T^2 + w_{L,i}T^3, \quad (11.16)$$

$$h_i^* = u_{V,i}T + v_{V,i}T^2 + w_{V,i}T^3, \quad (11.17)$$

where  $H_i^*$  = enthalpy of liquid, and  $h_i^*$  = enthalpy of vapor.

A set of important column characteristics can be determined by the following manner.

- (1) Input feed conditions, feed flow rates, and feed composition.
- (2) Several simulation runs are carried out by changing the column pressure, the flow rates of vapor and liquid flows within the column, the flow rates from the top and the bottom of the column, and the number of theoretical stages of the column to determine a set of desirable parameters of the column.
- (3) A column diameter is determined in the following way. The volumetric vapor flow rate can be calculated from the vapor flow rate within the column (molar flow rate) and pressure and temperature of the column. The vapor velocity within the column can then be calculated from the volumetric vapor flow rate by dividing the column diameter. The vapor velocity is a significant parameter for a series of column design. To decrease T inventory within the column, the diameter of the column should be decreased as much as possible. In the case where the vapor velocity exceeds a certain value (the flooding point), the pressure drop across the column becomes so large that liquid never flows down from the top to the bottom of the column. (This phenomenon is well known as the flooding in chemical engineering.) The column diameter is usually selected so that the vapor velocity is set at 60–70 % of the flooding point. By applying this value, we can avoid the flooding and can get a margin for the control of the column.
- (4) The column height is then determined. The number of theoretical stages needed is determined by the simulation results. The HETP (Height Equivalent to a Theoretical Plate) values have been measured by a series of trial runs. The

column height can finally be determined by multiplying the number of theoretical stages to the HETP value.

## 11.4 Experimental Data of the Cryogenic Distillation Column

For designing the cryogenic distillation column, as described in the preceded section, the flooding point and the HETP value shall be determined experimentally.

Several workers have determined the HETP values experimentally [10–14]. Figure 11.5 shows the effect of the vapor velocity in the column on the HETP values. Experimental conditions are presented in Table 11.4. Although the HETP values are fluctuating, they do not seem to depend on the vapor velocity. Figure 11.6 shows how the HETP values changed with a reflux ratio which is defined as the ratio of the flow rates of the top product flow of the column and the vapor flow in the column. No major effect of the reflux ratio on the HETP value was observed in the figure. Most of previous data were obtained for a small column with its packed height of 50 cm as shown in Table 11.4. An actual scale cryogenic distillation system (3 ~ 5 m in column height) was constructed in Los Alamos National Laboratory (LANL) [15, 16]. Using this system, a series of data were obtained under a Japan-US joint research program as shown in Fig. 11.7. The calculated values by the simulation in the preceded section are given in the figure for comparison. The experimental conditions are listed in Table 11.5. The

**Fig. 11.5** Effect of vapor velocity on HETP (Height Equivalent to a Theoretical Plate)

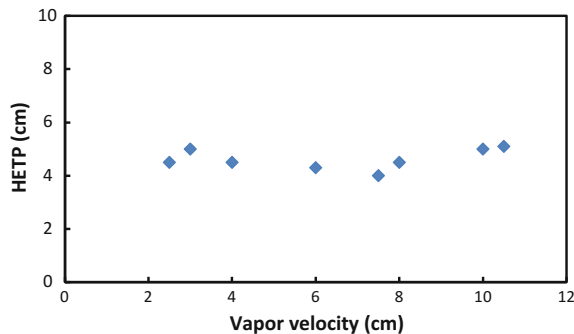


**Table 11.4** Column conditions for experimental data in Figs. 11.7 and 11.8

Distillation column	
Inner diameter	2 cm
Packed height	50 cm
Packings	3 mm Dixon gauge ring
Pressure	40–200 kPa
Composition	H-D-T (50:50:1)

**Fig. 11.6** Effect of reflux ratio on HETP (Feed flow rate = 4 mol/h)

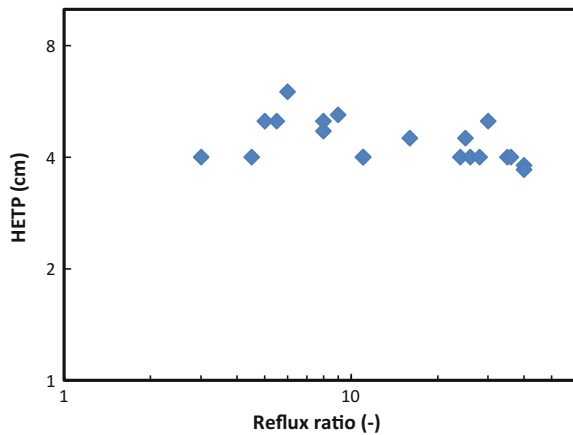


**Fig. 11.7** Change of molecular fraction of hydrogen isotopes in vapor phase from the bottom to the top of the LANL column

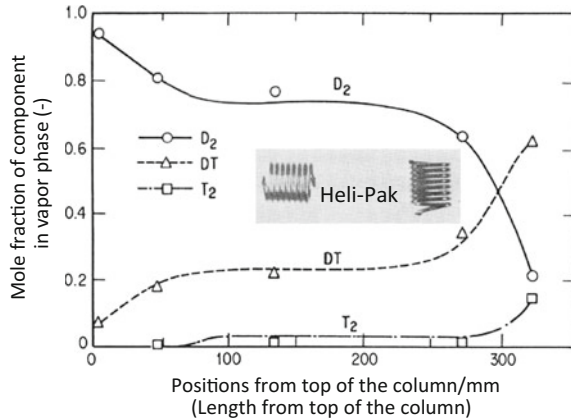


**Table 11.5** Experimental conditions to give data in Fig. 11.7

Distillation columns	
Inner diameter	2.5 cm
Packed height	3.2 m
Packings	4.4 mm Heli-Pak
Pressure	84.6 kPa
Composition	D-T (50:50)
Flow rate	
Top	3.1 mol/h
Bottom	1.8 mol/h
Vapor velocity	2.2 cm/s
HETP	4 cm
Composition	D-T (50:50)

compositions of the vapor within the column are in close agreement with the calculated values as shown in Fig. 11.7, and the validity of the simulation methods are thus demonstrated. As shown in Table 11.5, the packed height is 3.2 m and is much larger than that of the column of Table 11.4 (50 cm). However, HETP of Fig. 11.7 (4 cm) is almost the same as that of Figs. 11.5 and 11.6 (4–6 cm). This means that the column height is not a major factor to alter the HETP value.

For the flooding point, there have been no clear data. No clear inflection point for the pressure drop has been observed up to the vapor velocity of 20 cm/s. We can choose 20 cm/s as the vapor velocity of the column as a design condition.

## 11.5 Summary of the Cryogenic Distillation Column

The cryogenic distillation system is very likely to be employed as an isotope separation system in a DEMO fusion reactor. The distillation technique is well developed, and basic R&D studies to use the technique for the hydrogen isotope separation have already been completed. The simulation method has been developed as described in preceding section. A set of basic data required for designing the column has also been obtained. An actual scale of the column system was also constructed and was demonstrated at LANL. Subsequently, several new systems were constructed in EU, the USA, and Japan. A main remaining subject is to demonstrate the system for a long and continuous operation with handling large amount of T safely. This is one of the main missions of ITER for future application of the cryogenic distillation column as ISS of a DEMO reactor.

The cryogenic distillation column would have the largest T inventory in the fusion fuel cycle system, because the column contains a large amount of liquid hydrogen [2]. Therefore the column has a potential hazard, and the demonstration of long-term safe operation is a quite important subject in ITER. A new type of packing having a new structure may increase surface area of the packing. To use a new surface treatment, method of packing may decrease the liquid inventory holding the packing. This new type of packing can allow us to reduce the column size and T inventory. Maintenance and inspection of the column for the long-term operation are also important subjects. The cryogenic distillation column is a key component of the fusion fuel cycle system and is indispensable to overcome these subjects.

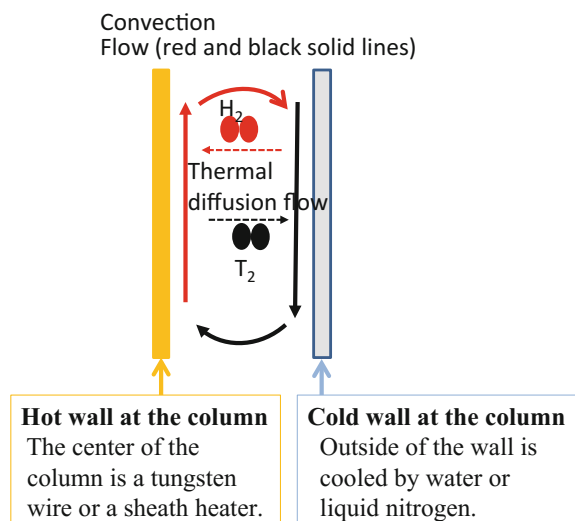
## 11.6 Other Isotope Separation Method

An isotope separation system is also needed to remove and recover T in exhausts from any T handling facilities. Although the cryogenic distillation system seems the best for the fuel cycle system for its capability to handle large T flow rate, it is complicated and expensive. For smaller flow rates, there could be several other

methods. A gas chromatography method which is often used to analyze hydrogen isotopes is a promising one. Although it cannot be operated continuously and is difficult to handle a large flow rate in its single column use, the flow rate can be increased to several times by using a large column and/or multiple columns. Some basic studies have been carried out to apply this method to the hydrogen isotope separation [17, 18].

Thermal diffusion column can be also a possible isotope separation system. The structure of the column is quite simple and can be operated continuously. Figure 11.8 shows a conceptual structure of the column. A heavier isotope such as T moves to a cold wall, and a lighter isotope such as H moves to a hot wall because of the difference in their thermal diffusivity. Within the column, there is a convective flow caused by thermal gradient. The heavier isotope is accordingly enriched to the bottom of the column, and the lighter isotope is enriched to the top of the column. The column was first developed to separate uranium isotopes [19]. A large difference in the thermal diffusivity among hydrogen isotopes gives much larger separation factor compared to the uranium separation. Yamamoto et al. [20] have studied the thermal diffusion column in detail. They have developed a two-dimensional simulation model for the column [20]. From their study, it has been pointed that the separation factor of the column can be increased by using a larger diameter hot wall (for instance, a sheath heater). We can also get a larger separation factor by cooling the outside of the column wall to liquid nitrogen temperature. They have achieved quite large separation factor in H/D or H/T separation with a typical flow rate of  $10 \text{ cm}^3/\text{min}$  for the thermal diffusion column by using the above modifications of the column.

**Fig. 11.8** Conceptual structure of thermal diffusion column



## References

1. Y. Iwai et al., *Fusion Eng. Des.* **61–62**, 553–556 (2002)
2. M. Glugla et al., *Fusion Eng. Des.* **82**, 472–487 (2007)
3. E.W. Thiele et al., *Ind. Eng. Chem.* **25**, 28–32 (1983)
4. M. Kinoshita, PhD Dissertation, Kyoto University, 1983
5. M. Kinoshita, *Fusion Technol.* **6**, 574–579 (1984)
6. T. Yamanishi et al., *J. Chem. Eng. Jpn.* **26**, 1–6 (1992)
7. T. Yamanishi et al., *J. Nucl. Sci. Technol.* **31**, 562–565 (1994)
8. T. Yamanishi et al., *J. Nucl. Sci. Technol.* **34**, 375–380 (1997)
9. P.C. Souers, *Cryogenic Hydrogen Data Pertinent to Magnetic Fusion Energy*, Lawrence Livermore National Laboratory Report, UCRL-52628 (1997), Livermore, Calif. 94550 (1979)
10. J.R. Bartlit et al., *Cryogenics* **19**, 275–278 (1979)
11. W. R. Wilkes, MLM-2502 (1978)
12. T. Yamanishi et al., *Fusion Eng. Des.* **10**, 319–322 (1989)
13. T. Yamanishi et al., *Fusion Technol.* **20**, 419–423 (1991)
14. T. Yamanishi et al., *Fusion Technol.* **21**, 948–952 (1992)
15. T. Yamanishi et al., *Fusion Technol.* **14**, 489–494 (1988)
16. Y. Iwai et al., *Fusion Eng. Des.* **61**, 553–556 (2003)
17. E.H. Carter et al., *J. Phys. Chem.* **67**, 1512–1516 (1963)
18. H. Frischmuth et al., Fifth Topical Meeting on the Technology of Fusion Energy, Knoxville, April 26–28, 1983
19. W.M. Rutherford et al., *Fusion Technol.* **8**, 2778–2881 (1985)
20. I. Yamamoto et al., *J. Nucl. Sci. Technol.* **27**, 631–636 (1990)

# Chapter 12

## Evaluation Method of Tritium Breeding Ratio Using Neutron Transport Equation

Hideaki Matsuura and Masabumi Nishikawa

**Abstract** The breeding blanket is the only place to produce tritium (T) in a fusion reactor. It is necessary to recover bred T in the blanket effectively because no T in the natural resources is usable as the fuel in a fusion reactor. Fortunately, T can be produced by the reaction between neutron and lithium in the blanket placed surrounding the fusion chamber with. The T breeding ratio attainable in the blanket should be large enough to cover whole T consumed for steady operation of a fusion reactor. In this chapter, T breeding in a blanket zone and the evaluation method of the T breeding ratio are introduced.

**Keywords** Tritium breeding ratio · Neutron transport · Simulation · Neutron flux · Plasma zone · Blanket zone · Neutron multiplier

### 12.1 Roles of Blanket and Importance of Slowing-Down and Multiplication of Fusion Neutrons

For a D-T thermonuclear fusion reactor to be energy source, “blanket” plays critical roles, i.e., energy carried by neutrons produced by fusion reactions is converted into heat and, at the same time, the neutrons react with a tritium (T) breeding material to breed T fuel. Because of limited resources of T, attaining fuel self-sufficiency is “must” for steady operation of the reactor as the energy source.

In D-T fusion, two fusion reactions occur as:



---

H. Matsuura (✉)

Department of Applied Quantum Physics and Nuclear Engineering,  
Kyushu University, 744 Motooka, Fukuoka 819-0395, Japan  
e-mail: mat@nucl.kyushu-u.ac.jp

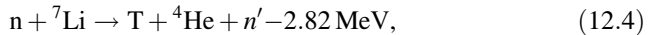
M. Nishikawa

Department of Advanced Energy Engineering Science, Kyushu University,  
6-1 Kasuga-Koen, Kasuga-Shi, Fukuoka 816-8580, Japan



They are referred as the D-T reaction ( $T(d, n){}^4He$ ) and the D-D reaction ( $D(d, n){}^3He$ ), respectively. Neutrons produced by the two reactions initially have 14 and 2.5 MeV, respectively, for the D-T and D-D reactions (they are referred as D-T neutrons and D-D neutrons, respectively), and travel into the blanket to deposit their energy as heat. Hence, effective energy conversion from the kinetic energy of the neutrons into heat, i.e., slowing-down process of the neutrons in the blanket is critically important for power production. It should be noted that the reaction cross section is nearly 100 times larger for the D-T reaction than the D-D reaction, or the number of neutrons produced by the latter is less than 1 % of the total production. Therefore, the D-T neutrons dominate in both T breeding and heat generation.

During the slowing-down process, the neutrons react with a T-breeding material, mostly lithium (Li), to generate T. Natural Li includes both  ${}^6Li$  (7.5 %) and  ${}^7Li$  (92.5 %) and both generate T as:



where  $n'$  represents a neutron generated from the compound nucleus intermediately formed by the  $n + {}^7Li$  nuclear reaction, i.e., the energy of  $n'$  is different from that of the source neutron  $n$ . The reaction cross sections for the above reactions are significantly changed with neutron energy as shown in Figs. 12.1 and 12.2, for reactions (12.3) and (12.4), respectively. The cross section of the former is much

**Fig. 12.1** Cross section for  ${}^6Li(n, \alpha)T$  reaction as a function of neutron energy in the laboratory system (taken from JENDL-4.0)

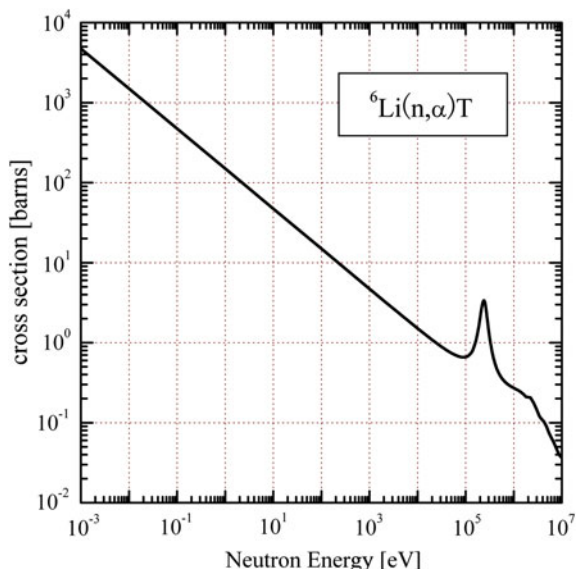
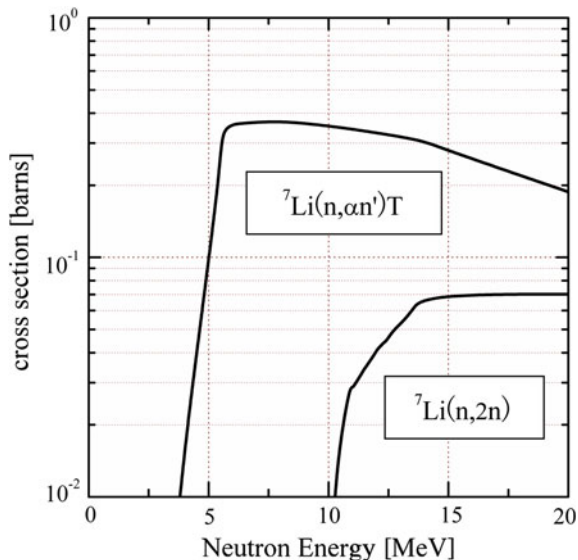


**Fig. 12.2** Cross sections for  ${}^7\text{Li}(\text{n}, \alpha\text{n})\text{T}$  and  ${}^7\text{Li}(\text{n}, 2\text{n})$  reactions as a function of neutron energy in the laboratory system (taken from JENDL-4.0)



larger than that of the latter, while the abundant ratio is opposite. Therefore, using  ${}^6\text{Li}$ -enriched one as the breeder is optional. It should be noted that the cross section of the reaction (12.3) increases with decreasing the neutron energy reaching nearly a thousand barn for thermal (0.025 eV) neutrons. In this respect, the slowing down is favored. On the other hand, the reaction (12.4) occurs only with neutrons having energies above  $\sim 3$  MeV (referred as a threshold reaction) and its reaction cross section is higher for higher neutron energy. Furthermore, neutrons with energy of more than 10 MeV induces another reaction referred as a neutron multiplication reaction ( $\text{n}, 2\text{n}$ ) with  ${}^7\text{Li}$  nucleus (see Fig. 12.2).

It should be noted that in the reactions (12.3) and (12.4), basically one T is generated by consuming one neutron. Since one T is burned in a D-T fusion reaction to produce one neutron, the fuel self-sufficiency is not attained owing to T loss by its decay with 5 %/year and any loss in recovery process of bred T. Therefore, multiplication of neutrons is required. To do this, we introduce neutron multipliers such as  ${}^9\text{Be}$  and  $\text{Pb}$  in the blanket. There exist many possible channels for the neutron multiplication, i.e.,  $(\text{n}, 2\text{n})$  reactions, for example:



Neutron energy dependence of these reaction cross sections are shown, respectively, in Figs. 12.3 and 12.4 which are taken from ENDF/B-VII.1 [1] and JENDL-4.0 [2], respectively. The both reactions are the threshold reactions, and neutrons with more than  $\sim 2.5$  MeV ( ${}^9\text{Be}$ ) and  $\sim 7$  MeV ( ${}^{208}\text{Pb}$ ) energy can

**Fig. 12.3** Cross section of  $(n, 2n)$  reactions for  $^{9}\text{Be}$  target as a function of neutron energy in the laboratory system (taken from ENDF/B-VII.1)

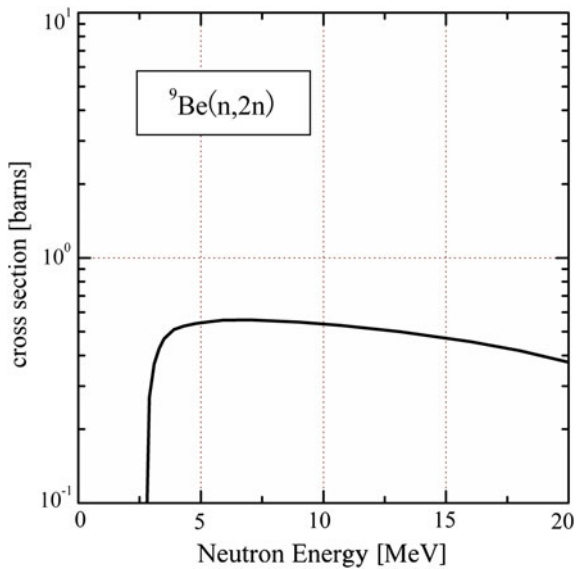
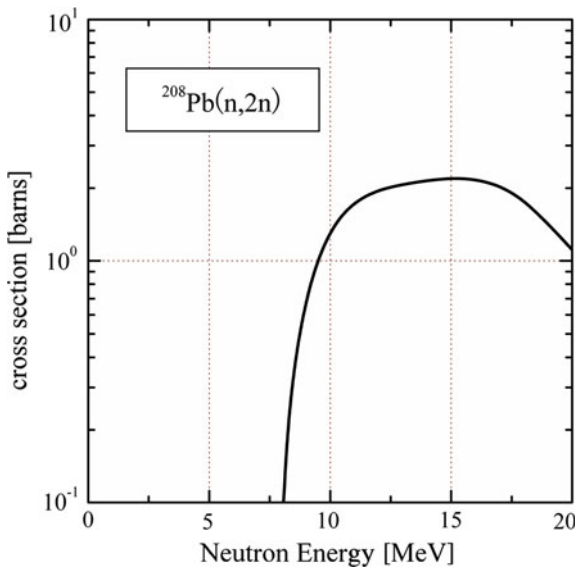


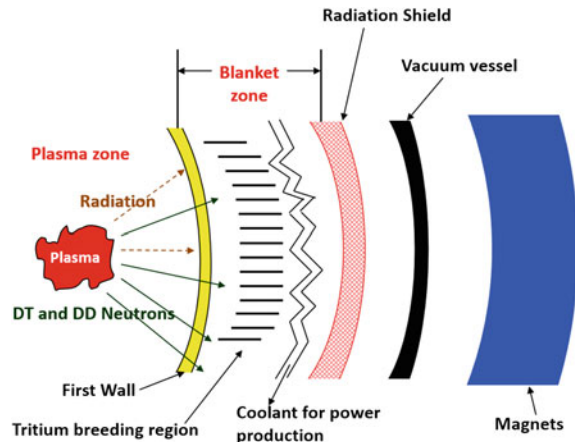
**Fig. 12.4** Cross section of  $(n, 2n)$  reaction for  $^{208}\text{Pb}$  target as a function of neutron energy in the laboratory system (taken from JENDL-4.0)



multiply neutrons. It should be noted that the D-D neutrons with their energy less than 2.5 MeV hardly contribute to the neutron multiplications.

As such, energy of neutrons plays the critical role on T breeding. In order to realize the self-sufficiency in T breeding and high efficiency in energy conversion simultaneously, both selection of components (breeding materials, neutron multipliers, coolant, and structure materials) and geometrical structure of blanket

**Fig. 12.5** Schematic view of the reactor system



including its reactor coverage must be optimized. To do this, we have to clarify (1) slowing-down process, starting from neutron produced in the reactor core with the highest energy, penetrating into blanket through first wall, (2) loss or multiplication during the slowing-down process, and (3) accompanied heat generation and T production. The schematic view of the reactor system is shown in Fig. 12.5. In this chapter, at first methodology to do this (neutron transport equation adopted to a fusion reactor system with Li as the main breeding material) is introduced, and followed how T breeding changes with blanket design (of course the blanket design depends on the plasma design). Finally, possible breeding rates in a reactor are discussed.

## 12.2 The Neutron Transport Equation

To evaluate the performance of T breeding in a blanket zone, we have to know how many  $n + {}^6\text{Li}$  (12.3) and  $n + {}^7\text{Li}$  (12.4) reactions occur per neutron injected into the blanket area as a function of position  $\vec{r}$  in it. To know this, we have to grasp how many neutrons exist per unit volume with energy  $E$  at the position  $\vec{r}$ . The neutrons slow down and react with Li in the blanket zone, but most of them are initially produced in the plasma zone with spatial profile and with various directions. Sometimes the neutron emission spectrum can be changed from Gaussian distribution and, especially in a torus device, both of the intensity and incident angle distribution to the first wall depend on positions at the first wall. To accurately grasp the comprehensive performance of the fusion blanket in a fusion device and to design the plasma and blanket system, it is desirable that three-dimensional neutron transport analysis is carried out including both plasma and blanket regions. In this chapter, we consider the neutron behavior in both plasma and blanket zones (see Fig. 12.6). The number of neutrons in the volume element  $dV$  at a position,  $\vec{r}$ ,

**Fig. 12.6** Schematic view of the slow-down process of neutrons in plasma and blanket zones

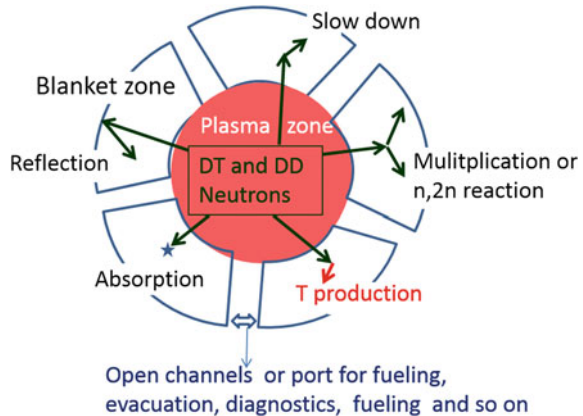
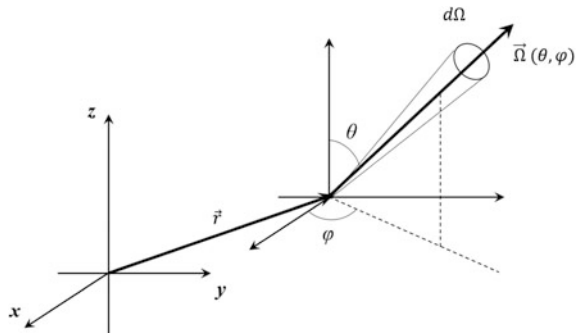


**Fig. 12.7** Coordinates of position and direction of motion of a neutron



moving to directions within  $d\Omega$  about  $\vec{\Omega}$  and having energies in  $dE$  about  $E$  at time  $t$  can be expressed as  $N(\vec{r}, E, \vec{\Omega}, t)dV dE d\Omega$ , using a physical scalar quantity  $N(\vec{r}, E, \vec{\Omega}, t)$  which is called “angular neutron density.” Here,  $\vec{\Omega}$  is a unit vector in the moving direction;  $\vec{v} = |\vec{v}|\vec{\Omega}$ . In Fig. 12.7, coordinates of the neutron position and the moving direction are indicated. Here, the element of solid angle  $d\Omega$  can also be written using the angles in the spherical coordinate  $\theta$  and  $\phi$  as  $d\Omega = \sin \theta d\theta d\phi$ . The angular neutron flux  $\Phi(\vec{r}, E, \vec{\Omega}, t)$  is defined as the product of  $|\vec{v}|$  and  $N(\vec{r}, E, \vec{\Omega}, t)$ , i.e.,  $\Phi(\vec{r}, E, \vec{\Omega}, t) \equiv |\vec{v}|N(\vec{r}, E, \vec{\Omega}, t)$ , which implies probable number of neutrons flowing toward the direction of  $\vec{\Omega}$  per unit area at the position  $\vec{r}$  with the energy  $E$  (or speed  $|\vec{v}|$ ) at time  $t$  per unit solid angle per unit energy per unit time. The equilibrium angular neutron flux can be determined by solving the following steady-state Boltzmann transport equation.

$$\vec{\Omega} \cdot \nabla \Phi(\vec{r}, E, \vec{\Omega}) + \Sigma_i \Phi(\vec{r}, E, \vec{\Omega}) = \int \Sigma_s(\vec{r}; E' \rightarrow E, \vec{\Omega}' \rightarrow \vec{\Omega}) \Phi(\vec{r}, E', \vec{\Omega}') dE' d\vec{\Omega}' + S(\vec{r}, E, \vec{\Omega}) . \quad (12.7)$$

The equation describes the balance of the number of neutrons, which are contained in the unit phase space element centered at  $\vec{r}$  and  $E$  at time  $t$ , i.e., each term has a dimension of neutrons/s/cm<sup>3</sup>/eV/sr. In the following discussion, we refer each term in Eq. (12.7) as a circled number written below the equation. They respectively represent the following:

- ① The net number of neutrons flowing out from the unit phase space element per unit time, due to streaming of the neutrons with velocity  $\vec{v} = |\vec{v}|\vec{\Omega}$ .
- ② The disappearance rate of neutrons due to (a) absorption and (b) scattering reactions per unit phase space element.
  - (a) neutron disappearance rate due to absorption reactions by background nuclei.
  - (b) neutron outflow rate due to scattering by background nuclei [the scattering accompanies the change of neutron energy].
- ③ The number of neutrons coming into the unit phase space element centered at  $E$  per unit time as a result of scattering with the background nuclei from the other velocity region. Some neutrons are coming into the unit phase space element centered at  $E$  losing (or obtaining) their energy due to the scattering with the background nuclei.
- ④ The neutron production rate due to the D-T and D-D fusion reactions in the plasma and the neutron multiplication, e.g., ( $n, 2n$ ), reactions, in the blanket area. The fusion neutron source does not depend on the angular neutron flux, but the neutron source due to the neutron multiplication reaction is a function of the angular neutron flux itself.

Here  $\Sigma_t$  in term ② represents the macroscopic total cross section in which all kinds of scattering and absorption reactions are included.  $\Sigma_s(E' \rightarrow E, \vec{\Omega}' \rightarrow \vec{\Omega})$  in term ③ can be expressed as a product of the macroscopic scattering cross section  $\Sigma_s(\vec{r}, E')$  and the probability density function  $P(E' \rightarrow E, \vec{\Omega}' \rightarrow \vec{\Omega})$  as  $\Sigma_s(\vec{r}, E' \rightarrow E, \vec{\Omega}' \rightarrow \vec{\Omega}) = \Sigma_s(\vec{r}, E')P(E' \rightarrow E, \vec{\Omega}' \rightarrow \vec{\Omega})$ . The probability density function  $P$  implies the probability for the neutron moving toward the direction  $\vec{\Omega}'$  with energy  $E'$  changing its direction to  $\vec{\Omega}$  and energy to  $E$  as a result of a scattering event. The probability density function  $P$  satisfies the following condition;

$$\int P(E' \rightarrow E, \vec{\Omega}' \rightarrow \vec{\Omega}) dE d\Omega = 1, \quad (12.8)$$

and can be obtained via complicated classical kinetics calculation as a function of scattering angle in the center of mass system. In Monte Carlo simulations, the scattering angle can be determined by generating random numbers in a computer, referring to the differential cross sections as a weight function. When the scattering

**Table 12.1** Physical Quantities

Cross section (microscopic cross section)	$\sigma$	$\text{cm}^2$
Macroscopic cross section	$\Sigma$	$\text{cm}^{-1}$
Reaction rate in unit volume	$R$	$\text{cm}^{-3}\text{s}^{-1}$
Unit vector in the direction of motion	$\vec{\Omega}$	—
Angular neutron density	$N(\vec{r}, E, \vec{\Omega}, t)$	$\text{cm}^{-3} \text{eV}^{-1} \text{sr}^{-1}$
Angular neutron flux	$\Phi(\vec{r}, E, \vec{\Omega}, t)$	$\text{cm}^{-2} \text{s}^{-1} \text{eV}^{-1} \text{sr}^{-1}$
Differential cross section	$\Sigma_s(E' \rightarrow E, \vec{\Omega}' \rightarrow \vec{\Omega})$	$\text{cm}^{-1} \text{eV}^{-1} \text{sr}^{-1}$
Probability density function	$P(E' \rightarrow E, \vec{\Omega}' \rightarrow \vec{\Omega})$	$\text{eV}^{-1} \text{sr}^{-1}$
Neutron number density	$n$	$\text{cm}^{-3}$
Reaction rate coefficient	$\langle \sigma v \rangle$	$\text{cm}^3 \text{s}^{-1}$

is isotropic in the center of mass system, the probability density function  $P$  can be reduced into the following simple form:

$$P(E' \rightarrow E) = \begin{cases} \frac{1}{(1-\alpha)E'} & \alpha E' < E < E' \\ 0 & \text{others} \end{cases}, \quad (12.9)$$

where  $\alpha \equiv [(A - 1)/(A + 1)]^2$ . Here, “ $A$ ” represents the mass number of a neutron colliding nuclei. Physical quantities used in the neutron transport equation and evaluation of T amount produced are summarized in Table 12.1.

The solution of the Boltzmann transport equation  $\Phi(\vec{r}, E, \vec{\Omega})$  should be obtained so as to satisfy both conservation of the number of neutrons and their power balance with sufficient accuracy. If we simply integrate Eq. (12.7) overall the six-dimensional phase space, we can obtain the conservation equation for the number of neutrons in the plasma and blanket zones. In this case, two terms obtained by integrating term ②-(b) and term ③ are canceled out with each other. A term obtained by integrating term ① represents the loss rate of the neutrons from the plasma and blanket zones, and a term obtained by integrating ②-(a) denotes the loss rate of the neutrons by the neutron absorption reactions, e.g.,  $n + {}^6\text{Li}$  reaction. The total loss rate of neutrons obtained by adding the integrated terms ① and ②-(a) must be equal to the neutron production rate obtained by integrating term ④.

On the other hand, if we integrate Eq. (12.7) after multiplying energy  $E$  overall the six-dimensional phase space, an equation giving the power balance in the plasma and blanket zones can be obtained. In this case, the power obtained by subtracting the term ②-(b) from ③ represents the deposited power from energetic neutrons to blanket materials, e.g., coolant, structural and T-breeding materials. Integrated power lost from the plasma and blanket zones (given by integration of ①), by neutron absorption reactions [given by integration of ②-(a)] and by deposition into blanket materials equal to the source power (given by integration of ④) by fusion and neutron multiplication reactions. In order to satisfy the power balance equation and to establish the equilibrium state in the system, the deposited power

must be removed by coolants, thus additional equation to consider the power balance for blanket system should be solved simultaneously with the neutron transport equation, i.e., Eq. (12.7), to design the system.

In a burning plasma, the angular fluxes of plasma ions would be obtained by solving similar Boltzmann-type equations, e.g., the Fokker-Planck equation, for each ion specie considering interactions with background plasma ions and electrons. The equations must be solved for every ion species. In such case, the background plasma condition is constantly changed, and the equations are essentially nonlinear retaining interactions between the same ion species. For neutron transport problems in a blanket zone, on the other hand, we usually solve the Boltzmann equation only for neutrons, assuming energy of the background nuclei are considerably low (they are approximately standstill with small thermal motions) compared with averaged neutron energy. In addition, the density of neutrons is much smaller compared with those of the background nuclei, and thus the interactions between the neutrons are usually neglected. In such neutron transport simulation in the plasma and blanket zones, it is necessary to determine what kind of background nuclei (materials) exist in which position with how much energy (temperature). In other words, detailed information for all components in the blanket zone is required in advance to make accurate evaluation of the amount of T produced.

To solve neutron transport equations, the Monte Carlo simulation method is a powerful tool. In the simulation, a certain number of neutrons are generated as test particles corresponding to the probability density for the specified space, energy, time, and then they start random walk obeying the physical laws between the neutron and background nucleus. The neutron behaviors in each event during interactions with background nucleus are determined using random numbers so that it satisfies physical laws. To perform the simulation, as mentioned before, spatial distribution of background nuclei which interact with neutrons, i.e., shape, position, and composition of each material, density, temperature of each materials, must be exactly set in the calculation space according to the blanket zone designed. In addition, adequate boundary conditions must be adopted. For the simplest case, either perfect reflection, i.e., neutrons are reflected with the same reflection angle as incident angle or no reflection is employed at the boundary of the blanket zone. By collecting the information from the large number of histories for each neutron behavior, we can estimate physical quantities, i.e., solution of the neutron transport equation, statistically.

In the simulation, determined physical quantities always involve statistical uncertainties. To decrease the statistical uncertainties, the number of source neutrons must be increased to confirm the results converging, while this increases computational CPU time and requires optimization.

### 12.3 Tritium Production Rate and Heat Generation in Blanket Zone

By solving the Boltzmann neutron transport equation, we can obtain the angular neutron flux. Then using the angular neutron flux, we can evaluate the reaction rates for all of the neutron absorption reactions as well as the deposited power from the neutrons to background nuclei in the blanket zone. One of the most concerned physical quantities would be a T production rate. The reaction rates  $R_T(^6\text{Li})$  for  $n + ^6\text{Li}$  reaction (12.3) and  $R_T(^7\text{Li})$  for  $n + ^7\text{Li}$  reaction (12.4) are related to the angular neutron flux as:

$$R_T(^6\text{Li}) \equiv \int \Sigma_{^6\text{Li}} \Phi(\vec{r}, E, \vec{\Omega}) dE d\Omega d\vec{r}, \quad (12.10)$$

$$R_T(^7\text{Li}) \equiv \int \Sigma_{^7\text{Li}} \Phi(\vec{r}, E, \vec{\Omega}) dE d\Omega d\vec{r}, \quad (12.11)$$

where

$$\Sigma_{^6\text{Li}} = n_{^6\text{Li}}(\vec{r}) \sigma_{^6\text{Li}}(E), \quad (12.12)$$

$$\Sigma_{^7\text{Li}} = n_{^7\text{Li}}(\vec{r}) \sigma_{^7\text{Li}}(E), \quad (12.13)$$

respectively. Here,  $\Sigma_{^6\text{Li}}$ ,  $\Sigma_{^7\text{Li}}$  are the macroscopic cross sections for  $n + ^6\text{Li}$  (12.3) and  $n + ^7\text{Li}$  (12.4) reactions, and  $n_{^6\text{Li}}$ ,  $n_{^7\text{Li}}$  are the number densities of  $^6\text{Li}$  and  $^7\text{Li}$  nuclei in the blanket zone, respectively.

It should be noted that the  $n + ^6\text{Li}$  reaction produces energy as shown in Eq. (12.3) in the form of the kinetic energy of alpha particle and T produced. The energy generated by  $n + ^6\text{Li}$  reactions per unit time and unit volume,  $W(^6\text{Li})$ , is written as:

$$W(^6\text{Li}) \equiv Q_{^6\text{Li}} \int \Sigma_{^6\text{Li}} \Phi(\vec{r}, E, \vec{\Omega}) dE d\Omega d\vec{r}, \quad (12.14)$$

where  $Q_{^6\text{Li}}$  is 4.78 MeV. There are many kinds of energy production reactions depending on materials used as structural and coolant in the blanket zone. Here, it should be noted that there are endoergic reactions such as the  $n + ^7\text{Li}$  (12.4) reaction. The energy gain per a Li nucleus is determined depending on the ratio of the reaction rates given by Eqs. (12.10) and (12.11). The ratio depends on neutron flux and  $^6\text{Li}$  enrichment in Li used (macroscopic cross sections). When 100 %  $^6\text{Li}$ -enriched Li compound is used, the energy gain per a Li nucleus would be 4.78 MeV (if a small amount of  $^7\text{Li}$  production by neutron-Be reaction is neglected). When natural abundant Li is assumed, i.e., 7.5 %  $^6\text{Li}$  enrichment, the energy gain would become -1.9 MeV if the same reaction rates for  $^6\text{Li}$  and  $^7\text{Li}$  reactions per a Li are assumed. In addition, to accurately evaluate the heat generation, energy

production via  $(n, \gamma)$  reactions should also be considered. When neutrons with large kinetic energy compared with thermal energy react with breeding materials, their initial kinetic energy should be reflected in the evaluation of the total heat generation by considering the non-Gaussian energy spectrum of the produced nuclei. In order to more precisely evaluate the heat generation in the blanket zone, we should keep in mind that neutron irradiation causes nuclear transmutation of some constituent elements of structural materials resulting unstable nuclei (radio isotopes). Such radio isotopes continuously release energy via radioactive decay process and contribute to the heating power. In a reduced activation ferritic–martensitic steel (RAFM), which is a candidate structure material of a fusion reactor,  $^{56}\text{Mn}$  ( $T_{1/2} = 2.58$  h) is one of the dominant activated species releasing 3.7 MeV energy by each  $\beta$  decay. In W to be used as armors of divertor,  $^{187}\text{W}$  ( $T_{1/2} = 23.7$  h) would be an important nucleus (1.3 MeV energy is released by each  $\beta$ -decay) [3]. We cannot artificially control the release energy nor decay lifetime of the radioisotopes, and the release of their decay heat continues even after the reactor shutdown, which concerns safety.

## 12.4 Tritium Breeding Ratio and Blanket Design

One of the most important parameters to describe the performance of T breeding in a blanket system is the tritium breeding ratio (TBR). TBR can be defined as the ratio of a T production rate in the blanket zone to a T consumption rate in the plasma zone. The T consumption or burning rate in whole plasma region of a D-T reactor can be written as:

$$R_{\text{DT}} = \int n_{\text{D}} n_{\text{T}} \langle \sigma v \rangle_{\text{DT}} d\vec{r}, \quad (12.15)$$

where  $\langle \sigma v \rangle_{\text{DT}}$  is the reaction rate coefficient of the D-T reaction. If we assume the Maxwellian distribution for velocities of D and T,  $\langle \sigma v \rangle_{\text{DT}}$  is a function of only the plasma temperature (see Chap. 4). Since fuel ion density and plasma temperature have a space profile in the confined plasma, the D-T reaction rate in whole plasma region (12.15) is a function of the position  $\vec{r}$ . The detail of the fuel consumption is described in Chap. 4.

From Eqs. (12.10), (12.11), and (12.15), TBR can be defined as:

$$\text{TBR} \equiv \frac{R_{\text{T}}(^6\text{Li}) + R_{\text{T}}(^7\text{Li})}{R_{\text{DT}}} = \frac{\sum_i \int \Sigma_i \Phi(\vec{r}, E, \vec{\Omega}) dE d\Omega d\vec{r}}{\int n_{\text{D}} n_{\text{T}} \langle \sigma v \rangle_{\text{DT}} d\vec{r}}, \quad (12.16)$$

which is usually referred as “net TBR” for a reactor as a whole, while “local TBR” is defined in the following.

It should be noted that neutron flux at the first wall is not homogeneous and changes with locations in a tokamak-type reactor with a torus-shaped vacuum vessel. At the midplane of the torus or the equatorial plane including the toroidal axis (center of the plasma), the neutron flux is the highest and decreases poloidally to both the top and the bottom directions. This is mainly because that plasma volume which comes into the view is different depending on the toroidal position of the first wall. Because of limited abilities of heat removal by coolant and fixed surface area of a local blanket module, higher heat load requires larger volume of cooling equipment and accordingly, the TBR tends to decrease. Thus, TBR changes with the location and we call TBR at the specific location as “local TBR”. Because the T consumption rate equals to the 14-MeV neutron production rate, the local TBR can be simply evaluated as

$$\text{local TBR} \approx \frac{\sum_i \int_{V_{\text{local}}} \Sigma_{^i\text{Li}} \Phi(\vec{r}, E, \vec{\Omega}) dE d\Omega d\vec{r}}{\int_{S_{\text{local}}} \Phi_{14}(\vec{r}, E, \vec{\Omega}) dE d\Omega dS}, \quad (12.17)$$

where  $S_{\text{local}}$  represents a specific area of a T breeding blanket exposed to certain flux of the 14-MeV neutrons and  $V_{\text{local}}$  is the local volume underneath in the blanket where T is produced (via both  $n + {}^6\text{Li}$  and  $n + {}^7\text{Li}$  reactions) by the incoming neutrons. The denominator in Eq. (12.17) means the surface integral over  $S_{\text{local}}$ . Here,  $\Phi_{14}(\vec{r}, E, \vec{\Omega})$  represents the angular neutron flux formed only by the fusion (D-T reaction) source component.

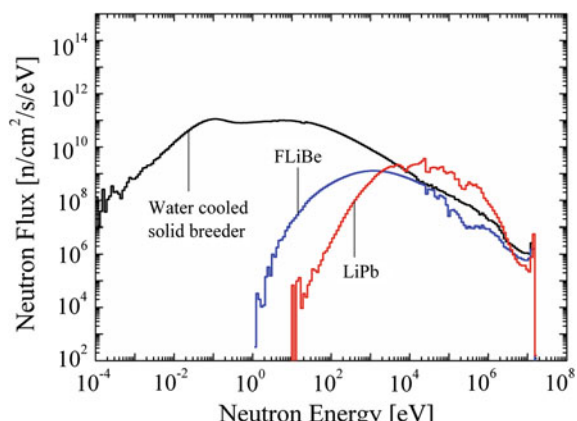
In addition, there are many ports on the first wall for installation of diagnosing apparatuses, plasma heating and fueling equipment, and divertor, where T cannot be produced, i.e., the local TBR becomes zero. Therefore, increasing blanket coverage or “coverage ratio” (fraction of the surface area of the T breeding blanket to all surface area of the surrounding vacuum vessel) is quite important to increase the net TBR. In a fusion reactor, the coverage ratio is likely to be  $0.8 \sim 0.9$ . If we consider frames and ribs of the blanket modules and a gap between the modules, the ratio may be further reduced [4]. (On the other hand, in inertial confinement fusion, the coverage ratio could be nearly  $\sim 1.0$ .) For example, in a typical design of a DEMO reactor, i.e., SlimCS [4], the local TBR is evaluated from  $\sim 1.33$  to  $\sim 1.56$  depending on the neutron wall load. Assuming 85 % of the coverage of the blanket with the local TBR given above and 95 % of the T recovery rate, the net TBR becomes 1.07–1.26. Therefore, the net TBR of above  $\sim 1.05$  to compensate T decay would be achievable. Nevertheless, significant improvement in blanket design and T recovery are required to attain the net TBR over  $\sim 1.05$  in a reactor. (See Chap. 3)

“Slowing-down” and “multiplication” of fusion-produced neutrons in the blanket zone change with selections of component of the blanket, neutron moderators, multipliers, coolant, and T breeding materials. As one of the promising blanket systems, a solid breeder blanket system with water as coolant,  $\text{Li}_2\text{TiO}_3$  as a T breeder, and  ${}^9\text{Be}$  as a neutron multiplier, has been developed [4]. In the

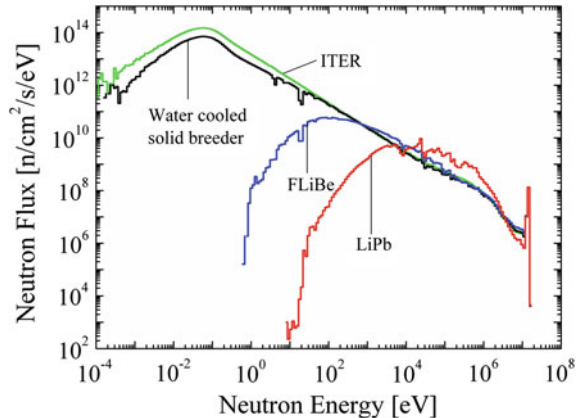
water-cooled solid blanket system, the water plays two important roles as neutron moderator and coolant. To improve TBR, a high-performance blanket design using beryllides ( $\text{Be}_{12}\text{W}$ ,  $\text{Be}_{12}\text{Ti}$ , and  $\text{Be}_{12}\text{V}$ ) as mixed pack with a T breeding material has been proposed [5]. As another promising candidate, a liquid lithium and Pb blanket system has also been investigated [6]. In this system, Pb and Li are chosen as the neutron multiplier and T breeding material, respectively, and an alloy of  $\text{Li}_{0.17}\text{-Pb}_{0.83}$  is adopted. In this system, either helium gas cooling or self-cooling with the liquid Li-Pb is employed. Since the neutron slowing-down performance of Pb is inferior to that of water, the total volume of the liquid Li-Pb blanket system to obtain the same TBR as the water-cooled solid breeder blanket tends to be larger, while the structure of the blanket system of the former can be simplified compared with the latter. A blanket system using FLiBe ( $\text{LiF}-\text{BeF}_2$ ) as neutron multiplier and T breeder has also been studied [7, 8]. In this system, helium gas is a candidate coolant. The system can be simplified as that of the Li-Pb blanket system, and the neutron moderation performance is higher than the Li-Pb blanket to some extent. However, introduction of additional neutron multiplier, e.g., Be, would be required to improve the T breeding performance to be in a comparable level with other blanket systems.

Figure 12.8 compares typical neutron fluxes at the blanket zone (T breeding region) calculated with the above-described method for three blanket systems, i.e., (a) a water-cooled solid breeder blanket ( $\text{Li}_2\text{TiO}_3$  with  $\text{Be}_{12}\text{Ti}$ ), (b) a Li-Pb blanket and (c) a FLiBe (with additional Be metal) blanket. In the calculation, the neutron wall load was fixed as  $2 \text{ MW/m}^2$ , and the volume of the blanket zone was determined so that the “local TBR” becomes the same value, i.e., 1.45. The calculation was made using the continuous energy Monte Carlo neutron transport code MVP [9]. One can see that in the Li-Pb blanket fraction of energetic neutrons in the neutron spectrum is larger than that of the other blanket systems. On the contrary, neutrons in the water-cooled solid breeder blanket are well moderated. This is because that the neutron moderation performance of water is superior to that of Pb. For the Li-Pb blanket, the required volume of the blanket zone to attain the same

**Fig. 12.8** Typical neutron flux at the blanket zone calculated with MVP code for (a) water-cooled solid breeder ( $\text{Li}_2\text{TiO}_3$  with  $\text{Be}_{12}\text{Ti}$ ), (b) Li-Pb and (c) FLiBe (with additional Be metal) blanket systems



**Fig. 12.9** Typical neutron flux at the plasma zone calculated with MVP code for (a) water-cooled solid breeder ( $\text{Li}_2\text{TiO}_3$  with  $\text{Be}_{12}\text{Ti}$ ), (b) Li-Pb and (c) FLiBe (with additional Be metal) blanket systems. The results are compared with the one for ITER shielding blanket [10]



TBR increases and for the water-cooled solid breeder blanket, the required volume becomes small. This is because the T production rate of the  $n + {}^6\text{Li}$  reaction becomes large in the well-moderated neutron spectrum (see Fig. 12.5). The typical neutron fluxes at the plasma zone of the fusion reactor with breeders of (a) the water-cooled solid, (b) Li-Pb, and (c) FLiBe are exhibited in Fig. 12.9. The neutron flux at the plasma zone includes the slowing-down and produced neutrons in the blanket zone. All conditions used for the calculation are the same as those in Fig. 12.8. Since there are no thermal neutron absorption reactions at the plasma zone, thermal component in the neutron spectrum for each blanket system becomes larger compared with those given in Fig. 12.8. For reference, the neutron spectra of one typical ITER shielding blanket are given in Fig. 12.9, which is evaluated for the same wall load. Since the blanket designed for ITER contains cooling water layer [10], the neutron spectrum in the plasma zone is almost similar as the one for water-cooled solid breeding blanket.

As shown in Figs. 12.8 and 12.9, different blanket systems have clearly different neutron fluxes at the blanket zone depending on their constructions. In order to increase TBR, we have to optimize materials selection and combination of T breeding materials and neutron multipliers, and structural design of the blanket system. At the same time, it is necessary to consider the heat removal performance (the heat energy is produced by various kinds of nuclear reactions, decay heat, and deposited (slowing down) neutron energy). With the current blanket design for DEMO, the local TBR of  $\sim 1.33$  to  $\sim 1.56$  and the net TBR of  $\sim 1.05$  seem attainable [4]. However, the net TBR of 1.05 might not compensate the loss by T decay ( $\sim 5\%$  per year). Therefore, in addition to appropriate materials selection, increase in the heat removal capability and/or decrease in heat load by changing reactor design, e.g., reducing thermal output power or increasing surface area of the first wall (coverage ratio), are important as explained in the former paragraph.

## 12.5 Summary

T production efficiency in a breeding blanket consists of the efficiency in neutron usage for T production with  $n + Li$  reaction and the efficiency in recovery process of bred T from the Li compounds. In this chapter, T breeding in the blanket by neutrons produced by D-T reactions is mainly discussed. To describe behavior of the neutron in the blanket, the Boltzmann-type neutron transport equation is introduced and solved numerically to evaluate TBR (tritium breeding ratio).

Methods to solve the Boltzmann transport equation and obtain the angular neutron flux have been developed for analyzing neutron transport in a fission reactor. Various techniques to solve the neutron transport equation were investigated, and simulation codes have been developed. The codes were validated by comparing with experimental data. In fusion blanket systems, as was described in this chapter, neutron production and multiplication are the main topics in the simulation, and those codes developed for fission were modified to include T production in fusion blanket systems. Referring typical neutron fluxes emitted from D-T burning core, neutron transport, and consequent tritium production and neutron multiplication in some blanket systems were simulated. Since the neutron flux at the blanket zone is varied depending on constructions of a blanket system, complete information for all components and geometrical structure of the blanket system are required for the evaluation of TBR with the simulation of neutron transport. Heat generated in the blanket zone should be effectively transferred to coolant for electric power generation. Therefore, local heat generation in the blanket zone should be simultaneously determined together with T production rate. To do this, full sets of nuclear data for production of heat and T are required. Although the nuclear data are provided recently in the typical nuclear data library, JENDL, they are not well validated, yet.

Since fuel self-sufficiency is quite sensitive, as discussed in Chap. 4, the accuracy of TBR is quite important. At present, we cannot help saying that uncertainty in the simulation is still large. The accuracy of the simulation including uncertainties for nuclear data should be experimentally validated. The ITER project provides opportunity to test whole over the T breeding concepts including such a neutron transport simulation. Through the validation in ITER project, features for several kinds of blanket systems would be clarified, and required modification of the blanket system would be done to satisfy the fuel sufficiency.

**Acknowledgments** The authors would like to acknowledge useful comments and discussions with Prof. Y. Nakao and K. Iwamura. Special thank also go to prof. T. Tanabe for helpful comments and advices.

## References

1. M.B. Chadwick et al., Nucl. Data Sheets **112**, 2887 (2011)
2. K. Shibata et al., J. Nucl. Sci. Technol. **48**, 1 (2011)
3. Y. Someya, K. Tobita, Plasma Fusion Res. **7**, 2405066 (2012)
4. K. Tobita et al., Nucl. Fusion **49**, 075029 (2009)
5. H. Yamada et al., Fusion Eng. Des. **69**, 269 (2003)
6. L. Palermo et al., Fusion Eng. Des. **87**, 1019 (2012)
7. M.E. Sawan, M.Z. Youssef, Fusion Eng. Des. **81**, 505 (2006)
8. C.P.C. Wong et al., Fusion Eng. Des. **72**, 245 (2004)
9. Y.Nagaya et al., JAERI 1348 (2005)
10. A.R. Raffray, Fusion Eng. Des. **87**, 769 (2012)

# Chapter 13

## Recovery of Tritium Bred in Blanket

Kazunari Katayama and Masabumi Nishikawa

**Abstract** In order to ensure tritium (T) fuel self-sufficiency in a fusion power plant, key issues are full recovery of T generated in breeder materials and minimization of T loss in all fuel cycle systems. To realize the full recovery, T behavior in the breeder materials has to be understood, and the optimal T extraction system has to be designed. In this chapter, firstly, solid breeder materials and liquid breeder materials are introduced. Then, characteristics of T release from the solid breeder materials are explained, and a T release model is introduced. Finally, tritium extraction from liquid breeder materials is briefly explained.

**Keywords** Blanket · Tritium breeding · Solid breeder · Liquid breeder · Tritium release behavior · Tritium recovery

### 13.1 Blanket

#### 13.1.1 Functions of Blanket

Important components referred as “Blanket” are placed surrounding plasma in the vacuum chamber. Its roles are T production, heat generation, and radiation shielding. Various types of T breeding and heat generation systems have been proposed so far. As for example, two types of blanket system are schematically drawn in Figs. 13.1 and 13.2.

---

K. Katayama (✉) · M. Nishikawa  
Interdisciplinary Graduate School of Engineering Sciences, Kyushu University,  
6-1 Kasuga-Kouen, Kasuga, Fukuoka 816-8580, Japan  
e-mail: kadzu@nucl.kyushu-u.ac.jp

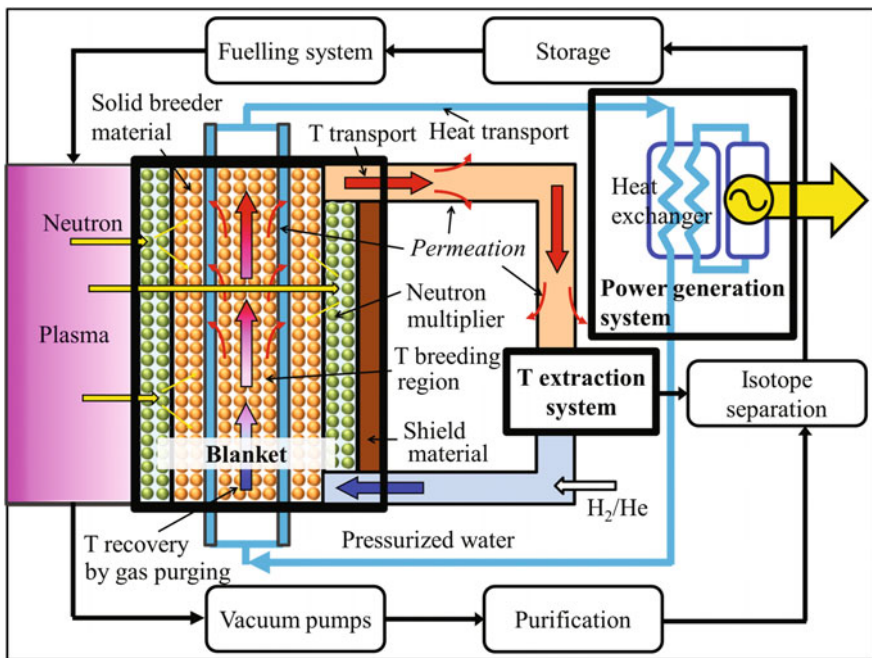


**Fig. 13.1** Schematic diagram of T breeding and power generation system using solid breeder blanket with water cooling

${}^4\text{He}$  and neutron are produced by the D-T nuclear reaction in the core plasma. Only neutrons pass through plasma-facing walls and penetrate into the blanket structure to give their energy to the blanket components as heat. A coolant removes the deposited heat in the blanket and transports it to an electric power generator.

Since T hardly exists in nature, it is necessary to be produced by the nuclear reaction of Li and neutron in the blanket. In the D-T fusion reaction, consumption of one T generates one neutron. In order to sustain the operation of the fusion reactor, more than one T has to be produced by using one generated neutron. However, a part of the neutrons are absorbed to other materials than Li. Additionally, a part of produced T cannot be used as fuel due to losses in the fuel cycle components and by radioactive decay. Therefore, neutron multipliers such as beryllium (Be) or lead (Pb) are employed to produce T with enough margins. Detailed physics and mechanism for T production are given in Chap. 12.

The blanket essentially has a function of the neutron-shielding because neutron is decelerated and absorbed in the blanket structural materials. Consequently, the blanket suppresses radiation damages of any components outside of the blanket, such as the vacuum vessel and the superconducting magnet, which is quite sensitive to heat and radiation damages. The radiation shielding is indispensable for workers, too. In this respect, coverage of a reactor by the blanket should be as large as possible.

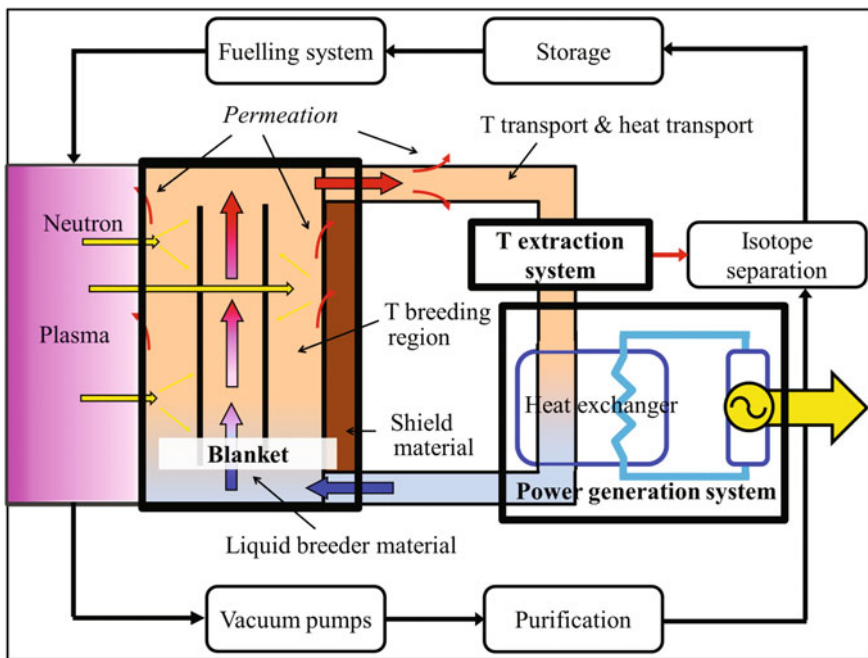


**Fig. 13.2** Schematic diagram of T breeding and power generation system using liquid breeder blanket with self-cooling capability

### 13.1.2 Tritium Breeding and Heat Transport

Various types of blanket have been designed with different T breeder materials and coolants. In a “solid blanket” which uses solid breeder materials such as  $\text{Li}_2\text{TiO}_3$  and  $\text{Li}_4\text{SiO}_4$ , T generated in the breeder materials is recovered by gas purging, and then T is extracted from the purge gas in a T extraction system. In a “liquid blanket system” which uses liquid breeder materials such as Li, LiPb, and Flibe, the liquid breeder materials carry T by themselves to the T extraction system.

A thermofluid (or coolant), either gas or liquid, is required for the transport of the generated heat in the blanket to a power generation system. A gas cooling blanket uses helium (He) as the coolant. A water cooling blanket uses pressurized light water or supercritical water to improve heat removal efficiency. Utilization of a liquid breeder material as a coolant, referred as a self-cooling blanket, simplifies the system configuration, because the breeder material transports both heat and T. A dual cooling blanket uses both He gas and a liquid breeder material as coolants. Although the liquid blanket is attractive because of simpler configuration and easy Li supply, there remain concerns such as corrosion of structural materials (chemical corrosion by Li and erosion by led), large T permeation for LiPb and Flibe, large T

inventory for Li, and MHD (Magneto-Hydro-Dynamics) pressure drop. A few different types of test blanket modules have been proposed by ITER participating parties and will be examined in ITER.

## 13.2 Tritium Breeder Materials

Characteristics required for breeder materials are as follows:

- High atomic density of Li;
- Inclusion of neutron multiplier;
- High chemical stability and compatibility with structural materials and coolant;
- Exclusion of any nuclides having a large neutron absorption cross section other than Li and neutron multiplier;
- Easy recovery of T;
- Small T inventory

In addition, some specific properties are required corresponding to solid breeder materials and liquid breeder materials.

### 13.2.1 Solid Breeder Materials

Generally, solid breeder materials are sintered into pebbles with a few mm in diameter consisting of crystal grains with micron size. High thermal conductivity, small thermal expansion, and small radiation swelling are required for the solid breeder materials.

The candidate solid breeder materials are  $\text{Li}_2\text{O}$ ,  $\text{Li}_2\text{TiO}_3$ ,  $\text{Li}_4\text{SiO}_4$ ,  $\text{Li}_2\text{ZrO}_3$ , and  $\text{LiAlO}_2$ . A photograph of sintered pebbles of  $\text{Li}_2\text{TiO}_3$  is shown in Fig. 13.3 together with their SEM image. Characteristics of these materials are shown in Table 13.1 [1].  $\text{Li}_2\text{O}$  has high Li atomic density, high thermal conductivity, and high melting point. However,  $\text{Li}_2\text{O}$  readily reacts with  $\text{H}_2\text{O}$ , generating  $\text{LiOH}$ . Because the vapor pressure of  $\text{LiOH}$  is much higher than that of  $\text{Li}_2\text{O}$ , the generation of  $\text{LiOH}$  causes reduction in T breeding ratio (TBR) by evaporation of  $\text{LiOH}$ . Furthermore, because  $\text{LiOH}$  is chemically active, corrosion of structure materials by  $\text{LiOH}$  is concerned.  $\text{Li}_2\text{TiO}_3$  is chemically stable and shows good T release property.  $\text{Li}_2\text{ZrO}_3$  is also chemically stable with good T release property, while activation of Zr by neutron irradiation is relatively large. The Li atomic density of  $\text{LiAlO}_2$  is low and the tritium release property is not good. The Li atomic density of  $\text{Li}_4\text{SiO}_4$  is relatively high and the T release property is relatively good.  $\text{Li}_2\text{TiO}_3$  and  $\text{Li}_4\text{SiO}_4$  are candidate materials in the ITER test blanket. In order to reduce T inventory and to enhance T release from T breeder pebbles, grain sizes in the pebbles must be optimized. They are about 100  $\mu\text{m}$  for  $\text{Li}_4\text{SiO}_4$ , about 10  $\mu\text{m}$  for  $\text{Li}_2\text{TiO}_3$  and

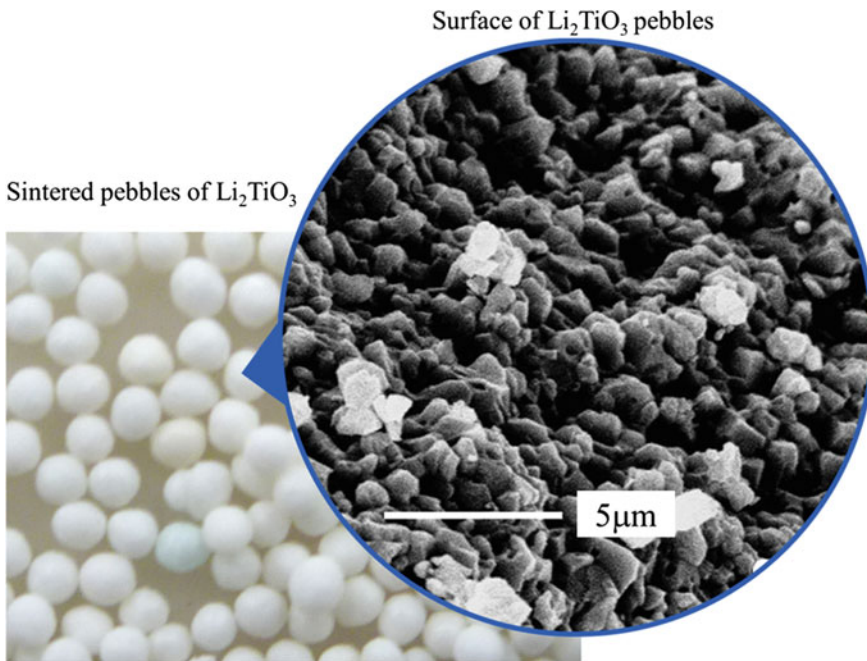


**Fig. 13.3** Photograph of sintered pebbles of  $\text{Li}_2\text{TiO}_3$  and SEM image

$\text{Li}_2\text{ZrO}_3$ , 10–100  $\mu\text{m}$  for  $\text{LiAlO}_2$ . The optimum grain size depends on the T recovering temperature [2].

### 13.2.2 *Liquid Breeder Materials*

Liquid breeder materials have advantages such as tolerance to irradiation damage and allowance of continuous operation in T recovering and Li supplying. Main candidates of the liquid breeder materials are Li, LiPb, and Flibe ( $2\text{LiF-BeF}_2$ ). Their characteristics are shown in Table 13.2. Li has high chemical activity, high T solubility, and large MHD pressure drop due to their conductive nature. In spite of its highest Li density, Li has disadvantages; high T solubility makes T extraction difficult, high chemical activity limits selection of structural materials, and large MHD drop requires insulation coating on surfaces of cooling channels. Although LiPb also requires the insulation coating, its chemical activity is much less than Li. In addition, low T solubility of LiPb reduces T inventory and makes T extraction easier. Nevertheless, its low solubility increases equilibrium dissociation pressure of T and consequently increases T permeation. Hence, the development of T permeation barrier with good compatibility with LiPb is necessary. Although Pb plays the

**Table 13.1** Properties of solid breeder materials [1]

	Preferable	Li <sub>2</sub> O	Li <sub>2</sub> TiO <sub>3</sub>	Li <sub>2</sub> ZrO <sub>3</sub>	Li <sub>4</sub> SiO <sub>4</sub>	$\gamma$ -LiAlO <sub>2</sub>
Melting point [K]	Higher	1692	1808	1888	1523	1883
Density [g/cm <sup>3</sup> ]	Lower	2.02	3.43	4.15	2.21	2.55
Li density [g/cm <sup>3</sup> ]	Higher	0.94	0.43	0.38	0.51	0.27
Thermal conductivity at 500 °C [W/m°C]	Higher	4.7	1.8	0.75	2.4	2.4
Thermal expansion coefficient at 500 °C [ $\delta L/L_0$ %]	Smaller	1.25	0.8	0.50	1.15	0.54
Reactivity with water	Lower	High	Stable	Stable	Low	Low
Tritium retention time at 400 °C [h]	Shorter	8.0	2.0	1.1	7.0	50
Swelling [ $\delta V/V_0$ %] <sup>*</sup>	Lower	7.0	–	<0.7	1.7	<0.5
Activated products by neutron absorption	Less	<sup>16</sup> O (n, p):7 s	<sup>46</sup> Ti(n,p):84 d <sup>47</sup> Ti(n,p):3.4 d <sup>48</sup> Ti(n,p):1.8 d	<sup>90</sup> Zr(n,p):64 h <sup>91</sup> Zr(n,p):57 d <sup>94</sup> Zr (n,2n): $10^6$ y <sup>96</sup> Zr(n,2n):64 d	<sup>28</sup> Si(n,2n):4 s <sup>29</sup> Si(n,p):6 m <sup>30</sup> Si(n, $\alpha$ ):9 m	<sup>27</sup> Al(n,2n):6 s <sup>27</sup> Al(n,p):9.5 m <sup>27</sup> Al(n, $\alpha$ ):15 h

<sup>\*</sup>Li burn-up ratio is assumed to be 3 at % at 500 °C

role of a neutron multiplier, the neutron-induced <sup>210</sup>Po and <sup>203</sup>Hg give radiological concern. The chemical stability of Flibe is better than LiPb. However, TF generated in Flibe by the following reactions



are very much corrosive to the structural metals, and hence its reduction is indispensable. It has been suggested that TF concentration can be kept low by the redox control of Flibe by adding Be [3]. Although the T solubility of LiPb is known to be as low as Flibe, the solubility data of hydrogen isotopes are widely scattered in more than 4 orders of magnitude. For the installation of the LiPb blanket in ITER, determination of reliable data of the solubility is urgently required.

**Table 13.2** Comparison of properties of three liquid breeder materials [1]

	Li (500 K)	$\text{Li}_{17}\text{Pb}_{83}$ (513 K)	Flibe ( $\text{Li}_2\text{BeF}_4$ ) (800 K)
Density (g/cm <sup>3</sup> )	0.509	9.59	1.99
Li Density (g/cm <sup>3</sup> )	0.509	0.065	0.279
Melting point (K)	453	508	732
Thermal conductivity (W/m/K)	41.4	12.2	1.00
Specific heat at constant pressure (kJ/kg/K)	4.33	0.19	2.39
Electric resistivity ( $\Omega\cdot\text{cm}$ )	27.6	124	$5.88 \times 10^5$
Viscosity (mPa·s)	0.558	2.86	7.50
Characteristic of T release behavior	High T solubility and difficult to recover T	Low T solubility and high T permeation rate	Low T solubility and high T permeation rate
Reactivity with $\text{H}_2\text{O}$ and Air	High	Low	Stable
Compatibility with structural materials	Low	Lower than Li	Fluorination and elution of metals with HF or TF generation

### 13.3 T Release Behavior from Solid Breeder Materials

Understanding of T release behavior from breeder materials is essential to develop the efficient recovery of T generated in them.

For the solid breeder materials, various investigations about T release from breeding materials, such as basic laboratory studies, and in-pile and out-pile T extraction from irradiated breeding materials have been performed and T release models have been proposed. Adsorption of ubiquitous  $\text{H}_2\text{O}$  which forms hydroxyl groups on the surface of the solid breeder materials makes T release from them very complex due to interactions of T with H in the hydroxyl groups. The porous nature of the solid breeders enhances the adsorption of  $\text{H}_2\text{O}$  and other impurity gases. In this section, experimental results and numerical simulations on the T release processes from the solid breeder materials are introduced based on a model proposed by Nishikawa [4].

The handling of liquid breeder materials is harder than that of solid breeder materials and remains as the most important technical issue to develop liquid breeder materials. Moreover, understanding of behavior of hydrogen isotopes in the flowing liquid breeder materials is insufficient and more experimental data are awaited.

### 13.3.1 T Migration Process in Pebbles

T generated in Li ceramic pebbles is recovered and transported to a T extraction system with a purge gas. Most T generated in the Li pebbles remains in grains constructing the pebble, while a few T is directly emitted to the gas phase with recoil energy of the nuclear reaction. Figure 13.4 schematically shows T migration process from the inside of the grains of a pebble to the outside through open pores. T generated in the grains diffuses to their surfaces and/or grain boundaries. Then, T is released to the interconnected pores constructed by the network of the grain boundaries and finally reaches geometrical surfaces of the pebble to be removed by the purge gas. Since T is generated continuously in the pebbles, a certain amount of T is constantly retained in them. This amount is referred to “T inventory” and should be kept as low as possible from viewpoints of efficient T recovery and T safety.

### 13.3.2 Influence of Surface Reactions on T Release

How is T released actually from neutron-irradiated solid breeder materials? Thermal neutron irradiation experiments using nuclear fission reactors indicated that the majority of T was released as HTO from the solid breeder materials. Figures 13.5 and 13.6 show time traces of concentration of T thermally released in the purge gas, respectively, from  $\text{Li}_2\text{TiO}_3$  and  $\text{LiAlO}_2$  that were irradiated with thermal neutrons at

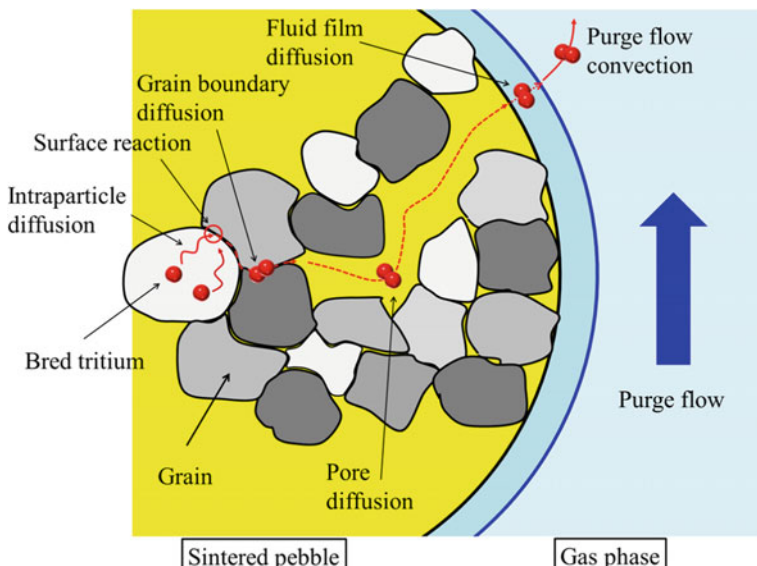


**Fig. 13.4** Schematic drawing of T migration pathway in a pebble

**Fig. 13.5** Time trace of thermally released T concentration in purge gas from  $\text{Li}_2\text{TiO}_3$  irradiated with thermal neutrons at JRR-3 reactor

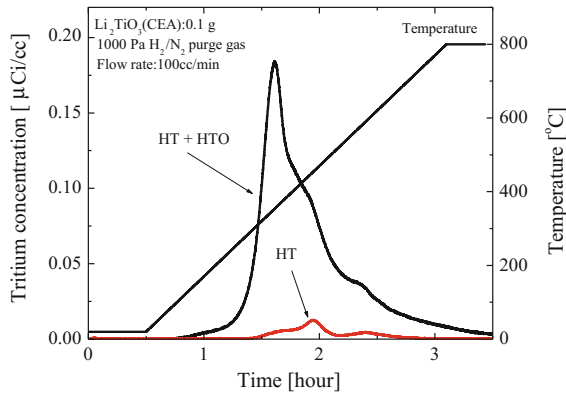
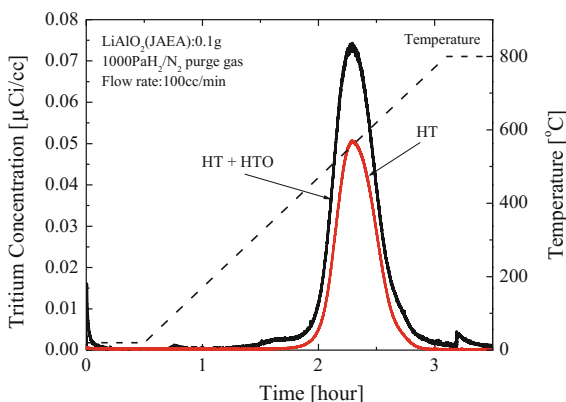


**Fig. 13.6** Time trace of thermally released T concentration in purge gas from  $\text{LiAlO}_2$  irradiated with thermal neutrons at JRR-3 reactor



the JRR-3 reactor in JAEA [5]. The time traces are referred as T release curves hereafter. Although in these experiments,  $\text{H}_2$  was added in the purge gas to enhance T release as HT, T was dominantly released as HTO for  $\text{Li}_2\text{TiO}_3$ , while as HT for  $\text{LiAlO}_2$ . The main difference in such release behavior can be attributed to the difference of surface release processes as described in following sections in which three processes, (a) surface adsorption/desorption of water, (b) water formation on the surface, and (c) isotope exchange between T on the surface and  $\text{H}_2/\text{H}_2\text{O}$  in the purge gas, are separately described.

#### (a) Adsorption/desorption of water vapor

In any breeder materials and on their surfaces as well as in purge gasses, some amounts of water and/or impurities with hydroxyl groups are always present. They are referred as “surface water” and play a critically important role for T recovery from the breeder materials. T reached at the grain surfaces replaces H atom in the surface water by isotope exchange reactions. The surface water is phenomenologically assigned to be constructed of three components, (1) physically adsorbed

water, (2) chemically adsorbed water, and (3) structural water as described in the followings [6],

### (1) Physically adsorbed water

The amount of the physical adsorbed water,  $q_{\text{ad,p}}$  [mol/m<sup>2</sup>], changes reversibly with vapor pressure in the gas phase at a given temperature and is represented by the Langmuir isotherm equation:

$$q_{\text{ad,p}} = \frac{b \exp(-Q_{\text{ad,p}}/RT)P}{(1 + aP)}, \quad (13.3)$$

where  $a$  [1/Pa] and  $b$  [mol/m<sup>2</sup>/Pa] are the Langmuir constants, and  $Q_{\text{ad,p}}$  [J/mol],  $T$  [K], and  $P$  [Pa] are heat of adsorption, temperature, and vapor pressure, respectively.

### (2) Chemically adsorbed water

The chemically adsorbed water  $q_{\text{ad,c}}$  [mol/m<sup>2</sup>] is hard to remove with a dry gas purge at the same temperature as it is adsorbed. In other words, heating is required to desorb it, and its amount is represented by:

$$q_{\text{ad,c}} = c \exp(-Q_{\text{ad,c}}/RT)P^{1/2}. \quad (13.4)$$

Here, dissociative adsorption of water vapor is considered,  $Q_{\text{ad,c}}$  [J/mol] is activation energy of the dissociative adsorption, and  $c$  [mol/m<sup>2</sup> Pa<sup>1/2</sup>] a constant.

### (3) Structural water

The structural water represents any water included in breeder materials such as crystal water and any chemical groups containing hydrogen as hydroxyl groups strongly bound to the surface. T is isotopically exchanged with H in the structural water. Accordingly, the amount of the structural water,  $q_{\text{str}}$  [mol/m<sup>2</sup>], does not depend on the vapor pressure of the gas phase as:

$$q_{\text{str}} = d f(T), \quad (13.5)$$

where  $d$  [mol/m<sup>2</sup>] is a constant,  $f[T]$  is a function of temperature.

Thus, the total amount of the surface water  $q_s$  is given by:

$$q_s = q_{\text{ad,p}} + q_{\text{ad,c}} + q_{\text{str}}. \quad (13.6)$$

State of surface water and T under a dry gas atmosphere and additional heating condition is schematically drawn in Fig. 13.7. Purging with a dry gas at the same temperature at which T was sorbed can remove T in the physically adsorbed water, while T in both the chemically adsorbed water and the structural water remains on the surface. The dry gas purging at higher temperatures than the temperature at

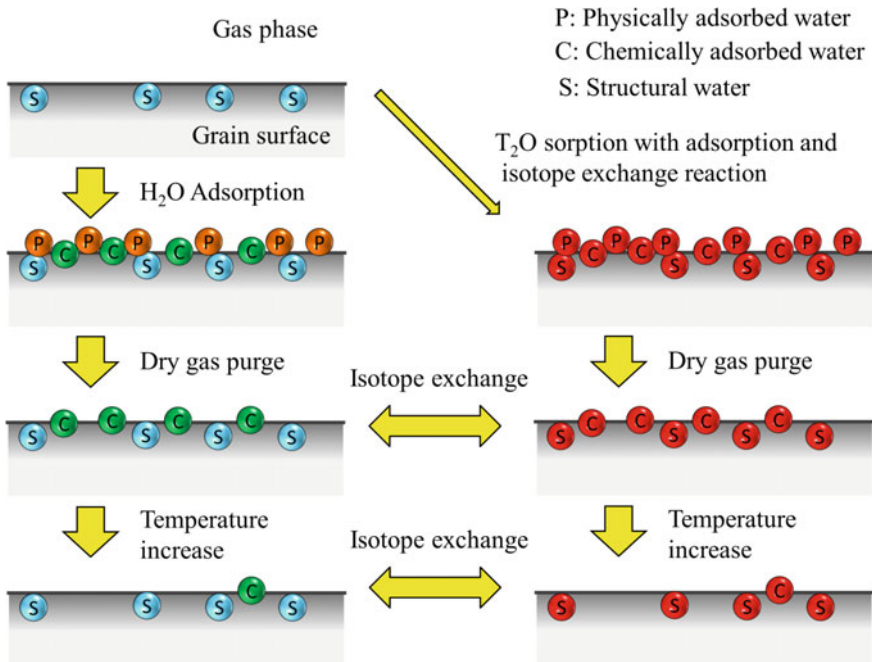


Fig. 13.7 Schematic drawing of state of surface water and T

which  $T_2O$  was sorbed can remove T in the physically or chemically adsorbed water but T in the structural water remains. Purging with a gas containing  $H_2$  or  $H_2O$  can remove T in all kinds of surface water with isotope exchange reactions.

### (b) Water formation reaction

The release curves of water vapor from  $Li_2TiO_3$  by purging with the dry Ar gas and the dry  $H_2/N_2$  gas are compared in Fig. 13.8. During the purging, the temperature was raised from room temperature to 900 °C with a constant heating rate [7]. The first peak appeared before heating is attributed to the release of the physically adsorbed water. The other peaks appeared after the heating are attributed to the release of chemically adsorbed water. Two peaks appeared above 400 °C only for the dry  $H_2/N_2$  gas purging are attributed to the release of HTO vapor generated with the reaction of  $H_2$  and  $Li_2TiO_3$ .

In any solid breeders, the water formation is always observed. The amount of the generated water is different in each breeder so as its release behavior. The control of moisture (water vapor) level as well as  $H_2$  level in purge gas is a quite important factor to recover T from the solid breeders.

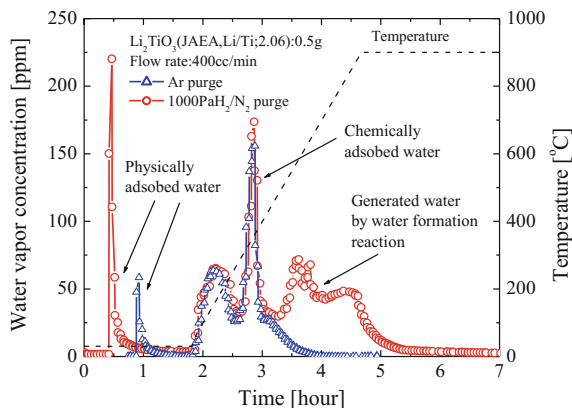


Fig. 13.8 Release of water vapor from  $\text{Li}_2\text{TiO}_3$  in dry Ar flow and in dry  $\text{H}_2/\text{N}_2$  flow

### (c) Isotope exchange reaction

As mentioned above, since solid breeders basically holds T at the surface as hydroxyl groups and adsorbed water, an isotope exchange reaction of H with T is a very important reaction for T release.

The isotope exchange reactions are schematically shown in Fig. 13.9. The isotope exchange reaction between the molecular form of H (either HT or  $\text{H}_2$ ) in the gas phase and T in surface water, or the isotope exchange reaction between the molecular form of T (either HT or  $\text{T}_2$ ) and H in the surface water is referred to as the isotope exchange reaction 1 (EX1).

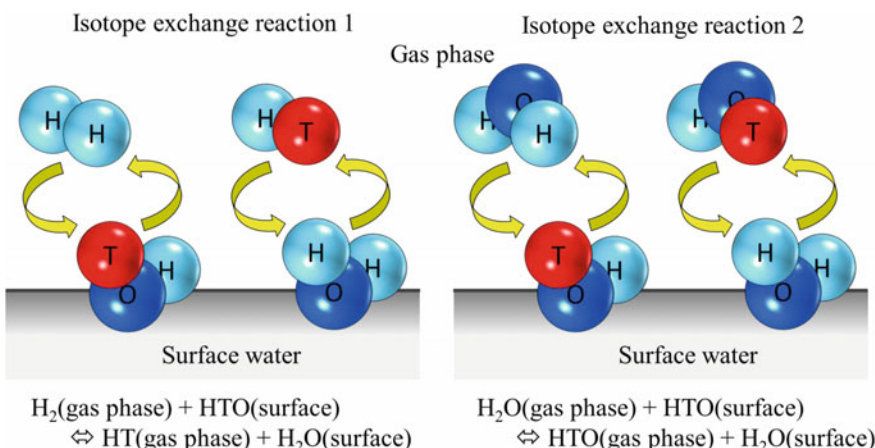
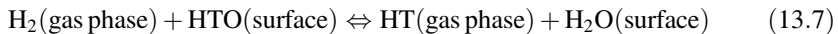


Fig. 13.9 Schematic drawing of isotope exchange reactions



The isotope exchange reaction between H in water vapor (either HTO or H<sub>2</sub>O) in the gas phase and T in surface water, or the isotope exchange reaction between T in water vapor (either HTO or T<sub>2</sub>O) in the gas phase and H in surface water is referred to as the isotope exchange reaction 2 (EX2).



The isotope exchange reaction proceeds until T/H ratio in the surface water and T/H ratio in the gas phase reach the equilibrium. The reaction rate of EX2 is faster than that of EX1. At room temperature, EX2 proceeds quickly, while EX1 hardly occurs.

### ***13.3.3 T Mass Transfer Processes and T Inventory***

Both fundamental laboratory researches on T behavior in solid breeder materials and experiments on T recovery from solid breeder materials under neutron irradiation using fission reactors have shown that surface reactions on the grains, which are described in Sect. 13.3.2, dominate T release behavior. Since H<sub>2</sub> is most probably added in a purge gas to enhance T release as the form of HT by EX1, the water formation reaction with H<sub>2</sub> have to be taken into account. T transfer processes and chemical reactions in overall T release behavior are key factors to simulate the T release behavior and explained in the following:

- (1) T generation in the crystal grain.
- (2) T diffusion in the crystal grain.
- (3) Interaction of diffusing T with irradiation defects formed in the crystal grain.
- (4) T transfer from inside to surface of the crystal grain.
- (5) Absorption of T in the crystal grain.
- (6) Adsorption/desorption of HTO and H<sub>2</sub>O on the crystal grain surface.
- (7) Isotope exchange reaction between H<sub>2</sub> in gas phase and T on the crystal grain surface (EX1).
- (8) Isotope exchange reaction between H<sub>2</sub>O in the gas phase and T on the crystal grain surface (EX2).
- (9) Water formation reaction on the crystal grain surface with H<sub>2</sub> in the gas phase.
- (10) Mass transfer of hydrogen isotopes and water vapor through the interconnected pores to geometrical surfaces of the pebbles.
- (11) Mass transfer of hydrogen isotopes and water vapor through fluid film formed between geometrical surfaces of the pebbles and the purge gas flow.

From the aspect of T safety, the suppression of T inventory in the blanket is quite important. The T inventory in a solid breeder material is categorized to “diffusion inventory,” “absorption inventory,” “surface inventory,” and “micropore

inventory.” Among all processes given above, the processes of (1)–(4) are assorted to diffusion inventory, corresponding to the amount of T in the inside of crystal grains when the breeder material has no absorption capacity. The process (5) corresponds to absorption inventory, which is the amount of T absorbed into the inside of crystal grains from the gas phase. Most of absorption inventory can be attributed to HTO absorbed on the surface. In reality, the absorption inventory is quite insignificant;  $\text{Li}_2\text{O}$  absorbs water vapor only at high temperatures and  $\text{Li}_2\text{TiO}_3$ ,  $\text{LiAlO}_2$ ,  $\text{Li}_2\text{ZrO}_3$ , and  $\text{Li}_4\text{SiO}_4$  have no detectable absorption of water vapor and molecular form hydrogen. Surface inventory, caused by the processes (6)–(9), is the amount of T on the surface of crystal grains. Micropore inventory, which is attributed to process (10), is the amount of T migrating in the pores of sintered pebbles. Basically, the diffusion inventory and the surface inventory dominate the total T inventory in a solid breeder material, which is, in consequence, governed by surface reaction rates, diffusivity, and the size of crystal grains.

### 13.3.4 Chemical Form of T Recovered in a Purge Gas

Chemical form of T, either HTO or HT, plays a quite important role for T extraction from the purge gas. Furthermore, the mechanism of T permeation caused by HTO and HT is quite different. Therefore, it is important to evaluate the ratio of HTO to HT in the purge gas because the ratio gives a large impact on designing a T extraction system and evaluating T permeation. Nishikawa et al. [8] describe that the chemical forms of T recovered in the purge gas are different depending on the processes of (6)–(9) in the previous section. To enhance the T recovery as HT, addition of  $\text{H}_2$  of about 100 Pa into the purge gas has been proposed. However, elimination of HTO production is not possible, because a small amount of water vapor is always included in the purge gas, or incorporated with desorbed water from the system wall. Furthermore, the reaction rate of EX2 is much faster than that of EX1 at low temperature. Figures 13.5 and 13.6 indicate the T release from neutron-irradiated  $\text{Li}_2\text{TiO}_3$  and  $\text{LiAlO}_2$  at JRR-3 reactor in JAEA [5]. One can see that the significant amount of T was released as HTO, even though the purge gas contains  $\text{H}_2$ . EX1 has almost no contribution on T recovery from the breeder material at low temperature even when 1000–10,000 ppm of hydrogen is added to the purge gas, because its reaction rate is quite slow at temperatures lower than 600 K. On the contrary, EX2 works effectively to T recovery from the grain surface as HTO even when only a small amount of water vapor is included in the purge gas because its reaction rate is fast even at the room temperature. T trapped on the adsorbed water is released as the chemical form of HTO through desorption reaction with increasing temperature. Accordingly, at temperatures lower than

600 K, the main chemical form of T released into the purge gas is HTO. At higher temperatures, the release of T as HT increases because the reaction rate of EX1 becomes fast. The water formation reaction, however, becomes significant at the grain surface at temperatures higher than 750 K, and this reaction supplies water vapor to the purge gas when  $H_2$  is added to the purge gas. Increase in water vapor concentration in the purge gas promotes the release of T as HTO. Because T diffusivity in  $Li_2TiO_3$  is relatively large, the majority of T migrates from the inside of the grain to the surface water at low temperatures and is successively released as HTO as shown in Fig. 13.5. On the other hand, because T diffusivity in  $LiAlO_2$  is relatively small, the T transfer from the inside of the grain to the surface water does not occur sufficiently at low temperatures although the adsorbed water vapor is released. When the temperature becomes high, the T migration from the inside of the grain to the surface water effectively occurs and also the reaction rate of EX1 becomes fast. Consequently, the release of T as HT becomes comparable or larger than that of HTO as shown in Fig. 13.6.

### 13.3.5 Simulation of T Release

In order to analyze the T release from breeder materials, as described above, T diffusion in the grain and surface reaction (rates) are critically important. There are large data scattering in reported T diffusivities in solid breeder materials. The main cause of the scattering is likely insufficient consideration of surface reactions. Nishikawa et al. [4] have experimentally determined the capacity of water adsorption/desorption and reaction rates of water formation and the isotope exchanges, EX1 and EX2, and proposed a new model schematically shown in Fig. 13.10. In their model, generated T diffuses from the grain bulk to the interfacial layer and then transfers to the surface water. The latter process is suppressed by resistance in mass transfer from the inside of the grain to the surface water [4], which is schematically shown in Fig. 13.10. They have succeeded to analyze experimental release curves of generated T in various types of solid breeder materials by thermal neutron irradiation obtained with out-pile experiments as shown in Figs. 13.11, 13.12, and 13.13 [5]. Furthermore, they concluded that effects of the processes of (10) and (11) are negligible [9, 10]. One can see that the Nishikawa model given by symbolled lines in the figures well represents the experimental release curves of generated T from 4 kinds of solid breeder materials under different purge gas conditions and the model is used in JAEA.

In DEMO and commercial fusion reactors, the solid breeder materials will be used at a high temperature for a long time. The amount of Li in the solid breeder material decreases with the operation time because of Li burn-up and Li evaporation. However, the influence of the Li loss on the T release behavior has been hardly

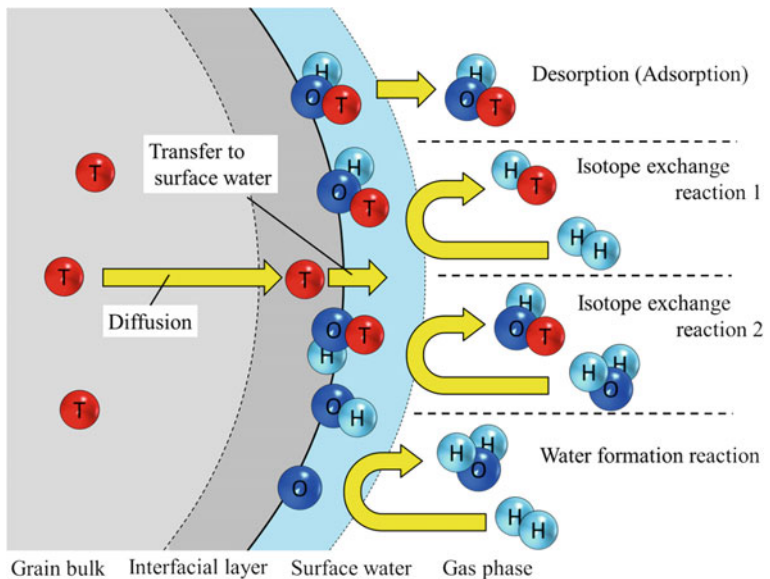
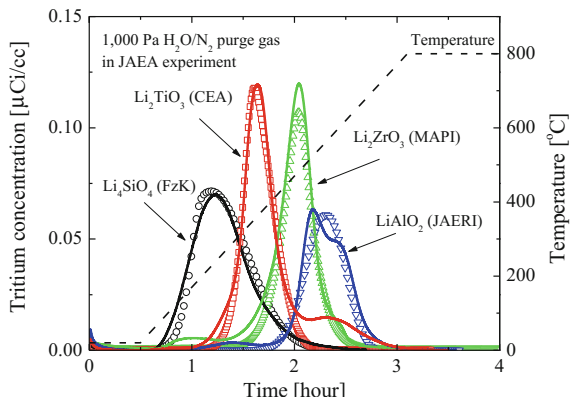


**Fig. 13.10** Schematic drawing of a model for T release from solid breeder materials

**Fig. 13.11** Comparison of experiments and simulations for T release curves in humidified gas flow (*solid lines* are the experimental results and *symbolled lines* are calculated ones)



studied yet [7, 11]. To compensate the Li loss,  $\text{Li}_{2+x}\text{TiO}_{3+y}$  with excess Li has been developed as an advanced T breeder material [12]. The Li loss from  $\text{Li}_{2+x}\text{TiO}_{3+y}$  by the evaporation does not seem to give a large impact on T behavior because the amount of evaporated Li is a few wt % even at a high temperature of 900 °C. Another concern is effects of neutron irradiation on T release from breeding materials. Defects and damages generated by the neutron irradiation and He recoils, and He remaining in the breeder material should significantly influence the T release. Although some efforts have been done to observe the effects, it is hard to quantify their effects [13, 14].

**Fig. 13.12** Comparison of experiments and simulations for T release curves in Dry N<sub>2</sub> gas flow (solid lines are the experimental results and symbolled lines are calculated ones)

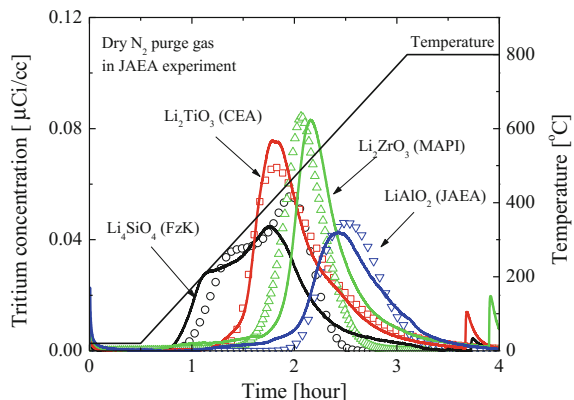
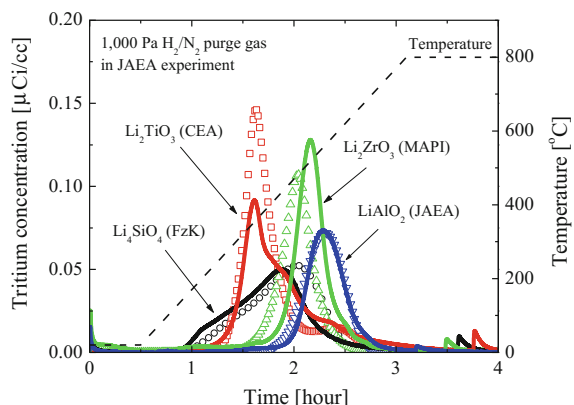


**Fig. 13.13** Comparison of experiments and simulations for T release curves in Dry H<sub>2</sub> gas flow (solid lines are the experimental results and symbolled lines are calculated ones)



### 13.4 Permeation of Generated T

T generated in the breeding region in a blanket is transported to a T extraction system as shown in Figs. 13.1 and 13.2. Since T permeates metals at high temperatures, loss of T by the T permeation in the breeding region and in the transport region concerns the fuel self-sufficiency. A reduced activation ferritic martensitic stainless steel such as F82H would be used in the breeding region, and an austenite stainless steel would be used in the transport region. Since T permeability of the ferritic martensitic stainless steel is larger than that of the austenite stainless steel, the permeation rate of the generated T to coolant has to be suppressed from viewpoints of efficient T recovery and safety. Therefore, the development of permeation barriers is an important issue as described in Chap. 9. In particular, the permeation barrier is essential for a liquid breeder blanket using LiPb or Flibe. Owing to very low T solubility in these materials, an equilibrium pressure of T

becomes very high. Accordingly, T permeation rate from the breeding region to the coolant region becomes very large.

It should be noted that water vapor released from solid breeder materials oxidizes the surface of the blanket wall and cooling tubes (pipes). The surface oxide layers that appeared on an austenite stainless steel are dominated with chromium oxide and reduce T permeation rate, while the oxide layers formed on F82H dominated with iron oxide do not seem to reduce T permeation rate [15].

To enhance T recovery from the breeder materials, intentional addition of water vapor into the purge gas instead of gaseous hydrogen is quite effective. In this case, T is mainly released as HTO via EX2 under continuous supply of the water vapor at the surface accompanying surface oxidation. Accordingly, the T permeation could be significantly suppressed compared to the hydrogen gas addition. Nevertheless, T uptake in the oxide layers becomes large to increase T inventory. Furthermore, T recovered as HTO has to be converted to HT by a water processing system to be used as fuel, which forces additional load on the water processing system.

## 13.5 T Extraction Method

### 13.5.1 *T Extraction from a Purge Gas*

Various methods to extract T from the gas phase are explained in Chap. 6 in detail. Materials and methods used for T extraction are summarized in Fig. 13.14. In DEMO and commercial fusion reactors, T extraction by a low-temperature physical adsorption method is not suitable because the purge gas temperature will be significantly high. A Pd alloy membrane diffuser method is one of the most attractive methods and allows a continuous recovering which is preferable to introduce the bred T into a fuel cycle smoothly. Unfortunately, the presence of water vapor in the purge gas causes the formation of oxide layer on the membrane surface, which reduces its permeability [15]. To maintain original performance of the membrane, the reduction of water vapor and oxygen in the inlet gas may be required.

### 13.5.2 *T Extraction from Liquid Breeder Materials*

Comparing to the T recovery from solid breeder materials, that from liquid breeder materials has not been established well. As already described, there are two different liquid blanket concepts, i.e., (1) a self-cooling blanket in which the liquid breeder material concurrently works as coolant or (2) an independent cooling blanket which employs an additional cooling mechanism such as the solid breeder case. In this section, the former which is simpler than the latter as seen in the comparison of

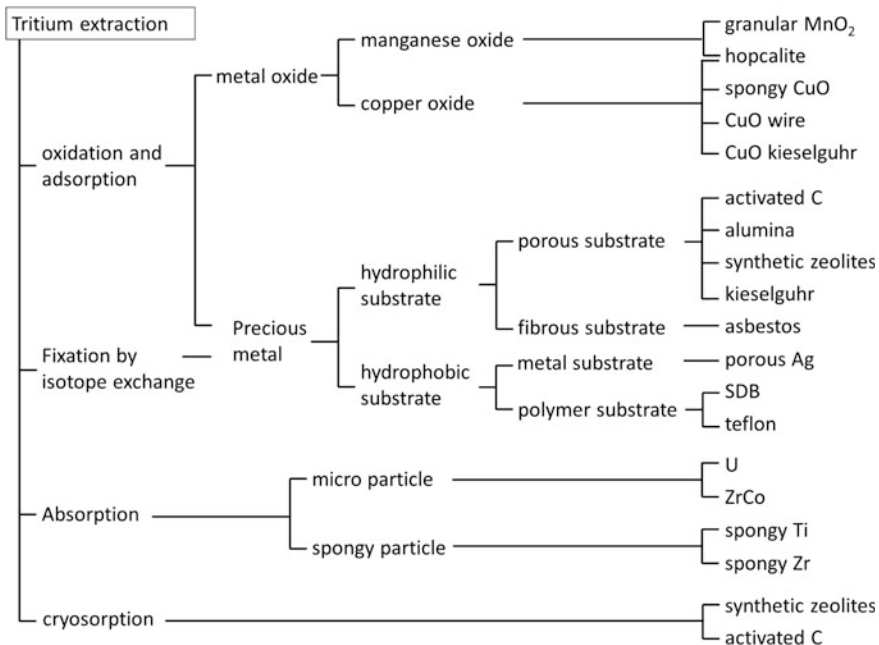


**Fig. 13.14** Materials used for T extraction with gas purging

Figs. 13.1 and 13.2 is described in detail. Among three candidate liquid breeder materials, in Table 13.2, T behavior in Li is separated from those of LiPb and Flibe. T solubilities of the latter two are much lower than that of Li. Accordingly, their T inventories are lower and T extraction is easier. On the other hand, T permeation is concerned because their T equilibrium pressure is high. Therefore, T recovery system is installed upstream of a heat exchanger in order to reduce the T permeation in the heat exchanger. Different from LiPb and Flibe, T solubility in Li is quite high which makes T extraction quite difficult. For Li, safety issue would not be the T permeation but large T inventory in the blanket. It requires significant R&D efforts to realize the self-cooling liquid breeder blanket [16–19]. In the following, T extraction methods from liquid breeder materials are summarized.

### (1) Permeation window

T is extracted by permeation through a thin metallic membrane having high permeability. Nb and Fe are attractive materials as the permeation membrane from viewpoints of not only T permeability but also compatibility with liquid breeder materials. In this method, surface reactions of T uptake from the breeder material to the membrane play a critical role. Precipitation of impurities on the membrane surface significantly suppresses the permeation rate. Tanaka et al. [20] have found that the hydrogen permeation rate of a Nb membrane dipped into liquid Li containing H is two orders of magnitude lower than that estimated for diffusion-limited

permeation. Such reduction was attributed to the formation of nitride layers on the Nb membrane surface. In a case, that SUS304 is used as a membrane, the T permeation rate decreased with operation time owing to the precipitation of oxide layers on its surface [21]. In the case of  $\alpha$ Fe used with LiPb, the oxide layers were formed but the layers could be removed at 500 °C by hydrogen intentionally added with above 1000 ppm to recover the permeation rate [22]. Thus, for long-term utilization of the permeation membrane and impurities such as nitrogen and oxygen in liquid breeder materials should be controlled.

### (2) Gas purging

For a gas purging extraction system, to increase contacting area of liquid breeder material to a purge gas is quite important, and several types of contacting methods are proposed such as droplet contacting, counter current contacting, and bubbling. In a droplet contactor, T is recovered from free falling small droplets or mist of the liquid breeder material into a counter current purge gas or by direct vacuum extraction [23]. To realize this, the feasibility of formation of the small droplets and their stability remain to be clarified. Fukada et al. [24] proposed a counter current extraction tower packed with metallic Raschig rings to extract T generated and dissolved in LiPb as shown in Fig. 13.15. They have found that D<sub>2</sub> addition in He purge gas is effective to achieve a faster rate of T recovery from the LiPb flow.

### (3) Hot trap (gettering)

Some metals, such as yttrium (Y), of which hydride has lower hydrogen dissociation pressure than that of Li hydride, can extract T from Li contacted to them.

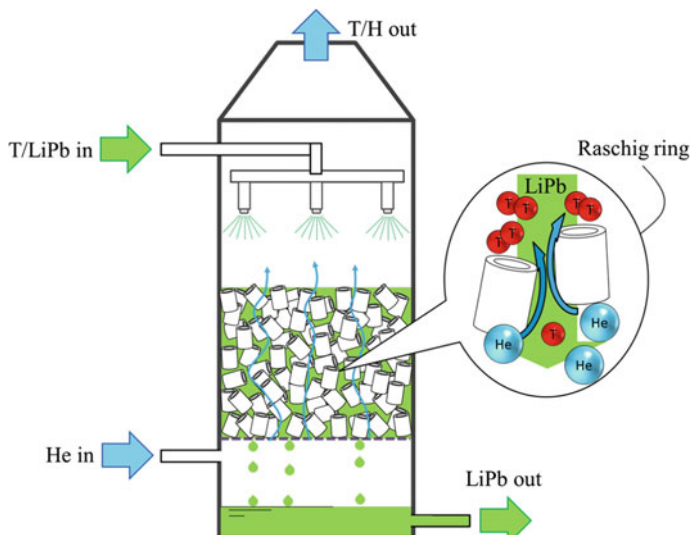


**Fig. 13.15** Schematic diagram of a counter current extraction tower

The method, referred to as a hot trap method or gettering is advantageous for its simplicity. When Li flows through a Y pebble packed bed, T dissolved in Li is extracted to the Y pebbles [25, 26]. Since the formation of surface oxide or nitride deteriorates the T extraction rate, an impurity removal system is necessary in the Li cycle for the effective T extraction. However, a high temperature is required for the T extraction from Y because the dissociation pressure of Y tritide is very low. Furthermore, T extraction from Y by gas purging takes a long time.

#### (4) Molten salt extraction

The molten salt extraction consists of three steps. First, Li containing T is mixed with a molten salt mixture of lithium halides such as LiF, LiCl, and LiBr, and T is transferred to the molten salt side by the solvent extraction mechanism. Second,  $T_2$  is recovered from the molten salt mixture into the purge gas by electrolysis. Third,  $T_2$  in the purge gas is extracted into a metal getter [27]. However, the electrolysis increases the operation cost significantly compared with the above-mentioned methods.

#### (5) Cold trap

If the temperature of the Li breeder is lowered, T dissolved in it precipitates as LiT before it is fully solidified. Then LiT can be removed by filtering. Addition of H in the Li breeder would enhance hydride precipitation and increase T extraction efficiency. Although extracting hydrogen from the hydride precipitates is done by simple heating, released hydrogen contains both H and T, which requires additional isotope separation.

## 13.6 Summary and Future Prospect

To construct a D-T fusion reactor ensuring T fuel self-sufficiency and T safety, understanding of behavior of T in breeder materials is an important issue. For solid breeder materials, T release is controlled with both T diffusion processes inside of the crystal grains and reaction processes at the surface of the crystal grains such as water adsorption/desorption and isotope exchange reactions. Taking these into account, Nishikawa et al. [4, 8] have made a new T release model which is successfully applied to simulate the T release behavior from the solid breeder materials irradiated by neutron in a fission reactor. For simulating T behavior in the DEMO blanket condition, additional processes such as the interaction of irradiation defects and generated T, and the influences of Li burn-up on T behavior must be considered. Compared to the solid breeder materials, liquid breeder materials are behind in R&D. However, the liquid breeder materials have various attractive characters. Hence, international research activities for their compatibility with structural materials and for T transport-phenomena under fluidized condition have been promoted.

Various T extraction methods from a purge gas and from liquid breeder materials have been proposed with demonstration of their practical uses. Still significant

R&D efforts are required in order to optimize each T extraction method. When DEMO blanket condition becomes more exact or realistic, suitable T extraction methods will be selected taking safety, economical availability, and reliability into account.

## References

1. M. Seki, et al., *Kakuyugouro Kougaku Gairon*. Nikkan Kogyo Shimbun, Ltd (2001)
2. H. Yamasaki et al., *Fusion Sci. Tech.* **60**, 1151–1154 (2011)
3. S. Fukada et al., *J. Nucl. Mater.* **367–370**, 1190–1196 (2007)
4. T. Kinjyo et al., *Fusion Eng. Des.* **81**, 573–577 (2006)
5. T. Kinjyo, Study on tritium release behavior from solid breeder materials of D-T fusion reactor. PhD Dissertation, Kyushu University (2007)
6. M. Nishikawa et al., *J. Nucl. Mater.* **277**, 99–105 (2000)
7. K. Katayama et al., *Fusion Eng. Des.* **87**, 927–931 (2012)
8. M. Nishikawa et al., *J. Nucl. Mater.* **325**, 87–93 (2004)
9. M. Nishikawa et al., *J. Nucl. Mater.* **246**, 1–8 (1997)
10. M. Nishikawa, A. Baba, *J. Nucl. Mater.* **257**, 162–171 (1998)
11. H. Kashimura et al., *Fusion Eng. Des.* **88**, 2202–2205 (2013)
12. T. Hoshino, M. Nakamichi, *Fusion Eng. Des.* **87**, 486–492 (2012)
13. K. Okuno, H. Kudo, *J. Nucl. Mater.* **138**, 31–35 (1986)
14. K. Okuno, M. Kobayashi et al., *Fusion Eng. Des.* **86**, 2358–2361 (2011)
15. H. Yamasaki et al., *Fusion Eng. Des.* **87**, 525–529 (2012)
16. S. Fukada, M. Nishikawa, Annual Report of Hydrogen Isotope Research Center. Toyama University, Japan, vol. 14 (1994)
17. H. Moriyama et al., *Fusion Eng. Des.* **28**, 226–239 (1995)
18. A. Suzuki, *J. Plasma Fusion Res.* **76**, 1029–1035 (2000)
19. M. Nishikawa et al., *J. Plasma Fusion Res.* **79**, 678–686 (2003)
20. S. Tanaka et al., *J. Nucl. Mater.* **97**, 59–66 (1981)
21. T. Terai et al., *J. Nucl. Mater.* **191–194**, 272–276 (1992)
22. T. Terai, et al., Fusion Technology, in *Proceedings of the 17th Symposium On Fusion Technology*, Rome, Italy, 14–18 Sept 1992, pp. 1518–1522
23. G. Pierini et al., *Fusion Technol.* **1**, 463–471 (1984)
24. S. Fukada et al., *Fusion Eng. Des.* **83**, 747–751 (2008)
25. J.B. Talbot et al., *J. Nucl. Mater.* **103&104**, 681–686 (1981)
26. S. Shigeharu et al., *Plasma Fusion Res.* **7**, 2405080 (2012)
27. W.F. Calaway, *Fusion Technol.* **39**, 63–74 (1978)

**Part III**

**Tritium Issues Relating Safety**



# Chapter 14

## Safety Confinement System

Kazunari Katayama and Masabumi Nishikawa

**Abstract** A large amount of T is used as a fuel in a fusion reactor, but its release to the environment is rigidly regulated to be quite low by law. In order to protect workers, the public, and the environment from radiation of T, it is very important to confine T safely. The first section explains basics of radiation protection and indicates specified values relating to T safety confinement such as dose limit. T has a property of permeating easily through even metals. Therefore, the T release to the environment is suppressed by multiple confinements system based on the concept of defense in depth. The multiple-confinement system has been adopted in many T handling facilities in the world and operated successfully for many years. The second section explains the concept and practical configuration of the multiple confinements system in the present T handling facilities and a fusion power plant. In the fusion power plant, various kinds of wastes contaminated by T would be generated. It is necessary to pay careful attention in handling of these T contaminated wastes. The third section explains the management and processing of the T contaminated wastes.

**Keywords** T confinement · T safety · Defense in depth · Multiple confinements system · T contaminated waste

### 14.1 Basic Concepts of Radiation Protection

#### 14.1.1 ALARA Concept

In order to ensure radiation safety of a fusion reactor, radiological protection from T and activated materials by neutron irradiation is the most important issue. The basic concept to protect human being from radiation is suggested by a non-governmental

---

K. Katayama (✉) · M. Nishikawa  
Interdisciplinary Graduate School of Engineering Sciences, Kyushu University, 6-1  
Kasuga-Kouen, Kasuga, Fukuoka 816-8580, Japan  
e-mail: kadzu@nucl.kyushu-u.ac.jp

international organizer, the International Commission on Radiological Protection (ICRP), based on the latest scientific data. After the discussion by experts of radiology on radiation genetics based on various animal experimental data and the epidemiological analysis of Hiroshima–Nagasaki atomic bomb survivors, the radiological protection concepts were proposed and have been updated. Many countries respect ICRP recommendations and employ them as their national regulations. The following sentence in the recommendation is famous as ALARA concept [1].

“The likelihood of incurring exposures, the number of people exposed, and the magnitude of their individual doses should all be kept As Low As Reasonably Achievable (ALARA), taking into account economic and societal factors”.

#### ***14.1.2 Deterministic Effects and Stochastic Effects***

It is known that there are two types of harmful effect by radiation. Severity of each effect against radiation dose is shown in Fig. 14.1. One is “deterministic effect.” A threshold value of the radiation dose exists in each organ and tela, and if the doses exceed the threshold, symptoms appear clearly. The severity of the radiation effect

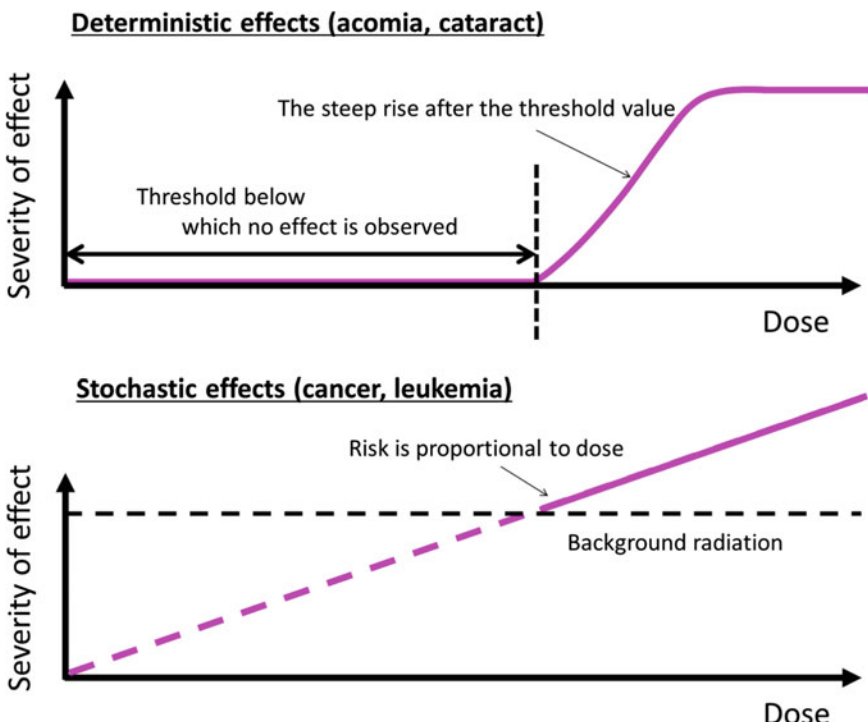


**Fig. 14.1** Deterministic effects and stochastic effects

increases with increasing the doses. If the doses can be suppressed to be below the threshold, the radiation effect can be prevented. When a high dose of radiation is exposed in a short period, the disorder will be appeared in mucosa of skin or gut and spinal marrow. This effect is referred to as “acute disorder” and appears sometimes after several years or ten years of the exposure. The possibility to appear the symptom increases depending on the cumulative dose, even if the radiation dose is not high. This type of effects is referred to as “stochastic effect.” As of now, it is said that stochastic effect by the radiation dose below around 100 mSv is unclear. ICRP assumes that the incidence of the stochastic effects increases proportionally to the radiation dose. This assumption is referred to as “linear non-threshold (LNT) model”.

### 14.1.3 Radiation Exposure

As shown in Fig. 14.2, there are two types of radiation exposure. One is external exposure, and another is internal exposure. Radiation exposure by radioactive materials taken into the body is referred to as “internal exposure”. Radiation exposure when a radiation source is outside of the body is referred to as “external exposure”. Because the energy of  $\beta$  ray from T is low, the radiological effect by the external exposure of T is quite weak. Hence, the protection of the internal exposure of T is mainly concerned.

#### (a) Internal Exposure

Internal exposure is caused by radioactive materials entered in human body through inhalation, ingestion, absorption, or injection. Followings are basic protection mechanisms against the internal radiation exposure.

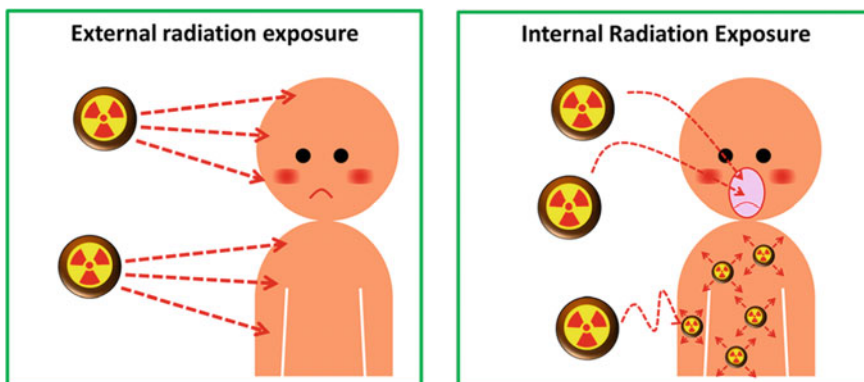


Fig. 14.2 External and internal radiation exposure

- Isolating radioactive materials from the workers by physical barriers.
- Wearing respiratory protective equipment to avoid an inhalation of radioactive materials or and radioactive dust.
- Ventilating air to reduce the contamination level of the work area.
- Monitoring the concentration of radioactive materials in the air appropriately.
- Prohibiting to eat and drink in any contaminated areas.

A certain amount of T leakage from any T handling systems containing a large amount of T cannot be avoided. As to a fusion power plant, at various occasions, such as the maintenance of fuel processing equipment, the replacement of in-vessel components such as divertor and blanket, and the disposal processing of wastes, workers have to handle T contaminated materials in open space. The internal exposure of the workers must be reduced following to the ALARA concept. Equipment and tools for radiological protection in T handling are explained in the next section.

(b) External exposure

Basic concepts of the protection against external exposure are as follows:

- Reducing the amount of radioactive materials handled by the workers.
- Keeping enough distance between the radiation source and their body.
- Putting the shielding material between the radiation source and their body.
- Shortening the radiation exposure time.

During operation of a fusion reactor, the workers cannot enter the reactor building due to high radiation dose. During the maintenance and the repair of activated in-vessel components, the hot cell building becomes the high radiation area in addition to the reactor building. Moreover, a certain amount of activated dust will be scattered in the transportation process of the in-vessel components from the reactor building to the hot cell building. Evaluation of the contamination level and strict access control at possible contaminated areas in these buildings is important to protect the workers from radiation exposure.

#### **14.1.4 Radiation Protection from T**

The maximum energy of  $\beta$  ray from T is 18.6 keV, and the mean energy is 5.7 keV. It is known that the range of the  $\beta$  ray in tissue is less than 6  $\mu\text{m}$  but the thickness of skin is around 70  $\mu\text{m}$ . Therefore, the external exposure of T is not hazardous. The radiotoxicity of T for the internal exposure varies depending on chemical form of T. The radiotoxicity of HTO caused by inhalation is 10,000 times larger than that of HT. Furthermore, the radiotoxicity of OBT, which is organically bound T, caused by the inhalation is 22,800 times larger than that of HT [2]. Owing to the egestion

of water, the amount of HTO in the body reduces exponentially with a half-life of ~ 10 days [3].

Equipment and clothing to protect workers from the internal exposure are briefly explained below. Various tools are used for the radiation protection in T handling facilities in the world. Appropriate use or selection of the tools according to T amount handled in a system is quite important.

#### (a) Fume hood and glove box

A fume hood in which a small amount of T is handled equips a local ventilation system. When T is released or a T including material is handled in the hood, any gases including T released in the hood are transported to the exhaust system together with air coming into the hood from the open window of the hood. In order to prevent the spreading of contaminated air from the hood to the room through the front space, the ingress rate of the air from the front space into the fume hood is controlled not to regurgitate.

Different from the fume hood, a glove box is an airtight container and materials containing T inside the box are handled by gloves. The box is usually kept at negative pressures around 100–300 Pa lower than the atmosphere. The materials handled in the glove box are brought in or taken out through a pass box equipped with the glove box. The inside of the pass box can be evacuated or filled with an inert gas to avoid the release of T to the outside. When the radioactivity level is low and the probability of spreading T by handling is little, a simplified acrylic glove box is used without the ventilation system. The ventilation system is connected to a detritiation system (DS), which is explained in the next section.

#### (b) Personal protective clothing

When workers go in T contaminated area or handle directly T contaminated materials and/or equipment, protective clothing such as a smock, gloves, and shoe covers are required.

**Smock:** The smock or laboratory coat is adequate for a worker in a room where T activity is low or T is handled in fume hoods or glove boxes. If contamination levels are not low, an overall is worn instead of the smock. Such clothing is generally reusable after washing. Disposable smocks or laboratory coats are also commercially available.

**Gloves:** Workers wear gloves to minimize the uptake of T through their skin at handling contaminated or potentially contaminated subjects by T. The gloves are usually made of latex or polyvinyl chloride (PVC). PVC is preferred because of its lower permeability to HTO and HT and its low chemical reactivity. Depending on T activity, gloves may be worn doubly or triply with the outermost one being exchanged at proper intervals. In case of the triple use, the innermost could be cotton gloves, the second, polyethylene gloves, and the outermost, elbow-length latex gloves to protect the upper arm. It should be noted that the gloves, after handling contaminated subjects, should be kept off from any uncontaminated surfaces to avoid cross-contamination.

**Boots:** Generally, wearing of boots or shoe covers is always required in any laboratory rooms for handling radioactive materials. However, in some laboratories, where T is handled in the glove boxes or fume hoods, the wearing may not be required. However, from a viewpoint of suppression of spread of T contamination, it is better to wear them in any T handling rooms.

**Mask:** In order to avoid inhalation of T contaminated gases or dust, wearing a mask is important. A cotton mask is worn with a smock when T contamination level is low. A mask with the double-layered cotton clothes is usually used, and a piece of wet cotton cloth is inserted between the layers so that HTO is expected to be captured in the wet cotton by an isotope exchange reaction with H<sub>2</sub>O for a short while, even if workers breathe the T contaminated air unintentionally.

When the contamination level of T in the atmosphere of a working room is potentially high, a full face mask is used together with wearing an overall. The full face mask equips a filter to adsorb airborne T such as HTO and CH<sub>3</sub>T. The principal hazard in a T handling room is a sudden release of airborne T, which can be drawn in a breath of workers and can be adsorbed through skin. When the sudden T release happens, the workers are immediately evacuated from the room. During evacuating, the overall can suppress intake of T. When a person works in highly contaminated atmosphere or handles highly contaminated materials by T in open space, a full face mask with fresh air supply is used with full plastic suits.

**Plastic suits:** Plastic suits are made with low T permeability materials such as PVC and Tyvek (high-density polyethylene) and have high airtightness. Fresh air is supplied from a ventilation system via connected tubes for inhalation, cooling, and keeping positive pressure against the penetration of T contaminated air. A plastic suit with a full face mask with a ventilation system can protect a human body from T inhalation and absorption significantly. However, it takes a long time to conduct a task with plastic suits compared with the further simplified protective clothing because it is hard to move quickly and delicately with a plastic suit. In a fusion power plant, highly contaminated materials with T are handled. With considering risks of not only internal exposure by T but also external exposure by high dose  $\beta$  and  $\gamma$ , personal protective clothing has to be selected properly.

### **14.1.5 Dose Limit of T**

Radiation exposures are categorized into following three [1].

- (a) Occupational exposure: Radiation exposures of workers incurred as a result of their work.
- (b) Medical exposure of patients: Radiation exposures of patients under diagnostic, interventional, and therapeutic procedures.
- (c) Public exposure: Radiation exposures of the public other than occupational exposures and medical exposures.

**Table 14.1** Recommended dose limits in planned exposure situation<sup>a</sup> [1]

Type of limit	Occupational	Public
Effective dose	20 mSv per year, averaged over defined periods of 5 years <sup>e</sup>	1 mSv in a year <sup>f</sup>
<b>Annual equivalent dose in:</b>		
Lens of the eye <sup>b</sup>	150 mSv	15 mSv
Skin <sup>c,d</sup>	500 mSv	50 mSv
Hands and feet	500 mSv	—

<sup>a</sup>Limits on effective dose are for the sum of the relevant effective doses from external exposure in the specified time period and the committed effective dose from intakes of radionuclides in the same period. For adults, the committed effective dose is computed for a 50-year period after intake, whereas for children, it is computed for the period up to age 70 years

<sup>b</sup>This limit is currently being reviewed by an ICRP task Group

<sup>c</sup>The limitation on effective dose provides sufficient protection for the skin against stochastic effects

<sup>d</sup>Averaged over 1 cm<sup>2</sup> area of skin regardless of the area exposed

<sup>e</sup>With the further provision that the effective dose should not exceed 50 mSv in any single year. Additional restrictions apply to the occupational exposure of pregnant women

<sup>f</sup>In special circumstances, a higher value of effective dose could be allowed in a single year, provided that the average over 5 years does not exceed 1 mSv per year

Radiation exposure situations are also categorized into following three [1].

- (a) Planned exposure situation: A radioactive source is used with deliberation.
- (b) Emergency exposure situation: Urgent action is required to avoid undesirable consequences.
- (c) Existing exposure situation: Radiation sources already exist before the radiation exposure control begins. Prolonged radiation exposure after emergency exposure situation is included.

Dose limits recommended by ICRP [1] for the occupational exposure and the public exposure are shown in Table 14.1. Based on these recommended doses, the safe design of a fusion power plant will be carried out.

#### 14.1.6 Derived Air Concentration

The hazard of radioactive materials is evaluated by its radiotoxicity rather than its chemical toxicity. The radiotoxicity of a radioactive material is expressed by an effective dose coefficient, which is derived with considering radiation dose and a tissue-weighting factor, metabolic, and biokinetic information. The effective dose coefficients for inhalation of T for a worker are compared with those of some radioactive gases in Tables 14.2 and 14.3 [4].

**Table 14.2** Effective dose coefficients ( $e$ ) for inhalation of radioactive gasses including T and radioisotopes of carbon and iodine for workers [4]

Nuclide/chemical form	$T_{1/2}$	Effective dose coefficient, $e$ (Sv/Bq)
<b>Hydrogen</b>		
Organically bound tritium(OBT)	12.35 y	$4.1 \times 10^{-11}$
Tritium gas		$1.8 \times 10^{-15a}$
Tritiated methane		$1.8 \times 10^{-13}$
Tritiated water		$1.8 \times 10^{-11b}$
<b>Carbon</b>		
C-11 CO <sub>2</sub>	20.38 m	$2.2 \times 10^{-12}$
CO		$1.2 \times 10^{-12}$
Methane		$2.7 \times 10^{-14}$
Organic gases/vapors		$3.2 \times 10^{-12}$
C-14 CO <sub>2</sub>	5730 y	$6.5 \times 10^{-12}$
CO		$8.0 \times 10^{-13}$
Methane		$2.9 \times 10^{-12}$
Organic gases/vapors		$5.8 \times 10^{-10}$
I-129 CH <sub>3</sub> I	$1.57 \times 10^7$ y	$7.4 \times 10^{-8}$
I <sub>2</sub>		$9.6 \times 10^{-8}$
I-131 CH <sub>3</sub> I	8.04 d	$1.5 \times 10^{-8}$
I <sub>2</sub>		$2.0 \times 10^{-8}$
I-133 CH <sub>3</sub> I	20.8 h	$3.1 \times 10^{-9}$
I <sub>2</sub>		$4.0 \times 10^{-9}$

<sup>a</sup>The value may be increased approximately 20 % by irradiation from gas in the lungs<sup>b</sup>The value does not include effects of absorption through skins**Table 14.3** Effective dose rate coefficients ( $e'$ ) for inhalation of radioactive inert gases for workers [4]

Nuclide/chemical form	$T_{1/2}$	$e'$ (Sv/day per Bq/m <sup>3</sup> )
<b>Argon</b>		
Ar-37	35.02 y	$4.1 \times 10^{-15}$
Ar-39	269 y	$1.1 \times 10^{-11}$
Ar-41	1.827 h	$5.3 \times 10^{-9}$
<b>Krypton</b>		
Kr-74	11.50 m	$4.5 \times 10^{-9}$
Kr-76	14.8 h	$1.6 \times 10^{-9}$
Kr-88	2.84 h	$8.4 \times 10^{-9}$
<b>Xenon</b>		
Xe-121	40.1 m	$7.5 \times 10^{-9}$
Xe-123	2.08 h	$2.4 \times 10^{-9}$
Xe-138	14.17 m	$4.7 \times 10^{-9}$

The intake limit of radioactive materials for a worker in a year (Bq) is referred to as “annual limit on intake (ALI)”. ALI of a radionuclide  $j$  is derived by the following equation:

$$ALI_j = \frac{E_{\text{limit}}}{e}, \quad (14.1)$$

where  $e$  is the effective dose coefficient (Sv/Bq) of  $j$  for a worker. ALI should be based on the dose limit of 20 mSv/year averaged over 5 years without exceeding 50 mSv in any single year. The value of ALI divided by the total volume of air that inhaled by a worker in a working year (Bq/m<sup>3</sup>) is referred to as “derived air concentration (DAC)”. When it is assumed that a worker’s breathing rate is 1.1 m<sup>3</sup>/h and an annual working time is 2000 h, an annual air intake by the worker is 2200 m<sup>3</sup>. Then, DAC of the radionuclide  $j$  is given by the following equation:

$$DAC_j = \frac{ALI_j}{2200}, \quad (14.2)$$

The concept of DAC is utilized for area classification for safe control in ITER [5].

US Department of Energy (DOE) indicates DAC for T in DOE HANDBOOK [6] as follows. The DAC for T is T concentration in the area that would give approximately a 50 mSv dose for a worker who works in the contaminated area over a one-year period and is given by the following formula:

$$DAC \left( \frac{\text{Bq}}{\text{m}^3} \right) = \frac{50 \text{ (mSv)}}{e} \cdot \frac{1}{2400 \text{ (m}^3\text{)}}, \quad (14.3)$$

where 2400 m<sup>3</sup> is averaged breathing volume for a worker over 1 year which is derived from 0.02 m<sup>3</sup>/min × 60 min/hr × 40 h/wk × 50 wk/yr. DAC for HTO (includes a 50 % allowance for skin absorption) is 7 × 10<sup>5</sup> Bq/m<sup>3</sup>, and DAC for HT is 9 × 10<sup>9</sup> Bq/m<sup>3</sup>.

Many countries respect ICRP recommendations and take the recommendations as national regulations. In Japan, the laws relating to radiation protection were enacted based on the 1990 Recommendations referred to as “Publication 60” [7]. The regulation limits in air and effluent for T are established by Laws Concerning the Prevention from Radiation Hazards due to Radioisotopes and Others as shown in Table 14.4.

When a fusion power plant will be constructed in Japan, T concentration in workspace, exhaust gas, and effluent water shall be regulated based on the values listed if these are not updated.

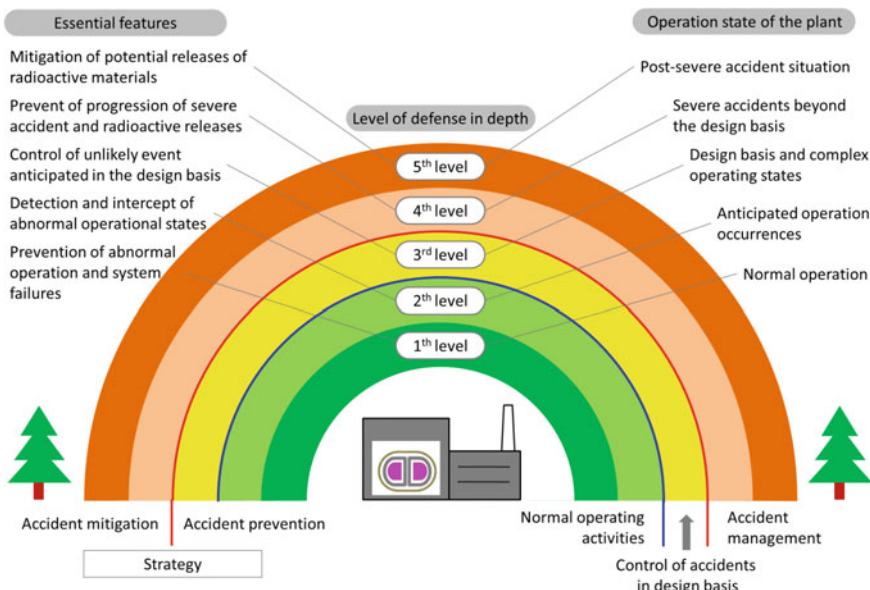
**Table 14.4** T regulation limits in air and effluent in Japan

Nuclide/chemical form	Controlled area Air (Bq/cm <sup>3</sup> ) average a week	Boundary Air (Bq/cm <sup>3</sup> ) average a month	Effluent (Bq/cm <sup>3</sup> ) average a month
Tritium gas	10,000	70	—
Tritiated methane	100	0.7	—
Tritiated water	0.8	0.005	60
OBT	0.5	0.003	20
Other tritium compound	0.7	0.003	40

## 14.2 Multiple Confinements System

### 14.2.1 Concept of Defense in Depth

A concept referred to as “defense in depth” has been applied for confinement of radioactive materials in nuclear installations. The T confinement system in a fusion power plant is established based on this concept. Figure 14.3 shows the conceptual illustration of defense in depth that is generally structured in five levels. Objectives and means in each level indicated by International Atomic Energy Agency (IAEA) are summarized in Table 14.5 [8]. Should one level fail, the subsequent level comes

**Fig. 14.3** Concept of defense in depth

**Table 14.5** Levels of defense in depth [8]

Levels of defense in depth	Objective	Essential means
Level 1	Prevention of abnormal operation and failures	Conservative design and high quality in construction
Level 2	Control of abnormal operation and detection of failures	Control, limiting, and protection systems and other surveillance features
Level 3	Control of accidents within the design basis	Engineered safety features and accident procedures
Level 4	Control of severe plant conditions, including prevention of accident progression and mitigation of the consequences of severe accidents	Complementary measures and accident management
Level 5	Mitigation of radiological consequences of significant releases of radioactive materials	Off-site emergency response

into play. The objective of the first level of protection is the prevention of abnormal operations and system failures. If the first level fails, the abnormal operations are controlled or the system failures are detected by the second level of protection. Should the second level fail, the third level ensures that safety functions are further performed by activating specific safety systems and other safety features. Should the third level fail, the fourth level limits accident progression through accident management, so as to prevent or mitigate severe accident conditions with external releases of radioactive materials. The last objective (fifth level of protection) is the mitigation of the radiological consequences of significant external releases through the off-site emergency response. The strategy for defense in depth is twofold: the first, to prevent accidents and, the second, if the prevention fails, to limit their potential consequences and prevent any evolution to more serious conditions.

#### **14.2.2 Characteristics of Fission and Fusion Reactors on Safety**

In fission and fusion reactors, the most important safety issue is to minimize the release of radioactive materials to the environment. The following three are the fundamental rules to keep safety in a fission reactor [9].

- **Reactor shutdown:** When an abnormal event occurs, fission chain reactions are stopped immediately.
- **Reactor cooling:** Decay heat by fission products (FP) is removed by cooling to prevent the damage of physical barriers to contain FP.
- **Radiation confinement:** Radioactive materials are confined in the fission reactor to protect the public against radiation exposure.

In case of a fusion reactor, DT fusion reaction stops without active shutdown operation when an abnormal event occurs in the reactor core. Furthermore, decay heat of activated materials can be removed without active cooling operation because the decay heat is much less than that of a fission reactor. Therefore, the importance of “shutdown” and “cooling” is lower than “confinement”. From the viewpoint of safety in the fusion reactor, the confinement of T and other radioactive materials is the most important issue.

### **14.2.3 T Confinement in T Handling Facilities**

In the safety operation of a fusion power plant, the most important issue is to confine T in the plant. Several large-scale T handling facilities have been constructed mainly to perform R&D for T handling in a fusion reactor, and various results and experiences for the T handling have been accumulated. In this section, T confinement methods applied in existing T handling facilities are explained and T confinement strategy in a fusion power plant is discussed. The following are fundamental and important points for handling T safely.

1. To equip multiple physical barriers.
2. To maintain the air flow from T low-concentration space toward T high concentration space.
3. To limit T inventory in any compartments.
4. To install T monitoring and detritiating systems in each compartment.
5. To design an appropriate detritiation system for each compartment considering the amount of T and its chemical form handled.
6. To avoid spreading T contamination.

To avoid wide spreading of T in an accident, the building is divided into several spaces for T safety management. The space is referred to as “compartment” here, and each compartment is airtight and is physically isolated in emergency.

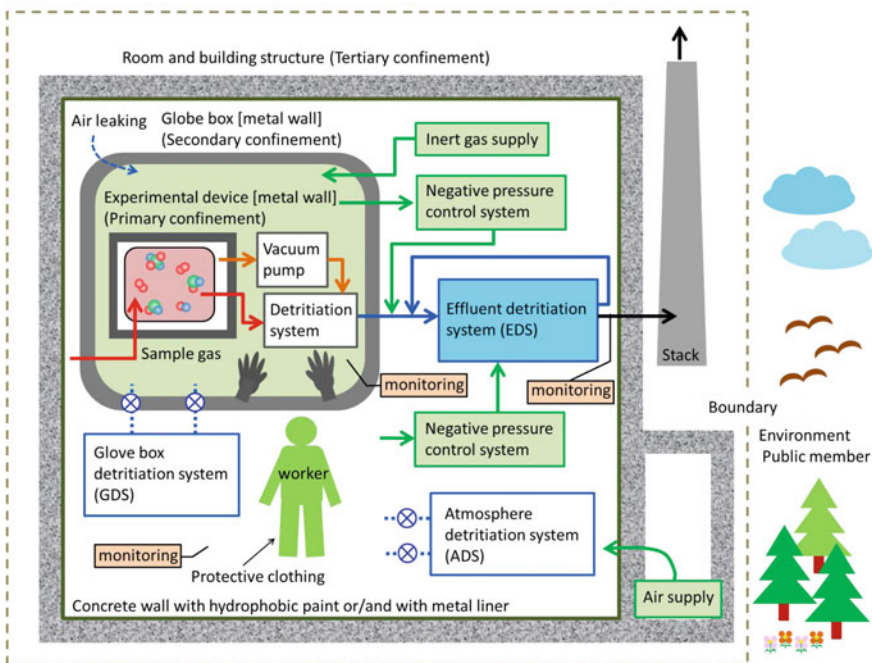
#### **14.2.3.1 Triple Confinement System**

Figure 14.4a shows the concept of triple confinements of T in one compartment. The primary confinement owes T handling equipment and connecting pipes. The equipment and pipes are set in a glove box or a negatively pressurized room as the secondary confinement system. The tertiary confinement is ensured by a concrete wall of the building. An independent DS is installed in each confinement system. The exhaust gas through ventilation of each system is detritiated and is released to the environment from the stack via filters, blowers, and T monitors. Figure 14.4b, c conceptually show the countermeasure for unintentional T release into the glove box and for T leakage to the workspace, respectively. In the next paragraphs, each confinement system is explained.

### (a) Primary confinement system

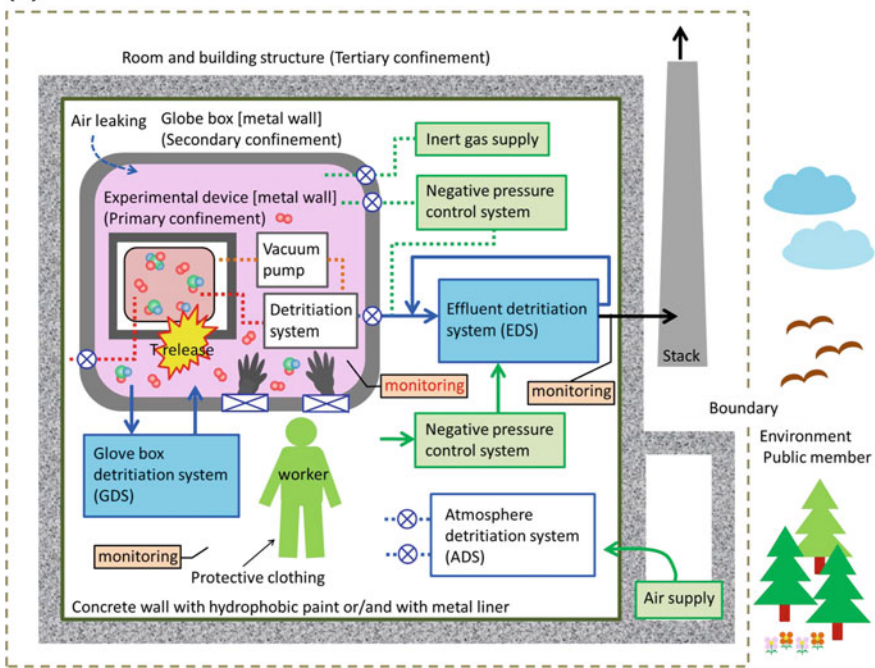
T handling equipment and pipes are consisting of airtight parts to ensure the primary confinement. The airtightness must be confirmed with pressurized leak tests or evacuated leak tests. When the equipment and pipes are operated at higher temperatures, T permeation through their wall is unavoidable, which requires double-layered wall or tube structure. The space between the layers or tubes is purged by an inert gas or evacuated by a vacuum pump, and the permeated T is removed by DS to suppress T release to the outer space. All working gases in any T handling systems are processed by DS before their exhaustion. Exhausted gasses from DS are further processed by an effluent detritiation system (EDS). Even if a malfunction occurs in DS, T can be recovered by EDS. T concentrations in the exhausted gases and waters from any T handling systems are always monitored by an ionization chamber or a proportional counter. When observed T concentration exceeds the preset concentration, the system operation is suspended and a cause of the malfunction of DS is pursued. The confirmation of normal operation of DS is very important from a viewpoint of T confinement.

**(a)**

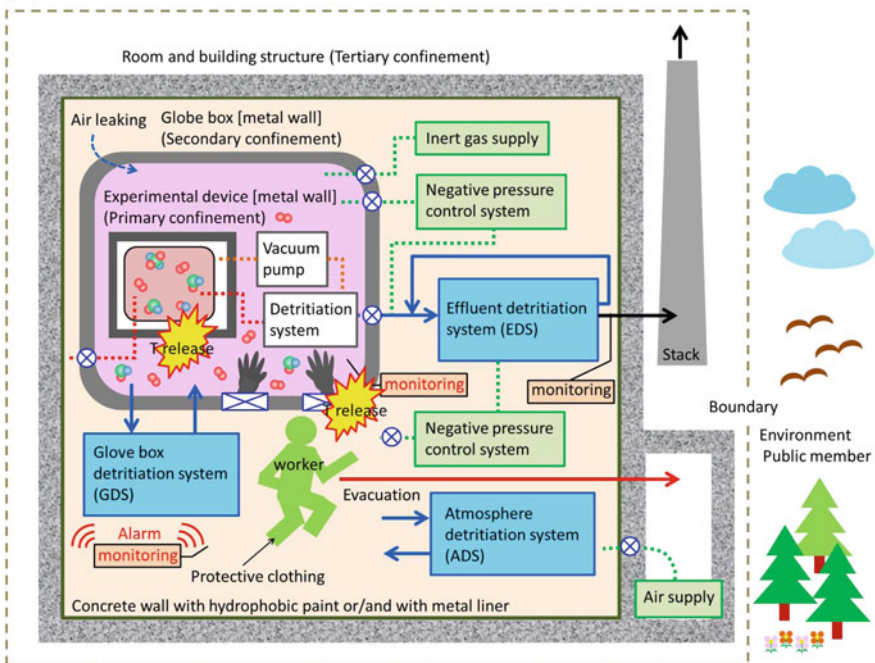


**Fig. 14.4 a** Explanatory drawing of a triple confinement for T under the normal operation. **b** Explanatory drawing of a triple confinement for T under the unintentional T release into the glove box. **c** Explanatory drawing of a triple confinement for T under the accidental T leakage to the workspace

(b)



(c)

**Fig. 14.4** (continued)

(b) Secondary confinement system

A glove box, which works as the secondary confinement system, mainly consists of observation windows, a glove-installation port, and a pass box. Airtight feed-through is also equipped for power supply to operate experimental apparatus in the box. In order to avoid hydrogen explosion, the glove box is usually filled by an inert gas with installation of equipment to maintain the negative pressure and to adjust the purity of the inert gas against the air leakage, together with DS and a monitoring system. The glove box is often ventilated in order to dilute inside T concentration. A fresh inert gas is supplied into the glove box, and a potentially contaminated inert gas is exhausted. The ventilation is also necessary for the temperature management in the glove box. The pass box is used for taking experimental samples or tools in and out of the glove box avoiding its directly opening to air. The atmosphere of the pass box is separately controlled from that of the glove box. Since water vapor permeates gloves made of polymer films faster than hydrogen, the worker wears double or triple gloves on his hands with occasional replacements. In order to avoid T contamination of his hands, the gloves are replaced with new one at proper intervals.

When the T concentration in the exhausted gas from the glove box becomes higher than the preset limit concentration, the negative pressure control system is automatically shut off and the glove box detritiation system (GDS) is launched to remove T in the glove box with closed ventilation. Such situation is shown in Fig. 14.4b. The negative pressure in the glove box is maintained by GDS. Because T permeation through the equipped gloves is promoted due to the increase in T pressure in the glove box, the ports for the gloves are closed immediately. While the T concentration is gradually decreased by GDS, the worker needs to pay attention to a T room monitor whether T leaks to the room or not.

(c) Tertiary confinement system

The concrete walls of rooms or building ensure tertiary confinement and are the last boundary to the environment. Airtight and waterproof coating usually cover the inner surface of the wall. In case that T activity used in the room is high, a metal liner may be installed on the wall. The negative pressure against neighboring environment is maintained so that T leakage to the environments is suppressed even if T is released from the T handling systems or glove boxes. Constantly, a fresh air is fed by air supply equipment and the potentially contaminated air is exhausted to EDS by a blower. The air in the building is designed to flow from low contamination area to high contamination area. When a T monitor detects high T concentration, alarm sounds immediately. The worker stops to work and escapees promptly. The negative pressure control system and the air supply system are

automatically shut off, and the atmosphere detritiation system (ADS) is launched to remove T in the room with closed ventilation. The negative pressure in the room is maintained by ADS. Such situation is shown in Fig. 14.4c. DS of the tertiary confinement system is very important to avoid T leakage to the environment. DS must be designed to work soundly even in fire emergency. It is known that it takes a long time to remove T retained in concrete walls. Prompt T recovery from the atmosphere is required in order to restore normal situation quickly after accidental T leakage.

#### **14.2.3.2 Experiences of T Handling**

Major T handling facilities presently operated for R&D of T handling in a fusion power plant are summarized in Table 14.6. It should be noted that the allowable amount of T in each facility is far less than that in ITER which will use the similar amount of T as used in a fusion power plant. Therefore, extrapolation or applicability of the present experience of T handling to that in ITER or a reactor is not certain, and hence, all T handling systems in ITER will be the first test bed to safely handle the huge amount of T.

#### **14.2.4 T Confinement in a Fusion Power Plant**

Although basic concepts to confine T in a fusion power plant are same as those in the present T handling facilities, a huge amount of T in the fusion power plant forces T handling facilities not only to scale up but also to have some different concepts/methods. For handling of a small amount or tracer level of T, simple experimental equipment is installed in a glove box. To handle the huge amount of T, on the other hand, complicated T processing systems will be installed in glove boxes with remote controlling so that no workers stay or enter the room containing

**Table 14.6** Major T handling facilities in the world [10]

Country	Institute ·facility	Allowance (g)	DS for primary confinement ( $m^3/h$ )	DS for secondary confinement (B) ( $m^3/h$ )	DS for final confinement ( $m^3/h$ )
Japan	JAEA·TPL	62	20	150	300
Germany	FzK·TLK	40	120	50	by (A) (B)
USA	LANL·TSTS	200	90	by (A)	2500
USA	PPPL·TFTR	5	85	17	1700
UK	EURATOM·JET	90	500	by (A)	by (A)
France	IILE·ITER	3000	700	150	3000–4500

DS: Detritiation system

the glove boxes, except for maintenance and inspection. In this section, T confinement methods in a fusion power plant are discussed taking into account the characteristic of each T processing system.

#### 14.2.4.1 T Confinement in Each Subsystem

A fusion power plant consists of various T processing subsystems, and as an example, a conceptual drawing of a fusion power plant configuration with solid breeder and water cooling is shown in Fig. 14.5. In each subsystem, chemical forms and physical states of T flowing in and out are often significantly different. In this section, T confinement in each subsystem is described referring defense in depth with consideration of T release or leakage from primary, secondary, tertiary confinements, and final release to the environment.

##### (a) Fuel cycle system

The fuel cycle system consisting of various subsystems connected by pipes constitutes the primary confinement system. All subsystems are designed to confine T well so that T leakage or permeation to the outside of the subsystems should be little under their normal operation. In the followings, concerns of each subsystem on T confinement are noted.

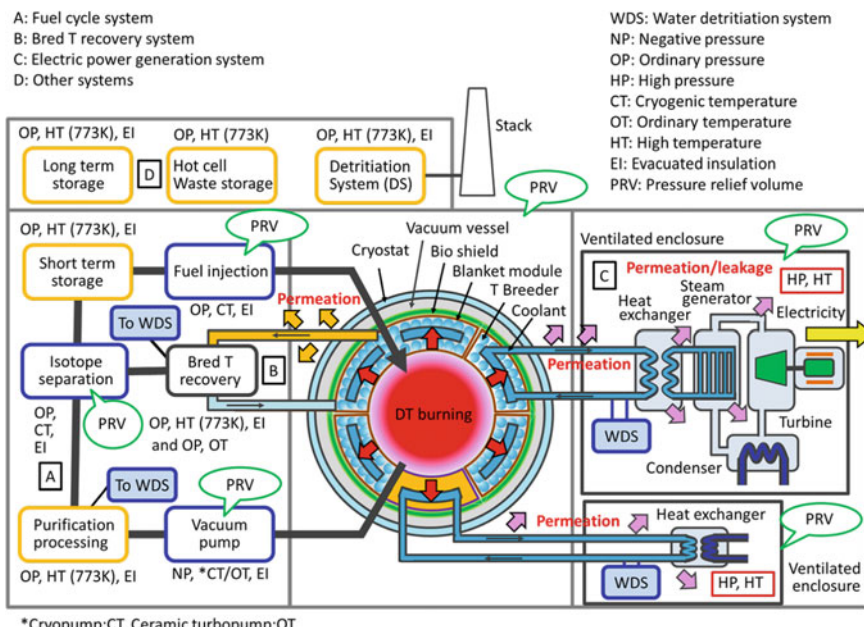


**Fig. 14.5** Conceptual drawing of a fusion power plant configuration with solid breeder and water cooling

A fusion reactor constructed of a large vacuum vessel has the largest T inventory except for T reservoir. Therefore, it is extremely important to maintain the structure soundness of the vacuum vessel. As the primary confinement system, the vacuum vessel is protected from any damage given by abnormal plasma event such as disruption, a pressure rise accompanied by the fracture of cooling pipes, and a temperature rise by the loss of coolant in its cooling system. When water is used as the coolant, it is necessary to consider the safety guarantee for reactions of hot water with any materials used in the vacuum vessel. Possible emergency events at the vessel are release of activated dust at the vacuum break and coolant contaminated with T at the troubles of cooling tubes.

Cryo-sorption pumps and ceramic turbo-molecular pumps are candidates to be employed in vacuum exhaust systems. The cryo-sorption pumps will be used in ITER. Their T inventory is relatively large because all exhaust gases including T are temporarily stored on the adsorbent panel at cryogenic temperatures. A pressure relief system is required against a pressure rise by refrigerator trouble with the cryo-sorption pump. For DEMO or commercial reactors, the development of a ceramic turbo-molecular pump with a large exhaust capacity is expected. T inventory in ceramic turbo-molecular pumps is smaller than that in cryo-pumps because T exhausted from the vacuum vessel is continuously transported to the fuel purification system. For both vacuum exhaust systems, T leakage or permeation under their normal operation is little because T is treated at low/ordinary temperatures and negative pressure.

A fuel purification system is explained in Chap. 6. The reaction container is insulated by vacuum because T permeation and leakage from the container are not negligible. T permeated in the vacuum region is continuously recovered in DS. Assuming the failure of the vacuum insulation, the processing equipment would be installed in a ventilated enclosure (VE).

As an isotope separation system, a cryogenic distillation method is a primary candidate because of its large processing capacity, while its T inventory becomes relatively large because of liquidation of the fuels for the distillation. The reaction container is insulated by vacuum to maintain cryogenic temperature effectively. A pressure relief system is required against a pressure rise by the refrigerator trouble. A constant T leakage or permeation is little because T is treated at a low temperature and ordinary pressure.

$T_2$ ,  $D_2$ , or DT prepared in the isotope separation system is stored in hydrogen storage alloys once, and it is transported to fueling systems as needed. ZrCo or U beds that can release T by heating of around 500 °C are used. Insuring against the failure of the vacuum insulation and considering a large T inventory, the storage bed would be installed in VE.

The fueling systems include gas puff, ice pellet injection, and neutral beam injection (NBI). As to the gas puff system, there are no particular concerns relating to T confinement. As to the ice pellet injection system, ice pellets of  $T_2$  and  $D_2$  or DT have to be manufactured continuously at cryogenic temperatures. In the NBI system, a cryo-sorption pump is used to maintain the injection port at high vacuum

condition. In the ice pellet manufacturing system and NBI system, a pressure relief system is required against a pressure rise by the refrigerator trouble.

(b) Bred T recovery system

Bred T recovery systems in solid/liquid blanket are explained in Chap. 13. In a solid breeder blanket, the partial pressure of bred T in the purge gas is kept to be low to suppress T permeation into a coolant. In a liquid breeder blanket using LiPb or Flibe as a coolant, the double-tube structure may be required in the pipes/tubes on which LiPb or Flibe flows in order to suppress T permeation to the outside. In a liquid breeder blanket using Li as a coolant, large T inventory is main concern.

(c) Electric power generation system

The heat generated in the blanket and carried by the coolant is converted to electric energy in a power generation system. At the same time, a part of the bred T and also a part of the energetic T implanted in the plasma facing wall permeate into the coolant, and T permeating into the coolant is finally transported to turbines in the power generation system. Therefore, the suppression of the T permeation into the coolant is the most effective countermeasure to avoid the T contamination of the power generation system.

(d) T storage system

The T long-term storage system stores about a month's fuel and supplies T to the fuel cycle system as needed. A large amount of T is subdivided into about 100 g each, and T is stored stably in hydrogen storage alloys as hydride. The long-term storage system is important from a viewpoint of security, too. It is necessary to manage storage beds appropriately so that its safety confinement system is not destroyed by any external factors. The storage beds should be distributed dispersely in a plant so that a large amount of T is not lost by one accident.

#### 14.2.4.2 Detritiation System

(a) Detritiation of contaminated atmosphere

DS consists of the atmosphere detritiation system (ADS) and EDS. As explained in the previous section, T released in a work space at an abnormal event is recovered by the closed recirculation using ADS. The exhaust gas by normal ventilating in each enclosure or compartment is processed in EDS. Figure 14.6a shows the case that this method is applied in both ADS and EDS. Generally, a catalytic oxidation–water adsorption method is applied in both ADS and EDS. This detritiation method is commonly used in existing large-scale T handling facilities. The catalytic reaction bed consists of two catalytic layers at 200 and 500 °C. The first catalytic layer can oxidize HT, and the second one can oxidize hydrocarbon. The generated HTO is recovered in the adsorption bed. In the normal operation, the exhaust gas for maintaining the negative pressure in the compartment is transported

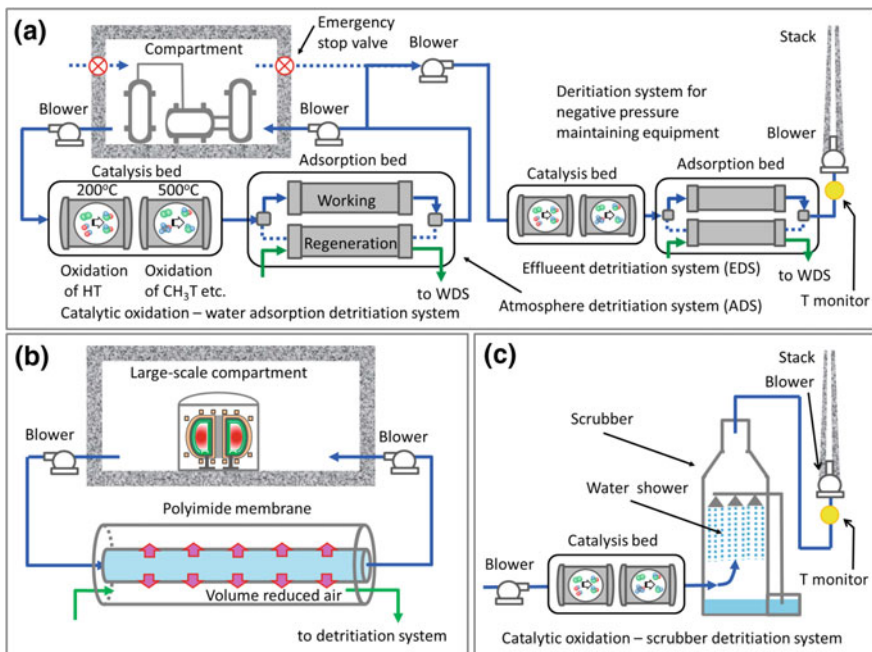


**Fig. 14.6** Explanatory drawing of detritiation systems (DS). **a** A catalytic oxidation–water adsorption method. **b** DS using polyimide membrane. **c** A catalytic oxidation–water exchange (scrubber) method

to EDS and is released from a stack into the environment after T concentration is monitored. When the T monitor detects high T contamination, the emergency isolation valve is automatically shut down and a closed ventilating by ADS is launched. After the T concentration decreases sufficiently, the isolation valve is opened and the system returns to the normal operation. In order to maintain the negative pressure in a compartment during closed ventilation by ADS, a part of the circulating gas flows to EDS.

Duplicated adsorption beds are necessarily installed in the system. When one bed is adsorbing T, another is desorbing T by heating. Although an adsorption/desorption operation is a batch-type process, continuous processing is possible by repeating adsorption and desorption alternately. The adsorption operation has to be terminated before the breakthrough of HTO in the bed. Considering adsorption capacity of the bed and the averaged humidity in the compartment, the switching time of adsorption and desorption is planned appropriately. T concentration in the outlet gas of the adsorption bed is monitored, and when the T concentration increases unintentionally, the adsorption bed is switched to another one immediately.

A part of the released T flows into EDS until the emergency isolation valve is completely closed after the T leak occurs. Numbers of T monitors and their locations to be installed are determined in the consideration of the size of a compartment and a

ventilation-air flow in it. If T monitors and emergency isolation valves do not work, a large amount of released T is introduced in EDS. Therefore, EDS should have enough detritiation capacity to avoid T release to the environment even in emergency. When T leaks to a compartment (room), it is known that T recovery rate in a wet atmosphere condition is faster than that in dry atmosphere condition.

In the wet atmosphere condition, the majority of the leaked T is retained in the water vapor adsorbed on the wall. When the ventilation by ADS starts, T is removed together with adsorbed water vapor quickly. On the other hand, in the dry atmosphere condition, the majority of leaked T is retained on the wall surface as structural water such as OH basis and crystal water by the isotope exchange reaction. Then, it takes long time to remove T by dry gas circulation by ADS. To quickly recover T after the T leakage accident, it is effective to adjust the humidity of the supplied air. However, it should be avoided to raise the humidity of the atmosphere excessively because a load to the adsorption bed in DS increases.

For a large space such as a fusion reactor building, EDS becomes very large because throughput of processing air is large. To miniaturize a whole EDS system from a viewpoint of cost, the method that utilizes a polyimide membrane has been proposed [11]. The schematic diagram of the polyimide method is shown in Fig. 14.6b. Permeation rates of hydrogen and water vapor through the polyimide membrane are much larger than that of nitrogen. Therefore, the volume reduction in processing air and the condensation of HT or HTO are possible. Consequently, the air passed through the polyimide membrane can be processed by a smaller-scale catalytic oxidation–water adsorption method. A catalytic oxidation–water exchange (scrubber) method is also available as DS. The schematic diagram of this method is shown in Fig. 14.6c. The failure probability of this method is lower than that of the catalytic oxidation–water adsorption method because there is no switching operation of adsorption and regeneration. Since some metals such as Ti, Zr, and U absorb a large amount of hydrogen isotopes as hydrides, metal getter beds can be used as DS for a small compartment such as a glove box or a metallic enclosure. T is recovered by contacting to these metals.

A catalytic oxidation–water adsorption equipment is very important system from a viewpoint of T confinement. Even in blackout situation, ADS is required to work well without heating of the catalyst beds. However, an HT oxidation efficiency of the catalyst bed decreases at room temperature because of the adsorption of generated water vapor. To solve this issue, installation of an additional adsorption bed in the upstream of the catalyst bed has been proposed to suppress influence of the water vapor [12]. As for an alternative way of the HT oxidation, a bioreactor using creature reactions in natural soils has been also proposed. Recently, the catalyst which works even at room temperature was developed [13]. It is also necessary to confirm that these methods work well for various occasions, particularly in a fire accident.

#### (b) Detritiation of contaminated water

T concentration in T contaminated water in a fusion power plant distributes very widely and is categorized into exhaust water and reuse water. When the T

concentration is low, it is exhausted with dilution until the T concentration becomes lower than the regulation limit. When the T concentration is high, it is processed in the water detritiation system (WDS). In WDS, T is recovered from the contaminated water and the processed water still containing T with relatively low concentration is reused in the fusion power plant. Details of WDS are explained in Chap. 6.

#### 14.2.4.3 Structural Configuration of Building

To image a fusion power plant building, a conceptual drawing on which main equipment are properly positioned is shown in Fig. 14.7. The figure also shows the multiple confinement concepts in the fusion power plant. A reactor vessel is one of the primary confinements, and concrete walls of the reactor building are the secondary confinement. Hot cells for maintenance and repairing and T fuel processing systems are independently placed in neighboring buildings constructed of concrete to ensure multiple confinements.

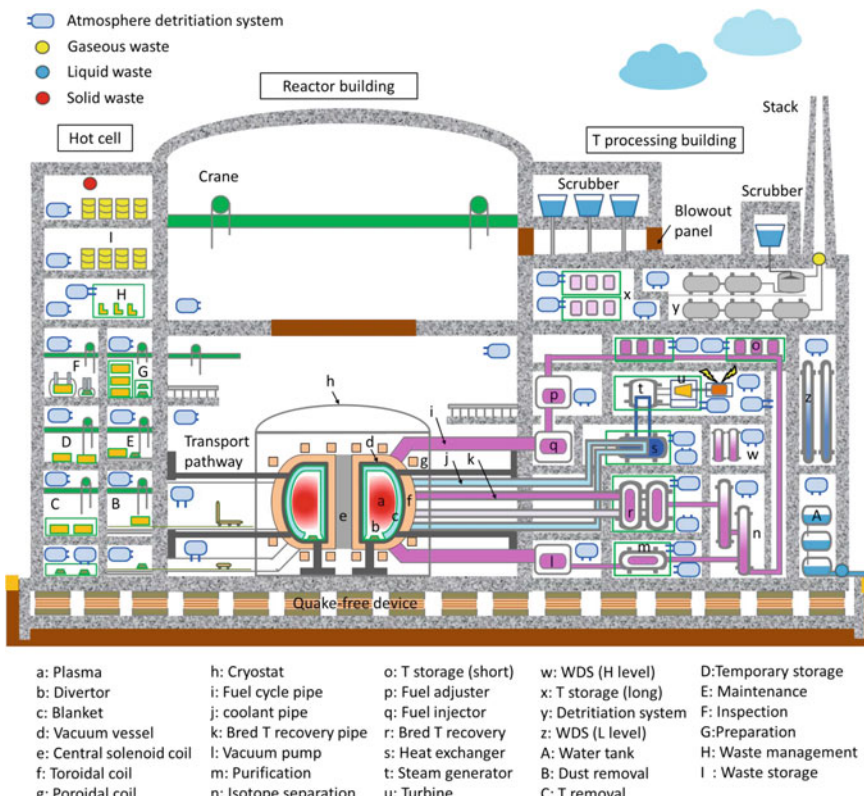


Fig. 14.7 Conceptual drawing of a fusion power plant building

The reactor is placed at the central building which has a large volume and a high ceiling because a crane is necessary for assembly and repair of the reactor. The hot cells are designed to be in a multistoried building. Sizes and weights of components to be handled in the hot cell building decrease for upper floors. The T processing building contains all subsystems for fuel recycling, storage and detritiation separately in its airtight compartment rooms. Some subsystems in which a certain amount of T is constantly leaked are additionally contained in an airtight metal VE. Independent DS and T monitors are installed in each room. Because WDS is large-scale equipment having a water tank on the top of the equipment, it may be reasonable to be installed in the adjoining separated building. Eventually, the detritiated effluent gas is exhausted from a stack to the environment after confirmation of T concentration and radiation dose being under the regulation limit.

In normal operation, there are three kinds of routes that T is potentially released to the environment. First one is the release of gaseous waste from a stack, second one is the disposal of water used or generated in the plant, and third one is the disposal of solid wastes. As mentioned in the previous section, the regulation limit of HT in air is  $70 \text{ Bq}/\text{cm}^3$ , the regulation limit of HTO in air is  $0.005 \text{ Bq}/\text{cm}^3$ , the regulation limit of T in effluent water is  $60 \text{ Bq}/\text{cm}^3$ , and the surface regulation limit for solids is  $4 \text{ Bq}/\text{cm}^2$ , in Japan. Under the strict concentration management, the release of waste to the environment must be carried out.

Because a large amount of T contaminated water is present in a fusion power plant, it is necessary to prepare for off-normal events or severe accidents preventing the release of the contaminated water to the environment. In this respect, it is critically important to maintain soundness of the building structure for the radiation protection of the public and the environment. The seismic isolation structure may be required in the building. Even if the pressure rise occurs by the coolant discharge, the soundness of the building has to be maintained. A large space of the reactor building is effective for the mitigation of the pressure rise. An emergency air vent function may be required in the building structure. In order to suppress the release of radioactive materials such as T, activated Ar, and dust, water scrubbers should be equipped in the vent function.

To lay clay or an adsorbent having a high hydrogen isotope exchange capacity in the surrounding ground may be effective as a countermeasure against the penetration of T into the ground. The spreading of T in the soil can be mitigated by recovering the clay or the adsorbent layer after the T leakage accident immediately.

#### 14.2.4.4 T Monitoring

Concepts and methods of T measurements or monitoring are totally different depending on T concentration or T activity level (see Chaps. 7 and 8 in detail). In the primary confinement, i.e., a reactor vessel and fuel processing equipment, T is dominant component and T monitoring provides information to judge whether normal processing is being carried out in each equipment or not. In the secondary confinement, any increase in its T concentration may indicate off-normal events in

the primary confinement that requires attention and countermeasure. The tertiary confinement is generally set at working area, and hence, the T activity in the working area is always monitored for radiological protection of workers.

Routine monitoring during normal operations provides information that the work area is safe, and it gives an immediate indication of changes in radiological situation. When a worker handles contaminated materials in maintenance activities, monitoring provides an immediate indication and warning of unexpected increase in T activity. Monitoring also indicates necessary radiological protection for succeeding works and workers, for example, allowable staying time in the working area and required protective clothing.

T release from a stack should be as low as possible and continuously monitored. The total amount of released T for a given period must be under the regulation limit. An ionization chamber is often used as an online stack monitor. However, the ionization chamber cannot determine the source of T or chemical forms of T released from the stack. The regulation limits for the T release are specified for chemical forms of T, such as HT, HTO,  $\text{CH}_3\text{T}$ , and OBT (organic compound). Since OBT is the most hazardous among all, T exhausted from the stack is equated to be OBT and regulated T activity in the exhausted gas from the stack to be under 0.003 Bq/cm<sup>3</sup> in the Tritium Process Laboratory (TPL) in JAEA [14, 15].

A part of the exhausted gas is regularly introduced into the oxidation-collection system, which consists of water bubblers and catalyst beds to allow the separate detection of HTO, HT, and OBT. And then, integrated amounts of T in all chemical forms are evaluated every month by a liquid scintillation counter, in order to confirm that the T release is under the regulation limit.

Surfaces of any T handling equipment or walls of working rooms are easily contaminated by T and are the most possible pathway of T uptake for workers. The surface monitoring by a smear method must be routinely performed (see Chap. 7).

#### 14.2.4.5 T Inventory

Since the quantity of T inventory directly connects T safety in a fusion power plant, its evaluation and reduction following to the ALARA concept are critically important. Present estimation of the T inventory in a fusion power plant is nearly 1 kg each in the vacuum vessel, in the fuel cycle system, and in the hot cell and 15 kg in the long-term storage, while those in ITER are evaluated to be 330 g in in-vessel components (plasma facing components, dust, codeposited, etc.), 120 g in cryo-sorption pumps, 55 g in fuel injection systems [pellet fueling (45 g) and gas fueling (10 g)], 30 g in fuel purification systems, 220 g in an isotope separation system, 10 g in a water de-tritiation system, and 200 g in a hot cell [16]. The maximum T leakage in the Tokamak building is assumed to be 70 g, and the maximum T release from a stack to the environment is evaluated to be below 7 g assuming 90 % or more recovery in DS. Following this release rate, annual radiation exposure of the public at the ITER site boundary can be suppressed under

1 mSv, which is the recommended value by ICRP. Besides, an emergency radiation exposure limit of the public is recommended to be 50 mSv/week by IAEA.

The main difference in the T inventory of ITER and a fusion power plant is caused by the long-term storage, which is considerably larger in the latter. Since the long-term storage should be separated from the reactor building, the risk caused by T leakage in normal operation is not much different between the two. Accidental T release to the environment totally depends on the accidental scenario. T behavior in the surrounding area after the release from the plant is discussed in Chap. 15 in detail. Anyway, the plant should be designed to keep the public exposure at the site boundary is below the recommended value by the international organization such as ICRP and IAEA.

## 14.3 Management of T Contaminated Wastes

This section focuses on the management of T contaminated wastes (materials) except the T contaminated water which is discussed in the previous section.

### 14.3.1 *Wastes in a Fusion Power Plant*

Radioactive wastes generated in a fusion power plant are classified into following three categories.

- (a) Activated wastes with T contamination: Most of in-vessel components such as blanket and divertor retain a large amount of T escaping from plasma at elevated temperatures. At the same time, they are highly activated by neutron irradiation. Therefore, any wastes occasionally removed from the reactor vessel, for maintenance and repairing, are mostly activated with T contamination.
- (b) Activated waste without T contamination: Most materials in the reactor building cannot be escaped from the neutron activation, because the penetration depth of neutron is too large to be completely shielded. Most of out-vessel components are also n-irradiated but are not exposed to T except the severe accident of the reactor including T release. Structural materials of superconducting coils and the cryostat are activated by neutrons but are not contaminated by T.

These activated wastes except those from the reactor vessel and blanket are classified to the low-level radioactive waste according to the classification criterion of a fission power plant. The low-level radioactive waste is allowed to employ geological disposal in a rather shallow depth different from the high level radioactive waste which has to be confined at a depth of around 500 m for hundreds

of thousands of year. However, the volume of low-level radioactive waste generated in a fusion power plant is larger than that generated in a fission power plant because n-activation area of a fission power plant is limited in the reactor core region by shielding due to cooling water.

- (c) Wastes contaminated only with T: Most of T processing systems shall be installed outside of the reactor building. Therefore, any wastes from those systems are not activated, although they are potentially contaminated by T and require housekeeping and radiological protection tools in their handling. The concrete walls in the T processing building and the hot cell building will are potentially T contaminated wastes after the long-time plant operation. T contaminated level will spreads in very wide ranges.

### ***14.3.2 Management of Activated and T Contaminated Wastes***

#### **14.3.2.1 T Safety in Maintenance Process**

Since both divertor and blanket will be highly activated and tritiated, remote handling is indispensable. Moreover, their large size does not allow on-site repairing. Therefore, they are cut into some sectors and drawn out from the vacuum vessel through the maintenance ports equipped between the toroidal magnetic field coils. Each sector is put on the carrier referred to as “cask” and transferred to a hot cell. To suppress the spreading of T contamination during the transportation and to reduce T inventory in the hot cell, in-vessel T removal is recommended as discussed in Sect. 14.3.2.2. Particular concerns are deposited layers and dusts on the surfaces of all in-vessel components, which retains significant amount of T and neutron activated. The airtight pathway has to be constructed from the vacuum vessel to the hot cell so that T and dust are not dispersed widely to the reactor building. The transport processes of the in-vessel component to the hot cell by remote handling for ITER are described in Ref [17].

Conceptual compartments in a hot cell are indicated in the left-hand side of Fig. 14.7. At first, activated dust adhering on the in-vessel components is removed at dust removal area. Subsequently, the components are heated at higher temperatures than the on-site baking temperature to remove residual T at T removal area. The components are stored in temporary storage area until their radioactivity decreases low enough for maintenance works, and then, damaged or eroded parts are repaired or replaced at maintenance area. Replacement of armor tiles on the first wall and refill of solid breeder pebbles are routinely performed. In a case of a liquid breeder blanket, all breeders may be ejected from the loop to confirm erosion and corrosion situation in the structural materials. At that time, a part of liquid breeder such as LiPb and Flibe may become waste. The component of which the

maintenance process is completed is inspected the soundness of the function through the examinations such as a leak test and a stress test at inspection area. The component which passed the inspection is put in preparation area and is transported in the vacuum vessel at suitable timing. The wastes generated in the maintenance process including significantly damaged blanket and divertor are stored at waste management area for a while to reduce their radioactivity.

A large space is required for repairing and replacing works. For keeping the negative pressure and ventilating the contaminated air and cooling the decay heat, the work load of DS becomes large. In case of high T contaminated wastes, possible T release from them with temperature rise caused by the decay heat should be concerned and continuous T monitoring and concentration control are required in the waste management area.

#### 14.3.2.2 T Recovery from in-Vessel Components

T removal process for in-vessel components in ITER is shown in Fig. 14.8. On-site baking temperature is designed to be 200 °C for vacuum vessel, 240 °C for first wall, and 350 °C for divertor [18]. Various T removal techniques have been studied so far, such as D<sub>2</sub> soaking, laser radiation, and melting. T must be also removed

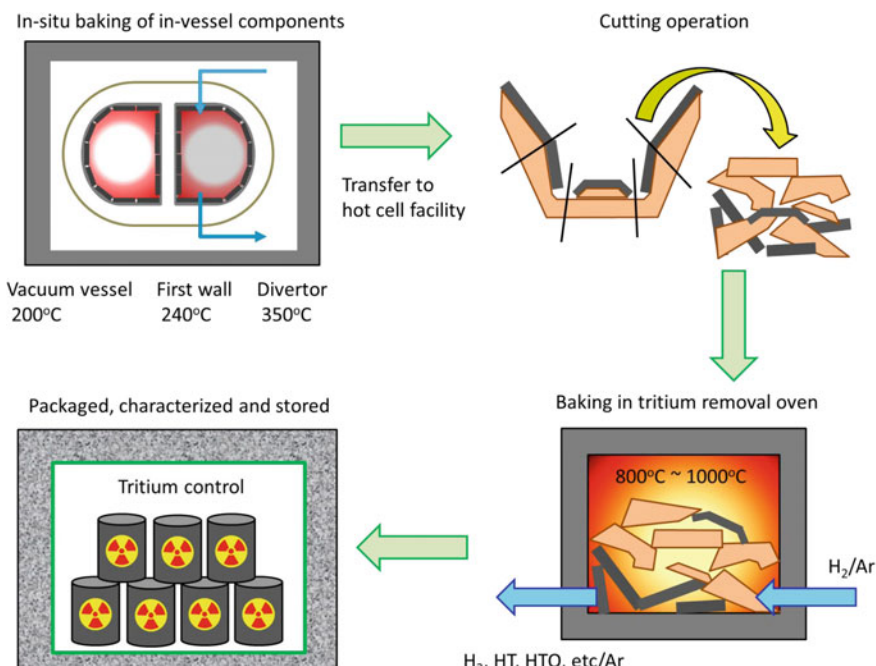


Fig. 14.8 T recovery process for in-vessel components in ITER

from the components after transfer from the reactor to the hot cell. The most promising method of the T removal is thermal desorption in an oven at 800–1000 °C in a mixture of hydrogen and argon from viewpoints of efficiency, safety, and easy operation. The components are cut into small parts to be installed in the oven by a remote handling technique. After detritiation, the materials are packed into an airtight container such as a drum can. After their storage for approximately a few 10 years until their radioactivities are decayed significantly, the materials could be processed for recycling.

### ***14.3.3 Management of Non-activated and T Contaminated Waste***

#### **14.3.3.1 Fuel Processing System**

Among various T processing systems except the plasma facing components, two systems, a fuel refining system using Pd membranes and an isotope separation system applying cryogenic distillation, require particular care on T inventory and T safety. In the former, owing to its higher temperature operation, T penetration in deep inside of the system wall and even permeation are concerns. Detritiation of the system wall could be done by heating. However, it is difficult to completely remove T from high T contaminated metals only by heating even if the heating is continued for a long time. Hence, the walls should be packed into an airtight container for disposal even after their detritiation. In the later, owing to the operation at low temperature or cryogenic temperature, T retained on the surface of the system wall becomes quite large. Therefore, T retained on the surface can be removed by etching or polishing of the surface layer. However, T contaminated dust is generated in these processing systems.

#### **14.3.3.2 Concrete**

Since most of the T processing systems are installed in compartments or rooms surrounded by concrete walls, the surface of the concrete is easily contaminated by T. Therefore, the concrete accounts for a large percentage in the wastes generated in decommissioning of a fusion power plant. It retains a large amount of H as structural water, and T taken-up at its surface easily replaces with H in the concrete during the plant operation. Because concrete is porous material, any gases including T can penetrate deeply, resulting in T contamination in deep inside of the concrete. The contamination of the wall surface can be found easily by a smear method, while that of the wall inside is not easy to evaluate. Core extraction by drilling is used to monitor T contamination inside the concrete. The sample cores are immersed in water to be monitored by a liquid scintillation counter.

Even in case of demolition of the reactor building, T release to the environment should be kept as low as possible. To do this, the whole building may be enclosed in a tent or a simple temporary building, and cutting and dismantling may be done under a water-sprayed condition. The water generated in this process has to be collected in a storage tank, and then, it is exhausted after its T concentration is confirmed to be under the regulation limit. The effective detritiation method of a concrete building has to be established on the practical scale.

#### 14.3.3.3 Radiation Protective Tools

In a fusion power plant, the majority of T processing systems are installed in compartments or rooms maintained at negative pressure with a ventilation system. For their repair or maintenance, workers directly handle them wearing personal protective clothing and gloves in the room. Therefore, these closing and gloves are contaminated by T, i.e., generating T contaminated wastes in every maintenance works. Since they are mainly composed of plastic, cellulose, and rubber, T retained in them are in chemical forms of either HTO and/or OBT (organic binding T). Different from HTO, OBT is difficult to remove by water soaking or water vapor purging. Therefore, the volume of the wastes in a fusion power plant becomes much larger than those in existing large-scale T handling facilities, and reduction in their volume is an important issue for the disposal.

Combustion is an effective method for detritiation or volume reduction with recovering T as HTO. However, the combustion of plastic generates chemically toxic gases such as tritiated chlorides. Therefore, recovery of chemically toxic components as well as HTO from the released gas by the combustion is mandatory. Generally, catalytic oxidation employed in the combustion enhances the oxidation of the toxic gases to be HTO and other oxides which can be removed by a water adsorption method or a water exchange method. Since remaining ash after the combustion still contains T, it is packed in an airtight container and safely stored as T contaminated wastes.

Nevertheless, incomplete combustion is concerned and improvement to attain full combustion is required to use the combustion method as the volume reduction. Volume reduction by compression would be one option. Still the compressed wastes should be stored in an airtight container because OBT is hard to be removed. In JET, the volume reduction in plastic wastes by the plasma arc method with centrifugal separation and gasification was performed. Afterward, the components in the exhaust gas were analyzed [19] and found the combustion was incomplete.

#### 14.3.4 Disposal of Radioactive Wastes

In Sect. 14.3.1, T contaminated wastes are classified into three categories. For the disposal of the wastes, here, they are further separated into four groups as follows.

The disposal of radioactive wastes generated in a fusion power plant is performed in accordance with the methods of the waste disposal developed for a fission power plant. Different from the fission, however, the fusion generates no high level wastes mainly composed of FP of which activity is quite high and requires geological disposal, i.e., buried in the tunnel which was excavated to a depth of 300 m or more with artificial barriers and natural barrier such as sand and rock (called an isolation landfill type disposal). The wastes from a fusion reactor are categorized into four types according to their radioactivity levels. A conceptual drawing of waste management is shown in Fig. 14.9.

#### (1) Waste with activity below clearance level

Solid wastes of which radioactivity level is less than clearance level are equated to industrial wastes and are excluded from radiation protection regulation. In a fusion power plant, the radioactivity level of cryostats and other instruments outside a reactor is likely below the clearance level.

#### (2) Low and (3) extremely low wastes

If species and concentration of radioactive nuclides in any wastes meet the necessity for burying standard, near-surface burial disposal of the wastes is carried

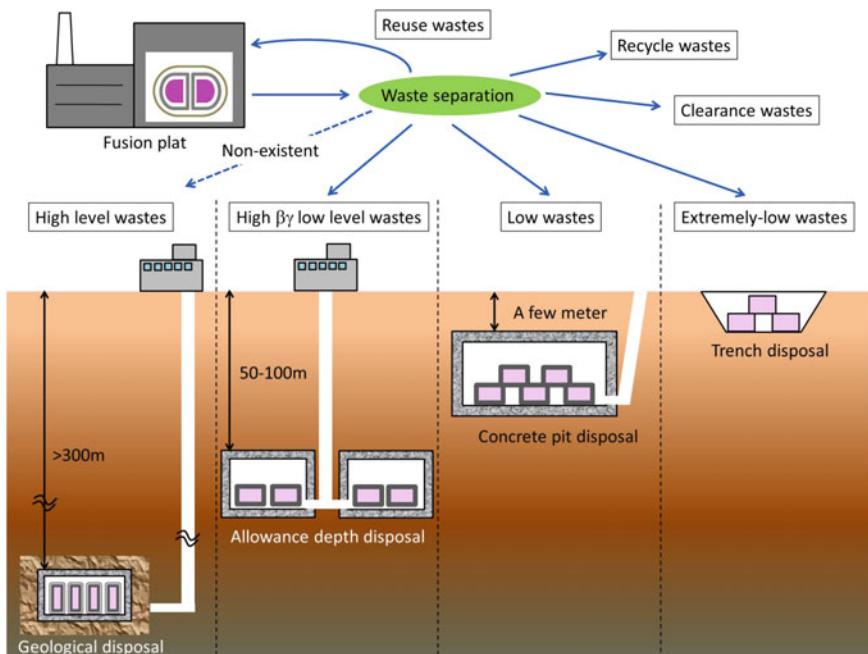


**Fig. 14.9** Conceptual drawing of waste management

out by using concrete pits or simple trenches. Many of radioactive wastes from a fusion power plant are classified into low or extremely low-level wastes.

#### (4) High $\beta/\gamma$ low-level wastes

Any wastes whose activity exceeds the upper limit to allow the concrete pit burial disposal are categorized as high  $\beta/\gamma$  low-level wastes. Most of structural materials of a fusion reactor including the blanket are categorized as this level and disposed with a method called as a controlled landfill type; i.e., the wastes were enclosed in artificial barriers such as a metal container and are buried in the tunnel which was excavated to the depth (underground 50–100 m) well separated from general underground use.

### ***14.3.5 Reuse and Recycle of Radioactive Materials***

From the aspect of material recycling, all used components/materials in a reactor system are classified into three categories depending on their activation levels by neutron irradiation, “reusable,” “recyclable,” and “disposal” materials. “Reusable” means that the component is used as it is. “Recyclable” means that materials constituting the component are refined and utilized for different uses or purposes. Under general regulatory control concept, radioactive materials whose surface dose rate is less than about 10 mSv/h can be recycled to be used by remote handling [20]. According to the assessment by SEAPP (safety and environmental assessments of fusion power), in a fusion reactor built by low activated ferrite steel which reduced impurity density, all low-level wastes can be reused after 100 years’ storage [10].

Owing to its short decay time of T, only  $\sim 1\%$  of T in them remains after 100 years’ storage. Therefore, the reuse and recycle of T contaminated materials without the n-activation are separately considered. Basically, the reuse of T handling equipment that are non-activated are possible if the soundness of materials and the function as the equipment are maintained after their detritiation (decommission) mostly done by vacuum heating. Alternatively, the equipment can be reused after the long storage for disintegration of T in an airtight room or an airtight metallic enclosure with DS. To be recycled, the equipment is dismantled into components and they are heated or melted to reform which accompanies T release.

To maintain high T breeding ratio, burned Li in blankets should be replenished. Moreover, Li in ceramic pebbles should be recycled or reused because its resources are not enough. Therefore, a Li recycling system should be established. The key is to establish an efficient method to melt Li pebbles and remove T and other impurities. Liquid breeders such as LiPb and Flibe are reusable owing to their nature [21].

## 14.4 Summary

The most important issue to secure the safety of a fusion power plant is confinement of T. The basic concept to protect workers, the public, and the environment from the radiation exposure is defense in depth. Accordingly, multiple-confinement concept is employed with multiple physical barriers and independent detritiation systems. Key issues are to keep soundness of the physical barriers and the function of the detritiation systems even at off-normal events.

Experiences to handle T safely with robust confinement have been acquired in large-scale T handling facilities existing in the world without severe accidents. Therefore, it can be said that basic techniques for T confinement have already been established.

However, T amount handled in a fusion power plant is much larger than that of the present T handling facilities. This forces most of T handling equipment in the plant to be larger compared with those used in the present facilities and consequently requires large volume of rooms and/or glove boxes to ensure T confinement. This makes T confinement harder accompanying larger permeation and possible leakage of T. At the same time, materials to be detritiated in detritiation systems significantly increase. Furthermore, wider ranges of T contamination levels require independent operations with different concepts depending on the T contamination level. Key issues are to develop reliable detritiation systems attaining a higher decommission factor (DF) and to avoid cross-contamination.

To do this, practicing large amount T handling is indispensable. In this respect, ITER is the first opportunity to get T handling experiences of highly activated and/or T contaminated materials. Nevertheless, for personnel training and the technical improvement, training facilities and mock-up systems handling a large amount of T equivalent to that used in a real fusion fuel cycle system seem indispensable before the construction of T handling systems of ITER.

## References

1. Publication 103. Ann. ICRP **37**, 2–4 (2007)
2. Publication 72. Ann. ICRP **26**, 1 (1995)
3. Publication 30. Ann. ICRP **2**, 3–4 (1979)
4. Publication 119. Ann. ICRP **41(s)** (2012)
5. Final report of the ITER EDA, IAEA, VIENNA, 2001
6. Tritium handling and safe storage, DOE-HDBK-1129-2008, 2008. Evaluation of Facilities Handling Tritium Part of the Tritium Studies Project INFO-0796, Feb. 2010
7. Publication 60. Ann. ICRP **21**, 1–3 (1991)
8. DEFENCE IN DEPTH IN NUCLEAR SAFETY INSAG-10 IAEA VIENA, 1996
9. Outline of safety design (case of BWR), JNES (2005)
10. “Genshiryoku Handbook”, Ohmsha (2007). (in Japanese)
11. T. Hayashi et al., Fusion Eng. Des. **39–40**, 901–907 (1998)
12. T. Takeishi et al., Radioisotopes **45**, 537–544 (1996)

13. Y. Iwai et al., *Plasma Fusion Res.* **9**, 332–337 (2010). (SERIES)
14. H. Nishi, *J. Plasma Fusion Res.* **79**, 1078–1084 (2003). (in Japanese)
15. Y. Hatano, *J. Plasma Fusion Res.* **86**, 173–184 (2010). (in Japanese)
16. D. Murdoch et al., *Fusion Eng. Des.* **75–79**, 667–671 (2005)
17. A. Dammann et al., *Fusion Eng. Des.* **98–99**, 1457–1460 (2015)
18. S. Rosanvallon et al., *Fusion Sci. Technol.* **60**, 855–860 (2011)
19. L.A. Bernstein et al., in *Study of JET Soft Housekeeping Waste Volume Reduction by Plasma Arc Centrifuge and Gasification in Countercurrent Regime Methods*, EFDA-JET-PR (09) 47
20. K. Tobita et al., *J. Nucl. Mater.* **329–333**, 1610–1614 (2004)
21. K. Tobita, *J. Plasma Fusion Res.* **80**, 959–961 (2004). (in Japanese)



# Chapter 15

## Behavior of Tritium Released to the Environment

Kazuyuki Noborio and Tetsuo Tanabe

**Abstract** Tritium release from a fusion reactor consists of chronic one during the normal operation and accidental one. Once tritium ( $T$ ) is released from the reactor, it disperses into environment. Because of its low energy of the  $\beta$ -electron released at  $T$  decay, internal exposure by  $T$  uptake (inhalation and ingestion) and its biological effects are major concerns. Therefore, it is quite important to estimate and/or understand how dispersed  $T$  is finally uptaken in and impact human living in surrounding area. In this chapter, numerical models developed to estimate concentration in the environmental elements, and their distribution of  $T$  released from a fusion plant are described. The analysis of  $T$  behavior in the environment starts from determining source terms, then follow analyses of spatial transportation by advection and diffusion and migration among environmental elements (compartments), and estimates uptake into human body and finally evaluates dose.

**Keywords** Tritium · Safety · Chronic release · Accidental release · Dispersion · Environment · Atmosphere · Numerical model · Does estimation

---

K. Noborio

Hydrogen Isotope Research Center, University of Toyama, Toyama, Japan  
e-mail: k.noborio@sakigakes.co.jp

K. Noborio

Sakigake Semiconductor Co., Ltd, 50 Onmaeda-Chou, Nishinanajo, Shimogoyo-Ku, Kyoto 600-8897, Japan

T. Tanabe (✉)

Interdisciplinary Graduate School of Engineering, Kyushu University, 6-1, Kasuga-Koen, Kasuga-City, Fukuoka 816-8580, Japan  
e-mail: tanabe@nucl.kyushu-u.ac.jp

## 15.1 Introduction

Commercial fusion power plants will release tritium (T) into environment even under normal operation. The release rate shall be controlled to be as small as possible by applying various techniques as described in previous chapters. However, it is impossible to make the release to be completely zero and it may be detectable in the periphery environment of the plants. The most important point is not to realize zero release, but to reduce influence on public health to be negligibly (acceptably) low. The influence depends on not only the release rate and the total quantity but also the conditions and situation such as release point, chemical form of T, and weather condition. It is required to analyze, understand, and control the T behavior in the environment.

Behavior of pollutants released into the environment from nuclear fission power plants, fire power plants, chemical plants, and other kinds of facilities has been well studied and understood. Accordingly, various techniques and models have been developed to analyze the behavior of these pollutants. Some of them can be applied to analyze the behavior of T released from a fusion power plant into the environment. However, we should pay special attention when treating T due to its distinctive characteristics in a fusion power plant and in the environment. In this chapter, numerical models developed to estimate concentration in the environmental elements and their distribution of T released from a fusion plant will be described. For assessment of human health impact by T, estimation of dose rate by T in atmosphere is not enough because exposure by T outside of the human body (external exposure) is negligibly small due to extremely low energy of  $\beta$  ray from T. It is more important to consider internal exposure by T uptake (inhalation and ingestion) and biological effects.

The analysis of T behavior in the environment consists of the following steps: determining source terms, analyzing spatial transportation by advection and diffusion, analyzing migration among environmental elements (compartments), and finally estimating uptake into human body and dose, as shown in Fig. 15.1.

The first step is to determine the T source terms: information on how much T is included in wastewater or exhaust air with their release rates, and from where and with what chemical form they are released. To determine the source terms, in other words, T migration path in a fusion plant should be clarified. The source terms can be specified by plant design, and therefore, at present, it is hard to estimate them for a commercial reactor installing an energy extraction system, which is not realized yet. Since the most important migration path is in blanket systems in a fusion plant, their concepts on T breeding and energy extraction are quite important for the T safety in designing a plant. Analysis on the migration paths in a fusion power plant will be described in the next Sect. 15.2.

After the determination of the source terms, behavior of T in the environment released from the fusion plant—spatial distribution of T for each chemical form in the atmosphere and concentration of T in each environmental element on the ground such as plants (vegetables), animals, and ground surface water—is traced.

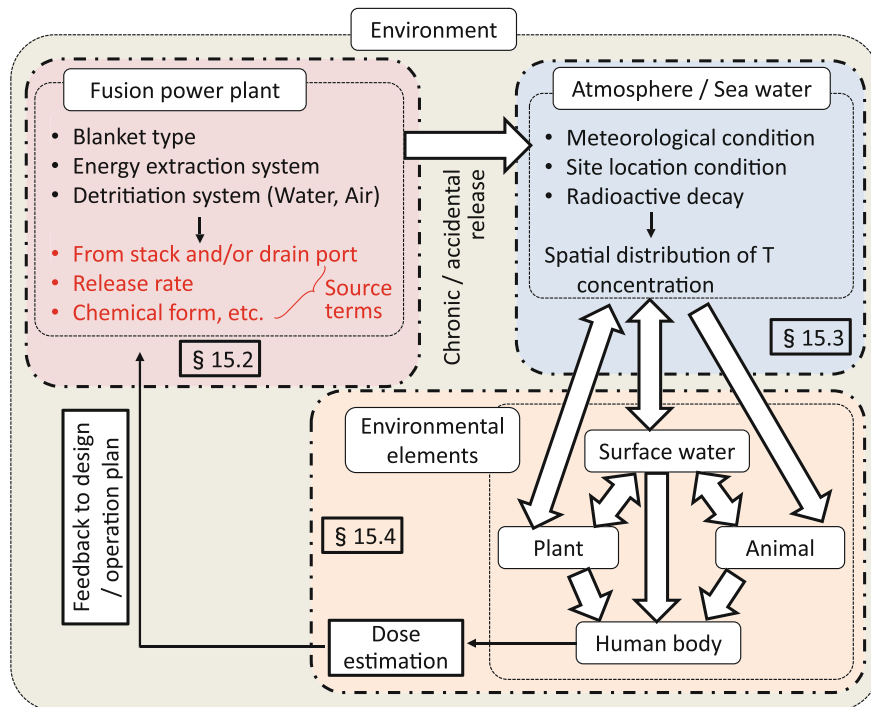


**Fig. 15.1** Flow diagram of analyzing behavior of T in the environment. Three boxed elements are separately explained in three Sects. 15.2, 15.3, and 15.4, respectively

Here, the trace is performed from two viewpoints: (a) spatial transportation by advection and diffusion and (b) migration among elements at each location. Due to the special characteristics of T, which will be described in Sect. 15.3, the spatial transportation in the environmental atmosphere and/or hydrosphere (sea, lake, river, underground water, etc.) is firstly estimated. Then, based on the estimated concentration in the atmosphere and hydrosphere, the T concentration in each environmental element, including human body, is estimated as described in Sect. 15.4. Traditional models and codes for the dispersion of pollutant materials in the atmosphere [1, 2], which have been well developed and are basis of application to the T transportation analysis, are introduced in Appendix.

## 15.2 Tritium Release from Fusion “Power Plant”

The most important purpose of a fusion power plant is, of course, to convert energy generated by fusion reactions into electricity or other useful energy forms. This requires thermo-fluid (coolant) such as water (pressurized, subcritical, and/or

vapor), gas, liquid metal, or molten salt to circulate in the plant. Tritium, bred in the blanket or permeating the first wall from fusion plasma, is incorporated into the thermo-fluid. Some of T in the thermo-fluid permeates through the heat exchanger wall to contaminate chronically the plant and is finally released into the vicinity environment of the plant. Estimation of the “source terms”, which is the first step of analyzing the behavior of T in the environment, is not easy even for the normal operation, because it cannot be correlated simply with fusion output power, T inventory, and other plant parameters. It is required to understand complicated migration path in the fusion plant for the estimation. At accidental events, T and other activated materials in the fusion plant might be released into the environment with quite different ways depending on accidental T release scenarios and the plant type as well.

In the following, the chronic T release during the normal operation and the accidental release from fusion power plants are described associating with the plant type.

### ***15.2.1 Chronic Tritium Release***

#### **15.2.1.1 Energy Extraction (Conversion) and Tritium Migration in Fusion Plants**

Handling of huge amount of T in the fusion power plant makes T confinement quite difficult. Furthermore, utilization of thermo-fluid in blanket systems in which T breeding and energy conversion are simultaneously done makes the confinement difficult as mentioned below.

Tritium incorporated in the thermo-fluid permeates or leaks to the next stage through the heat exchanger wall and is finally released into the external environment along with the waste heat. This T release is not avoidable so as the waste heat. To enhance the heat transfer, thinner wall and larger area of heat exchanger and higher operation temperature are better, while they increase T permeation. As such, the T migration path in a fusion power plant highly depends on the plant design. In particular, the blanket type, depending on materials used for T breeding and thermo-fluid (coolant), and energy extraction and conversion systems vary the migration path significantly. This means that the T migration analysis in a fusion power plant should be done considering the total system. Different combinations of breeders (breeding materials) and energy extraction mechanisms in designed reactors are listed in Table 15.1.

**Table 15.1** Various combinations of breeder and energy conversion system

Breeder	Thermo-fluid	Heat exchanger	Energy conversion	Design example
Solid	Water	SG	Steam turbine	Slim-CS [3]
Solid	Helium	IHX	Gas turbine	PPCS-B [4]
LM	Water	SG	Steam turbine	PPCS-A [4]
LM	He and LM	IHX	Steam turbine	ARIES-ST [5]
LM	LM	IHX	Gas turbine	ARIES-AT [6]
LM	LM	IHX	Fuel production by chemical reactions	GNOME [7]
LM	He	IHX	Gas turbine	—

LM—Liquid metal, SG—Steam generator, IHX—Intermediate heat exchanger

### 15.2.1.2 Simple Estimation of Tritium Migration in a Fusion Power Plant

T migration in a fusion power plant is roughly described here, assuming its steady-state operation for simplification. The “steady state” means that the T concentration and inventory of each subsystem and leakage or permeation rate stay constant (do not change in time). This assumption is applicable only for the case when the time constant required to reach the steady state in any subsystem is shorter than the operation period of the plant or the maintenance period of the blanket or other components.

A simplified flow model at a certain stage of multiple thermo-fluid loop stages with incoming/outgoing T flows are illustrated in Fig. 15.2. In this model, the permeation or leakage rate of T from the stage to the next stage,  $r_{\text{out}}$ , is assumed to be negligibly small compared with the original circulating T flow rate in the loop,  $fc$ , where  $f$  and  $c$  are flow rate or the thermo-fluid and T concentration in the thermo-fluid, respectively. This assumption is also indispensable to control T release into the environment as reasonably low level. According to this assumption, the incoming rate of T from the former stage,  $r_{\text{in}}$ , should equal to the recovering rate of T, which is expressed as  $\alpha fcp$ , where  $\alpha$  and  $p$  are the bypass ratio to the T recovery system and T recovery ratio, respectively. Therefore, the T concentration is expressed as:

$$c = \frac{r_{\text{in}}}{\alpha fp}. \quad (15.1)$$

Then, the T migration rate to the next stage,  $r_{\text{out}}$ , can be calculated by:

$$r_{\text{out}} = k \frac{S}{d} c^n, \quad (15.2)$$

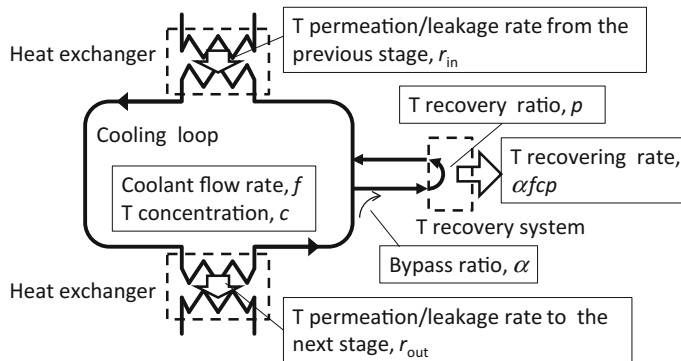
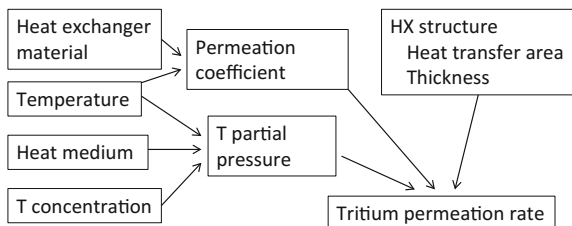


**Fig. 15.2** Schematic diagram of T flow through a stage of cooling (thermo-fluid) loops

where  $S$  and  $d$  are cross-sectional area and thickness of the permeation or leakage pathway (typically, heat exchanger),  $k$  and  $n$  are coefficients depending on the permeation mechanism; for example,  $n$  should be 0.5 for dissociative permeation and 1.0 for molecular leakage. Thus, the thermo-fluid, the operation temperature, and types and materials of heat exchangers affect the T permeation as shown in Fig. 15.3. These assumptions are so simple that the migration (permeation/leakage) rates can be calculated easily by hand or using a spreadsheet program. However, it should be noted that the input data are as important as an employed model in order to perform an accurate calculation.

As an example, T migration in the Slim-CS [3], a solid breeder and water-cooled reactor designed at Japan Atomic Energy Agency (JAEA), is analyzed here. Figure 15.4 shows the T flow and migration path together with their estimated values for breeding ratio in the blanket, permeation rate to the primary thermo-fluid (cooling water) through the cooling channels, permeation rate to the secondary steam/water loop through the steam generator, and leakage rate to seawater from the condenser. They are included to estimate the T release rate to seawater based on the designed parameters of the Slim-CS and conditions commonly used in PWR (pressurized-water reactor). Among all, the leakage or permeation rate is quite uncertain and can be significantly reduced by using permeation reduction techniques as described in the previous chapters.

**Fig. 15.3** Correlation of parameters which dominate T permeation through a heat exchanger



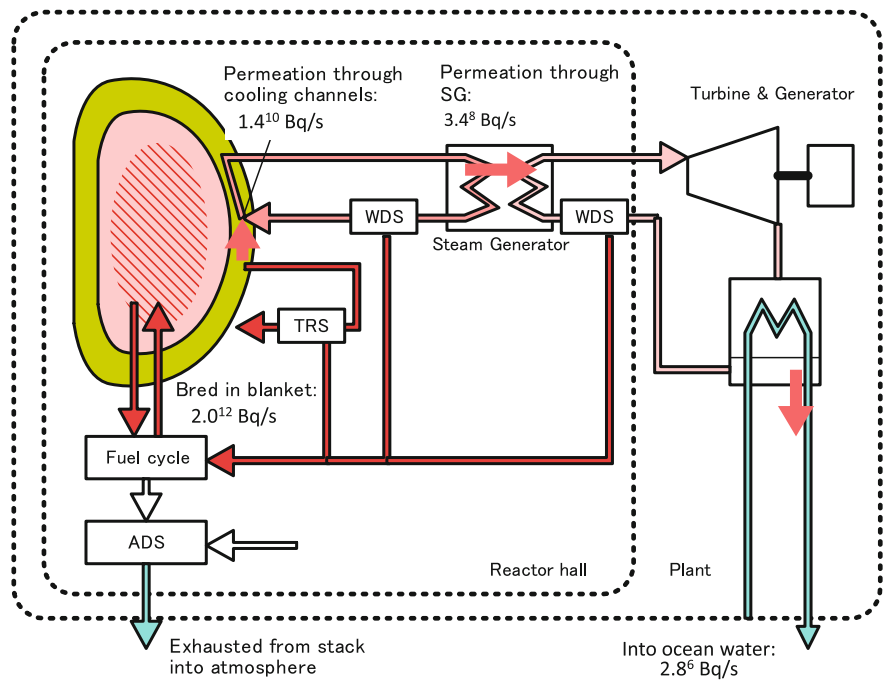


**Fig. 15.4** T flow in a solid breeder and water-cooled reactor system

### 15.2.1.3 Tritium Release from a Fusion Power Plant

The major migration path of T into the environment in the case of a solid breeder and water-cooled reactor might be accompanied with warm wastewater, as shown in Fig. 15.4. T in the wastewater is diluted to nearly the background level because of large flow rate of the wastewater (hundreds tons per second) if the location of the plant is facing to open coast and the intake of cooling seawater is well isolated from the outlet of wastewater. In contrast, if the location is at an enclosed bay and wastewater is released close to the intake, higher T accumulation may be detected due to multiple use of the local seawater. On the other hand, if the final waste heat is released from a cooling tower, where the heat of cooling water is removed by vaporization of the water, the exhausted water vapor from the tower will be highly contaminated if no countermeasures are taken. Installation of WDS (water detritiation system) will be indispensable.

Room air inside of a building containing any T processing systems can be always contaminated with T leaked from the systems. The contaminated air is ventilated and led to ADS (air detritiation system), while unrecovered T in ADS will be released to the environment from a stack. Therefore, ADS shall be designed to keep the T release rate below the regulation limit.

Anyhow, during the steady operation of a fusion plant, T is chronically released from fixed locations. T distribution originated from such chronic release can be analyzed by using a Gaussian plume model introduced in Appendix, giving release rate  $f$  at a particular location.

### **15.2.2 Accidental Tritium Release**

Manners of accidental T release are critically dependent on T inventory in components and locations of the accident. Most probable and serious accidents would be (if it could ever happen), respectively, leakage from and failure of the primary cooling system releasing its coolant (thermo-fluid) highly contaminated with T. For a water-cooled fusion plant, the inventory in the primary coolant water was estimated to be  $1.4 \times 10^{17}$  Bq (equivalent to 390 g-T) under assumption of the total water holdup in the cooling system being  $1000\text{ m}^3$ . The accidental spill or leakage for the water-cooled fusion plant can be mitigated with a suppression pool similar to the case of a BWR (boiling-water reactor).

For the ARIES-ST with a dual coolant (He and LiPb) system, the T inventories in LiPb and He coolants were estimated to be 16 g ( $5.7 \times 10^{15}$  Bq) and 1 g ( $3.6 \times 10^{14}$  Bq), respectively, by Khater et al. [8]. Because He is not condensable and anticipated time constant for a major break of the coolant piping is extremely short, it seems to be significantly difficult to mitigate the expansion and the protection of the building confinement. Liquid metals and other non-volatile fluids are expected to be much easier to keep T confinement in the case of any kinds of failure of the cooling system.

Although, the accidental release of the coolant containing T into the environment will be one of the most serious events for public safety, the countermeasure against the accidental release is essentially the same as that taken at normal operation but with quite different timescale, release rate, and total release. T confinement systems, such as buildings and glove-boxes and detritiation systems, finally dominate the environmental release, as far as they are intact. Therefore, the release scenario from these systems together with the nature of the source terms will have a major impact on the behavior of T released into the environment.

In many accidental scenarios, most of T is released for a short time. For such cases, a Gaussian puff model introduced in Appendix is applicable to estimate T distribution in the environment by giving the release position and the total release,  $q$ .

## **15.3 Characteristic Behavior of Tritium in the Environment**

As introduced in the previous section, T release events vary depending on the plant type and either during normal operation or at an accident. Furthermore, interactions of T released into the environment with elements in it, particularly water,

significantly change T migration in the environment. In order to understand T behavior in the environment, the traditional model introduced in Appendix is modified considering both the interaction of T with ubiquitous water and the radioactive decay of T with half-life of 12.3 years as described in this section.

### ***15.3.1 Hydrogen Isotopes in the Natural Environment***

As written in Chap. 2, T is an isotope of hydrogen, one of the most popular elements in the nature. Though large amount of T was introduced into the atmosphere by nuclear weapons tests from 1950s to 1960s, the T concentration in the environment has decayed owing to its short lifetime to be nearly the steady-state level balanced between production by cosmic rays and its decay, approximately the order of  $1 \text{ kBq/m}^3$  in natural water.

The regulation limits for T in water vary from country to country. For example, that of Japan is  $60 \text{ MBq/m}^3$  in discharged water or  $20 \text{ kBq/m}^3$  in drinking water.

Major chemical forms of hydrogen isotopes in the natural environment are ubiquitous water (vapor, liquid, and solid) and organic compounds (hydrocarbons). Hydrogen atom (H) and T atom in any chemical forms are possibly replaced mutually by isotopic exchange reactions. The tritiated water is referred as HTO and the tritiated organic material as OBT (Organically Bound Tritium). Therefore, T released into the environment easily spreads and circulates in the nature or hydrological cycle; water evaporates from ocean and ground surface, condenses and falls as rain or snow, pools in lakes and rivers, and flows into the oceans, as shown in Fig. 15.5. Plants take up water to use photosynthesis of hydrocarbon with  $\text{CO}_2$ . Human beings ingest water, plants and animals. For the assessment of T safety, both T in the hydrologic cycle and T uptake of human being should be taken into account. In the hydrological cycle, major water inventory is in oceans (97 %), and a tiny amount is in the atmosphere and biosphere (0.001 and 0.00004 %, respectively). However, for human life, the latter are quite important.

Although hydrogen with an elemental form ( $\text{H}_2$ ) rarely exists in nature, HT would dominate in emergency T release from a fusion reactor. While, in its normal operation, HTO release from stack or with wastewater will be dominant. HT is hardly oxidized in the atmosphere, but is oxidized into HTO by soil bacterium at ground surface.

### ***15.3.2 Absorption of HTO in the Atmosphere to Large Quantity of Environmental Water***

When waste water containing HTO is released into the sea, it will be immediately diluted into huge amount of seawater. Therefore, the isotopic ratio of T to H in the seawater becomes negligibly low. On the other hand, when it is released as HTO vapor from a stack or a cooling tower into the atmosphere, it will be dispersed instead

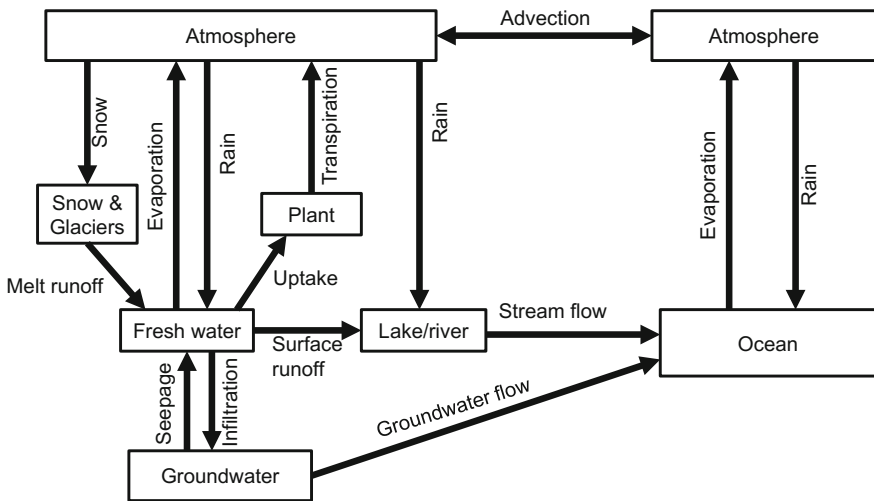
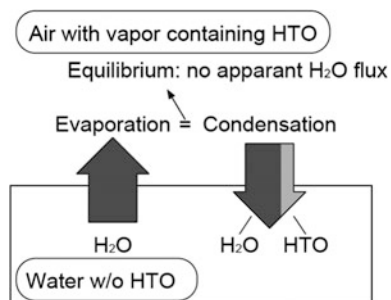


Fig. 15.5 Hydrologic cycle on the earth

of the dilution. In this case, T concentration in the atmosphere, which is expressed in units of  $\text{Bq}/\text{m}^3$ , decreases with time or distance from the release point, but the isotopic ratio of T to H shows slower decrease than that appeared in the dilution into water.

Consider interaction between water vapor containing HTO in the atmosphere and large pure water surface. If the partial pressure of the water vapor in the atmosphere is equivalent to the saturated vapor pressure at that temperature, there is no difference between incoming and outgoing water fluxes at boundary surface between the atmosphere and the water. However, HTO flux from the atmosphere to the water surface appears as illustrated in Fig. 15.6. This HTO flux appears even if evaporation is dominant. This is referred as chemical diffusion caused by concentration gradients (difference in the concentration of T/H in the atmosphere and in the water). Thus, when treating T migration in the atmosphere, T flux by condensation onto the large water surface and consequent reduction of T concentration in the atmosphere are essential.

Fig. 15.6 Evaporation and condensation of water containing HTO



### 15.3.3 Modification of Traditional Models Considering Tritium Absorption to Water Surface

The HTO vapor released into the atmosphere behaves like gas puff or plume, which migrates and expands into the environment. Some of the plumes touching the ground are reflected. The reflection of the plume at the ground surface is assumed to be handled by the basic Gaussian distribution models as given in Appendix based on little flux loss by absorption at the surface. However, HTO vapor touching the water surface must be fully absorbed into the water. This requires modification of the model to include the effect of the reflection and/or absorption, as a coefficient  $\alpha$ . Thus, the Gaussian plume model expressed as Eq. 15.19 in Appendix is modified as:

$$c(x, y, z) = \frac{f}{2\pi u \sigma_y \sigma_z} \exp\left(-\frac{y^2}{2\sigma_y^2}\right) \left\{ \exp\left(-\frac{(z-h)^2}{2\sigma_z^2}\right) + \alpha \exp\left(-\frac{(z+h)^2}{2\sigma_z^2}\right) \right\}. \quad (15.3)$$

Parameters in Eq. 15.3 ( $f$ ,  $u$ ,  $h$ ,  $\sigma_y$ , and  $\sigma_z$ ) and their dependence on meteorological conditions are described in Appendix. The effect of the coefficient  $\alpha$  on the vertical profile of the T concentration is shown in Fig. 15.7. When  $\alpha = 1$ , Eq. 15.3 is equivalent to Eq. 15.19, i.e., corresponding to the total reflection. While for  $\alpha = -1$ , the last term of Eq. 15.3 becomes a sink placed at  $z = -h$  (virtual sink), and Eq. 15.3 expresses full absorption in which the T concentration at the ground level ( $z = 0$ ) is zero.

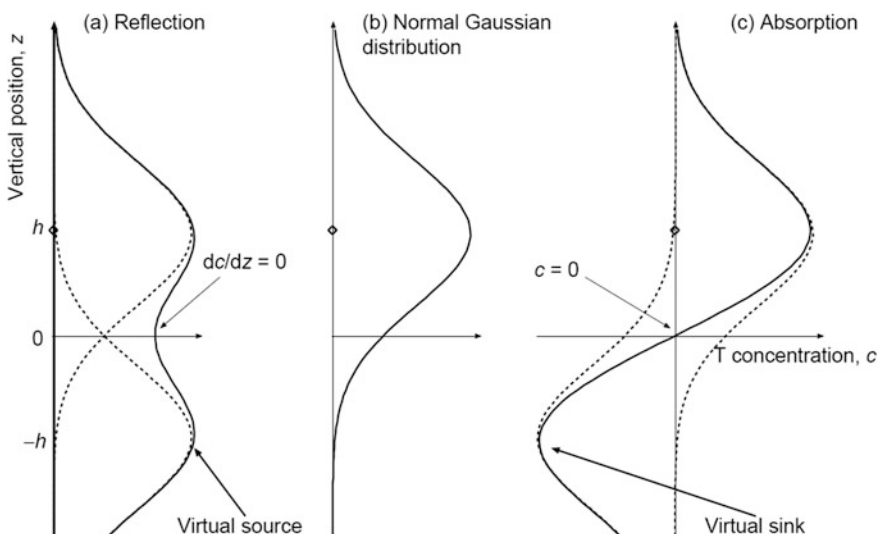


**Fig. 15.7** Vertical distribution of T concentration by the Gaussian distribution model for different ground surface conditions, **a** full reflection, **b** normal model, and **c** full absorption

Figure 15.8 shows a result calculated with the Gaussian plume model expressed as Eq. 15.3, indicating the distribution of T concentration along  $x$ -axis (wind direction) for different surface condition,  $\alpha$ . It is clear that the T distribution is strongly affected by the surface condition. Surface condition of reflection by the surface ( $\alpha = 1$ ) and absorption on the surface ( $\alpha = -1$ ) result in larger and smaller concentrations in the atmosphere than that calculated with normal Gaussian plume model, respectively. In this manner, the spatial distribution of T concentration in the atmosphere for various surface conditions can be estimated. However, this modification is not enough to be applied to realistic geographical condition including complicated coastline, for example. Advanced models considering geographical formation with aquatic and land areas have also been developed [9].

### 15.3.4 Effect of Radioactive Decay

One of the most important objectives of the analyses given above is to estimate annual dose by released T for safety regulation, while its accumulation for multi-year operation is not taken into account well. Since the half-life of T (12.3 years) is roughly comparable with designed lifetime of a plant, sequential accumulation of the released T for several dozen years should be considered.

In the case of chronic release, assuming a closed system where T inflows chronically with constant rate  $f$ , the accumulation rate of T in the system is given as:

$$\frac{dn}{dt} = -\frac{\ln(2)}{\tau} n(t) + f, \quad (15.4)$$

where  $n(t)$  and  $\tau$  are total amount of T in the system at time  $t$  and the half-life of T, respectively. Solving Eq. 15.4,  $n(t)$  is given as:

$$n(t) = \frac{\tau f}{\ln(2)} \left( 1 - \exp \left( -\frac{\ln(2)t}{\tau} \right) \right). \quad (15.5)$$

**Fig. 15.8** Distribution of T concentration normalized by  $f/u$  along  $x$ -axis at  $z = 2$  m (observation point) and  $y = 0$  m for different surface conditions with stability class of D, when the release height ( $h$ ) is 100 m

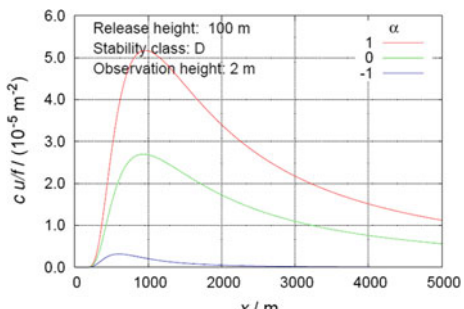
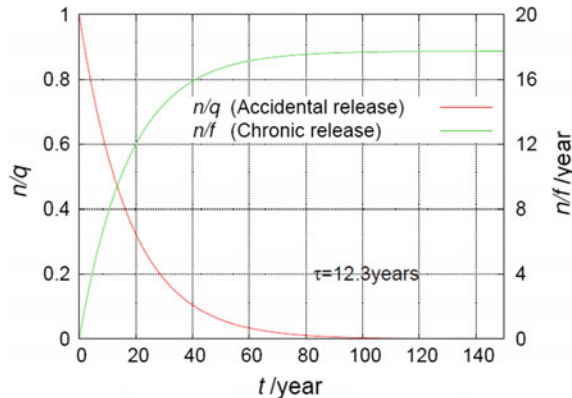


**Fig. 15.9** Time sequences of normalized T concentration in the environment for the chronic release ( $n/f$ ) given by Eq 17.5 and accidental release ( $n/q$ ) by Eq. 17.6



As shown in Fig. 15.9, in the case of the chronic release, T concentration in the closed system increases for the first 50 years and then saturates, i.e., the source term and decay term become equivalent.

On the other hand, in the case of accidental (instantaneous) release, the T concentration simply decays with the half-life time of T expressed as:

$$n(t) = \left(\frac{1}{2}\right)^{\frac{t}{\tau}} q, \quad (15.6)$$

where  $q$  is total released amount of T and plotted in Fig. 15.9 as well.

## 15.4 Migration of Tritium Among the Environmental Elements and Effect on Public Health

One of the final purposes of analyzing the behavior of T released into the environment is to find a way to reduce its influence on public health. Though harmful rumors in an occasion of T release often result in serious impact on local society, only direct impact on the human body is discussed here.

Based on the estimated T concentration in the atmosphere as described above, T migration among environmental elements and final uptake in the human body are investigated considering various migration pathways. A model introduced here is to reveal only local migration of T (migration among the environmental elements at each evaluation point), without horizontal transports, as shown in Fig. 15.10.

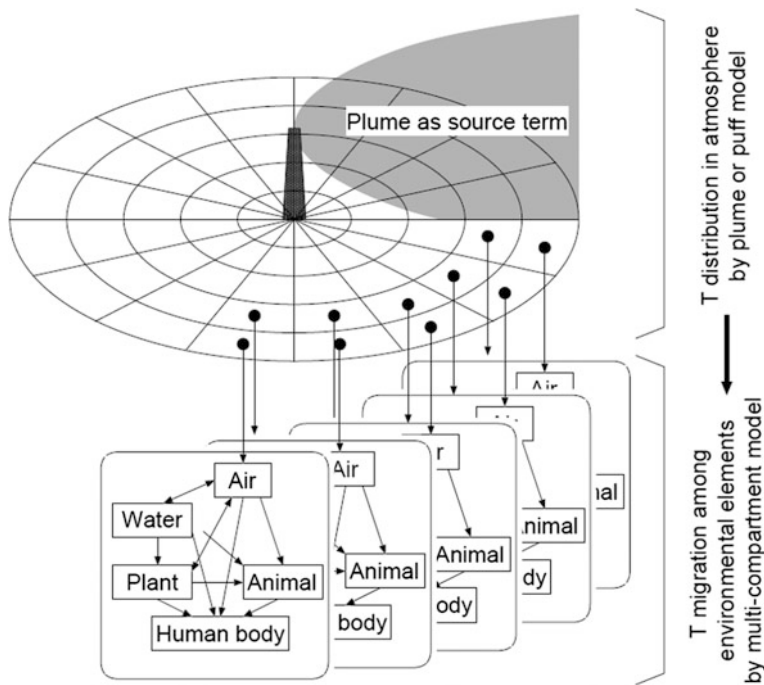


**Fig. 15.10** Flow diagram of a T migration model among environmental elements. T concentration in each element at each location is calculated by considering migration among the elements and T uptake of each element from the environment

### 15.4.1 Tritium Desorption and Reemission Between Ground Elements and Atmosphere

T transport from atmosphere to ground surface mainly consists of two mechanisms: deposition by rainfalls (wet deposition) and dry deposition. Because HTO is caught up and falls as raindrop or snow, the former mechanism is the dominant during raining or snowing. The T flux by the rain falls,  $\phi_{\text{wet}}$ , is expressed as:

$$\phi_{\text{wet}} = \beta c_{\text{air}} h_{\text{eff}}, \quad (15.7)$$

where  $\beta$  is a kinetic constant for precipitation of HTO into a water droplet with the dimension of time inverse calculated by the precipitation intensity;  $c_{\text{air}}$  and  $h_{\text{eff}}$  are the T concentration in the atmosphere calculated by above-introduced plume/puff model and an effective fall height of the rain drop, respectively. The dry deposition takes place for both chemical forms, HTO and HT. Based on the “velocity model,” the deposition flux,  $\phi_{\text{dry}}$ , should be directly related to  $c_{\text{air}}$  with a rate constant of  $v_{\text{dep}}$ , as:

$$\phi_{\text{dry}} = v_{\text{dep}} c_{\text{air}}. \quad (15.8)$$

This model is only applicable when the T concentration in a ground element considered is negligibly low. If not, the following “resistance model” should be employed;

$$\phi_{\text{dry}} = v_{\text{ex}}(c_{\text{air}} - rc_{\text{sur}}), \quad (15.9)$$

where  $v_{\text{ex}}$ ,  $r$ , and  $c_{\text{sur}}$  are a rate constant, a coefficient to match different dimensions of  $c_{\text{air}}$  and  $c_{\text{sur}}$ , and the concentration of the ground element, respectively. Generally, the deposition rate to ground element is too small to change the concentration in the atmosphere. However, if the deposition rate is large enough, the decrease in the concentration in the atmosphere should be considered.

There is another flow of T transport in reverse direction, reemission from ground elements to the atmosphere through evaporation from ground water surface and transpiration from plant leaves. Their contribution can be described by “secondary plume” model, and the total concentration in atmosphere is calculated by superposing the original plume and the secondary plumes from everywhere in the analysis area.

When the plume dispersed onto huge water surface such as sea and a large lake, HTO included in the plume just near the surface easily condenses onto the water surface, even if the evaporation from the water surface is dominant, as already described in Sect. 15.3.2. Since the HTO fraction in water vapor above the water surface should be negligibly small, the migration from the large water surface to other ground elements can be neglected.

### 15.4.2 Multicompartment Model

A simplified model, a multicompartment model, is introduced here. In the model, elements in the environment are categorized into several “compartments” and T distribution in each compartment such as groundwater and vegetable is assumed to be uniform. Then, only the T migration among the compartments is analyzed. Assuming T concentration in a compartment is uniform, each compartment is connected with each other by migration fluxes as shown in Fig. 15.11. This model seems rough; however, the simplification contributes to get realistic results in many cases because sophisticated but maybe realistic models require plenty numbers of input data, which sometimes causes unrealistic results.

The migration flux of T from a compartment  $i$  to another one  $j$ ,  $\phi_{i,j}$ , is calculated from the concentration of the two compartments,  $c_i$  and  $c_j$ . In the simplest case, the flux is assumed to be proportional to the source concentration,  $c_i$ , expressed as:

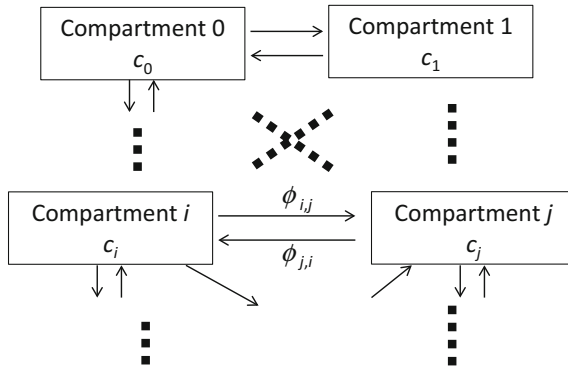


**Fig. 15.11** Multicompartments model

$$\phi_{ij} = vc_i, \quad (15.10)$$

where  $v$  is a rate constant with the dimension of velocity. This velocity model is consistent with both wet and dry deposition models, as given by Eqs. 15.7 and 15.8. This model is available for the limited case when  $c_j$  is negligibly small compared with  $c_i$ .

On the other hand, when  $c_j$  is comparable with  $c_i$ , the velocity model cannot reflect the actual phenomena, and the following resistance model same as Eq. 15.9 should be introduced;

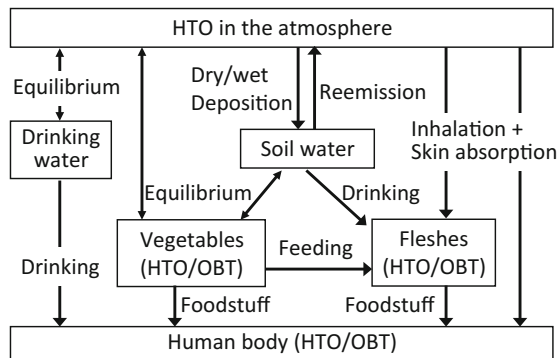
$$\phi_{ij} = w(c_i - kc_j), \quad (15.11)$$

where  $w$  is a proportionality coefficient and  $k$  is a coefficient needed if  $c_i$  and  $c_j$  have different dimensions (for example, considering transfer from atmosphere to ground surface, the concentration in the atmosphere is expressed as a volume density but that on the surface is an area density).

The above models expressed as Eqs. 15.10 and 15.11 are based on assumption that decrease in  $c_i$  and increase in  $c_j$  caused by the migration are negligibly small during the analyzing time. If the assumption is not effective, equations should be modified to be time dependent.

As an example, a code named as NORMTRI [10] is introduced here. The code is based on the above migration model of T released as HTO and HT into environmental atmosphere and considers all possible pathways of environmental T to human body. The HTO part of the pathways is shown in Fig. 15.12. Different from the models described above, migrations among the environmental compartments are simplified, and the concentration in each compartment is assumed to be equilibrated with those in other compartments as follows. Further details are described in Ref. [10].

**Fig. 15.12** T migration pathway from HTO in the atmosphere to human body modeled in NORMTRI, redrawn from Fig. 1 of [10]



### Surface water (drinking and soil)

Drinking water for human and animals is originated from either surface water or ground water. The tritiated water (HTO) concentration in the surface water is assumed to be equivalent with that in air moisture. HTO concentration in the groundwater is derived by multiplying a reduction factor,  $r_w$  (in between 0 and 1 for clean ground water and the surface water, respectively), to the concentration in the surface water. Then, the HTO concentration in drinking water,  $c_{\text{wat}}$ , is expressed as:

$$c_{\text{wat}} = \frac{C_{\text{air, ay}}}{h_{\text{a, ay}}} r_w, \quad (15.12)$$

where  $C_{\text{air, ay}}$  is averaged HTO concentration in air within a whole year and  $h_{\text{a, ay}}$  is averaged volumetric absolute humidity within a whole year.

### Plants (vegetables and forages)

Tritium in some representative plants, such as foodstuffs for human or animals, is considered in NORMTRI. The plants are divided into two categories: greens and root vegetables. The HTO and OBT concentrations in each vegetable are separately calculated from T concentrations in soil water and/or air humidity based on the fractions of organic matter and water of each plant. The T concentrations are also different depending on the plant categories of the vegetables and seasons in a year (vegetation or winter).

During the vegetation period, the HTO concentration in the greens is calculated based on the mean HTO concentration in air moisture and the soil water. Their contribution is determined by relative humidity,  $h_r$ ; if  $h_r = 100\%$ , for example, all of HTO in the greens originates from air moisture. The OBT concentration is obtained by assuming that T/H atomic ratio in the organic material is equivalent to that in air moisture and the surface water.

The HTO concentration in the edible parts (tubers) of the root vegetables during vegetation period is assumed to originate solely from HTO in the soil water. The OBT concentration is calculated according to the same procedure as the greens, because the organic materials are photosynthesized at leaves.

During the winter, it is assumed that any vegetables are not cultivated and stocked ones are consumed. Therefore, both HTO and OBT concentrations in the leafy and root plants are same as in the vegetation period at beginning of the winter. Then, they are determined by multiplying with the radioactive decay factor taking the time difference between harvesting and consumption or feeding into account.

### **Meat (from beef, pork, sheep, and chicken) and milk**

In NORMTRI, it is assumed that the T concentration in organic compartment of animals as well as that in water compartment is in equilibrium with the incoming water and feedstuffs. The incoming pathways are inhalation air, skin absorption, and the feeding materials. The HTO concentration in fleshes (animal meat) is calculated by adding the entire T uptake weighted by its relative fraction of the total uptake of water. The OBT concentration is calculated with the similar way as described above, except for a reduction factor taking into account the number of hydrogen atoms between the organic and inorganic fractions. In addition, the change in feeding habit and radioactive decay during the winter period is considered.

The general approach to calculate the T concentration in milk is in accordance with that used for the fleshes because of equilibrium with the animal (cow) body.

#### ***15.4.3 Dose Estimation***

On standard approach of dose estimation, the dose is calculated by summing up T uptake multiplied with a dose conversion factor (DCF) for each incoming pathway for every chemical form (HTO or OBT). The pathways into human body are almost same as those into animals (inhalation, skin-absorption, drinking water, and ingestion). The dose is evaluated under a “conservative” assumption that the objective person keeps staying at the specific location (evaluation point), and taking all breathing air, drinking water, and eating foods originated there. Although content and amounts of intakes of foodstuff, breathing rate, and many other factors depend on individuals, a “standard” human in that society is assumed for the dose evaluation. Nevertheless, this analysis is deeply related with culture and food habit; for example, a staple food in many Asian countries is rice, but that in other countries may be wheat, barley, corn, potato, or others. In addition, the T uptake is quite differently dependent on where the drinking water comes either from surface water or from underground water.

The existing approach to estimate the impact of T in the environment on human bodies is based on annual dose calculated by multiplication of T uptake and the DCF as mentioned above under the assumption that the T uptake distributes uniformly in a human body or each organ. However, the possible impact on human health caused by such low levels of T exposure appears in carcinogenesis or leukemia, initiated by damaging DNA. Tritium just adjacent or in the cell nucleus can damage their DNA since the mean free path of  $\beta$  ray from T in water is less than

5  $\mu\text{m}$ , which is shorter than the human cell size ranging from 10  $\mu\text{m}$  to 50  $\mu\text{m}$ . Therefore, distribution of T in the cell is important to estimate the stochastic risk.

An advanced approach considering transfer of T into DNA from foodstuff and drinking water is under development, which can assess the risk caused by low-dose irradiation of T [11]. In the approach, *Escherichia coli* was cultivated with tritiated water or tritiated glucose, and then T concentration in DNA was measured. Based on the results, the transfer coefficient of T (from foodstuff and drinking water to DNA) was estimated. By using this transfer coefficient, contribution of OBT to the T concentration in DNA was estimated to be 67 %, which is greater than the contribution of OBT to the T dose calculated by applying the conventional approach, 26 %. This result suggests necessity of new approach to estimate the stochastic risk, in addition to the conventional dose estimation.

## 15.5 Summary

This chapter introduced a simple approach to estimate source terms for T released from a fusion power plant, dispersion models of released T in the atmosphere, and T migration model among environmental elements, considering final uptake to human body through inhalation and ingestion.

It was indicated that major part of T released from a fusion power plant during normal operation is incorporated in thermo-fluids along with release of waste heat. This permeated T is chronically released from stack, cooling tower, or wastewater outlet as elemental HT and/or HTO. In addition, there could be accidental T release. Although, the release scenarios at the accidents change depending on the plant design and accident types, T is possibly released in very short time with a quite high release rate compared with the chronological release.

The released T will be isotopically diluted in the case of release into seawater, while it will be dispersed broadly by advection and diffusion in the case of release into the atmosphere. The modified Gaussian plume and puff models considering absorption into large water surface were indicated to be useful to estimate T distribution in the atmosphere.

The total uptake of T into human body, which is necessary to estimate dose by internal exposure, inhalation (from air), and ingestion (from foods and water), is estimated by using a compartment model. In this model, the T concentration in each environmental compartment on the ground is estimated by considering migration among each compartment and between the compartments and atmosphere.

Combination of these models makes us to understand the environmental behavior of T and then to control the impact on public health by feeding back the results to the plant design including ambient geographical conditions of the plant.

## Appendix: Analysis of Tritium Behavior in the Atmosphere

The analysis introduced in the main text for T release, transportation, migration, uptake into lives, and so on in surrounding area of a fusion power plant is based on Gaussian puff and plume models which have been well developed for analyzing transportation of air pollutant in the atmosphere. Here, the models are explained in a little detail with modifications of them to analyze the T transportation. Details of the T transportation analysis are in the main text.

### Transportation by Advection and Diffusion

Dispersion of T released into the vicinity atmosphere is affected by the meteorological conditions such as wind velocity and solar irradiation, which vary from hour to hour. Therefore, it is hard to analyze and predict the dispersion behavior accurately.

In liquid, gas, or solid that is in static condition, solutes (atoms and molecules) in them diffuse driven by molecular motion, which can be solved analytically by applying Fick's law with their diffusion coefficients. On the other hand, in the case of dispersion in atmosphere, the solute is carried by air which moves intricately and far faster than molecular diffusion. This is called "turbulent diffusion" and is multiscale phenomenon ranging from molecular motion ( $\sim 10^{-7}$  m) to global scale ( $\sim 10^7$  m). Therefore, it is quite hard to analyze completely and to trace all atmospheric molecules in the analyzing area. However, if focusing attention on limited time and spatial scales, the phenomena of the interested region can be analyzed by using simple functions or coefficients as representatives of other scaling phenomena. A lot of analyzing models have been developed for many kinds of scales in time and space; we should select the appropriate one depending on the interest. To analyze T behavior released from a fusion plant during normal operation, for example, the scales might be orders of  $\sim 10$  years and  $\sim 100$  km.

### Introduction of Traditional Tritium Dispersion Models and Codes

A Gaussian dispersion model is very simple and therefore has been used for the prediction of migration of air pollutant such as industrial fumes. It has been modified for analyzing transportation of radioactive materials in both chronic and accidental releases from a nuclear fission power plant. In particular, a Gaussian plume model is adopted to estimate dispersion of radioactive materials released from a fission power plant in the "Meteorological Guide for Safety Analysis of

Nuclear Power Reactor Facilities” [12] which guides how to assess a plan for construction of a nuclear fission power plant in Japan.

### (a) Gaussian puff model

In the Gaussian puff model, the pollutant matter is assumed to be released instantaneously at a time and to expand into a flat spherical puff, the center of which is moving along the wind. The spatial distribution of the matter in the puff is assumed to form the normal (Gaussian) distribution, which satisfies the diffusion equation by Fick’s law. This model is usually applied to the case of the instantaneous release of the pollutant matter such as accidental release. Furthermore, this is the base of subsequently explained plume models to analyze chronic release of pollutants.

#### Calm condition

Consider that pollutant with the total amount of  $q$  is instantaneously released at time,  $t = 0$ , from a point  $(x_0, y_0, z_0)$  in flat calm. The pollutant expands with time following the Gaussian distribution. Therefore, the concentration of the pollutant in air,  $c$ , at an observation point  $(x, y, z)$  at time  $t$  is expressed as:

$$c(x, y, z, t) = \frac{q}{(2\pi)^{\frac{3}{2}}\sigma_x\sigma_y\sigma_z} \exp\left(-\frac{(x - x_0)^2}{2\sigma_x^2}\right) \exp\left(-\frac{(y - y_0)^2}{2\sigma_y^2}\right) \exp\left(-\frac{(z - z_0)^2}{2\sigma_z^2}\right), \quad (15.13)$$

where  $\sigma_x$ ,  $\sigma_y$ , and  $\sigma_z$  are dispersion parameters for  $x$ ,  $y$ , and  $z$  directions, respectively. The dispersion parameters increase with time. Equation 15.13 is equivalent to a solution of the diffusion equation:

$$\frac{\partial c}{\partial t} = D\nabla^2 c, \quad (15.14)$$

where  $D$  is the diffusion coefficient of the pollutant in air. If the dispersion parameters can be converted from the diffusion coefficient as:

$$\sigma_x = \sigma_y = \sigma_z = \sqrt{2tD}. \quad (15.15)$$

#### Wind-blown condition

Under a wind-blown condition, the puff is considered to move along the wind velocity,  $\mathbf{u}$ . By taking coordinates, so that the  $x$ -axis is parallel to the wind direction and assuming that the release point is  $(0, 0, h)$ , for simplification, the center of the puff at a time,  $t$ , moves to  $(u(t), 0, h)$ . Then, the following equation expressing the concentration of the pollutant in air is obtained by substituting the center of the moving puff into Eq. 15.13 as:

$$c(x, y, z, t) = \frac{q}{(2\pi)^{\frac{3}{2}}\sigma_x\sigma_y\sigma_z} \exp\left(-\frac{(x-ut)^2}{2\sigma_x^2}\right) \exp\left(-\frac{y^2}{2\sigma_y^2}\right) \exp\left(-\frac{(z-h)^2}{2\sigma_z^2}\right). \quad (15.16)$$

If the wind velocity changes with time, the spatial distribution of the concentration can be obtained by substituting  $(x_0, y_0, z_0) = \int_0^t u(t) dt$  into Eq. 15.13 as well.

### Reflection by the ground surface

The above-mentioned puff model, expressed as Eqs. 15.13 or 15.16, does not include the effect of interaction of the pollutant with the ground surface. In many cases of air pollutions, when the puff of the pollutant touches the ground surface, the absorption of the pollutant onto the surface is negligibly small. This means that the vertical ( $z$ ) flux to the surface is zero, and therefore the concentration gradient along the vertical axis at the ground level should be zero. This condition can be reproduced by introducing an imaginary source at the inverted position of the original source to the ground surface,  $(0, 0, -h)$  as:

$$c = \frac{q}{(2\pi)^{\frac{3}{2}}\sigma_x\sigma_y\sigma_z} \exp\left(-\frac{(x-ut)^2}{2\sigma_x^2}\right) \exp\left(-\frac{y^2}{2\sigma_y^2}\right) \left\{ \exp\left(-\frac{(z-h)^2}{2\sigma_z^2}\right) + \exp\left(-\frac{(z+h)^2}{2\sigma_z^2}\right) \right\}. \quad (15.17)$$

The last term represents the imaginary source, and we can see that Eq. 15.17 satisfies  $\partial c / \partial z|_{z=0} = 0$ . However, in the case of the water surface, HTO should be immediately absorbed without reflection different from the land surface. This must be taken into account in case of release and dispersion of T from a fusion plant as discussed in the main text.

### (b) Gaussian plume model

Assuming a steady-state release with a constant release rate from a fixed point and a stable weather condition, the pollutant can be recognized as superposition of multiinfinitesimal puffs released continuously, each of which is expressed by Eq. 15.17. Here is assumed that the concentration distribution does not change in time, different from the puff model. For simplification, the  $x$ -axis is set parallel to the wind direction and the release point to be  $(0, 0, h)$ . By defining the release rate (released amount of the pollutant per unit time) as  $f$ , the released amount during an infinitesimal period from  $t$  to  $t + dt$  is  $f dt$ , and the concentration of the micro puff given during this period,  $dc$  is expressed as:

$$dc = \frac{f dt}{(2\pi)^{\frac{3}{2}}\sigma_x\sigma_y\sigma_z} \exp\left(-\frac{(x-ut)^2}{2\sigma_x^2}\right) \exp\left(-\frac{y^2}{2\sigma_y^2}\right) \left\{ \exp\left(-\frac{(z-h)^2}{2\sigma_z^2}\right) + \exp\left(-\frac{(z+h)^2}{2\sigma_z^2}\right) \right\}. \quad (15.18)$$

We can obtain the concentration profile by integrating dc with time, as:

$$\begin{aligned}
 c(x, y, z) &= \int_{t=-\infty}^{t=\infty} dc \\
 &= \frac{f}{(2\pi)^{\frac{3}{2}}\sigma_x\sigma_y\sigma_z} \exp\left(-\frac{y^2}{2\sigma_y^2}\right) \left\{ \exp\left(-\frac{(z-h)^2}{2\sigma_z^2}\right) + \exp\left(-\frac{(z+h)^2}{2\sigma_z^2}\right) \right\} \int_{-\infty}^{\infty} \exp\left(-\frac{(x-ut)^2}{2\sigma_x^2}\right) dt \\
 &= \frac{f}{2\pi u\sigma_y\sigma_z} \exp\left(-\frac{y^2}{2\sigma_y^2}\right) \left\{ \exp\left(-\frac{(z-h)^2}{2\sigma_z^2}\right) + \exp\left(-\frac{(z+h)^2}{2\sigma_z^2}\right) \right\}.
 \end{aligned} \tag{15.19}$$

At first glance, Eq. 15.19 does not seem to include the downwind distance ( $x$ ). However, the dispersion coefficients,  $\sigma_y$  and  $\sigma_z$ , are functions of  $x$ ; therefore,  $c$  is still the function of  $x$ .

### (c) Dispersion coefficient, $\sigma$

The horizontal and vertical dispersion coefficients,  $\sigma_y$  and  $\sigma_z$ , in the above-mentioned Gaussian plume model are functions of the downwind distance  $x$  and classifications of the atmospheric stability described below. The plume spreads with increasing the distance from the release origin and having stronger atmospheric turbulence. The horizontal dispersion is far greater than the vertical one. Several methods to determine the coefficients have been established. Here, two typical methods, one using reference curves and the other using approximate expressions, are introduced.

#### Classification of atmospheric stability

In order to determine the dispersion coefficients, it is required to evaluate how stable or how turbulent the atmosphere is. The dispersion will be small in stable atmosphere and will be accelerated in turbulent atmosphere. The stability of the atmosphere is classified by an index, “atmospheric stability class.” This index is categorized into 6 levels (A–F; F is the most stable) by evaluating wind speed and sunshine during the day or cloudiness during the night as given in Table 15.2 by Pasquill [1]. This classification is determined based on the fact that strong sunshine during daytime causes strong updraft airflow, and that clear sky during night results in stable atmosphere due to radiation cooling of ground surface.

**Table 15.2** Atmospheric stability class [1]

Surface wind speed at 10 m [m/s]	Day			Night	
	Incoming solar radiation			Thinly overcast or $\geq 4/8$ low cloud	$\leq 3/8$ cloud
	Strong	Moderate	Slight		
<2	A	A–B	B	N.D.	N.D.
2–3	A–B	B	C	E	F
3–5	B	B–C	C	D	E
5–6	C	C–D	D	D	D
>6	C	D	D	D	D

### Pasquill-Gifford curves

The first method to estimate the dispersion coefficients is referring the Pasquill-Gifford curves after determining the atmospheric stability class. The curves were graphically presented by Turner [2], and approximation formulas were proposed by Green et al. [13] as shown in Fig. 15.13.

### Sutton's formula

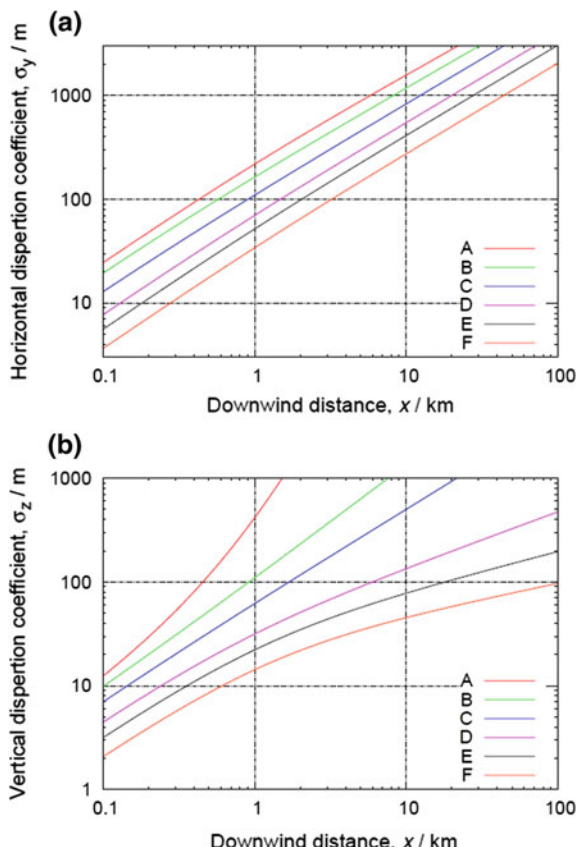
Another method, proposed by Sutton [14], is to express the dispersion parameters by power functions of the downwind distance,  $x$ , as:

$$\sigma_y = \frac{C_y}{\sqrt{2}}(x/m)^{(1-n/2)} \text{ m} \quad (15.20)$$

$$\sigma_z = \frac{C_z}{\sqrt{2}}(x/m)^{(1-n/2)} \text{ m}. \quad (15.21)$$

A similar method is employed in the atmospheric dispersion submodule of the NORMTRI code [10] which was developed to calculate the behavior of T released into the environment under a normal operation. In that model,  $\sigma_y$  and  $\sigma_z$  are expressed as:

**Fig. 15.13** Pasquill-Gifford curves, **a** horizontal and **b** vertical dispersion coefficients as functions of downwind distance and atmospheric stability



$$\sigma_y = P_y \cdot (x/m)^{Q_y}, \quad \text{and} \quad \sigma_z = P_z \cdot (x/m)^{Q_z}, \quad (15.22)$$

where  $P_y$ ,  $Q_y$ ,  $P_z$ , and  $Q_z$  are shown in Table 15.3 with the atmospheric stability, assuming the release height of 100 m and smooth and uniform ground surface.

### Maximum ground concentration

One of the most interesting points when designing the site boundary of a fusion power plant may be how high the maximum T concentration in the atmosphere at the ground level will be and where the maximum concentration will be observed. These issues can be solved by using the Gaussian plume model as follows. The maximal concentration on the ground surface must appear on the  $x$ -axis. Assuming that the dispersion coefficients are given by Eq. 15.22, and substituting Eq. 15.22 and  $y = z = 0$  m into Eq. 15.19, the concentration at the ground level along the  $x$ -axis is presented by:

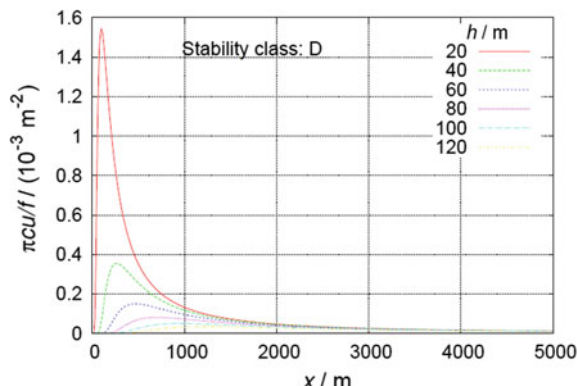
$$c(x, 0, 0) = \frac{f}{\pi u P_y P_z (x/m)^{(Q_y + Q_z)}} \exp\left(-\frac{h^2}{2P_z^2} (x/m)^{-2Q_z}\right). \quad (15.23)$$

In the case of the stability class of “D,” for example, the concentration at the ground-level changes with the downwind distance for different release heights is

**Table 15.3** Dispersion parameters depending on the atmospheric stability class

	Stability class					
	A	B	C	D	E	F
$P_y/m$	0.946	0.826	0.586	0.418	0.297	0.235
$Q_y$	0.796	0.796	0.796	0.796	0.796	0.796
$P_z/m$	1.321	0.950	0.700	0.520	0.382	0.311
$Q_z$	0.711	0.711	0.711	0.711	0.711	0.711

**Fig. 15.14** Concentration along  $x$ -axis for different release heights when the atmospheric stability is class D



shown in Fig. 15.14. As the release point becomes higher, the maximum of the concentration decreases, while the downwind distance  $x$  giving the maximum becomes longer.

The above-mentioned Gaussian puff and plume models are primitive; however, they have an advantage that the concentration in the atmosphere at an arbitrary point can be calculated uniquely without iterative computations. They have been used to calculate the distribution of air pollutants for long time and are still used with appropriate modifications.

## References

1. F. Pasquill, The estimation of the dispersion of windborne material. *Meteorol. Mag.* **90**, 33–49 (1961)
2. D.B. Turner, *Workbook of Atmospheric Dispersion Estimates*, U.S. Department of Health, Education, and Welfare (1970)
3. K. Tobita et al., Compact DEMO SlimCS: design progress and issues. *Nucl. Fusion* **47**, 892–899 (2007)
4. D. Maisonnier et al., DEMO and fusion power plant conceptual studies in Europe. *Fusion Eng. Des.* **81**, 1123–1130 (2006)
5. F. Najmabadi, The ARIES Team, “spherical torus concept as power plants—the ARIES-ST study”. *Fusion Eng. Des.* **65**, 143–164 (2003)
6. A.R. Raffray, Advanced power core system for the ARIES-AT power plant. *Fusion Eng. Des.* **82**, 136–217 (2007)
7. K. Ibano, Design studies of innovatively small fusion reactor based on biomass-fusion hybrid concept: GNOME. *Fusion Eng. Des.* **86**, 2779–2782 (2011)
8. H.Y. Khater et al., ARIES-ST safety design and analysis. *Fusion Eng. Des.* **65**, 285–301 (2003)
9. T. Shibata et al., Model of environmental tritium behavior and effect of aquatic system in Japan, in *Proceedings of Symposium on Fusion Engineering* (2009)
10. W. Raskov, *Description of NORMTRI: a Computer Program for Assessing the Off-Site Consequences from Air-Borne Released Tritium during Normal Operation of Nuclear Facilities*, KfK-Report 5364, Kernforschungszentrum Karlsruhe (1994). ISSN 0303-4003
11. T. Shibata et al., Tritium concentration in the environment and genomic DNA. *Fusion Sci. Technol.* **60**, 1200–1203 (2011)
12. Japan Nuclear Safety Commission, Meteorological Guide for Safety Analysis of Nuclear Power Reactor Facilities (1982)
13. A.E.S. Green, R.P. Singhal, R. Venkateswar, Analytic extensions of the Gaussian Plume model. *J. Air Pollut. Control Assoc.* **30**(7), 773–776 (1980)
14. O.G. Sutton, The theoretical distribution of airborne pollution from factory chimneys. *Q. J. R. Meteorol. Soc.* **73**, 317–318, 426–436 (1947)

# Index

## A

Absorption, 13, 19, 44, 55, 56, 129, 130, 146, 210–212, 222, 231–234, 237, 238, 263, 264, 266, 270, 276, 278, 285, 299, 302, 304, 305, 339–341, 348, 349, 352  
Accelerator mass spectrometry (AMS), 112, 159  
Accident, 13, 18, 19, 23, 120, 307, 308, 315, 317, 319, 321, 328, 338  
Accidental release, 334, 338, 343, 350, 351  
Activated material, 15, 18, 297, 308, 334  
Activation energy for diffusion, 209, 210, 220  
Active charge exchange (ACX), 198, 201, 203  
Adsorbed water, 237, 282, 283, 286, 287, 317  
Adsorption, 22, 55, 56, 130, 133, 141, 155, 208, 220, 234, 237, 240, 279, 281, 282, 285, 287, 290, 293, 315–317, 325  
Advanced fusion fuels, 74  
Air detritiation system (ADS), 337  
ALARA concept, 24, 120, 125, 297, 300, 320  
 $\alpha$ -particle, 75, 80, 84, 85  
 $\alpha$ -particle power, 80  
Annual dose, 342, 348  
Antineutrino, 27, 29  
ARIES-ST, 335, 338  
ASDEX-upgrade, 103, 105  
Astrophysical *S*-factor, 76  
Atmosphere, 19, 22, 41, 55, 57, 62, 84, 120, 124, 153, 154, 159, 208, 232, 239, 282, 301, 302, 311, 312, 317, 332, 333, 339, 340, 343, 344, 346, 347, 349–351, 353, 355  
Atmosphere detritiation system (ADS), 312, 315, 317  
Auger electron spectroscopy (AES), 138  
Austenitic stainless steel, 237  
Austenitic steel, 220  
Autoradiography, 151, 160  
Auxiliary heating, 81

## B

Balmer-alpha, 186  
Balmer lines, 36, 187  
Barrier, 20, 21, 23, 67, 74, 76, 221, 225, 234, 300, 328  
Barrier penetration factor, 75  
<sup>9</sup>Be, 259, 260, 268  
Beam emission spectroscopy (BES), 199, 197  
Beryllides, 269  
Beryllium (Be), 15, 120, 128, 150, 274  
Beryllium wall, 15, 150, 151  
 $\beta$ -counting, 30  
 $\beta$ -decay, 138  
 $\beta$ -electron, 19, 22, 27, 29, 30, 43, 45, 47, 133, 137, 138, 140, 141, 144–148, 150, 155, 157–160, 234, 238  
 $\beta$ -limit, 80  
 $\beta$ -ray induced X-ray spectrometry (BIXA), 146, 150, 159  
Be<sub>12</sub>Ti, 269  
Biological effect, 332  
Blanket, 12, 14, 20, 45, 81, 119, 121, 128, 220, 243, 257, 264, 267, 269, 270, 273, 274, 289, 294, 322  
Blanket coverage, 69, 268  
Blanket system (BS), 11, 15, 20, 33, 45, 50, 52, 55, 58, 62, 63, 65, 67, 96, 119, 120, 128–130, 132, 216, 223, 224, 232, 243, 261, 265, 267–271, 273, 332, 334  
Boiling point (BP), 28, 133, 245, 248, 249  
Boltzmann neutron transport equation, 266  
Boundary condition, 213, 265  
Branching ratio, 186, 189  
Break-even, 8, 24, 82, 83, 90  
Breeding, 6, 23, 33, 47, 52, 63, 65, 223, 261  
Breeding blanket, 91, 108, 220, 223, 257, 270  
Breeding material, 43, 51, 66, 120, 128, 260, 267, 270, 279, 288, 334

- Breeding ratio, 11, 34, 50–53, 61, 67, 336  
 Bremsstrahlung, 36, 79, 81, 144, 145, 150, 154, 159, 160  
 Bulk retention, 107, 110, 111, 113, 114  
 Bulk tritium, 44  
 Burning, 11, 14, 45, 49, 63, 73, 122  
 Burning core, 36, 87, 271  
 Burning efficiency, 17, 20, 23, 33, 35, 41, 45, 46, 49, 50, 52–54, 60, 61, 63, 65, 67–69, 89, 112, 121, 122, 152  
 Burning plasma, 7, 14, 15, 23, 27, 35, 36, 45, 46, 49, 54, 59, 61, 63, 64, 90, 91, 93, 112, 122, 165, 166, 197, 265  
 Burning rate, 36, 267  
 Burn parameter, 90
- C**  
 Calm condition, 351  
 Calorimetry, 111, 127, 138, 146, 157, 161  
 Canada Deuterium Uranium (CANDU), 32, 33, 58, 238  
 Carbides, 221  
 Carbon, 46, 50, 57, 94–96, 100–102, 104, 106, 113, 125, 182, 196, 202, 208, 219, 304  
 Carbon wall, 102  
 Central hotspot ignition, 86  
 Ceramics, 123, 125, 126, 130, 207, 208, 216, 221, 222, 233, 234, 240, 280, 314, 327  
 $\text{CH}_4$ , 95, 96, 100, 125, 143  
 Charge exchange excitation, 198  
 Charge exchange recombination spectroscopy (CXRS), 197, 203  
 Chemical decontamination, 17, 19, 231, 232, 235, 237, 239  
 Chemical diffusion, 22, 40, 44, 87, 107, 124, 207, 210–212, 215, 219, 224, 225, 233, 234, 239  
 Chemical exchange column, 131–133  
 Chemical potential, 74, 76, 161, 183, 208, 225, 254, 307, 311, 322  
 Chemical quenching, 149, 156, 238  
 Chemical sputtering, 96, 100, 101, 114  
 Chemiluminescence, 156  
 Chronic release, 216, 342, 351  
 Chronic Tritium release, 334  
 Cleanup, 119  
 Cold trap, 157, 232, 293  
 Color quenching, 156  
 Column height, 251, 252, 254  
 Combustion, 105, 157, 158, 325  
 Combustion method, 138, 157, 325  
 Compact toroidal injection (CTI), 59, 122  
 Compartment, 308, 315, 316, 322, 345, 346, 348, 349  
 Compound nucleus, 258  
 Concrete, 233–235, 312, 318, 322, 324, 327  
 Confinement, 8, 13, 46, 73, 79, 81, 83, 85, 91, 112, 268, 297, 306, 308, 312, 313, 315, 320, 338  
 Confinement parameter, 82, 83, 85, 89, 90  
 Contaminated area, 161, 235, 300, 305  
 Contaminated material, 19, 41, 235, 239, 300, 302, 320, 328  
 Contamination, 17–20, 41, 42, 52, 140, 153, 161, 231–235, 237–240, 300, 302, 311, 321, 324  
 Coolant, 12, 16, 62, 121, 132, 153, 232, 264, 268, 275, 276, 314, 315, 319, 338  
 Corrosion, 21, 45, 216, 223, 275, 322  
 Coulomb barrier, 6, 7, 76  
 Coulomb potential barrier, 74, 75  
 Counter measure, 308, 315, 319, 338  
 Coverage, 69, 101, 196, 261, 270, 274  
 Cross contamination, 17, 19, 41, 301  
 Cross section, 63, 74, 201, 258, 259, 263, 264, 266, 336  
 Cryogenic adsorption, 130  
 Cryogenic distillation, 243, 244, 246, 247, 252, 254, 324  
 Cryo-sorption, 61, 314, 320  
 Crystal grain, 276, 285, 286, 293  
 Cutoff frequency, 173, 174
- D**  
 Damping rate ( $\gamma$ ), 180, 181  
 D/C, 101–103  
 DD discharge, 102, 103, 105, 106  
 D-D reaction, 6, 74, 75, 238  
 De Broglie wavelength, 76  
 Decay heat, 13, 15, 30, 45, 128, 146, 307, 323  
 Decay term, 343  
 Decontamination, 23, 153, 231, 232, 234, 235, 237, 238, 240  
 Decontamination factor (DF), 20, 23  
 Defect, 22, 99, 108, 224, 234  
 Defense in depth, 23, 297, 306, 307, 313, 328  
 DEMO, 8, 18, 33, 45, 64, 65, 69, 108, 113, 121, 122, 126, 132, 133, 134, 254, 268, 270, 287, 290, 293, 294, 314  
 Density limit, 80  
 Deposition, 14, 96, 102, 103, 197, 344, 346  
 Detritiation, 17, 41, 54, 120, 121, 232, 244, 308, 309, 315, 316, 318, 325, 328, 338  
 Detritiation factor (DF), 126

- D-<sup>3</sup>He reaction, 6, 74, 76  
Differential cross section, 264  
Diffuser, 124, 290  
Diffusion, 40, 102, 110, 123, 138, 210, 218, 225, 226, 237, 255, 286, 349  
Diffusion coefficients, 40, 350  
Diffusivity, 39, 41, 216, 218, 220, 225, 237, 255, 287  
Discrimination electric circuit, 170  
Disintegration, 19, 43, 139, 149, 327  
Dispersion, 333, 349–355  
Disposal, 231, 239, 319, 324, 325, 327  
Dissociation, 76, 127, 189, 216, 293  
Dissolution, 29, 207, 226, 234  
Distillation system, 244, 245, 246  
Divertor, 14, 20, 63, 96, 102, 114, 166, 167, 195, 300, 323  
DNA, 348  
D<sub>2</sub>O, 59, 216, 238  
Does, 18, 35, 66, 69, 75, 89, 120, 148, 282  
Does estimation, 348, 349  
Doping neutral beams (DNB), 202–204  
Drinking water, 20, 43, 347, 348  
D-T burning, 165  
DTO, 59, 216  
D/T ratio, 35, 36, 46, 64, 112, 180  
D-T reaction, 6, 74, 76, 271  
Dust, 18, 124, 125, 300, 302, 319, 320, 322  
Dynamic inventory, 57, 58  
Dynamic retention, 99, 100, 102
- E**  
Effluent tritiation system (EDS), 309, 311, 315–317  
Einstein transition probability, 186, 190  
Elastic recoil detection analysis (ERDA), 157  
Electric power, 12, 16, 62, 274  
Electron impact excitation, 186, 197, 199  
Electron ionization rate coefficient, 181, 182  
ELMy mode, 166  
Energy confinement time ( $\tau_E$ ), 35, 81, 83, 85  
Energy conversion, 11, 12, 15, 258  
Energy flow, 84  
Energy gain, 10, 24, 91, 266  
Enthalpy of solution, 210, 216, 221  
Environment, 17, 32, 120, 126, 153, 208, 223, 243, 246, 307, 311, 319, 321, 327, 332, 333  
Environmental element, 332, 343  
Equilibrator, 244  
Equilibrium dissociation pressure, 127, 277  
Erosion, 18, 94–96, 102, 106, 114, 275, 322  
Er<sub>2</sub>O<sub>3</sub>, 222  
Excitation rate coefficient, 186
- Exhaust, 17, 46, 57, 62, 124, 165, 308, 311, 314, 319, 337  
Exhaust processing system (EPS), 52  
Exposure, 99, 133, 151, 191, 193, 207, 214, 216, 226, 299, 300, 302, 303, 332  
External exposure, 299, 300
- F**  
Fabry-Perot interferometer, 187  
Fading, 151  
Fast ignition, 87  
Feed back fueling, 54  
Feritic steel, 6, 220  
First wall, 14, 67, 96, 101, 114, 224, 261, 270, 334  
Fission product (FP), 12, 13, 17, 307  
Fission reactor, 12, 15, 16, 62, 280, 308  
Flibe, 269, 270, 275, 277, 291, 322  
Fluor, 149  
Fokker-Planck equation, 265  
Fractional burn-up, 73, 87, 89–91  
Fraction of the hydrogen, 174  
Fuel, 6, 7, 10, 13, 17, 20, 21, 29, 37, 47, 49–52, 54, 58, 59, 62, 63, 66, 68, 70, 76, 84–87, 89, 90, 93, 95, 99, 108–110, 112, 120, 124, 126, 185, 244, 271, 297, 320  
Fuel cycle, 45, 65, 91, 121, 126, 246, 254, 290, 315, 328  
Fuel depletion, 87, 89  
Fuel exhauste, 7, 14  
Fuel flow, 52, 69, 152  
Fuel gain, 91  
Fueling, 22, 35, 45, 59, 61, 66, 89, 91, 97, 119, 120, 122, 134, 184, 203, 314, 320  
Fueling control, 97, 114  
Fueling efficiency, 50, 61  
Fueling system, 33  
Fuel injection, 87, 119, 120, 320  
Fuel pellet, 85  
Fuel retention, 21, 45, 51, 63, 66, 103, 106, 109, 110  
Fuel self-sufficiency, 6, 12, 15, 47, 52, 59, 63, 65, 66, 67, 69, 91, 112, 158, 271, 293  
Fuel throughput, 17, 20, 59, 63, 68, 89, 152, 165  
Fusion core plasma, 73, 83  
Fusion neutronics source (FNS), 172  
Fusion plant, 65, 152, 332, 334, 338, 352  
Fusion power, 4, 14, 18, 45, 79, 84, 91, 166, 273, 297, 303, 308, 312, 313, 318, 332–334, 349, 355  
Fusion reactor, 4, 7, 15, 22, 33, 45, 54, 60, 97, 119, 124, 139, 207, 223, 237, 240, 244, 270, 308, 327

**G**

Gamov energy, 75, 78  
 Gas chromatography, 126, 140, 142, 154, 244  
 Gas cooling, 269, 275  
 Gas driven permeation (GDP), 212, 214, 223, 225  
 Gas puff, 46, 63, 122, 152, 177, 314, 341  
 Gas separation, 38  
 Gaussian distribution, 261, 341  
 Gaussian plume model, 338, 341, 342, 350, 355  
 Gaussian puff model, 338, 351  
 Geometrical cross-section, 76  
 Glove box, 19, 21, 42, 134, 153, 239, 301, 302, 308, 311, 312, 317, 328  
 Grain, 100, 110, 113, 221, 222, 280, 285, 287  
 Grain boundary, 222  
 Graphite, 45, 110, 175, 190  
 Gravimetric method, 138, 140  
 Ground, 149, 183, 189, 319, 332, 339, 345, 352  
 Ground water, 345, 347, 348

**H**

Half-life, 27, 28, 32, 339  
 H/C, 96, 101  
 He ash, 14, 17, 59, 120  
 Heat generation, 258, 261, 266, 273  
 Heat of Solution, 22  
 Heat transport, 275  
 Height equivalent to a theoretical plate (HETP), 251, 253  
 Helium (He), 49, 94, 275  
 Helium 3 ( $^3\text{He}$ ), 5, 6, 32, 74, 76, 124, 141, 144, 258  
 HH discharge, 103, 105, 106  
 High field side (HFS), 174, 175  
 High level waste, 326  
 H mode, 166  
 Horizontal transport, 343  
 Hot trap, 292, 293  
 HTO, 19, 20, 32, 42, 62, 129, 130, 133, 152, 155, 157, 232, 237, 283, 286, 290, 302, 319, 325, 339, 344, 347, 349  
 Human, 4, 43, 332, 339, 346, 347, 349  
 Human being, 30, 297  
 Human body, 19, 42, 299, 333, 343  
 Hydride, 126, 129, 292, 315  
 Hydrocarbon, 19, 20, 46, 62, 101, 124, 232, 339  
 Hydrogen, 3, 10, 19, 27, 29, 31, 34, 37, 44, 55, 74, 79, 95, 97, 98, 100, 103, 108, 124, 127, 129, 131, 138, 143, 176, 177, 207–210,

214, 215, 219, 221, 222, 243, 245, 255, 285, 311, 339  
 Hydrogen diffusivity, 218  
 Hydrogen embrittlement, 29, 39, 124, 215, 220  
 Hydrogen explosion, 57  
 Hydrogen permeability, 40, 213, 220, 222  
 Hydrogen plasma, 23, 36, 208  
 Hydrogen production, 29, 33  
 Hydrogen property, 276, 297  
 Hydrogen recycling, 97  
 Hydrogen retention, 106, 109  
 Hydrogen solubility, 211, 220, 221  
 Hydrologic cycle, 339, 340  
 Hydrosphere, 333

**I**

Ice pellet, 19, 22, 30, 45, 64, 314  
 Ignition, 10, 73, 81, 85–87  
 Imaging plate (IP), 151, 160  
 Incident flux, 34, 96, 172, 215  
 Incoming rate, 335  
 Inertial confinement, 8, 10, 73, 108  
 Inertial confinement fusion (ICF), 8, 10, 79, 84, 86, 90, 91, 108  
 Infra-red (IR) lines, 195  
 Ingestion, 299, 332, 348  
 Inhalation, 299, 300, 302, 348, 349  
 Initial inventory, 33, 57, 67, 110  
 Internal exposure, 231, 299, 300, 349  
 International commission on radiological protection (ICRP), 17, 18, 24, 298, 303, 321  
 In-vessel component, 18, 111, 300, 321–323  
 In-vessel fuel retention, 45, 109  
 In-vessel inventory, 23, 64, 109  
 Ion cyclotron frequency, 173, 174  
 Ion–ion hybrid cutoff layer (IIHCL), 174, 175  
 Ion–ion hybrid resonance, 173, 174  
 Ion–ion hybrid resonance layer (IIHRL), 174  
 Ion ionization rate coefficient, 182  
 Ionization chamber, 56, 111, 146, 147, 154, 309, 320  
 Ionization current, 147, 148  
 Ion pump, 93, 154  
 Iron, 4, 142, 290  
 Isotope, 284, 293, 302, 314, 317, 320, 339  
 Isotope effect, 23, 34, 35, 40, 47, 217, 221  
 Isotope exchange reaction, 19, 42, 128, 281, 284, 285, 293  
 Isotope separation, 20, 33, 51, 55, 66, 119, 120, 129, 243, 244, 254, 314, 324  
 Isotope separation system (ISS), 52  
 Isotopic effect, 28, 39, 41, 112  
 Isotopic exchange, 19, 58, 235, 339

- Isotopic replacement, 20, 41, 42, 44, 55, 105, 233, 237  
Isotopologues, 141, 142, 152, 166, 190, 193  
ITER, 8, 9, 15, 17, 18, 20, 24, 33, 47, 54, 58, 83, 96, 106, 108, 111, 113, 121, 125, 129, 132, 146, 165, 166, 177, 184, 203, 204, 240, 245, 254, 271
- J**  
JET, 36, 96, 102, 104, 105, 123, 160, 171, 182, 183, 199, 200, 238  
JET Mark-II, 100  
JT-60U, 103, 105, 109, 110
- K**  
Kinetic energy, 15, 73, 78, 113, 150, 267  
Kinetic theory, 52, 112, 208
- L**  
Last closed flux surface (LCFS), 190  
Lawson criterion, 8, 81  
LiAlO<sub>2</sub>, 276, 277, 281, 286  
Li ceramic pebble, 276, 280  
LiOH, 276  
LiPb, 123, 275, 277, 278, 291, 292, 315, 327, 338  
Liquid breeder, 123, 273, 275, 277, 279, 292, 315, 327  
Liquid cooling, 16, 123, 138  
Liquid lithium, 269  
Liquid scintillator, 148, 156, 161  
Liquid scintillation analyzer (LSA), 148  
Liquid scintillation counter, 320, 324  
Li<sub>4</sub>SiO<sub>4</sub>, 275, 276, 286  
Lithium Lead (LiPb), 62  
Lithium (Li), 33, 62, 258  
Li<sub>2</sub>TiO<sub>3</sub>, 268, 270, 275, 276, 281, 284, 287  
Li<sub>2</sub>ZrO<sub>3</sub>, 276–278  
L mode, 166  
Local TBR, 267, 268, 270  
Low activation, 15, 20, 62  
Low-field side (LFS), 175, 176  
Low level waste, 326, 327  
Low Partial Pressure, 226
- M**  
Magnetic confinement, 64, 108  
Magnetic confinement fusion (MCF), 8, 79  
Magnetic proton recoil spectrometer (MPRS), 170  
Magnetic resonance (NMR) spectroscopy, 238  
Maintenance, 59, 120, 239, 300, 318, 322, 335  
Mass spectrometer, 140, 141  
Maxwell-Boltzmann distribution, 77  
Maxwell velocity distributions, 181  
Meat, 348  
Membrane, 125, 133, 220, 291, 316, 317  
Memory effect, 56, 57, 140, 161  
Metal, 16, 18, 19, 29, 101, 110, 124, 129, 208, 210, 215–217, 220, 225, 234, 278, 317, 338  
Metal bed, 126  
Metal jet diffusion pump, 123  
Metallic wall, 57, 102  
Methane, 96, 124–126, 234, 306  
MHD spectroscopy, 173, 178, 179  
Migration, 100, 224, 232, 234, 280, 332, 335, 345, 347, 350  
Migration path, 332, 334, 337  
Migration rate, 234  
Moisture, 105, 239, 347  
Molecular Fulcher-Band, 189  
Molecular kinetics, 34  
Molecular spectroscopy, 37  
Molecular vibration, 37  
Monitoring, 17, 154, 161, 300, 311, 319, 320  
Multichannel analyzer, 149, 191  
Multi compartments model, 346  
Multiple confinement, 23, 153, 297, 318  
Multi-stage contamination, 41
- N**  
Nafion, 133  
NaI scintillation detector, 150  
Natural abundance, 7, 32, 75  
Net TBR, 69, 267, 268, 270  
Neutral beam injection (NBI), 59, 122, 175, 314  
Neutral density, 181  
Neutral particle analyzer (NPA), 180, 185  
Neutron, 6  
Neutron activation, 113, 161, 172, 321  
Neutron damage, 114  
Neutron density, 262, 264  
Neutron flux, 171, 172, 262, 264, 266, 268, 270  
Neutron multiplier, 11, 34, 96, 259, 269, 270, 278  
Neutron power, 81  
Neutron production rate, 63, 168, 172, 263, 264, 268  
Neutron shielding, 195, 270, 274  
Neutron spectrum, 269, 270  
Newton-Raphson method, 248  
NIF, 10, 86, 91  
Normal operation, 17, 307, 309, 313, 315  
NORMTRI, 346, 347, 354  
Nuclear data, 271  
Nuclear fusion, 3, 73, 152, 257

- Nuclear reaction, 4, 11, 12, 33, 74, 168, 270, 280  
 Nuclear reaction analysis (NRA), 157  
 Nuclear waste, 11, 12  
 Nuclear weapon, 32, 339  
 Numerical model, 332
- O**  
 OH, 44, 216, 233, 235, 237, 317  
 Operating temperature, 110, 114  
 Organic, 19, 31, 42, 130, 137, 156, 233, 238, 347, 348  
 Organic bound tritium (OBT), 19, 20, 31, 42, 152, 234, 300, 306, 320, 325, 348  
 Original plume, 345  
 Orthogonal polarization components, 200  
 OT, 44, 233, 234  
 Out-gassing, 52, 111  
 Oxide, 20, 43, 59, 128, 154, 215, 225, 233, 234, 290, 292, 325  
 Oxide layer, 216, 234, 290, 292  
 Oxygen, 94, 100, 125, 155, 158, 214, 290
- P**  
 Palladium diffuser, 124, 125, 129  
 Palladium (Pd), 124, 125  
 Partial pressure, 128, 226, 315, 340  
 Particle confinement time ( $\tau_p$ ), 91, 93  
 Passive charge exchange (PCX), 201  
 Pb, 11, 15, 80, 124, 259, 269, 277  
 Pd-Ag alloy, 124  
 Pebble, 128, 276, 277, 280, 285, 327  
 Pellet, 10, 59, 63, 122, 123, 315, 320  
 Pellet injection, 59, 64, 122, 314  
 Penetration, 19, 43, 45, 102, 110, 150, 160, 321, 324  
 Permeability, 20, 39, 40, 212, 219–222, 291, 302  
 Permeation, 17, 19, 20, 31, 55, 66, 108, 161, 207, 210, 212, 215, 216, 219, 220, 222, 225, 289, 291, 292, 314, 334, 336  
 Permeation barrier, 20, 62, 220, 225, 232, 289  
 Permeation window, 291  
 Phase velocity, 173  
 Photoluminescence, 156  
 Photon flux, 186, 198, 199  
 Photostimulated luminescence (PSL), 151  
 Physical decontamination, 235  
 Physical sputtering, 94, 96, 235  
 Plasma confinement, 9, 80, 83, 166  
 Plasma-Driven Permeation (PDP), 214, 221, 226  
 Plasma-facing material (PFM), 223
- Plasma facing surface, 14, 20, 41, 63, 93, 97, 103, 107, 113, 161  
 Plasma surface interaction, 93  
 Plasma wall interaction, 93, 113  
 Plume, 338, 341, 342, 345  
 Polarization angel, 200  
 Poloidal mode number, 178  
 Power balance, 264  
 Power generation, 7, 12, 23, 58, 110, 315  
 Pressurized-water reactor (PWR), 336  
 Principle quantum level, 186  
 Prompt redeposition, 94, 96, 102  
 Proportional counter, 138, 147, 148, 155, 309  
 Protection, 24, 233, 297, 300, 307, 320  
 Public exposure, 20, 31, 303, 321  
 Public health, 332, 343, 349  
 Public safety, 18, 19, 23, 59, 338  
 Pulse height analyzer, 149  
 Pump, 15, 24, 35, 52, 61, 123, 309, 314, 320  
 Pumping, 35, 47, 59, 61, 63, 96, 102, 109, 119, 120, 123, 154, 239  
 Purge gas, 237, 239, 275, 280, 281, 283, 285–287, 290, 292, 293, 315  
 Purification, 61, 129, 219, 220, 314, 320  
 PVT measurement, 23
- Q**  
 Q-branch, 190, 193  
 Quantum effect, 37, 40  
 Quench correction, 156  
 Quenching, 149, 150, 156, 158, 238  
 Q-value, 73, 75, 81, 88
- R**  
 Radiated power, 79  
 Radiation damage, 274  
 Radiation does, 231  
 Radiation effects, 224  
 Radiation-induced diffusion, 225  
 Radiation shielding, 273  
 Radioactivity, 6, 12, 18, 20, 22, 27, 54, 55, 60, 69, 120, 137, 139, 140, 142, 147, 148, 151, 156, 161, 231, 246, 301, 322, 326  
 Radiochemical reaction, 234  
 Raman spectroscopy, 38, 142, 143, 238  
 Rate equation, 186, 189  
 Reaction cross section, 6, 258  
 Reaction rate, 6, 12, 13, 35, 73, 77, 79, 96, 111, 237, 264, 266, 267, 285–287  
 Reactor, 6, 13, 15–17, 20, 33, 45, 52, 57, 59, 63, 69, 89, 106, 113, 114, 120, 125, 132, 140, 221, 238, 257, 274, 293, 314, 324, 326, 337  
 Reactor core, 13–15, 120, 122, 261, 308, 322

- Reactor vessel, 15, 17–19, 21, 24, 34, 37, 44, 45, 85, 93, 95, 100, 114, 158, 224, 318, 319, 321  
Recombination, 147, 189, 191, 209, 210, 212, 215, 219  
Recombination rate coefficient, 181  
Recovery, 7, 11, 20, 53, 58, 59, 62, 64, 66–69, 107, 110, 113, 114, 120, 121, 128–131, 239, 259, 268, 271, 273, 276, 279, 320, 325  
Recycle, 45, 47, 327  
Recycling, 35, 41, 63, 97, 98, 113, 189, 324  
Recycling coefficient, 50  
Recycling system, 15, 17, 18, 59, 327  
Redeposited layer, 69, 95, 96, 102–104, 107, 109, 111, 113, 114  
Redeposition, 63, 94, 96, 102, 106, 109, 114  
Reemission, 41, 97–101, 108, 344, 345  
Reflected waves, 174  
Reflection, 41, 98, 205, 265, 341, 342, 352  
Reflectometry, 173, 177  
Regulation, 17–19, 21, 30, 55, 57, 58, 61, 120, 126, 127, 134, 153, 161, 231, 232, 239, 298, 305, 318–320, 325, 326, 337, 339, 342  
Release rate, 46, 54, 112, 320, 332, 337, 338, 349, 352  
Remote area, 102, 105, 113  
Reprocessing, 20  
Reservoir, 19, 50, 64, 127, 140, 314  
Residence time, 60, 61, 64, 66, 67  
Residual gas, 50, 93, 94, 124  
Retention, 24, 46, 52, 57, 62, 69, 96, 99, 104, 109, 112, 224  
Retention mechanism, 109, 114  
Retention rate, 45, 46, 50, 52, 58, 63, 66, 99, 103, 104, 110, 112  
Retention time, 57, 278  
Reuse, 51, 121, 130, 140, 153, 240, 317, 327  
Risk, 302, 321, 349  
Rotational and vibrational levels, 37, 38  
Rotational population, 190  
Rotational quantum number, 190  
Roughing pump, 124  
Rutherford backscattering spectrometry (RBS), 157
- S**  
Safety, 6, 12, 15, 17–20, 23, 24, 27, 29, 30, 41, 45, 47, 55, 58, 59, 69, 93, 99, 108, 111, 113, 137, 153, 158, 165, 231, 289, 307, 308, 314, 324, 328  
Safety factor, 178, 181  
Saturated wall, 101, 103  
Saturation concentration, 101–103, 110  
Scintillation, 138, 149, 150, 238  
Scintillation cocktail, 149, 150, 156, 161  
Scintillator, 146, 149, 156, 158, 170, 183  
Scrape-off layer, 63, 93, 94  
Sea water, 7  
Secondary electron multiplier (SEM), 141, 276, 277  
Secondary ion mass spectrometry (SIMS), 138, 157  
Secondary plume, 345  
Self-ignition, 82, 89  
Self-radiolysis, 44, 45, 47, 155  
Separation factor, 126, 131, 133, 134, 243, 244, 245, 248, 255  
Sequential process, 84  
Shadowed area, 63, 69, 94, 96, 101, 104, 107, 109, 113, 114  
Shock ignition (SI), 87  
Sieverts' law, 208, 214  
SlimCS, 268, 335, 336  
Slowing-down, 257, 261, 268–270  
Smear, 44, 161, 320, 324  
Solid breeder, 128, 268–270, 273, 275, 276, 278, 283, 285, 287, 288, 290, 293, 313, 315, 322, 336, 337  
Solubility, 39, 41, 43, 208, 210, 216, 220, 221, 225, 233, 237, 277  
Source term, 332, 334, 338, 343, 349  
Spin isomers, 29, 38  
Sputtering, 94–96, 101, 113, 157  
Sputtering yield, 94, 96  
Stage, 10, 76, 84, 197, 246–249, 251, 334–336  
Stage model, 246, 247, 249  
Stainless Steel, 159, 182, 195, 216, 220, 225, 237, 289  
Stark multiplet, 200  
Static inventory, 57, 58  
Steel, 15, 151, 196, 216, 220, 222, 237, 289, 327  
Stopping power, 144, 145  
Storage and delivery system (SDS), 52–54, 58, 62, 69, 120, 126  
Structural water, 282, 317, 324  
Superheterodyne reflectometer, 174  
Surface contamination, 55, 148, 161, 219, 233  
Surface Impurity, 14, 44, 94, 111, 113, 114, 155, 210, 233, 293, 327  
Surface reaction, 212, 219, 221, 233, 280, 285–287, 291  
Surface-saturated layer, 102, 107  
Surface tritium, 43  
Surface uptake, 232, 233  
Surface water, 32, 234, 281–284, 287, 332, 347, 348  
Surrounding area, 321, 350

- Swipe assay, 161
- T**
- T accountancy, 18, 22, 31, 54, 55, 69, 127, 153, 158, 161
  - TAE frequency, 178
  - $\tau_E$ , 81–83, 88
  - $\tau_p$ , 88
  - T breeder material, 119, 275, 288
  - T breeding, 7, 15, 16, 23, 27, 33, 34, 45, 51, 53, 59, 60, 62, 67, 69, 107, 120, 257, 258, 260, 261, 267–269, 271, 273, 274, 327, 332, 334
  - T breeding ratio (TBR), 33, 267, 269, 270
  - T burning, 15, 23, 33, 35, 36, 47, 58, 67, 68
  - T concentration, 45, 56, 124, 126, 130, 132, 138, 139, 142, 146, 153, 154, 159, 188, 239, 244, 246, 249, 281, 305, 309, 311, 316, 317, 319, 325, 333, 335, 339–341, 343–345, 347–349, 355
  - T confinement, 20, 23, 59, 134, 308, 309, 313, 314, 317, 328, 334, 338
  - T contaminated waste, 231, 297, 321–325
  - T decay, 30, 32, 45, 66, 113, 137, 144, 268, 270
  - T distribution, 104, 151, 158, 160, 237, 338, 345, 349
  - Temperature Gradient, 224, 226
  - TEXTOR, 37, 38, 103, 105, 190, 201
  - T extraction, 66, 157, 273, 275, 277, 279, 286, 289–291, 293
  - TFTR, 83, 103, 104, 121, 160, 187, 188, 238
  - T handling, 7, 16–19, 21, 23, 31, 44, 52, 54, 55, 57, 60, 67, 69, 124, 127, 134, 148, 153, 154, 158, 161, 165, 231, 233, 235, 238, 240, 254, 297, 300–302, 308, 311, 312, 315, 320, 328
  - Theoretical stage, 246, 248, 251
  - Thermal diffusion, 126, 243, 244
  - Thermal diffusion column, 255
  - Thermal power, 49, 81
  - Thermo-fluid, 333–336, 338, 349
  - Thermomigration, 224
  - Thermonuclear, 8, 10, 73, 84
  - Thermo nuclear fusion, 77–79
  - Throughput, 11, 17, 20, 44, 49–51, 53, 55, 57, 60, 61, 63, 66, 68, 69, 89, 93, 121, 152, 165, 203, 317
  - Time-of-flight (TOF) spectrometer, 170, 172
  - T inventory, 18, 19, 29, 32, 33, 44–46, 55, 57–62, 64, 66, 69, 97, 99, 101, 106–114, 127, 129, 130, 153, 165, 234, 251, 254, 276, 280, 285, 290, 291, 308, 314, 315, 320–322, 324, 334, 338
  - T leakage, 55, 129, 300, 308, 309, 311–314, 317, 319–321
  - T monitor, 143, 146, 154, 308, 311, 316, 319, 323
  - $T_2O$ , 44, 216, 283, 285
  - TOF sphere, 170, 172
  - Tokamak, 8, 9, 14, 17, 21, 33, 50, 57, 63, 79, 80, 90, 96, 97, 102, 103, 106, 109–112, 174, 175, 180, 190, 199, 268, 320
  - Tokamak exhaust process (TEP), 54, 59, 120, 124, 126, 129, 130, 244
  - Tokamak exhaust system (TES), 63, 120
  - Tore Supra, 104
  - Toroidal Alfvén eigenmode(TAE), 173, 178, 179, 180, 184
  - Toroidal mode number, 178–180
  - T permeation, 20, 21, 121, 124, 131, 216, 232, 275, 277, 279, 286, 289–292, 309, 311, 314, 315, 336
  - T processing, 34, 52, 55, 59, 65, 66, 120, 123, 127, 153, 161, 312, 313, 319, 322, 324, 325, 337
  - Traditional tritium dispersion models, 350
  - Transmission coefficient, 181, 182, 184
  - Transportation by advection and diffusion, 332, 333, 350
  - Trap, 99, 154, 157, 237, 292
  - Trapping, 41, 99, 107, 114, 220, 221, 224, 232, 234
  - Trap system, 154
  - T recovery, 54, 62, 64, 66, 67, 128, 129, 131, 232, 235, 268, 280, 281, 285, 286, 289–292, 312, 315, 317, 323, 335
  - T refining, 33, 66, 124, 324
  - T release, 17, 45, 120, 127–129, 153, 161, 233, 234, 239, 273, 276, 279, 280, 281, 284–288, 293, 297, 302, 307–309, 313, 315, 317, 320, 321, 323, 325, 327, 332, 334–336, 338, 339, 343, 346, 349, 350, 354
  - T removal, 58, 106, 114, 120, 130, 131, 133, 322, 323
  - T resource, 6, 12, 15, 23, 45, 55, 62, 67
  - T retention, 33, 44, 45, 55, 60, 67–69, 95, 96, 102–104, 106, 107, 109, 113, 158
  - Tri-diagonal method, 247, 249
  - Triple product (T ntE), 8, 9, 83, 90

- Tritiated water, 20, 42, 45, 47, 62, 119, 120, 128, 131, 133, 153, 155, 231, 232, 235, 237, 304, 306, 339, 347, 349  
Tritium accountancy, 165  
Tritium breeding ratio (TBR), 34, 65, 67, 128, 267, 268, 270, 271, 276  
Tritium burning, 45, 46, 54, 61  
Tritium confinement, 22, 208  
Tritium handling, 11, 15, 19, 23, 41, 45, 55, 111, 237  
Tritium inventory, 34, 45, 62, 65, 106, 111  
Tritium leakage, 17, 19–21, 120  
Tritium management, 113  
Tritium measurement, 30, 139  
Tritium migration, 334  
Tritium permeation, 216, 221, 223–225  
Tritium plasma, 7, 8, 22, 35  
Tritium processing, 20, 55, 56, 220  
Tritium processing laboratory (TPL), 127, 128, 239, 312, 320  
Tritium recovery, 52, 53, 61, 62, 128  
Tritium refining, 51, 59, 63  
Tritium removal, 119  
Tritium reprocessing, 20  
Tritium separation, 51, 61, 96  
T safety, 23, 33, 39, 57, 59, 62, 67, 69, 91, 97, 98, 104, 110, 120, 148, 158, 280, 285, 293, 297, 308, 320, 322, 324, 339  
Tungsten (W), 14, 94, 107, 221  
Tunneling, 6, 41, 75, 76  
T uptake, 233, 237, 240, 290, 291, 320, 344, 348  
Turbo-molecular pump (TMP), 35
- U**  
Ubiquitous water, 18, 31, 41, 44, 47, 55, 233, 339  
Uranium (U), 12, 127, 255
- V**  
Vacuum duct, 94  
Vacuum vessel (VV), 20, 46, 51, 52, 57, 58, 61, 63, 104, 109, 111, 112, 122, 128, 130, 179, 268, 274, 314, 320, 322, 323  
Vanadium (V), 220  
Vapor, 22, 43, 124, 125, 128–131, 133, 138, 216, 231, 239, 244, 246, 248, 249, 251–253, 276, 281–287, 290, 311, 317, 325, 334, 337, 339–341, 345  
Vapor-liquid equilibrium, 131, 247, 249  
Vegetable, 332, 345, 347  
Velocity model, 344, 346  
Ventilation, 54, 59, 232, 301, 302, 308, 311, 312, 316, 317, 325  
Vibrational level, 190  
Volumetric method, 127, 140, 154
- W**  
Wall effect, 156  
Wall inventory, 46, 101, 112  
Wall pumping, 63, 97, 101, 102, 109  
Wall retention, 46, 52, 53, 60–63, 66, 67, 109  
Wall saturation, 103  
Waste disposal, 326  
Waste heat, 334, 337, 349  
Waste management, 323, 326  
Waste water, 339  
Water cooling, 20, 62, 274, 275, 313  
Water de-tritiation system (WDS), 121, 131, 132, 243, 244  
Water formation reaction, 283, 285, 287  
Water surface, 340, 341, 345, 349, 352  
Weak interaction, 74  
Wind-blown condition, 351  
WKB approximation, 177  
WKB calculation, 75  
Worker, 18, 24, 231, 252, 274, 297, 300–305, 311, 312, 320, 325, 328  
W-value, 148
- X**  
X-ray photoelectron spectroscopy (XPS), 138
- Y**  
Yttrium (Y), 292
- Z**  
Zeeman patterns, 193  
Zeolite, 130, 133  
Zero release, 332  
Zirconium (Zr), 127, 129  
ZrCo, 127, 129, 314  
ZrO<sub>2</sub>, 222

